Development and Characterisation of Novel Nanoparticle-Loaded Contact Lenses for the Treatment of Posterior Segment Diseases of the Eye

Dan Chau Thuy Nguyen

A dissertation submitted to the South East Technological University for the fulfilment of the Doctor of Philosophy (PhD) degree.

09th February, 2023

Prepared under the supervision of Prof. Peter McLoughlin, Dr. Richie Ryan, Dr. Joseph Dowling, and Dr. Laurence Fitzhenry.

Ocular Therapeutics Research Group, Pharmaceutical & Molecular Biotechnology Research Centre, Department of Science, South East Technological University.

DECLARATION

I hereby certify that this material, which I now submit for assessment is entirely my own work and has not been taken from the work of others, save to the extent that such work has been cited and acknowledged within the text of my work.

Signed: __Dan Chau Thuy Nguyen___

ID No.: _____20060182_____

Date: ____09th February, 2023____

ACKNOWLEDGEMENTS

I want to express my most sincere appreciation and deepest gratitude for the support and help to the following people, who in one way or another have contributed to making my study possible:

Primarily, I would like to express my sincere gratefulness to my principal supervisor Dr. Laurence Fitzhenry, my co-supervisors Prof. Peter McLoughlin and Dr. Richie Ryan and my enterprise mentor/supervisor Dr. Joseph Dowling for their expertise, understanding, continuous support, guidance, motivation, and advice which benefits me hugely in my completion and the success of this research.

I wish to further my thanks to all the staff in the Pharmaceutical Molecular Biotechnology Research Centre and Department of Science for all their expertise in various scientific areas and for their training and help on the use of FT-IR, HPLC, TGA, DSC, XRD and other instruments, as well as their great input into my projects. I could not have completed this study without them. I also want to thank to all my friends for their friendliness, thoughtfulness and being there for me throughout my research.

My sincere thanks also go to everyone in the Research and Development Department, Quality Control and Monomer Departments at Bausch and Lomb for their continuous support throughout my project. I would also like to thank Professor Ana Paula Serro and her teams at the BIOMAT research group, for their expertise, training, and excellent advice on a large part of my work carried out in Chapter 2.

And especially, I would like to gratefully acknowledge the gratitude, the huge support and love from my family: my mother: Công Huyền Tôn Nữ Diệm Phương, my father: Nguyễn Hoài Bắc, and my brother: Nguyễn Minh Triết; and my fiancé Gerard Gilroy and his mother Marian Gilroy and father Frank Gilroy. They all have helped me to be who I am now and kept me going, this work would not have been possible without them.

Last but not least, I also would like to acknowledge the funding from Irish Research Council – Enterprise Partnership Scheme with Bausch + Lomb Ireland of this project.

ABSTRACT

Treatment of ocular diseases face challenges such as low drug bioavailability from topical routes and side effects from intravitreal injection (e.g., retinal detachment and infection). The sophisticated ocular anatomy, while protecting the eye, also prevents therapeutic compound from readily reaching the target site. This project aims to address these challenges through the development of a hydrogel soft contact lens (SCL) impregnated with drug:cyclodextrin complex-loaded biodegradable and biocompatible polymeric nanoparticles (NPs) designed for controlled release and enhanced corneal permeation.

Daily disposable hydrogel SCLs (nesofilcon A materials) were successfully fabricated at an academic research lab utilising a comparable process to an industrial commercialized lens manufacturing approach. Naringenin (NAR) was chosen as the drug in this study because of its antioxidant and anti-inflammatory activities as an ocular therapeutic. NAR-loaded SCLs exhibited comparable critical lens parameters with >98% optical transparency, >75% water content, a lens diameter of 14.10-14.20 mm and a Young's modulus of 0.51-0.55 MPa. A controlled daily drug delivery was achieved within the estimated therapeutic range of 17.88 – 54.42 µg NAR/day.

In order to improve ocular bioavailability and permeation of NAR, a NAR:SBE-ß-CD (sulfobutyl ether-β-cyclodextrin) inclusion complex was formed using a freeze-drying monophasic system approach. A notable increase (6480-fold) in NAR aqueous solubility was obtained arising from complexation. In addition, this complex was used in the synthesis of a NAR-loaded chitosan (CS) NP through an ionic gelation process (333.3 ± 26.6 nm, +22.0 ± 4.3 mV, and a PDI of 0.0777 ± 0.0580). NAR-loaded CS NPs had a %encapsulation efficiency of 37.4 ± 4.0%, while providing a sustained drug release for 30 days through a diffusion-controlled mechanism.

These two drug carrier systems were subsequently loaded into the developed SCLs. Based on the characterized physicochemical properties of the loaded SCLs, a 'soak and release' approach was determined to be the optimum method. The release mechanism of NAR in complex- and NP-loaded SCLs was governed by both diffusion and swelling, with a drug release rate of 45.95 ± 2.06 and 45.96 ± 5.18 µg NAR/day, respectively.

The results from this research demonstrated that the developed models could act as promising drug delivery systems to provide a more sustained, less invasive, and controlled delivery of a drug or supplement to the eye. Outcomes from this work suggest potential areas for future work that can lead to the commercialization of the studied technologies.

TABLE OF CONTENTS

LIST OF FIGURES

LIST OF TABLES

LIST OF ABBREVIATIONS

Abbreviations	Full name	Abbreviations	Full name
AFM	Atomic Force Microscopy	MI	Molecular imprinting
AIBN	Azobisisobutyronitrile	MW	Molecular weight
AMA	Allyl methacrylate	NAR	Naringenin
AMD	Age-related macular degeneration	NM(s)	Nanomaterial(s)
AML	Aamlodipine	NP(s)	Nanoparticle(s)
API	Active pharmaceutical ingredient	NVP	N-vinyl pyrrolidone
BAB	Blood aqueous barrier	ODD	Ocular drug delivery
BC	Bruch's membrane choroid	ODDS	Ocular drug delivery system
BRB	Blood retinal barrier	PDI	Polydispersity index
CD	Cyclodextrin	PEG-DA	Poly-ethylene glycol diacrylate
CEP	Commercial Enterprise Product	pHEMA	poly2-hydroxy ethyl methacrylate
CL	Contact lens	PLTF	Pre-lens tear film
CNV	Choroidal Neovascularization	POLTF	Post-lens tear film
CS	Chitosan	RPE	Retinal pigment epithelium
CsA	Cyclosporin A	SBE-β-CD	Sulfobutylether-β-Cyclodextrin
DED	Dry-eye disease	SCL(s)	Soft contact lens(es)
DLS	Dynamic Light Scattering	SEM	Scanning Electron Microscopy
DR	Diabetic retinopathy	SiHy	Silicone hydrogel
DSC	Differential Scanning Calorimetry	TBA	Tert-butyl alcohol
EE	Encapsulation Efficiency	TEER	Transepithelial/endothelial electric resistance
EGDMA	Ethylene glycol dimethacrylate	TEM	Transmission Electron Microscopy
EWC	Equilibrium Water Content	TFLL	Tear film lipid layer
FRP	Free radical polymerisation	Tg	Glass transition temperature
HA	Hyaluronic acid	TGA	Thermogravimetric analysis
HEMA	2-hydroxy ethyl methacrylate	TMA	Thermal Mechanical Analysis
HPMC	Hydroxypropyl methylcellulose	VEGF	Vascular endothelial growth factor
IOP	Intraocular Pressure	WM	Waterford Made (lenses made in SETU)
M/T	Monomer to Template ratio	XRD	X-ray diffraction

CHAPTER 1

INTRODUCTION TO

OCULAR DRUG DELIVERY

1 INTRODUCTION TO OCULAR DRUG DELIVERY

In a recent report by the World Health Organization (WHO), it was reported that there are at least 2.2 billion people worldwide with either vision impairment diseases or blindness [1]. The fact that the eye is such a sophisticated organ, with a high level of protection from various biological barriers, along with limitations from the blinking reflex and the renewal rate of the lachrymal fluid, has meant that controlled ocular drug delivery (ODD) has been a significant challenge for scientists [2]. Overcoming such challenges is imperative for effective treatment of various vision-threatening disorders, such as age-related macular degeneration (AMD), diabetic retinopathy (DR), as well as conditions related to quality of life such as dry-eye disease (DED).

Treatment of ocular disorders have often relied upon topical delivery strategies, which are frequently associated with low drug bioavailability [3]. Where relevant, intravitreal or periocular routes have been employed, which, while improving therapeutic bioavailability, can result in a higher number of side effects (e.g., increased intraocular pressure, retinal detachment, infections, etc.) [4-6]. The increased emergence of nanotechnology and nanoscience methods in biopharmaceutical applications has resulted in the research of several novel, safe, patient-friendly formulations, and drug delivery carriers/techniques [7-9]. Such methods not only enhance the efficacy of the ODD system (ODDS) but could also possess lower toxicity as compared to conventional approaches. In addition, by using a therapeutic soft contact lens (SCL) as an ocular drug delivery system, the drug bioavailability can increase from less than 5% in topical administration up to 50% [10, 11]. The first therapeutic-loaded contact lens, Acuvue® Theravision®, was marketed in 2021, which is a ketotifen-loaded hydrogel lens (etafilcon A) from Johnson & Johnson Inc. [12]. This product has increased the interest in the development of various therapeutic-loaded lenses to provide better care for patients who need vision correction and suffer from various ocular diseases.

1.1 Ocular Diseases and Their Treatment

The aging population, together with the rise in obesity and diabetes have resulted in a continuous increase in the prevalence of ocular diseases that lead to visual impairment and blindness [13]. While those that are related to vision loss are mainly due to damage in the posterior segment [14], diseases that affect the anterior segment of the eye are the leading causes of ocular morbidity [15]. This section will provide an overview of the anatomy of the eye, some common ocular diseases, particularly concentrating on the ones that affect the posterior segment of the eye, as well as the mechanism of ocular absorption and various current treatment approaches for eye disease.

1.1.1 The Anatomy of the eye

The eye is one of the most significant and complex sensory organs in the body and is generally divided into the anterior and posterior segments [16]. Including the choroid, neural retina, retinal pigment epithelium (RPE), sclera and vitreous humour, the posterior segment accounts for two-thirds of the ocular space. The anterior segment comprises the aqueous humour, conjunctiva, cornea, ciliary body, lens and iris [16]. The anterior-to-posterior diameter is approximately 24-25 mm and in total, has a mass of roughly 7.5 grams [17]. The eyes are isolated and highly protected due to their unique anatomy and physiology, schematically represented in Figure 1.1 [18, 19].

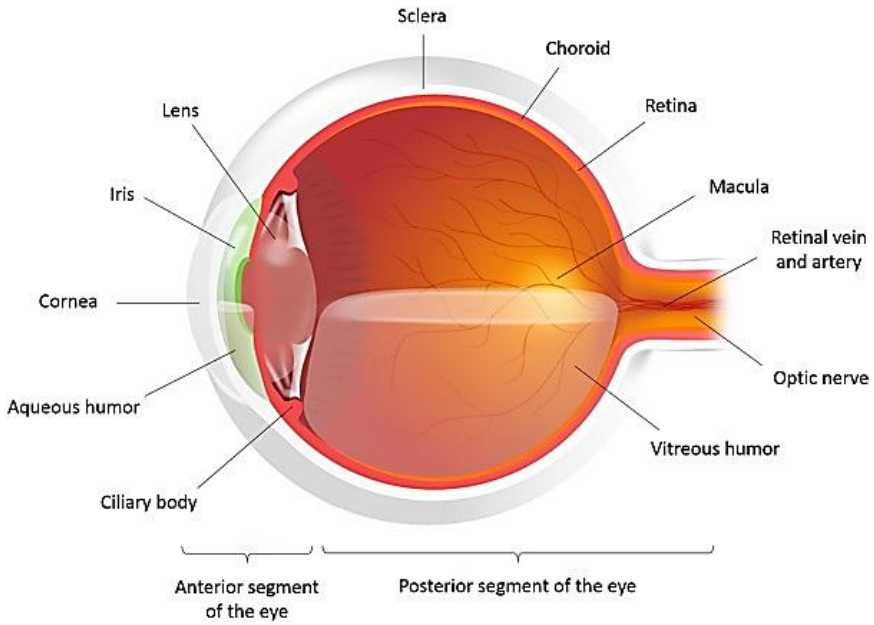

Figure 1.1: Anatomy of the eye [19].

The eye is protected against the permeation of drug particles and foreign bodies due to its sophisticated anatomy [16]. Therefore, to develop a more effective treatment for ocular diseases, an understanding of the various limitations and challenges in ODD is essential. This section aims to give a deeper insight into the anatomy of the eye, of both the anterior and posterior segments, and the corresponding physiology of each tissue, thereby providing an understanding of the potential obstacles that can limit drug delivery to the eye.

1.1.1.1 The anterior segment of the eye

The tear film, along with the cornea and conjunctiva, are the first tissues that interact with the external environment and that are important to ocular health in humans [20]. The tear film contains three layers, which are the lipid, aqueous and mucin layers (Figure 1.2a). Each layer in the tear film has different compounds, including proteins, lipids, electrolytes, mucins, and water. These components not only protect the eye from external pathogenic microbes but also provide nutrients, as well as eliminate waste from the eye. Tear film instability is the main cause of dry-eye disease (DED), one of the most common ocular disorders of the anterior segment [20].

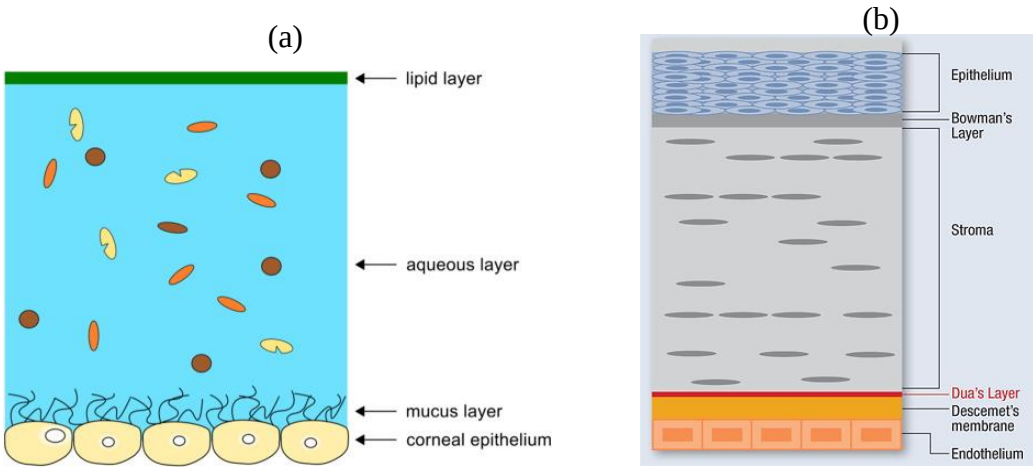

Figure 1.2: (a) Schematic representation of the tear film in contact with the cornea [21] and (b) the six layers of the cornea [22].

The outermost layer, which is also known as the tear film lipid layer (TFLL), contains a mix of both polar and nonpolar lipids. Generally, it is assumed that the lipids in this layer are mainly secreted by the Meibomian glands [20, 21, 23], with the possible exception of phospholipids, since there is no evidence on the origin of phospholipids in the tear film [23, 24]. In an aqueous environment, phospholipids act as amphiphiles

to keep both polar and non-polar layers together. As such, while polar lipids in this layer reduce the surface tension in high concentrations, non-polar lipids tend to repel water [25]. The major functions of this layer are to prevent the evaporation of the tears from ocular surface and stabilize the tear film. Thus, alterations in thickness, distribution and pattern in this layer are often listed as an important stage in the so-called “cascade of inflammation” of DED [21].

The middle layer is the aqueous layer, which forms the bulk of the tear film and is secreted from the lacrimal glands. This layer contains electrolytes, water and proteins [23]. It has an ability to remove epithelial debris, toxins and foreign bodies, together with supplying supplements and oxygen to the underlying avascular corneal tissue [23]. The main proteins are tear lipocalin [26] and lysosome [27]. Lipocalin molecules can help during tear film spreading since they are surface active and amphiphilic [26], while lysosome is active in antimicrobial activity. The aqueous layer also contains soluble mucins that assist throughout film re-spreading [21].

The innermost layer of the tear film is the mucus layer, which consists of secreted mucins, water and electrolytes produced by conjunctival goblet cells [20]. Mucins, also known as a type glycoproteins, function as antioxidants produced by epithelial cells are anchored to the epithelium, which have a molecular weight (MW) ranging from 5×10^4 to 4×10^6 kDa [28]. This layer is active in lubrication and helps prevent the cornea from being damaged during blinking, in addition to the prevention of microbial and bacterial contamination [20].

The cornea is a thin, transparent, and sensitive tissue, which is directly exposed to the external environment [16]. Although it is devoid of blood vessels, the corneal epithelium and endothelium cells are metabolically involved in wound healing. The cornea has six layers in total, including: the epithelium, the Bowman’s layer, stroma, Dua’s layer, Descemet’s membrane and the endothelium [18].

The conjunctiva is a highly vascularized, and semi-transparent tissue that facilitates ocular lubrication by generating mucus, and also helps with tear film adhesion [16]. It lines the palpebral conjunctiva (i.e., inner surface of the eyelids) and the bulbar conjunctiva (i.e., scleral surface of the globe) [29]. It is comprised of the lymphatic

cells which are below the epithelium and has an ability to provide mucus to the tear film, while protecting the ocular surface from pathogens.

Intraocular pressure is maintained by the continuous flow of the aqueous humour from anterior to posterior segments at the rate of 2-2.5 mL/min. The iris-ciliary body and lens (Figure 1.1) play a significant role for vision and offers protection to the retinal layer from UV radiation [16].

1.1.1.2 The posterior segment of the eye

The outer coat of the eyeball, the sclera, also known as the "white of the eye" acts as a primary protection to shield the intraocular contents, which contains collagen fibers, proteoglycans, and glycoproteins. It connects to the cornea through the limbus and has a thickness of 0.51-1 mm (Figure 1.1). Transscleral drug diffusion happens by permeating through porous spaces within the collagen aqueous network [30].

The retina, in the posterior segment of the eye, is a photosensitive tissue, a multi-layered sensor that has a well-organized laminar structure, and which plays a crucial role in converting light into a nerve signal in the central nervous system (Figure 1.3) [19].

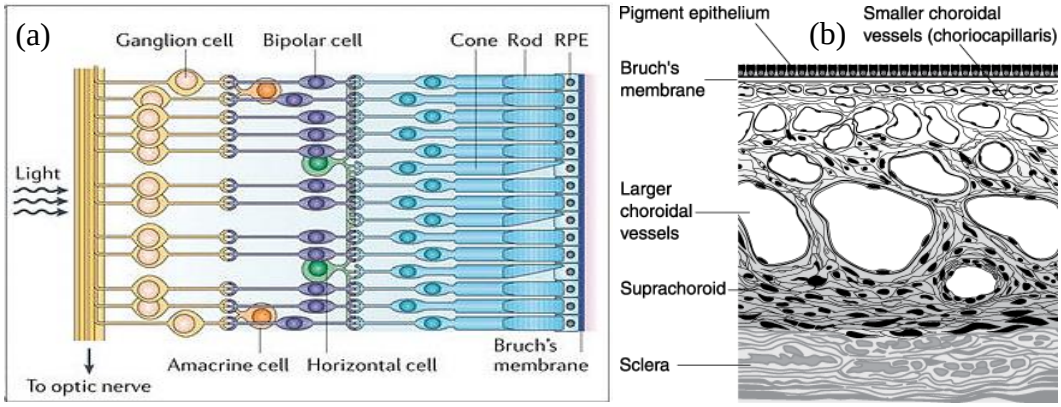

Figure 1.3: (a) Schematic representation of cellular structure of the retinal layer [31] and (b) cross-section image of choroid vessels [32].

The retina has a significant functional relationship with the retinal pigment epithelium (RPE) – a cellular monolayer located under the neural retina [33]. It is composed of tight, adherent and gap junctions and plays a key role in supporting the overlaying photoreceptor cells and protecting the blood-retina barrier [34].

This is due to the ability of RPE in forming a physical barrier that prevents the passage of molecules and ions through the paracellular space. RPE can proliferate under pathological conditions such as AMD [35]. It helps to protect the inner ocular tissues from oxidative damage, as well as releasing large numbers of growth factors such as vascular endothelial, ciliary neurotropic and platelet derived factors. Consequently, it conserves ocular immunity and visual functions, as reviewed by Cholkar *et al.* [16] and Strauss [34]. The RPE has a dark brown colour due to the presence of melanin, which is also presented in the uveal tract (i.e., iris, ciliary body, choroid) of the eye [36, 37]. Melanin was previously studied to reduce damage to the retina and internal nerves from ultraviolet light [37, 38]. In the retinal pigment epithelium, it is a mixed polymer synthesized from α-tyrosine [39]. Retinal melanin was also previously studied to exhibit photoprotective ability by neutralizing ROS as well as decreasing damages caused by free radicals [36]. In ocular pharmacokinetics and pharmacodynamics, melanin binding is an essential factor which was extensively reviewed by Rimpelä *et al.* [40]. This potential interaction between melanin and a therapeutic agent can result in drug accumulation to the pigmented tissue, and thus, would increase drug retention in the ocular tissues [41, 42].

The vitreous humour occupies most of the posterior segment of the eye, and is an avascular, transparent, thick, gel-like fluid (2-3 times more viscous than water) [16]. It comprises mainly hyaluronic acid (HA), proteoglycans (heparan sulphate), and collagen fibrils [18]. The viscosity of this fluid tends to decrease with age [16], which is due to the decrease of enzymatic collagen cross-links. Thus, this would contribute to the instability of the collagen network [43]. This is the main cause for posterior vitreous detachment, as well as contributing to the development of retinal detachment [44]. With the exception of the central retinal artery, the circulation of blood in the posterior segment depends mainly on the choroid vessels – a highly vascularized and innervated tissue that includes three parts: the suprachoroidal, a vascular layer and Bruch's membrane [16] (Figure 1.3b). This tissue can not only control temperature in the eye while maintaining the ocular pressure but can also nourish the photoreceptors' cells in the retina and supply blood to the anterior chamber [18, 19]. A study from Delplace *et al.* [19] indicated that the alterations in vascularization are related to AMD as well as DR, which results in the loss of photoreceptor cells.

1.1.2 Ocular diseases

1.1.2.1 Anterior segment eye diseases

Despite the continuous development in technology, there are still various challenges presented to the effective treatment of anterior segment diseases due to the aforementioned barriers in the eye. These pose an important problem to public health. Such conditions are DED, cataracts, infections, inflammations, etc. [45, 46].

One area where treatment has received noticeable attention is DED, a disease that affects approximately 1 in 11 people worldwide (prevalence of 9.1%) [47]. Instability of the tear film is one of the main causes of DED, which occurs when the eye is inadequately lubricated due to either insufficient tears, poor quality of tear production, or an increase in evaporation. This disease potentially hinders doing computer work, reading, other daily activities, and can also lead to vision loss [48].

A variety of lubricating drops and ointments, which require frequent re-application, are considered to be the current treatment for DED [49]. However, these do not cure the underlying disease process but just temporarily relieve the symptoms. As a result, many studies have been carried out in the field of researching and developing new technology for the effective treatment for DED. Those include the development of nanomaterials and the application of drug-loaded hydrogel materials such as contact lenses [10, 50-52].

1.1.2.2 Posterior segment eye diseases

Posterior segment disorders are commonly defined as diseases of the retina, choroid, and optic nerve, such as AMD, glaucoma and diabetic retinopathy (DR), etc. [53].

AMD is a leading cause of visual impairment among patients aged 45 to 85 years and accounts for 8.7% of blindness worldwide, which is equivalent to 196 million people in 2020 [54]. This number is expected to increase to 288 million in 2040. The exact pathophysiology of AMD is, however, not yet fully understood. It is generally considered to be a result of a complicated multifactorial interaction between metabolic, functional, genetic, and environmental factors [55-58]. AMD can be identified by the presence of drusen within the macula, which appears at the interface between the RPE

and inner collagenous zone of Bruch's membrane [56]. This is followed by choroidal neovascularization (CNV) and geographic atrophy (GA), which can also be referred to as dry or wet AMD, respectively [55-57].

- Dry (non-neovascular) AMD accounts for 85-90% of AMD cases [55]. However, it is less severe, and vision decreases over a longer period of time when compared to the wet form. It happens when drusen forms at the macular, which leads to atrophy of the RPE and eventually results in vision loss [55].
- Wet (neovascular) AMD accounts for 10-15% of AMD cases [55] and is characterized by the growth of new blood vessels from the choroid into the Bruch's membrane, followed by bleeding or leakage that interrupt the normal structure of the photoreceptor-RPE complex. This subsequently leads to severe vision loss, due to retinal damage caused by scar formation [58].

There are several moderately effective treatments for wet AMD that are available on the market. The mainstay of treatment for wet AMD is identified to be the application of intravitreal vascular endothelial growth factor (VEGF) inhibitors and is based on targeting choroidal neovascular membranes [59-61]. VEGF has an important role in many physiological processes. In the eye, VEGF plays a role in the development and trophic maintenance of the choriocapillaris [62], as well as in protecting retinal neurons from apoptosis in conditions of ischemia [63]. Current treatment for AMD involves intravitreal injection using anti-VEGF agents to effectively inhibit the formation of neovascular and reduce leakage of blood vessels. Anti-VEGF drugs can be classified as: RNA aptamer – pegaptanib sodium (Macugen®) [64], monoclonal antibodies including ranibizumab (Lucentis®) [65] and bevacizumab (Avastin®) [66], or fusion proteins including aflibercept (Eylea®; known as VEGF-Trap Eye) [67] and conbercept (Lumitin®) [68]. The change in visual acuity and central macular thickness (CMT) following treatment with intravitreal injections of aflibercept for 12 months in the treatment of neovascular AMD was assessed by Lim *et al.* [67]. An anatomical improvement in macular appearance was investigated to be greatest at Month 1, following by a sustained gain in the next 11 months. A reduction of 44.7 μm in CMT was obtained at Month 12. However, no statistically or clinically noticeably change in visual acuity was recorded [67].

In addition to the current anti-VEGF agents, there are several studies on the development of alternative therapeutic strategies in the treatment of AMD [69-72]. Of those, the use of natural products such as naringenin (NAR) have received considerable research focus due to their favourable pharmacological properties, such as anti-inflammatory and antioxidant behaviours [73, 74]. Oxidative stress is suggested to have an important role in the pathogenesis of AMD since the retina-RPE exists in an environment that is rich in an endogenous source of reactive oxygen species (ROS) [75]. This led to the use of antioxidants to reinforce the eye's defences against oxidative stress. NAR, a natural flavanone, was seen to significantly protect RPE from sodium iodate ($NaIO_3$) induced degeneration as well as prevent the formation of CNV [70]. Comparing to the control group (without $NaIO_3$ and/or NAR), the ERG (electroretinogram) C-waves of both $NaIO_3$ and $NaIO_3$+NAR groups fell to 37% and 57% of control group, respectively. The ERG is a non-invasive technique used in the measurement of the mass electrical response of the retina to light [76]. Moreover, in combination with laser treatment, NAR was shown to reduce the CNV formation by 47% as compared to the control group after four weeks [70].

DR is defined as an ocular manifestation of end-organ destruction in diabetes mellitus [77]. DR is one of the main causes for visual impairment and blindness with around 93 million people globally suffering from this condition. Of those, 17 million people with proliferative retinopathy defined by retinal or iris neovascularization, 21 million people with diabetic macular oedema characterized by the swelling of the macula, and 28 million people with sight-threatening non-proliferative retinopathy identified by microaneurysms, cotton wool and haemorrhage spots [78, 79]. Anti-VEGF treatments including ranibizumab, bevacizumab and aflibercept have the ability to reduce the risk of progression of proliferative DR [77].

Glaucoma is the second leading cause of global irreversible blindness, with approximately 60.5 million people affected worldwide [80]. The main risk factors associated with glaucoma are high intraocular pressure (IOP) and IOP variability. Up until now, the most common treatment for glaucoma is self-administration of topical eye-drops, which can help to manage and lower IOP (by 20-50%), while preventing progressive visual field loss by either increasing aqueous flow or decreasing aqueous production [80, 81].

1.1.3 Mechanisms of ocular absorption from anterior to posterior segments

There are three major pathways for the absorption of drugs through the eye, including the trans-corneal, transscleral and uveal routes, as summarised in Figure 1.4

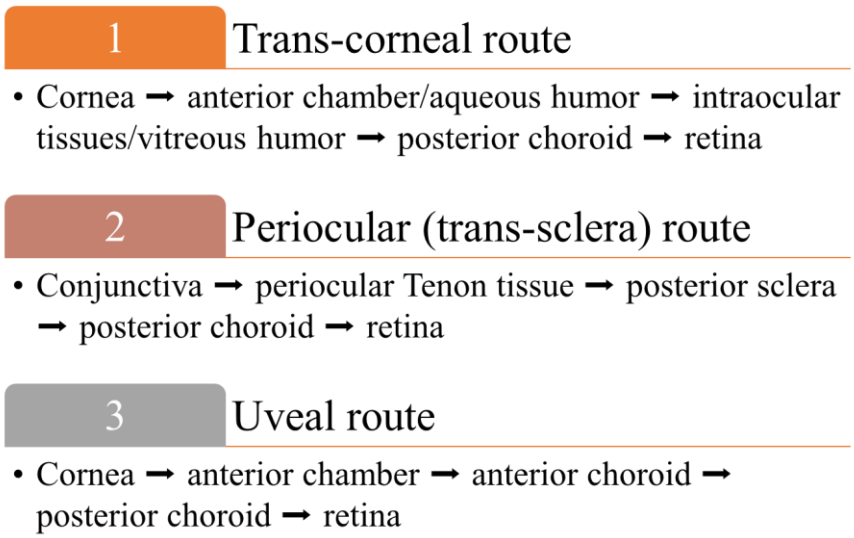

Figure 1.4: Main pathways for ocular absorption from anterior to posterior segments of the eye.

The major route where most of the drugs enter the eye is via the cornea, which occurs from the precorneal space through either paracellular or transcellular pathways [82]. The paracellular route, which can also be anatomically referred to as the intercellular space, is the main route for the passive penetration of ions in the corneal epithelium. The average pore size for Descemet's membrane is 38 nm, while it is 92 nm for the anterior basement membrane [83], which allows the diffusion of small hydrophilic compounds with MW <350 Da [84]. Characteristics such as the MW, lipophilicity and aqueous solubility of drugs play a vital role in the permeability of molecules through this route [82]. For transcellular pathways, the absorption of lipophilic drugs (e.g., propranolol) was shown to be noticeably higher than hydrophilic drugs (e.g., sotalol). Propranolol is a lipophilic drug (logP of 3.21) that was shown to have 10-fold higher absorption via transcellular pathways than a hydrophilic drug – sotalol with a logP of -0.62 [85].

For larger hydrophilic drugs (proteins or peptides) or those that have low corneal permeability, a non-corneal route (i.e., trans-scleral route) is more preferable [82]. The

conjunctiva shows a 17-times higher surface area than the cornea as reviewed by [30] Valera-Fernandez *et al.* Due to the wider intracellular area, the conjunctival absorption is higher than the cornea, allowing the passage of molecules up to 10 kDa. Permeation of both lipophilic and hydrophilic drugs through the sclera demonstrates a higher permeability than the cornea and conjunctiva [86, 87]. In addition, at physiological pH, proteoglycans within the sclera are negatively charged, and thus, it also allows the passage of negatively charged molecules [88].

1.1.4 Traditional ocular drug delivery systems

Ocular drug delivery (ODD) has remained a considerable challenge and has received significant attention from scientists due to its highly complex nature and the presence of various barriers, as mentioned in Sections 1.1.1 and 1.1.2. There are many different routes of ODD and each possess their own advantages and disadvantages (Figure 1.5) [89].

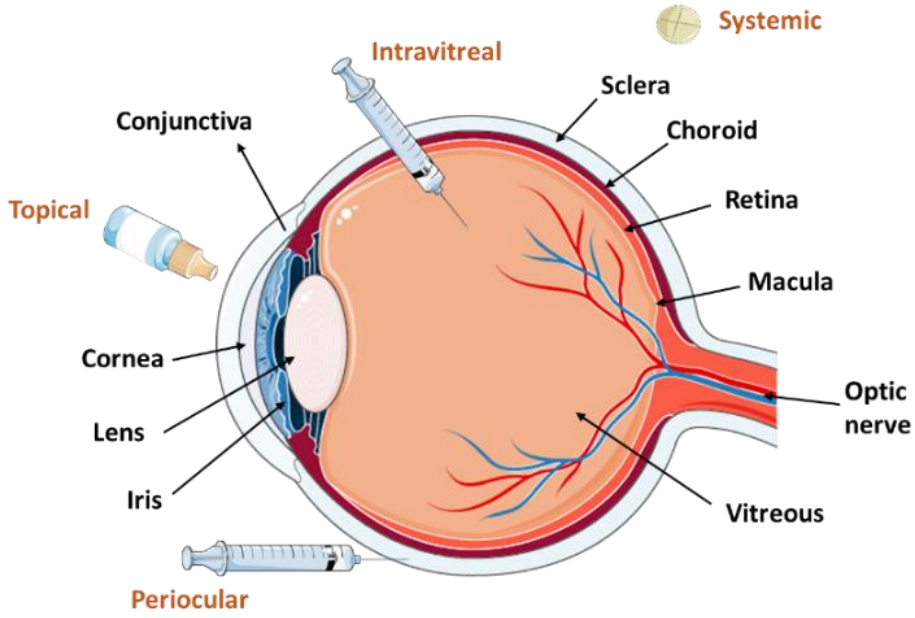

Figure 1.5: Traditional routes of drug administration to the eye (adapted from [90]).

Several studies have been conducted in this field, and there are six main characteristics that should be considered when developing an ODDS [7, 91-93], including:

- Good corneal penetration – good drug bioavailability.
- Controlled drug release – prolonged contact time.
- Targeted drug delivery.

- Low toxicity and minimal side effects.
- Comfortable and non-irritating.
- Patient friendly.

1.1.4.1 Topical drug delivery

The most preferred non-invasive route of ODD is topical administration, especially for treating diseases affecting the anterior segment of the eye. Several studies on various types of this system have been carried out such as eye drops [94], ointments [95], and emulsions [96]. Attributed to the ease of use and patient friendly, the eye drops market is predicted to dramatically increase in the near future, from $15,587 million in 2017 to $22,625 million in 2025 globally [97].

However, this route is known to have limited effectiveness [98, 99]. The main reasons for this are due to the high blinking frequency, high tear drainage and dilution that lead to drug loss in effective therapeutic concentration in the precorneal route, as well as nonspecific absorption [100]. Together with the sophisticated structure of the eye as described above, eye drops have very low residence time on the ocular surface, approximately 2-5 minutes, which results in more frequent applications. The average physiological turnover rate was determined to be 16%/min (for a normal epithelium) [101], which Gahl *et al.* [102] demonstrated that to achieve a sufficient therapeutic dosage of cysteamine, hourly application of eye drops was required. Additionally, treatment for DED [103] or inflammation (from post-cataract surgery) [104] using eye drops also required an application of one drop for each eye four times a day. This leads not only to a reduction in patient compliance, but also to a decrease in undesirable side effects (e.g., redness, blurry vision). Therefore, since only around 5% of the applied dose can reach the targeted tissue, different pathways are required for ODD to both anterior and posterior segments of the eye [105].

1.1.4.2 Oral drug delivery

Oral drug administration is commonly known as a potential non-invasive and patient-friendly route, which can be used in conjunction with topical administration to give a more effective treatment for chronic retinal diseases [89, 106]. Orally administered therapeutics (e.g., CF101 – an A_3 adenosine receptor agonist) [107] and supplements

(e.g., antioxidant [108], hyaluronic acid – HA [109]) were used to provide an effective treatment for DED. A combined supplement of both oral and topical HA was shown to provide a more efficient treatment for DED than topical HA alone [109].

This combination therapy demonstrated an enhancement in corneal epithelial wound healing and related symptoms. The ocular surface disease index for patients when using the combination therapy reduced significantly after 3 months in comparison to patients who only used topical HA, as shown in Figure 1.6.

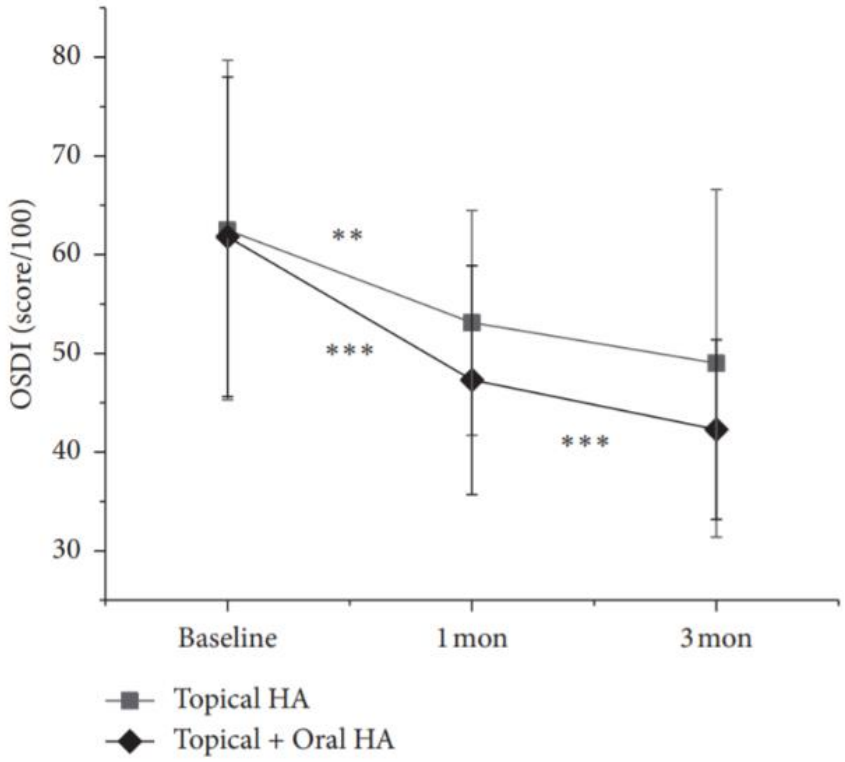

Figure 1.6: Changes in ocular surface disease index between two study groups in 3 months [109].

However, due to the presence of the tight junctions of the RPE, the major challenge for this approach is to effectively cross the blood-aqueous and blood-retinal barriers, which again, would restrict drug permeation and limit the accessibility to a lot of targeted ocular tissues. Thus, a higher dose is required to reach the required therapeutic efficacy, which can lead to possible systemic toxicity [110]. Consequently, more specific targeting ODDSs are required to effectively transport molecules through these barriers into deeper layers of the retina [111].

1.1.4.3 Intravitreal and periocular injections

Unlike ODD to the anterior segment of the eye, topical drug delivery to the posterior is restricted by the lipoidal nature of the corneal epithelium as a rate limiting barrier, systemic circulation absorption and pre-corneal drainage, etc. which leads to low drug bioavailability. One of the most effective approaches that has been identified to overcome the inefficiency of topical and systemic routes to tackle several ocular diseases in the retina, such as AMD, is injection through either intravitreal or periocular routes [89]. Periocular injection bypasses the corneal-conjunctival barrier, along with several barriers present in the posterior segment. This route, however, suffers from rapid drug elimination. Two studies indicated that therapeutics will be drained into systemic circulation through this route, resulting in a reduction in the ocular bioavailability [112, 113].

In comparison, the intravitreal route is said to be more advantageous as the therapeutic will be injected directly into the vitreous [89]. It has been applied widely in the delivery of anti-VEGF proteins such as bevacizumab [114], ranibizumab [114], and aflibercept [115] to wet AMD patients [116], which requires monthly or bimonthly injections. Another factor that has an influence on this approach is the surface charge of the particle. Kim *et al.* [117] observed the movement of intravitreally injected human serum albumin nanoparticle (NP) (HSA-NP). They found that, in comparison to the cationic HSA-NP, which was cationized by covalent coupling of ethylenediamine to carboxyl groups, the anionic HSA-NP showed a better permeation in the vitreous than cationic molecules (Figure 1.7). Anionic NPs could potentially penetrate better through the vitreal barrier in comparison to cationic NPs possibly due to electrostatic attraction between the cationic HAS-NPs and the negatively charged vitreal glycosaminoglycan [117].

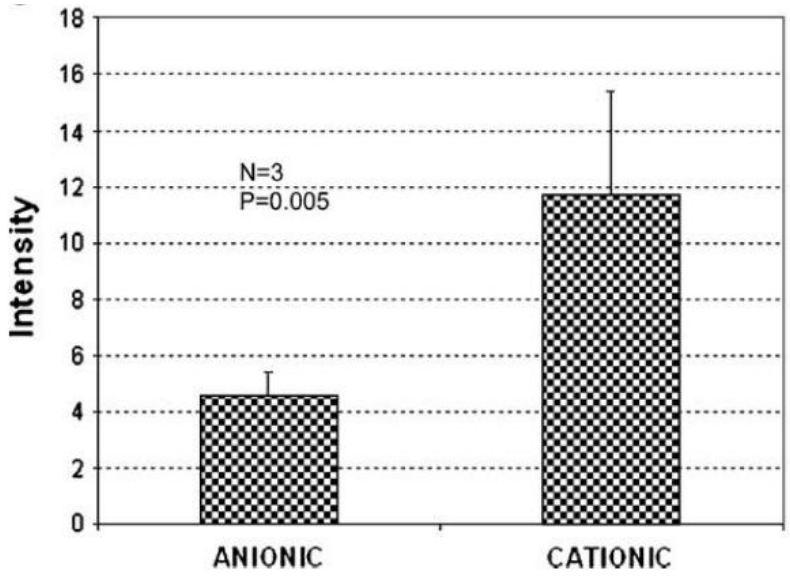

Figure 1.7: The average fluorescence intensity in the vitreous between the anionic and cationic HAS-NP injected eyes [117].

However, there are limitations associated with intravitreal injection therapy, such as retinal detachment [118] or infection [119], although, the recorded risk of these incidences is low. For instance, the risk of developing infectious endophthalmitis per intravitreal injection was seen to be 0.077% (1 per 1291 injections) [119]. Another substantial limitation of this approach is patient compliance. An appropriate follow-up in eye care is essential to ensure a better long-term result of anti-VEGF therapy. A study carried out by Gao *et al.* showed that around 1 in 4 DR patients did not come back to a clinic for further treatment after their first anti-VEGF injection after more than one year [120]. Therefore, such non-compliant practice could lead to a higher risk of further irrecoverable vision loss for those patients.

1.1.5 Challenges in ocular drug delivery

To achieve efficient drug delivery to the eye, with controlled release and targeted delivery, the ODDS has to be designed in such a way that it can overcome the barriers in the anterior and/or posterior segments of the eye. This section provides detail on the different types of ocular barriers, which can be categorized into static/physical and dynamic barriers, and the metabolic barrier (posterior segment only). The level to which these barriers impact on therapeutic bioavailability directs the different approaches to ODD [121].

1.1.5.1 Barriers to anterior segment drug delivery

Figure 1.8 shows the four main static barriers to ocular penetration present in the anterior segment, thereby limiting effective ODD to the internal tissues. The main components in the tear film layer are mucins, water and lipid; all of which will make this layer limit the entrance of the foreign object to the cornea and conjunctiva as described in Section 1.1.1 [122].

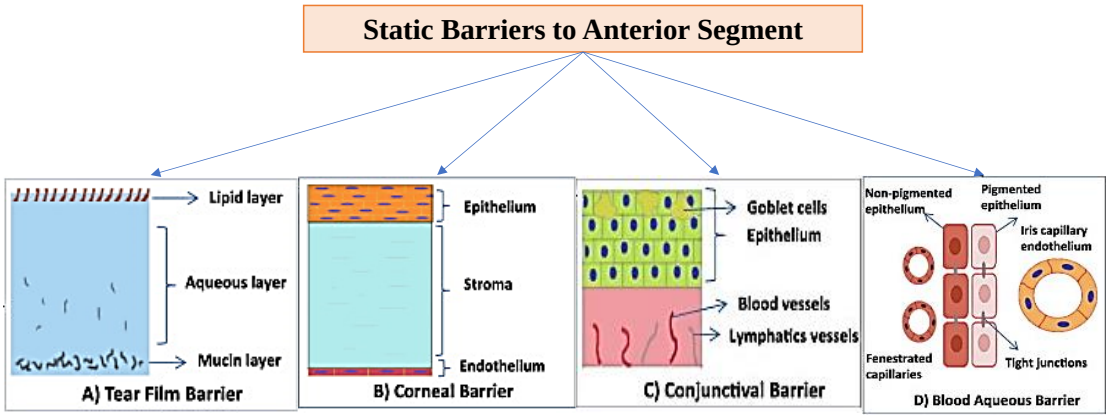

Figure 1.8: Examples of some static barriers in drug delivery to the anterior segment of the eye [122].

The complex structure of the cornea has been demonstrated in Section 1.1.1.1, which makes it act as a multilayered mechanical barrier that significantly prevents the permeation of drugs into deeper ocular tissues. Cholkar *et al.* states that the epithelium is a rate-limiting barrier that limits the penetration of macromolecules and hydrophilic drugs due to the presence of the superficial epithelial cell layers sealed by tight junctions [18]. This hinders the transport of hydrophilic macromolecules that are larger than 100 kDa in MW. Furthermore, with the presence of acid moieties in the mucins of this layer, the epithelium is said to have a negative charge at physiological pH (approximately 7.3-7.4) [123]. The stroma, which is the thickest layer that occupies 90% of the cornea, allows the permeation of hydrophilic compounds while preventing the diffusion of lipophilic drugs due to its hydrophilic nature. The main components in this layer are the open-structured collagen fibrils and mucopolysaccharides, which allow the permeation of large molecules of up to 500 kDa [123]. Due to the contrasting properties between the two layers in the cornea, any drug that is to cross should be amphiphilic with molecular weight less than 500 kDa; making it a significant challenge to achieve efficient ODD.

Aiming to improve the corneal penetration of acetazolamide (used in the treatment of glaucoma) through the topical route, chitosan/sodium tripolyphosphate (CS/TPP) nanoparticles (NPs) were developed as a drug nano-carrier [124]. The synthesized NPs had an average diameter of 188.46 ± 8.53 nm and a charge of +36.86 ± 0.70 mV. Transcorneal permeation studies carried out using goat cornea showed that the drug-loaded NPs provided nearly 2-fold increase in drug permeation compared with an aqueous solution of free drug of the same concentration (i.e., 2.11 ± 0.05% vs. 1.39 ± 0.01%). Since the corneal mucin layer is negatively charged, the positively charged drug-loaded NPs could increase the drug ocular bioavailability due to their electrostatic interactions [124]. This study also showed that the %transcorneal permeation was affected by particle size. NPs that had larger size than 230 nm showed a smaller %transcorneal permeation in comparison to free drug (NPs of size 239.66 ± 3.90, 264.2 ± 9.73 and 289.40 ± 6.36 nm gave the %transcorneal permeation values of 0.76 ± 0.01, 0.75 ± 0.01 and 0.73 ± 0.01, respectively) [124].

The conjunctival barrier also limits the entrance of drugs via the topical route, primarily due to its transepithelial/endothelial electric resistance (TEER), which is in the range of 0.75 to ~1.5 KΩcm^2 [16]. TEER is an accepted measurement of the integrity of the tight junction dynamics in cell culture models of endothelial and epithelial monolayers, which makes it a strong indicator of the integrity of cellular barriers [125]. Although, compared to the cornea, the conjunctiva has a higher paracellular permeability and is therefore a better route for ODD of peptides and oligonucleotides with MW up to 10000 [126]. Such an increase is due to the fact that the conjunctival epithelia contains pores that are twice as large in comparison to those in the cornea , and its total paracellular space is estimated to be 230 times greater than that of the cornea [126]. Based on rabbit eyes, Hamalainen *et al.* calculated that the epithelial pore diameter in corneal epithelium, palpebral and bulbar conjunctiva are 2.0 ± 0.2, 4.9 ± 2.5 and 3.0 ± 1.6 nm, respectively [126].

The other substantial barrier to anterior segment delivery is the tight junction created by the blood aqueous barrier (BAB), which is formed from the combination of the endothelial cells of the iris/ciliary blood vessels and the non-pigmented ciliary epithelium [127]. Small lipophilic molecules are more likely to be removed than larger hydrophilic molecules when crossing the BAB after escaping the tight junctions.

The dynamic barriers, such as tear drain, conjunctival lymph, and blood flow, as well as the aqueous humour, are also factors that limit ODD into the anterior segment. Further, the aqueous humour barrier can also lower the therapeutic bioavailability of larger hydrophilic drugs that penetrate into the eye [16]. This is due to the opposite flow directions from the topical route to the aqueous humour, and towards the cornea to the drug entrance.

1.1.5.2 Barriers to posterior segment drug delivery

As discussed in Section 1.1.1.2, the highly protective nature of the posterior segment of the eye that helps to prevent it from exogenous materials, also prevents the permeation of drugs to the retina. The barriers to the posterior segment delivery can be mainly divided into three categories: static, dynamic, and metabolic (Figure 1.9).

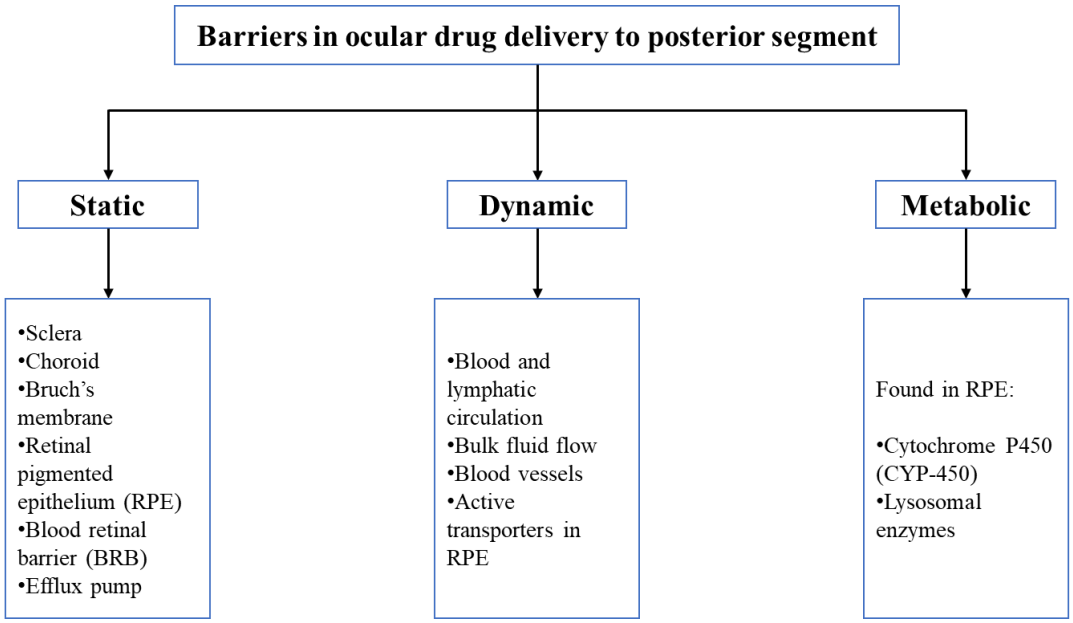

Figure 1.9: The main barriers to drug delivery to the posterior segment of the eye, summarised from references [16, 53, 121].

Numerous studies on *ex vivo* permeability of the sclera, Bruch's membrane and Bruch's membrane choroid (BC)-Retinal pigment epithelium (RPE) have been carried out [88, 128-130]. Increasing the molecular radius of analytes was shown to lead to an exponential decrease in permeability through the sclera [129], BC [130] and BC-RPE [130] barriers. The higher the molecular weight (MW) and molecular radius (MR) of a compound, the lower its scleral permeability [129].

For example, the permeability coefficient of sodium fluorescein (MW: 376 Da, MR: 0.5 nm) was measured to be 84.5 ± 16.1 x 10^{-6} cm/sec, while a value of 25.2 ± 5.1 x10^{-6} cm/sec was observed for fluorescein isothiocyanate dextran (FITC-D) 4 kDa (MW: 4400 Da, MR: 1.3 nm). In a study carried out by Pitkanen *et al.*, lipophilic ß-blockers were shown to cross the BC-RPE more readily when compared to hydrophilic atenolol and carboxyfluorescein (e.g. permeability coefficient of betaxolol (logD of 1.59) was 16.7 ± 4.5 x 10^{-6} cm/sec and atenolol (logD of -1.77) was 2.21 ± 0.5 x 10^{-6} cm/sec) [130]. When compared to FITC-dextran (80 kDa), RPE-choroid was 35 times more permeable to carboxyfluorescein (376 Da) [130].

Additionally, *in vitro* transscleral drug permeability in bovine and porcine eyes was carried out by Cheruvu and Kompella to study the influence of the choroid-Bruch's layer and solute lipophilicity [88] . By assessing various common solutes including ^{3}H-mannitol (neutral), budesonide (neutral), celecoxib (neutral), sodium fluorescein (anionic) and rhodamine 6G (cationic), particle charge was identified to have an influence on the permeability through the sclera and BC barriers. Because of the poor aqueous solubility of celecoxib and budesonide, permeability studies were conducted with 5 %w/v of hydroxypropyl-ß-cyclodextrin (HP-ß-CD). Permeability studies on the other solutes were also conducted with and without HP-ß-CD. The permeability coefficients across sclera and sclera-choroid-Bruch's layers in both eye models were in an order of ^{3}H-mannitol > fluorescein > budesonide > celecoxib > rhodamine 6G (with HP-ß-CD), and ^{3}H-mannitol > fluorescein > rhodamine 6G (without HP-ß-CD). It was suggested that the choroid-Bruch's layer was a more significant barrier to drug transport than sclera. As such, the presence of this layer resulted in a noticeable reduction in sclera permeability in both bovine and porcine models. A reduction by 2-, 8-, 16-, 36- and 50-fold for ^{3}H-mannitol, fluorescein, budesonide, celecoxib, and rhodamine 6G, respectively was obtained in the bovine model. A reduction by 2-, 7-, 15-, 33-, and 40-fold, respectively, for the solutes as listed above, was seen in porcine model [88].

Further, efflux pumps also act as major static barriers that would also limit the permeability of drug molecules to both anterior and posterior segments. At a cellular level, these actively reduce intracellular therapeutic concentrations [16].

The blood retinal barrier (BRB) (Figure 1.10) in the posterior segment can not only restrict topical drug delivery, but can also reduce the effectiveness of intravenous ODD [100]. It includes the inner BRB, which contains retinal capillary endothelial cells, and the outer BRB that comprises RPE cells [16], both with tight junctions of the non-leaky type [127]. This type of barrier gives selective penetration for highly lipophilic molecules [100] and very small molecules such as CO_2 or O_2 [16].

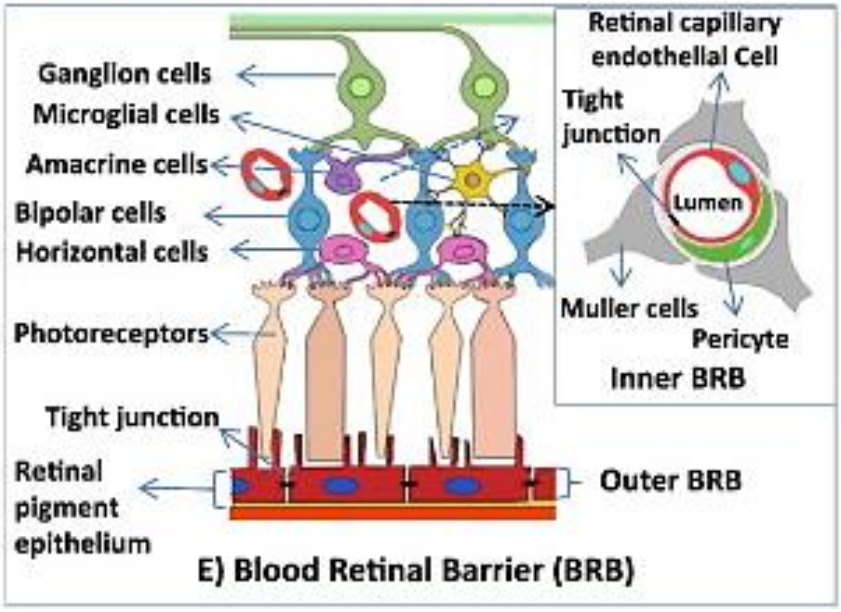

Figure 1.10: Diagram of blood retinal barrier [122].

The choroidal blood and lymph circulation are dynamic barriers to the posterior of the eye. This barrier actively prevents the entrance of lipophilic drugs into inner retinal tissues which would be eliminated through systemic and choroidal circulation [16]. On the other hand, there is evidence that hydrophilic therapeutics such as sodium fluorescein experienced elimination from this barrier to a much lesser extent [131].

Additionally, the posterior segment of the eye also contains several metabolic enzymes such as Cytochrome (CYP) P450 and lysosomal enzymes [121]. The main function of these is to protect the eye against the entry of xenobiotics – foreign substances that are extrinsic to the normal metabolism of a specific organism. However, they can also significantly lower therapeutic bioavailability, when moving across the RPE, by either degrading (lysosomal enzymes) or metabolising (CYP P450) macromolecular drugs [128].

1.2 Nanomaterials in Ocular Drug Delivery Systems

Due to several limitations in conventional ODD routes, such as intravitreal or topical, as discussed in Section 1.1.4, along with the natural barriers present in the eye, scientists have been continuously developing more controlled and targeted ocular drug delivery systems (ODDS). Of those, the applications of nanotechnology in ODDS such as polymeric and lipid nanoparticles (NPs), liposomes, etc. has received particular interest as a new solution for the problems of conventional ODD [132-138]. This approach could potentially both overcome ocular barriers and protect drugs from degradation, while increasing drug permeation. It could also improve the ability to achieve controlled release and targeted delivery of therapeutics [53]. This section will focus on discussing and summarizing the development, advantages, and up-to-date work of such novel ODDS for the treatment of common eye diseases.

Nanotechnology is a branch of technology that deals with matter on a molecular or atomic scale [3]. This has been applied widely in various fields such as science, engineering, etc. As part of this, the development of NPs as drug-carriers in ODD has received attention from scientists with an ultimate goal to improve the quality of human life [13]. Ali *et al.* [139] gave a definition for NPs or nanomaterials (NMs) as materials that have dimensions in the range of 1 to 1000 nm. NMs within the scope of this technology includes polymeric NPs [140], liposomes [133], and micelles [137]. Several main considerations in designing a nanocarrier system is demonstrated in (Figure 1.11) [141].

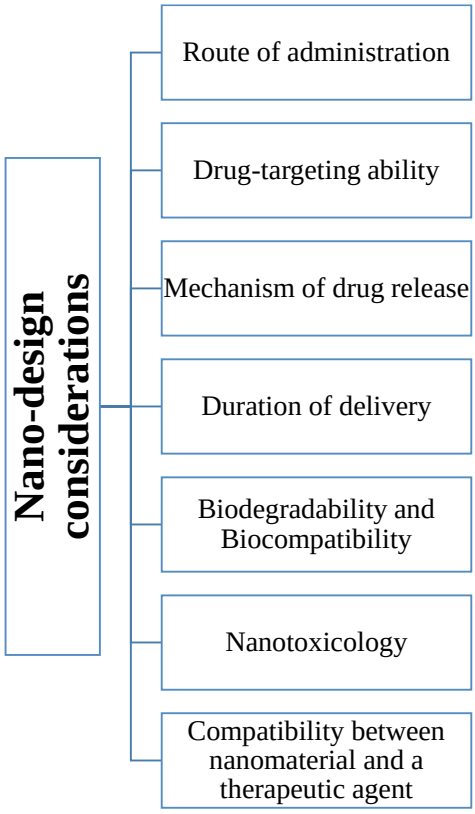

Figure 1.11: Main considerations in nano-design platforms (adapted from [141]).

1.2.1 Polysaccharide-based nanomaterials

Polysaccharide-based nanomaterials have received great attention in the development of therapeutic nanocarriers aiming to provide a more effective treatment for various diseases [140, 142-147]. Polysaccharides hold a large number of hydroxyl groups or other hydrophilic groups, such as amino groups in chitosan [148] and carboxyl groups in hyaluronic acid [149].

Chitosan (CS) (Figure 1.12), which is the most important derivative of the strongly polycationic chitin (poly(ß-(1→4)-N-acetyl-D-glucosamine)), has gained great attention in various fields such as the environment [150], food [151], cosmetic [152] and pharmaceutical (e.g. wound dressing) [153]. Deacetylation of chitin under 40-50% alkaline solution (e.g., sodium hydroxide) at 100-160 °C for a few hours is a common process in the preparation of CS [154-157]. The degree of deacetylation of CS can be up to 95%.

Because of its amine groups, CS is a weak base/polyelectrolyte (pka ~ 6.5), and so it is only soluble in dilute acidic solution (e.g., 1% CH_3COOH), which can potentially convert the glucosamine units into a soluble form of protonated amine [158]. This happens due to the protonation of the NH_2 functional group on the C-2 position of the D-glucosamine repeating unit, which leads to the removal of the acetyl moieties presented in the amine functional groups (Figure 1.12).

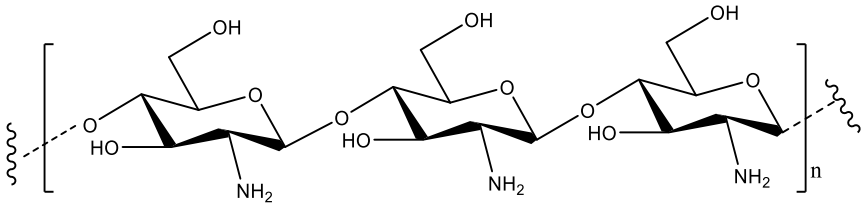

Figure 1.12: Chitosan molecular structure.

The pKa values of CS are in a range of 6.2 to 7. At pH 7.4 and above, the aqueous solubility of CS decreases [159]. Properties of CS depend on the distribution of the acetyl groups together with its molecular weight [160, 161]. CS is considered as a potential carrier in ODDS due to its inertness, biodegradability, biocompatibility, non-toxic and non-immunogenic properties, as well as antibacterial activity, which was extensively reviewed by Paliwal *et al.* [162], Morris *et al.* [163] and Badawy and Rabea [164]. CS positive charge can bind to the negative charge on the corneal surface, which results in enhancement in the residence time in the precorneal area while reducing clearance [165]. This property is known as mucoadhesion, and can be defined as the adhesion when one of the surfaces is mucus, which consists of water (>95%) and high molecular weight glycoprotein mucin [165]. The interaction between CS and mucin is dependent on the charge of the mucin, as well as the concentration, molecular weight, and charge of CS, in addition to the pH of the aqueous media [166, 167].

CS-based formulations such as NPs [144] or nanomicelles [168] have been applied in ocular applications, which results in a more controlled drug release and targeted delivery, as well as increasing therapeutic bioavailability. In order to enhance the bioavailability and efficacy of dorzolamide in glaucoma treatment, an *in situ* gel of CS NP was developed by Katiyar *et al.* [148]. The optimized drug-loaded CS NPs with 164 nm in size exhibited a 98.1% drug loading efficiency. Through an *ex vivo* study, a sustained drug release for the optimal *in* situ gel NP formulation was also obtained

(58% of drug release in 8 hours). Further, HET-CAM (hen's egg-chorioallantonic membrane test) assay test on this nanocarrier also demonstrated that it was a non-irritant [148]. Another investigation on CS NP, hyaluronic acid (HA)-coated CS NP, and dexamethasone-sodium-phosphate (DEX) was carried out by Kalam [132]. This work aimed to study the *in-vitro* trans-corneal permeation on excised-rabbit cornea and its impact on hydration level of cornea, *in vivo* ocular irritation, concentration of DEX after topical administration in tear and aqueous humour. Comparing to DEX-solution systems, both uncoated and coated NPs showed significantly prolonged release of drug in aqueous humour after 24 hours topical administration. The permeability coefficient for DEX-solution was 21.909 x 10^{-3} cm/h, and a value of 23.193 x10^{-3} cm/h was obtained for HA-coated CS NPs. They also resulted in higher tear concentration and higher bioavailability of DEX-solution (2548.563 ngmL^{-1}.h), about 1.83 and 2.14-fold higher observed for CS NPs (4674.413 ngmL^{-1}.h) and HA-coated CS NPs (5451.366 ngmL^{-1}.h), respectively). This phenomena was suggested to be due to the mucoadhesive property of both CS and HA [132].

HA (Figure 1.13) is an unbranched linear polysaccharide comprised of disaccharide units containing of glucuronic acid and N-acetylglucosamine [169] linked by ß(1-3) and ß(1-4) glycosidic bonds [170]. HA exists as a polyanion with a pKa value of 3.21 [171]. The molecular weight range of naturally occurring HA is 10^5 to 10^7 Dalton as reported by Balazs *et al.* [172].

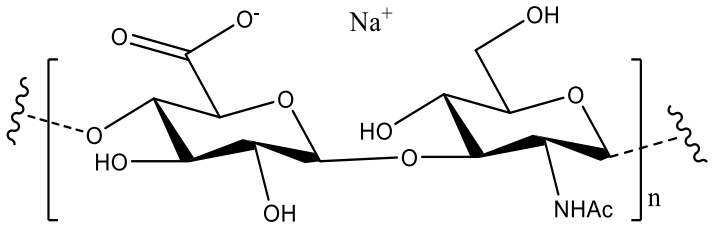

Figure 1.13: Sodium hyaluronate molecular structure.

HA has been shown to be biocompatible, biodegradable, non-immunogenic, non-inflammatory and non-toxic [169]. In the eye, HA can be found in the vitreous humor [173]. Due to its viscoeleastic and mucoadhesive properties, together with its high water-binding capacity and ability to enhance comfort, HA has been commonly used in various areas such as cosmetics [174], tissue engineering [175], pharmaceutical (arthritis treatment) [176] and drug delivery [177].

Silva *et al.* developed CS/HA NPs loaded with epoetin beta (EPOβ) for subconjunctival ocular delivery to potentially provide a more effective treatment for glaucoma [178]. The optimized drug-loaded CS/HA NPs had an average size of 289 ± 3 nm, with a surface charge of 39 ± 1 mV. The drug encapsulation efficiency was determined to be 38.4 ± 0.3 %. By carrying out *in vitro* release studies in simulated tear fluid (37 °C, pH 7.4), their study observed a EPOβ release rate of 60 – 70% from CS-HA NPs within the first 15 minutes, followed by a sustained drug release of approximately 90% within the next 6 hours. Moreover, the use of CS/HA NPs also showed to enhance the mucoadhesion and retention time of a therapeutic agent on the ocular surface. The *in vivo* study was conducted on healthy Wistar Hannover rats indicated no adverse reactions and no abnormalities could be observed for intraocular pressure during the assays. Furthermore, EPOβ presence was also detected in the retina 12-hour after the subconjunctival administration and remained detectable until day 21, which suggested that this developed model could act as a novel ODDS [178].

When compared to conventional drug formulations, the quality, as well as safety and efficacy profiles of drug-loaded NPs requires an assessment of various additional physicochemical properties [179-182]. These include but are not limited to chemical composition, particle size and shape, polydispersity index, surface coating and charge. Due to the interactions between plasma proteins and the surface of drug-loaded NP, it was postulated that the particle size and polydispersity could be significantly changed [181, 183]. Following the European Medicines Agency [184-186] and the Food and Drug Administration [183, 187] guidelines, the particle size, polydispersity, and size stability of drug-loaded NPs should be controlled in various stages and conditions (aqueous and biological media). The particle size distribution should be measured after formulation, along with investigating its reproducibility to assess batch-to-batch consistency, long-term stability of the NPs throughout storage, particle size in the final product administered to the patient, and changes upon interaction with physiological conditions (e.g., serum proteins).

1.2.2 Nanotoxicology

Nanotoxicology has remained a challenge to the application of potential nanomaterials in either pharmaceutical/medical device or medical fields. It is referred to as the study of potential negative interactions between NPs and biological systems in which they are applied [188]. A book chapter written by Khan and Shanker [189] mentioned that the large-scale production of nanomaterials and the proliferation of novel NPs with complex physical and chemical characteristics have made the study of nanotoxicology essential. Numerous studies have been carried out in this field, and two main points can be identified upon the application of NPs [190]:

- The formation of radicals [191]: due to the noticeably higher surface area to volume ratio, NPs which are highly reactive can lead to increased production of reactive oxygen species (ROS). This results in oxidative stress or inflammation, etc; which can damage proteins, membranes, and DNA in the human body.
- The undesirable permeation of NPs through the epidermis as well as other parts of the body can lead to toxic effects [192]. This may lead to the change in body distribution, passage through the blood-brain barrier, damage of brain cells [193], and activation of blood coagulation pathways [194].

Depending on various aspects derived from the physiochemical properties, physical properties and environmental conditions, a number of approaches, involving biological systems, have been proposed to have an effect on the toxicity of NPs [190]. For examples, the aforementioned features can be the diversified factors of modelling, physicochemical features of nanomaterials, and their biological influences [188]. According to EU Medical Devices Regulations [195], it is accepted that there is scientific uncertainty regarding the risks and benefits of nanomaterial use in medical devices. In the design and manufacture of devices using nanoparticles special care should be taken when there is a high or medium potential for internal exposure. Such devices should be subject to the most stringent conformity assessment procedures. Based on a recommendation from the commission in 2011 it is deemed necessary to introduce a uniform definition of the necessary flexibility to adapt that definition to scientific and technical progress and subsequent regulatory development at Union and international level [195].

1.3 Cyclodextrins in Ocular Drug Delivery

One of the main challenges in the discovery and development of many drugs is their hydrophobic nature, which can result in their poor aqueous solubility, and consequently, poor drug bioavailability at the active site. Fahr *et al.* stated in their review that approximately 40% of the marketed drugs and 60% of the compounds at research and development stage have been listed as poorly soluble in aqueous environments [196]. Many studies have been carried out in an attempt to increase the bioavailability of insoluble drugs, including the use of self-emulsification [197], micronization [198], salt formation [199], pH modification [200] and supramolecular complexation [201]. Of those, host-guest complexes have received a considerable attention in the development of a hydrophobic drug carrier since this approach can potentially increase the drugs solubility, stability, permeability, and bioavailability [202-204]. In this approach, cyclodextrins will form an inclusion complex with a hydrophobic molecule through non-covalent bonds, van der Waals forces, hydrophobic interactions and electrovalent bonds as reviewed by Del Valle [205].

Cyclodextrins (CDs) are cyclic oligosaccharides that have (α-1,4)-linked α-D-glucopyranose units [206] and contain a hydrophobic cavity and a hydrophilic outer surface composed of 6, 7 and 8 dextrose units leading to the formation of three parent CDs: α-, ß- and γ-CD (Figure 1.14).

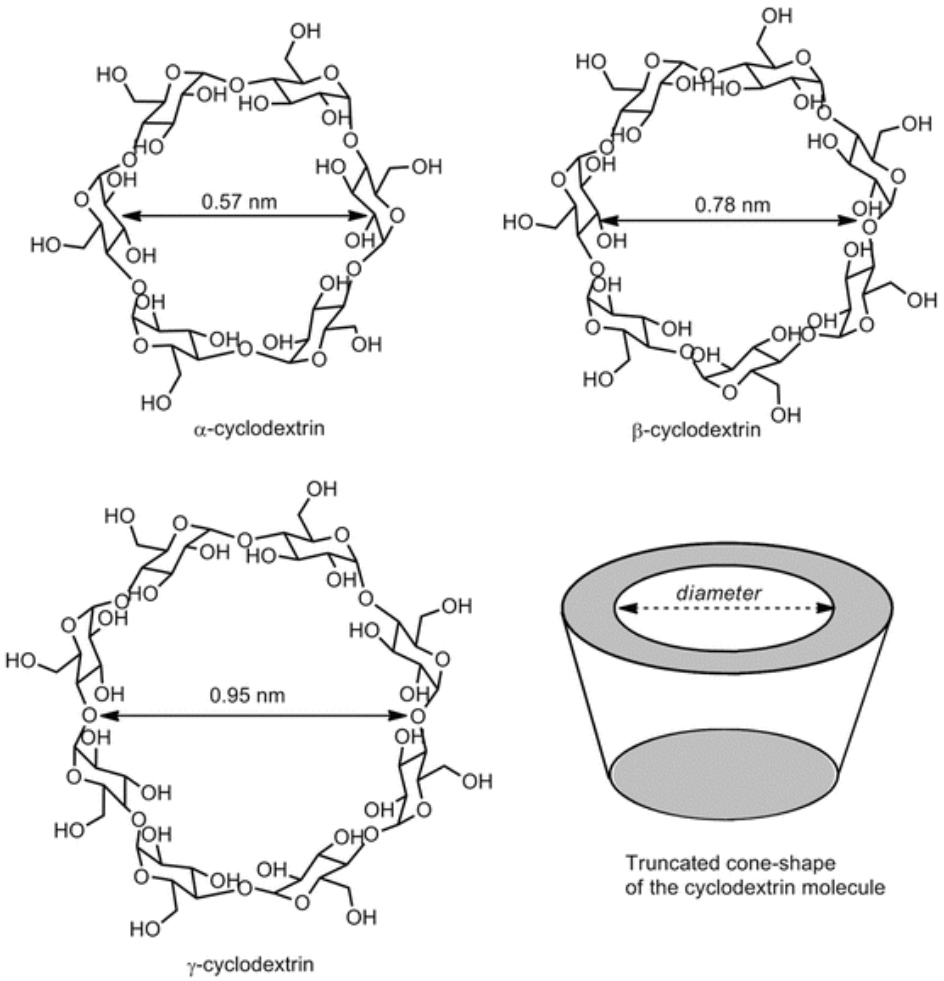

Figure 1.14: Chemical structures of 3 main types of cyclodextrin and their shape [207].

The hydrophobic cavity size can vary depending on the number of dextrose units [208]. This structure of CD gives it an ability to accommodate lipophilic moieties to form host-guest complexes with various hydrophobic analytes – the inclusion complexes [209]. In the area of ophthalmology, besides increasing the aqueous solubility of hydrophobic drugs such as corticosteroids and flavanones (e.g., naringenin) [206], CDs can also act as immunosuppressive agents and an enhancer for ocular permeability of drugs through the extremely lipophilic corneal epithelial membrane [210, 211]. CDs can significantly enhance the permeability of lipophilic drugs through the aqueous tear film to the epithelial surface [206]. Besides the parent α-CD, ß-CD, and γ-CD, there are several derivatized CDs prepared by substituting their hydroxyl groups with the desired functional moieties such as hydroxylpropyl (HP)-α/ß/ γ-CDs [212] and sulfobutyl ether (SBE)-ß-CD [204].

Four of the most common applications of CDs in ODD are: stabilizing the drug, reducing ocular irritation, improving ocular therapeutic permeability, and/or enhancing the solubilisation of the drug or the drug-CD complex [207]. A study carried out by Stancanelli *et al.* [213] investigated the use of a derivative ß-CD, SBE-ß-CD to form an inclusion complex with hydrophobic drugs (isoflavones: genistein (Gen) and daidzein (Dai)). Following the phase solubility (PS) study using the Higuchi and Connors model [214], the solubility diagrams obtained for both drugs suggested that complexes were formed with a 1:1 molar ratio (Figure 1.15(a) and (b)). The aqueous solubility of the hydrophobic drugs was significantly increased upon complexation with SBE-ß-CD as evidenced through the *in vitro* dissolution studies (over 90% of drugs dissolved in water in 15-30 minutes) (Figure 1.15(c)).

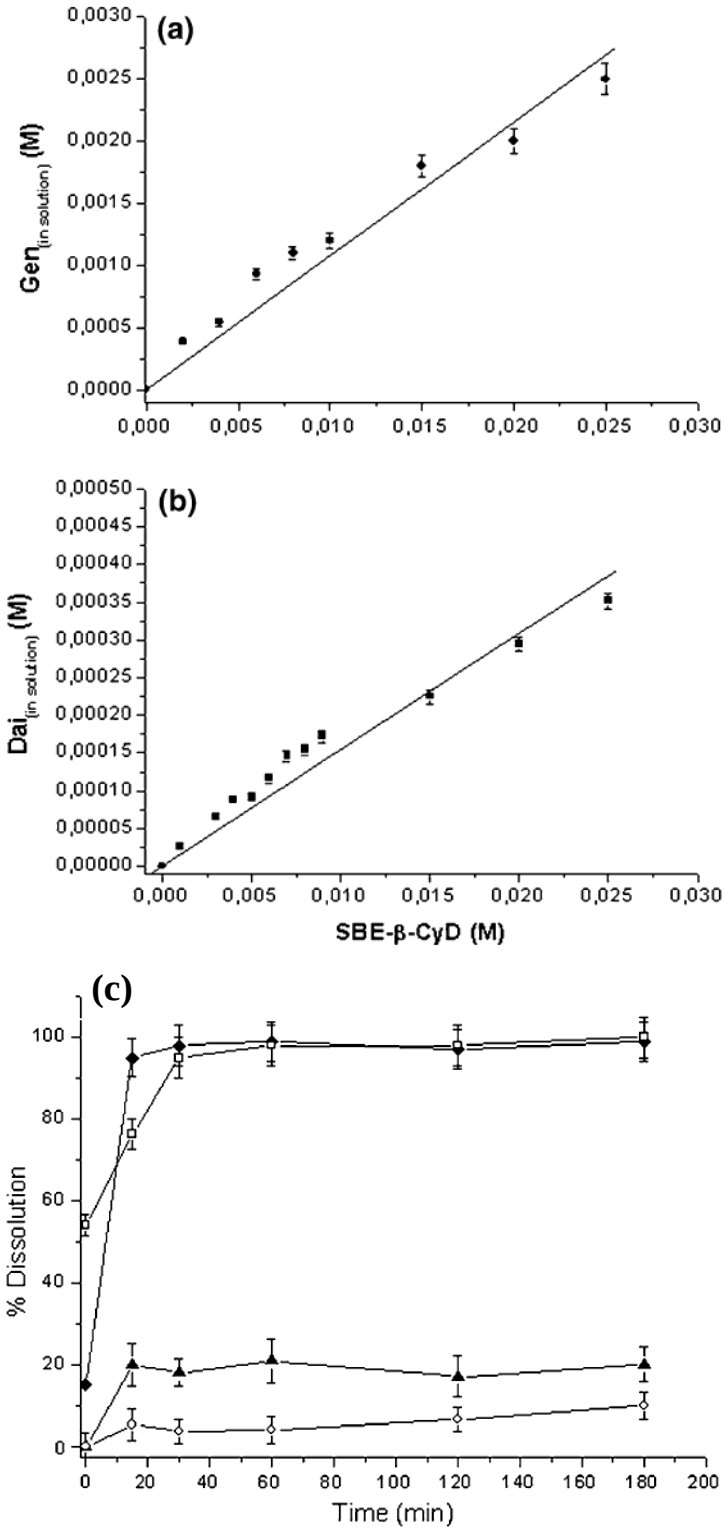

Figure 1.15: Phase solubility diagrams of Gen (a) and Dai (b) in the presence of increasing concentrations of SBE-ß-CD (0–25 mM) in water at 25.0 ± 0.1 °C; (c) Dissolution profile of free Gen (close triangles) and free Dai (open circles), SBE-ß-CD/Gen (close rhombus) and SBE-ß-CD/ Dai (open squares) 1:1 inclusion complexes in water at 37.0 ± 0.1 °C. Each value is the average of three different experiments ± standard deviation [213].

As mentioned in Section 1.1, the topical administration route is limited in usefulness due to low drug bioavailability. Aiming to address this challenge, Soni and Saini developed a new eye drop formulation based on aggregates formed by self-assembly of the drug (nepafenac):HP-ß-CD complexes in aqueous solution [215]. Nepafenac is a non-steroidal anti-inflammatory drug (NSAID) used in the treatment of the pain and inflammation associated with cataract surgery, which has low water solubility and low tissue permeability. Nepafenac is available in the market in the form of 0.1% and 0.3% ophthalmic suspension eye drops since it is sparingly soluble in water.

In order to prolong release potential for transmucosal ocular delivery of a hydrophobic drug – flurbiprofen (FLU), Shinde *et al.* synthesized FLU:HP-ß-CD complex-loaded N-trimethyl chitosan (TMS) and CS NPs for the treatment of bacterial conjunctivitis [216]. TMS is a water-soluble derivative of CS. The particle size and zeta potential of the TMC NPs (TMC:TPP ratio of 6:1) were determined to be 201.0 ± 1.6 nm and +13.9 ± 1.7 mV, respectively. Following complexation with HP-ß-CD, the solubility of FLU increased from 0.3 mM/L to 1.26 mM/L at 4.1 mM solution of HP-ß-CD. The FLU:HP-ß-CD encapsulation efficiency in the TMC NPs was 10.9 ± 1.5%. A biphasic release pattern with an initial burst period of 1 hour was observed, in which approximately 25% of FLU was released. This was followed by a sustained FLU release of around 54% over the period of 12 hours. The drug:CD complex-loaded CS NPs were also investigated in this study, with an average size of 361.2 ± 1.6 nm and a charge of +10.9 ± 0.4 mV. *In vitro* drug release of this nanoparticulate system showed an initial burst in the first hour with 44% of the drug released, followed by a sustained release of FLU for the next 12 hours (80% of drug was released) (Figure 1.16).

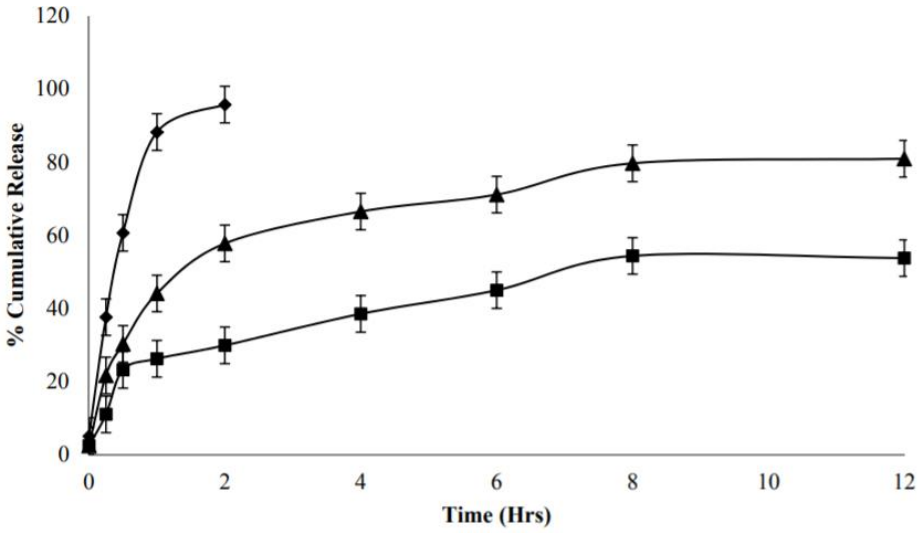

Figure 1.16: *In vitro* release profiles of free drug solution (diamond), drug:CD complex-loaded CS NPs (triangle) and drug:CD complex-loaded TMC NPs (square) [216].

Additionally, a HET-CAM test was performed to assess the ocular irritation potential of drug:CD complex-loaded TMC NPs and 0.1% TMC solution. Both of the two tested samples were observed to be non-irritant to the eye [216]. The anti-inflammatory potential of amlodipine (AML) on carrageenan-induced rabbit and the impact of SBE-ß-CD on corneal permeation were investigated by Nanda *et al.* [217]. The preparation of a hydroxypropyl methylcellulose (HPMC) ocular film was carried out after complexation of AML with ß-CD, HP-ß-CD and SBE-ß-CD. HPMC is a mucoadhesive, biodegradable polymer used in the ocular film which adhered to the conjunctival mucous membrane, while absorbing tear fluid from the surrounding environment. Consequently, HPMC can produce a gel layer to release the entrapped drug. Various techniques were employed to study the formation of the drug:CD inclusion complexes, including DSC, FT-IR and XRD. Presence of CD in the HPMC film was shown to increase water retention capacity. The hydration of the polymer matrix was followed by erosion and degradation. By complexing with CDs, the percentage matrix erosion decreased substantially with 73.05% for HPMC gel and 36.56% for HPMC complexed with SBE-ß-CD. In addition, by examining each formulation using scanning electron microscopy, it was shown that drug-loaded HPMC gel and drug-loaded CD-based gel provided smooth and homogenous surfaces due to an adequate solubility of AML into the polymeric network. Drug release of AML was significantly improved following the complexation with CDs, with the highest enhancement observed for SBE-ß-CD, as shown in Figure 1.17(a) [217]. This

was potentially due to the higher solubility of SBE-ß-CD in water in comparison to ß-CD.

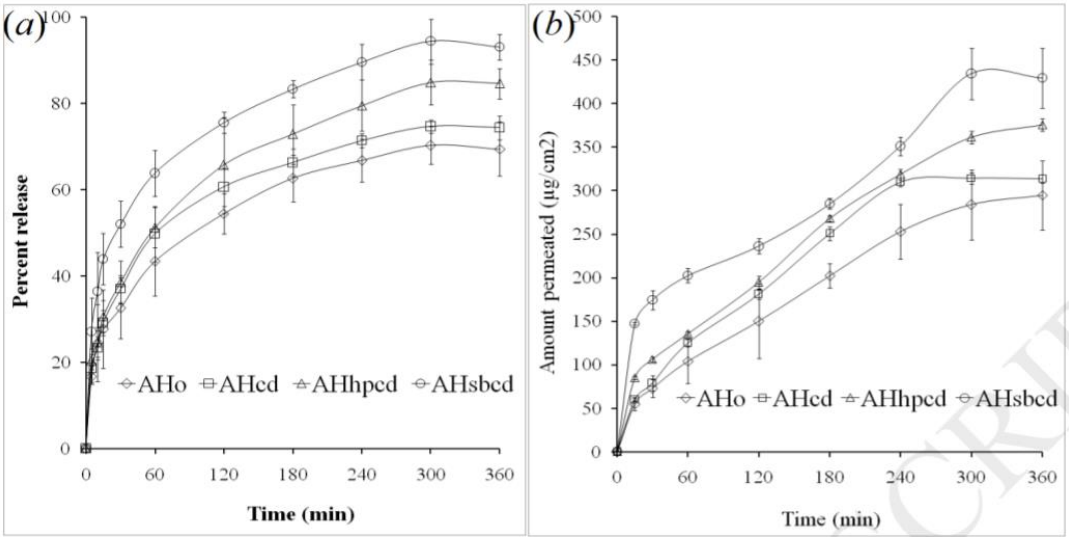

Figure 1.17: (a) *In vitro* drug release study and (b) *ex vivo* permeation on AHo: blank HPMC gel, AHcd: HPMC with ß-CD, AHhpcd: HPMC with HP-ß-CD and AHsbcd: HPMC with SBE-ß-CD (mean ± SD; n = 3) [217].

As could be seen in Figure 1.17, the AML release from the formulations was postulated to be highly diffusion controlled through the analysis of the kinetic study of drug release. Furthermore, AML ocular bioavailability near the cellular surface was increased since the CD complexation improved the solubility of the drug. The drug:SBE-ß-CD complex demonstrated a better permeation than the other two CD complexes due to highest steric hindrance and low-affinity binding. While higher binding ability resulted in a lower ocular drug diffusion, steric hindrance led to a loose binding of AML, and hence, higher drug permeation was achieved (Figure 1.17(b)) [217].

1.4 Contact Lenses as Ocular Drug Delivery Systems

Contact lenses (CLs) have been widely suggested to provide a much higher corneal bioavailability in comparison to eye-drops [218]. Because of the placement on the cornea with minimal mixing in the thin post-lens tear film (POLTF), which is between the lens and the cornea, soft contact lenses (SCLs) have been continuously developed and investigated as a novel vehicle for ODD (Figure 1.18) [219, 220]. Further, the concept of delivering medicines through hydrogel SCL or medical device has received

great interest because of their good biocompatibility, high water content, together with convenient use and an improvement in drug bioavailability (up to 35 times more than eye-drops) [218].

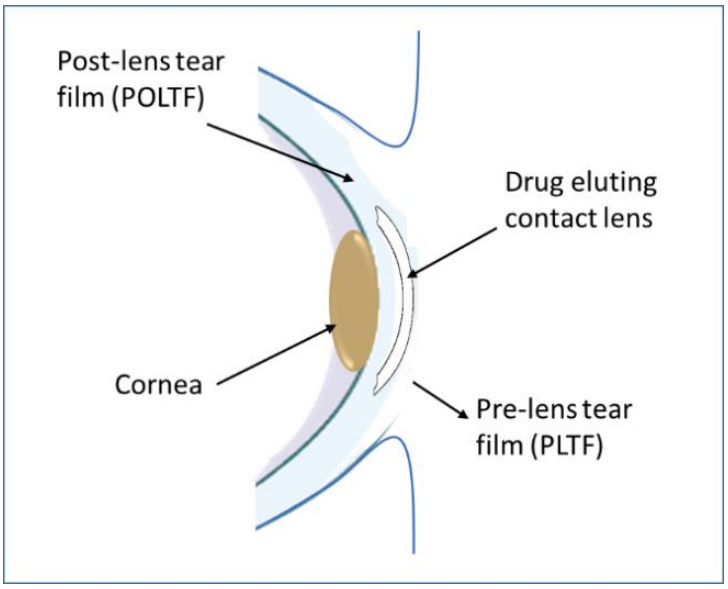

Figure 1.18: Schematic diagram of ocular drug delivery by contact lenses (adapted from [219]).

In order to fully discuss the potential of using SCLs as an ODDS, the history of CLs, the polymerization of CLs and their chemical and physical characterisation, as well as the manufacturing processes of CLs will be reviewed in this section.

1.4.1 The history of contact lenses

Materials used to make CLs, both rigid and soft, can be classified as biomaterials [221]. Figure 1.19 below reports the advancement of the contact lens market, from when a concept of the CL was first developed in 1508 by Da Vinci up to the present day, through various important historical timelines [222].

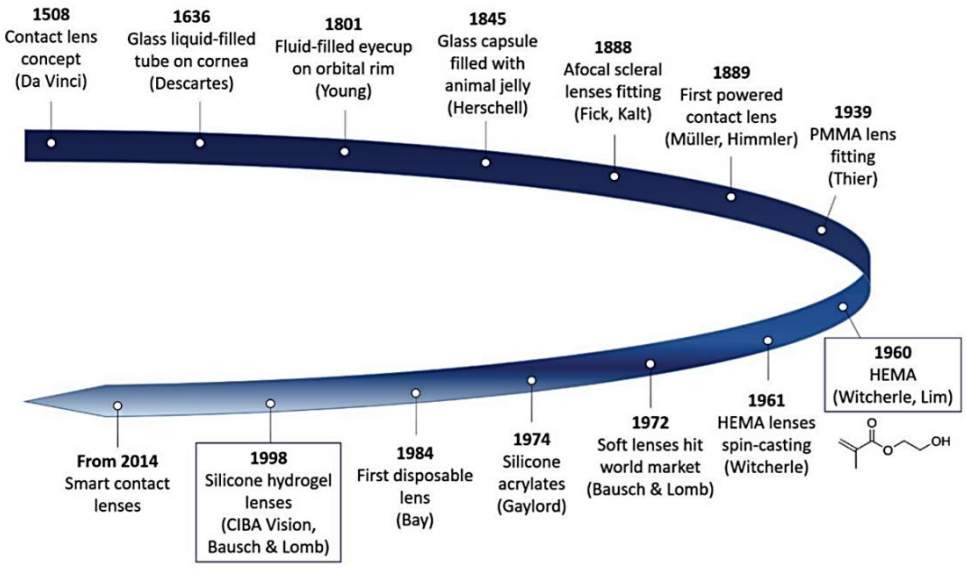

Figure 1.19: Historical timeline of the development of contact lens [222].

Since SCLs became widely available, a process led by Bausch+Lomb in the 1970s, they have had a considerable influence on the global market in this field [221, 222]. An article published in Contact Lens Spectrum in January 2020 provided an overview of general market trends in 2019 of CL fits and refits. The figure showed that 65% was silicone hydrogel (SiHy) materials while hydrogel SCLs accounted for 24% of the market in 2019 [223]. The explanation for this is that SiHy CLs exhibits almost identical comfort compared to hydrogel materials, while providing substantially higher oxygen and ionic permeabilities. In addition, SiHy CLs may also offer easier handling [224], reduce conjunctival redness [224], and also less protein deposition on the lens surface [225]. Hydrogel and SiHy materials will be further discussed later in Sections 1.4.2 and 1.4.3.

The following sections give a brief introduction to the different stages involved in the manufacturing processes of CLs, followed by various chemical, physical, and mechanical characteristics of SCLs.

1.4.2 Hydrogel

SCLs are known to be flexible as they are made from water-swollen, biocompatible, lightly cross-linked and hydrophilic polymers [221]. Hydrogels are a three-dimensional, hydrophilic, and cross-linked polymeric network [226, 227]. They can uptake and retain water or biologic fluids, which in turn increases their original mass

[228-230]. Hydrogels are classified as viscoelastic polymers, those that deform and recover in a time-dependent manner when a stress is applied to or removed from them. These materials represent an extremely versatile class of polymeric materials, those that can be produced using natural and/or synthetic polymers [229]. Moreover, they also exhibit diverse characteristics that can be applied in various biomedical fields (e.g., drug delivery [231], sensing applications and increasing the life-time of surface coatings [232], 3-D cell culture [233]) (Figure 1.20).

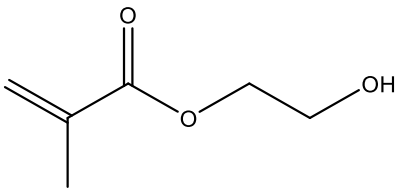

HEMA (2-hydroxyethyl methacrylate)

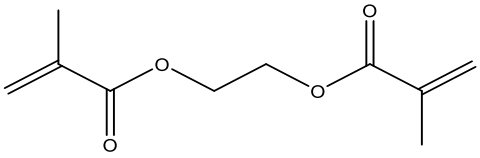

EGDMA (Ethylene glycol dimethacrylate)

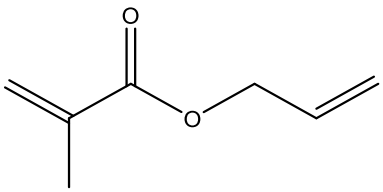

AMA (Allyl methacrylate)

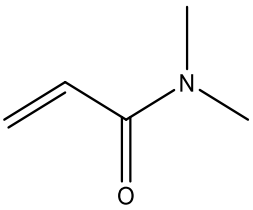

DMA (N,N-dimethylacrylamide)

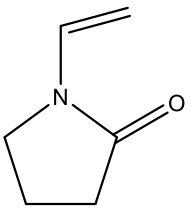

NVP (N-vinyl pyrrolidone)

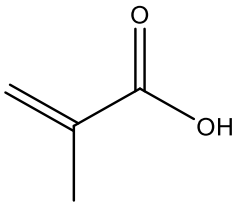

MAA (Methacrylic acid)

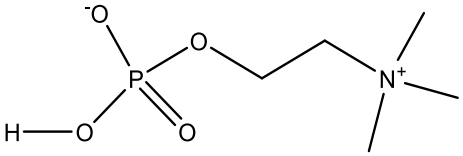

PC (Phosphorylcholine)

Figure 1.20: Monomers used in the manufacturing of hydrogel contact lenses.

Hydrogel complexation occurs mainly via hydrophilic ionic interactions between water molecules and polymeric long chain entities [227]. Hence, they are capable of absorbing large quantities of biological fluids or water. Hydrogels are considered an open and semipermeable system. They allow the movement of water and solute molecules, as well as ionized species. Hydrogels hold promising potential as sustained

ocular drug delivery systems (ODDSs), mainly due to their ability to swell in an aqueous solvent platform, thus, retaining solvents within a cross-linked gel network, along with other hydrophobic and hydrophilic agents, small molecules and macromolecules [226]. Moreover, they can also combine with micro- or nano-materials to enhance ODD, regardless of their solubility characteristics [234].

1.4.3 Silicone hydrogel

Silicone-based hydrogels encompasses silicone, siloxanes, fluorosiloxanes and their derivative materials. The chemical structure of a number of these are presented in Figure 1.21 [235].

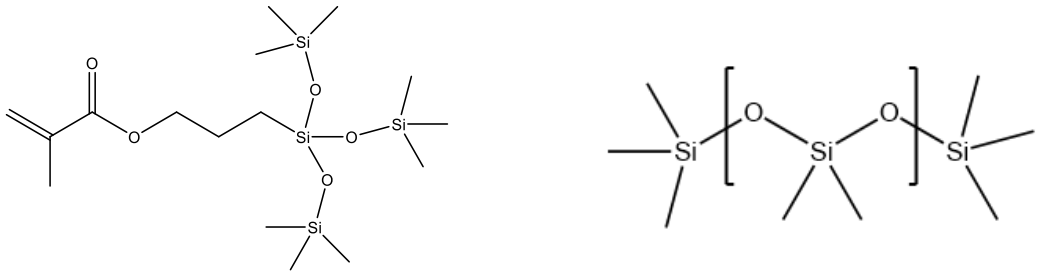

TRIS — Tris-(trimethyl-silyl-propyl-methacrylate)

PDMS — Hydroxyl-terminated polydimethylsiloxane

Figure 1.21: Monomers used in the manufacturing of silicone hydrogel contact lenses.

Due to the siloxy groups presented in SiHy structure, the hydrophilicity of this lens material is generally lower than most hydrogel materials, although these groups help to increase the D_k values (oxygen permeability) [236]. In order to improve the wettability of SiHy lenses, many different strategies such as plasma treatment or surface coatings [237, 238], and the inclusion of internal wetting agents [239, 240] have been used to mask the hydrophobic silicone from the tear film [241]. Due to this, the surface characteristics of SiHys are far more complex than those of hydrogels and also not associated directly with lens water content [236].

1.4.4 Lens polymerization

The principal chemical reaction process involved in the curing of contact lenses is chain polymerization, where most of the polymers involved are unsaturated (e.g., vinyl

monomers) (Figure 1.20). The monomers belonging to this group have one or more carbon-carbon double bond. Throughout the polymerization process, the monomer concentration gradually reduces over time, leading to a mixture containing: monomer, high molar mass polymer, and a low amount of growing chains [242].

The polymerization kinetics of hydrogels, such as poly-HEMA, poly-AMA, and poly-EGDMA, etc. have received special attention due to the presence of methacrylate groups in their structure. This results in relatively straightforward radical reactions, with the hydroxyl groups providing hydrophilicity [243]. Free radical polymerisation (FRP), which is a type of chain polymerization, is normally characterized by three distinct stages: initiation, propagation and termination [242].

1.4.4.1 Initiation

The initiation process is defined as the series of reactions that leads to the formation of initiating radicals. This happens by generating primary radicals, molecules that contain reactive unpaired electrons, and culminates in addition to the carbon-carbon double bond of a monomer [244] (Figure 1.22). Generally, the radical can be produced from the decomposition of an added initiator through different processes such as thermal heating/warming, reaction with other chemicals or radiation with either ultraviolet (UV) or infrared (IR) light [245, 246].

$$I_2 \rightarrow I^{\bullet} \rightarrow I\text{-}M^{\bullet} \rightarrow I\text{-}M\text{-}M^{\bullet} \rightarrow$$

$$\text{Secondary radical } I'^{\bullet} \rightarrow I'\text{-}M^{\bullet} \rightarrow I'\text{-}M\text{-}M^{\bullet} \rightarrow$$

Where: I is the concentration of the initiator, M is the concentration of monomer, and I and M are the active growing chains.

Figure 1.22: Schematic diagram represents the initiation process of free radicals.

Primary radicals, produced by either thermolysis or photolysis, can go through rearrangement or fragmentation that will lead to the formation of secondary radicals [244]. Further, they may also react with solvents or other species (e.g., oxygen) instead of monomer. The formation rate of radicals depends on different properties, including

temperature, the concentration of initiator, and the nature of other molecules [244, 246]. The overall conversion times, which indicate the time it takes for monomer mixture to convert into hydrogel polymer materials, in most polymerizations are relatively slow, and can take at least 30 minutes or much longer. This is due to the fact that the polymer growth process happens almost immediately after the initiation stage [246].

When radicals interact with monomers, these processes can happen via different types of reactions, such as tail addition, head addition, abstraction, or aromatic substitution. Moad's detailed study on the initiation stage of polymerization using Styrene (St) and methyl methacrylate (MMA), commercially relevant monomers, with each of three common initiators benzoyl peroxide (BPO), azobisisobutyronitrile (AIBN) and di-*t*-butyl peroxyoxalate (DBPOX), demonstrated the complexities of this stage (Figure 1.23) [244]. Moad reported that the initiation pathway is significantly dependant on the structure of both radical and monomer species.

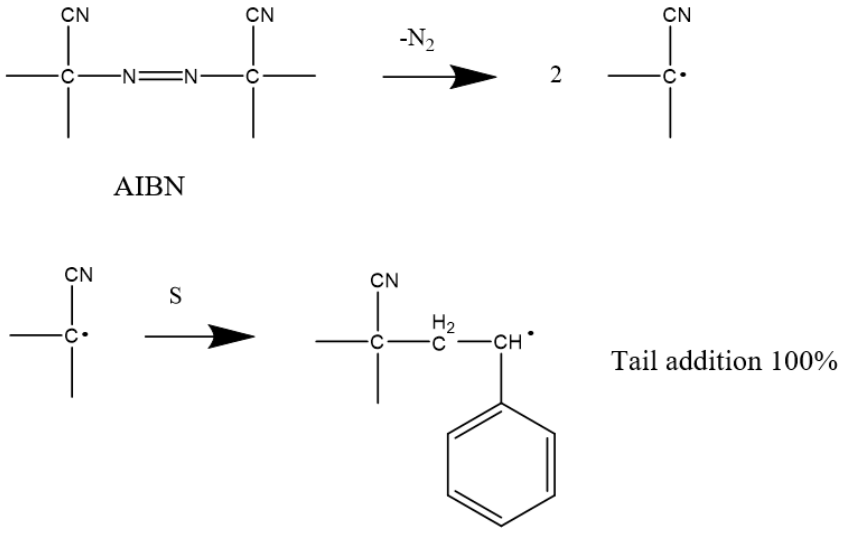

Figure 1.23: Decomposition of AIBN, and tail addition pathway in the reaction of AIBN with monomer (where S is styrene) [244].

1.4.4.2 Propagation

After the radical species is created, they can then combine with another monomer unit leading to the formation of a new compound. This stage is known as propagation of polymerization [242]. It includes a series of radical additions to the carbon-carbon

double bonds. By repeating this process many times so that thousands of monomer units are linked together, the polymer chain is propagated, resulting in a long chain radical [246] (Figure 1.24).

$$IM^{\bullet} + M \rightarrow IMM^{\bullet}$$

$$IM_n^{\bullet} + M \rightarrow IM^{\bullet}_{(n+1)}$$

Figure 1.24: A schematic diagram illustrates the propagation stage of the FRP process.

A propagating radical must have a high degree of specificity in its interaction with unsaturated systems, which hence, has an ability to give addition to the exclusion of side reactions that results in the growth of polymer chains [244]. Since the predominant head-to-tail structure may be broken by the head-to-head or tail-to-tail linkages (Figure 1.25), the addition to double bonds will not be totally regiospecific.

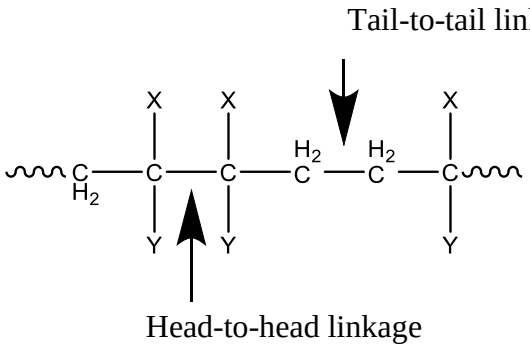

Figure 1.25: Schematic diagram represents head-to-head and tail-to-tail linkages.

1.4.4.3 Termination

Due to the high reactivity of free radicals, they can easily lose their reactivity in various ways. The polymerization process does not generally end until all the monomers have been used up. This stage can occur in four different ways and are depicted in Figure 1.26, including (a) mutual combination of two growing radicals [244], (2) disproportionation between growing radicals [244], (3) reaction with an initiator radical [246], and (4) chain transfer with a modifier [246].

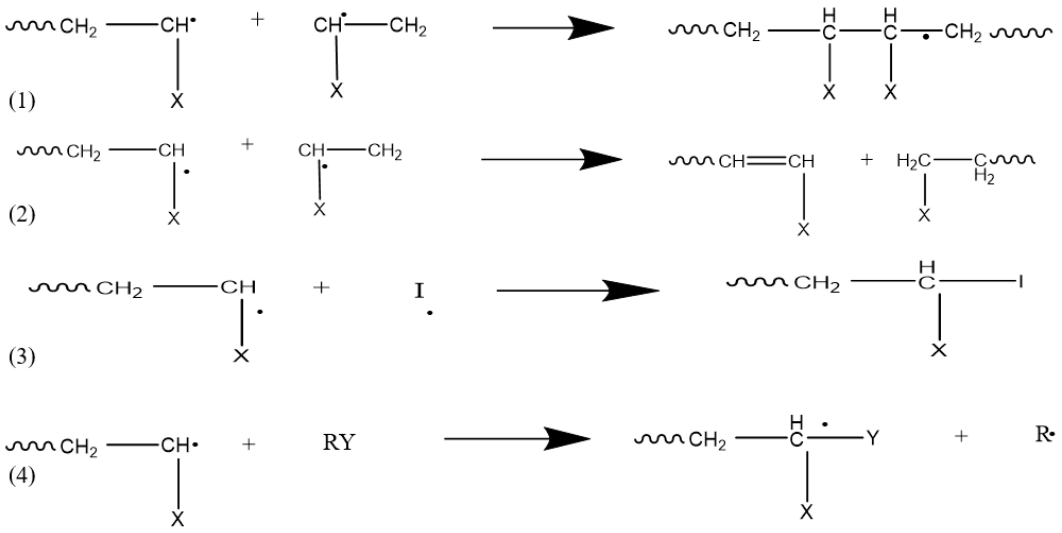

Figure 1.26: Schematic diagram illustrates the possible ways happen in termination step.

The most common and important termination mechanism in FRPs is radical-radical combination or disproportionation (1, 2). Before any chemical interaction can happen, the radical centres of the propagating species have to reach appropriate proximity. This means that there will be no single rate constant for termination in FRP [244, 246]. For step (1), this takes place when two growing molecules with free radicals meet and share the unpaired electrons, subsequently, form a stable covalent bond to render them unreactive. As for the disproportionation method of termination, as a result of the reactions between two radicals via hydrogen abstraction, two reactive products can be formed; in which one is saturated while the other is unsaturated [244].

1.4.5 Lens manufacture

1.4.5.1 Manufacturing of contact lenses

To fabricate SCLs at low cost, the manufacturing process of CLs plays a vital role. There are three main approaches used in the manufacture of CLs, including lathe cutting, spin casting and injection moulding (Figure 1.27).

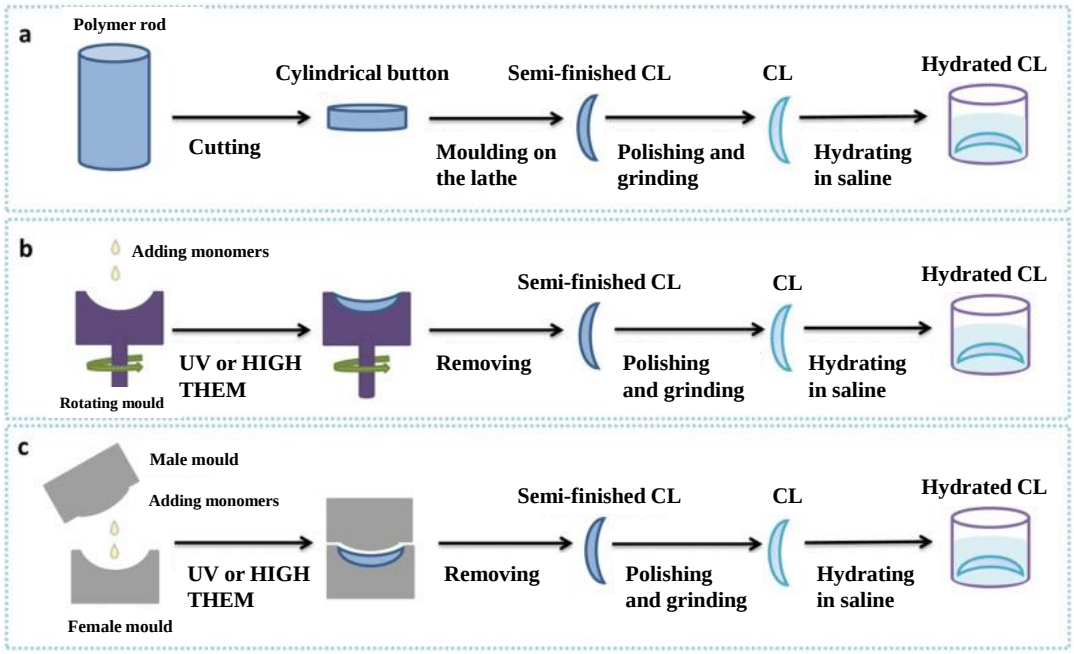

Figure 1.27: A summary of three different processes in making SCL (a) lathe-cutting, (b) spin casting and (c) injection moulding approaches [247].

Lathe cutting was originally used in the fabrication of rigid lenses before it was applied in the manufacture of SCLs. Compared to the other two approaches, this method is more expensive. The lathe cutting process involves the formation of an anhydrous polymer rod [248]. By cutting the polymer rod, a cylindrical button is produced which is then moulded into the CLs shape on the lathe. After being polished and ground, the lens will be hydrated to form the final SCLs [247, 248].

For the spin casting method, while the outside of the mould fixes the outer surface, the inner surface will be generated when the liquid monomer mixture undergoes centrifugal force [247]. After the injection of liquid into the centre of the rotating mould, it then goes through either thermal or UV light polymerization. The next steps of this process are similar to the lathe cutting approach, and include polishing, grinding, and hydration in saline/water. This method can be used in mass production due to its cost-effective process [248].

Injection moulding, known as cast moulding, is a process that requires several sets of matching anterior and posterior moulds that are manufactured using either polypropylene [247] or polystyrene [249]. Different lens properties and powers can be obtained by modifying the design of both mould parts. Label back vertex power of a

lens is defined as the dioptric power measured by focimeter either in air or in saline (Moire deflectometer or Hartmann methods), according to the current international standard [250]. This method involves the injection of liquid monomer mixture into the anterior mould, which is then capped with the posterior mould. The lens is then cured inside the mould [248]. The cured lens will then be either dry-released or wet released (i.e., cured moulds will be immersed in water until the lenses hydrated and come out of the mould) from the mould [251]. This is followed by extraction and hydration using water or water:solvent (e.g., alcohols) mixtures [252]. As stated by Xu *et al.* [247], injection moulding, due to its efficiency and lower cost production, has become a dominant technology for large-scale CL production, particularly in the field of disposable CLs.

1.4.5.2 Sterilization of contact lenses

One of the most important aspects to assure the quality, safety and efficacy of any biomedical device for potential commercial production is the sterilization process [253]. In medical device industries, infection arising from the manufactured medical devices have always remained a major problem. Thus, an efficient sterilization approach for all materials in contact with the body is crucial to reduce the incidence of these infections [230, 254]. Since soft biomaterials such as hydrogel SCLs are very sensitive to heat or irradiation, sterilization of these materials is especially challenging [254]. Depending on different natures and properties of specific material compositions and their applications, the most suitable sterilizing process can be identified.

Several studies [255-257] indicated that the sterilization process can eventually cause material degradation, potentially leading to further crosslinking of polymers or even toxic effects. There are a number of well-established terminal sterilization methods that have been used for hydrogel-based devices [258], which are described in Table 1.1.

Table 1.1: Established sterilisation methods for biomaterial devices.

Sterilization method	Advantages	Disadvantages	Ref.
Physical: *steam heat, dry heat*	Simple. Inexpensive.	The application is restricted to heat resistant hydrogels (e.g., silicone-based, acrylic-based).	[259]
Chemical: *alcohol, phenol, aldehyde*	Volatile. Does not leave residues.	Can be toxic, corrosive, and/or irritating. FDA issues.	[258, 260]
Gamma radiation (GR)	Highly penetrating. Allows operating at low temperature. Does not leave chemical residues. High sterility assurance level. Preferable in sterilizing SiHys.	High cost. Complicated process. Requires well-trained staff and special facilities. Unsuitable for radio-sensitive materials.	[261-263]
Gas sterilization *(e.g. ethylene oxide EtO, hydrogen peroxide HP)*	EtO: Highly efficient, adequate for heat and radiation sensitive materials. HP: Highly oxidizing agent.	EtO: Concerns on toxic and carcinogenic nature of EtO residues, which have to be removed, so increases processing times. HP: Material degradation or harmful changes in properties of materials.	[260, 264]
E-beam (electron beam)	Very safe method. An advanced technology. Allows operating at low temperature. Easy to control. High sterility assurance level. Preferable in sterilizing SiHys.	Needs an electron accelerator which is quite rare.	[262, 263]

Besides the above common sterilization approaches in biomedical device industries, several new methods have been researched and investigated to provide possible alternatives (e.g., plasma, ozone, high intensity UV and supercritical fluids) [230, 265]. The impact on different SiHy SCLs properties of the hydrated samples before and after drug-loading and sterilization under different conditions (e.g., steam heat, gamma irradiation and ozonation) was investigated by Galante *et al.* [266]. GR sterilization was investigated to reduce optical transparency for drug-loaded CLs (below 80%). Both GR and ozonation sterilisation approaches resulted in noticeable degradation of

all the drugs (i.e., levofloxacin, chlorhexidine, diclofenac and timolol) used in the study. As a result, these approaches were identified to be unsuitable in the application of ODD with steam heat sterilization to be the optimum approach since it showed the least impacts on the drug-loaded CLs [266].

1.4.6 Physicochemical and mechanical properties of soft contact lens

In order for particular SCLs to be feasible and acceptable in the commercial market, they must meet several important requirements in line with ISO-18369:2017 standards (4 parts) [267-270]. The requirements/tolerances for some of lens' critical properties of a commercial SCL from the ISO standards are summarized in Table 1.2.

Table 1.2: Tolerances for some of lens' critical properties from the relevant ISO standard [267].

ISO standard number: 18369-2:2017	
Lens' property	**Requirements/Tolerance**
Back optic zone radius/base curve equivalent/ equivalent posterior radius of curvature	± 0.20 mm
Sagittal depth	± 0.05 mm absolute (control value)
Total diameter	± 0.20 mm absolute (control value)
Centre thickness (t_C)	Thickness >0.10 mm: ±(0.015 mm + 0.05t_C) Thickness ≤0.10 mm: ±(0.010 mm + 0.10t_C)
Spherical Power	Power ≤10.00 D: ± 0.25 D 10.00 D < Power <20.00 D: ± 0.50 D Power >20.00 D: ± 1.00 D
Spectral transmittance in the visible region	± 5% absolute (control value)
Refractive index	± 0.005 absolute (control value)
Water content	± 2% absolute (control value)
Oxygen permeability	± 20% absolute (control value)

1.4.6.1 Thermal analysis of SCLs

Thermal analysis is one of the most common analytical techniques used in the characterization of polymeric materials. By heating the sample in a certain temperature range at a specific rate, its structure and properties can be analysed [271-273]. This analysis includes the use of differential scanning calorimetry (DSC), thermogravimetric analysis (TGA) and thermal mechanical analysis (TMA) [273]. These techniques allow the determination of polymer structure, water content, and the influence of the cross-linking process as well as the degradation mechanism of polymers. Thermal analysis also provides information on the relationship between material structure and its thermal stability. Both TGA and DSC are essential and powerful analytical techniques in the thermal characterization of polymeric materials, such as: glass transition (T_g), thermal stability, polymorphism, degradation temperature, etc. [272].

Besides determining the degradation temperature of materials, TGA has generally been applied in the determination of the total quantity of water in an equilibrated gel, including identifying the temperature at which the water is lost and to define if this is dependent on the heating rate [274]. DSC is a thermal analysis technique that provides information on the thermal properties of materials based on the rate at which they adsorb heat energy compared to a reference material. In other words, this technique investigates the response of a tested polymer to heating. It is applied widely to study either the melting of a crystalline polymer or the glass transition of an amorphous polymer [271].

Polymers can go through three distinct transitions during heating, including a glass transition (T_g), crystallization (T_c) and melting (T_m), although not all materials will experience all three (Figure 1.28).

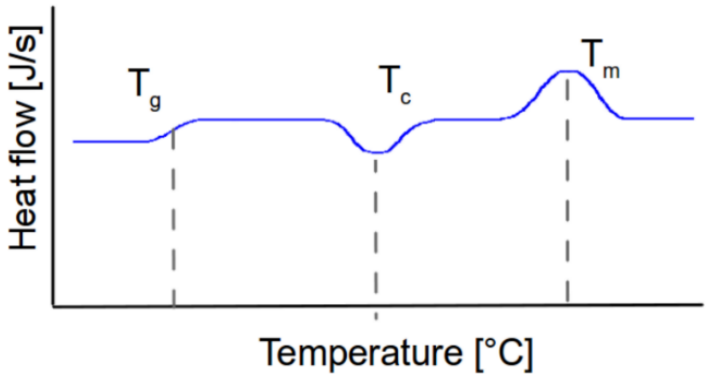

Figure 1.28: Schematic diagram represents three main thermal transitions that a material that can experience throughout DSC analysis [171].

The glass transition temperature (T_g) is defined as a second order pseudo transition, which provides important information in the study of amorphous and crystalline materials [275]. T_g is the temperature when the brittle and glassy material become less rigid and more rubbery [276]. Above the T_g, the polymers have more mobility and when they reach a certain temperature, where they gain enough energy to move into ordered management and undergo crystallization, this temperature is known as crystallisation temperature (T_c) [171]. It is an exothermic process. As the temperature increases, the polymer chains can move around freely again and reach another thermal transition, called melting. At melting temperature (T_m), the energy added during this time is used to melt the crystalline regions and since it requires the absorption of heat, it is an endothermic process [171]. While all three transition peaks can be observed for crystalline polymers, purely amorphous polymers will only go through a glass transition. The characteristics of polymers are essentially impacted by their level of crystallinity and morphology [271]. As such, polymers with a high level of crystallinity will have a higher glass transition temperature (T_g), which implies that they will have higher modulus, toughness, stiffness, tensile strength, hardness, and more resistance to solvents, although their strength would be less affected.

An investigation into the glass transition and water dynamics in a hydrated HA hydrogel crosslinked by divinyl sufone (DVS) at various hydration levels, using DSC was carried out by Panagopoulou *et al.* [277]. The group also examined the implementation of dielectric relaxation spectroscopy (DRS) and water sorption-desorption (ESI) measurements. The DSC data from this study indicated that the T_g of a material would reduce due to plasticization by water molecules (T_g went down from

-48 °C to -80 °C). However, when water was recrystallized, the T_g stopped decreasing. This indicated that the glass transition was based on the combined motion of uncrystallised water molecules at primary sorption sites and segments of the HA chains. A study carried out by Bennour and Louzri also used DSC and TGA analysis as part of their investigation into the swelling properties and thermal behaviour of Poly(N,N-Dimethylacrylamide-*co*-Maleic Acid) based hydrogels (PDMA-MA) [274]. It was observed that the developed hydrogels degraded in two main stages that were associated with the loss of water (Stage 1) and polymer degradation (Stage 2). The TGA data implied that the maximum degradation temperature of polymers increased with an increase of NMBA (N,N-methylenebisacrylamide) content, which was due to an increase in crosslink density. Similar trends with the T_g values of tested hydrogels were also seen. As such, the higher the amount of NMBA (8, 15, 29, 33 and 38 mol%), the higher the T_g values of PDMA-MA. As an example, the T_g at 8 mol% of NMBA is 126 °C, while T_g of 158 °C was obtained at 38 mol% NMBA. The reason for this was attributed to the movement restrictions of polymer segments, which was due to the high crosslink density.

In addition, DSC has also been widely used to study and monitor the kinetics of radical polymerization [242]. The biggest advantage of such an approach is the ability of continuously recording the variation of the reaction rate with time during the measurements of the amount of heat released. Several works were carried out using DSC to investigate the polymerization kinetics of HEMA and its copolymers with several dimethacrylate monomers (e.g., EGDMA, or DEGMA) [278-282]. Another study carried out by Ning *et al.* [279] used DSC to monitor the reaction process of HEMA in a mixture (with BMA-butyl methacrylate and BPO-benzoyl peroxide as an initiator). When the polymerization of HEMA was initiated (at 100-150 °C), the formed pHEMA generated an interpenetrating network with the synthesized polymethacrylate through H-bonds. This study also demonstrated the effect of DSC heating rate on the polymerization of HEMA, which demonstrated that a faster heating rate could accelerate the polymerization of HEMA (Figure 1.29).

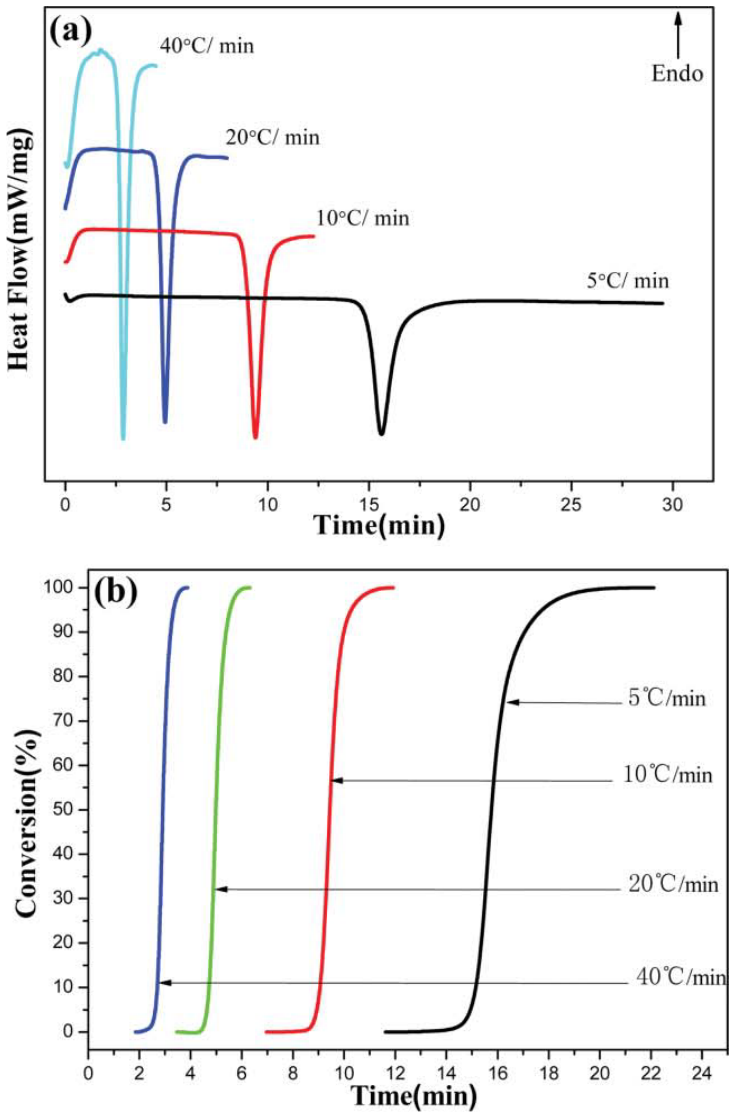

Figure 1.29: Schematic diagram illustrates the impact of heating rate on (a) conversation temperature of HEMA and (b) the fractional conversion as a function of time [279].

1.4.6.2 Light transmission of SCLs

To achieve optimum visual performance, SCL materials must be transparent. This characteristic is generally expressed as the percentage transmission of the visible electromagnetic spectrum. For hydrogels, the main materials used in the manufacturing of SCLs can transmit over 90% of light in the visible part of the spectrum [52, 283, 284]. When microphase separation of water happens, referred to as the area of varying refractive index (RI) formed within the gel, a hydrogel tends to lose its transparency.

The most common methods in the determination of the absorption or transmission spectrum of CLs involves the use of bench-top spectrometer, with the tested CLs attached to a suitable cuvette placed in the fixed light path of the system [285]. Kapoor *et al.* [286] investigated the effect of drug (cyclosporine A) concentration on the transparency of 200 µm thick pHEMA hydrogels. The results indicated that the optical clarity was maintained (>95%) if the drug loading was less than 0.4% (close to the drug limit of solubility in pHEMA). As the drug concentration increased, it could be observed that the gels turned hazy and almost opaque [286]. In another study carried out by Paradiso *et al.*, the optical transparency of a pHEMA-based hydrogel material loaded with drug (levofloxacin) was assessed before and after coating with a liposome layer [284]. Liposome-based coating (average size of 103 ± 8 nm) was developed to provide a more controlled drug release from the SCLs. Measurement of optical clarity was carried out within visible light range in the spectral transmittance (i.e., 400-700 nm). The pHEMA hydrogel %transmittance was measured to be 99.0 ± 0.2%. Following the coating of liposomes, the hydrogel transmittance decreased to 98.7 ± 0.3% for the DMPC (liposomes of 1,2-dimyristoyl-sn-glycero-3-phosphocholine) coating layer, and 97.6 ± 0.4% for the DMPC+CHOL (cholesterol) coating layer.

1.4.6.3 Equilibrium water content of SCLs

The ability of the hydrogel or SiHy to bind water in its equilibrium state is called the equilibrium water content (EWC) [287]. Water content is defined as a mass fraction present in a hydrated material, which has been fully equilibrated at room temperature as stated in the ISO 18369-4:2017 standard [250]. Water content of SCLs is a vital property since it is closely related to their comfort and oxygen permeability. The higher the water content, the higher the oxygen permeability of hydrogels [288]. The equilibrium water content (EWC) of a hydrogel can be calculated according to the following equation (Equation 1.1):

$$\text{EWC} = \frac{\text{weight of water in polymer}}{\text{total weight of hydrated polymer}} \text{ x } 100 \qquad \textbf{Equation 1.1}$$

Alternatively, the surface EWC can also be calculated basing on its relationship with the refractive index (RI) value of hydrogel SCLs as discussed in Section 1.4.6.4. Further, the EWC value of hydrogels is also intimately related to the oxygen and ionic permeability of a CL [52]. One of the main limitations that hinders the CL market

growth is related to dehydration issues of the ocular surface caused by CLs [289, 290]. SCL dehydration can lead to several problems, such as: changes in lens parameters [291, 292], and changes in oxygen [293, 294] and ionic permeability [295]. There are three main factors that can affect the EWC of the hydrogel lens, including ocular surface, lens material and environmental conditions [296-298]. Those that in turn can cause an impact on CL fitting behaviour, spoliation, and tolerance [291, 297].

Two of the most common methods in determining the EWC are gravimetric techniques [299, 300] and refractometry [291, 301, 302]. The swelling kinetics of the hydrogels in the polycaprolactone-based NPs loaded SCLs (pHEMA) carried out by Nasr *et al.* [303] were done gravimetrically in phosphate buffer solution (pH 7.4). An increase in %EWC was observed following an increase in the concentration of added NPs (74.8% EWC with a 7.5%wt NP loading). However, a high concentration of incorporated NPs (10-15 %wt) led to a reduction in the swelling ability of the hydrogels. Two main factors that influenced the swelling behavior of SCLs were suggested to be the hydrophobic content of NPs and the physical crosslinking between the hydrogel lenses and the NPs. As such, an increase in water content could be observed following the addition of hydrophilic monomer (e.g., NVP) due to stronger binding ability of lactam groups in pyrrolidone groups. In addition, at a constant concentration of NVP monomer, by increasing the amount of crosslinker (PEG-DA, polyethylene glycol diacrylate), the %EWC of the lenses also increased. For example, for hydrogel lenses prepared at a ratio of 10:4:03 (HEMA:NVP:PEG-DA), the %EWC was 51.4%, at a ratio of 10:4:0.8 (HEMA:NVP:PEG-DA), the %EWC increased to 59.7% and the highest %EWC was measured for the lenses prepared at a ratio of 10:6:0.8 (HEMA:NVP:PEG-DA), which was 67.1%. However, too high an amount of incorporated NPs (10%-15% wt) led to a reduction in the swelling ability of the hydrogels (e.g. 49.90 %EWC with a 10%wt NP loading). [303].

1.4.6.4 Refractive index of SCLs

Besides optical transparency, ideal hydrogel materials used in the manufacturing of SLCs must provide a refractive index (RI) that is similar to the cornea RI (i.e., an RI that is near to 1.37) [221]. RI is conventionally measured using a refractometry technique, in which the RI of a material is determined by measuring the critical angle between the material and a glass of higher or known RI [304]. RI not only is important

from the optical point of view, but it is also an essential parameter from a physiological perspective. This is due to the fact that RI is a measurable value that reflects the alterations in the EWC of polymers [302]. The quoted reference values for RI for commercial hydrogel and silicone-hydrogel CLs, which were determined in Varikooty *et al.* [305] and Lira *et al.* [306], to be in the range of 1.40 to 1.43.

According to ISO 18369-4:2017 [307], the RI of the CL material should be measured at either 589 nm (sodium D-line) or at 546.1 nm (mercury E-line). There are many methodologies involved in the determination of RI based on the lens shape and measuring conditions (dry, blotted or immersed). The technique of determining the RI of the hydrogel materials is also noted under this ISO standard, which uses the calibrated Abbe refractometer or an equivalent instrument at room temperature. It was reported that by measuring the RI/EWC of SCLs during wear can help to define whether the dehydration is linked to the onset of symptoms of discomfort or dryness. This study evaluated the RI of lotrafilcon B and etafilcon A lenses. *In vivo* RI values at baselines for lotrafilcon B and etafilcon A were 1.422 ± 0.004 and 1.405 ± 0.002, respectively. The results showed a statistically significant change *in vivo* across the day for etafilcon A lens ($P < 0.01$) but not for lotrafilcon B lens ($P > 0.05$) [305].

1.4.6.5 Fluid and ionic permeability of SCLs

It is essential to obtain an adequate ion permeability (D_{ion}) in SCLs to ensure the formation of a fluid hydrodynamic boundary layer, which in turn, decreases the direct abrasion between the lens and the eye [303]. Adequate lens movement can only be maintained when there is a minimum level of ionic permeability. The permeation of ions in polymeric membranes encompasses the dissociation of ion from salt. As such, it includes the movement of anion and cation to the aqueous medium, and eventually, spreading of the ions in the confined water within the polymer matrix [308]. This property is vital since it allows the post lens tear film (PLTF) to reform between blinks, and for metabolic waste removal [309], hence, reducing the possibility of the elastic SCLs from binding to the cornea [310]. A major part of the tear film is known to contain sodium ions. As cited by Pozuelo *et al.* [308], for extended wear SCLs, the effective ion diffusivity (D_{ion}) should be larger than $1.5x10^{-6}$ mm^2/min to ensure homeostasis of ion concentration between the lens and cornea. As such, the lens would be free from abrasion and friction [308].

Ionic permeability of SCLs were generally measured using a modified conductivity meter in several studies [308, 311-313]. As an example, the hydrated lens was attached to the bottom of the donor tube, which was filled with 24 mL of saline solution (130 mM). This was then placed on top of an acceptor compartment that had 32 mL of deionized water. After securing the position of the two cells, they were placed horizontally. The conductivity probe was placed inside the acceptor part to measure the conductivity over a specified time. This whole set-up (except for the conductivity meter) was placed in an oven at 36 °C [312]. The data was then calculated to give the D_{ion} based on the concentration of Na^+ ions that had travelled through the lens into the water in a specific time interval [308, 311].

Based on the methodology cited by Peng *et al.* [313], work done by Maulvi *et al.* [314] demonstrated a noticeable reduction in D_{ion} with the NP-laden ring implant in hydrogel CLs and also with the increase in ratios of timolol to ethyl cellulose. This could be explained by the presence of hydrophobic ethyl cellulose NPs. In addition, it also pointed out that the ion flux diffusion coefficients would decrease in the presence of NPs. However, since the D_{ion} value was still higher than $1.5x10^{-6}$ mm^2/min, the developed modified lens would be still fit for use [314]. Nasra *et al.* also reported the impact on ionic permeability of drug-loaded NPs loaded hydrogel [303]. The D_{ion} values for blank CLs and CLs with 7.5% NPs loaded were calculated to be 1.71×10^{-3} and 2.83×10^{-3} mm^2/min, which were both larger than the critical value as mentioned above. Their study also stated that following an increase in water uptake, the salt diffusion coefficient would also increase.

Ionic permeability of two hydrogels for drug release was reported by Paradiso *et al.* [315]. Due to higher swelling capacity, the TRIS/NVP/HEMA hydrogel had a higher ionic permeability than HEMA/PVP hydrogel (5×10^{-7} vs. $8 \times 10^{-8} \pm 2 \times 10^{-8}$ cm^2/s). The impact on lens (ACUVUE® OASYS®) ion permeability post-vitamin E and drug loading was investigated in a work carried out by Sekar *et al.* [316]. Upon the incorporation of vitamin E, a minor decrease in this value was observed in experiments (e.g., 0.65 ± 0.04 vs $0.50 \pm 0.1 \times 10^{-4}$ mm^2/min for control lens and lens with 10% vitamin E loading, respectively).

While ionic permeability is an important parameter of CL that directly correlated to comfort and was quoted in several studies in the development of pharmaceutical-loaded CLs, there are currently no ISO standards on both the measurement method and tolerance of this property.

1.4.6.6 Oxygen permeability of SCLs

Most cornea oxygen is derived from the atmosphere. Therefore, in order to sustain corneal integrity and provide sufficient defense against infection [303], SCL materials are generally oxygen permeable (D_k) due to their high water content, which is a key factor in governing the clinical success of such materials [317, 318]. As stated in ISO 18369-1:2017 oxygen permeability (D_k) is defined as the "oxygen flux (j) under specified conditions through contact lens material of unit thickness when subjected to unit pressure difference". The ISO unit of D_k is 10^{-11} $(cm^2/s)[mlO_2/(ml \times hPa)]$, and is called the "$D_k$ unit" [268]. "D" is the diffusion coefficient of the material, whereas "k" represents the solubility coefficient. D_k is an intrinsic physical property of a material, which demonstrates the rate of oxygen flow through that material, as defined by Lebow and Campbell-Burns [319]. The D_k value of a material is directly dependent on its water content. As an example, a D_k value of 8 D_k was recorded for Softlens 04 (38.6% water content), while for a Duragel 75 lens that has 75% water content, the oxygen permeability value was determined to be 40 D_k [320].

This observation was also in agreement with a study carried out by Young and Benjamin [321]. Their work investigated the relationship between material water content and D_k of 35 conventional hydrogel materials based on the general format of ANSI Z80.20:1998 and ISO 9913-1:1996. Silicone hydrogel CLs (SiHys), on the other hand, were noted to have an inverse relationship between water content and D_k (at 35 °C) as cited by Efron *et al.* [322]. Focus Night and Day SiHys of water content 23 ± 3.2% provided 162.0 ± 9.8 D_k. A D_k value of 75.2 ± 9.8 D_k was recorded for Acuvue Advance SiHys that had 46.5 ± 1.1% water content.

According to ISO 18369-4:2017 [270], the two main methodologies for determining the D_k value are the polarographic method [323] and the coulometric method. The oxygen permeability of olopatadine-loaded (used in the treatment of the allergic conjunctivitis) biomimetic acrylic hydrogels was investigated by immersing the discs

in 0.9% NaCl solution for 48 hours [323]. The oxygen permeability was measured using a Createch Permeometer model 210T (Redher Development Co., Castro Valley, CA, USA) at 100% humidity at room temperature. Biomimetic acrylic hydrogel CL, a lens designed to mimic the active site of the H_1-receptor (for which olopatadine acts as a selective antagonist), was synthesized by combining the selected monomers and applying a molecular imprinting technique. In comparison to the control hydrogel materials, non-imprinted and imprinted biomimetic olopatadine-eluted CLs showed no significant difference with lenses all within the typical values of HEMA-based lenses (45-56 D_k) [323].

There are various parameters associated with the successful measurement of this property after the insertion of CLs for a short period of time. Such parameters include the reservoir of oxygen in the polarographic electrode [324, 325]; the material and thickness of the membrane [324, 326, 327]; the duration of exposure leading to the reduction of oxygen tension (i.e. the partial pressure of the dissolved oxygen) [328, 329]; the time between exposure and measurement [324, 330]; the surrounding corneal environment (temperature [331] and oxygen tension [332]); pH, osmolarity and buffering condition of tear [318]; corneal conditions (location [333], thickness [324, 333] and health [334]). The acceptable values for oxygen transmissivity of SCLs are around 25 D_k units for open eyes and 75 up to 200 D_k units for closed eyes, even though the results may vary slightly depending on the measurement approach [303, 321, 335, 336]. These are recommended figures to prevent corneal edema while providing sufficient oxygen to the cornea. Nasra *et al.* [303] measured the D_k of hydrogels with and without drug-loading. The concentration of oxygen was measured using an OX-TRAN® Model 2/21 from Mocon. At a 200 µm thickness, the hydrogel with 7.5% drug loading gave a D_k of 28.3 ± 1.3 [(10^{-11} (cm^2/s).(ml O_2/(ml mm Hg)] compared to 27.4 ± 2.2 [(10^{-11} (cm^2/s).(ml O_2/(ml mm Hg)] for the control lens [303]. As outlined in Table 1, the ISO tolerance for oxygen permeability is within 20% of the control value, thus, the Dk value of drug-loaded hydrogel in this study was in an acceptable range.

1.4.6.7 Wettability of SCLs

Wettability is the tendency of a surface to wetting, in other words, it demonstrates the ability of one fluid to spread on or adhere to a solid surface in the presence of other immiscible fluids [337]. In this system, there are three distinctive phases and three surface/interfacial tensions that must be taken into consideration: γ_{sv}: solid and vapour phase, γ_{sl}: solid and liquid phase, and γ_{lv}: liquid and vapour phase. These interactions can be demonstrated through Young's model (Figure 1.30).

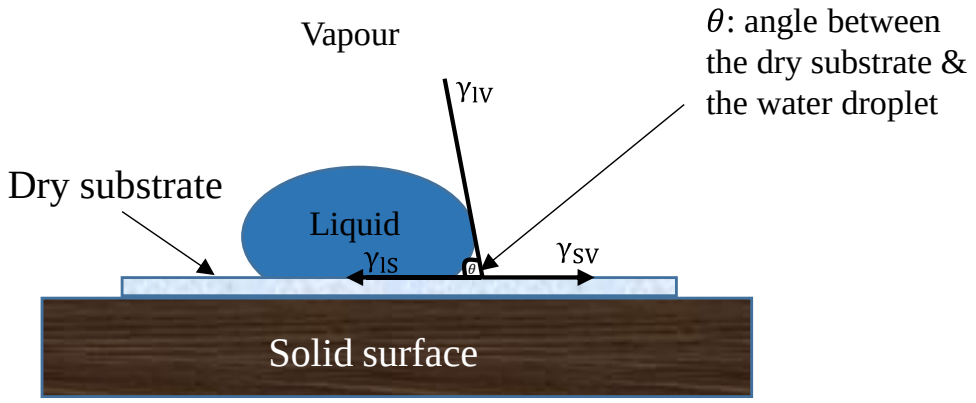

Figure 1.30: Young's model in the measurement of wettability.

The most common method used in the determination of the wettability behaviour of a solid surface, particularly the SCL surface, is to measure contact angle (CA). CA is defined by the angle (θ) formed at the base of the liquid drop on a solid surface. The cosine of the CA in equilibrium (θ_e) with a gas phase can be calculated using Young's equation (Equation 1.2).

$$\cos\theta_e = \frac{\gamma_{sv} - \gamma_{sl}}{\gamma_{lv}} \qquad \textbf{Equation 1.2}$$

A lower CA value means better wettability, which in turn improves the stability of the tear film spread over the lens surface [338]. This is because the liquid can spread more easily with relatively lower energy. There are three critical factors that influence the measurement of CA, including the surface tension of the wetting liquid, the surface tension of the solid, and the interfacial tension between the two surfaces. Whilst the impact of the vapour phase on the surface energy of the liquid and solid when exposed to air is negligible, the molecular involvement of the solid and liquid phase is critical since it defines the interfacial tension between them [337]. CL wettability can be

measured in many ways, with the most common two approaches being the sessile drop technique and the captive bubble technique.

The sessile drop technique is an optical-based tensiometry technique that involves the placement of a liquid droplet onto a substrate of interest (e.g., contact lens) (Figure 1.31). The droplet can be formed by using a computer-controlled syringe, which will give a reproducible chosen test volume. A tested specimen is placed on the movable stage that is directly below the syringe, the images or videos of the experiment are recorded simultaneously by a camera focused on the stage over specified periods from which the CA can be established [337].

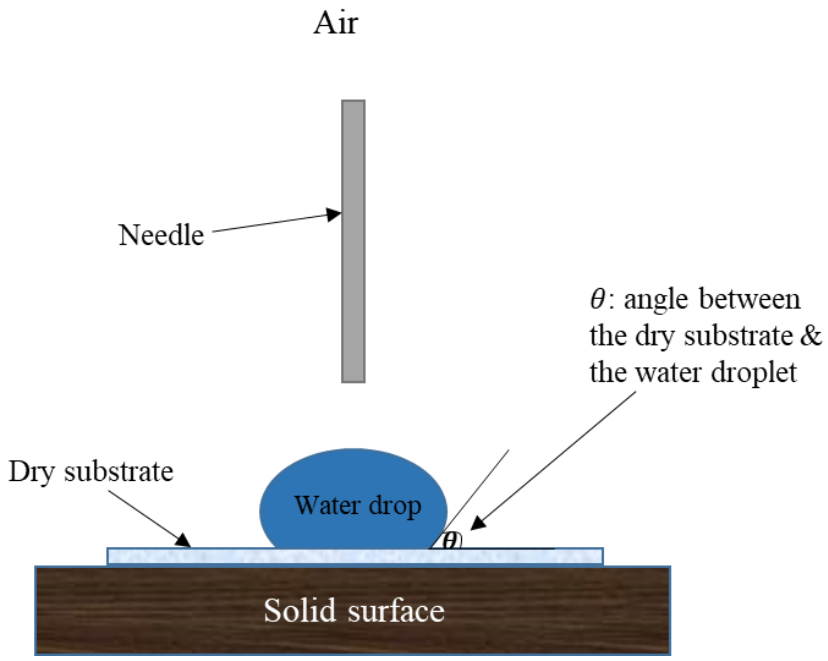

Figure 1.31: A view of the sessile drop technique applied to the analysis of CLs.

The second approach is the captive bubble technique, which can be referred to as an "inverted" sessile drop [337]. With this method, the tested material is immersed in a probe fluid (generally water), and air (or another immiscible liquid) is introduced to form the droplet (Figure 1.32). As the air bubbles encounter the surface of the tested object, a solid-liquid interface will be created. Similar to the sessile drop technique, the images of the formed CA at this interface can be captured and measured using similar instrumentation and software. Although the sessile drop method is one of the most common approaches used in determining the wettability, the hydrogel material must be dried. However, as the CLs must be in a hydrated state before placing in human eyes, it is more appropriate to investigate the CA in similar conditions.

Therefore, the captive bubble method is preferable in determining the wettability of SCLs [339].

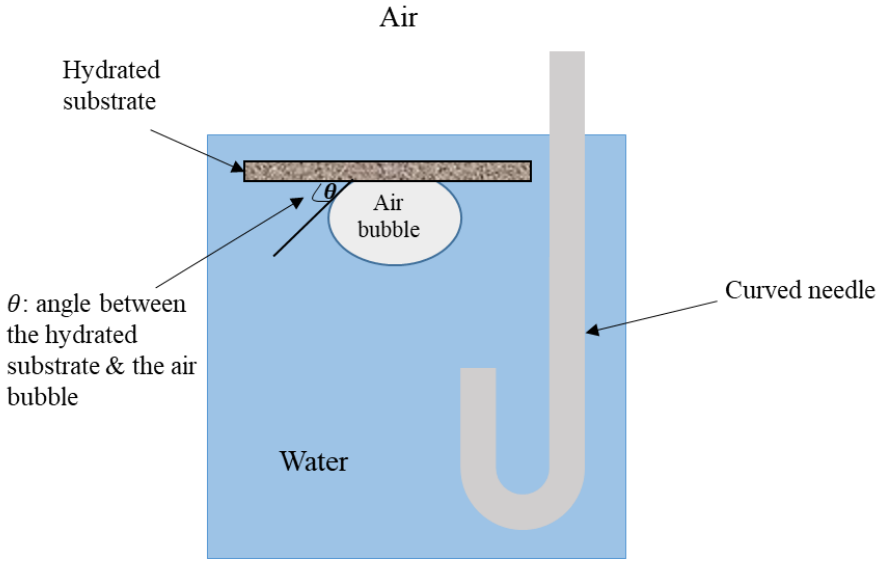

Figure 1.32: A view of the captive bubble technique.

1.4.6.8 Mechanical properties of SCLs

The mechanical properties of hydrogel CLs are extremely significant since they are related directly to comfort, visual performance, fitting characteristics, physiological impact, durability and handleability of the lenses as reviewed by Bhamra *et al.* [340]. One of the key properties of SCLs is the ability to maintain their physical dimensions and shape upon the application of external forces. Stresses in the lens material can cause a loss in optical transparency, discomfort, or even complete disintegration [341].

A study carried out by Efron [342] demonstrated that the CLs must be cut into a standard shape before its tensile properties can be investigated. Then, a tensile stress (N/m^2) or load per unit area of that minimum cross-section can be applied, which will subsequently lead to the elongation of the materials. The extent of this elongation is referred to as tensile strain, which is a dimensionless unit. The material will continue to elongate as long as the strain is applied until it reaches a yield point, when there will then be an increase in strain without a further increase in stress. This point indicates the degree of stress the material can hold without being deformed permanently.

The tensile strength (TS) of the material can be determined through the tensile stress where the stress is applied past the yield point until breakage. The elasticity or a Young's modulus (E) of the material can be calculated by dividing the stress by the strain (Equation 1.3). The higher the E value, the harder and stiffer the material [341].

$$\mathrm{E} = \frac{\text{stress}}{\text{strain}} \qquad \textbf{Equation 1.3}$$

The modulus of a hydrogel material demonstrates the extent to which its deformation will occur due to eyelid movement, along with indicating the influence on fitting behaviours of the lens and its comfort [341]. A study done by Tighe [343] implied that while the tensile strength relates to the durability and resistance to the handling of SCLs, the shear and compression force due to eyelid motion give a different type of deformation, which was determined to be 2.6 x 10^4 dynes/cm^2. This deforming force can be reproduced by using a calibrated flat probe in conjunction with a micro-indentation apparatus designed for work on paint film.

A common mechanical testing instrumentation used in the determination of SCL mechanical properties is the tensile strength machine. A study carried out by Tranoudis *et al.* [341] used the Instron 1122 Testing Instrument with a loading cell of 5 kN. The specimens of identical width (3 mm) were cut from individual CLs using a sharp utility knife. Each test specimen was then flattened between two thin plastic sheets. The biggest challenge of such a method was identified to be the consistency of the specimen's dimensions. If small flaws were created throughout the preparation of the samples, the test results would be unreliable. A range of tensile strength values of 1.23-5.87 kg/cm^2 across eight types of SCLs with various water content was obtained. This work suggested a way to overcome this issue using a 'plastic window frame', which allowed the specimen to be cut and handled better while transferring to the instrument. Furthermore, to minimize the dehydration of the materials, instead of using a complicated process of taking the measurement in solution, the film of water on the surface of the lens remained intact so the dehydration of the hydrogel would be negligible [341].

1.4.6.9 Coefficient of Friction of SCLs

When discussing the lens surface properties, besides CA and wettability, its frictional features also play an important role in clinical implications [344]. Friction can be defined as the resistance that a solid surface encounters when it moves over another. Subsequently, these solid surfaces can go through 'wear and tear' that can be reduced if there is adequate lubrication between the surfaces. There are several factors that can lead to an increase in friction between the lens and the eyelid margin, including dehydration, spoliation, poor tear film properties or irregularities of the ocular surface. Such characteristics can be measured using the coefficient of friction (CoF), which is the ratio of the required force to initiate or sustain sliding to the normal force while holding the two surfaces together. CoF is usually symbolized by the Greek letter μ, is dimensionless and can be calculated based on Equation 1.4.

$$\mu = \frac{\text{Frictional force}}{\text{Normal force}} \qquad \textbf{Equation 1.4}$$

The CoF of SCLs has been analyzed *in vivo* to correlate with subjective comfort [344]. Thus, the lens comfort can be predicted from *in vitro* tribological data. CoF can be impacted by the measurement conditions such as speed, contact pressure, the chemical/biological composition of the lubricating fluid, as well as the sliding counter-surface [344]. These properties should resemble those existing between the eyelid and cornea. In addition, the mechanical properties of hydrogels are easily influenced by water content and humidity, whereas contact pressure is known to cause redistribution and/or reduction of water content of hydrogel materials. Thus, low contact pressure conditions are preferential in carrying out tribological testing [345].

With sliding speed up to around 10 cm/s throughout blinking, the range of contact pressure that the eyelid exerts on the cornea has been cited to be 1 to 7 kPa [344]. Whilst, several studies showed that the contact pressure could be estimated to be in a range of 3.5 – 4 kPa with an average blinking speed of 12 cm/s [346, 347]. The combination of low contact pressure and high speeds with relatively low frictional forces has made it challenging to measure the tribological properties of SCL appropriately. The CoF of pHEMA was demonstrated to be in a range of 0.060 – 0.115 using a custom-built pin-on-disk tribometer, with a contact pressure of 3.5 kPa in the

work carried out by Nairn and Jiang [346]. Another study carried out by Freeman *et al.* [348] cited the CoF of flat disks of pHEMA hydrogels to be in a range of 0.02 – 1.7 over various applied load, lubrication, hydrogel crosslink density, and degree of hydration.

The friction coefficient of SCLs Etafilcon A was investigated by Rennie *et al.* [345]. Using a micro-tribometer, the tests were set-up at 10-50 mN of normal load at speeds from 63 to 6280 µm/s, using a 1 mm radius glass sphere as a pin. The contact pressure for this study was identified to be around 54 to 120 kPa, which was an order of magnitude higher than the expected values, while the speeds were an order of magnitude lower. This work also examined various factors that can influence the frictional force in a microtribological contact with a saturated hydrogel. It was identified that the viscoelastic nature of the hydrogel, viscous shearing of the packaging solution, and the interfacial shear between the glass sphere and CLs all contributed to the CoF value.

1.4.7 Incorporation of Analytes into Soft Contact Lens

Contact lenses as ODDS (Figure 1.33) have been suggested to be more beneficial than eye drops due to an increase in the residence time of the therapeutics in the tear film. This approach could lead to an enhancement in therapeutic bioavailability as extensively reviewed by Xu *et al.* [247].

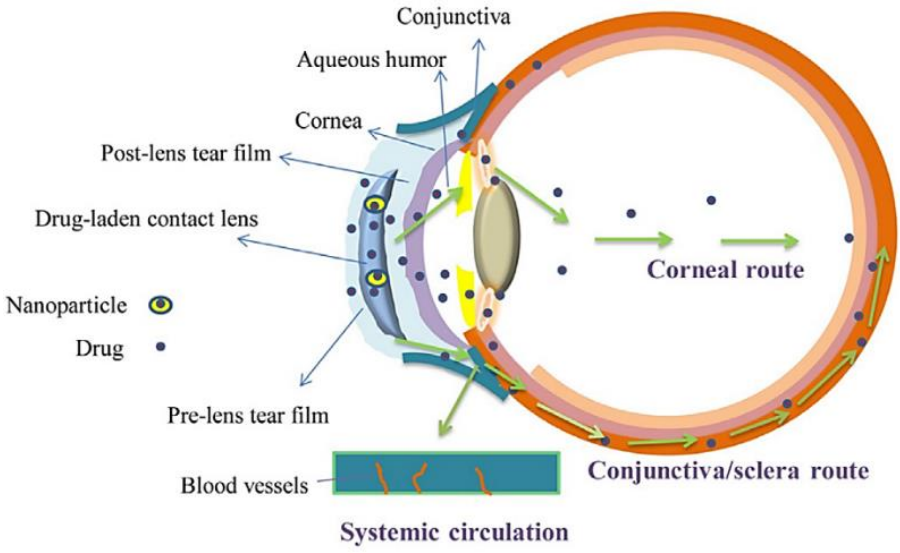

Figure 1.33: Schematic diagram of a contact lens used as an ocular drug delivery system [247].

There are several methodologies and technologies used to create CL-based ODDS which were extensively reviewed [219, 220, 288]. Such approaches include 'soak and release', molecularly imprinted CL, NPs-loaded CL, and surface modified CL. Additionally, with the improvement of the soft daily-disposable CL market worldwide [219, 220], as well as extended wear CL, the implications of this technology can reduce redness and irritation as it limits the eye contact with other preservatives in the topical formulations. Various techniques used in the design and development of contact lens-based DDS, along with the potential of hydrogel SCLs in drug delivery to the posterior segment of the eye will be addressed in this section.

1.4.7.1 'Soak and release' method

A majority of early studies on the incorporation of drugs into SCLs focused on soaking the lenses in drug solution, followed by insertion of the lenses in the eye [11, 349-351]. This approach is widely known as the 'soak and release' method, and is the simplest and the cheapest approach to loading drugs into CLs (Figure 1.34) [247].

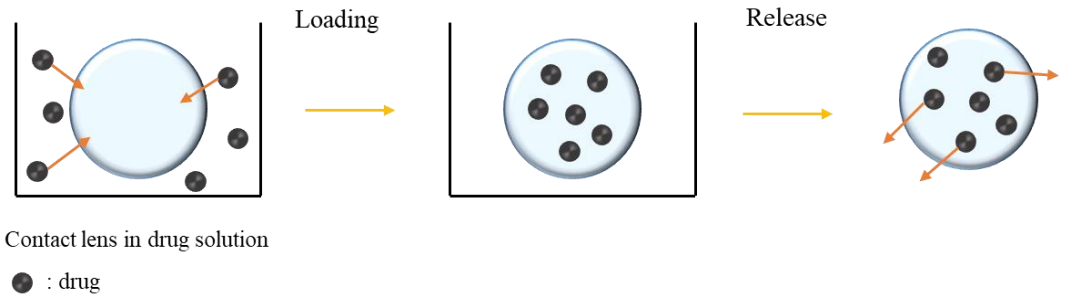

Figure 1.34: Schematic diagram of the 'soak and release' method of integrating drug into a contact lens.

In this approach, the primary driving force for drug loading into the CL is said to be molecular diffusion, which is involved in the mechanism of the drug release from the CL [247]. This is due to the difference in drug concentration between the aqueous phase of CL and soaking solutions. Specifically, as described by Kakisu *et al.* [352], a cationic or anionic compound in the SCL matrix will firstly form an ionic complex with the drug molecule in its solution. After applying the SCL to the eye, components in tear fluid including sodium, chloride, etc. will replace the drug content over time. Consequently, this leads to a sustained drug release from the SCL. The 'soak and release' approach has been applied successfully in loading ophthalmic drugs such as

timolol [353], dexamethasone [354], pilocarpine [355], pirfinedone [356], aminoglycosides and fluoroquinolones [357].

Maulvi *et al.* [311] investigated the drug loading and release from HA-loaded hydrogel sheets. The hydrogel sheets were soaked for 48 hours in 2 mL of HA solution of various concentrations (0.25, 0.5 and 0.75% wt) prepared in stimulated tear fluid (STF is made of NaCl, $NaHCO_3$, $CaCl_2$ and KCl). This was followed by blotting the lenses with tissue paper to remove the excess HA solution from the surface. Swelling behaviour of the soaked lenses increased with increase in concentration of HA in the soaking solution (e.g., 80.7 ± 2.9% in blank sample, 82.3 ± 1.2% in 0.25 %wt HA solution and 85.7 ± 1.6% in 0.75 %wt HA solution). Optical transparency and ion permeability of the lenses before and after soaking in HA solution showed a statistically non-significant change. A higher concentration of HA in the soaking solution resulted in a higher loading value after soaking (35.9 ± 2.3, 58.0 ± 1.6 and 81.2 ± 2.0 μg for 0.25, 0.5 and 0.75 %wt HA in soaking solution, respectively). However, it should be noted that when the HA concentration went above 0.75 %wt, the solution become too viscous to handle. A rapid release of HA in the first 6 hours was demonstrated. Moreover, a higher concentration of HA in the soaking solution resulted in a higher percentage release in the initial hours (Figure 1.35) [311].

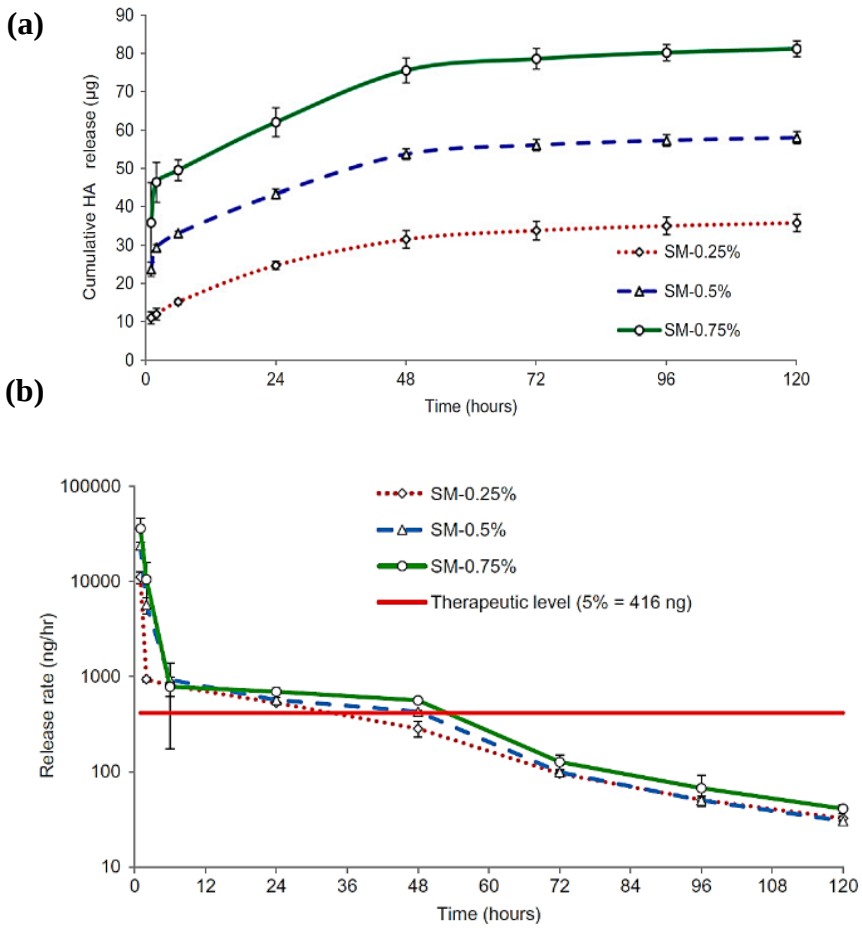

Figure 1.35: (a) Cumulative HA release from hydrogel sheets loaded by a soaking method; (b) release rate (ng/h) of HA from soaked hydrogel sheets using cumulative release data. Therapeutic release rate was calculated based on 5% absorption from eye drops. Data are shown as mean ± SD (n = 3) [311].

The results from Figure 1.35 demonstrated the limitation of a 'soak and release' approach in preparing HA-loaded SCLs for ocular drug delivery (ODD). The high molecular weight of HA prevented it from penetrating the aqueous channels of the hydrogels and only adsorbed on the surface. Therefore, no significant enhancement in release duration could be obtained [311].

In order to prepare drug-loaded CLs, Zhu *et al.* [358] immersed the dry CLs in 1 mL aqueous drug (betaxolol hydrochloride, BH) solution (5 mg/mL), kept at 25 °C in the dark for 3 days. While an increase in drug concentration from 0.5 to 5 mg/mL led to an increase in drug loading (DL) and loading efficiency (LE), further increasing the drug concentration resulted in a slight increase in DL with LE remaining unchanged. However, when the concentration increased up to 50 mg/mL, a reduction in LE was

observed which indicated an increase in drug wastage. Equilibrium of the loading process was reached after 12 hours. Nevertheless, when the incubation time increased to 72 hours, although no further increase in drug loading was observed, a reduction in standard deviation was observed (Figure 1.36). However, this approach was found to suffer from several limitations including low drug LE, short drug release duration and poor storage stability. As such, more than 80% of the drug was released within 2 hours in STF, with complete drug release taking place in 4 hours (Figure 1.36D). A similar observation was made for drug release in phosphate buffered saline (PBS), which has been used as a CL packaging solution (Figure 1.36D) [358].

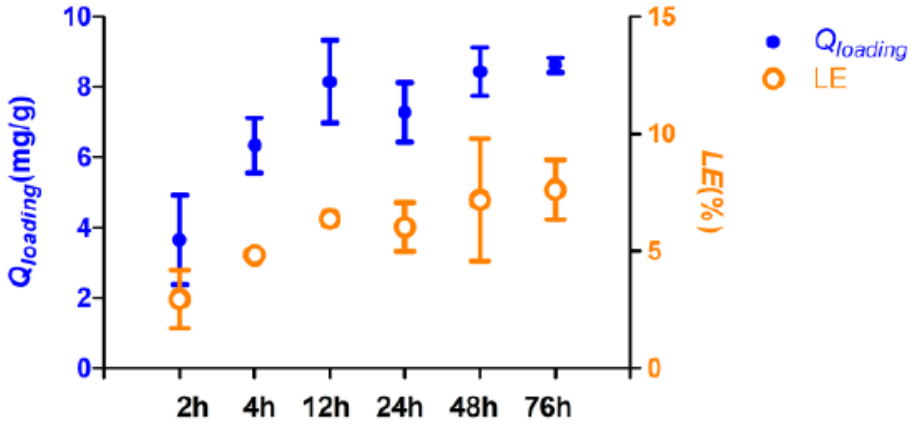

A

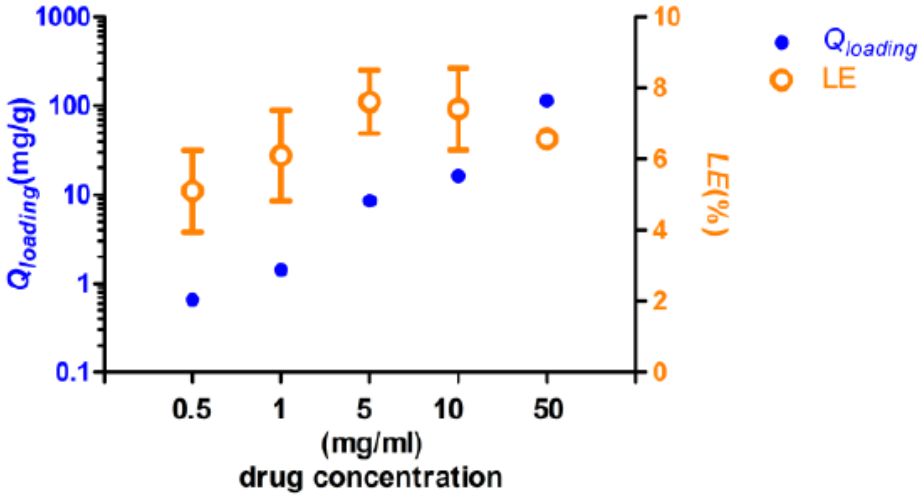

B

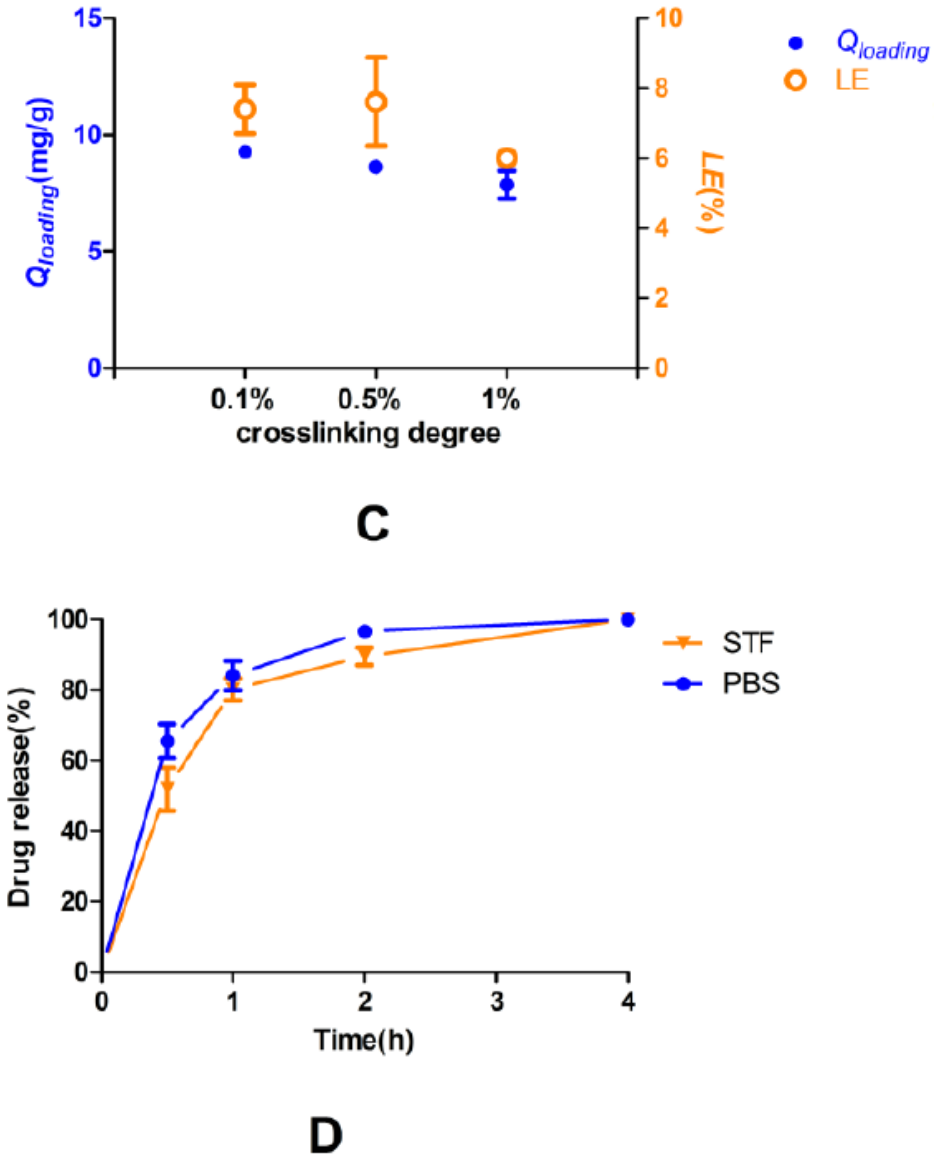

Figure 1.36: Influence of loading time (A), soaked solution concentration (B), and crosslinking degree of CLs (C) on drug loading amounts (left Y) and efficiency (right Y) using the soaking method and drug release from soaked CLs with 0.5% crosslinking degree in STF (simulated tear film, pH 8) or PBS (phosphate buffered saline, pH 6.8). Values are shown as mean ± SD (n = 3) [311, 358].

An alternative approach to enhancing the soaking method has been extensively carried out and developed to overcome burst release limitations. Since the release of drug through the soaking method is mainly based on molecular diffusion, creating a diffusion barrier in the lens polymer matrix can result in the prolongation of drug release [219, 247, 288]. This involves the incorporation of vitamin E (VE) aggregates into CLs to form barriers to drug diffusion that force the drug molecules to diffuse

through the ‘tortuous’ path around the barriers [10, 359]. This resulted in an increase in therapeutic release times from hours to several days. VE is a biocompatible hydrophobic liquid and a strong antioxidant, which also has therapeutic benefits [10]. Further, VE-laden silicone CLs have been shown to improve the UV blocking ability of conventional lenses, and thus, effectively prevent the penetration of UVR to protect the cornea [10, 360].

Although VE has been demonstrated to be a potential biocompatible diffusion barrier that can extend the release duration of various therapeutics, there are a few limitations associated with this approach for the development of therapeutic CLs. As such, the incorporation of VE into the lens matrix can lead to the reduction in ion and oxygen permeability, changes in mechanical properties (e.g., increase in storage modulus), and protein adsorption issues, due to the hydrophobic nature of VE [361].

1.4.7.2 Molecular imprinting

The concept of molecular imprinting (MI) through the imprinting of organic polymers was first introduced by Wulff’s research group in 1972, which is now established and used by various research groups [362]. Its concept involves binding the polymerizable functional groups to a suitable template molecule, which is then copolymerized, resulting in highly cross-linked polymers with fixed-arrangement chains. This is followed by the removal of template molecules to obtain polymers with well-defined cavities, those that are complementary to and have an affinity for the original target molecule [362] (Figure 1.37).

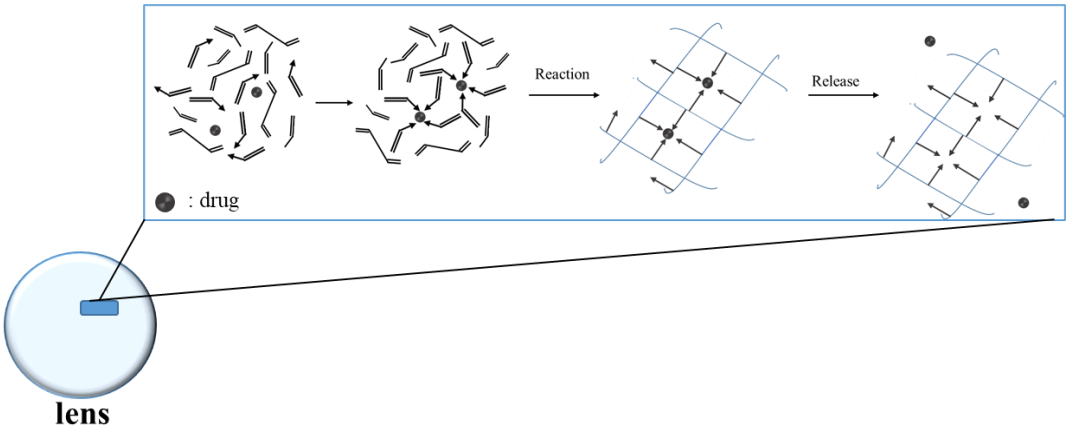

Figure 1.37: Schematic illustration of molecular imprinting drugs.

As reviewed by White and Byrne [363], owing to the number and strength of interactions between the analyte and polymer, together with the crosslinking structure and mobility of polymer chains, the formation of imprinted networks can result in a more controlled release profile. Several studies indicated that the drug affinity and its release pattern can be controlled by the type and ratio of monomers of the polymer matrix [349, 363, 364]. Commonly used functional monomers include acrylic acid (AA), acrylamide (AM), methacrylic acid (MAA), methyl methacrylate (MMA), and N-vinyl-2-pyrrolidone (NVP) [350, 365-370]. Through hydrogen bonding, hydrophobic or ionic interactions, these functional monomers can interact with the drug. While lacking of functional monomers will lead to non-imprinting, excessive functional monomers can cause the drugs to be retained rather than released [364]. As discussed in Section 1.3, the cross-linker can improve the mechanical strength of the CLs, too much cross-linking agent will slow the drug release rate due to network structure stiffness [369].

MI technology has been successfully investigated by researchers to increase the drug loading and the drug release time from hydrogel matrices [335, 367, 371, 372]. There are several factors that can cause the increase in partitioning due to imprinting, including temperature, pressure, initiator concentration and degree of crosslinking [219]. The importance of the functional monomer to template (M/T) ratio in the optimization of imprinted CLs design was assessed [364, 365, 373]. A slower *in vitro* release with 50% timolol being released in three days (2-fold increase in release duration) was observed with an increase in M/T ratios (1:16 to 1:32) for MAA-based systems [364]. Tieppo *et al.* [373] reported a dramatic decrease in the release rate of sodium diclofenac (from 11.72 µg/h to 6.75 µg/h during the first 48 hours) from imprinted CLs by increasing M/T ratio up to 10.5, where zero-order release was achieved. This strategy was applied in the treatment of DES using 120 kDa hydroxypropyl methylcellulose (HPMC). The release duration was extended up to 60 days with a rate of 16 µg/day, and was found to depend essentially on the M/T ratio [369].

A study by Pereira-da-Mota *et al.* [374] demonstrated the development of imprinted and non-imprinted HEMA hydrogels with and without the presence of various functional monomers for the incorporation of atorvastatin as a promising ODDS. Their

work showed that comparing to the non-imprinted hydrogels bearing AEMA (2-aminoethyl methacrylate hydrochloride) and APMA (N-(3-aminopropyl) methacrylate hydrochloride) functional monomers, imprinted hydrogels exhibited minor increases in the amount of drug loading. This suggested that both monomers possessed the highest affinity for atorvastatin. Hence, the imprinting effect was minimal in this case. The MI approach was shown to effectively extend the release duration of multiple therapeutics through SiHy CLs for post-cataract surgery and uveitis treatment. Lenses were fabricated using MI for the incorporation of diclofenac sodium, dexamethasone sodium phosphate, bromfenac sodium, and moxifloxacin. A controlled release duration of one week with 11.4 ± 2.8, 6.8 ± 1.9, 28.2 ± 8.6, and 14.0 ± 5.0 µg/day from the four aforementioned therapeutics-loaded lens, respectively, was demonstrated by DiPasquale *et al.* [375].

1.4.7.3 Nanoparticle-laden therapeutic contact lens

NP-loaded SCLs have been investigated as nanocarriers to extend drug release in the eye. This technique is based on the ability of NPs (e.g., polymeric NPs [376], lipid NPs, liposomes [377]) to encapsulate or entrap drug and control its release rate from CLs. In this delivery system, the drug may first diffuse through the NPs to reach the CL matrix, and consequently, it moves through the hydrogel matrix to reach the tissue as shown in Figure 1.38 [378].

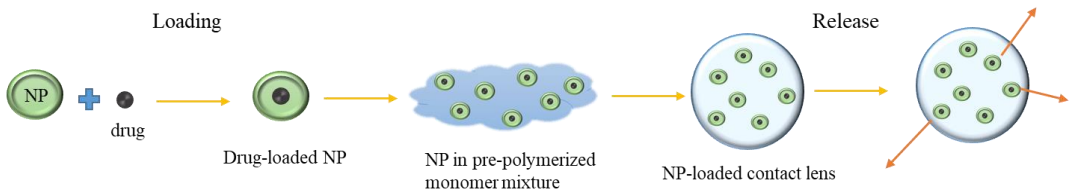

Figure 1.38: Schematic of drug release from NPs-laden CLs.

One commonly used technique is direct-entrapment of drug-loaded NPs into the lens matrix [52, 283, 311]. After the preparation of drug-loaded NPs, they are dispersed into the monomer mixture followed by polymerization to form a NP-loaded CL [378, 379]. To load the prepared NPs by this method, a specified mass fraction of NPs was added to the pre-polymerized monomer mixture before being purged with nitrogen. This was followed by injecting the mixture into lens moulds for curing under UV light.

As an example, a dexamethasone sodium phosphate (DXP)-loaded CS NPs laden pHEMA lenses were successfully prepared using this technique (Figure 1.39) [283].

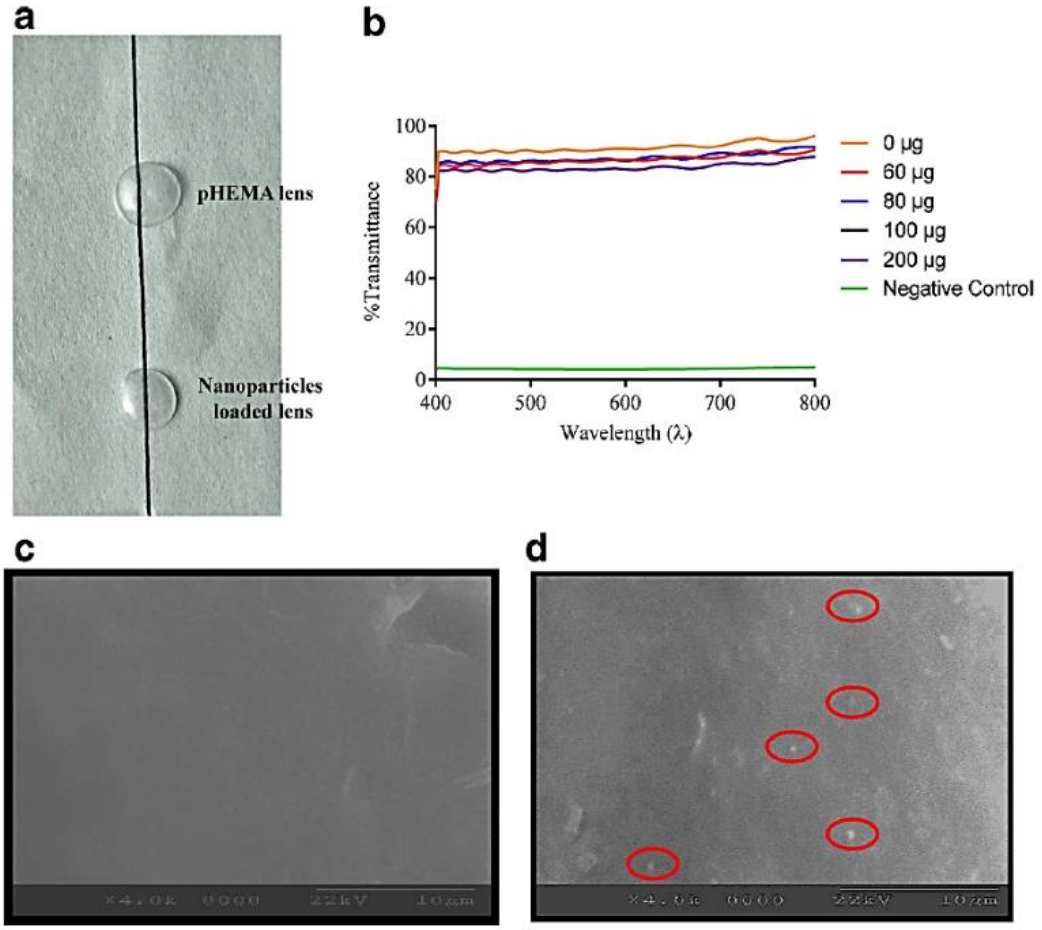

Figure 1.39: (a) Image of unloaded and drug-loaded CS NPs laden pHEMA lenses; (b) Optical transparency of the pHEMA lenses with varying amount of drug loaded CS NPs; and SEM images of (c) unloaded pHEMA lens and (d) drug-loaded CS NPs laden pHEMA lens [283].

Similar lens diameters of around 10 mm and lens centre thickness of 50 µm were obtained for both types of pHEMA lenses (Figure 1.39(a)). The addition of drug-loaded CS NPs did not affect the optical transparency of the lenses (95-98% transmittance relative to the unloaded CLs) (Figure 1.39(b)). The surfaces of unloaded and NP-loaded CLs were assessed by SEM to be similar to each other (Figure 1.39(c) and (d)) [283].

Alternatively, a different approach was used in this application including the addition of both the surfactant and drugs into the monomer mixture to create micelles throughout the polymerization [137, 380]. In order to overcome the burst release of

drugs and the limited drug loading capacity, Mun *et al.* [137] investigated a cholesterol-hyaluronate (C-HA) micelle-loaded hydrogel CL (pHEMA) for the delivery of cyclosporine. The diameter of C-HA micelle was analysed to be 290 ± 35.95 nm with a negative charge of -17.4 ± 3 mV. The drug-loaded C-HA micelle was then incorporated into the CL mixture prior to curing. The developed formulation provided a slight decrease in light transmittance (95% vs 90% for non-loaded and loaded-micelle lenses, respectively), and an increase in equilibrium water content (39% vs 43% for non-loaded and loaded-micelle lenses, respectively). A significant improvement in lens wettability (48.07° vs 39.6° for non-loaded and loaded-micelle lenses, respectively) and mechanical strength (C-HA micelle-loaded pHEMA lens was more stretchable than NP-loaded pHEMA lens) for the drug-loaded micelle lens was obtained. Cyclosporine was shown to be released in a controlled manner (50%) for more than 12 days through an *in vitro* study in this particular model [137].

Another approach to loading an analyte into CLs is surface immobilization of CLs with the analytes [381, 382]. Surface immobilization of CLs HA binding peptides was observed to locally attract and concentrate exogenous HA, while creating a thin HA-coated layer that can retain moisture on the surface of the lens [383]. Additionally, via electrostatic interactions using the layer-by-layer (LbL) technique, CL surface properties including wettability, dehydration and resistance to protein sorption could improve through the deposition of a self-assembled CS/HA multilayer coating [384]. This approach was also used to reduce bacterial cell adhesion on SCLs, which results in changes to the CL surface stiffness and roughness, surface hydrophilicity/hydrophobicity, and surface charge and charge density [385]. Korogiannaki *et al.* [386] recently demonstrated the preparation of covalent immobilization of HA on the surface of model pHEMA (poly(hydroxyethyl methacrylate) hydrogels using thiol-ene “click” chemistry. It includes the reaction of thiol with an α, ß-unsaturated derivative or an unreactive olefin via a base/nucleophile-catalysed Michael addition reaction or anti-Markovnikov’s radical addition mechanism [387]. Using a phosphine-mediated Michael addition thiol-ene “click” mechanism, surface grafting of HA-SH (thiolated HA) onto an ArcpHEMA hydrogel (acrylated pHEMA) surface was demonstrated (Figure 1.40).

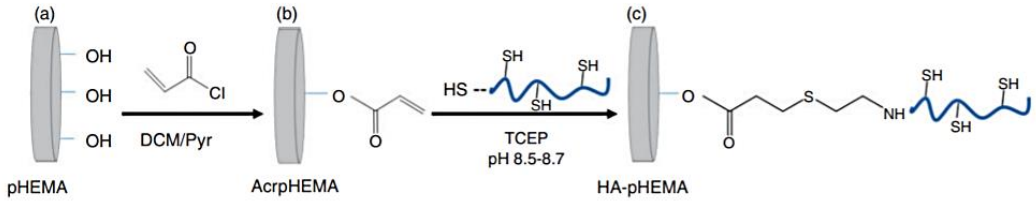

Figure 1.40: Schematic diagram illustrating the synthesis of surface grafted HA-pHEMA hydrogel via phosphine-mediated thiol-ene "click" chemistry [386].

A nucleophile-mediated Michael addition mechanism offers several advantages including mild reaction conditions with a low amount of catalyst (phosphine) required, while providing high functional group and oxygen tolerance, chemo-selectivity, bio-orthogonality and conversion [387, 388]. The successful immobilization of HA was confirmed by FT-IR and low resolution X-ray photoelectron microscopy [386]. The contact angles of the blank pHEMA hydrogels (control), ArcpHEMA and HA-grafted HEMA samples were 37.5 ± 1.8 °C, 45.1 ± 2.6 °C, and 14.5 ± 1.3 °C, respectively. The modified lenses demonstrated good biocompatibility for human corneal epithelial cells (HCEC) as determined by *in vitro* testing. Results from this study suggested that this method resulted in non-toxic materials, more wettable surfaces with enhanced water-retentive and antifouling abilities, while maintaining lens optical clarity (>92%) (Figure 1.41) [386].

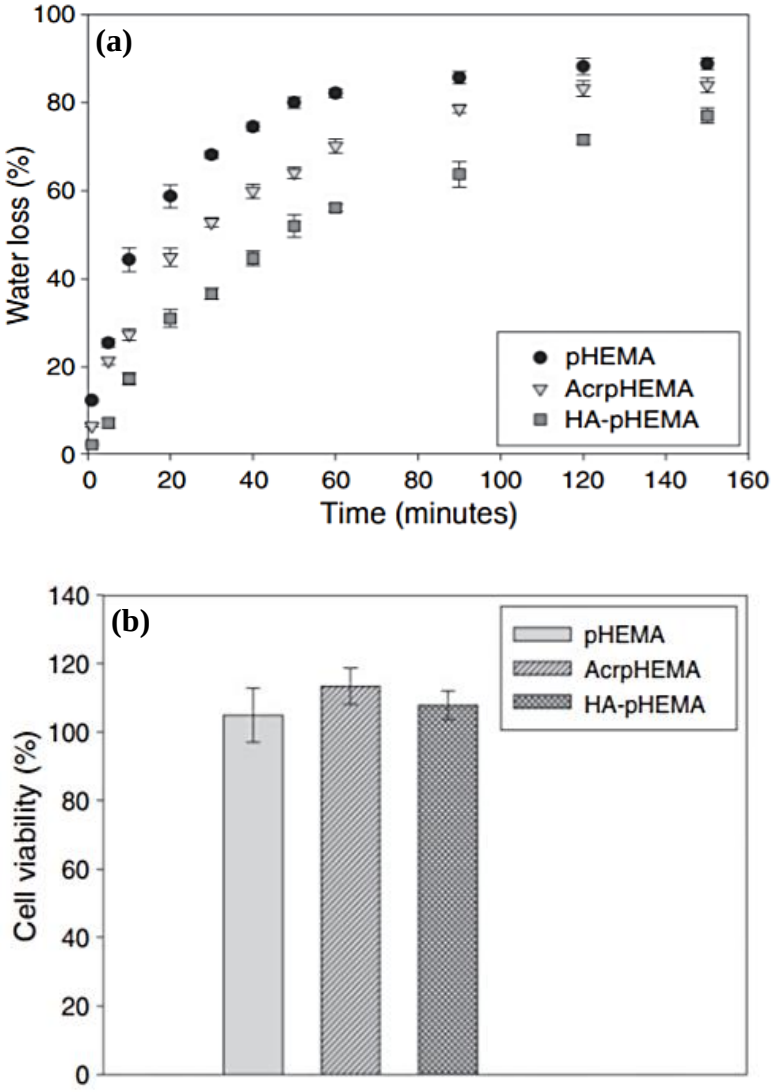

Figure 1.41: (a) The dehydration profile (n = 6) expressed as water loss (%) (T = 24 °C and relative humidity = 30%) from and (b) Cell viability (%) (n = 4) of the HCEC upon incubation with the unmodified pHEMA, acrylated pHEMA (AcrpHEMA) and HA-pHEMA hydrogels [386].

A different approach to the preparation of LbL deposition, based on natural polymers (CS, HA, polylysine hydrobromide-PLL and alginate-ALG), to provide a controlled and sustained drug release from silicone hydrogel (SiHy) materials while minimizing bacterial growth was introduced in a study by Silva *et al.* [389]. The model drugs were moxifloxacin hydrochloride (MXF), chlorhexidine diacetate monohydrate (CHX) and diclofenac sodium salt (DIC). The crosslinked SiHys were prepared using TRIS (3-tris (trimethylsilyloxy) silylpropyl 2-methylprop-2-enoate), NVP (N-vinyl pyrrolidone), HEMA, EGDMA (ethylene glycol dimethacrylate) and initiator AIBN (2,2'-azobis(2-methylpropionitrile)) (i.e., TRIS/NVP/HEMA). Three types of LbL coatings were

employed in this study with EDC (1-ethyl-3-(3-dimethylaminopropyl) carbodiimide hydrochloride) acting as crosslinkers for the carboxyl groups of the ALG and HA, and the amine group of PLL and CS, including ALG/PLL(EDC), HA(EDC)/CS and HA/PLL(EDC)+drug. In all cases, initially, the drug-loaded SiHys were coated with PEI (branched poly(ethylenimine)) by soaking the sample for 5 min in a 20 mM PEI solution to enhance the stability and uniformity of the subsequent layers. In the visible region, the transmittance of all coated samples was above 90%. No irritation of all the coated SiHy materials was observed through the results from HET-CAM test. Among the three drugs, controlled release of DIC was achieved following the LbL processes in comparison to the control lenses (without coating layer), and a reduction of bacterial growth was observed in this work.

In addition to the above approaches, one study carried out by Maulvi *et al*. [390] introduced another method which is drug encapsulated microemulsion and silica shell NPs. The silica shell NP-loaded hydrogels were prepared from the microemulsion using octyltrimethoxysilane. Due to the presence of a porous silica membrane at the liquid interface of the microemulsion, prolonged ocular drug delivery was facilitated. Compared to the hydrogel with direct drug entrapment, microemulsion and silica shell formulations did not show substantial impacts on lens optical transmittance and physical properties. With a much lower drug loading (65 µg for silica shell NP-loaded lens, 100 µg for microemulsion-loaded lens, and 125-500 µg for direct drug-loaded lens), only silica shell NP-loaded hydrogels showed extended drug release up to 9 days that still achieved the therapeutic level (105 ng/h). Cytotoxicity and animal studies were carried out to confirm the safety of all formulations within this study [390]. The cell line used in this study was rabbit corneal epithelial cell lines ATCC®CCL60™, and the animal study was carried out on healthy Swiss albino mice and white New Zealand rabbit.

A number of studies [391-393] demonstrated that this technology not only can prevent interaction of the drug with the polymerization mixture but also can provide additional resistance to drug release. Hence, this approach could deliver drugs at a controlled rate for extended periods. Further, NP-loaded CLs can also be considered as an effective method to avoid the degradation of drug during the sterilization and storage processes

[51]. To date, several types of NPs have been successfully loaded into SCLs, including polymeric NPs [394], liposomes [392], micelles [380] and microemulsions [391].

1.5 Novel Aspects and Scope of This Study

Due to the unique and sophisticated anatomy of the eye, along with the limitations in current eye diseases treatment, there is a need for a new ODDS. The novel aspect of this research involves the development of a prophylactic SCL of commercial quality to act as a therapeutic and non-therapeutic (i.e., supplement) carrier to the eye, which can release a compound that may potentially protect the retina from degeneration, while enhancing eye comfort.

A lab-scale manufacturing process for soft hydrogel CL that will exhibit the same critical lens parameters as a commercial lens will be assessed in this work. It is of scientific interest that the developed lens in this study is NVP-based, while the majority of hydrogel materials used in the development of therapeutic lens are HEMA-based. Many current works on the development of therapeutic soft contact lens use flat sheets of lens materials, which do not have the same physical geometry, dimensions, thickness, and shape as a contact lens. Whereas, for those that fabricated SCL using a lens mould, most of them only used an approximate lens material (e.g., HEMA-based monomer) rather than a commercial formulation (e.g., nesofilcon A monomer). With the ability to manufacture commercial quality contact lens at an academic lab utilizing a comparable commercial process, this will facilitate future study on the incorporation of therapeutics and particles to produce a novel ocular drug delivery system.

Drug-, complex- and NP-laden SCLs were formulated and developed for a sustained drug release and targeted drug delivery. To this end, two different approaches which are direct entrapment, and ‘soak and release’ were employed in the preparation of pharmaceutical-loaded SCLs. This part was essential to identify the optimum incorporating method to maintain the lens critical properties, while ensuring the therapeutically relevant drug loading concentration.

The above information supports the novel aspects of this study. These are worthy of extensive investigation to identify the possibility of using such a nano-drug carrier to provide a treatment approach for diseases that affect the posterior segment of the eye.

This research conducted a study into the development and characterisation of novel biodegradable and biocompatible drug:cyclodextrin complexes and drug-loaded NPs, incorporated into soft hydrogel CLs. This will act as a potential ocular drug delivery system that can provide targeted delivery and sustained release of a chosen therapeutic to treat posterior segment eye diseases. This thesis includes seven chapters which are outlined as below:

Chapter 1 outlined the literature review on ocular drug delivery.

Chapter 2 focused on developing a reproducible methodology of manufacturing CLs, which have comparable properties to commercial lenses. Subsequently, the manufactured CLs were fully characterized dimensionally, thermally, chemically, and mechanically and compared with the control lenses (commercial products).

Chapter 3 investigated the fabrication of drug-loaded SCLs of commercial quality, which were capable of providing a sustained and controlled release of a drug within its estimated therapeutic window.

Chapter 4 concentrated on the formulation and characterization of hydrophobic drug-cyclodextrin inclusion complexes. These were then fully characterized using various techniques such as thermogravimetric analysis, differential scanning calorimetry, and Fourier Transform infrared spectroscopy. The amount of drug loading in the drug:cyclodextrin complexes was subsequently determined using suitable chromatographic conditions.

Chapter 5 aimed to formulate and optimize drug-loaded polymeric nanoparticles (NPs) to investigate their physicochemical properties, their drug encapsulation efficiency as well as their *in vitro* release profile.

Chapter 6 demonstrated the fabrication, development and optimization of drug:cyclodextrin complex- and NP-loaded CLs that are capable of providing a sustained drug release while maintaining critical commercialized lens properties.

Chapter 7 describes the potential future work and areas that can be further investigated based on the completion of the studies carried out in the previous five chapters. It also provided the conclusion of the thesis and the associated publications.

CHAPTER 2

MANUFACTURING AND CHARACTERISATION OF SOFT HYDROGEL CONTACT LENSES

2 MANUFACTURING AND CHARACTERISATION OF SOFT HYDROGEL CONTACT LENSES

2.1 Introduction

Chapter 1 outlined how the treatment of ocular disorders have often relied upon a topical delivery strategy. As detailed, this approach is often associated with low drug bioavailability [3]. Where clinically relevant, intravitreal or periocular routes have been employed [395], which, while improving therapeutic bioavailability, can result in a higher number of systemic adverse effects and ocular complications [396]. As reviewed by this author, several studies have demonstrated controlled and sustained drug delivery using contact lenses, while examining their critical physical properties such as swelling, optical transparency, ionic permeability, modulus, refractive index, wettability, and morphological characterisation [218]. Hydrogels are commonly used in the manufacture of soft daily disposable contact lenses (SCLs), which have been investigated in various biomedical applications such as ocular drug delivery systems (ODDS) [218]. The functionality of SCL on the human eye is determined by the interaction between the polymer and the water that the polymer binds or adsorbs [397].

By using a therapeutic SCL as an ODDS, drug bioavailability can increase from less than 5% in topical administration up to 50% [10, 11]. The first therapeutic-loaded contact lens, Acuvue® Theravision®, a ketotifen-loaded hydrogel lens (etafilcon A) by Johnson & Johnson Inc., reached the market in 2021 as mentioned in Chapter 1[12]. This product has enhanced interest in the development of therapeutic-loaded SCLs to provide better care for patients who need vision correction and suffer from ocular conditions. In this work, a daily disposable SCL (Nesofilcon A material, Biotrue® ONEDay) was chosen. Nesofilcon A lenses are daily disposable SCLs that are capable of maintaining almost 100% moisture for 16 hours [398]. Daily disposable CLs were chosen in this study since a smaller loading of a therapeutic agent would be needed in comparison to a longer wear-duration SCL, and hence, it was postulated that this would enable the retention of lens' critical properties better.

Chapter 2 outlines the development of a reproducible lab-based method to manufacture hydrogel SCLs, which results in a lens that exhibits comparable critical properties to a chosen commercial lens from the Enterprise Partner (EP) – Bausch+Lomb (B+L), the

co-funder of this research, i.e., Biotrue® OneDay daily disposable (DD) SCLs. The first stage of this work focused on the characterisation and investigation of an appropriately chosen lens formulation, while examining manufacturing process parameters that included: thermal curing, polymerisation kinetics, the importance of hydration, extraction, and the sterilization process on formed lens properties. To fabricate the SCLs with reproducible physicochemical properties, size, shape, and optical power, the lens manufacturing processes are required to be robust. Therefore, a well-controlled free radical polymerisation plays a vital role in achieving a functional SCL. Manufacturing of SCLs through thermal curing was carried out using commercial lens moulds and a monomer mixture provided by the EP.

The second stage of this study involved the characterisation of the finished lens produced in an academic lab, labelled the WM lens (i.e., lens fabricated onsite using a forced convection Memmert oven). These were fully characterised based on the relevant ISO standards [399, 400] to ensure that they could potentially function as an optical device and have comparable properties to the chosen control (i.e., commercial) lens from the EP (abbreviated as CEP lens). Such properties included optical transmittance, equilibrium water content, refractive index, wettability, tensile modulus, ionic permeability, and dimensional parameters (diameter, sagittal depth, centre thickness, and roundness), and optical power. This was important to ensure the produced lens was fit for use as an optical device as well as drug delivery vehicles.

Many studies on the development of therapeutic SCL were executed using the hydrogel or SiHy flat thin film model to investigate the potential of this technology as an ODDS as reviewed by this author [218]. These models did not have the same physical geometry, dimensions, thickness, and shape as a contact lens. Hence, to drive this technology forward, it is essential to study the capability of therapeutic SCL using the actual lens that exhibits similar critical properties and geometry as commercial ones. Since this work demonstrates the ability to manufacture commercial quality CLs on-site, this will facilitate future studies into the incorporation of analytes and particles to produce a novel ODDS.

2.2 Research Aims and Objectives

The aims and objectives of this chapter are:

- To develop a reproducible commercial-quality methodology of manufacturing SCLs for investigation.
- To fully characterize dimensional, thermal, chemical, and mechanical properties of the WM SCLs, to ensure comparable properties to commercial lenses (Biotrue® ONEday SCLs) and thus provide a clear baseline for the incorporation of drug delivery technologies to the lens.
- To compare different sterilization techniques: non-sterilization vs. heat vs. gamma radiation, and their effects on contact lens properties as a predictor for the potential scale up of any drug delivery devices developed.

2.3 Experimental Methodology

2.3.1 Materials

Monomer components, nesofilcon A pre-polymerized monomer mixture, Biotrue® ONEday contact lens' moulds and contact lens (-3.00 SVS was used as the control lens throughout this study), N-vinyl pyrrolidone (NVP, >97% purity, BASF Ireland), 2-hydroxyethyl methacrylate (HEMA, >99% purity, Evonik Industries/Bimax Chemicals), ethylene glycol dimethacrylate (EGDMA, >98% purity, Evonik Industries), allyl methacrylate (AMA, >99% purity, Evonik Industries), t-Butyl-hydroxycyclohexyl methacrylate (TBE, >97% purity, Arran Chemicals), 1,4-Bis(4-(2-methacryloxyethyl)phenylamino)anthraquinone (IMVT/In-monomer Vis Tint, >95% purity, Arran Chemicals), poloxamer 407 dimethacrylate (purity: not specified, Polysciences), propylene glycol (PG, >99.8% purity, Dow Chemicals), 2,2'-Azobisisobutyronitrile (AIBN/Vazo 64, >96% purity, The Chemours Company), 2-[3-(2H-Benzotrialzol-2-yl)-2-hydroxyphenyl]ethyl methacrylate (UV Blocker, >96% purity, Sigma Aldrich, Melrob Limited) were provided by Bausch + Lomb Ireland Ltd (Waterford City, Ireland). Naringenin (>98% purity) and acetic acid (>99% purity) were purchased from Sigma-Aldrich Ireland (Wicklow, Ireland). PBS (phosphate buffered saline tablets, purity: not specified) and Methanol (HPLC grade, >99% purity) were purchased from Fisher Scientific (Dublin, Ireland). Ultrapure deionized water obtained from WhiteWater equipment (Dublin, Ireland).

2.3.2 Contact lens manufacture

The full preparation process of making SCLs is presented in Figure 2.1.

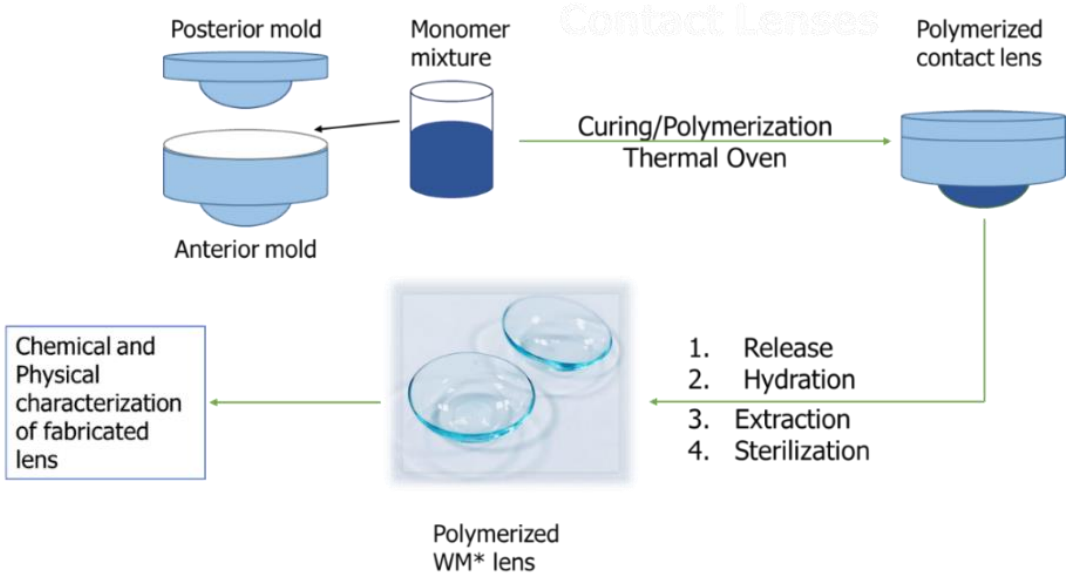

Figure 2.1: Schematic diagram of the contact lens manufacturing (WM lens = lens made at the academic lab).

2.3.2.1 Monomer fill

The polypropylene moulds and the support trays and towers provided by B+L Ireland Ltd. were used to manufacture the SCLs at the academic lab (Figure 2.2).

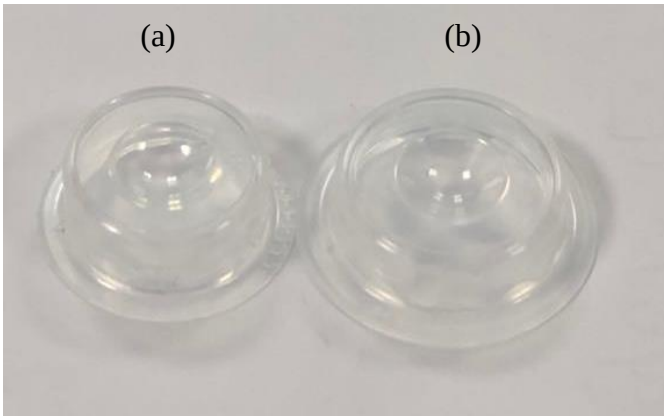

Figure 2.2: Moulds provided by Bausch+Lomb Ireland: (a) anterior (bottom) mould; (b) posterior (top) mould.

The pre-polymerization monomer mixture (nesofilcon A material) with the initiator (AIBN) was obtained from the enterprise partner. The volume of pre-polymerization monomer mixture to fill the mould was 23 µL, based on the mould specifications from the EP. This volume provided enough monomer mixture to form a complete lens while leaving a small 1-2 mm tab of excess monomer to ensure a good lens edge profile (Figure 2.3).

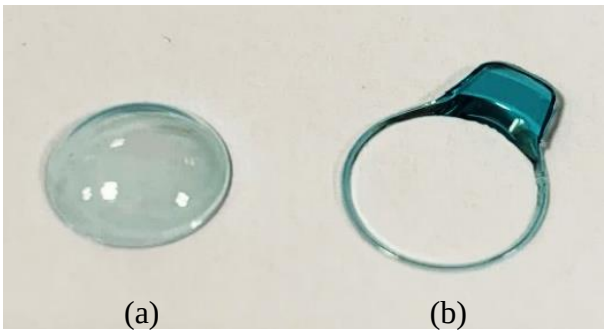

Figure 2.3: Image representing the post-curing (a) WM lens and (b) WM lens tab post-curing.

2.3.2.2 Thermal curing of contact lens

The curing of SCL was carried out using three different oven systems.

In the first trial, a previously developed stainless steel oxygen depletion chamber, which was built by Suir Precision Engineering Ltd, Waterford was used to cure lenses (220 mm diameter, 65 mm high and 316L). After placing the filled moulds inside the chamber and sealing its lid, the curing chamber was put inside a Heraeus Vacutherm oven to be cured (Figure 2.4).

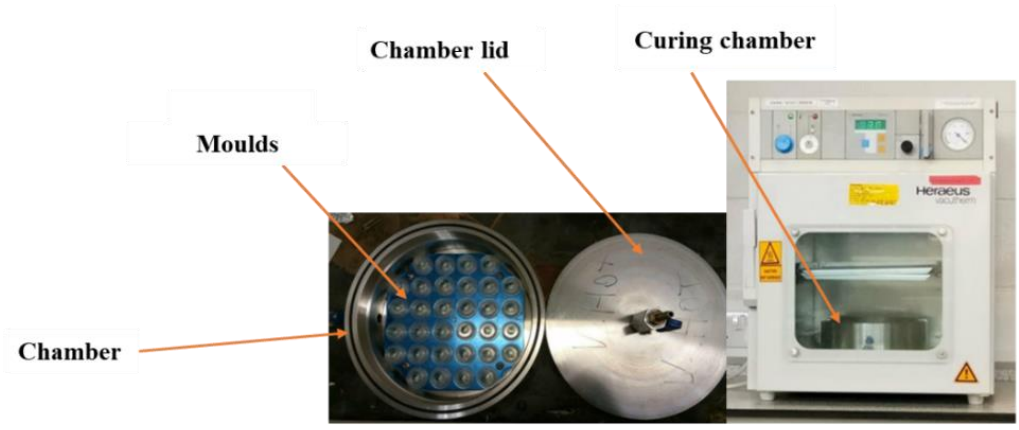

Figure 2.4: Oxygen depletion chamber (left) and Heraeus vacutherm oven with chamber inside (right).

In the second trial, instead of using an oxygen depletion chamber, trays of filled moulds were placed directly into a mould tower (Figure 2.5) and placed inside the Heraeus vacutherm oven. An ambient gaseous environment was employed. The curing temperature profile was monitored using a k-type thermocouple connected to Pico Data Logger. The temperatures were recorded and stored on a computer every 0.1 s for the full curing cycle.

Figure 2.5: Lens mould tower (left) and Heraeus vacutherm oven with mould tower inside (right).

In the third trial, the set-up was similar to trial two. However, a Memmert forced convection oven (UF50Plus, 50L capacity, Lennox, Ireland), which allowed a programmed temperature profile, was instead used to cure SCLs. An ambient gaseous environment was employed, and the curing temperature profile was obtained using a k-type thermocouple. The filled and capped moulds were thermally cured according to the curing cycle (in the second and third trials, Figure 2.6).

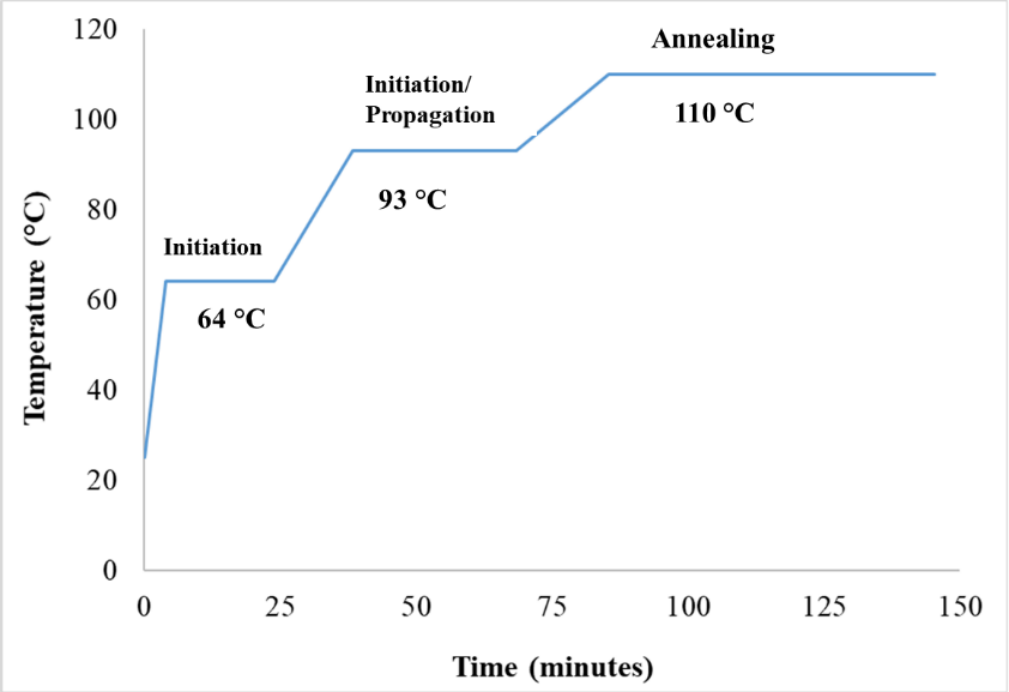

Figure 2.6: Memmert curing cycle profile and stage of polymerization throughout the process.

2.3.2.3 Hydration, Extraction and Sterilization of contact lens

Once the curing cycle was complete, the tower of moulds was allowed to cool for at least 30 minutes inside the chamber. Lenses were then removed from the moulds using a dry-release process. Here, the cured moulds were placed on a compressor, as shown in Figure 2.7.

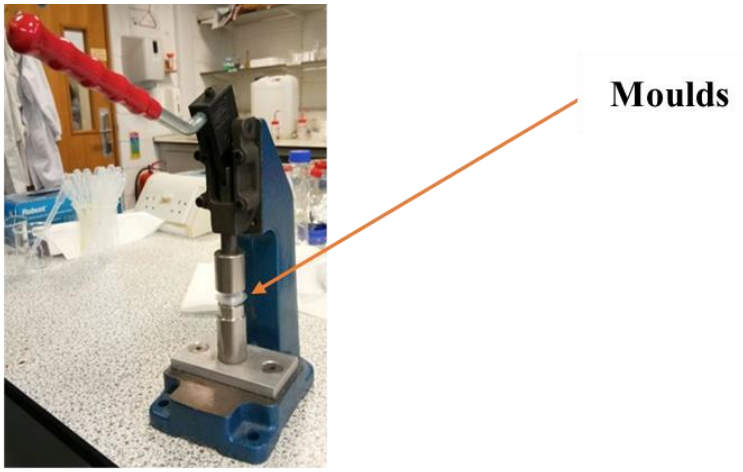

Figure 2.7: Compressor to release cured lens from moulds.

Lenses were then hydrated in 2 mL of 60 °C DI H_2O and the extraction process was carried out by washing each lens three times using 60 °C DI H_2O (2 mL each time) in a tray. The finished products were subjected to two types of sterilization, including: thermal sterilization (autoclave) and gamma radiation sterilization.

For thermal sterilization (autoclave, HV-50L, HCM/Lennox, Ireland), approximately 10-20 lenses were placed in a beaker containing 50 mL ultrapure water. The beaker was then placed inside the autoclave for 66 minutes at 123 °C.

Gamma radiation sterilization was carried out at the BIOMAT Research Group, Superior Tecnico Lisboa, Portugal. 10 WM lenses were placed in a sealed 10 mL glass vial filled with ultrapure water. The sterilized conditions [401] were set at:

- Dose debit: 5.02 kGy/h.
- Total dose: 25 kGy.

2.3.3 Contact lens characterisation

The WM lenses were characterized along with the CEP lenses for comparison. A total of five characterization methodologies were carried out at the BIOMAT Research Group at the Instituto Superior Técnico Lisboa, Lisbon, Portugal. These tests included: equilibrium water content, optical transparency, ionic permeability, contact angle, and tensile modulus. Dimensional analysis and refractive index (RI) measurement were carried out in Bausch+Lomb Ireland, Waterford City. The remaining characterisation techniques were carried out at the Pharmaceutical and Molecular Biotechnology Research Centre (PMBRC), SETU.

Besides the dry and non-sterilized lenses, it should be noted that only lenses that went through thermal sterilization process were used within this section. Lenses that were sterilized using gamma sterilization were not characterized due to their unfavourable physicochemical properties as described in detail in Section 2.4.1.

2.3.3.1 Dimensional analysis of hydrogel SCLs

Lens dimensional parameters: diameter, sagittal depth, roundness, spherical power, and centre thickness, were assessed. Values presented are averages of ten (10) lenses. Except for centre thickness measurement, which was done on-site, the rest of the tests was carried out in the Enterprise Partner lab using the following instrument:

- Vertexometer (PL-2, Nikon): Power (based on SOP provided by the EP):

When the unit was first turned on, the target was appropriately aligned with the screen. The center horizontal mire (longer than the other mires) was positioned directly on the 0° target line and the center vertical mire line directly on the 90° line. The Ø4.50mm aperture paddle fixture (BL000011177) was placed on the stage to simulate actual measurement conditions. Initially, the hydrated lens was examined to ensure that it was free from particulates and was blotted on lint-free blotting paper to remove excess solution (the lens was placed concave upwards). The lens was then placed concave facing downwards and centred on the measuring paddle. Before carrying out the measurement, the readout was covered, and the focus knob was adjusted to blur the image on the screen. Within 10 seconds after blotting, lens power was measured by adjusting the focus until the image came into sharp focus and recorded by uncovering the readout.

- SNAP (QVI, RAM Optical Instrumentation by Quality Vision International): diameter, roundness, and sagittal depth (based on SOP provided by the EP):

The experiment was carried out using the 'MeasureX2D' software. The lenses were placed in a water cell, which was filled slightly below the upper fill line. Lenses were placed in the appropriate slots provided in the water cell, concave side up and were allowed to sit in solution for 3 minutes. Each lens was then placed onto the pedestal within the four location marks concave side down and allowed to settle fully before measurement.

- Centre thickness (ET-3, REHDER Development company):

Lens centre thickness was measured using the Micrometer Calliper measurement tool through magnified glass at 5X in air at room temperature. The generated results were comparative only and may not be reflective of the true value of nesofilcon A lenses. Centre thickness results depend on the force used during the measurement due to the sponge type nature of the material.

2.3.3.2 Thermal analysis of hydrogel SCLs

Thermogravimetric analysis (TGA): Dynamic weight loss tests were conducted using a TA Q50 thermogravimetric analyser (TGA, TA Instruments, UK). 1-5 mg of

sample was accurately weighed into an aluminium pan for analysis. All samples were analysed over a temperature range of 20-600 °C at a rate of 10 °C/min, under a constant N_2 flow of 50 mL/min. A calibration with indium was carried out before testing any samples to ensure the accuracy and precision of the measurements. Values presented are averages of three (3) lenses per sample type.

Differential Scanning Calorimetry (DSC): A DSC (Q2000 model, TA Instruments, UK) was used in this study. Approximately 2-10 mg of each sample (either pre-polymerized monomer mixture, physical mixture, or dry lens) was accurately weighed into a sample pan. An empty aluminium pan was used as a reference. A calibration with indium was carried out before testing any samples to ensure the accuracy and precision of the measurements. The pan lid was pierced with a pin to ensure no pressure build up within the pan during the experiment. Values presented are averages of three (3) lenses per sample type. The method was set-up with the required parameters under a constant N_2 flow of 50 mL/min (Table 2.1).

Table 2.1: Parameters for differential scanning calorimetry analysis.

Monomer component + Initiator		**Contact lenses (dry state)**	
Test parameter	**Setting**	**Test parameter**	**Setting**
Equilibrate	20 °C	Equilibrate	20 °C
Ramp rate	10° C/min 64 °C	Ramp rate	5 °C/min to 200 °C
Isothermal	20 mins	Contact lenses (hydrated state): each lens was desalinated in DI H_2O for 24 hours.	
Ramp rate	2 °C/min to 93 °C		
Isothermal	30 mins	Initial temperature	-50 °C
Ramp rate	1 °C/min to 110 °C	Equilibrate	-45 °C
Isothermal	60 mins	Ramp rate	10 °C/min to 50 °C

2.3.3.3 Equilibrium water content of hydrogel SCLs

CL swelling studies evaluated the equilibrium water content (EWC) over a three-hour period. Three measurements were carried out for each type of lens at three different temperatures, 4 °C, 20 °C and 36 °C. This method was based on the work of Topete *et al.* [402]. CLs were first dried for 24 hours in a convection oven at 36 °C. The dry lenses (W_D) were weighed. They were then immersed in DI H_2O in separate containers.

At specific intervals of time, each sample was carefully blotted with white paper (that should be free from residues) and weighed immediately (W_w). The equilibrium water content (%EWC) was calculated based on Equation 2.1 [52] and each measurement was carried out in triplicate:

$$\%EWC = \frac{W_w - W_D}{W_w} \times 100 \qquad \textbf{Equation 2.1}$$

2.3.3.4 Light transmission of hydrogel SCLs

A Multiskan GO UV Vis spectrometer (Thermo Scientific, Portugal) was used to measure the light transmission through the hydrated WM and CEP lenses. Measurement was carried out using a wavelength range from 800-400 nm at 1 nm intervals and referenced to air. Lenses were suspended in the light path using a quartz cuvette. Values presented are averages of three measurements for each lens type.

2.3.3.5 Refractive index analysis of hydrogel SCLs

The refractometer (ATR-L, Schmidt Haensch, Germany) with a wavelength of 546.1 nm (Mercury line) was used to measure the refractive index (RI) of all lenses. Temperature was controlled at 20 °C throughout the measurement. Tested lenses were immersed in ultrapure water for at least 30 minutes prior to testing. To verify the performance of the refractometer, the RI of water was measured prior to testing samples, which was determined to be 1.333. The hydrated individual lens was then placed directly on top of the lens holder, which was attached to an appropriate spring to create a force to push the lens in contact with the prism. Values presented are averages of ten (10) lenses per sample type.

2.3.3.6 Ionic permeability of hydrogel SCLs

Ionic permeability of the hydrated SCLs was determined by measuring the conductivity (in µS/cm) every 30 minutes, for at least 12 hours, using a conductivity meter (HI2003 Edge$^{EC®}$, HANA Instruments, Portugal) at 36 °C. The hydrated hydrogel was measured in a poly(methyl methacrylate) horizontal cell with two sides: the donor compartment containing 24 mL of saline solution (0.9% v/v) and the acceptor compartment containing 32 mL of DI water.

The ionic permeability, D_{ion}, was calculated based on Equation 2.2 [389] and each measurement was carried out in triplicate:

$$\frac{FV}{A} = D_{ion}\frac{dC}{dx} \quad => \quad D_{ion} = \frac{FV}{A}\frac{dx}{dC} \qquad \textbf{Equation 2.2}$$

Where F is the rate of ion transport, V is the volume of the receiver solution, A is the area of the hydrogel sample and dC/dx represents the initial NaCl concentration gradient across the hydrogel.

2.3.3.7 Optical Microscopic characterisation of hydrogel SCLs

An optical microscope (OM) (Olympus DP71, Olympus BX51- U-LH100HG, Ireland) was used to examine the SCL surface (post hydration vs. post thermal sterilization) of WM lenses and CEP lenses. Each lens was laid flat on top of the glass slide prior to each observation. The images were taken in 'visible light mode' on the FM. This was carried out at two magnifications: 400X and 1000X.

2.3.3.8 Contact angle measurement of hydrogel SCLs

The goniometer is an instrument commonly used to measure the contact angle (CA) of a specimen. Contact angles of captive air bubbles lying underneath the substrates immersed in water were measured to determine the wettability of SCL samples (Section 1.4.6.7, Chapter 1). The desalinated, hydrated SCL was flattened and placed horizontally in a measuring cell containing DI H_2O. A micrometre syringe with a curved needle was used to create air bubbles underneath the surface of the hydrogels. A video camera (jAi CV-A50, Leica, Spain) mounted on a microscope Wild M3Z (Leica Microsystems, Germany) was used to acquire the images which were analysed with ADSA software (Axisymmetric Drop Shape Analysis, Applied Surface Thermodynamics Research Associates, Toronto, Canada). Values presented are averages of eight (8) lenses per sample type. The experiment was set-up as shown in Figure 2.8.

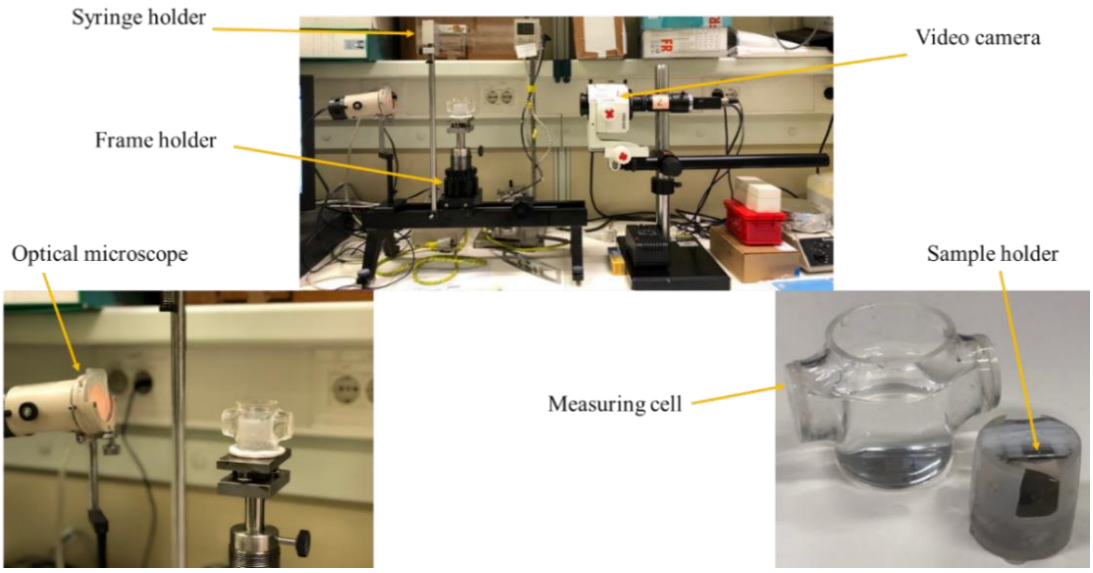

Figure 2.8: Experimental set-up for contact angle measurement for SCLs used in this study.

2.3.3.9 Tensile modulus of hydrogel SCLs

Each hydrated lens was cut into a dog-bone shape using a 'dog-bone' shaped cutting template (Figure 2.9). The OPTIMUM-Press Manual Universal DDP10 was used to cut the lenses to obtain a more consistent applied force. The TA.XT Express Enhanced (Stable Micro System, Portugal) instrument was used in this study to measure the tensile properties of the lenses. Tensile grips (which were modified with sponges) were used to stretch the lens until breakage occurred. In order to eliminate any ambiguity from the slope area used, the modulus can be derived from a tangent within the first 10% of the extension range, which was previously used by Kim *et al.* [403] to measure the mechanical properties of commercial lenses. The velocity of the two grips was set to 0.11 mm/s and the applied force was 1 g. Values presented are averages of ten measurements for each lens.

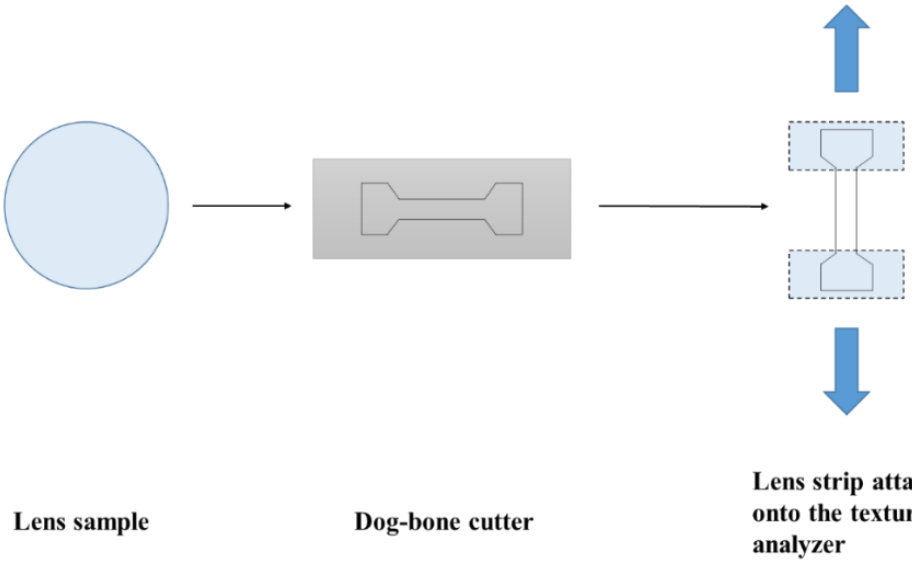

Figure 2.9: Schematic diagram of a lens being cut using a dog-bone cutter.

This experiment was carried out using tensile test grips to apply a tensile stress-load per unit area of minimum cross-section with a velocity of 0.11 mm/s. Since a SCL is very easy to break, the grips were adjusted with soft sponges on all sides (Figure 2.10).

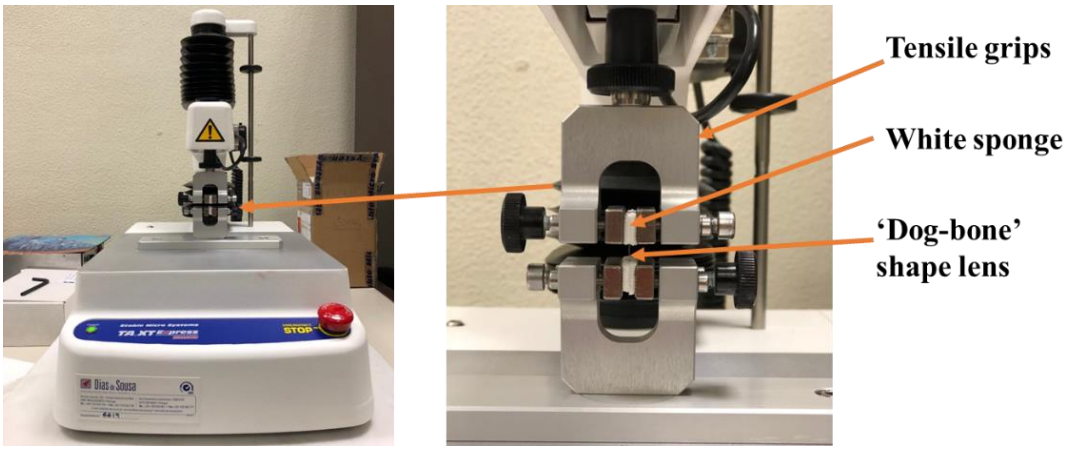

Figure 2.10: Experimental set-up for mechanical testing: instrument (left) and grips that hold the 'dog-bone' shape lens using sponge to protect the lens from breaking by grips prior to starting the test (right).

2.3.3.10 Fourier-transform infrared spectroscopic analysis of hydrogel SCLs

A calibration with polystyrene sample was carried out before testing any samples to ensure the accuracy and precision of the measurements. Each sample was scanned 64 times and the spectrum was recorded in a range of 600-4000 cm^{-1}, with a resolution of 2 cm^{-1}. Monomer spectra were recorded using FT-IR spectrophotometer (660-IR, Varian, USA):

- Solid monomers (Poloxamer, UV Blocker, Tint, Vazo 64, Extractables from dry lens and finished product): KBr disc: A small quantity (2-4 mg) was finely ground in a 1:5 ratio with KBr. This mixture was then made into solid disc (applied pressure: 3 N for 3 minutes) for further analysis.
- Liquid monomer (NVP, HEMA, AMA, EGDMA, TBE, PG): a six reflection ZnSe crystal with a 45° angle of incidence (70 mm x 10 mm) was used: A thin layer of liquid monomer was injected on top of the ATR crystal to cover the entire crystal surface.

For SCLs, spectra were recorded using FT-IR spectrophotometer equipped with an attenuated total reflectance (ATR) microscope (610, Varian, USA). The spectrum was obtained upon contacting the Ge crystal and the surface of the lens. Since the detector for this approach was extremely sensitive (MCT High Sensitivity detector), cooling with liquid N_2 was required to obtain the signal prior to the measurement.

2.3.3.11 Extractable characterisation of hydrogel SCLs

The methanol extractable content of SCLs produced was evaluated gravimetrically. 30-500 lenses from each type were tested and analysed over four days:

Day 1 (Desalination: for lenses stored in BBS solution): 30 lenses were removed from the blister and rinsed with DI water. The lenses were then left in a beaker with DI water overnight.

Day 2: The lenses were separated and dried overnight in an oven at 36 °C.

Day 3: The dry weight (W_D) of beaker was recorded. 30 dried lenses were placed in the beaker and the weight (W_L) was recorded. The sample weight (W_S), which was

calculated by subtracting the W_L to $W_{D,}$ was used to determine the required volume of added methanol ($V_{MeOH} = W_S$ x 60). After adding MeOH, the beaker was covered with Parafilm and allowed to stand for 18 hours.

Day 4: The lenses were removed from the MeOH. The beaker was placed on a hot plate to evaporate to dryness. This was followed by drying the beaker at 105 °C for an hour. After cooling in a desiccator, the weight of the beaker was recorded to calculate the %Residue as per Equation 2.3 based on a referenced document from the Enterprise Partner:

$$\%\text{Residue} = \frac{\text{Residue weight}}{\text{Sample weight}} \text{ x } 100 \qquad \textbf{Equation 2.3}$$

2.3.4 Statistical analysis

A paired t-test (two-tailed) was used to compare various lens properties between the WM lenses and the CEP lenses. All analyses were performed using Minitab 17, where a p-value < 0.05 was considered statistically significant.

2.4 Results and Discussion

2.4.1 Contact lens manufacture

A suitable polymeric material is important in the manufacturing of SCLs. The polymer can then be formed through various polymerization mechanisms (e.g., radical and catalytic), as previously discussed in Section 1.4.3. To develop a reproducible manufacturing method for SCLs, three thermal curing approaches were investigated. Further, to produce a lens with the same critical parameters as the CEP lens from the EP, mimicking the same curing environment played a vital role. Therefore, the optimum polymerisation conditions were determined based on the curing temperature profile in each trial, which was measured using a k-type thermocouple and Pico Data Logger.

Due to their simple structure, low cost and strong robustness, a thermocouple sensor is commonly used for dynamic temperature measurement in harsh environments [404]. Since the thermocouples measure the temperature based on the heat balance, it must be in direct contact with the object to be measured [404, 405].

The k-type thermocouple was identified to be effective for measuring temperature change during polymerization [405-408]. In this study, the k-type thermocouple wire was placed inside and at the centre of the moulds. To stabilise the thermocouple wire position inside the mould and transfer heat from the mould surface, a small quantity (~50 µL) of pre-polymerization monomer mixture was injected into the mould and cured prior to further measurement of the curing temperature profile. A similar approach was carried out by Alkurt *et al.* [405, 406]. Since the output from the thermocouple was fed directly to a computer through the Pico Data Logger at 0.1 s intervals for the full cycle, the temperature values were recorded in real time. Dynamic mapping and real-time temperature monitoring of a system can provide valuable information on system control, failure analysis, product quality, and process improvement [409, 410].

In the present study, for the first approach, 32 lenses were placed in the curing chamber that was capable of nitrogen purging. Due to the thickness of the chamber (as described in Section 2.3.3), it was postulated that it would take much longer for the heat to transfer to inside the curing chamber. Therefore, this would affect the curing process of the lens. The heating rate in this approach was determined to be 0.3 °C/min, which was noticeably different from the control condition (i.e., condition from CEP curing profile), which is 1-10 °C/min depending on the curing stage (control cycle). Hence, it took much longer to reach the final temperature of the curing cycle that is 110 °C, compared to the control cycle (e.g., 5.5 hours vs. 1.4 hours, Figure 2.11).

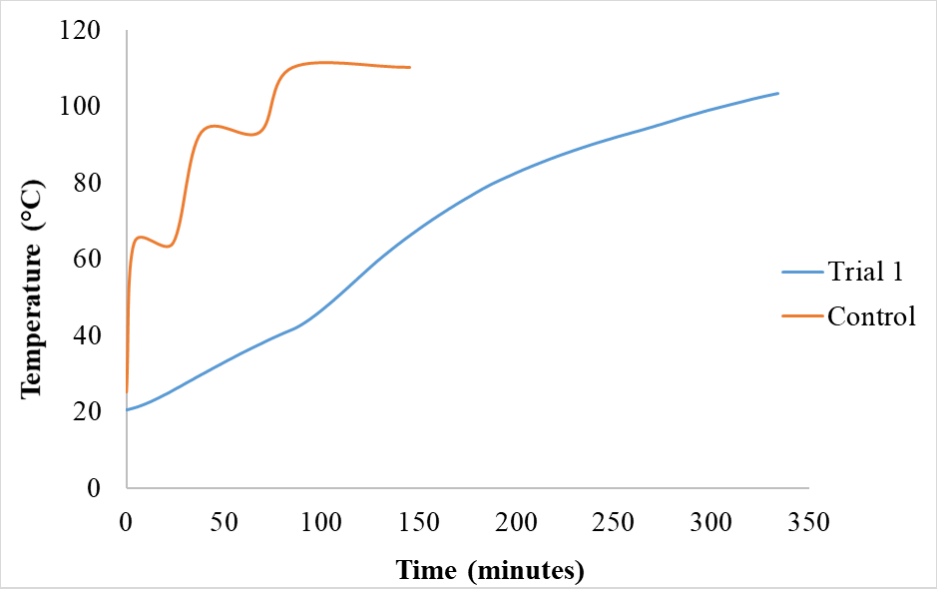

Figure 2.11: Curing temperature profiles of the first trial in the curing chamber versus the referenced profile of the control cycle.

The acceptance criteria of lens diameter for the CEP lens are 14.2 ± 0.2 mm. Thermally curing inside the chamber was determined to be unsuitable due to production of smaller lens (post thermal sterilization) with larger variations (~13.45 ± 0.7 mm in diameter, n = 10) and challenges in the release process. The percentage of successful lenses that could be released was only 33.3% (i.e.,10 out of 30 lenses were released without being broken). The majority of lenses stuck to the mould and could not be released.

A second trial was carried out by curing trays of lenses in the lens holder tower (Figure 2.5). This adjustment facilitated direct lens contact with the heat inside the oven. Although the temperature profile in this trial was closer to the control cycle, a lack of temperature control, which was due to the capability of the equipment, resulted in a different curing temperature profile compared to the control ones. While the required heating rate was 1-10 °C/min (depending on the curing stage) to mimic the curing condition of the control lens, the Heraeus Vacutherm could only provide a constant heating rate of 1.45 °C/min for the entire curing cycle (Figure 2.12).

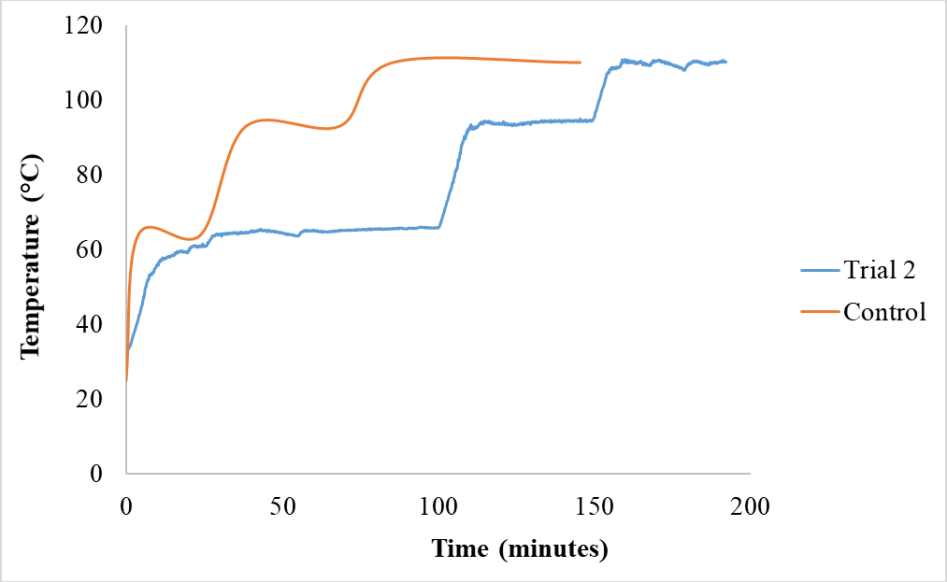

Figure 2.12: Curing temperature profiles of the second trial in the curing chamber versus the referenced profile of the control cycle.

In order to produce the closest curing system to the Enterprise Partner, with a reasonable cost, the Memmert UF50Plus forced convection oven was used as it allowed programming of the appropriate curing profile (Figure 2.6). However, due to the restriction of the set-up of this oven system, the lenses were cured under ambient environmental conditions. The curing profile in this trial is presented in Figure 2.13.

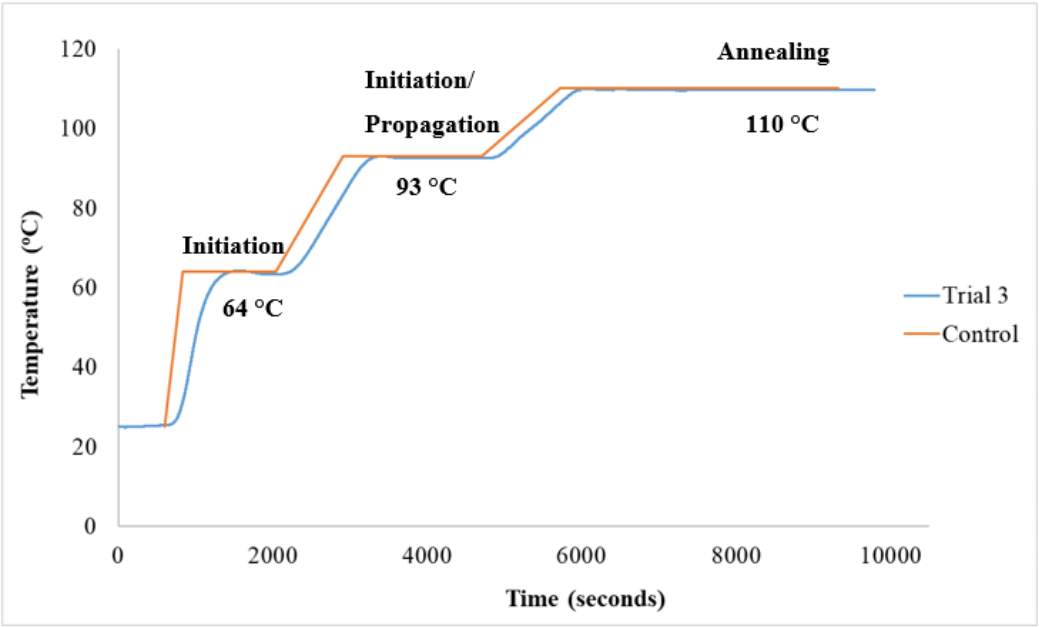

Figure 2.13: Curing cycle profile of Memmert oven (Trial 3) vs control cycle.

As could be observed in Figures 2.11 – 2.13, the curing cycle from Trial 3 provided the closest curing profile to the control cycle (i.e., curing cycle carried out by the EP). Hence, this curing approach was determined to be the optimum method in the manufacturing of WM lenses on-site.

To remove unpolymerized residue that might be present after polymerization [251, 411], the hydrated lens was washed three times using 60 °C DI H_2O. The extracted lenses were then sterilized using two methods: autoclave (heat sterilization) at 123 °C for 66 minutes (Figure 2.14) and gamma radiation. As mentioned in Section 1.4.5.2, in order to be commercially relevant, the quality, safety and efficacy of the produced lens must be guaranteed [253].

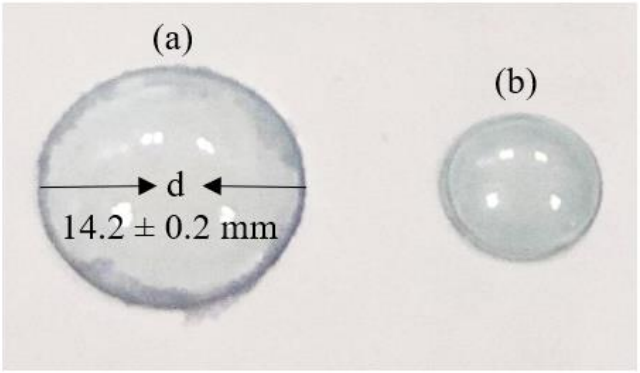

Figure 2.14: Images of (a) hydrated lens (post thermal sterilization) and (b) dry lens (post curing).

It should be noted that after sterilizing using gamma radiation, the WM lenses turned yellow. The discoloration was suggested to be attributed to the formation of macroradicals such as phenoxyl and phenyl produced by the irradiation process [401]. This phenomenon was commonly seen in lenses sterilized by gamma radiation, which potentially indicates the degradation process of materials [412]. In addition, lenses that were sterilized by gamma radiation were found to be very brittle and flimsy. Therefore, no further characterisations on these lenses were carried out.

2.4.2 Chemical properties of contact lens

2.4.2.1 Thermal investigation on polymerization kinetics of hydrogel SCLs

A controlled and repeatable polymerisation process is essential in producing a commercial-quality lens as mentioned in Section 2.4.1. Hence, to obtain an insight into the polymerisation kinetics of the WM lens, pre-polymerization monomer mixture and eight individual monomers including NVP, HEMA, EGDMA, AMA, TBE/PG, UV Blocker, Poloxamer and IMVT with the presence of an adequate amount of initiator (AIBN) were polymerized and analysed by differential scanning calorimetry (DSC). DSC, as mentioned in Section 1.3.4, has been used for monitoring polymerization reactions for several systems [242]. The DSC temperature programme was set to the same as the CEP curing temperature profile (Figure 2.13). The reaction exotherm (normalized-Q) in W/g at a constant temperature was recorded as a function of time [413].

Due to the addition reaction to the monomer's double bond, free radical polymerization of vinyl monomers produces a substantial heat release (polymerization enthalpy). To investigate the radical polymerization of NVP and poly(methacrylic acid) using AIBN as an initiator, Koetsier *et al.* [414] carried out the polymerizations at 50, 60 and 70 °C, which resulted in an almost identical trend. The bulk radical polymerization of NVP with AIBN was also carried out at 60 °C by Wan *et al.* [415]. The optimum amount of AIBN is an essential factor to determine whether the monomer mixture would be cured completely to obtain the highest possible amounts of polymer. The effect of AIBN concentration on the conversion of NVP after polymerizing at 80 °C was investigated by Devasia *et al.* [416]. Their study showed that the lower the initiator concentration, the lower the yield of the polymer, due to a lower concentration of radicals produced, thus resulting in a slower rate of polymerization. The mass of AIBN used to initiate this polymerization was calculated based on Equation 2.4 (according to the Enterprise Partner's standard).

Grams of initiator required = monomer net weight in grams x 0.00418 **Equation 2.4**

A common FRP reaction includes three stages that are initiation (i.e., decomposition of an initiator to form the primary radicals), propagation (of radicals by reacting with

monomer molecules) and termination (of two macro-radicals to form polymer chains) [413]. The DSC thermogram of the pre-polymerized monomer mixture is presented in Figure 2.15.

An investigation on the polymerization kinetics of each monomer component with the presence of AIBN was carried out to study the polymerization kinetics of the pre-polymerization monomer mixture (Figure 2.16). Therefore, the intensities of each exothermic reaction in the individual component reactions did not reflect those in the lens monomer mixture. This analysis aimed to provide insight into the polymerization process of the monomer mixture, to determine which component was correlated to the first and second stages of polymerisation.

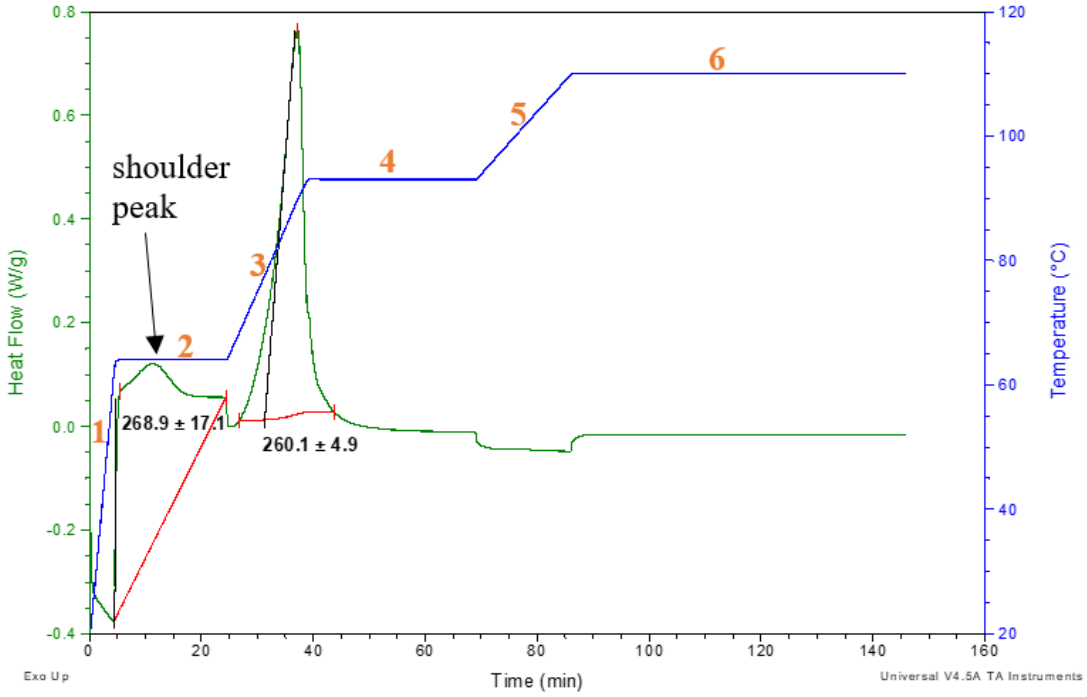

Figure 2.15: Polymerization kinetic of pre-polymerization monomer mixture with AIBN as a function of time (n = 3).

Figure 2.15 displays the heat evolved during the polymerisation through two exothermic peaks which indicated a free radical polymerisation process initiated by AIBN [242]. This observation indicated that there were two polymerization processes happening throughout the curing of SCLs of the chosen formulation. The peaks were integrated to measure the reaction enthalpy (J/g) and the peak temperature for each polymerisation reaction (T_P). There was no energy release at Stage 1 of the process (ramp 10 °C/min from 20 °C to 64 °C). An exothermic peak, which indicated the start

of the propagation, occurred at Stage 2 (isothermal at 64 °C for 20 minutes), which produced a reaction enthalpy of 268.9 ± 17.1 J/g. This energy release occurred due to the decomposition of AIBN initiator, which produced free radicals at approximately 64 °C to initiate the polymerization process to give a rapid increase in energy involved in the reaction [242, 414].

When the polymerization process proceeded into Stage 3 (ramp 2 °C/min to 93 °C), a noticeable amount of heat release, 260.1 ± 4.9 J/g, was recorded, indicating the propagation stage of the reaction. This stage corresponded to the initiation of NVP, AMA and EGDMA monomers that release heat in the system (Figure 2.16(b)). In addition, due to a lack of C=C in their structures, four other lens components including UV Blocker, Poloxamer, IMVT and TBE/PG did not participate in the polymerization processes (Figure 2.16(a)). Since NVP accounts for over 75% of the monomer mixture, the majority of the lens is cured at this step following the initiation of NVP. Stage 4 of the polymerization (isothermal at 93 °C for 30 minutes) showed a heat release solely from EGDMA (Figure 2.16(c)). This step is essential to increase the overall conversion of the pre-polymerization monomers. At a higher reaction temperature, both monomers and polymer network exhibit sufficient energy to overcome the limitation of diffusion [243]. Stages 5 (ramp 1 °C/min to 110 °C) and 6 (isothermal at 110 °C for 60 minutes) of the polymerization process recorded minimal heat release from the system, indicating that the reaction had entered the termination/completion stage.

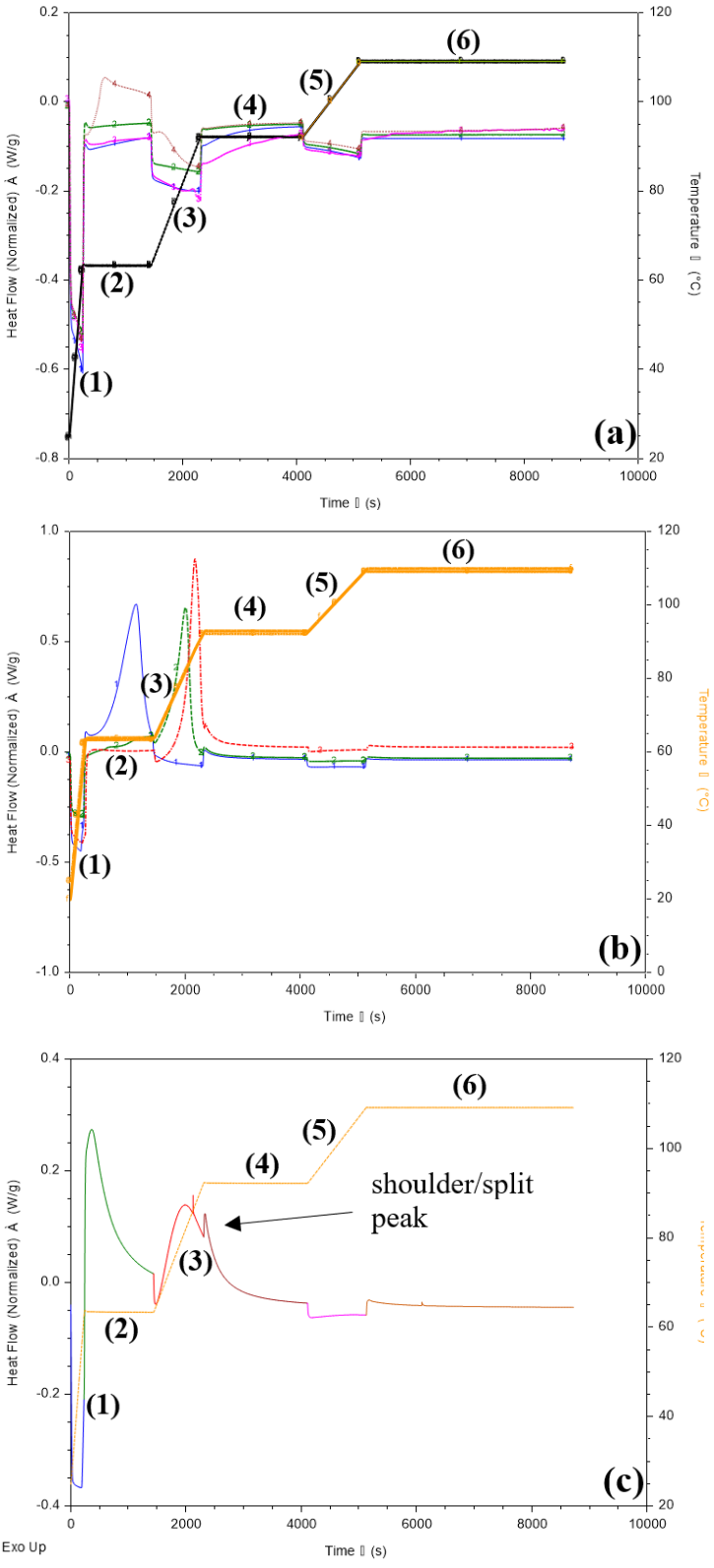

Figure 2.16: DSC thermograms of each individual monomer with AIBN: (a) UV Blocker (pink-dash dot line), Poloxamer (green-dash line), IMVT (blue-solid line) and TBE/PG (red-short dash line), (b) AMA (red-dash dot line), NVP (green-dash line) and HEMA (blue-solid line), and (c) EGDMA as a function of temperature (left) and time (right).

As can be observed in Figure 2.16(c), only the exothermic peak of the curing reaction of EGDMA had a shoulder/split peak. It was suggested that this type of free radical polymerization was a diffusion-controlled reaction [242]. As the chemical cross-linking of the polymer matrix increased, diffusion through the matrix was considered as a limiting factor since higher degree of crosslinking could result in more residual vinyl groups in the network [243]. Thus, the isothermal conversion and the associated heat release would be decreased. It was postulated that the presence of shoulder peak or peak splitting from EGDMA was due to a later reaction of the trapped monomers and pendant vinyls, which could limit both the reaction rate and final conversion. In addition to EGDMA, HEMA was the second monomer that initiated at Stage 2 of the polymerization process due to the decomposition of AIBN at 64 °C [242].

Thermal analysis using DSC was previously used to assess the impact of the amount of drug-loaded nanoparticles (NPs) loading into SCLs on the polymerization kinetics of the lens monomer mixture [242, 417]. This study presented baseline kinetic data for further analysis in the preparation of pharmaceutical-loaded NPs laden SCLs as discussed in Chapters 3 and 6.

2.4.2.2 Thermogravimetric analysis of hydrogel SCLs

Thermogravimetric analysis (TGA) was carried out to examine the loss in mass of the sample over time as the temperature was increased to 600 °C at 10 °C/min rate. TGA analysis was also carried out to compare the degradation behaviour between CEP and WM lenses (Figure 2.17).

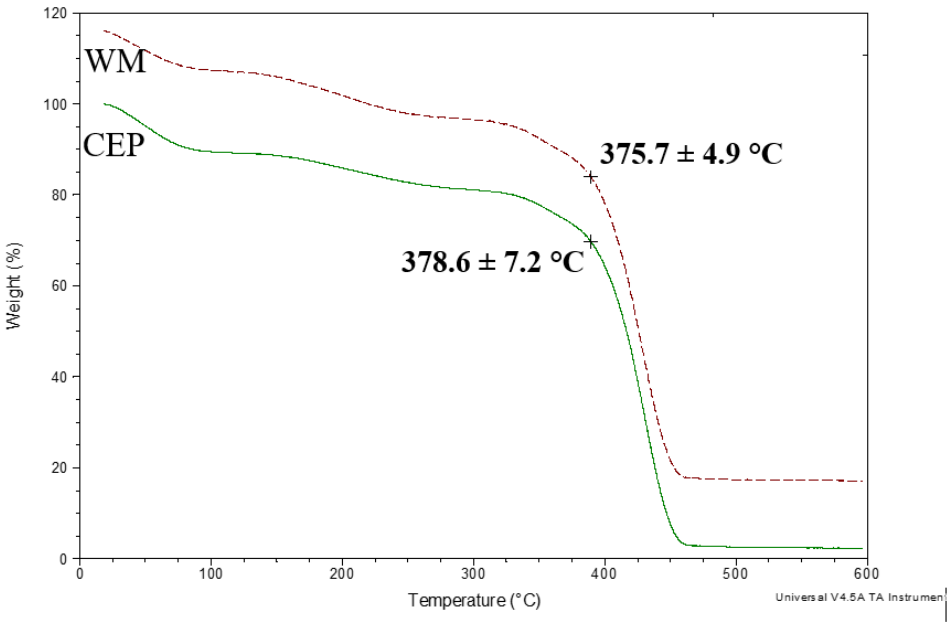

Figure 2.17: TGA thermogram for the CEP lens (green-solid line) vs the WM lens (red-short-dash line) (n = 3).

Figure 2.17 shows that both CEP and WM lenses behaved in a similar fashion (p-value > 0.05 for their degradation temperatures). The major mass loss, associated with lens decomposition took place at 378.6 ± 7.2 °C and 375.7 ± 4.9 °C for both the CEP lenses and WM lenses, respectively. Rao *et al.* [418] demonstrated that pure PVP (poly-vinylpyrrolidone), which is a major component of the studied lens material (i.e., NVP), had two degradation temperatures. The first one was at 250 °C, and the second one (with degradation of over 50% by weight) was identified to be 420 °C. In a different study carried out by Du *et al.* [419], pure PVP was shown to start decomposing at about 380 °C. Their study also showed that this decomposition temperature reduced by 30 °C for PVP coated on Platinum (Pt) nanoparticles, suggesting that temperature range of a material is dependent on its composition. A degraded temperature of the lens material used in this work was 20 °C higher than pure that of PVP. This was postulated due to the interactions between various monomer components in the lens pre-polymerization mixture, as well as a different percentage of NVP presented in the mixture.

2.4.2.3 Differential scanning calorimetry of hydrogel SCLs

The thermotropic behaviour of both dry (Figure 2.18) and hydrated (Figure 2.19) SCLs was investigated throughout this study. The DSC cycle used in this study was previously used to determine the T_g value of a hydrogel material [378, 420].

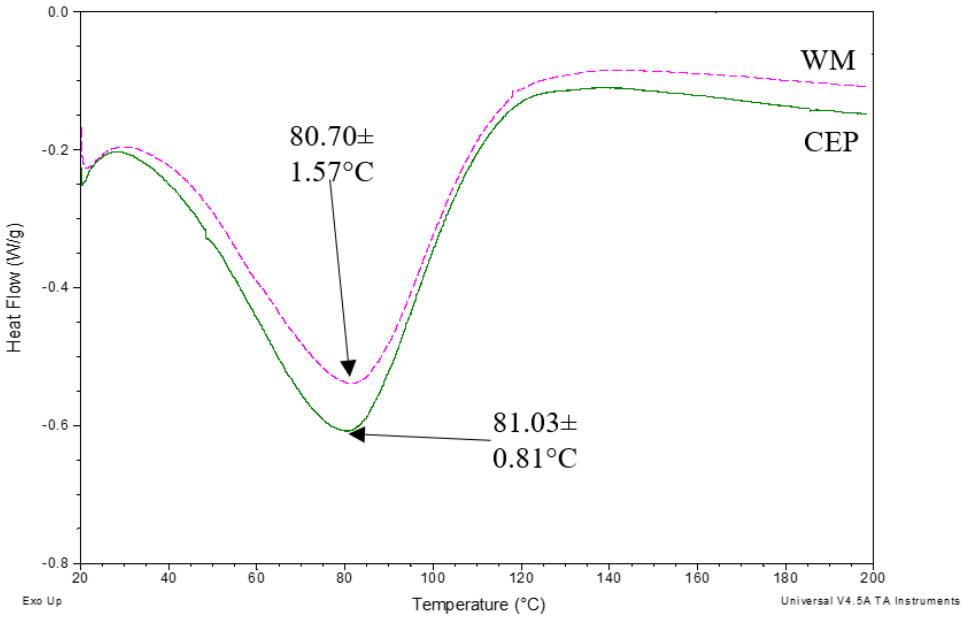

Figure 2.18: DSC thermograms of dry CEP (green) and dry WM (purple) lenses (n = 3).

The glass transition temperature (T_g), as described in Section 1.3.4, is defined as a second order pseudo transition, which provides important information in the study of amorphous and crystalline materials. The thermograms obtained for the CEP and WM dry lenses showed an average T_g of 81.03 ± 0.81 °C and 80.70 ± 1.57 °C, respectively. Hence, it could be observed that the fabricated WM lens in the dry state produced comparable thermotropic behaviour to the CEP lens. The literature value T_g for 10 kDa PVP polymer falls in a range between 66 °C to 124 °C [421]. However, this value is dependent on the molecular weight (MW) of PVP and can also vary upon interacting with the other seven monomer components in the pre-polymerization mixture [421-423]. Using TGA, DSC and FT-IR, Çaykara *et al.* [422] investigated the influences of composition on the thermal behaviour of pHEMA homopolymer. Compared to a pHEMA-co-itaconic acid (pHEMA/IA) copolymer, an increase in T_g values (88 to 117 °C) and degradation temperature (271 to 300 °C) was observed. Due to the wide range of MW of PVP, its effect on the T_g was examined by Buera *et al.* [421].

Since T_g values depend on various factors such as experimental approach (e.g., drying method, heating rate, etc.) and matrix properties (e.g., degree of cross-linking and MW distribution), only T_g values of a material obtained from systems where experimental method and material characteristics are similar should be compared to each other. To assess the thermotropic behaviour of the hydrated WM lenses, thermal analysis was carried out with the heating cycle ranging from -50 to 50 °C [420] (Figure 2.19).

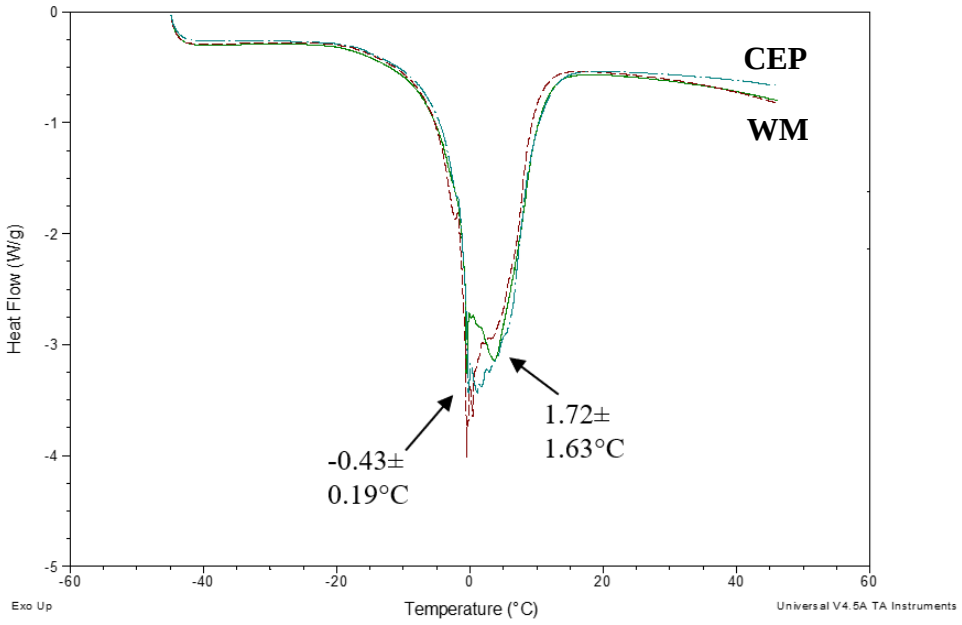

Figure 2.19: DSC thermograms of CEP and WM hydrated lenses (post thermal sterilization) (n =3). (Note: the three lines together denoted to thermograms from WM lenses).

The thermograms obtained for WM lenses showed the appearance of two peaks, which can be related to the fusion of water upon the interaction with the hydrogel network. Work by Tranoudis and Efron [397] implied that there are three states of water that can occur within the hydrated polymer systems, based on the interactions between the water molecules and the polymer matrix, including tightly bound, loosely bound and free water. Tightly bound water is non-freezable under normal characterization conditions (below -93 °C). This is associated with water molecules that strongly interact with ionic residues of the polymer matrix or directly bind to the polar groups of the matrix via hydrogen bonding. Loosely bound water has a fusion temperature lower than 0 °C. It varies slightly depending on the amount of water present in the hydrated hydrogel and how water molecules bind to the polymer matrix. This state refers to water molecules that only loosely bond to the polymer matrix. Free water

corresponds to water molecules that do not have any interactions with the polymer matrix. As a result, it generally freezes at or above 0 °C.

Thus, from the obtained thermogram (Figure 2.19), it was postulated that the first peak at -0.43 ± 0.19 °C was attributed to loosely bound water, while the second peak at 1.72 ± 1.63 °C represents the free water molecules. A similar observation was noted in a work carried out by Silva *et al.* [420]. Their work investigated the DSC behaviour of hydrated HEMA/PVP hydrogel samples, demonstrating two peaks at approximately -2 °C and 5 °C.

2.4.2.4 Equilibrium water content of hydrogel SCLs

This value indicates the comfort of SCLs and is also closely related to their dehydration, which is a vital factor that can impact the lens comfort [424]. The amount of dehydration and the time to reach equilibrium are influenced by several elements, including: the maximum water content of the polymer [425, 426], the lens thickness [291, 295, 425, 427], the temperature and relative humidity [292], and also the volume and tonicity of the wearers' tears [428, 429].

To determine the lens hydrophilicity and water uptake, swelling studies were carried out on the WM lens and the CEP lens. This was to gain a greater insight into swelling kinetics and to have a better understanding of the impact of temperature on hydrogel matrices in the absence of drug [266]. The percentage EWC and its standard deviation for each lens type at three different temperatures are tabulated in Table 2.2.

Except for %EWC of the CEP lenses at 4 °C (p-value = 0.06), %EWC in the remaining systems was found to be a statistically significant difference from the stated 78% water content of Biotrue® ONEday SCLs (p-value < 0.05). A difference in this value was expected due to the nature of this methodology. On the other hand, low standard deviation in %EWC values implied that the WM lenses were manufactured uniformly. Both WM and CEP lenses equilibrated after 5 minutes (at 25 and 36 °C) with the %EWC not changing significantly afterwards. When the lenses were immersed in 4 °C water, they were visually observed that the lenses were not fully hydrated after five minutes. Hence, the first measurement was carried out after 10 minutes.

The obtained data demonstrated that %EWC values of the WM lenses were similar to those obtained in the CEP lenses at 25 °C and 36 °C (p-values = 0.27 at 25 °C and 0.55 at 36 °C). However, the average %EWC of the WM lenses at 4 °C was found to be statistically different from the CEP lenses (p-value < 0.05). The reason for this observation was postulated to be due to unfavourable hydrogen bonding between the polymer and water compared to polymer-polymer interactions, which happens at higher temperature. The degree of swelling in both WM lenses and control lenses decreased with increasing temperature when the temperature went from 4 °C to 25 °C, and from 25 °C to 36 °C (p-value < 0.05). This behaviour of hydrogels was previously assessed by Topete *et al.* [402]. Two materials commercially available including CI26Y (intraocular lenses) and Definitive 50 (SCLs) were chosen for their study. After 50 hours, the %swelling of Definitive 50 SCLs significantly increased from around 70% at 36 °C to 130% at 25 °C and to approximately 160% at 4 °C. As for CI26Y, temperature effect on its swelling ability was statistically less significant (29% at 36 °C to 31% at 25 °C and to approximately 36% at 4 °C).

Table 2.2: Percentage equilibrium water content of SCLs in different conditions over three hours interval at three different temperatures in DI H_2O (n = 3).

Temperature (°C)	**4 °C**				**25 °C**				**36 °C**			
Lens type	**WM**		**CEP**		**WM**		**CEP**		**WM**		**CEP**	
Time (minutes)	**%EWC**	**Std Dev**	**%EWC**	**Std dev**	**%EWC**	**Std Dev**	**%EWC**	**Std Dev**	**%EWC**	**Std Dev**	**%EWC**	**Std Dev**
5	-	-	-	-	75.81	0.19	76.51	0.73	75.48	0.35	75.59	0.28
10	77.99	0.41	77.56	0.07	76.69	0.27	76.88	0.72	75.63	0.44	75.90	0.12
15	-	-	-	-	76.70	0.49	76.37	0.65	75.82	0.30	76.09	0.28
20	78.26	0.18	77.72	0.20	77.00	0.27	76.30	0.70	75.91	0.37	76.17	0.27
25	-	-	-	-	76.71	0.53	76.59	0.76	75.96	0.40	76.23	0.26
30	78.30	0.22	77.83	0.21	76.69	0.45	77.28	0.34	76.41	0.79	76.37	0.27
40	78.36	0.16	77.88	0.22	-	-	-	-	-	-	-	-
50	78.41	0.16	78.17	0.19	-	-	-	-	-	-	-	-
60	78.46	0.14	78.22	0.08	76.25	0.38	77.04	0.37	76.43	0.78	76.44	0.27
90	78.48	0.15	78.40	0.21	76.25	0.25	76.24	0.46	76.52	0.80	76.48	0.31
120	78.52	0.13	78.49	0.11	76.32	0.40	76.15	0.28	76.64	0.77	76.52	0.32
150	78.55	0.10	78.52	0.14	76.22	0.31	76.70	0.24	76.65	0.79	76.56	0.33
180	78.61	0.12	78.54	0.10	76.47	0.30	76.80	0.22	76.67	0.76	76.63	0.30

2.4.2.5 Refractive index analysis of hydrogel SCLs

Refractometry measures the critical angle between the material and a glass of a higher and known refractive index (RI). As mentioned in Section 1.4.6.4, since the RI value is related to lens water content and dehydration, this figure can give an indication to lens fitting characteristics, oxygen permeability and lens parameters. As stated in ISO18369-4:2017 [400], the RI of CL materials should be measured at either 589 nm (sodium D-line) or 546.1 nm (mercury line). The required RI value for a commercial SCL typically should not exceed 1.55 [400]. The RI of water and BBS were measured to be 1.33453 and 1.33700, respectively. These values agree with work obtained by the Enterprise Partner. In addition, the RI of water at 589 nm, 20 °C and 1.0 bar (atmospheric pressure) was previously determined by Thormählen *et al.* [430] to be 1.33283. RI of the packaging solution (BBS) for Biotrue® ONEday lenses, which are the control lenses used in this study, was previously measured to be 1.33670 by the CLR 12-70 refractometer [431].

Table 2.3 demonstrates that the fabricated WM lenses produced a lower RI than the control commercial lenses (p-value < 0.005). However, following the ISO 18369-2 standard, this difference is within the tolerance limits for RI values of SCLs [399]. Hence, the WM lenses produced a comparable RI value to the control lenses, and so is suitable for commercialisation.

2.4.2.6 Light transmission of hydrogel SCLs

The SCL light transmission is directly related to its visual performance. Hence, this property was measured for both the unloaded and loaded lenses to examine its optical quality [432]. The lens must transmit over 90% of light in the visible spectrum to provide clear vision, as cited by Gulsen *et al.* [391]. The summary of result data from this study is given in Table 2.3. As was observed from the generated data, an average transmittance of 99% (in the visible region) relative to the control lenses was observed in all the WM lenses (p-value < 0.05). This result indicated that the WM lenses produced sufficient optical clarity for commercial use as ophthalmic medical devices.

Table 2.3: Physicochemical properties of the fabricated WM lenses vs. the control lens.

Sample	%T (n = 5)	Refractive index (n = 10)	Contact angle (°) (n = 8)	Tensile modulus (MPa) (n = 8)	Ionic permeability ($x10^{-6}$ cm^2/s) (n = 3)
CEP	99.04 ± 0.74	1.374 ± 0.000	48.54 ± 3.90	0.64 ± 0.04	0.91 ± 0.13
WM (heat ster.)	99.93 ± 0.82	1.373 ± 0.000	47.91 ± 4.40	0.71 ± 0.07	0.86 ± 0.20
WM (non-ster.)	99.98 ± 0.61	N/A	50.00 ± 1.09	0.76 ± 0.05	1.04 ± 0.11
ISO tolerance [399]	± 5% CEP	± 0.005 CEP	N/A	N/A	N/A

2.4.2.7 Ionic permeability of hydrogel SCLs

As discussed in Section 1.4.6.5, it is essential to obtain an adequate ion permeability (D_{ion}) in SCLs to ensure the formation of a fluid hydrodynamic boundary layer, which in turn, decreases the direct abrasion between the lens and the eye. Ionic permeability of SCLs has been measured using a modified conductivity meter in several studies [308, 311-313].

From the generated data (Table 2.3), it was observed that the thermal sterilization process did not affect ionic permeability of the WM lenses, with 0.86 x 10^{-6} ± 0.20 x 10^{-6} cm^2/s and 1.04 x 10^{-6} ± 0.11 x 10^{-6} cm^2/s for sterilized and non-sterilized WM lenses, respectively (p-value > 0.05). In addition, it was determined that there was no statistically significant difference in D_{ion} values between the WM lenses and the CEP lenses (0.91 x 10^{-6} ± 0.13 x 10^{-6} cm^2/s). Hence, the fabricated WM lenses were demonstrated to have the commercial quality in ionic permeability. This technique was previously used in a study carried out by Silva *et al.* [389]. Their study investigated the ionic permeability of the silicone hydrogel (SiHy) materials prepared using a layer-by-layer (LbL) deposition technique as described in Section 1.3.6. The average D_{ion} for coated sample was measured to be 4.5 $x10^{-7}$ ± 0.4 $x10^{-7}$ cm^2/s and for the uncoated sample was $5x10^{-7}$ ± $0.2x10^{-7}$ cm^2/s. Nonetheless, the D_{ion} of the developed WM lens and the CEP lens determined in this work agreed with the literature data on D_{ion} of hydrogel SCLs (0.9 – 2.5 x 10^{-6} cm^2/s) as reported by Gavara and Compan [317].

2.4.3 Physical and Mechanical properties of contact lens

2.4.3.1 Surface and matrix characterisation of hydrogel SCLs

The surface and matrix properties of the WM and CEP SCLs were examined through two different approaches. The first method used an optical microscope to investigate the effects of extraction and sterilization on the lens matrix (Figure 2.20).

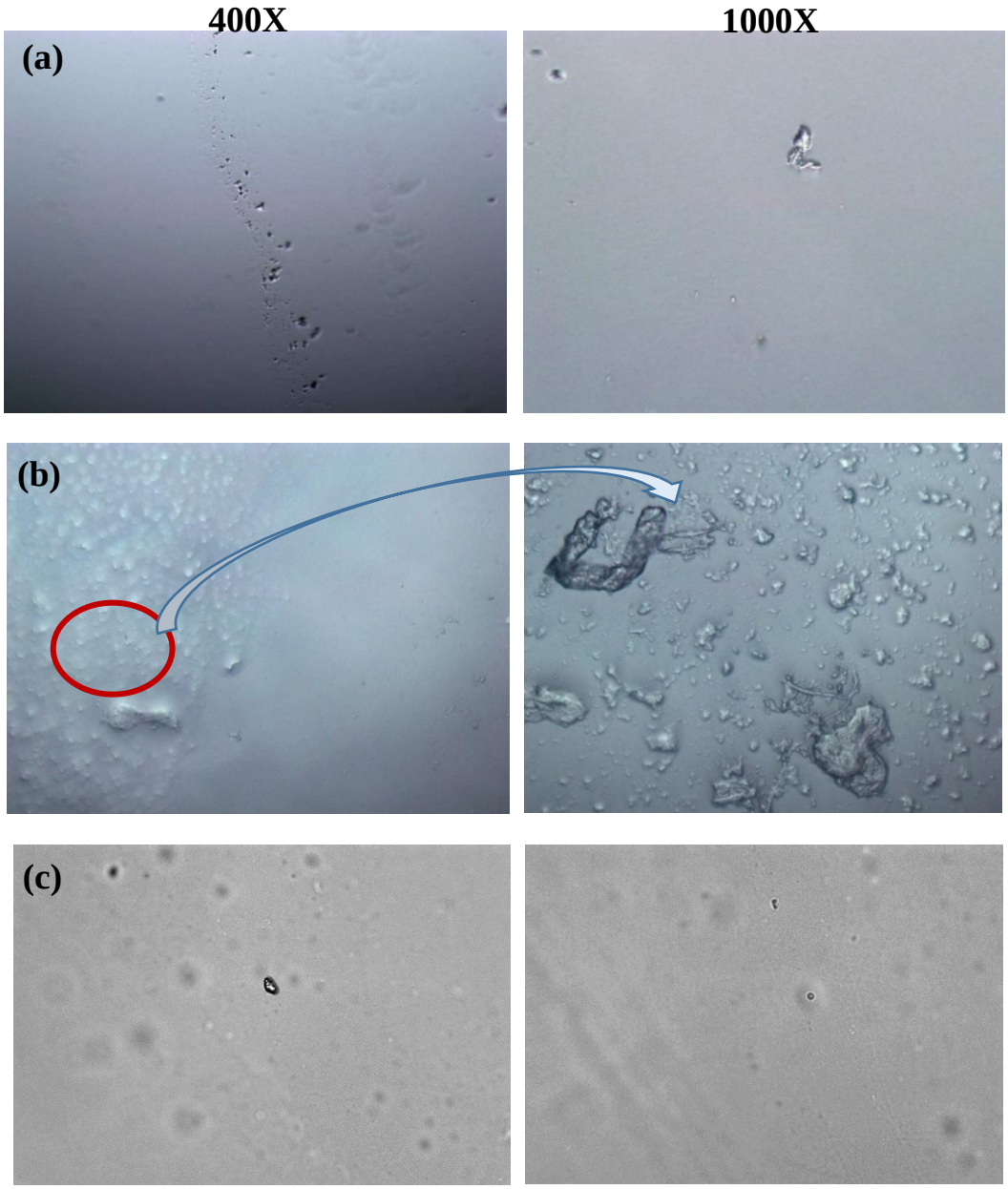

Figure 2.20: Microscopic images of a) CEP lens at 400X (left) and 1000X (right), b) WM lens that went through hydration only (no extraction and no sterilization) at 400X (left) and 1000X (right) and c) WM lens that went through hydration, extraction and sterilization (thermal sterilization) at 400X (left) and 1000X (right).

Microscopic images of both the CEP lenses and the WM lenses hydrated in water with and without going through the extraction and sterilization processes are shown in Figure 2.20. Analysis of the images demonstrated that there was a difference in the matrix of the hydrogel after it went through extraction and sterilization stages. Microscopic images of the commercial SCLs (i.e., CEP lenses) showed a homogenous matrix, whereas for those obtained from the WM lenses that were not extracted and sterilized, a rough matrix with numerous residues from partially unreacted/low molecular weight polymer could be observed [251, 411]. Nonetheless, upon extraction in 60 °C water three times and sterilization for 66 minutes at 123 °C, the microscopic images of the WM lenses were relatively similar to those of the CEP lenses. This experiment demonstrated the importance and effects of extraction and sterilization processes on the lens matrix in removing unpolymerized monomers or oligomers [251, 411].

The second approach for investigating lens surface property was to determine the wettability of SCLs through the measurements of contact angle using a goniometer. Wettability is a crucial characteristic since it indicates the spreading ability of the tear film along the material surface, which can affect the tribology of the SCLs. It is closely related to the comfort and performance of manufactured SCLs. The smaller the CA, the better the wetting ability of the material over a substrate [337]. CAs of the studied lenses in the hydrated state were measured by the captive bubble method (Table 2.3). The generated CA values in this study demonstrated that the fabricated WM lens has a comparable wettability to the CEP lens (47.91 ± 4.40° and 50.00 ± 1.09°, respectively, p-value > 0.05).

Using the same approach to measuring CAs of the hydrogel lenses, Silva *et al.* [420] showed significant deviations in each sample (e.g., the CA of TRIS/NVP/HEMA lens in albumin solution was 22° ± 6°). The values obtained for CA on the WM lenses regardless of sterilization approaches showed a statistically insignificant difference compared to CA of the control lenses (p-value > 0.05). The CA of the HEMA/PVP lenses (water content of 60.7 ± 0.3%) was previously determined to be 42° ± 3° using captive bubble method [420]. In addition, Lin *et al.* [338] cited that the acceptable range of CA of commercial SCLs as 11°-83°, demonstrating that the produced WM

lenses have a suitable hydrophilicity (CA of 47.91 ± 4.40°) to be used as ophthalmic medical devices.

Many studies use water as the medium for CS measurement [337, 386, 420], which was also carried out in this study. It was postulated that if the measurement was done in simulated tear fluid (STF), the lens matrix could potentially take up the components that are present in the solution, which would impact the outcome of the inherent wettability of the SCL material. Consequently, although tear fluid and water have distinctive characteristics, this study was carried out in water rather than STF to investigate the raw material property.

2.4.3.2 Tensile modulus of hydrogel SCLs

As described in Section 1.4.6.8, mechanical properties are a vital factor in optimising both vision quality and patient comfort. ISO 18369-1:2017 (E) [433] states that the tensile modulus (i.e., Young's modulus) of elastic material is a constant ratio between the tensile stress and the tensile strain, which should be in the range of linearity of elastic behaviour of the material. As cited by Bhamra and Tighe [340], this value is directly related to both handling and durability. This property of a material can be defined by a relationship between stress and strain, where stress is the load per unit area and strain is the extent of elongation. Young's modulus can then be calculated as a slope of a straight line through the linear range of the generated stress-strain curve [403]. The higher the modulus, the greater the lens stiffness and resistance to shape change [434].

The tensile moduli of three different types of lenses were examined including CEP lens, WM lens (non-sterilized lens) (WM-NS), and WM lens (thermal sterilized lens) (WM-TS). This study not only compared the mechanical properties of CEP lens vs WM lens, but also the impacts of thermal sterilization on lens modulus. The lens was fully hydrated prior to testing as described in Section 2.3.2. Figure 2.21 shows the stress vs strain curves for the aforementioned three lens types. The Young's moduli values (Table 2.3) generated for the three lens' systems at room temperature demonstrated that sterilization does not cause significant difference in the mechanical strength of the formed CLs (p-value = 0.10). The sterilized and non-sterilized WM lenses showed a higher Young's modulus values (0.71 ± 0.07 MPa and 0.76 ± 0.05

MPa, respectively) in comparison to the CEP lenses (0.64 ± 0.04 MPa, p-value < 0.05). The standard deviation was low in all cases, which implied that this technique is feasible in determining the hydrogel modulus, and WM lenses were produced consistently. The higher the modulus, the greater the lens stiffness and resistance to shape change [434].

As quoted in the Materials Data Book from Cambridge University Engineering Department [435], the Young's modulus value for hydrogels such as pHEMA is expected to be approximately 0.5 MPa, and 0.4-2.5 GPa is expected for thermoplastic and thermoset polymers (e.g. nylons, polyethylene, polystyrene, phenolics, etc.). The Young's modulus values in a range of 0.1-1.9 MPa were recorded for conventional hydrogel lenses, depending on the lens' components and its water content [340]. Since the Young's modulus values of the WM lenses from this experiment are within the range of other hydrogel materials with similar composition, they can be considered as appropriate material for commercialized SCLs.

On the other hand, as mentioned by Kim *et al.* [436], there are currently no reference materials available, and also no standardized measurement techniques for SCLs, and therefore validation and accuracy of such measurements are hard to achieve.

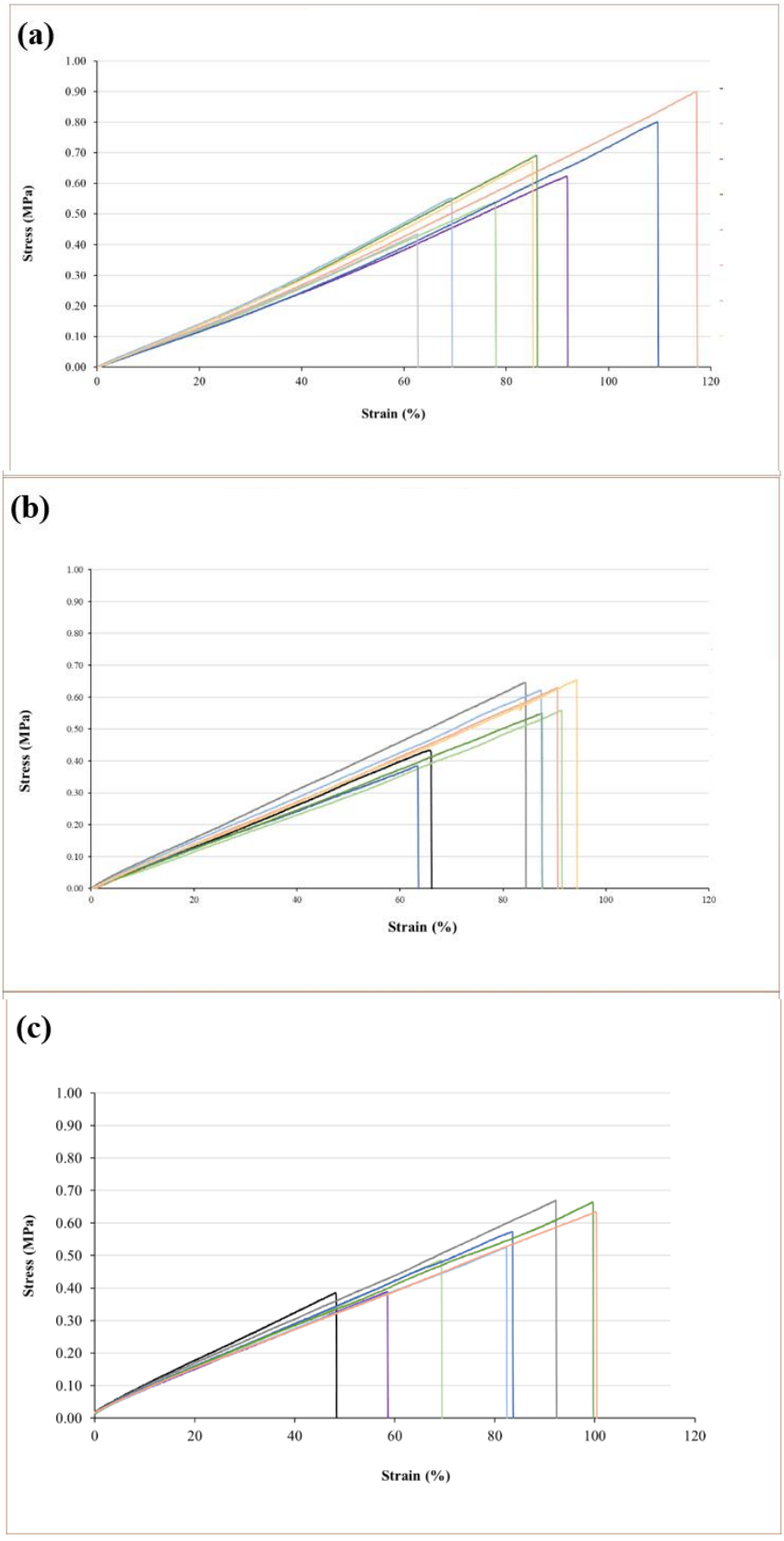

Figure 2.21: Stress vs Strain graph for (a) CEP lens, (b) WM-TS lens, and (c) WM-NS lenses (n = 8).

2.4.3.3 Fourier-transform infrared spectroscopic analysis of hydrogel SCLs

The spectroscopic characterization of hydrogel SCL and their monomer components was performed by Fourier-transform infrared spectroscopy (FT-IR). The FT-IR spectra of dry and wet lenses for both WM and CEP lenses are shown in Figure 2.22.

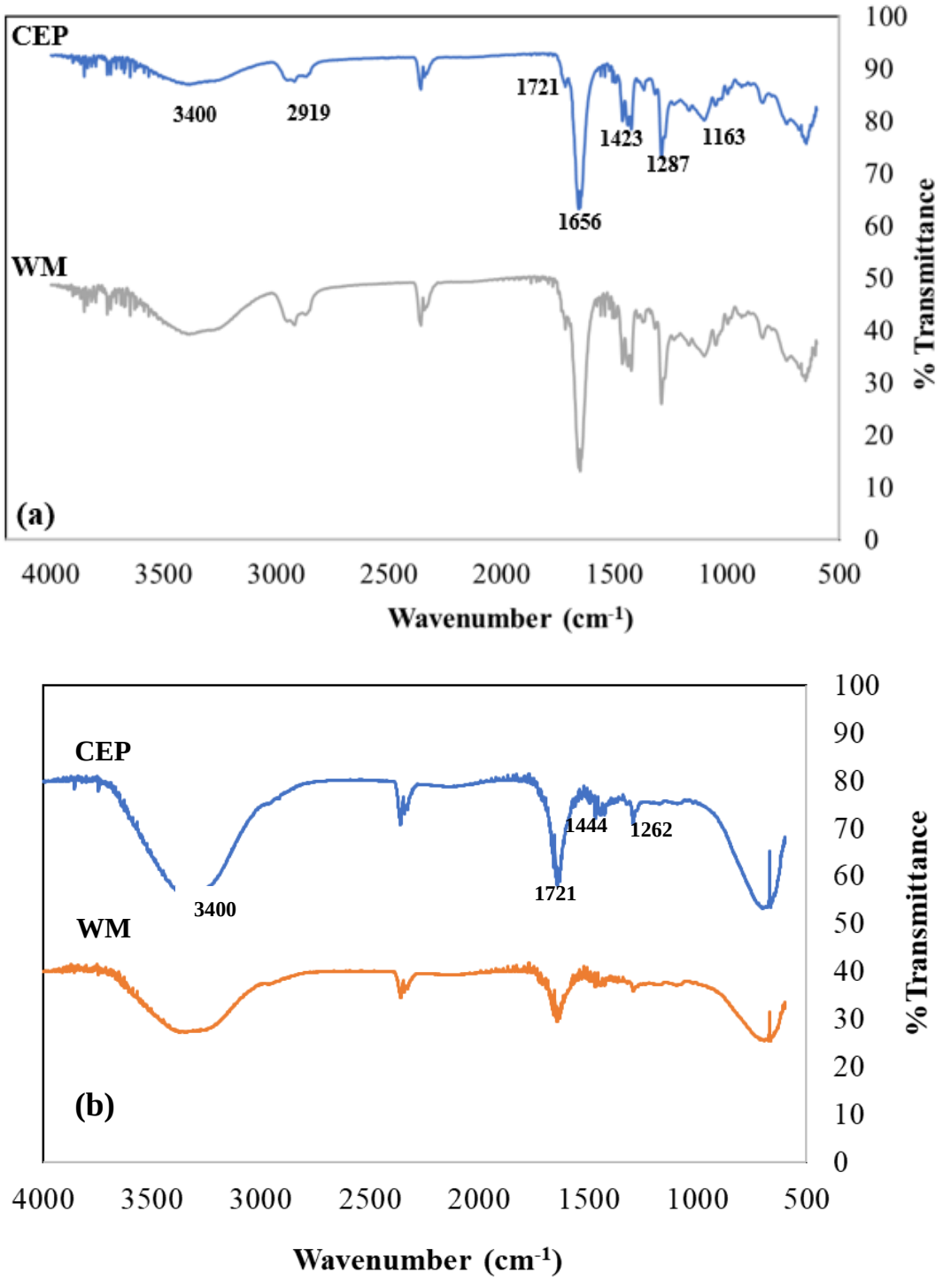

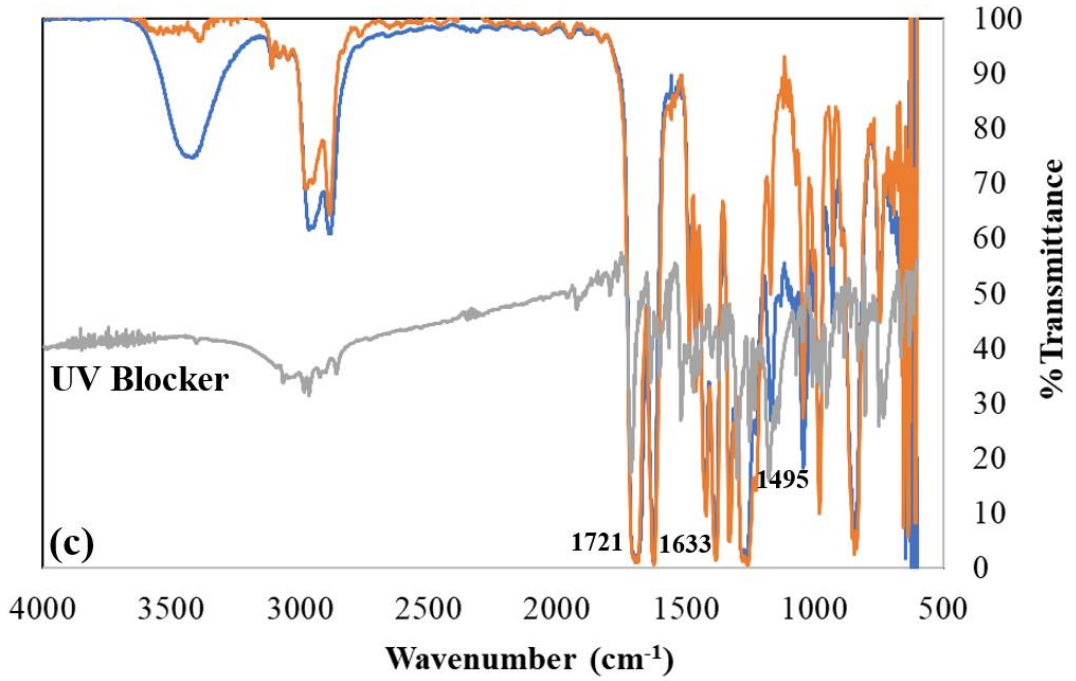

Figure 2.22: FT-IR spectrum of (a) dry CEP lens (blue) vs. dry WM lens (post curing) (grey), (b) wet CEP lens (blue) vs. wet WM lens (post thermal sterilization) (orange), and (c) raw materials including Nesofilcon A monomer (blue), NVP (orange) and UV Blocker (grey).

Because NVP is the main component in the monomer mixture (>75%), it was expected that the FTIR spectra of the WM lens and the control lens would exhibit the characteristic peaks of PVP. Table 2.4 lists the major characteristic peaks of the functional groups in the sample. Comparing the spectra of both the WM and CEP lenses obtained from dry lens, less peaks could be seen in the wet lens spectrum due to the presence of the intense and broad –OH stretching of H_2O at 3400 cm^{-1}. Moreover, it was expected to see less functionality in finished lenses since they went through extraction and sterilization stages, which would remove the majority of unreacted monomers presented in the lens matrix. The double peak at 2350-2400 cm^{-1} represents the CO_2 molecule. The characteristic C-H stretching for alkenes present in most monomeric components could be seen only in the dry form at 2919 cm^{-1} and could not be identified in the finished product spectrum. This indicated that the majority of the original monomer components had been fully cured and/or extracted after going through processing. An intense peak at 1721 cm^{-1} observed in both spectra represented the C=O stretching from the aliphatic ketones in NVP spectrum, which was also observed in other previous FTIR analysis on NVP [437-439] (Figure 22(c)). A distinctive peak representing the C=C stretch in cyclic alkenes

present in the UV Blocker monomer can be identified at 1495 cm^{-1} (Figure 2.22(c)). The two characteristic peaks (C-N stretching) indicative for NVP (the major monomer component of the formed CLs), which were at 1294 and 1262 cm^{-1}, could be seen in dry and wet forms of the lens, respectively.

Table 2.4: Spectral band assignment of the WM lens and the CEP lens in dry and wet states.

Ref. peak position (cm^{-1})	**Functional group**	**WM lens (dry)**	**CEP lens (dry)**	**WM lens (wet)**	**CEP lens (wet)**
3381 [437] 3396 [438]	O-H stretching	3400	3400	3400	3400
2933 [437] 2852 [438]	Aliphatic carbon (-CH_3, -CH_2)	2919	2919	-	-
1719 [437] 1701 [439] 1644 [438]	C=O stretching (pyrrolidone group)	1721	1721	1721	1721
1620 [437]	C=C stretching	1656	1656	1633	1633
1451 [437] 1423 and 1371 [438]	Deformation of aliphatic carbon (-CH_2)	1423	1423	1444	1444
1246 [437] 1279 [438]	C-N stretching	1287	1287	1262	1262
1151 and 1075 [437]	C-O-C stretching	1163-1100	1163-1100	1100	1100

Lai *et al.* [437] used FTIR to characterise their developed hydrogel lens (made from HEMA, MMA, NVP, DMMA, EGDMA and HMPP) to establish its chemical functional groups. This was carried out to observe the changes in characteristic peaks on FTIR spectra between the standard hydrogel lens and the tested lens (lens with silica nanosphere powders incorporated). Similar observations on the main functional groups between the developed WM lens, control lens and hydrogel lens from this study could be seen in Table 2.4 above. In both dry and wet forms, it could be observed that the WM lens gave the same spectra as the control lens. Hence, the fabricated lenses are shown to have the similar spectroscopic characteristics as the commercial lens.

2.4.4 Dimensional analysis of WM contact lenses

The produced WM lenses were dimensionally analysed at the EP research and development lab. This involved examining the effects of storage solution (water vs. borate buffered saline) on lens diameter, sagittal depth, roundness, and power. The developed WM lenses were hydrated, extracted, and stored in water, while BBS is the packaging solution used in the manufacture of the control lenses in the EP site. Therefore, it was essential to compare if different storage solutions would have an impact on lens dimensions. The schematic illustration of each of the dimensional parameters of the lens is shown in Figure 2.23 with the results obtained shown in Table 2.5.

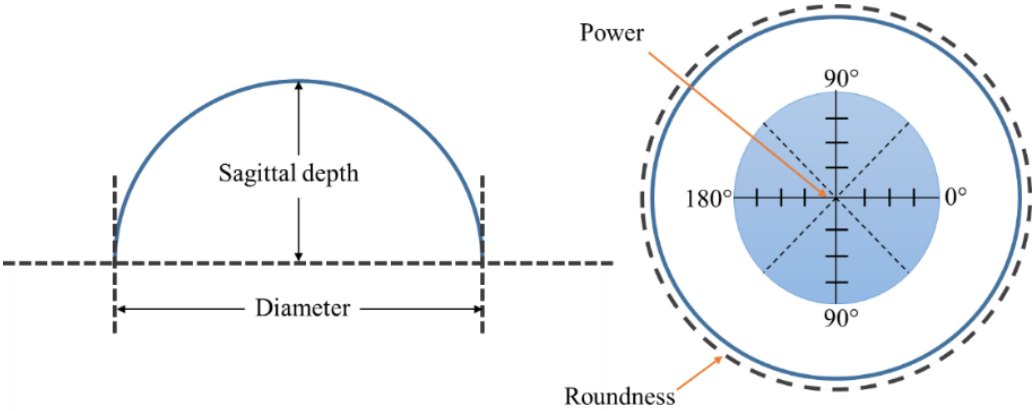

Figure 2.23: Schematic diagram illustrates a CL diameter, sagittal depth, roundness, and power.

Table 2.5: Contact lens dimensions and power in water and BBS (n = 10).

Lens type	Diameter (mm)	Sagittal depth (mm)	Centre thickness (mm)	Roundness	Spherical Power (D)
WM_{water}	14.30 ± 0.05	3.99 ± 0.07	0.120 ± 0.008	0.17 ± 0.07	-2.97 ± 0.18
WM_{BBS}	14.33 ± 0.07	3.98 ± 0.04	0.118 ± 0.009	0.22 ± 0.11	-2.83 ± 0.07
CEP	14.20 ± 0.20	3.80 ± 0.05	0.100 ± 0.020	< 0.400	-3.00 ± 0.25

The analysis showed a non-statistically significant difference in diameter (p-value: 0.34), sagittal depth (p-value: 0.53), power (p-value: 0.11) and roundness (p-value: 0.23) in the WM lenses immersed in BBS when compared with the lenses immersed

in water. When comparing to the CEP lenses, the fabricated WM lenses in both water and BBS gave the dimensions and power within the acceptable range. In addition, the tolerance limits for each dimensional parameter and power of all the measured lenses were within the acceptance criteria according to ISO 18369-2:2017 (E) [399].

2.4.5 Contact lens extractable testing

Extraction is a standard method to quantitatively determine the substances extractable from CL (extractables). The extractables are determined through the percentage of residue (by weight) after the lenses are extracted in a chosen solvent. Choosing an appropriate extraction solvent is important since it will have a direct impact on the matrix of the hydrogel. As stated in ISO 18369-4:2017 (E) [400], an ideal solvent should not degrade the CL material, since this will lead to the removal of both crosslinked and non-crosslinked materials. This in turn can lead to an inaccurate measurement of extractables. The solvent should have a solubility that is equal to or higher than the extracted medium solubility, while not reacting with the presented analytes. Because of these reasons, methanol is chosen to be a suitable solvent for this test. In addition, MeOH can swell the CL, which accelerates the extraction process.

The percentage residue is calculated from the difference between the original dry weight of sample and the extracted dry weight. This figure represents the amount of unreacted monomer after curing vs after sterilization. It demonstrated the impact that manufacturing processes cause on the formed CLs. After being extracted for 18 hours, the percentage residue for each lens type was calculated and recorded in Table 2.6.

Table 2.6: Percentage of methanol extractable residue from the CEP lenses vs. the WM lenses at different stages (post curing and post thermal sterilization).

Sample (n = 500)	%Residue	Sample (n = 120)	%Residue
CEP lenses (post thermal sterilization)	0.73	CEP lenses (post curing)	6.90
WM lenses (post thermal sterilization)	1.51	WM lenses (post curing)	9.79
WM lenses (post curing)	7.70		

The %Residue for WM lenses that did not go through extraction and sterilization showed a value 7 times higher than those that did. Higher %residue is expected in the dry lens since a substantial amount of unreacted monomers after curing should be extracted after three extraction cycles using 60 °C deionized water and a 60-minute thermal sterilization process [251, 411].

WM lenses had a higher %Residue when compared to CEP lenses before (9.79% and 6.90%, respectively) and after extraction and sterilization (1.51% and 0.73%, respectively). This could be due to two potential reasons. Firstly, it could be because of the lack of an N_2 purge in the current set-up for curing WM lenses compared to control lenses. The polymerization of SCLs is generally performed under inert gas such as nitrogen or argon to improve the polymerization rate of a CL [411, 440, 441]. As such, this process was patented to be used to remove unpolymerized monomers from a polymer. After 1.2 hours of nitrogen purging (flow rate at 44.8 lb/h), a significant reduction in ENB (ethylidene norbornene monomer, used in the production of ethylene polymers – e.g., ethylene propylene diene terpolymers) residue from 0.5% wt. to below 100 ppm wt. was recorded [441]. The second reason could be due to the difference in the rate of curing. Since the oven used to make WM lenses is much smaller in size compared to those used commercially, it would provide a faster curing rate that leads to a higher amount of extractables [442, 443]. As previously discussed in Section 1.4 (Chapter 1), a faster heating rate could accelerate the polymerization of a monomer [279]. This data is essential in assessing new CL materials and in evaluating and quantifying drug uptake, as well as during the pre-clinical examination programme.

2.5 Conclusions

A reproducible manufacturing method for hydrogel SCLs was successfully developed, which resulted in lenses (WM) that had comparable properties to the CEP lenses. Using a thermal initiator AIBN and a forced convection oven, hydrogel SCLs were successfully produced through a thermal polymerisation process. Due to the importance of obtaining a similar temperature curing profile as the chosen commercial lens formulation to obtain similar lens critical properties, an N_2 curing environment could not be employed. This was because of the limitation of the curing system which was not capable of carrying out the full curing cycle under an N_2 environment. To ensure the produced WM lenses were manufactured consistently and had comparable properties to the CEP lens, characterisation methodologies were developed to determine the physicochemical and mechanical properties of the lenses. Further, by employing the state-of-the-art infrastructure at the enterprise partner site, the dimensional properties of lenses and their optical power were also measured. An investigation into the polymerization kinetics of individual components in the monomer mixture and the pre-polymerization monomer mixture was carried out using DSC and FTIR.

The WM lens showed high optical transparency of 99.93% ± 0.82% (thermal sterilization) and a refractive index of 1.37332 ± 0.00018, which are similar to those obtained from the CEP lens (1.37422 ± 0.00025). Both lens systems had a similar water swelling ability as determined by an equilibrium water content (%EWC) study. Lenses reached equilibrium water content very quickly (after 5 minutes), which was 75-76% at 25 °C, which was expected due to the highly hydrophilic nature of the lens materials. Thermal and FT-IR analysis on WM lenses and control lenses also indicated the functional similarity between the two. Wettability of WM lens showed a comparable value to the commercial lens, indicating a high comfort material.

Both lens systems were further characterised to test their tensile modulus and ionic permeability. In addition, as evidenced through a matrix characterisation study using microscopy, hydration, and extraction steps in the manufacturing of lenses were shown to play an essential role in removing unreacted monomers from the lens surface. The effect of sterilization methods on lens properties was also investigated.

Thermal sterilization was identified to be the optimum approach, with lenses sterilized using gamma radiation resulting in unfavourable properties such as poor optical transparency (lens turned yellow) and low modulus (lens was easy to break). Lens dimensional parameters and optical power were measured consistently with diameters of 14.30 mm ± 0.05 mm and -2.97 D ± 0.18 D in water environment. These values are similar to those obtained from the chosen commercial lens which acted as a control lens (i.e., CEP lens) throughout this study. Through the analysis of unreacted monomers from lenses extracted in methanol, it was observed that after the lens went through hydration, extraction and sterilization processes, the amount of residue was significantly reduced.

By characterising and comparing the lens critical properties between in-house produced lenses with CEP lenses, this study demonstrated the feasibility of the developed lens fabrication system. This work allows for further in-depth development, investigation, optimization, and characterisation of novel ocular drug delivery systems. If the preformed commercial lenses were used, they would have been very limited in terms of the potential approaches to loading analyte into the lens. With the developed lens manufacturing system, future drug loading approaches can be modified more easily, and optimization of drug-loaded lens formulation can be more controlled.

Following the successful development of a SCL of commercial quality in this chapter, the next chapter will discuss the impacts of loading a therapeutic agent (i.e., naringenin) on the lens' critical parameters, and subsequently, the *in vitro* drug release profiles from the developed drug-loaded SCLs.

CHAPTER 3

CONTROLLED RELEASE OF NARINGENIN FROM NARINGENIN-LOADED SOFT HYDROGEL CONTACT LENS

3 CONTROLLED RELEASE OF NARINGENIN FROM NARINGENIN-LOADED SOFT HYDROGEL CONTACT LENS

3.1 Introduction

As discussed in Chapters 1 and 2, therapeutic SCLs have been extensively investigated as a promising non-invasive ocular drug delivery system (ODDS) due to their potential ability to increase drug ocular bioavailability. In this work, naringenin (NAR) was chosen as a potential therapeutic agent to be loaded into the SCL (nesofilcon A material) matrix.

Flavonoids, or bioflavonoids, are a group of polyphenols that are commonly observed in plants, fruits, and vegetables. The general structure of the flavonoids is characterized by a C_6-C_3-C_6 carbon skeleton, which consists of two benzene rings (the A and C rings) linked by a three-carbon B ring (Figure 3.1) [444-449]. Depending on the level of oxidation and pattern of substitution of the C ring, flavonoids can be divided into various classes that include flavanones, anthocyanidins, flavons and flavonols [447]. Individual compounds within a class can be differentiated based on the substitution pattern of the A and B rings. Unlike flavones and flavonols, flavanones lack conjugation between the A and B rings. Instead, they have a saturated heterocyclic C ring. As an example, the UV spectra of flavanones (e.g., naringenin) exhibit a very strong maximum absorption between 270 and 295 nm, specifically at 285 and 288 nm [450].

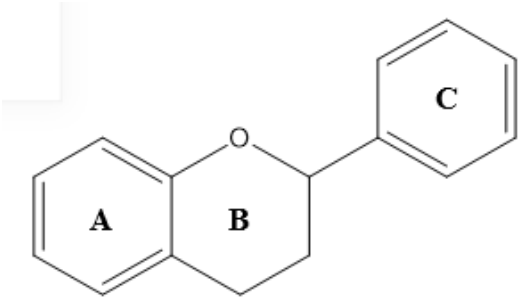

Figure 3.1: General structure of flavonoids.

Naringenin (NAR), 5,7-dihydroxy-2-(4-hydroxyphenyl)-2,3-dihydrochromen-4-one, is a type of flavonoid that has a molecular weight of 272.3 g/mol. NAR concentration varies from 1.47-11.15 mg/100 g in oranges and 14.17-53 mg/100g in grapefruit [451]. Having two hydroxyl groups at position 5 and 7 of the A ring and a carbonyl group at position 4 of the C ring (Figure 3.2), NAR can interact with iron and copper ions to quench free radicals and reactive oxygen species (ROS) as reviewed by Alam *et al.* [452].

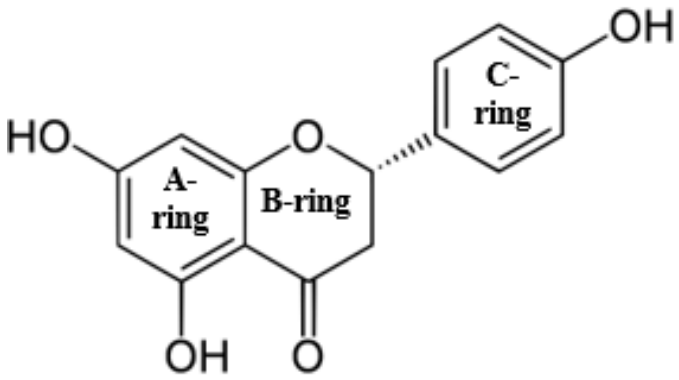

Figure 3.2: Molecular structure of naringenin.

NAR was shown to exhibit several protective effects such as antiestrogenic activity [453], inhibition of oxidative stress and UVB irradiation-induced skin damage [454]. NAR has also been shown to have anti-inflammatory and antioxidant properties, with an ability to reduce neutrophil-derived ROS [455]. By triggering the synthesis of reduced glutathione, the most abundant nonenzymatic antioxidant in cells, NAR can also enhance ROS detoxification [456]. NAR has been shown to tackle oxidative stress diseases such as cardiovascular, neurodegenerative, and age-related macular degeneration [74]. Administration of NAR can also reduce lipid peroxidation while increasing antioxidant levels [457]. As an eye-drop, with its anti-inflammatory and anti-oxidant properties, NAR at high dose (80 µg/eye) was found to inhibit corneal neovascularization [73]. Oguido *et al.* showed that daily treatment with NAR eye drops significantly reduced the area of neovascularization (mm^2) after 3 and 7 days from 500 to 250 mm^2 and from 900 to 300 mm^2, respectively [73]. Therefore, NAR has received increasing attention for ophthalmological applications via a topical route to treat posterior segment diseases [458, 459] (Figure 3.3).

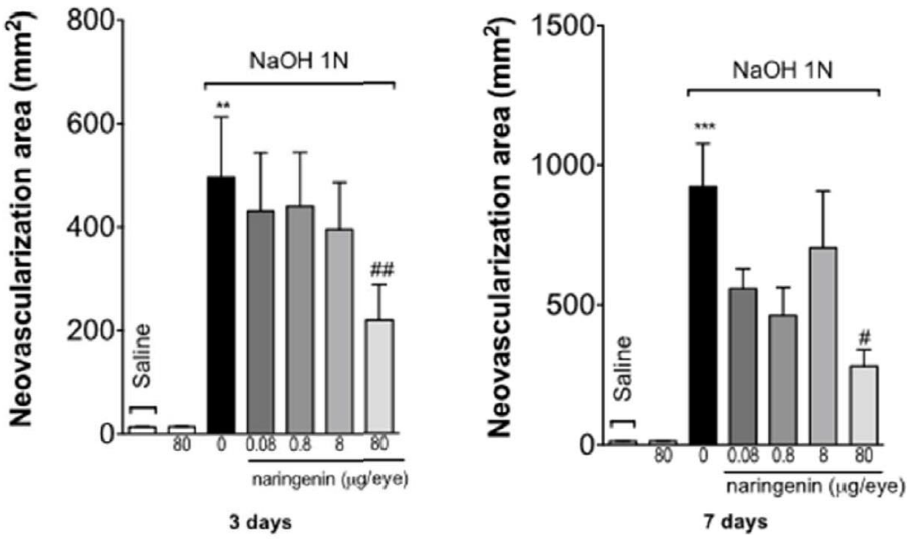

Figure 3.3: The effect of NAR on corneal area of neovascularization after alkali-induced corneal burn/vehicle, which was determined after 3 days (left) and 7 days (right). Results are provided as mean ± SD (n = 5) [73].

There are several methodologies and technologies used to create SCL-based ODDS, and these techniques have been extensively reviewed [220]. Such approaches include 'soak and release', direct entrapment, molecularly imprinted SCL, nanoparticle-loaded SCL, and surface modified SCL. Additionally, with the improvement of the daily-disposable SCL market worldwide, as well as extended wear SCL, this technology can potentially reduce redness and irritation as it limits the eye contact with other preservatives used in many topical formulations. Many early studies on the incorporation of drugs into SCLs focused on soaking the lenses in drug solution [460]. This approach is widely known as the 'soak and release' method, which is the simplest and the cheapest approach to loading drugs into SCLs. This technique was widely used in several studies to load the drug in the CLs [461-463]. Another commonly used approach in the preparation of drug-loaded SCL is by directly adding a therapeutic agent into the SCL by adding it into the pre-polymerized monomer mixture before polymerization, known as direct entrapment [51].

The current study involved the manufacture and characterization of a hydrogel SCL impregnated with NAR. Although there has been an extensive amount of work carried out on the development of therapeutic-loaded hydrogels, the majority of those did not involve the manufacturing of a commercial-quality SCL using a commercial-standard manufacturing process. Out of 50 articles published from 2016-2022 in various

scientific journals, 16 studies used a sheet of hydrogel/silicone hydrogel lens materials (e.g., [374, 464]), while another 18 studies used commercial lenses and modified those rather than fabricating them to commercial standards on-site (e.g., [93, 465]). It was noted that the remaining 16 studies used cast moulding techniques to fabricate a lens, and all used an approximation of commercial lens' polymeric materials rather than a commercial formulation. Furthermore, the synthesis of SCLs in those articles generally involved prolonged curing hours (e.g., 8-24 hours) and harsh extracting conditions (e.g., boiling water for 5 hours to 3 days [374, 461]). These lens manufacturing approaches, to the best of the author's knowledge, are not commonly used in the industrial manufacturing process of a commercial SCL. In addition, most of the hydrogel lenses that have been used are HEMA-based and are not commercial lens monomer mixtures, while in this study, the chosen monomer mixture formulation is predominantly NVP-based and was fabricated under the manufacturing process of a commercial lens. Therefore, it is of scientific value to investigate the impact of loading a therapeutic agent into a commercial hydrogel SCL. Furthermore, as mentioned by Brian Pall, a director at Johnson & Johnson Vision Care, there were various challenges with the commercialization of the first therapeutic SCLs [466]. After being successfully incorporated into the lens matrix, it is important to investigate whether the drug can diffuse out of the lens matrix once it is placed on the eye. Therefore, besides ensuring that the developed drug-loaded lens exhibits all the critical commercial lens parameters, the preliminary study should also include its release behavior.

The aim of this chapter was to investigate the feasibility of manufacturing NAR-loaded SCLs, prepared by both direct entrapment and 'soak and release' approaches, to act as a potential ODDS that has comparable properties to a commercial lens based on the relevant ISO standards.

3.2 Research Aims and Objectives

The aims and objectives of this chapter are:

- To manufacture NAR-loaded SCLs through two approaches: direct entrapment and 'soak and release'.
- To determine the amount of drug leaching throughout the lens manufacturing processes.
- To fully characterize NAR-loaded lens for its physicochemical, mechanical, and dimensional properties.
- To evaluate the *in vitro* release behavior of NAR-loaded lens and determine the kinetics of release through various mathematical models.
- To compare the properties and release behaviors of the NAR-loaded SCLs prepared using a direct entrapment approach vs. those prepared using a 'soak and release' approach.

3.3 Experimental Methodology

3.3.1 Materials

Monomer components, nesofilcon A pre-polymerized monomer mixture and Biotrue® ONEday contact lens' moulds and contact lens (-3.00 SVS was used as the control lens throughout this study) were provided by Bausch + Lomb Ireland Ltd (Ireland). Naringenin (>98% purity), acetic acid (≥99% purity) and Tween® 80 (polysorbate 80, CMC: 0.012 mM, purity: not specified) were purchased from Sigma-Aldrich Ireland (Ireland). PBS (phosphate buffered saline tablets, purity: not specified) and Methanol (HPLC grade, >99% purity) were purchased from Fisher Scientific (Ireland). Ultrapure deionized water obtained from WhiteWater equipment (Ireland) was used throughout the study.

3.3.2 Manufacturing of naringenin-loaded lenses

NAR was entrapped in the WM SCL by adding NAR directly into the pre-polymerized monomer mixture. Four batches of NAR-loaded lenses coded L1, L2, L3, and L4 were manufactured by adding 6.96, 5.66, 3.48 and 2.18 mg/mL of NAR in pre-polymerized monomer mixture.

NAR was entrapped in the WM SCL by soaking a lens in the drug solution. Two batches of NAR-loaded lenses coded L5 and L6 were manufactured by soaking each lens in 0.28 and 0.9 mg NAR in 3 mL 0.1% Tween® 80 in PBS, pH 7.4 for 72 hours. The NAR-loaded SCLs were manufactured using the procedure described in Section 2.2.1.

3.3.3 HPLC quantitation of naringenin

NAR was assayed by a gradient, reversed phase HPLC methodology using a Waters, Symmetry® C18 column (150 mm x 4.6 mm, 5 µm particle size). Method conditions were adapted from the study carried out by Zhang *et al.* [467] with a reduction in running time to 15 minutes. The mobile phase consisted of 0.1% acetic acid in water (A) and methanol (B), and each solvent was degassed in an ultrasonic bath for at least 45 minutes before use. Chromatographic separation was achieved using a gradient programme: 0-5 min (60:40 v/v A:B), 5-11 min (40:60 v/v A:B), 11-12.5 min (30:70 v/v A:B), and 12.5-15 min (60:40 v/v A:B). Column temperature was held constant at 30 °C with a 1 mL/min flow rate. The injection volume was 20 µL with each injection carried out in triplicate, and ultraviolet detection at 288 nm.

Limit of detection (LOD) and limit of quantitation (LOQ) of NAR were obtained using calibration curve analysis within the range of 0.05-0.5 µg/mL and were calculated based on Equations 3.1 and 3.2.

$$LOD = 3.3 \times \frac{S_y}{S} \qquad \textbf{Equation 3.1}$$

$$LOQ = 10 \times \frac{S_y}{S} \qquad \textbf{Equation 3.2}$$

Where: S_y is the standard deviation of y-intercepts of regression lines.

S is the slope of the calibration curve.

A stock solution of NAR (1 mg/mL) was prepared in MeOH. Appropriate dilutions were prepared from the above stock with MP to obtain dilutions in the range of 0.02 µg/mL to 50 µg/mL for the analysis.

3.3.4 Characterization of naringenin-loaded lenses

The following techniques were carried out as per methodologies described in Section 2.3.4, Chapter 2: thermogravimetric analysis (TGA, Q50 model, TA instrument, UK), differential scanning calorimetry (DSC, Q2000 model, TA instrument, UK) and Fourier-transform infrared spectroscopy (FT-IR, Varian-660 IR and ATR-610 model, Varian, USA), and lens characterization techniques, with the following deviations:

Light transmission: A Shimadzu UV-2401 PC, UV-Vis spectrophotometer was used to measure the light transmission.

Equilibrium water content: Three measurements were carried out for each type of lens at room temperature after one hour immersed in water.

Refractive index: The RFM340 refractometer (Bellingham+Stanley Ltd.) with a wavelength of 589 nm (sodium D-line) was used to measure the refractive index (RI) of all lenses as per ISO18369-4:2017 [400].

Wettability: A contact angle system G10 (Krüss Scientific, Germany) was used in this study.

Tensile modulus: The TA.XT Express Enhanced (Stable Micro System, UK) instrument was used in this study to measure the tensile properties of the lenses.

Lens' diameter: Lens diameter, sagittal depth and centre thickness were measured using the Micrometre Calliper measurement tool through magnified glass at 5X. Values presented are averages of ten measurements for each lens. The generated results are comparative only and may not be reflective of the true value of nesofilcon A lenses. Dimensional measurements are dependent on temperature and test solution, which were carried out in air at room temperature in this work. Centre thickness results depend on the force used during the measurement due to the sponge type nature of the material.

FT-IR: The KBr disc technique was used in this analysis.

DSC: All samples were analysed at 10 °C/min ramp rate from 0 °C to 200 °C.

Statistical analysis was carried out as per Section 2.3.4.

3.3.5 Investigating the thermal and aqueous stability of naringenin

3.3.5.1 Thermal stability of naringenin

TGA: Approximately 5 mg of NAR was accurately weighed into a sample pan. Each sample was analysed from 20 to 500 °C at 10 °C/min heating rate.

X-Ray Diffractometry: A X-Ray diffractometer, Bruker D8 Advance equipped with a copper source, operating at 4 kV and 40 mA using an SSD-160 detector, was used in this study. The instrument was operated in Bragg-Brentano geometry from 5-60° (2θ) with a CHC^{+} Temperature and Relative Humidity Chamber (Anton Parr). An Internal air scatter was equipped to limit beam divergence and reduce background interference. Prior to sample analysis the system was validated using a certified corundum reference standard. All samples were analysed using DIFFRAC.EVA software. XRD of NAR sample was analysed using the method described in Section 2.3.3.2 (non-ambient condition), using a 0.019° step size with 1s per step from 5 – 60° (2θ).

3.3.5.2 Aqueous stability of naringenin

The stability of NAR in the release media (i.e., PBS + 0.1% Tween® 80, pH 7.4) and in lens packaging solution (i.e., borate buffered saline, BBS) was investigated by implementing the HPLC method outlined in Section 1.3.5. Briefly, a NAR solution of 1 mg/mL was prepared in either release media or BBS in a 15 mL centrifuge tube and was placed in a 37 °C incubator (SI500 shaking incubator, Stuart, Ireland) and shaken at 50 rpm for over 7 days. After each day, an amount of NAR solution was withdrawn from the tube for HPLC analysis. In addition, NAR stability in water at 123 °C (based on the sterilization condition) was also assessed in this study by analysing the water solution of NAR-loaded lens after sterilisation.

3.3.6 In vitro release study of naringenin-loaded contact lenses

Soaked and directly entrapped NAR-loaded SCL (sterilized lens stored in DI water) were placed in 5 mL of 0.1% Tween® 80 in PBS in glass vials, kept at 37 °C in an incubator with shaking at 50 rpm. At a predetermined interval, 500 µL of release media was withdrawn and replaced immediately with the same volume of fresh release media

to maintain sink conditions. The time points used in this study were 5, 10, 15, 20, 25, 30, 40, 50 minutes, 1, 1.5, 2, 2.5, 3 – 8, 24, 48, 72, 96, 144, and 168 hours.

NAR concentration was determined by HPLC, according to the procedure described in Section 3.3.3. The percentage cumulative drug release from a lens was calculated using Equation 3.3.

$$\%\text{Cumulative drug release} = \left(\frac{Tested\ volume}{Bath\ volume} * P_t\right) + P_{tc} \quad \textbf{Equation 3.3}$$

Where: P_t and P_{tc} are the percentage release at time 't' and percentage release previous to time 't', respectively; Tested volume (mL): volume of release media was withdrawn at a specified interval for HPLC analysis; Bath volume (mL): total volume of release media in a glass vial.

3.4 Results and Discussion

As mentioned in Section 3.1, NAR ophthalmic drops were previously shown to treat retinal diseases. One such study, carried out by Lin *et al.*, demonstrated that 1 µg/mL NAR could increase the proliferation of retinal pigment epithelium cells while inhibiting the growth of human umbilical vein endothelial cells [468]. Therefore, it was essential to estimate the appropriate NAR concentrations to be used in this study that are within the therapeutic window appropriate to potentially treat posterior segment diseases. A required daily dose of approximately 500 µg was calculated based on the ocular pharmacokinetics of 1% NAR eye drops in rabbits [469]. In addition, the %drug clearance upon the application to the cornea and when it reached the retina, which was calculated to be ~99%, based on NAR pharmacokinetic study carried out by Lin *et al.* [469]. It is widely investigated that SCLs can significantly enhance drug residence time [220], and thus, as high as 50% ocular bioavailability could be observed in comparison to 1-5% ocular bioavailability in eye drops. Hence, the NAR therapeutic concentration range to be loaded into the developed SCLs was calculated for this study to be 14 – 66 µg/day.

Given that there are several processes involved in the fabrication of the SCLs, it is essential to quantify the amount of drug loss through each stage of the process, and subsequently, the precise amount of drug uptake in the lens. This would facilitate the ability to precisely quantify the amount of loaded NAR in the NAR-loaded lens for the

in vitro release. To accurately determine the amount of NAR present in the finished NAR-loaded lens before carrying out an *in vitro* release study, the amount of NAR loss through each stage of the process (i.e., drug leaching) was quantified. The percentage of NAR uptake in a finished NAR-loaded lens was quantified with respect to the initial amount of added NAR into the pre-polymerized monomer mixture (for direct entrapped lens), and the amount of added NAR into the soaking solution (for 'soak and release') lens (Table 3.1).

Table 3.1: Summary table illustrating an actual NAR loading concentration for L1-L6 lenses, the percentage drug loss through the manufacturing processes, and the percentage of NAR uptake for each lens type (n = 3).

Lens ID	%Drug present in the dry lens	%Drug loss through hydration, extraction, and sterilization steps	% NAR uptake	NAR (µg/lens)
L1	43.9 ± 9.0	17.65 ± 0.47	47.08 ± 3.32	23.54 ± 1.66
L2				28.45 ± 1.92
L3				39.63 ± 1.16
L4				51.14 ± 1.09
L5	N/A	33.45 ± 0.06	18.10 ± 1.50	15.45 ± 1.50
L6				55.51 ± 0.83

3.4.1 HPLC quantitation methods for the analysis of naringenin

A calibration curve was obtained by plotting peak area (mAu) versus concentration of NAR (µg/mL) giving a straight line over the entire concentration range, as presented in Figure 3.4. The calibration curve equation was identified to be y=56.741x + 1.6483, with a regression factor R^2 of 0.999. As could be observed in Figure 3.4, NAR calibration curve showed good linearity in a range of 0.05-25 µg/mL. LOD is determined as the lowest analyte concentration that can be reliably distinguished from the analytical noise and at which the detection of such analyte is feasible [470]. While LOQ is the lowest concentration at which the analyte can be quantitatively detected with a stated accuracy and precision [470]. Equations 3.1 and 3.2 were used to calculate the LOD and LOQ of NAR (Figure 3.5(b)), and these values were determined to be 0.044 and 0.133 µg/mL, respectively. To ensure the accuracy and sensitivity of each individual analysis [471], as well as to eliminate possible instrumental and experimental variations from day-to-day, a 10 µg/mL NAR standard was included in each analytical run.

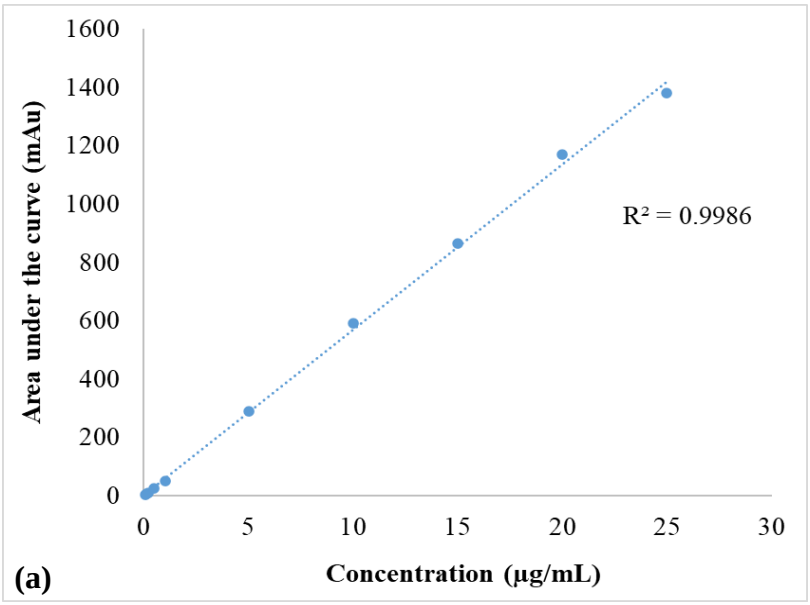

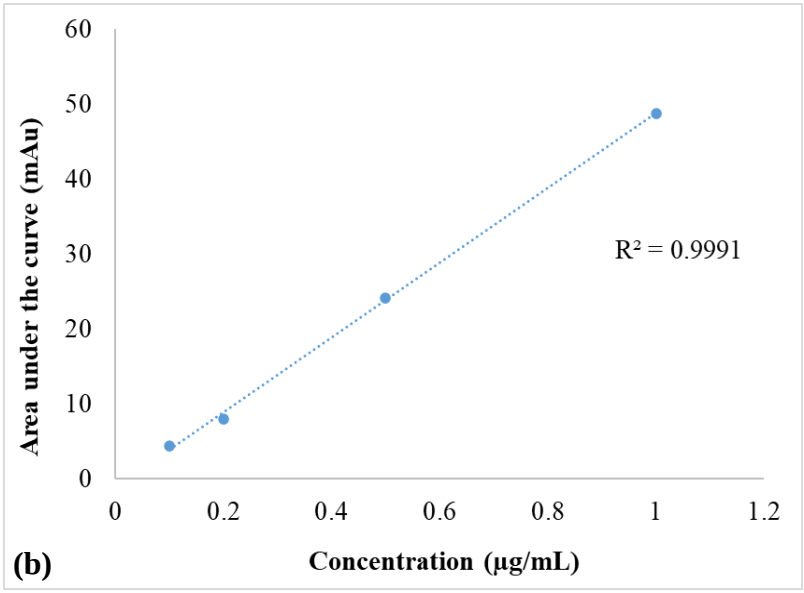

Figure 3.4: Calibration curve of NAR in the linear range (a) of 0.05-25 µg/mL and (b) 0.1 – 1 µg/mL. The regression factor value on each graph is recorded.

3.4.2 Investigating the thermal and aqueous stability of naringenin

3.4.2.1 Thermal stability of naringenin

It was essential to investigate the thermal stability of NAR to ensure its activity was maintained throughout the curing cycle, extraction, and sterilization steps. This was confirmed by TGA (Figure 3.5 (a)) and X-Ray Diffraction (Figure 3.5 (b)).

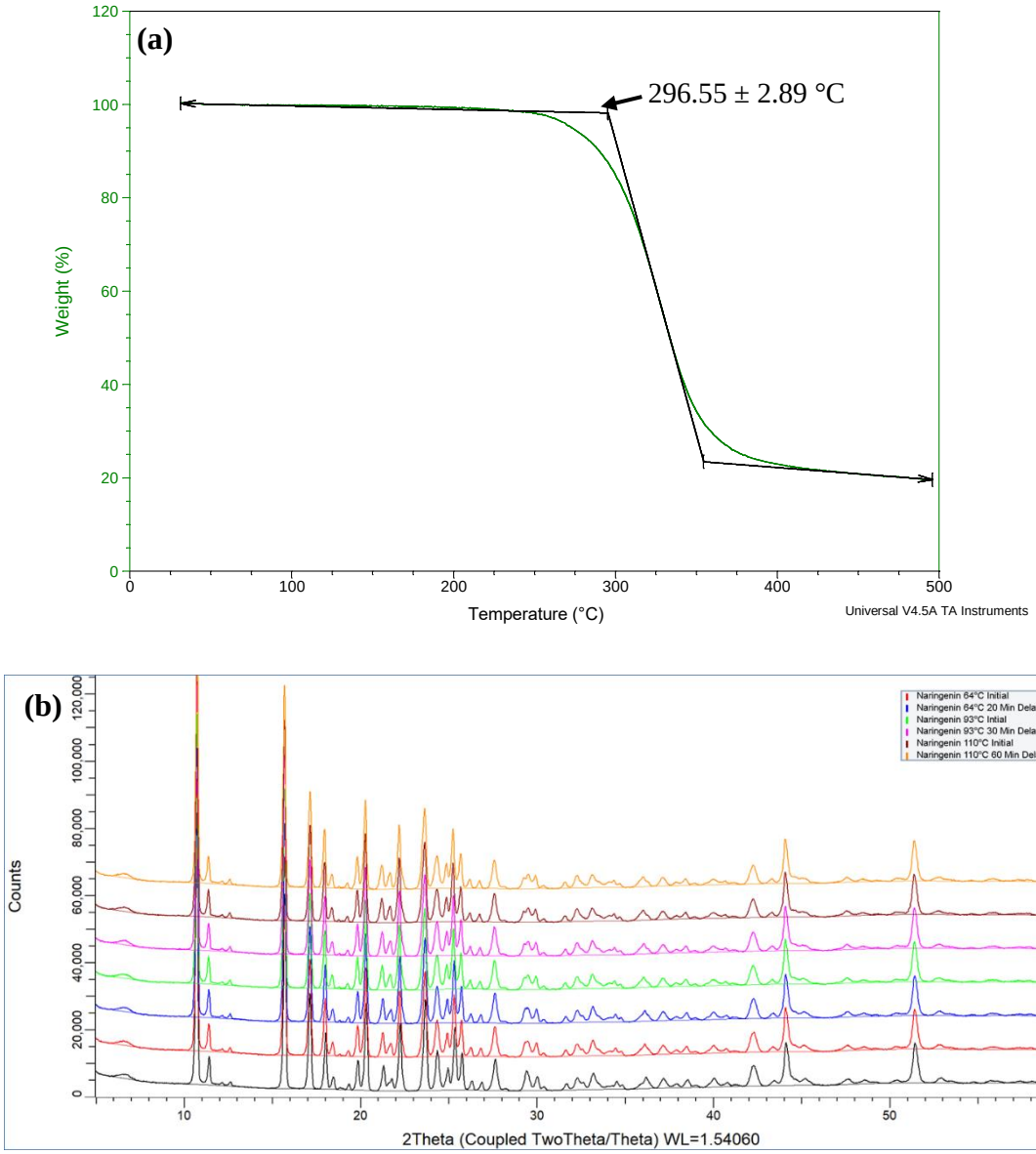

Figure 3.5: Naringenin thermal and crystalline profiles through (a) TGA (degradation temperature is recorded) and (b) XRD analysis.

As could be observed from the generated thermal graph (Figure 3.5(a)), NAR was thermally stable up to 296.55 ± 2.89 °C. Thermal degradation of NAR was previously investigated by Latos-Brozio *et al.* through the use of TGA [472]. Their study demonstrated that NAR started degrading at 290 °C.

XRD is commonly used to analyze the amorphous or crystalline state of materials, as well as their type of crystalline phase and chemical nature of a compound [473]. An XRD diffractogram of a number of drugs including budesonide, salmeterol xinafoate, ibrutinib and docetaxel showed sharp intensity peaks at 0-50°, indicating their

crystalline properties [144, 212, 474]. Figure 3.5(b) showed that the crystallinity of NAR was maintained throughout the whole curing cycle with strongly sharp peaks observed in the range of 2θ from 3° to 50°. A similar observation on NAR crystallinity was previously noted in Guan *et al.* work through XRD analysis [475].

3.4.2.1 Aqueous stability of naringenin

NAR stability in water and release media (i.e., PBS + 0.1% Tween® 80, pH 7.4) after sterilization was investigated using HPLC analysis. NAR concentration at Day 1 was analyzed using HPLC to be 0.04 ± 0.03 µg/mL in water and 152.5 ± 2.8 µg/mL in release media, and after 4 weeks, the values of 0.04 ± 0.03 µg/mL and 149.8 ± 3.6 µg/mL, respectively, were recorded (p-value > 0.05). The outcome from this analysis indicated NAR was stable in both water and release media at 37 °C for over 4 weeks. In addition, NAR stability in the lens packaging solution (i.e., borate buffered saline, pH 6.9-7.4) was determined to be stable for over 3 months (10.2 ± 1.4 µg/mL in Day 1 and 9.34 ± 1.74 µg/mL in Day 90). Stability of NAR in aqueous solution at various pHs (3.5, 6.5 and 8.5) was investigated by Lucas-Abellan *et al.* which demonstrated that NAR concentration remained stable for 48 hours in all the three pH conditions [476].

3.4.3 Polymerization kinetics of naringenin-loaded lenses

As mentioned in Chapter 2, a controlled and repeatable polymerisation process is essential in producing a commercial-quality lens. The polymerization kinetics of the blank pre-polymerized monomer mixture and its monomeric components were previously analysed in Chapter 2 (Section 2.4.3.1). In this section, the DSC data of the pre-polymerized monomer mixture with NAR (L1-L4 lenses) at various concentrations was investigated using the same method in Section 2.3.3.2, by the heat flow curves, where the heating rates matched the lens curing cycle. As expected to be seen in a radical polymerisation mechanism, the three stages included initiation (i.e., decomposition of an initiator to form the primary radicals), propagation (of radicals by reacting with monomer molecules) and termination (of two macro-radicals to form polymer chains) were observed in Figure 3.6 [413].

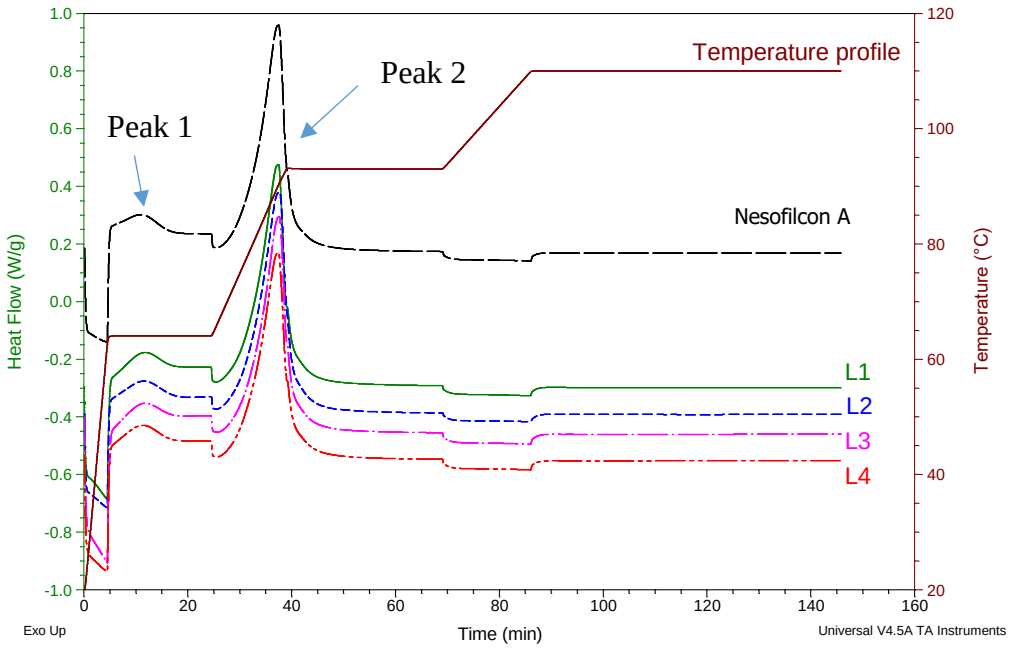

Figure 3.6: Polymerization kinetics of the pre-polymerization monomer mixture (without and with NAR, i.e., CEP/blank WM, and L1-L4 lenses) as a function of time (n = 3).

As could be observed from Figure 3.6, the polymerization kinetics of the lens pre-polymerization mixture with and without the presence of NAR provided similar thermal profiles. Following the thermal data generated from this experiment (Table 3.2), it was suggested that the addition of NAR did not significantly alter the polymerization of the pre-polymerized monomer mixture of the lens monomer. For an example, the reaction enthalpy values evolved from the first initiation process of the polymerization (Peak 1) were 268.9 ± 17.1 for nesofilcon A monomer and 278.2 ± 16.0 J/g for L1 lens. Therefore, it was suggested that the formulated NAR-loaded lens could potentially exhibit the lens' critical properties that are comparable to the CEP/blank WM lenses.

Table 3.2: Thermal data on peak temperatures and reaction enthalpy derived from the polymerization of pre-polymerized monomer mixture with and without the presence of NAR (n = 3, p-value > 0.05).

Sample	Peak 1		Peak 2	
	Temperature (°C)	Reaction enthalpy (J/g)	Temperature (°C)	Reaction enthalpy (J/g)
Nesofilcon A	63.99	268.9 ± 17.1	90.16 ± 0.27	260.1 ± 4.9
L1		278.2 ± 16.0	90.28 ± 0.08	261.8 ± 10.9
L2		302.8 ± 11.3	90.26 ± 0.10	261.2 ± 8.2
L3		305.8 ± 10.4	90.32 ± 0.11	251.3 ± 4.0
L4		284.2 ± 6.8	90.33 ± 0.04	245.7 ± 2.4

3.4.4 Physicochemical and mechanical analysis of naringenin-loaded lenses

3.4.4.1 Thermal analysis of naringenin-loaded SCLs

Thermogravimetric analysis (TGA) was used to determine the degradation temperature of each lens type in the dry state, with and without the presence of NAR (Figure 3.7).

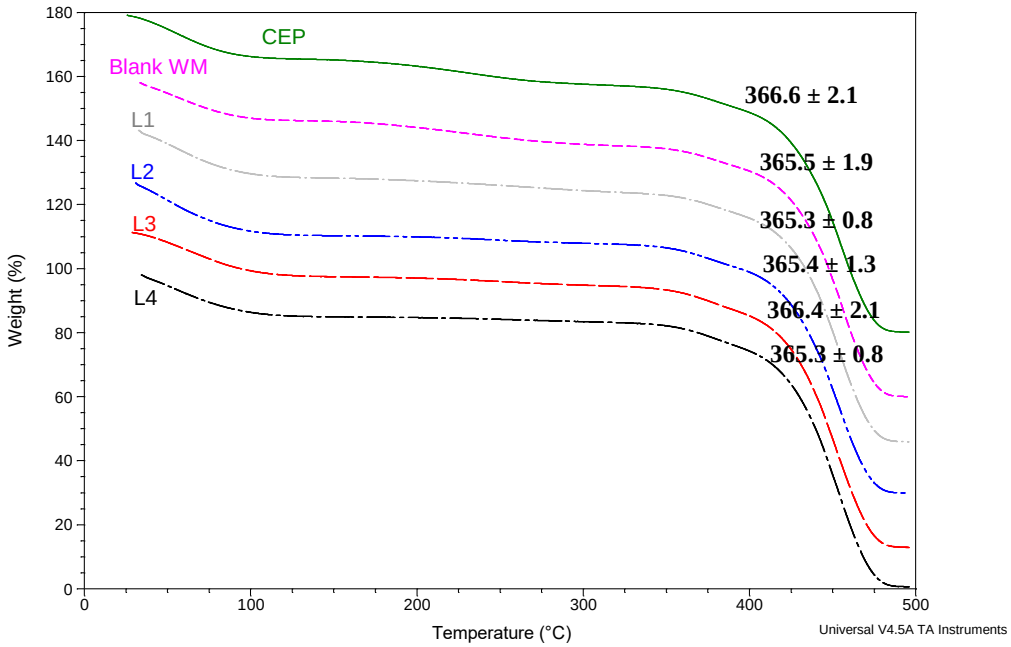

Figure 3.7: TGA thermograms of CEP, WM and L1-L4 lenses, in the dry state, with degradation temperatures (°C) illustrated in the figure for each lens type (n = 3).

TGA analysis of CEP and blank WM lenses was previously reported in Section 2.4.2.2 (Chapter 2), which had a degradation temperature at 365-368 °C. Figure 3.7 shows that all six lens systems maintained over 80% of their weight until 300 °C. No statistically significant different in the degradation temperature (i.e., weight loss) between all the four NAR-loaded lenses and the blank lenses could be observed (p-value > 0.05). TGA analysis was previously used to confirm the thermal stability and thermoplasticity of a hydrogel material [477-479]. For example, Zhao *et al.* demonstrated that the addition of epigallocatechin gallate into the pHEMA CL, for inhibition of bacterial adhesion, did not significantly alter the material fusibility, which showed a good thermal stability up to 300 °C [478].

The thermotropic behaviour of dry-state (Figure 3.8) SCLs was investigated throughout this study. DSC determines the material's glass transition temperature (T_g) by measuring material heat capacity as a function of temperature [480]. T_g correlates to the stiffness and flexibility of the polymer chains as it is determined by steric and electrostatic interactions [481]. The DSC cycle used in this study was previously used to determine the T_g value of a polymeric and hydrogel material [378, 420].

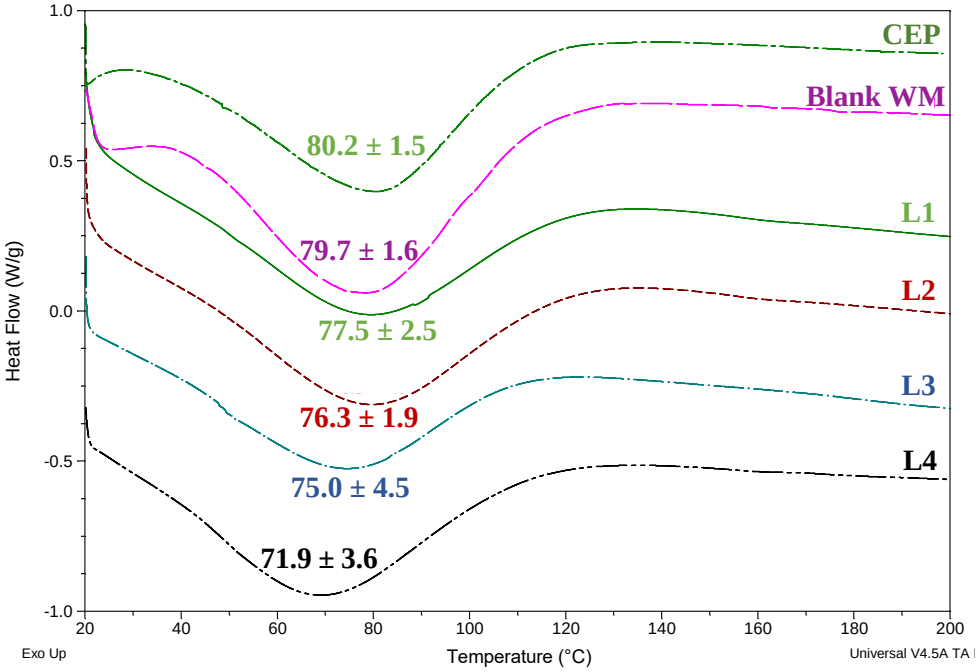

Figure 3.8: DSC thermograms of the CEP, blank WM, and NAR-loaded WM lenses (L1-L4 denoting different concentrations of NAR loaded through direct entrapment). All lens systems were in the dry state (n = 3) and the instrumental value for T_g is reported.

A reduction in the T_g value (Table 3.3) of the fabricated NAR-loaded lens was observed following the addition of NAR, and the higher the concentration of added NAR, the lower the T_g value (p-value < 0.05 for L4). This was believed to be due to the presence of NAR in the polymer matrix, which had a plasticizing effect [482]. T_g of a SCL is correlated to the lens' water content, and hence, this value can influence on-eye comfort, lens movement, as well as water, ion, and oxygen transport in the lens [483]. In polymers, the ability of a molecule to move within the matrix increases when the T_g of such material decreases, which is determined by the relaxation state of the polymer host matrix [484]. A lower T_g value indicates that there is less intermolecular constraint in the motion of the chain segment of the main polymer in the lens, and thus, the higher its water content [483, 484]. However, as can be observed from Table 3.3, the water content of all four concentrations of NAR-loaded lenses, prepared by a direct entrapment approach, showed no statistically significant difference to each other (p-value > 0.05).

The T_g of the fabricated lens (predominantly NVP-based) in this study was compared with the literature value T_g for PVP polymer of 10k Da, which falls in a range between 66-124 °C [421]. This value is dependent on the molecular weight of PVP and can also vary upon interacting with the other monomer components in the pre-polymerization mixture [423]. It should be noted that only T_g values of a material prepared using the same procedure should be compared to each other because they depend on various experimental factors (e.g., drying method, heating rate, as well as degree of cross-linking and MW distribution).

The hydrated state of the developed 'soak and release' NAR-loaded lenses (L5 and L6) was also analyzed using DSC at a different heating rate, with the aim of studying their thermotropic behaviours (Figure 3.9).

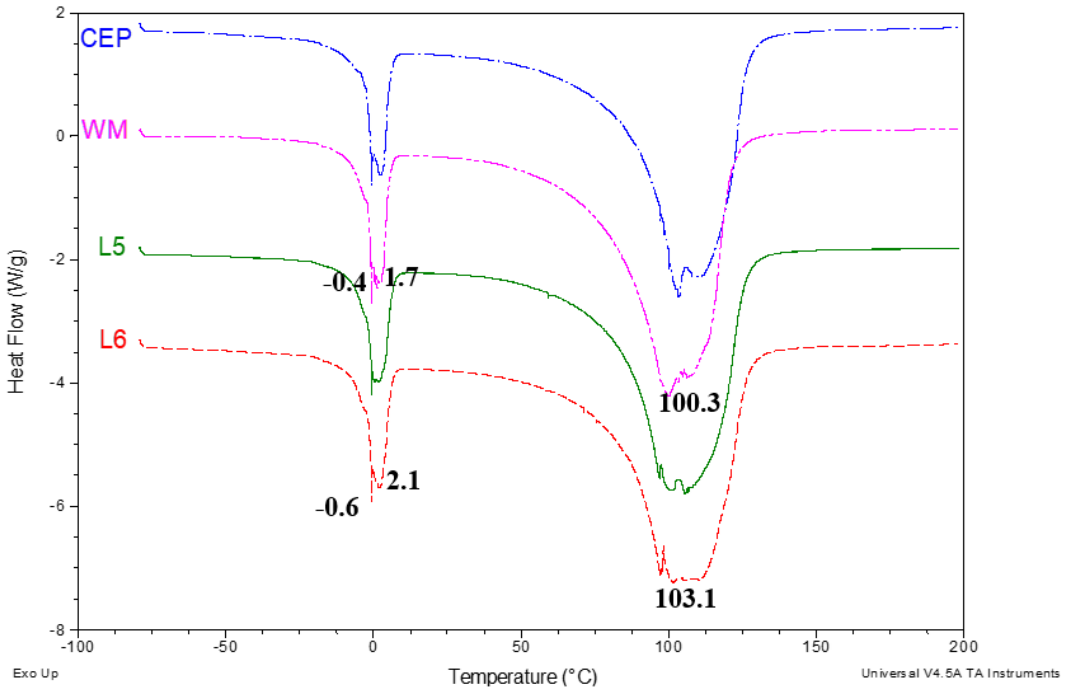

Figure 3.9: DSC thermograms of the CEP, blank WM, and L5 and L6 lenses. All lens' systems were in the hydrated state and the instrumental value for T_g is reported (n = 3).

Figure 3.9 shows that the thermograms obtained for L5 and L6 lenses were similar to those of CEP and blank WM lenses. As described in detail in Section 2.4.2.3 (Chapter 2), the two peaks that appeared before and after the 0 °C point are related to the fusion of water upon the interaction with the hydrogel network. It could be seen that there was no significant difference in the thermograms of the NAR-loaded lenses and the blank lenses (p-value > 0.05). For instance, loosely bound water appeared at -0.43 ± 0.19 °C and -0.65 ± 0.08 °C, while peaks at 1.72 ± 1.63 °C and 2.05 ± 0.89 °C indicated the presence of free water molecules, for blank WM and L6 lenses, respectively. A broad peak at around 100 °C was observed in all four lens systems, indicating the evaporation of water. T_g values of a hydrated hydrogel were also previously measured using DSC [477, 484, 485]. Using a similar method, Lira *et al.* determined the T_g of the hydrated lens (nesofilcon A) to be 24.86 °C [484]. However, in the present study, the T_g peak of each lens system could not be identified in their DSC thermogram (Figure 3.9). This was potentially due to the high-water content of the studied lenses, and as a consequence, this response was possibly masked and could not be detected.

3.4.4.2 Equilibrium water content of naringenin-loaded SCLs

The equilibrium water content (EWC) of a SCL is directly related to the lens comfort and is also closely related to their dehydration rate [218]. As discussed in the recently published review of the author [218], there are several limitations associated with this technique which could result in a significant difference between different operators. Hence, it should be noted that the value of the CEP lens in this test was for comparative purposes only; the published water content of nesofilcon A materials is 78% [398].

The average percentage EWC and its standard deviation for each lens type are tabulated in Table 3.3. The obtained data demonstrated that the %EWC values of the NAR-loaded WM lenses (e.g., 75.5 ± 0.6% for L1 lens) was similar to those obtained in the CEP and blank WM lenses, which were 76.0 ± 0.5% and 75.8 ± 0.2% at 25 °C, respectively (p-values > 0.05 at 25 °C), which was also within the ISO tolerance limits for water content of a SCL [399]. Additionally, low standard deviation in %EWC values implied that the WM lenses were manufactured uniformly. A statistically insignificant reduction in the percentage of equilibrium water content between the soaked timolol and HA lens (92.54% ± 3.54%), and the control lens (92.45% ± 3.76%) was previously observed [486]. For the treatment of glaucoma, Desai *et al.* investigated the co-delivery of timolol and hyaluronic acid from semi-circular ring-implanted CLs, which were made of 66.9% HEMA, 0.05% EGDMA, 31% DMA, 0.01% TRIS, 0.1% NVP and 0.05% Irgacure D [486].

3.4.4.3 Refractive index of naringenin-loaded SCLs

The required RI value for a commercial SCL should typically not exceed 1.55 [400]. An RI range of 1.37 – 1.43 was reported as reference values for commercial hydrogel and silicone hydrogel SCLs [302, 305]. Table 3.3 demonstrates that the fabricated WM NAR-loaded lenses produced similar RI values in comparison to the unloaded WM lens (p-value > 0.05), which was 1.373. This value agreed with previous work carried out on nesofilcon A lens, which showed an RI value of 1.3726 ± 0.0003 [484]. Additionally, following the ISO 18369-2 standard, this difference is within the tolerance limit (± 0.005) for RI values of SCLs [399]. Hence, the WM lenses with varying NAR concentrations produced a comparable RI value to the CEP lenses.

In addition, given that the standard deviation is low in both cases, the tests provided reproducible and reliable results. Even though the RI is one of the critical properties that commercial SCLs should be evaluated for according to the ISO 18369–1:2017 standard [433], this property has not been investigated in therapeutic-loaded SCL research.

3.4.4.4 Light transmission of naringenin-loaded SCLs

The optical clarity of the SCLs with the addition of NAR was assessed and as per Table 3.3, an average transmittance of over 97% (in the visible region) relative to the CEP lenses was observed in the fabricated NAR-loaded lenses (L1-L6 lenses) at different concentrations and was within the ISO tolerance limits for light transmission of a SCL [399]. This result indicated that the WM and NAR-loaded WM lenses produced by both direct entrapment and 'soak and release' approaches provided sufficient optical clarity for commercial use as ophthalmic medical devices. Similar observations were noted in previous works on therapeutic SCLs [374, 487]. For instance, the effect of loading cyclosporine A into pHEMA hydrogel on its light transmission was investigated by Kapoor *et al.* [380]. Given that there was sufficient drug solubility in the pHEMA matrix, the hydrogel optical clarity remained clear (>95%).

3.4.4.5 Contact angle measurement of naringenin-loaded SCLs

Wettability is a crucial characteristic since it determines the spreading ability of the tear film along the material surface as discussed in Section 1.4.6.7. From Table 3.3, it can be observed that the CA of the lens increased slightly with an increase in the amount of NAR loaded into the lens for the direct entrapment approach (p-value < 0.05). As an example, the CA value increased from 40.35° ± 0.66° in blank WM lens, to 42.23° ± 0.88° and 45.76° ± 0.87° for L1 and L4 lenses, respectively, which was expected due to the hydrophobicity of NAR. The CA of the HEMA/PVP lenses (water content: 60.7 ± 0.3%) was previously determined to be 42° ± 3° using a captive bubble method [420], and the CA range in Silva's work was between 40° – 46°. Lin *et al.* [338] cited that the acceptable range of CA of commercial SCLs is 11° – 83°, demonstrating that the produced WM lenses have a suitable hydrophilicity to be used as ophthalmic medical devices. The results in this work agree with several other studies that have also used water [337, 386, 420].

The wettability of the hydrated unloaded and drug-loaded CL (levofloxacin and chlorhexidine), with and without the addition of vitamin E (20%) was investigated by Paradiso *et al.* [488]. There was no statistically significant effect on the CA of the lens before and after the incorporation of drugs and/or vitamin E, with θ_{water} in a range between 30° and 40° [488].

Although tear fluid and water have distinctive characteristics, this study was carried out in water rather than simulated tear fluid (STF) to investigate the raw material's property. If the measurement was done in STF, the lens matrix could potentially take up the components that are present in the solution, which in turn could affect the outcome of the inherent wettability of the SCL material.

3.4.4.6 Tensile modulus of naringenin-loaded SCLs

As discussed in Section 1.4.6.8, it is essential to examine the modulus of a SCL upon incorporation of an analyte as this property is directly related to the lens' handling and durability. The Young's moduli of eight different types of lenses were investigated. From the generated data, calculations for mechanical properties of the material were carried out to determine the Young's Modulus of the SCLs. Generally, in the case of stress-strain graphs in experimental cases, the slope of the curve changes between the origin and terminus of the graph [340]. The Young's modulus values for the eight lens systems were compared (Table 3.3). All 7 types of fabricated lenses (e.g., 0.54 ± 0.06 MPa for CEP lens, and 0.53 ± 0.06 MPa for L4 lens) showed no statistically significant difference in modulus in comparison to the CEP lenses (0.53 ± 0.05 MPa, p-value > 0.05). The standard deviation was low in all cases, which implied that this technique is feasible for determining the hydrogel Young's moduli, and that WM lenses were produced consistently. Using a similar method, Toffoletto *et al*. examined the modulus of intraocular lens (pHEMA) before and after loading bromfenac sodium or dexamethasone sodium phosphate using a molecular imprinting approach [91]. When compared with the unloaded lens, the Young's modulus of the drug-loaded lens did not change significantly and were in a range of 3.5-4 MPa [91].

The Young's modulus value for hydrogels such as pHEMA is expected to be approximately 0.5 MPa [435], with a range of 0.1-1.9 MPa recorded for conventional hydrogel lenses, depending on the lens' components and its water content [340]. Since the Young's modulus values of the NAR-loaded WM lenses from this experiment are within the range of other hydrogel materials with similar composition, they could be considered as an appropriate material for commercialized hydrogel SCLs.

Table 3.3: Summary table of the fabricated lens' physicochemical and mechanical properties.

Lens sample	**%T (n = 3)**	**%EWC (n = 3)**	**Refractive index (n = 3)**	**Contact angle (°) (n = 10)**	**Young's modulus (MPa) (n = 10)**	**T_g (°C)** (n = 3)**	**Degradation temperature (°C) ** (n = 3)**
CEP	98.1 ± 0.7	76.0 ± 0.5	1.373 ± 0.000	41.22 ± 0.57	0.53 ± 0.05	80.2 ± 1.5	366.6 ± 2.1
WM	98.2 ± 0.8	75.8 ± 0.2	1.373 ± 0.000	40.35 ± 0.66	0.54 ± 0.06	79.7 ± 1.6	365.5 ± 1.9
L1	98.9 ± 0.5	75.5 ± 0.6	1.373 ± 0.000	42.23 ± 0.88^{+}	0.52 ± 0.04	77.5 ± 2.5	365.3 ± 0.8
L2	98.2 ± 0.4	75.4 ± 0.5	1.373 ± 0.000	44.33 ± 0.49^{+}	0.51 ± 0.05	76.3 ± 1.9	365.4 ± 1.3
L3	97.8 ± 0.3	75.1 ± 0.6	1.373 ± 0.000	46.03 ± 0.70^{+}	0.50 ± 0.06	75.0 ± 4.5	366.4 ± 2.1
L4	97.6 ± 0.5	75.6 ± 0.6	1.373 ± 0.000	45.76 ± 0.87^{+}	0.53 ± 0.06	71.9 ± 3.6^{+}	365.3 ± 0.8
L5	98.2 ± 0.8	75.8 ± 0.7	1.373 ± 0.000	45.52 ± 0.75	0.55 ± 0.08	N/A	N/A
L6	98.2 ± 0.6	75.9 ± 1.0	1.373 ± 0.000	44.47 ± 0.97^{+}	0.53 ± 0.07	N/A	NA
ISO tolerance [399]	± 5% absolute*	± 2% absolute*	± 0.005 absolute*	N/A	N/A	N/A	N/A

* : values from the blank WM lens.

$^{+}$: values exhibit a p-value < 0.05 in comparison to the CEP lens.

** : measurement was carried out on samples in the dry state only.

3.4.4.7 Fourier transform infrared spectroscopic analysis of naringenin-loaded SCLs

The spectroscopic characterization of hydrogel SCL and their monomer components was performed by Fourier-transform infrared spectroscopic analysis (FT-IR). The FT-IR spectra of NAR, CEP, blank WM, and L1-L4 lenses, all were in the dry state, are shown in Figure 3.10 and Table 3.4.

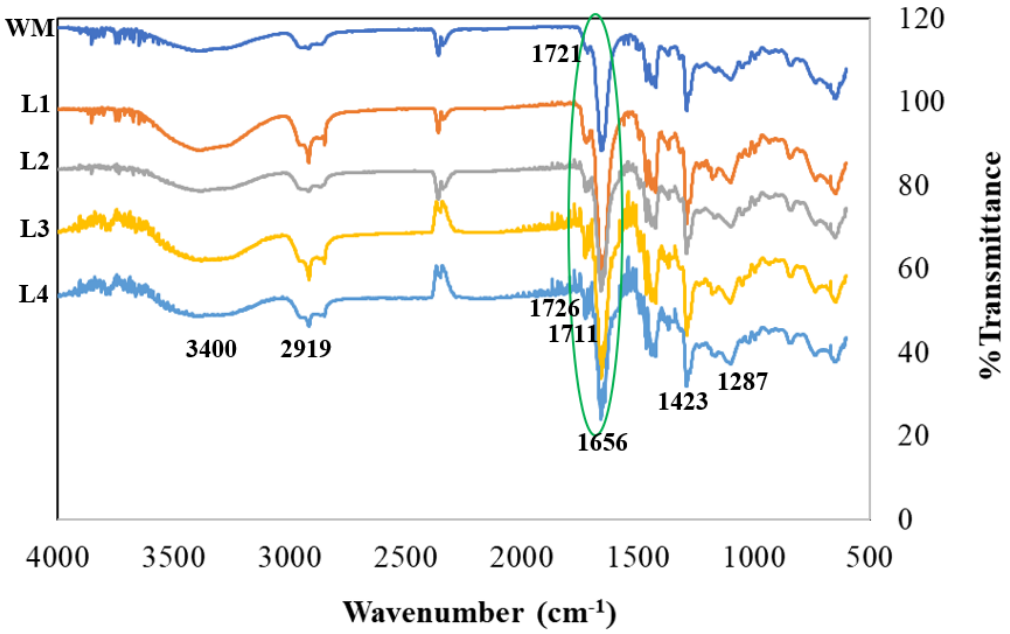

Figure 3.10: FT-IR spectra of blank WM, and L1-L4 lenses (all were in dry state).

Because NVP is the main component in the nesofilcon A monomer mixture, it was expected that the FTIR spectra of the developed WM lenses and the CEP lens would exhibit the characteristic peaks of PVP (poly-vinylpyrrolidone). For the developed NAR-loaded lenses formed through a direct entrapment approach, all characteristic bands present in FT-IR spectra of CEP and blank WM lenses appeared in the FT-IR spectrum of the obtained hydrogel. The two characteristic peaks (C-N stretching) at 1287 cm^{-1}, indicative of NVP (Figure 2.22(c)) was observed in all cases. A characteristic NAR peak at 1711 cm^{-1} (C=O stretch) [467, 489, 490] could be observed in the L3 and L4 lenses spectra (Figure 3.10), which was not visible in the FT-IR spectra of CEP, blank WM, as well as L1 and L2 lenses. This observation suggested that due to the low drug concentration in L1 and L2 in comparison to L3 and L4 lenses (e.g., 23.54 ± 1.66 µg/lens in L1 vs. 51.14 ± 1.09 µg/lens in L4), their FTIR spectra

showed no significant difference to the blank WM lens spectrum. Similar observations were noted in a work carried out by Pereira-da-Mota *et al.* [374], which investigated the potential interactions of atorvastatin-loaded pHEMA hydrogel through the use of FTIR analysis. Their study demonstrated that this technique was not sufficient to characterize the intermolecular interactions between atorvastatin and the pHEMA hydrogel matrix of the developed drug-loaded hydrogels due to the low drug content (i.e., 5.81 ± 0.12 mg/g of hydrogel) [374].

Table 3.4: Spectral band assignment of the blank WM, L1-L4 lenses, all were in a dry state.

Ref. peak position (cm^{-1})	**Functional group**	**WM**	**L1**	**L2**	**L3**	**L4**
3381 [437] 3396 [438]	O-H stretching	3400	3400	3400	3400	3400
2933 [437] 2852 [438]	Aliphatic carbon ($-CH_3$, $-CH_2$)	2919	2919	2919	2919	2919
1719 [437] 1701 [439] 1644 [438]	C=O stretching (pyrrolidone group)	1721	1722	1723	1725	1726
1711	C=O stretching	-	-	1711	1711	1711
1620 [437]	C=C stretching	1656	1657	1658	1659	1659
1451 [437] 1423 and 1371 [438]	Deformation of aliphatic carbon ($-CH_2$)	1423	1423	1423	1423	1423
1246 [437] 1279 [438]	C-N stretching	1287	1287	1287	1287	1287
1151 and 1075 [437]	C-O-C stretching	1163-1100	1163-1100	1163-1100	1163-1100	1163-1100

A shift in wavenumbers of the two characteristic peaks represented C=O stretching and C=C stretch could be seen in NAR-loaded lenses in comparison to blank WM lens. An intense peak at 1721 cm^{-1} observed in the CEP and blank WM lenses spectra represented the C=O stretching from an aliphatic ketone in NVP, which was also observed in other FTIR analysis on NVP [437-439], shifted to 1726 cm^{-1} in L4 lens spectrum. These observations indicated the presence of NAR within the lens matrix with possible weak dipole-dipole interaction between the lens' polymeric matrix and the drug. Based on this analysis, it was predicted that the drug release rate from the

developed NAR-loaded SCLs would be high, and a burst release might be observed. It was previously cited that the increase in crosslinker density within the hydrogel matrix would decrease the drug release rate, which was due to the fact that the drug had a strong interaction with the matrix, and thus, resulted in lesser and slower release [491].

3.4.5 In vitro release studies of naringenin-loaded lenses

Since NAR is sparingly soluble in aqueous solution, the *in vitro* release study of the NAR-loaded lens was carried out in 0.1% Tween® 80, in PBS (pH 7.4) to increase its water solubility, from 20.1 µg/mL (in PBS) to 152.5 µg/mL. Solubility and dissolution rate are vital factors to investigate the ocular bioavailability of a drug, and thus, it is essential to increase the dissolution of a poorly water-soluble drug (i.e., NAR). Tween® 80 has been commonly used in the development of ocular drug delivery [492] and *in vitro* release studies for different drug delivery systems to enhance the solubility of a therapeutic agent [7, 493]. Human tear film is comprised of three layers including: the outer lipid layer, the middle aqueous layer and the inner mucin layer that interacts with the corneal epithelial surface [20]. Each layer in the tear film contains different compounds, including proteins, polar and nonpolar lipids, electrolytes, mucins, and water. The most abundant lipids present in human tear fluid are phospholipids, free fatty acids (FFAs), triglycerides (TGs), cholesteryl esters (CEs), and wax esters [494]. Of those, FFAs, TGs and CEs are considered as neutral lipids. Hence 0.1% Tween® 80 was used in this study to ensure sink conditions were maintained for the release of NAR.

These drug release kinetic models were previously used in a number of studies in the same area [140, 143, 283, 358]. The percentage cumulative drug release (%) profiles for an initial daily release (24 hours) and a 7-day release for L1-L6 lenses are shown in Figure 3.11 below.

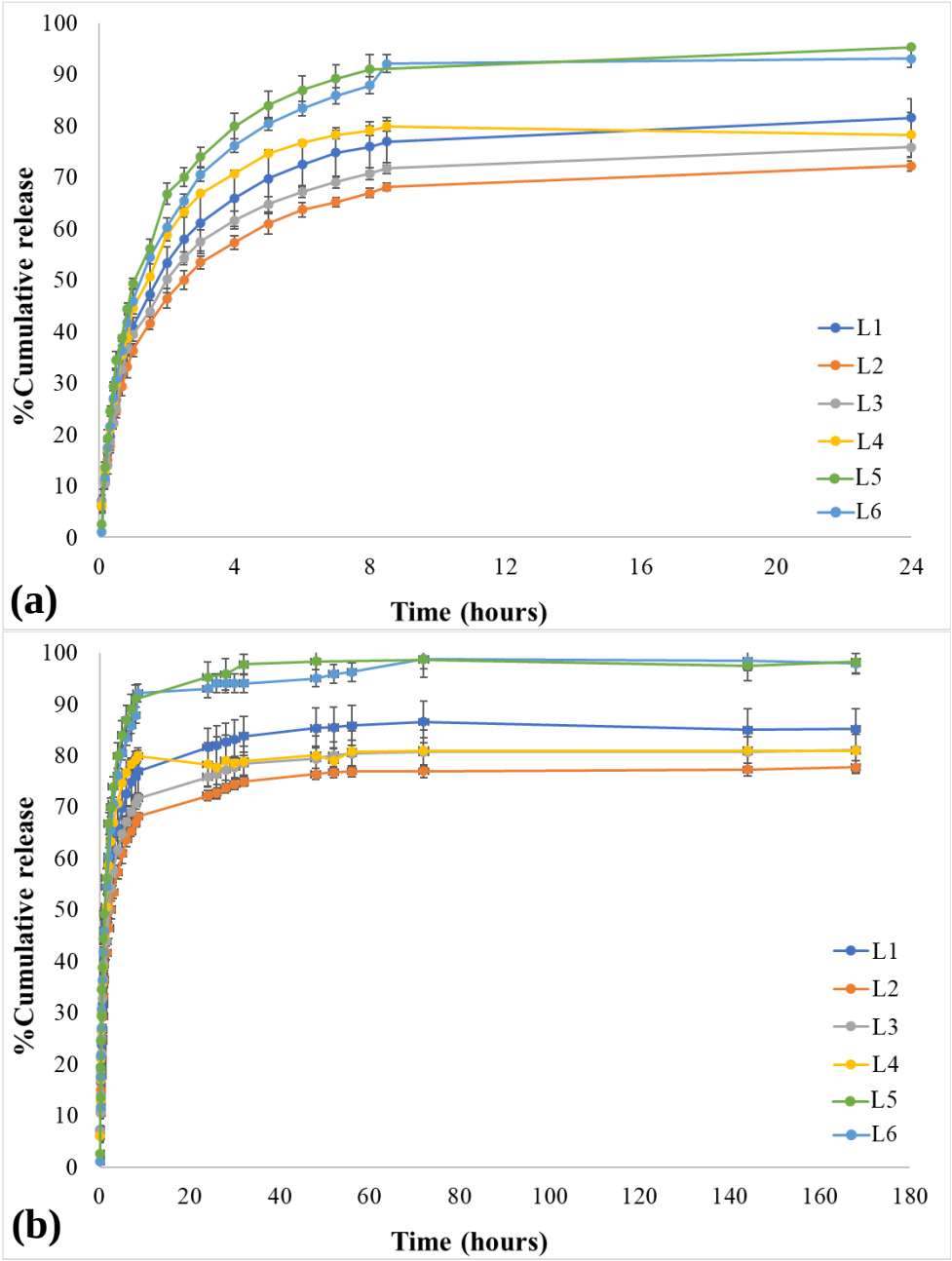

Figure 3.11: *In vitro* release profiles of NAR-loaded lenses in (a) 24 hours, and (b) 7 days, prepared by both direct entrapment and 'soak and release' approaches (n = 3).

As can be observed in Figure 3.11, all six batches showed a controlled and sustained NAR release in the first 24 hours, followed by a stabilized release of NAR over the next seven days. It also shows that there was no correlation between the loaded NAR concentration and the lens' release profile. The outcome demonstrated that NAR concentration released from the six developed NAR-loaded lens' systems is within the estimated therapeutic range, which was calculated at the end of the first 24 hours of

release (17.88, 19.04, 28.03, 40.46, 13.91 and 54.42 µg/day L1, L2, L3, L4, L5 and L6, respectively). Since this is a daily disposable SCL, the majority of drug would need to be released within a day for it to be therapeutically relevant. When compared with a different work on therapeutic SCL published previously [495], which investigated the *in vitro* release profiles of a hydrophilic drug naringin from the pHEMA hydrogel lenses, a different release pattern was observed. The work carried out by Kwak *et al.* demonstrated a sustained release of naringin from the hydrogel SCL for a month [495]. It is worth noting that the developed lens in this study is NVP-based, while many hydrogel materials used in the development of therapeutic lens are HEMA-based. Hence, it was expected that there would be a difference in lens' properties and behaviour upon the incorporation of a drug.

By applying various mathematical models: zero-order, first-order, Higuchi, and Korsmeyer-Peppas, the release mechanism of NAR-loaded lenses at various NAR concentrations was investigated. The applicability of all the models was tested up to 8 hours (i.e., 480 minutes, initial release). From the generated data, the correlation coefficient (R^2), diffusion exponent (n), and rate parameter (k) values (Table 3.5) were calculated to identify the best fit model to describe the release mechanism of the NAR-loaded lens.

Table 3.5: Kinetic release data for the first 8 hours obtained from zero order, first order, Higuchi and Korsmeyer-Peppas mathematical models from the prepared NAR-loaded lenses.

Lens type	**Drug release kinetic data**			
	Zero order (k unit: M/s)	**First order (k unit: 1/M)**	**Higuchi (k unit: $M/s^{1/2}$)**	**Korsmeyer-Peppas**
L1	R^2: 0.8114 k = 0.1373	R^2: 0.5939 k = 0.0015	R^2: 0.9433 k = 3.5792	R^2: 0.9533 n = 0.5001
L2	R^2:0.8120 k= 0.1182	R^2: 0.5814 k = 0.0015	R^2: 0.9432 k = 3.0794	R^2: 0.9451 n = 0.4893
L3	R^2: 0.7493 k = 0.1257	R^2: 0.5799 k = 0.0015	R^2: 0.9315 k = 3.2893	R^2: 0.9447 n = 0.4946
L4	R^2: 0.7808 k = 0.1426	R^2: 0.5492 k = 0.0015	R^2: 0.9247 k = 3.7497	R^2: 0.9292 n = 0.5096
L5	$R^{2:}$ 0.7865 k = 0.1650	$R^{2:}$ 0.4452 k = 0.0017	$R^{2:}$ 0.9275 k = 4.3298	$R^{2:}$ 0.8330 n = 0.5956
L6	$R^{2:}$ 0.7991 k = 0.1624	$R^{2:}$ 0.3920 k = 0.0019	$R^{2:}$ 0.9355 k = 4.2472	$R^{2:}$ 0.7727 n = 0.6759

As can be observed from Table 3.5, the initial release of NAR (in the first 8 hours) from the fabricated lens in all six systems indicated a good fit (highest R^2 values) for both Higuchi and Korsmeyer-Peppas models, suggesting that the mechanism of NAR release is mainly governed by diffusion. The diffusion exponent values 'n' obtained from the Korsmeyer-Peppas model for L5 and L6 lenses was higher than 0.5 (i.e., 0.6759 and 0.5956, respectively), indicating a non-Fickian release type. Hence, the mechanism of NAR release is governed by both diffusion and swelling for this system [496, 497]. L1-L4 lenses showed 'n' values that were very close to 0.5 (i.e., L1: 0.5001 and L4: 0.5096) or slightly less (i.e., L2:0.4893 and L3:0.4946), suggested that these systems are driven by diffusion mechanism through the swollen polymeric network. The above observation agrees with previous studies on drug-loaded hydrogels, suggesting that the release of drug from the hydrogel is governed by a diffusion-controlled mechanism. Work carried out by Pereira-da-Mota *et al.* on atorvastatin-loaded hydrogel (HEMA-based) demonstrated that the best fitted mathematical model for the developed system was Higuchi, with R^2 values are above 0.98 [374]. Aiming to investigate the novel material to be used in the development of therapeutic hydrogel lens, Jeencham *et al.* investigated the use of chitosan and regenerated silk fibroin blended films as SCL materials for the delivery of diclofenac sodium [498]. The *in vitro* drug release results from all tested drug-loaded hydrogels in Jeencham's study implied that Higuchi is the best fitted model.

The kinetic data from Table 3.5 also demonstrated that L5 and L6 exhibited a faster release rate in comparison to those fabricated using a direct entrapment approach. While the k values in the Higuchi model for L1-L4 lenses are in a range of 2.8-3.8 $M/s^{1/2}$, a value of 4.2-4.3 $M/s^{1/2}$ was obtained for L5 and L6 lenses. The obtained release patterns are as predicted from the FTIR analysis in Section 3.4.5.7 with regard to the impact of intermolecular interactions between NAR and polymer on *in vitro* release behavior of a drug-loaded SCL. By loading NAR into the lens using a direct entrapment approach, a higher crosslinking was expected in comparison to those prepared using a 'soak and release' approach. This observation was in agreement with a previous study by Maulvi *et al.* [460], which was potentially due to a loose binding of drug in the polymer matrix in the 'soak and release' lens in comparison to the lens prepared using a direct entrapment approach. Additionally, it has been suggested that the soaking duration of a lens in the drug solution could have an impact on the

distribution of drug throughout the lens matrix, which in turn, could potentially impact on the diffusivity of a drug and, therefore, its release profile [499].

3.4.6 Dimensional analysis of naringenin-loaded lenses

To evaluate the feasibility of commercialization of the developed drug-loaded SCLs, their dimensional properties were examined (e.g., lens diameter, sagittal depth, and centre thickness, Table 3.6). Due to the comparative nature of this test as noted in Section 2.4.4, it should be noted that the measured values for the CEP lens did not represent the true values of commercial nesofilcon A lens. The published dimensions for nesofilcon A lens are: 14.20 mm in diameter, sagittal depth of 3.820 mm and centre thickness of 0.100 mm [398].

Table 3.6: Diameter, sagittal depth, and centre thickness values of the CEP and developed SCLs (n = 10).

Lens type	Diameter (mm)	Sagittal depth (mm)	Centre thickness (mm)
CEP	14.18 ± 0.10	3.82 ± 0.09	0.116 ± 0.008
WM	14.15 ± 0.09	3.79 ± 0.06	0.117 ± 0.008
L1	14.03 ± 0.08	3.91 ± 0.07	0.116 ± 0.008^{+}
L2	14.09 ± 0.10^{+}	3.77 ± 0.11^{+}	0.118 ± 0.007^{+}
L3	14.12 ± 0.05^{+}	3.83 ± 0.08^{+}	0.128 ± 0.006
L4	14.08 ± 0.09^{+}	3.75 ± 0.14	0.128 ± 0.009^{+}
L5	14.13 ± 0.07	3.80 ± 0.08	0.122 ± 0.007
L6	14.13 ± 0.09^{+}	3.86 ± 0.12^{+}	0.124 ± 0.007^{+}
ISO tolerance limit [399]	± 0.20 absolute*	± 0.05 absolute*	± 0.010 + 0.10 absolute*

* : values from the blank WM lens.
$^{+}$: values exhibit a p-value < 0.05 in comparison to the CEP/blank WM lens.

As outlined in Section 3.3.4, this was carried out with a simple mechanical measurement tool, thus, the use of more sophisticated measuring devices (e.g., SNAP system, as outlined in Section 2.3.3.1, Chapter 2) would be required for commercialized measurement. The impact of drug loading on lens diameter and centre thickness was previously investigated by Gade *et al.* [500]. Using a solvent casting technique with stainless steel mould, an SCL, made of chitosan, polyethylene glycol 400, and glycerol, was manufactured and had a diameter of 13.96 ± 0.17 mm with 241 ± 9 µm centre thickness.

An addition of moxifloxacin resulted in a reduction in both lens diameter (13.17 ± 0.25 mm) and thickness (211 ± 4 µm), while an increase in lens diameter (14.03 ± 0.03 mm) and decrease in lens thickness (127 ± 5 µm) were observed for dexamethasone loaded SCL. The observation from that study could potentially attribute to the hydrophilic nature of moxifloxacin and hydrophobicity of dexamethasone, which would lead to a different interaction with the lens monomer mixture [500].

The tolerance limits for each dimensional parameter of all the measured developed SCLs, with and without NAR, were within the acceptance criteria according to ISO 18369-2:2017 (E) [399]. Hence, the results (Table 3.6) demonstrated that the developed NAR-loaded lens exhibited what could be adequate lens dimensional properties for commercialization. All six developed NAR-loaded SCLs are visually observed to be similar to the blank WM lens, which was previously shown to be equivalent to the commercial CEP lens (Figure 3.12)

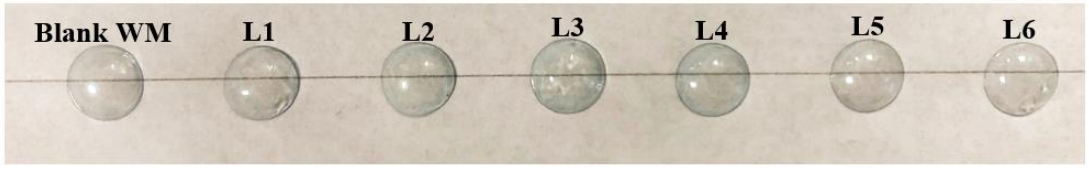

Figure 3.12: Images of SCLs without (Blank WM) and with NAR at various concentrations (L1-L6), all lenses are at hydrated state.

3.5 Conclusions

The development of therapeutic-loaded hydrogel SCLs for the controlled release of a drug has received considerable focus as an alternative approach to eye drops to treat various ocular diseases. This work was carried out using a commercial-standard process to manufacture a SCL to ensure the developed lens exhibited all the critical properties that are required of a commercial lens.

Due to the favorable ocular pharmacology and pharmacokinetics of NAR in the treatment of posterior segment diseases, topical installation of NAR through daily disposable SCLs can potentially act as an effective alternative delivery system. This work investigated the feasibility for use of a NAR-loaded hydrogel contact lens fabricated using direct entrapment and 'soak and release' approaches to provide an extended release of NAR to treat diseases affecting the back of the eye. All the formulated NAR-lens' batches were found to be suitable as a daily disposable SCL with respect to optical clarity, physicochemical, and dimensional properties when compared to the unloaded CEP lens (nesofilcon A). *In vitro* release studies under sink conditions showed that the loaded NAR in the lens can be released in a controlled manner for 24 hours within the estimated therapeutic window. Therefore, the outcome from this work suggested that the developed NAR-loaded SCLs can potentially be used as an alternative ocular drug delivery system to treat posterior segment diseases of the eye caused by oxidative stress.

To improve the ocular bioavailability of NAR, which is significantly hindered by its low aqueous solubility, the next chapter of this work focuses on the development, preparation and characterization of an inclusion drug:cyclodextrin complex (i.e., sulfobutyl ether-ß-cyclodextrin). Additionally, with the purpose of increasing the controlled release and targeted delivery of NAR and to develop a more effective drug delivery system to treat retinal diseases, the development of NAR:CD complex in Chapter 4 would be incorporated into the developed SCLs of commercial quality.

CHAPTER 4

FORMULATION AND OPTIMIZATION OF NARINGENIN:CYCLODEXTRIN INCLUSION COMPLEXES

4 FORMULATION AND OPTIMIZATION OF NARINGENIN:CYCLODEXTRIN INCLUSION COMPLEXES

4.1 Introduction

Topical administration of NAR, which had hydroxypropyl-ß-CD (HP-ß-CD) as an ingredient, was shown to markedly reverse $NaIO_3$-induced retinal pigment epithelium degeneration and laser-induced choroidal neovascularization [469]. This was proposed to be due to a strong increase of ocular blood flow and its antioxidant activity. The results of pharmacokinetic experiments indicated that NAR penetrated both cornea and conjunctiva/sclera into the posterior segment (T_{max} of aqueous humour-time of maximum concentration was 0.75 h and C_{max} of aqueous humour-maximum concentration was 1325.69 ± 239.34 ng/mL) [469].

The use of NAR is limited by its low water solubility and bioavailability [501]. It was reported that the absolute bioavailability of NAR was only 4% in rabbits when orally administered, where it was postulated that the low bioavailability was due to its poor solubility in gastro-intestinal fluid [502]. Although several studies were carried out to improve its water solubility and stability by using nano-dispersion [503] or enzymatic condensation [504] techniques, the solubility of NAR was not sufficiently improved. As an example, following the enzymatic hydrolysis processes at high temperature (303 K) and pressure (160 MPa), the maximum solubility of NAR was only increased by 3-fold to 1.5 M (in acetate buffer at 303 K) [504]. In addition, it is challenging for most drugs to reach therapeutic levels in intraocular tissues due to various barriers, as discussed in Chapter 1. Therefore, an efficient and non-toxic drug carrier merits investigation. The use of cyclodextrin (CD) to form an inclusion complex with the drug was found to be a promising approach to improve versatility, thermal stability, loading and controlled releasing profiles for many poorly water-soluble drugs [505-507].

As mentioned in Section 1.3, derivatized CDs from the three parent groups have been shown to improve the inclusion capacity as well as solubility in an aqueous environment. SBE-ß-CD is a polyanionic ß-CD derivative composed of 7 α-D glucopyranose units with a molecular weight of approximately 2163 g/mol [508]. With an average of 7 substitutions, it possesses much greater water solubility compared to

its parent ß-CD. In addition, due to the hydrophobic butyl side arms that extend the hydrophobic cavity of SBE-ß-CD, the inclusion ability of this CD is generally greater than its parent CD (Figure 4.1). Compared to commercial eye drops (8558.77 ± 2701.00 µg/mL.min), the inclusion complex formulation (15803.40 ± 2478.08 µg/mL.min) was 1.7 to 1.8-fold higher in chloramphenicol (CHL) pharmacokinetic parameters in rabbit tear fluid. In addition, ocular irritation tests of the CHL:SBE-ß-CD eye drops were also carried out, which indicated a good comfort profile [509].

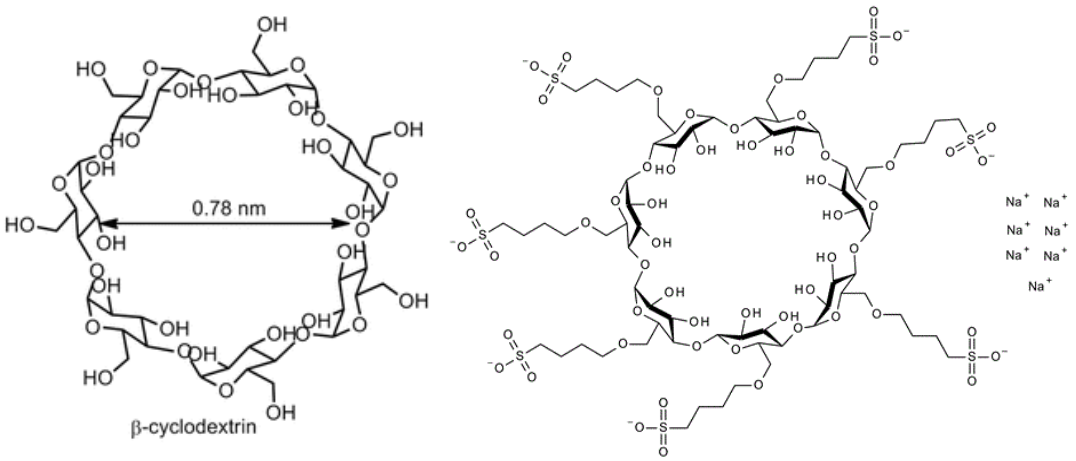

Figure 4.1: Molecular structure of ß-CD (left) [207] and SBE-ß-CD (right).

This chapter will investigate the formation of an inclusion complex of NAR:SBE-ß-CD to increase NAR aqueous solubility, with the aim of enhancing the drug penetration and bioavailability of NAR (Figure 4.2). Subsequently, this developed inclusion complex will be incorporated into the developed WM hydrophilic soft contact lenses (SCLs) to develop an ODDS that can provide a targeted delivery of NAR, while enhancing its permeation within the eye to reach the posterior segment of the eye more readily than NAR alone.

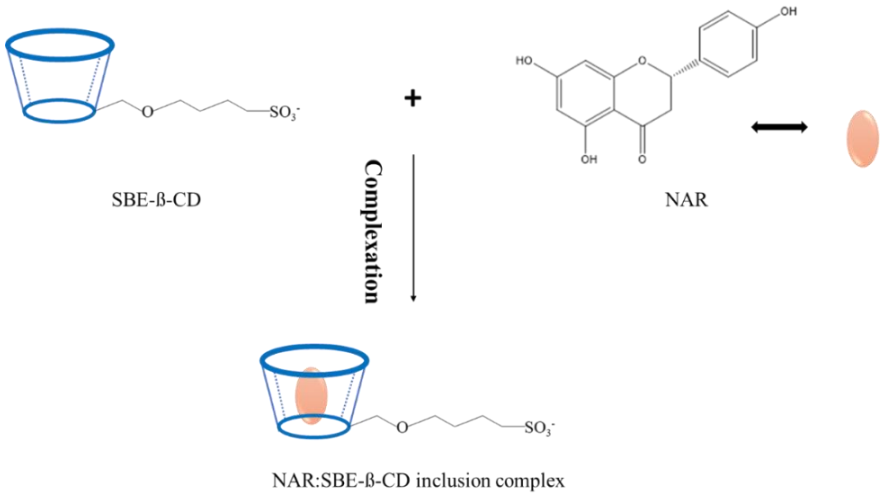

Figure 4.2: Schematic representation of the formation of NAR:SBE-ß-CD (1:1) complex.

A phase solubility (PS) study using both the Higuchi and Connors model and the Benesi-Hildebrand model was employed to establish the complex stoichiometry for the preparation of an inclusion complex of NAR with SBE-ß-CD. The complexes were prepared using a method developed by Wang *et al.* [212], by freeze-drying of a monophasic system. The formation of the drug-CD complexes was fully characterized using TGA, DSC and FT-IR to identify the optimum system for future study in subsequent chapters. Further, the solubility of the optimum complexes in water were also identified. Subsequently, the amount of NAR presented in 1 mg of the inclusion complex was determined using appropriate HPLC conditions.

4.2 Research Aims and Objectives

The aims and objectives of this chapter are:

- To identify the optimum NAR:SBE-ß-CD complexation stoichiometry and concentration ratio to formulate NAR:SBE-ß-CD complexes.
- To determine the optimum complexation method for the formation of NAR:CD inclusion complexes.
- To fully characterize the physicochemical properties of the formed NAR:CD inclusion complexes.
- To enhance NAR aqueous solubility by forming an inclusion complex with SBE-ß-CD.
- To determine the amount of drug recovery in the formed NAR:SBE-ß-CD inclusion complexes.

4.3 Experimental Methodology

4.3.1 Materials

Naringenin (>98% purity), and acetic acid (>99% purity) were purchased from Sigma-Aldrich Ireland (Wicklow, Ireland). Sulfobutylether-b-cyclodextrin (>98% purity) was purchased from Carbosynth (Ireland). Methanol (HPLC grade, 99% purity) were purchased from Fisher Scientific (Dublin, Ireland). Tert-butyl alcohol (>99.5%) was purchased from Acros (Ireland). Absolute ethanol was purchased from Lennox (Ireland). Ultrapure deionized water obtained from WhiteWater equipment (Dublin, Ireland) was used throughout the study.

4.3.2 Phase solubility studies of the NAR:CD inclusion complex

HPLC analysis of NAR was carried out as per Section 3.3.3 (Chapter 3).

4.3.2.1 Higuchi and Connors model (H-C model)

The experimental design was carried out based on the phase solubility (PS) studies of Higuchi and Connors [467]. Briefly, an excess amount of NAR (~8 mg) was accurately weighed into 1.5 mL vials. To three of those vials, 1 mL of ultrapure water was added to determine the intrinsic solubility of NAR. The remaining vials were used for the phase solubility study in triplicate. Eight concentrations of SBE-ß-CD (1-25 mM) were dissolved in 1 mL of ultrapure water and added to the vials. Two approaches were employed to mix the contents of the vial, the use of a roller (low profile roller, Stovall Life Science, USA) and the use of a shaker (SI500, Stuart, UK). For the shaker instrument, vials were placed vertically inside the shaker and the temperature inside the chamber was controlled and monitored. The vials were shaken at 25 °C and 36 °C at 150 rpm. For the roller instrument, vials were placed horizontally on top of the roller and the speed was set to 33 rpm. The temperature was controlled by the attached incubator to the system. In both methods, after mixing for 72 hours, the solutions were then filtered through a 0.45 µm membrane nylon filter and diluted appropriately. After dilution, samples were analysed using the HPLC method outlined in Section 3.3.3. From the linear phase solubility plot (concentrations of SBE-ß-CD vs. NAR in

mmol/L), the apparent binding constant ($K_{1:1}$), complexation efficiency (CE) and drug:cyclodextrin ratio (D:CD) were calculated according to Equations 4.1 – 4.3 [510]:

$$K_{1:1} = \frac{\text{slope}}{[S_0(1-\text{slope})]} \qquad \textbf{Equation 4.1}$$

$$CE = S_0 \times K_{1:1} = \frac{[D/CD]}{[CD]} = \frac{\text{Slope}}{(1-\text{Slope})} \qquad \textbf{Equation 4.2}$$

$$D{:}CD = 1 : \left(1 + \frac{1}{CE}\right) \qquad \textbf{Equation 4.3}$$

Where: $K_{1:1}$: the apparent stability constant (M^{-1}), S_0: intrinsic solubility of a drug (mg/mL), CE: complexation efficiency.

4.3.2.2 Benesi-Hildebrand model

To assess the possibility of SBE-ß-CD aggregation, the Benesi-Hildebrand model was applied to compare with the phase solubility obtained from the H-C model. The experimental methodology in the B-H model was similar to the H-C method. However, the concentration range of the SBE-ß-CD was smaller, at 20-125 µM. Based on the results obtained from the H-C study, only the roller method was used to carry out this experiment.

4.3.3 Naringenin:cyclodextrin complex formulation

The required stoichiometric amount of NAR and SBE-ß-CD (1:3 molar ratio, Table 4.1) was weighed out into two separate vials. A total of four solvent systems used to form the complex were investigated, including: tert-butyl alcohol (TBA), EtOH, and water with and without heat.

For the organic solvent systems, various concentrations of NAR (1-10 mg/mL) were dissolved in organic solvent. The required amount of SBE-ß-CD was dissolved in water and mixed with the drug-in-organic solvent solution. For water-only systems, various concentrations of NAR (1-5 mg/mL) were dissolved in SBE-ß-CD solution. The drug concentration in the co-solvent used in this study is detailed in Table 4.1.

Table 4.1: Various solvent/co-solvent systems and drug:CD concentrations used in the preparation of inclusion complexes.

Sample	Solvent system (D:CD)	D:CD concentration (mg/mL)
1	EtOH:H_2O	10:247.05
2		5:123.53
3		2.5:61.75
4	TBA:H_2O	5:123.53
5		2.5:61.75
6		1:24.71
7	H_2O	5:123.53
8		2.5:61.75
9		1:24.71
10	H_2O (heat at 60 °C for 3 hours)	5:123.53
11		1:24.71

Removal of organic solvent was carried out by evaporation prior to the lyophilisation process. Several trials for the formulation of drug:CD complexes were carried out as noted in Table 4.2.

Table 4.2: Different work-up and evaporation approaches in the formation of inclusion complexes.

Trials	Work-up approach	Organic solvent evaporating approach
1	After adding CD solution to drug solution, the mixture was stirred overnight or 3 hours (for water-heat system only).	Constant flow of N_2 gas on the surface of the monophase system
2		Rotary evaporator: 35 °C
3		Vacuum centrifuge (Scanspeed 32, Scanvac, Malaysia): 40 °C with speed set at 1500 rpm.

For the complex prepared in the water system (heat and no-heat), instead of an evaporation step, the solvent system was filtered through a 0.45 µm nylon membrane filter post stirring. It was subsequently freeze-dried for further analysis. The samples were freeze-dried without cryoprotectant. This was because in two trial batches, when 1% of cryoprotectant (trehalose) was used, a precipitation could be observed prior to freeze-drying.

4.3.4 Characterization of naringenin:cyclodextrin complex

A physical mixture (PM) was prepared by homogenously mixing an accurate amount of NAR and SBE-ß-CD (1:3 molar ratio) in a 10 mL vial.

The following techniques were carried out as per methodologies described in Section 2.3.4: thermogravimetric analysis (TGA), differential scanning calorimetry (DSC) and Fourier-transform infrared spectroscopy (FT-IR), with the following deviations:

- FT-IR: only the KBr disc technique was used in this analysis.
- DSC: all samples were analysed at 10 °C/min ramp rate from 20 °C - 300 °C.

Statistical analysis was carried out as per Section 2.3.4.

4.3.5 Quantification of naringenin in the inclusion complexes

For the freeze-dried sample, an investigation into the optimum solvent system to break the complexes to accurately quantify the amount of NAR was carried out. Full details of this study are shown in Table 4.3.

The chromatographic conditions for this experiment were the same as outlined in Section 3.3.3. Briefly, 10 µL of each solvent system at each stage (e.g., post stirring and post-centrifuge/post-filtration) was withdrawn and pipetted into a HPLC vial, which was diluted using 990 µL of MP.

Table 4.3: Details of experimental set-up for the analysis of the amount of drug in 1 mg of the complex.

Batch # (n = 3)	**MeOH (µL)**	**Water (µL)**	**Batch # (n = 3)**	**Water (µL)**	**DMSO (µL)**
1	1000	-	8	1000	-
2	800	200	9	900	100
3	600	400	10	800	200
4	400	600	11	600	400
5	200	800	12	400	600
6	200	800	13	200	800
7	100	900	14	-	1000

After preparing the stock solutions as per Table 4.3, appropriate dilutions (1:5 v/v) in mobile phase were prepared for chromatographic analysis.

4.4 Results and Discussion

4.4.1 Phase solubility studies of the NAR:CD inclusion complex

4.4.1.1 Higuchi and Connors model (H-C model)

Before commencing the full study on phase solubility of NAR and sulfobutylether-ß-cyclodextrin (SBE-ß-CD), an investigation to determine the most suitable technique between the roller shaker methods was carried out. Based on the linear range from previous studies on NAR in Section 3.4.1, three concentrations were chosen (0, 5 and 15 mM SBE-ß-CD) to run using both approaches for comparison. The outcomes from this study indicated that there was a vast variation in NAR concentration in NAR:SBE-ß-CD complexes between each run for both methods. A thermometer was placed in the roller and shaker chambers when the experiment was carried out to monitor temperature throughout the experiment. While the temperature was controlled at 25 °C ± 1 °C inside the roller chamber, an offset (higher) of 6-8 °C was observed inside the shaker chamber across all three runs.

In both approaches, the highest standard deviation was observed at 15 mM CD. NAR concentration was determined to be 6.822 ± 0.632 mM in the roller method, while in the shaker method, a concentration of 8.903 ± 1.340 mM of NAR was determined. Therefore, since the temperature was better controlled using the roller method and the variation was also less than the shaker method, the roller method was chosen to be the most suitable approach for the phase solubility study. It should be noted that the speed used in this study for the roller method was chosen to be 33 rpm (maximum speed of the system). The results are detailed in Table 4.4.

Table 4.4: NAR concentration at three SBE-ß-CD concentrations generated by the roller and shaker methods (n = 3).

[CD] (mM)	**[NAR] (mM)**	
	Roller method	**Shaker method**
0	0.013 ± 0.009	0.013 ± 0.008
5	1.596 ± 0.491	2.269 ± 0.519
15	6.822 ± 0.632	8.903 ± 1.340

The phase solubility diagrams of NAR:SBE-β-CD complexes prepared using the roller method (at 25 °C and 36 °) are shown in Figure 4.3.

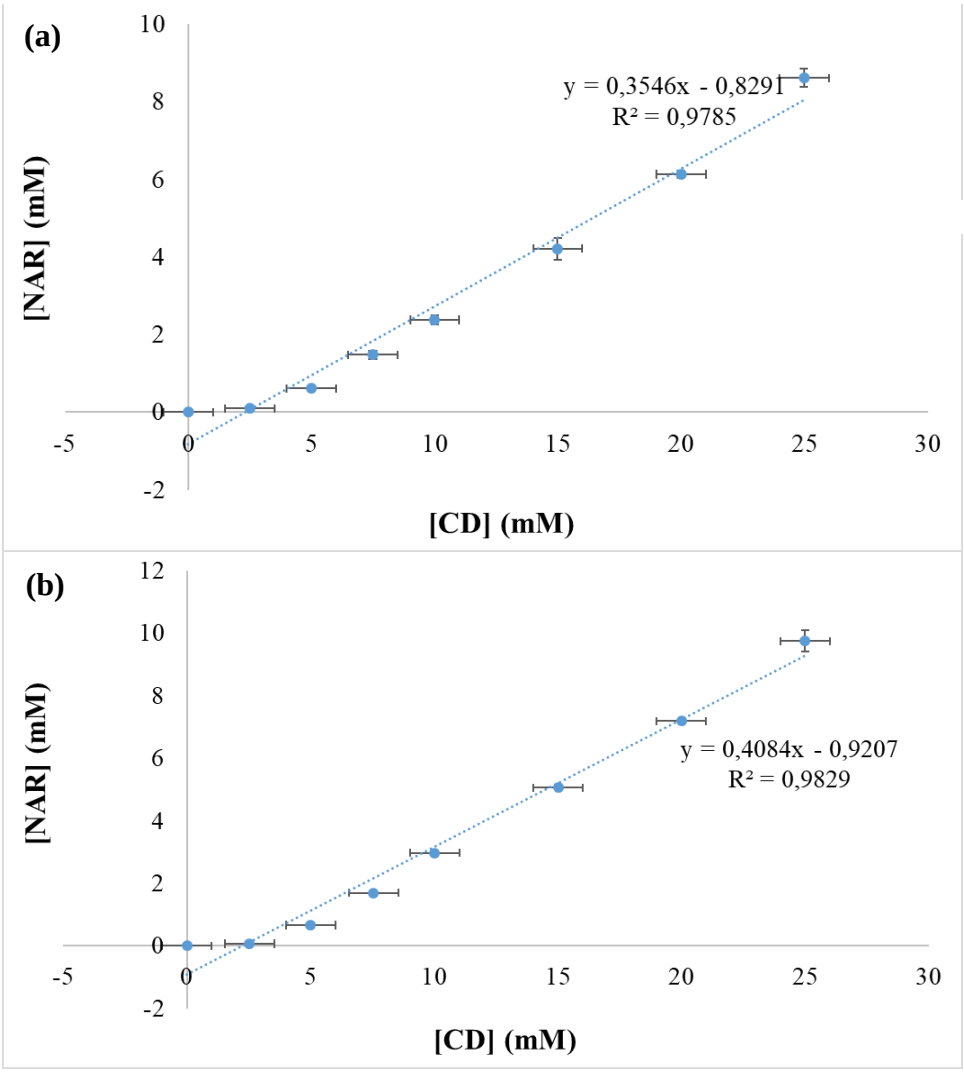

Figure 4.3: Higuchi and Connors phase solubility plots using the roller method (n = 3) at (a) 25 °C, (b) 36 °C.

The trend obtained from the graphs can be classified as type A_L (linear diagram) according to the Higuchi and Connors classification system [214] and was observed in several PS studies for drug:CD systems [212, 467, 509, 511]. As can be observed from the graphs, the apparent solubility of NAR increased linearly as the concentration of SBE-ß-CD increased across the studied concentration range. The intrinsic solubility of NAR was determined to be 0.0005 mg/mL at 25 °C and 0.002 mg/mL at 36 °C, which were in a similar range to the previously reported values, 0.0003 mg/mL at 25 °C and 0.0006 mg/mL at 36 °C [501, 512, 513].

Due to high water solubility and the large hydrophobic cavity of SBE-ß-CD, the water solubility of NAR was statistically improved following the addition of SBE-ß-CD. The solubility study was carried out by gradually dissolving 10 mg of complex in water, which resulted in a concentration of 80 mg of complex per mL, equivalent to 3.24 mg/mL of NAR. A substantial increase in NAR solubility from 0.0005 mg/mL to 3.24 mg/mL was observed after forming an inclusion complex with SBE-ß-CD, which is equivalent to a 6480-fold enhancement in NAR solubility. Yang *et al.* [506] assessed the solubilizing effect of various CDs on the solubilisation of NAR. Their study indicated that the solubility of the NAR:ß-CD complex was dramatically increased from 4.38 µg/mL (intrinsic solubility) to 1.34, 1.52 and 1.60 mg/mL, which is equivalent to a 306-, 347-, and 365-fold increase in NAR solubility, respectively, by complexing with ß-CD, trimethyl-ß-CD and dimethyl-ß-CD, respectively. The difference in the magnitude of increase in solubility between the present study (0.5 µg/mL) and Yang *et al.* (4.38 µg/mL) was due to the difference in the recorded intrinsic solubility of NAR.

In addition, since the slope (Figure 4.3) was less than 1, this indicated that a 1:1 complex between NAR and SBE-ß-CD was formed [212, 467]. Two temperatures, 25 and 36 °C, were studied in this work to determine the apparent stability constant ($K_{1:1}$) values of the formed NAR:CD complex. $K_{1:1}$ values obtained by Zhang *et al.* utilizing experimental conditions for a PS study on NAR and SBE-ß-CD were 4427 M^{-1} and 2959 M^{-1} at 25 and 36 °C, respectively [467]. The binding constant values from the present study were significantly lower (1001.76 ± 94.02 M^{-1} at 25 °C and 434.22 ± 11.09 M^{-1} at 36 °C). As the $K_{1:1}$ constant is defined by the slope and the intrinsic solubility (S_0) of the drug in the aqueous complexation medium based on Equation 4.1, the intercept (S_{int}) of the PS diagram should ideally be the same as S_0 [214]. However, since the $K_{1:1}$ value is very sensitive to the composition of the aqueous complexation medium, along with high inaccuracies associated with measuring the S_0 of a compound, these constants are often inaccurate and difficult to replicate [510].

It is commonly believed that an inclusion complex between a molecule and CD is always formed as some lipophilic moiety of the molecule enters the hydrophobic cavity of CD [510]. Many studies have demonstrated that the most common stoichiometry for drug:CD complexes is 1:1, which were determined based on the

Higuchi and Connors model [144, 467, 505, 509]. PS studies on budesonide and salmeterol xinafoate in ß-CD and HP-ß-CD (2-hydroxylpropyl) aqueous solution with various concentrations was investigated by Wang *et al.* [212]. The shaker method approach at 37 °C was used and the PS diagrams in both cases indicated the formation of 1:1 complex. The PS studies at various temperatures (e.g., 30 °C, 37 ° and 45 °C) of flavanones including NAR and hesperetin in methylated-ß-CD solution were carried out by Sangpheak *et al.* [514] with a linear relationship in PS studies for all complexes (Figure 4.4).

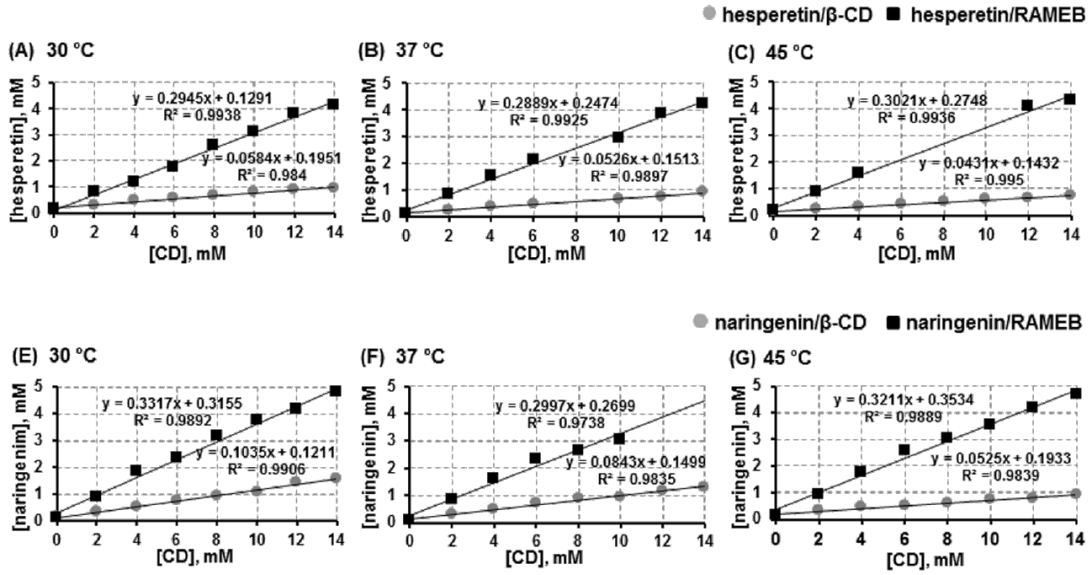

Figure 4.4: Phase solubility study of hesperetin and naringenin with ß-CD and RAMEB (the randomly methylated-ß-CD) in water at 30 °C, 37 °C and 45 °C [514].

Loftsson *et al.* proposed a more accurate way to determine the solubilizing efficiency of CD, which is to determine its complexation efficiency (CE) [510]. CE represents the concentration ratio between CD in a complex and free CD. Using the CE to determine the NAR:CD molar ratio was postulated to be more accurate since CD was shown to have an ability to form not only inclusion complexes but also non-inclusion complexes [510]. Depending on the solvent system used, various types of complexes can co-exist. Additionally, pure CD and CD complexes were noted to form aggregates, those that were able to solubilize hydrophobic molecules through a micellar-type mechanism [515, 516]. Further, Duan *et al.* [517] also cited that common pharmaceutical excipients like buffer salts or polymers can also be involved in the formation of the complex. As this value is calculated only from the slope of the PS plot, it is independent of both S_0 and S_{int}.

From the calculated CE value in this study, the NAR:CD molar ratio that is correlated to the expected amount in the formulation can be calculated. Generally, the CE values of poorly soluble lipophilic drug forming complexes with a chosen CD are below 1.5 with an average value of around 0.3 [518]. Based on Equation 4.2, the CE values for the complexes formed at 25 and 36 °C were calculated to be 0.55 ± 0.01 and 0.68 ± 0.01, respectively. Subsequently, the corresponding NAR:CD molar ratio for each system was calculated (Equation 4.3) to be 1:3. This value indicated that in order to form a 1:1 inclusion complex between NAR and SBE-ß-CD, a molar ratio of 1:3 NAR:CD in the complexation medium is required. Therefore, the NAR:CD complexes were prepared in a concentration ratio of 1:3 as detailed in Table 4.5.

Table 4.5: Molar ratio and mass ratio calculations for NAR and SBE-ß-CD.

	Drug (naringenin)	**Cyclodextrin (SBE-ß-CD)**
Molar ratio	1	3
M.W (g/mol)	272.26	2242.05
Mass ratio	272.26	6726.15
Mass ratio between D:CD	1 : 24.71	

4.4.1.2 Benesi-Hildebrand model

The phase solubility diagrams for NAR in an SBE-ß-CD inclusion complex system prepared using roller methods at 25 °C are shown in Figure 4.5.

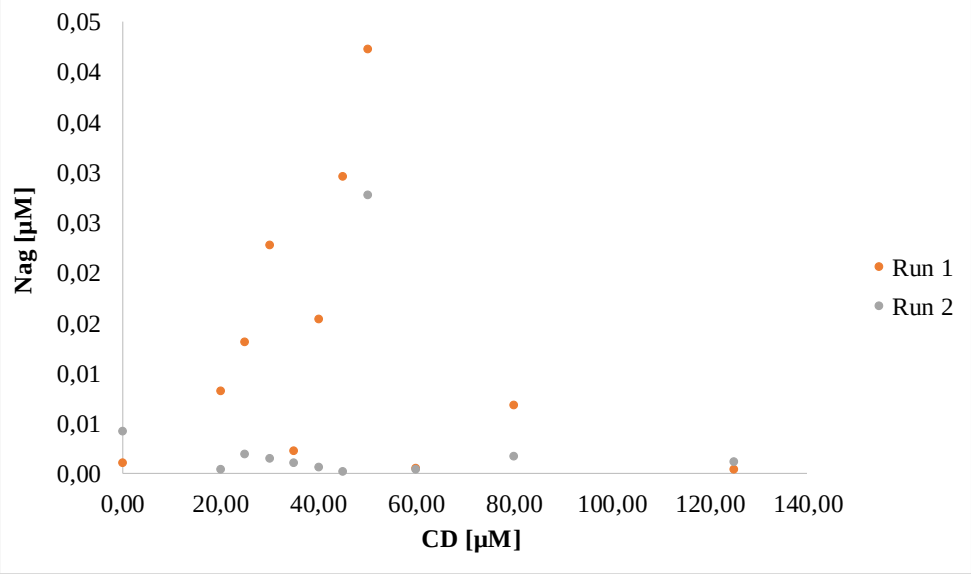

Figure 4.5: Benesi-Hildebrand phase solubility plots at 25 °C (n = 2).

As can be seen from the plot in Figure 4.5, the correlation of NAR across 11 different concentrations of SBE-ß-CD was poor. No correlation could be observed and so the binding constant $K_{1:1}$ could not be calculated in this case. A study carried out by Yang *et al.* [519] cited that this method not only results in high relative error but also has a low success rate. As a result, the poor correlation observed through this model could be expected. Therefore, the B-H phase solubility model was unsuitable to be used to study the binding characteristics between NAR and SBE-ß-CD.

4.4.2 Formation of the naringenin:cyclodextrin inclusion complex

Various approaches have been implemented in the formulation of hydrophobic drug-cyclodextrin (CD) complexes. The solvent evaporation technique requires excessive organic solvent use and also requires the removal of residual solvents [212], while the grinding and slurry approach is time-consuming [212, 520, 521], the co-precipitation method is not suitable for heat sensitive drugs since it needs high temperature with a large amount of CD [212, 521, 522]. In order to overcome these limitations, a different approach in preparing an inclusion complex was identified to be freeze-drying of a monophasic system as introduced through the study of Wang *et al.* [212]. Budesonide and salmeterol were complexed with ß-CD and HP-ß-CD, respectively using a TBA:water system, and utilizing a freeze-drying approach. The phase solubility profiles of the aforementioned study, based on Higuchi and Connors model, indicated that a 1:1 complex was formed in all cases [212].

Although EtOH has a negative long-term effect on the corneal surface, it is widely used in ocular surface surgeries [523]. TBA is a good solvent for hydrophobic drugs which can also improve the stability of water labile therapeutics [212], with recorded vapour pressure of 26.8 mmHg at 20 °C and melting point of 24 °C [524]. Furthermore, TBA could also enhance sublimation rates that in turn prevented the sample from reaching its collapse temperature (i.e., the maximum allowable temperature of a sample) [525]. Together with its low toxicity profile and miscibility with water, TBA is considered as an ideal freeze-drying solvent. A range of NAR concentrations, from 1 mg/mL to 10 mg/mL was investigated throughout this study (as noted in Table 4.1) to determine the potential maximum NAR concentration that was able to form a complex with SBE-ß-CD. It was observed that the high drug concentration in the EtOH:water system (10 mg/mL), TBA:water system (10 and 5 mg/mL), and heat and

no-heat water systems (10 mg/mL) did not result in a clear solution, and the precipitation could be seen. This observation suggested these concentrations went past the maximum solubility of NAR and resulted in the formation of insoluble complexes. Hence, these concentrations were not used for further study.

It is essential to determine an optimal ratio between organic solvent:water to ensure the physical stability of both drug and CD in order to promote the formation of a drug:CD complex. It was determined that SBE-ß-CD was sparingly soluble in most organic solvents including TBA and EtOH, while NAR has a very limited solubility in water. To ensure an equal strength of co-solvent between water and organic medium to obtain a clear solution, a 1:1 v/v ratio was used. A lipophilic drug can partition into the cavity of CD through various intermolecular interactions, those such as hydrogen bonding, hydrophobic, and van der Waals interactions [212, 526].

Due to the limitation of the available freeze-drying system (freeze-dryer, FreeZone 2.5, Labconco, USA) that only reaches to approximately -50 °C, the organic solvent was evaporated off as much as possible prior to this step. This is because most organic solvents have a higher freezing point than -50 °C, which could be trapped in the pump of the freeze-dryer and damage it. A total of 3 approaches were examined to identify the optimum method for evaporating organic solvent in this study, which were N_2 gas, rotary evaporator, and vacuum centrifugation (Table 4.2). While only one sample could be used at a time with rotary evaporator, the use of N_2 gas was unfavourable due to the challenge of maintaining a constant flow of gas from batch to batch.

Evaporating the solvent from the NAR:CD mixture using a vacuum centrifuge also resulted in a homogenous monophase solution. Therefore, it was determined to be the optimum approach to use in the preparation of NAR:CD complexes. The centrifugation temperature was determined to be 40 °C. Temperatures below 40 °C resulted in prolonged centrifugation time (i.e., at 30-35 °C, it took ~8-10 hours to evaporate ~2 mL). Higher temperature, on the other hand, could cause the sample to degrade. Since both EtOH and TBA have lower boiling points (78 °C and 82 °C, respectively) than water, they would evaporate before water. Therefore, once the volume in the tubes decreased by half, the system at this time should only contain water.

The formation of NAR:CD complexes was carried out using a 1:3 ratio following the results from the Higuchi and Connors phase solubility study. Four different systems included EtOH:water, tert-butyl alcohol (TBA):water and water only (with and without heat) were assessed in this study, as summarised in Table 4.6. These complexes were then characterized to identify the optimum system that would be used in the formulation of NAR-loaded chitosan nanoparticles (Chapter 5) and complex-loaded SCLs (Chapter 6).

Table 4.6: Co-solvent systems and NAR:CD concentrations used in the preparation of complexes.

Co-solvent system	Weight in 1 mL (mg)		Naringenin concentration (mg/mL)
	Cyclodextrin	Naringenin	
Water:TBA	61.75	2.50	1.25
	24.71	1.00	0.50
Water:EtOH	123.53	5.00	2.50
	61.75	2.50	1.25
Water (no heat)	123.53	5.00	5.00
	24.71	1.00	1.00
Water (heat at 60 °C)	123.53	5.00	5.00
	24.71	1.00	1.00

4.4.3 Characterization of NAR:SBE-ß-CD complex

4.4.3.1 Thermogravimetric analysis

The thermal properties of raw materials (NAR and SBE-ß-CD), a physical mixture of the two, and the NAR:SBE-ß-CD complexes formed under various solvent systems

were investigated by thermogravimetric analysis (TGA) (

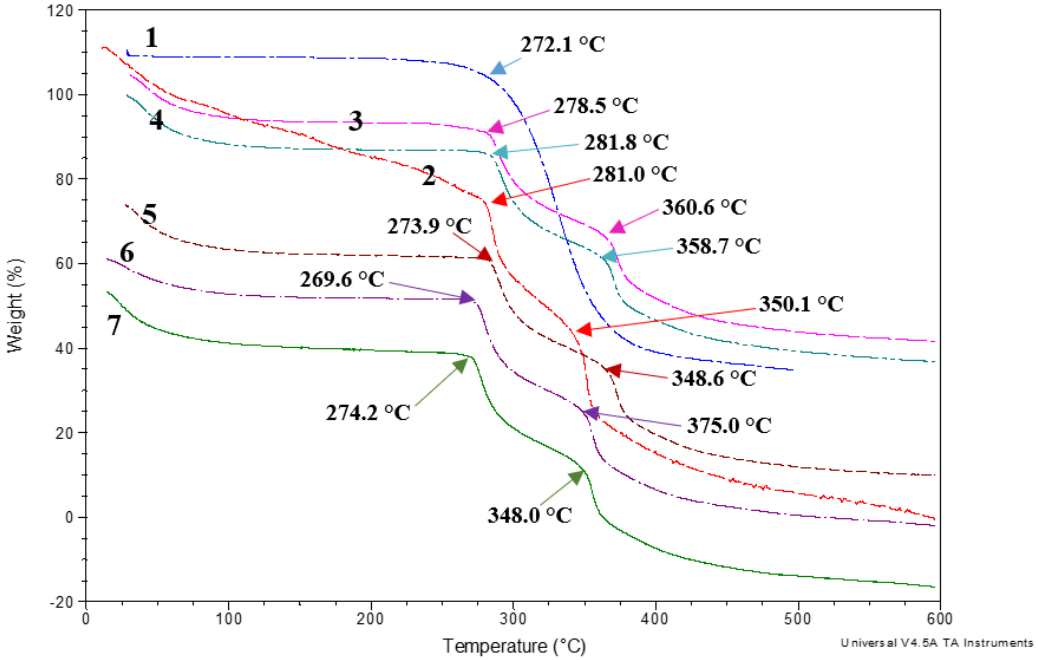

Figure 4.6).

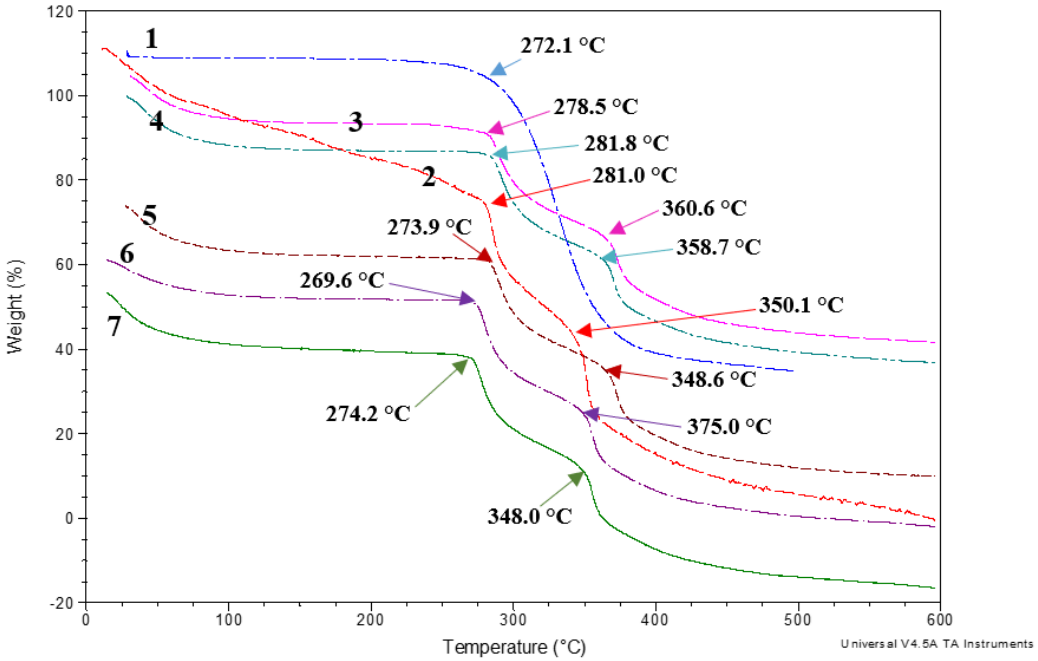

Figure 4.6: TGA of naringenin (1, blue), physical mixture (3, pink), SBE-ß-CD (4, teal), and inclusion complex formed in a TBA:water co-solvent system (2, red), EtOH:water co-solvent system (7, green), water system (5, maroon) and water-heat system (6, purple) (n = 3).

TGA was carried out to investigate the thermal stability of the raw materials and the inclusion complexes formed using various co-solvent systems. The TG curves in

Figure 4.6 indicate that NAR decomposed at 272.1 ± 4.7 °C. Thermal stability of flavanone and its derivative (6-hydroxyflavanone) was studied by Ferreira *et al.* [527]. Their work showed that the flavanone derivative exhibited a higher stability compared to its parent compound flavanone, which exhibited a mass loss at around 250 °C while in flavanone, degradation started at around 200 °C. NAR was expected to exhibit a higher thermal stability than both flavanone and 6-hydroxyflavanone since its molecular weight was higher (272 vs. 224, 240 g/mol, respectively) [527]. As for SBE-ß-CD, the first degradation point was found to be within a wide range between 70-80 °C, is associated with the loss of loosely bound water. Two degradation points could be observed at 278.5 ± 9.7 °C and 355.3 ± 12.4 °C for SBE-ß-CD. A similar degradation temperature of SBE-ß-CD was seen at around 270 °C in a study by Bettinetti *et al.* [528]. The physical mixture exhibited a similar trend to NAR and SBE-ß-CD with the two degradation temperatures at 278.5 ± 7.4 °C and 360.6 ± 9.1 °C.

In this study, a statistically significant increase in the first degradation point of the complex formed in the TBA:water co-solvent system was observed in comparison to NAR (281.0 vs. 272.1 °C, p-value < 0.05). This suggests that complexation of NAR and SBE-ß-CD results in a material that exhibits higher decomposition temperatures and was in agreement with previous studies [529, 530]. Following the formation of the inclusion of *cis*-jasmine in ß-CD, the thermal stability of *cis*-jasmine was enhanced. *Cis*-jasmine started degrading at 30 °C and the decomposition of the *cis*-jasmine-ß-CD complex began at 227.5 °C [529]. On the other hand, the first degradation temperature from the NAR:CD complexes formed in the remaining three systems showed a statistically insignificant difference (p-value > 0.05) to NAR, which indicated that the complexes formed were not as stable as complex formed using TBA:water system.

4.4.3.2 Differential scanning calorimetry

Thermal analysis by DSC has been widely applied by various research groups to examine the complexation of an antioxidant and CD complexes. A DSC thermogram of each component included in the preparation of the inclusion complex, which are NAR, SBE-ß-CD, and physical mixture, is shown in Figure 4.7.

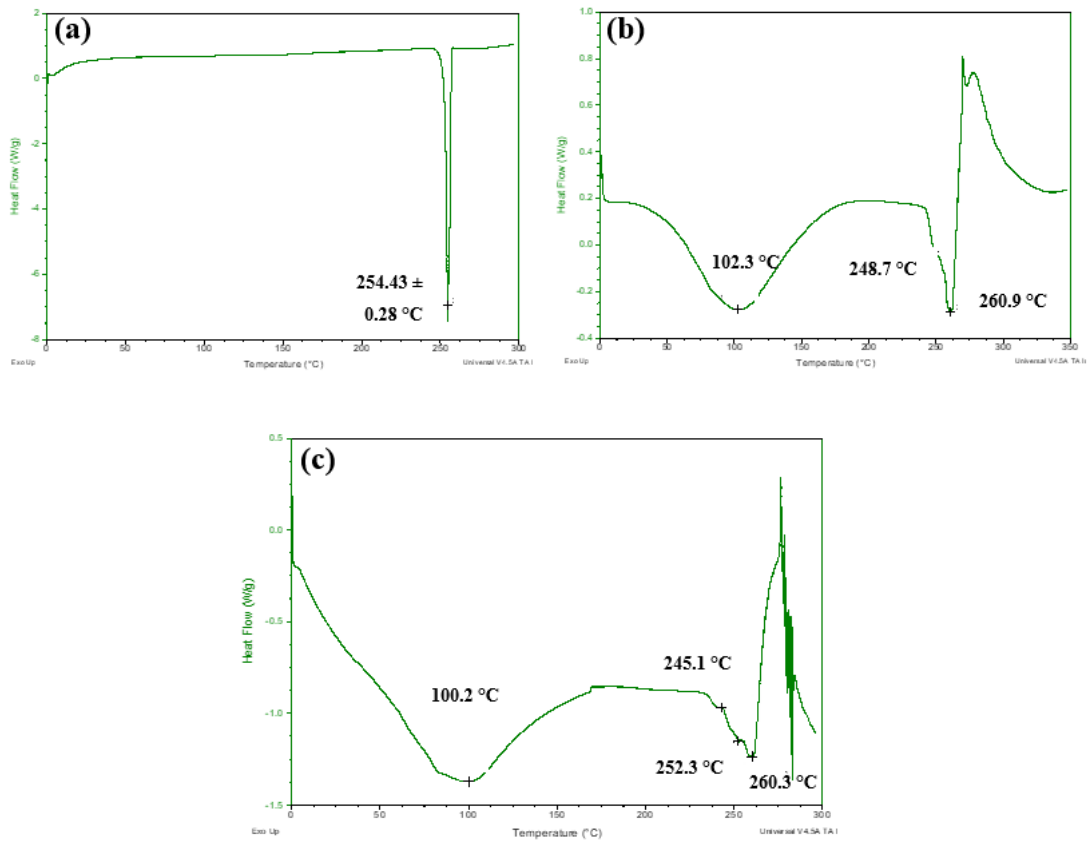

Figure 4.7: DSC thermograms of (a) naringenin, (b) SBE-ß-CD and (c) physical mixture (n = 3).

It could be seen that NAR demonstrated a sharp endothermic peak at 254.43 ± 0.28 °C corresponding to its melting point, a property illustrative of a highly crystalline compound as recorded in Section 3.4.2.1. The thermal analysis of SBE-ß-CD showed a broad endothermic peak around 102.3 ± 6.49 °C corresponding to the liberation of crystalline water, and distinctive melting/decomposition peaks could be seen at 248.7 ± 0.78 and 260.9 ± 0.9 °C. Even though the SBE-ß-CD DSC thermogram varied between studies, it could be seen that its melting/degradation points occurred at two temperatures such as at 232 °C and 240 °C [467], 212 °C and 258 °C [505], 260 °C and 270 °C [528], and 218 °C and 230 °C [531]. As for the NAR and SBE-ß-CD physical mixture that was prepared using a 1:3 ratio, its thermogram was very similar to that of SBE-ß-CD. However, a small melting peak at around 252.3 ± 2.6 °C could still be seen which was not present in SBE-ß-CD thermogram, suggesting the presence of NAR. This observation suggested that there was no inclusion complex formed between SBE-ß-CD and NAR.

A small shift in drug melting point in the PM was previously seen in a study carried out by Zhao *et al.* [144]. The melting peak of ibrutinib was 159.2 °C, which shifted to 155.8 °C in the PM of ibrutinib, SBE-ß-CD and chitosan.

Figure 4.8 presents the DSC thermograms of the four NAR:CD complexes formed in the four co-solvent systems. DSC has been used to identify the formation of inclusion complex based on the disappearance of the drug endothermic peak [201, 467, 505, 531]. As can be observed from **Figure 4.8**, each different co-solvent system used in the preparation of the inclusion complexes resulted in different thermograms.

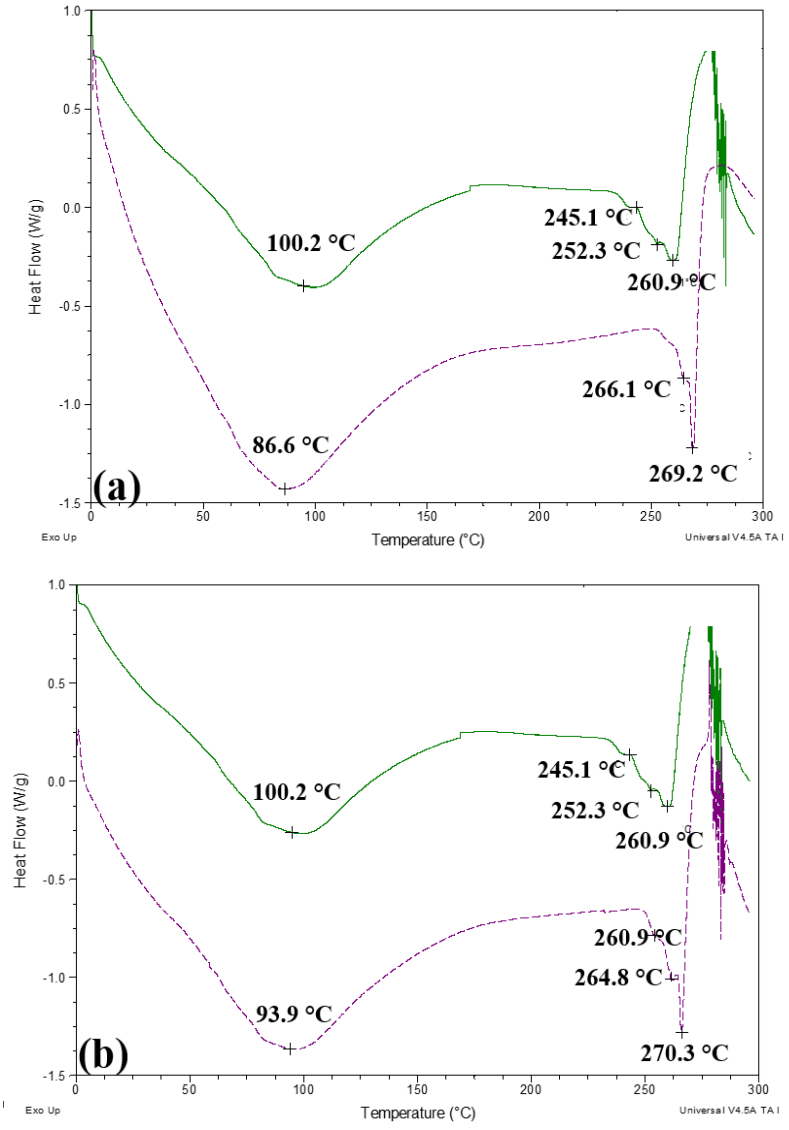

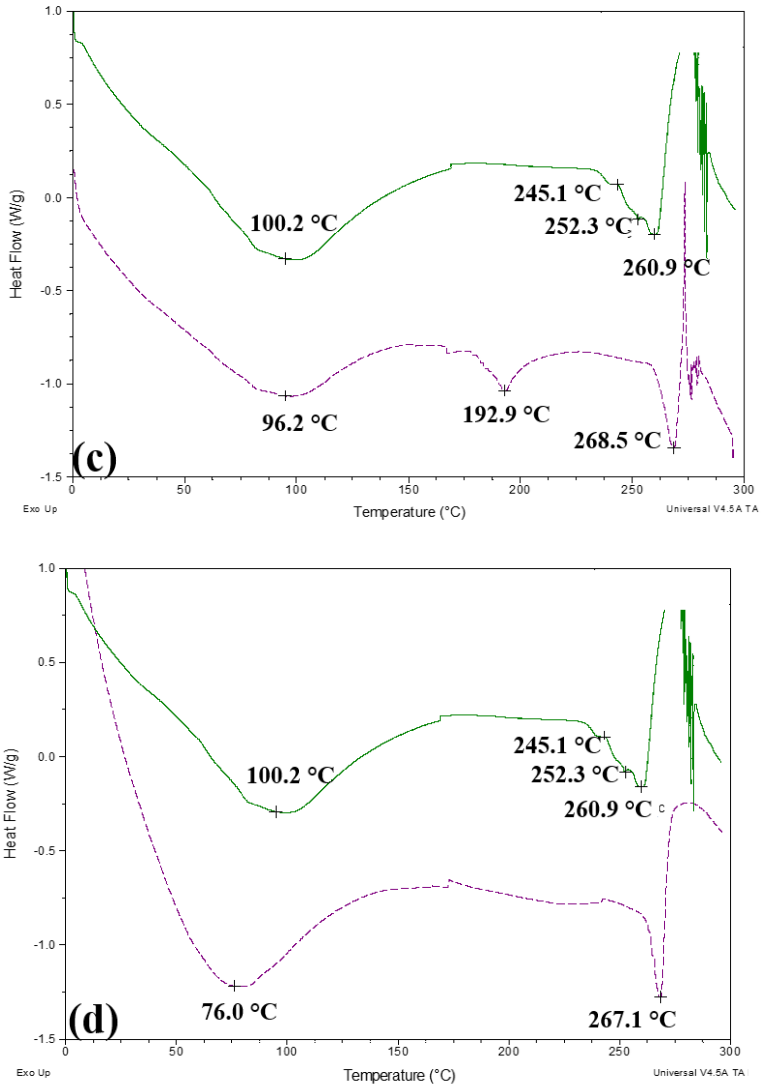

Figure 4.8: DSC thermograms of the various inclusion complexes (2.5 mg/mL) prepared using different solvent/co-solvent systems (purple-short-dash line) with the PM (green-solid line) (a) water complex, (b) water-heat complex, (c) EtOH:water complex, and (d) TBA:water complex (n = 3).

For water-heat system, the characteristic melting peak of SBE-ß-CD could still be seen, although it shifted from 245.1 °C to 260.9 °C for the first melting peak, and 260.9 °C and 270.3 °C for the second melting peak (p-value < 0.05), respectively. A similar shift in both melting peaks of SBE-ß-CD was also observed in the complexes prepared in water system with heat. Additionally, melting peaks of NAR were still visible in the DSC thermograms for water with and without heat systems, which were at 264.8 ± 2.4 °C and 266.1 ± 2.4 °C, respectively. These observations suggested that both systems were unsuitable to be used in the formation of stable inclusion complexes. In the case of the complex formed in the EtOH:water system, a completely different curve was

observed, illustrating a loss of loosely bound water at 96.2 ± 0.8 °C, and two melting peaks at 192.9 ± 0.2 °C and 268.5 ± 0.4 °C, suggesting the formation of an unknown molecule in the system.

For the NAR:CD complex formed in the TBA:water system, the peaks corresponding to both the melting point of NAR and the two melting/decomposing peaks for SBE-ß-CD as seen in the PM thermogram disappeared. Instead, a new peak at 267.1 ± 2.0 °C was observed, which was at a higher temperature (p-value < 0.05) in comparison to the SBE-ß-CD degradation peaks (245.1 ± 0.8 °C and 260.9 ± 0.9 °C). This indicated the formation of an inclusion complex between the drug and CD, which was also observed in the previous studies carried out by Zhang *et al.* [467] and Ficarra *et al.* [532]. As an example, a disappearance of the sharp melting peak of hespertin was also noted in the DSC thermogram of the inclusion complex formed from ß-CD and hespertin [532]. Therefore, the TBA:water system was determined to be the optimum approach in the preparation of the NAR:SBE-ß-CD inclusion complexes for this study.

4.4.3.3 Fourier-transform infrared spectroscopy

The FT-IR spectra of all NAR:CD complexes were compared with those of NAR, SBE-ß-CD, and the PM for characteristic absorption bands (Figure 4.9).

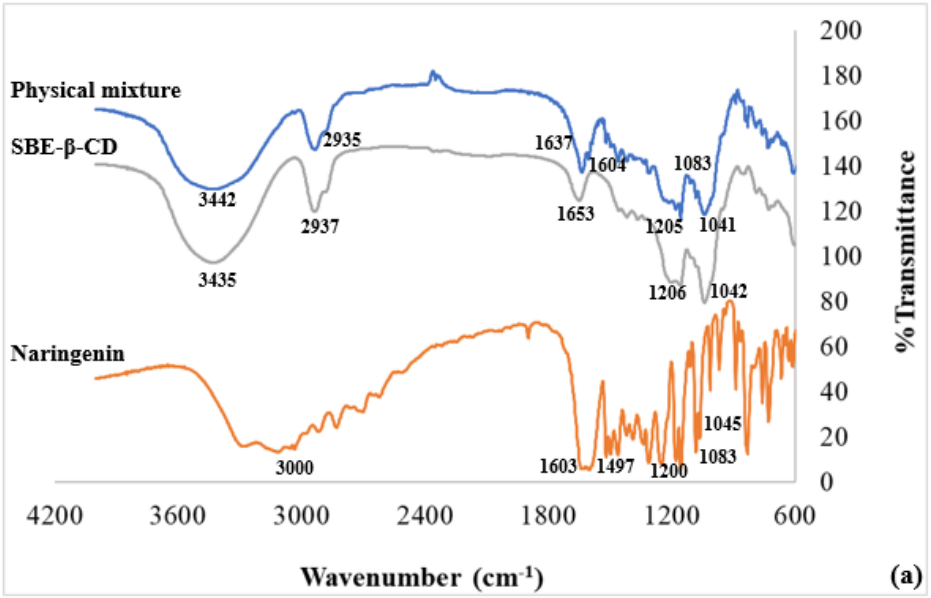
Physical mixture
SBE-β-CD
Naringenin
3442
3435
2935
2937
1637
1653
1604
1205
1083
1041
1206
1042
3000
1603
1497
1200
1045
1083
% Transmittance
Wavenumber (cm-1)
(a)

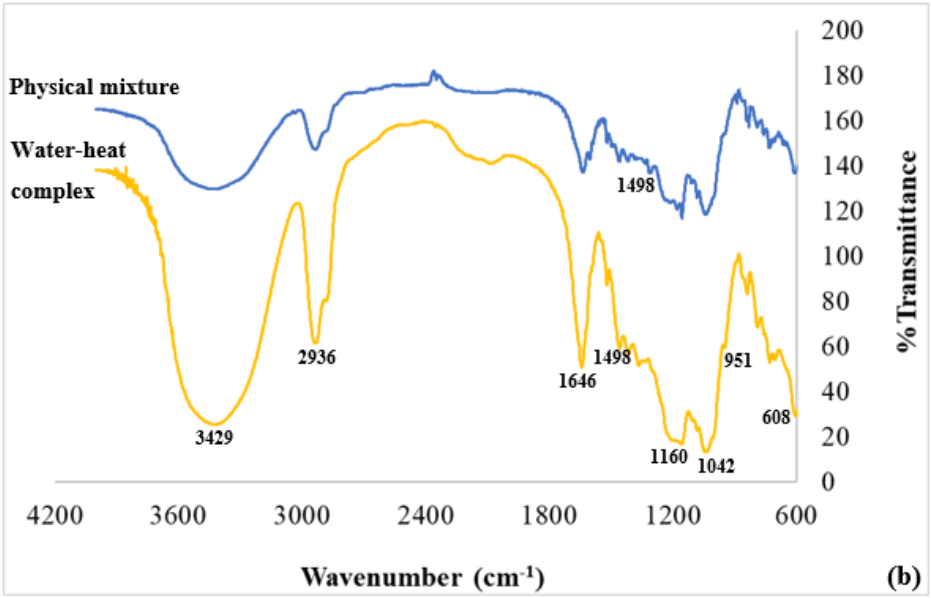
Physical mixture
Water-heat complex
1498
3429
2936
1646
1498
951
608
1160
1042
% Transmittance
Wavenumber (cm-1)
(b)

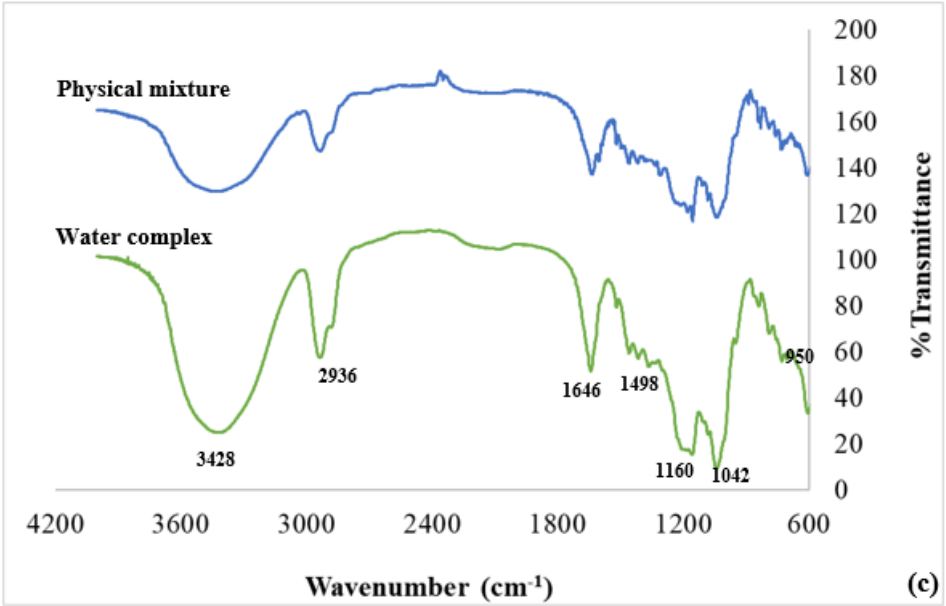
Physical mixture
Water complex
3428
2936
1646
1498
950
1160
1042
% Transmittance
Wavenumber (cm-1)
(c)

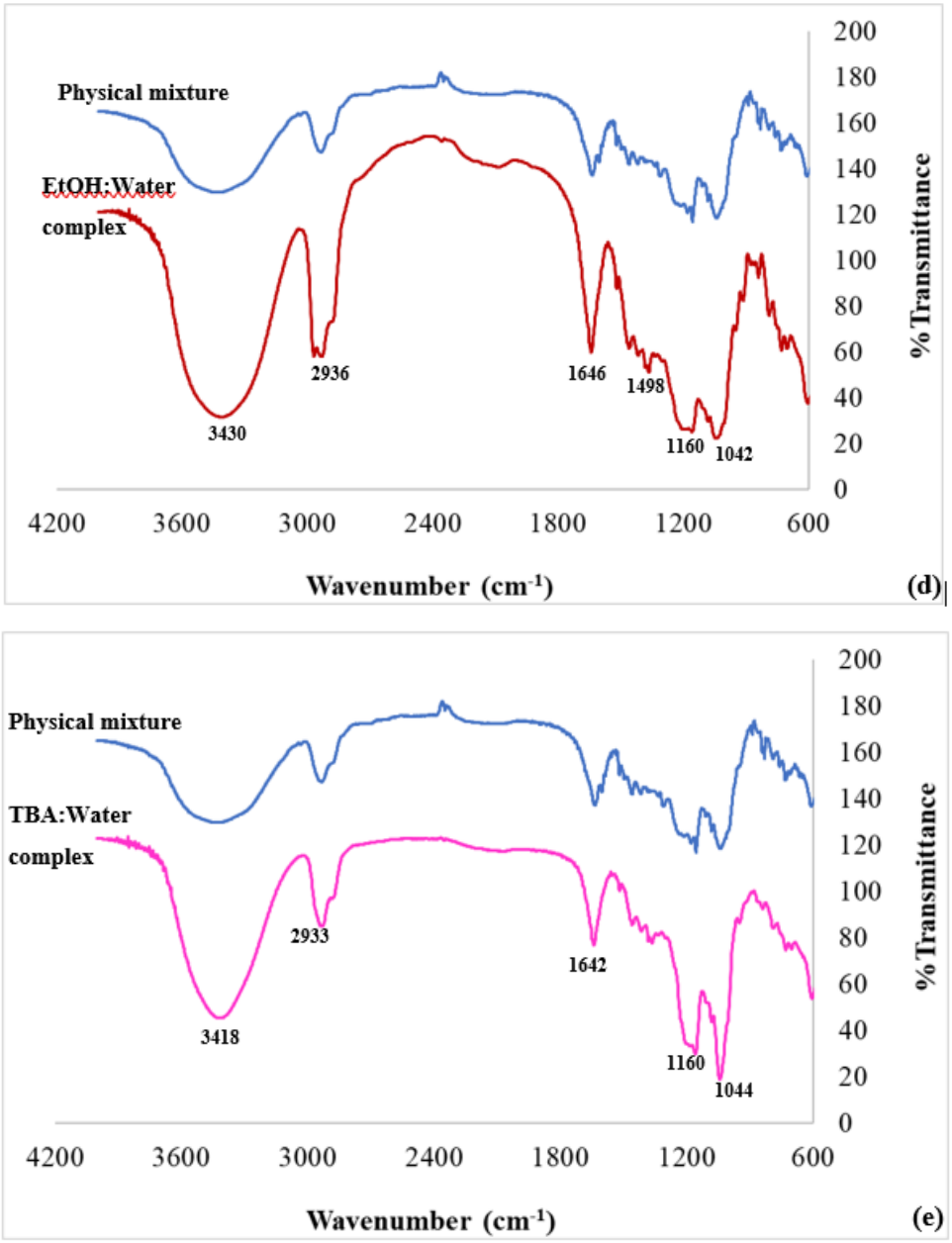

Figure 4.9: Representative FTIR spectra of a) raw materials including NAR, SBE-ß-CD and physical mixture, and various inclusion complexes prepared using different solvent/co-solvent systems, b) Water-heat, c) Water-no heat, d) EtOH:water and e) TBA:water.

The NAR spectrum showed various key peaks including: O-H stretching (3290 cm^{-1}), aromatic C-H stretching (3030 cm^{-1}), C=O stretching (1626 and 1640 cm^{-1}), and aromatic C=C stretching (between 1020 cm^{-1} and 1500 cm^{-1}) [467, 489, 490]. The SBE-ß-CD spectrum is characterized by a broad and intense peak representing O-H stretching (3430 cm^{-1}), C-H vibration (2910 cm^{-1}), CH_2 vibration at 2810 cm^{-1}, C-H stretching (1208 cm^{-1}), C-O stretching vibration (1035 cm^{-1}), and sulfoxide stretching (1042 cm^{1}).

This observation of SBE-ß-CD spectrum was in agreement with previous studies [144, 467, 505, 531]. The PM FT-IR spectrum showed a superposition spectrum of both compounds, the main functional groups bands for NAR and SBE-ß-CD were visible. It should be noted that the peak at position ~1041 cm^{-1} could represent either C-O stretching, or sulfoxide stretch (SBE-ß-CD), or C-O stretching (A ring in NAR structure). FTIR analysis has been applied widely by different research groups to investigate changes in characteristic functional groups in complexation studies [201, 213, 533, 534]. The key changes in functional groups and shift of bands of individual component upon complexation are noted in Table 4.7.

The FT-IR spectra of all the inclusion complexes formed using various co-solvent systems showed that the characteristic peaks of NAR at 1603 (C=C aromatic), 1500 (C=C aromatic), 1179 (HCC bending from A- and B- rings), 1388 and 1083 (C-O stretching from B-ring) and 889 (COO bending from B-ring) cm^{-1} had disappeared. Moreover, the characteristic peak at 1206 cm^{-1} represented C-H stretching in SBE-ß-CD also disappeared in the spectra of the complexes. In addition to the disappearance of those characteristic peaks, the absorption intensity of other peaks in the complex's spectra were reduced significantly with a shift in various functional group peaks also observed. All of these spectral changes indicated the formation of complexes as shown in the work carried out by Ficarra *et al.* [532]. Their study showed that following the complexation of NAR in ß-CD, a reduction in the intensity of the aromatic bands of NAR at 1510 and 1601 cm^{-1} was observed. In this study, a shift in a peak from 1041 cm^{-1}, which either represented functional groups in SBE-ß-CD or NAR, to 1044 cm^{-1} was observed in the TBA:water complex and to 1042 cm^{-1} in the other three systems. A shift in the characteristic C-H peak in SBE-ß-CD was also observed from 1653 cm^{-1} to 1642 cm^{-1} (the TBA:water complex) and 1646 cm^{-1} for the other three complexes. This indicated the interaction between NAR and SBE-ß-CD, and thus, the formation of new non-covalent interactions between drug and SBE-ß-CD as supported from previous studies on the inclusion complex of CDs and drug [506, 535].

Table 4.7: Summary of FT-IR analysis of starting materials and complexes [201, 213, 505, 531, 533-537].

Ref. frequency (cm^{-1})	Functional group	Raw materials (cm^{-1})			Complex system (cm^{-1})			
		Naringenin	SBE-ß-CD	Physical mixture	TBA	EtOH	Water	Water-heat
3446.4	O-H stretching	-	3435	3442	3418	3430	3428	3429
3100-2800	C-H stretching	3000	2937 – 2892	2935	2933	2936	2936	2936
1604	C=C aromatic	1603	-	1604	x	x	x	x
1644-1655	H-O-H (from water)	-	1653	1637	1642	1646	1646	1646
1500	C=C aromatic	1497	-	1498	x	1498	1498	1498
1205	C-H stretching	-	1206	1205	x	x	x	x
1200	OH phenolic NAR	1200	-	1181	1160	1160	1160	1161
1618-1019	C-C stretching (rings)	1618-1013	-	1604-1041	x	x	x	x
1183	HCC bending (A and B rings)	1179	-	1181	x	x	x	x
1283-1161	HOC bending (A ring)	1311-1155	-	1157	1160	1160	1160	1161
1388, 1083 and 971	CO stretching (B ring)	1388, 1083	-	1083	x	x	x	x
1040.7	C-O stretching	-	1042	1041	1044	1042	1042	1042
1040	Sulfoxide stretch	-						
1034 and 824	CO stretching(A ring)	1045	-	1041	1044	1042	1042	1042
996, 964 and 745	HCCC torsion (C ring)	969, 759	-	890, 760	950	951	950	951
896	COO bending (B ring)	889	-	890	x	x	x	X

As can be observed in Table 4.7, a bigger shift in all of the main characteristic bands could be observed in the TBA:water system compared to the others. Moreover, some of the characteristic bands present in NAR and SBE-ß-CD spectra were not observed in spectra of the formed complexes. Thus, this analysis implied the formation of a NAR:CD complex. Similar observations were made in previous research. Using a different drug (nintedanib) to form an inclusion complex with SBE-ß-CD, a similar observation on the FT-IR study was observed in the work carried out by Vaidya *et al.* [536]. The complex spectrum showed that the characteristic peaks of the drug had disappeared. This indicated that some functional groups of the drug were included in the cavity of SBE-ß-CD through the formation of a molecular complex. To examine the interaction within the inclusion complex formed by chrysin (a polyphenol from the flavonoid class, 5,7-dihydroxy flavones) and SBE-ß-CD, Kulkarni *et al.* [201] also used FTIR analysis to identify the changes in the complex spectrum compared to the two starting materials and physical mixture spectra. The variation in the intensities and the shift in peaks of the innate H-O-H and C-H absorption bands in the complex spectrum postulated the breaking of some hydrogen bonds, while generating of specific new ones in the inclusion complex.

A schematic illustration of the formation of the inclusion complexes of NAR in SBE-ß-CD is depicted in Figure 4.10.

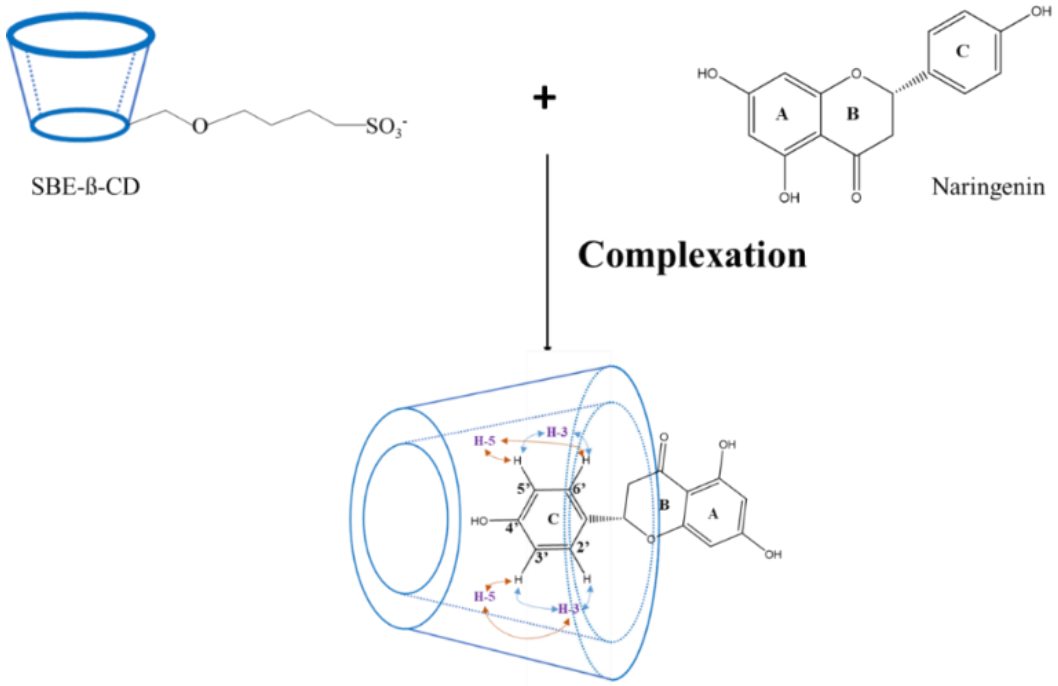

Figure 4.10: Schematic representation of the possible inclusion mode of SBE-ß-CD and naringenin and significant correlations of drug-CD inclusion complexes (adapted from Yang *et al.* study [506], based on a two-dimensional nuclear magnetic resonance (NMR) spectroscopic study).

4.4.4 Quantification of naringenin in complexes

Using the same chromatographic conditions as described Section 3.3.3 (Chapter 3), the percentage recovery of NAR in the formed inclusion complexes was investigated. Since the complex was prepared using a 1:3 NAR:CD molar ratio following the phase solubility study, the expected amount of NAR in 1 mg/mL of inclusion complex was calculated to be 38.89 µg/mL, given that 1 mg of NAR and 24.71 mg of SBE-ß-CD were used to prepare the complex.

Since accurately measuring the recovered amount of drug presented in a complex plays a vital role in the drug encapsulation efficiency study, an extensive investigation into the solubility of the complex formed was carried out. The optimum solvent combination from Table 4.3 was determined to be 200 µL MeOH : 800 µL water, which resulted in a 98.1 ± 2.4% of NAR quantified from 1 mg of formed NAR:SBE-ß-CD inclusion complex, which was equivalent to 38.9 ± 0.9 µg NAR.

4.5 Conclusions

In this chapter, a host-guest system containing NAR and SBE-ß-CD was successfully prepared and characterized. The formation of a hydrophobic drug and CD inclusion complex was investigated through phase solubility studies and prepared by a monophasic cosolvent approach.

The LOD and LOQ values of NAR were determined by HPLC method to be 0.044 µg/mL and 0.133 µg/mL, respectively. To identify the optimum stoichiometric ratio between NAR and SBE-ß-CD, a phase solubility study was carried out. This study utilised both the Higuchi and Connors and the Benesi-Hildebrand models. Due to the high variations and non-linear responses observed, the Benesi-Hildebrand model was concluded to be unsuitable to model this system. The impacts of process parameters including temperature and mixing techniques (shaker vs. roller) on the outcome of the phase solubility were also studied. The results from this work indicated that the optimum mixing approach was a roller method at 33 rpm. Intrinsic solubility of NAR in water was determined to be 0.0005 g/L at 25 °C and 0.002 g/L at 36 °C. With an increase in temperature, the binding constant decreased from 1001.7 ± 94.0 at 25 ° to 434.2 ± 11.1 at 36 °C.

The optimum NAR:SBE-ß-CD concentration ratio was determined to be 1:3 at 25 °C and the stoichiometry of the complexes was determined to be 1:1 according to the Higuchi and Connors model. This was followed by the preparation of complexes using two different approaches, one by mixing two components in water and heating at 60 °C, and the other by lyophilisation of a monophasic solution. Freeze-drying of a TBA:water co-solvent system (after evaporation of TBA) was shown to be the best approach for the preparation of a complex through various physical characterization techniques including TGA, DSC, and FT-IR. The maximum solubility of the NAR:SBE-ß-CD complex in water was determined to be 80 mg/mL, which was equivalent to 3.24 mg/mL of NAR in water. The solubility of NAR increased 6480-fold following the complexation with SBE-ß-CD when compared to its intrinsic solubility (0.0005 mg/L at 25 °C). By re-dissolving the formed complex in different solvent mixtures (MeOH, water and DMSO), HPLC analysis was performed to quantify the amount of drug present in 1 mg of the freeze-dried complex.

By redissolving the formed complex in various co-solvent systems, the NAR concentration recovered from 1 mg of NAR:SBE-ß-CD inclusion complex was determined to be 38.9 ± 0.9 µg.

Aiming to enhance the permeation of a therapeutic and its ocular bioavailability, the developed NAR:SBE-ß-CD complex will be loaded into the developed soft hydrogel contact lens in Chapter 6. The complex will be entrapped in the lens matrix by both direct entrapment and 'soak and release' approaches as described in Chapter 3.

Based on the successful preparation of a NAR:SBE-ß-CD complex, the next chapter will focus on the formulation and optimization of a novel biocompatible and biodegradable nanoparticle as a drug carrier. To this end, this drug-loaded nanoparticle system will be fully characterized to evaluate drug encapsulation efficiency/drug loading, and *in vitro* drug release behaviour of the developed nanomaterials. Consequently, this novel drug carrier can potentially sustain and control the release of NAR in the posterior segment of the eye to maintain ocular health, while preventing various eye diseases such as AMD.

CHAPTER 5

FORMULATION AND OPTIMIZATION OF NARINGENIN-LOADED CHITOSAN NANOPARTICLES FOR CONTROLLED DRUG RELEASE

5 FORMULATION AND OPTIMIZATION OF NARINGENIN-LOADED CHITOSAN NANOPARTICLES FOR CONTROLLED DRUG RELEASE

5.1 Introduction

As mentioned in Section 1.2, advances in nanotechnology and nanoscience have resulted in the development of several novel, safe, patient-friendly formulations, and drug delivery techniques. Nanoparticles (NPs) have been investigated as a potential novel drug delivery system in pharmaceutical research [538-540], specifically as an ocular drug delivery system (ODDS) [7, 541, 542]. Several advantages of using NPs as ODD vehicles have been evaluated, including: improving targeted drug delivery into cells [543], and co-delivery of two or more drugs for combination therapy [540]. Biodegradable and biocompatible natural polymers such as chitosan (CS), hyaluronic acid (HA) and ß-cyclodextrin (ß-CD) and its derivatives (e.g., sulfobutyl ether-ß-cyclodextrin, SBE-ß-CD) have been widely used in the preparation of novel ocular drug delivery systems [203, 204, 544].

CS, as introduced in Section 1.2.1, is a non-toxic, biodegradable and biocompatible cationic polymer [545]. The abundant amino groups of CS make it readily available for functionalization [546, 547]. By cross-linking with other anionic materials such as SBE-ß-CD or sodium alginate to form CS NPs, the formation of nano-carriers that can provide controlled release and targeted delivery of a therapeutic can be facilitated [467]. CS NPs were shown to increase the corneal penetration of drugs, which in turn improves their therapeutic effects for different diseases [548]. In addition, due to the interaction between cationic CS and the anionic cornea and conjunctiva, an enhancement in the concentration and residence time of drugs can be obtained, Collado-Gonzalez *et al.* [549]. Additionally, CS has been shown to act as a penetration enhancer since it can transiently open the tight junctions between cells [550].

A polyanionic derivative of ß-CD, SBE-ß-CD, has a greater water solubility as well as inclusion ability than the parent ß-CD, which is because of its hydrophobic butyl side arms and the sulphated sodium salt present in the molecule (Figure 5.1) [144]. SBE-ß-CD, being polyanionic, can form NPs with cationic CS by ionic gelation [144].

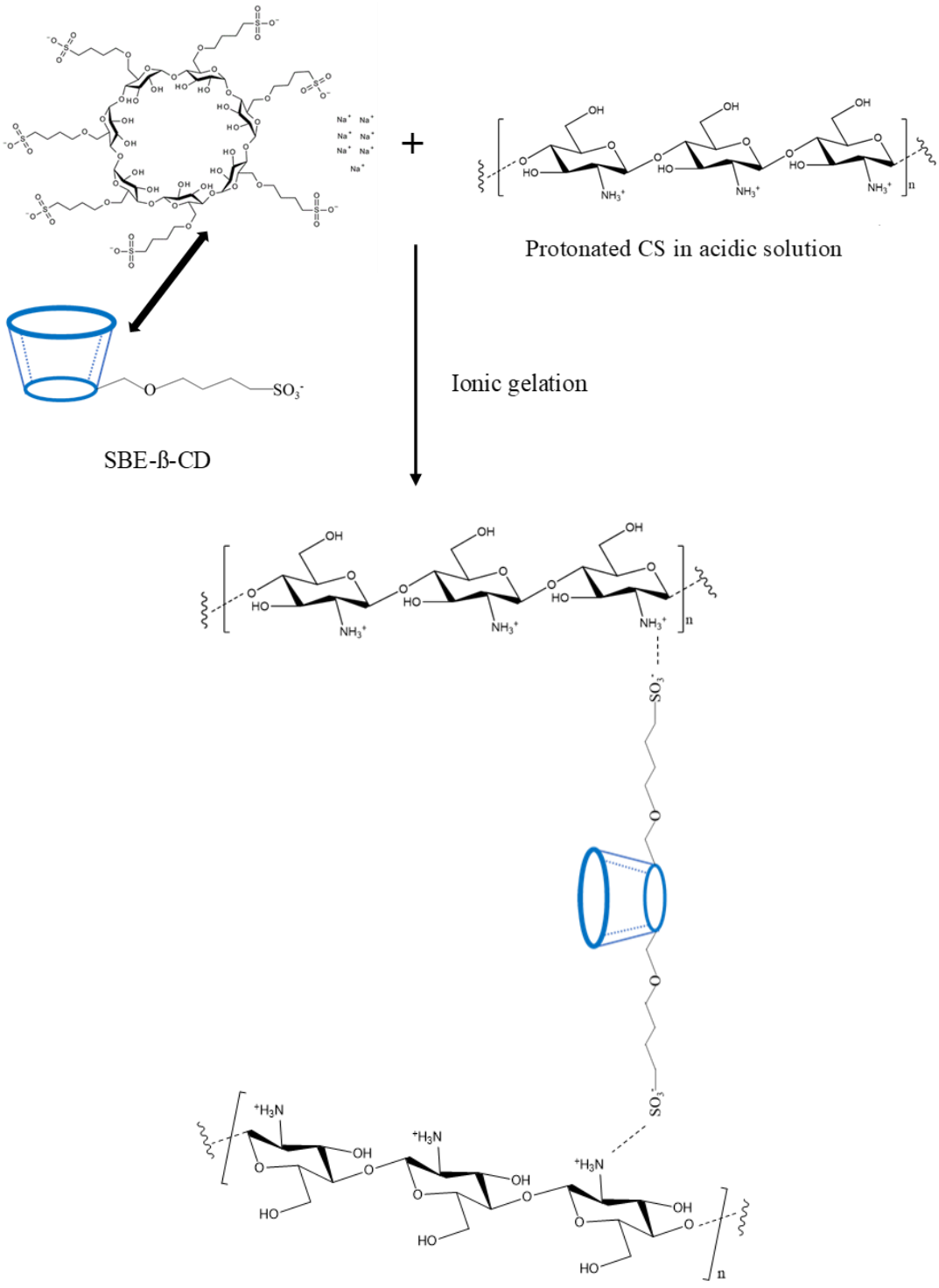

Figure 5.1: Schematic diagram illustrating the potential route for formation of a CS NP through crosslinking with SBE-ß-CD utilising an ionic gelation method.

In addition, SBE-ß-CD itself can act as a crosslinker. CS/SBE-ß-CD NPs were prepared using the ionic gelation method. The main advantage of this method has been reported to be the ability of forming particles under mild conditions, without the use of any harmful organic solvents, heat, or vigorous agitation [551].

The formation of CS NPs is attributed to polyelectrolyte interactions that leads to electrostatic cross-linking between the free amino groups of CS and the anionic sulfobutyl groups of SBE-ß-CD [144] (Figure 5.1). As discussed in Section 1.2.1, the use of polymeric NP as a drug carrier can result in an enhancement in both drug bioavailability and a more controlled and targeted release profile. Utilising the advantages of both CS and SBE-ß-CD, and combining these as a drug carrier, can result in several advantages such as size specificity, permeation enhancement, and mucoadhesive properties. In addition, such nanocarriers can also support and enhance the delivery of a hydrophobic drug. To this end, these drug-loaded NPs will be incorporated into the developed WM hydrophilic soft contact lenses (SCLs) as synthesised and characterised earlier in this research (Chapter 2), to develop a novel ODDS that can provide a sustained release and targeted delivery of naringenin (NAR). NAR, as previously discussed in Chapters 3 and 4, is a flavonoid and is a potent antioxidant [457].

The purpose of this chapter was to synthesize NAR-loaded CS/SBE-ß-CD NPs (i.e., NAR-CS NPs) via the ionic gelation method with the potential to promote eye health and/or prevent and treat ocular diseases such as AMD. The resulting NPs were evaluated by several techniques to assess their stability and physicochemical properties, including particle size, zeta potential, polydispersity index, as well as thermal and structural characterization. Drug encapsulation efficiency and loading capacity of the synthesized NPs was investigated by both a direct (e.g., measuring the amount of drug presented in the formed NPs) and an indirect (e.g., measuring the amount of free drug in supernatant) approaches. This study concluded with an investigation into drug *in vitro* release profiles of the formulated NAR-CS NPs.

5.2 Research Aims and Objectives

The aims and objectives of this chapter were:

- To synthesize and optimize CS/SBE-ß-CD NPs with and without drug, via the ionic gelation technique.
- To characterize the physicochemical properties of the developed NPs using dynamic light scattering, thermal gravimetric analysis, differential scanning calorimetry and Fourier-transform infrared spectroscopy.
- To determine the drug encapsulation efficiency and drug loading of the NAR-CS NPs.
- To investigate the *in vitro* release profile of the developed NAR-CS NPs.

5.3 Experimental Methodology

5.3.1 Materials

Water-soluble CS (10-100 kDa, ≥90% deacetylation), and SBE-ß-CD (>98% purity) were purchased from Carbosynth (Ireland). CS (10-100 kDa, ≥ 75% deacetylation), NAR (>98% purity), acetic acid (99% purity), DMSO (dimethyl sulfoxide, 99% purity), and lysozyme (from egg white) were purchased from Sigma Aldrich (Ireland). Methanol (HPLC grade, >99.9% purity) was purchased from Honeywell (Ireland).

5.3.2 Synthesis of polymeric nanoparticles

CS NPs were prepared using the ionic gelation method with SBE-ß-CD [144, 204] as the crosslinking agent. Briefly, 50 mg of CS was dissolved in 25 mL of 0.1% acetic acid (adjusted to pH 5 using dilute NaOH). 22.5 mg of SBE-ß-CD was dissolved in 2.5 mL of ultrapure water. The SBE-ß-CD solution was slowly added dropwise into the CS solution resulting in a 1:2 mass ratio of CS:CD, under vigorous stirring. Two types of low molecular weight (MW, 10-100 kDa) CS were used including conventional CS (≥ 75% deacetylation, CS_1) and water-soluble CS (≥ 90% deacetylation, CS_2).

The reaction mixture was left to stir overnight at room temperature. To optimize the NP yield, two centrifugation speeds at 15000 and 18000 rpm were used. The formulated nano-formulations were freeze-dried (FreeZone 2.5 freeze-dryer, Labconco, USA) with the presence of 2% trehalose as a cryoprotectant. Figure 5.2 presents the different steps in the preparation of CS NP.

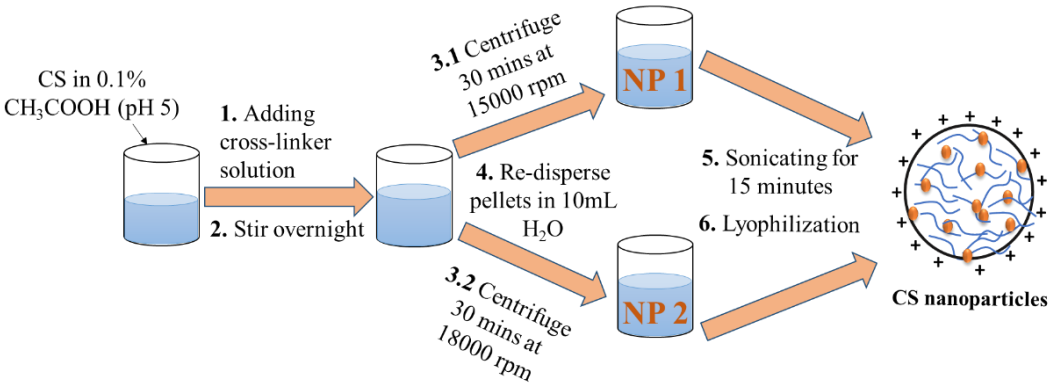

Figure 5.2: Schematic illustration of the preparation of CS NP using SBE-ß-CD as a cross-linker using centrifugation at 15000 rpm (NP 1) and 18000 rpm (NP 2).

Drug loaded CS NPs were prepared using the same method with the following adjustment: 23.45 mg of the NAR:CD complex was used to cross-link with CS solution.

5.3.3 Nanoparticle physicochemical characterization

A physical mixture (PM) was prepared by homogenously mixing CS and NAR:CD complex at a 2.1:1 mass ratio. This mass ratio was based on the mass ratio between CS:complex used in the formation of NAR-CS NPs as described in Section 1.3.2. The following techniques were carried out as per methodologies described in Section 2.3.4: thermogravimetric analysis (TGA, Q50 model, TA instruments, UK), differential scanning calorimetry (DSC, Q2000 model, TA instruments, UK) and Fourier-transform infrared spectroscopy (FT-IR, Varian 660-IR, Varian, USA), with the following deviations:

- FT-IR: only the KBr disc technique was used in this analysis.
- DSC: all samples were analyzed at 10 °C/min ramp rate from 0 °C to 300 °C.

Statistical analysis on the changes in the particle's average diameter and charge between unloaded and NAR-CS NPs was carried out as per Chapter 2, Section 2.3.4.

The hydrodynamic diameter (Z-average size), polydispersity index (PDI), and zeta potential of all NPs were analysed using a NanoWave II (Microtrac) instrument. The refractive index of the fluid was set to 1.333 (water), and the particle refractive index was set to 1.526 (CS NP). Each run was carried out in triplicate with a run time of 60 seconds per run. Prior to the measurement, samples were appropriately diluted with ultrapure water so that the concentration range was within 0.1 – 10 loading index. The electrophoretic mobility was determined at room temperature. Prior to the analysis of the NPs, reference standards for size (silica NPs) and zeta potential (alumina NPs) were run to ensure the instrument perform accurately.

5.3.4 Naringenin encapsulation efficiency and loading capacity in naringenin-loaded nanoparticles

Percentage of NAR loading (i.e., drug loading capacity) of NAR-CS NPs was calculated according to Equation 5.1 below:

$$\%\text{Drug loading} = \frac{\text{Total NAR added} - \text{free NAR}}{\text{Weight of added CS}} \text{ x } 100 \quad \textbf{Equation 5.1}$$

The encapsulation efficiency of NAR was determined by both direct and indirect methods. The amount of NAR in the drug-loaded NPs was measured by HPLC analysis, using the same method as described in Section 3.3.3 (Chapter 3).

Indirect method: the drug content of the NP was determined by the separation of drug-loaded NP from the aqueous solution that contained non-associated NAR. The nano-formulation was centrifuged twice (SIGMA 3-18 KS, Sigma Aldrich, Ireland). Firstly, the drug-loaded NP solution was centrifuged at 3000 rpm for 15 minutes, while the pellets were used to analyse the amount of non-associated NAR (unbound drug 1), the supernatant was used in the next centrifugation at 15000 rpm for 30 minutes. Then, after centrifuging the solution at 15000 rpm, the concentration of unbound NAR (unbound drug 2) in the supernatant was measured. The % encapsulation efficiency (%EE) was calculated using Equation 5.2 [467].

$$\%EE = \frac{[W_{total\ drug} - W_{unbound\ drug\ 1+2}]}{W_{total\ drug}} \times 100 \qquad \textbf{Equation 5.2}$$

Direct method: the NAR content of the NP was determined by degrading the drug-loaded NP (pellets after centrifugation of the solution at 15000 rpm). To identify the best possible solvent to break the NP, different solvent systems, along with the use of sonication, were investigated as detailed in Table 5.1.

Table 5.1: Details of the experimental solvent combinations for the analysis of drug encapsulation efficiency from NAR-CS NPs (n = 3).

Run #	Pellets dispersion (µL)	MeOH (µL)	Water (µL)	DMSO (µL)	0.1M HCl	Lysozyme (µL)$^{+}$
1	100	300	600	-	-	-
2	100	450	450	-	-	-
3	100	600	300	-	-	-
4	100	-	-	900	-	-
5	100	450	-	-	450	-
6	100	-	-	-	-	900
7	100	450	-	-	-	450

$^{+}$: Lysozyme solution was prepared at 2.5 mg/mL in phosphate buffered saline (PBS, pH 7.4).

5.3.5 In vitro release study of naringenin-loaded nanoparticles

NAR stability in the release medium (i.e., PBS+0.1% Tween® 80, as per Section 3.3.6, Chapter 3) at 37 °C was investigated for three months. At specific intervals (24, 48, 72, 96, 120 and 144 hours, weeks 2, 3, and 4, months 2 and 3), a sample of NAR was withdrawn and subjected to HPLC analysis.

The drug release studies from NAR-CS NPs were carried out in the release medium. 1 mL of release medium was distributed into 2 mL microcentrifuge tubes containing nanosuspension equivalent to 11 µg of NAR. These microcentrifuge tubes were placed in a shaker with continuous agitation at 150 rpm at 37 °C (SI500 shaking incubator, Stuart, Ireland). At every sampling point, a microcentrifuge tube was taken and centrifuged at 15,000 rpm for 15 min and the drug presented in the supernatant was quantified by HPLC using the method described in Section 3.3.3 (Chapter 3). The

percentage cumulative drug release from the NAR-CS NP was calculated following the below equation (Equation 5.3):

$$\%\text{Cumulative drug release} = \left(\frac{Tested\ volume}{Bath\ volume} * P_t\right) + P_{tc} \qquad \textbf{Equation 5.3}$$

Where: P_t and P_{tc} are the percentage released at time 't' and percentage released before time 't', respectively; Tested volume (mL): volume of release media withdrawn at a specified interval for HPLC analysis; Bath volume (mL): total volume of release media in a glass vial.

5.4 Results and Discussion

5.4.1 Formation of chitosan nanoparticles

Low molecular weight (MW) CS in a range of 10-100 kDa was chosen to be used in the formulation of CS NPs. The particle size of the NPs was previously cited to be affected by CS MW, whereas their zeta potential, overall shape and size distribution remained constant [552, 553]. Almalik *et al.* demonstrated that the NPs average diameter was gradually increased with a higher CS MW (Figure 5.3) [552].

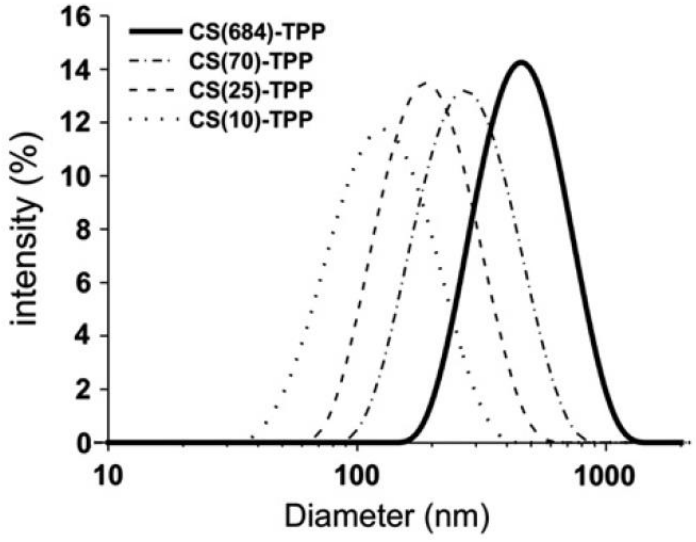

Figure 5.3: Size distribution of CS NPs prepared from different CS molecular weights [552].

Initially, CS_1 was used in the formulation. However, it did not give a monodispersed solution. DLS data on this type of NPs resulted in only 55% of the distribution under 365 nm with the rest in the micron-range (5 µm). When CS_2 was used in the formulation of NPs, a more uniform size (95% of the distribution was under 360 nm) was obtained. Therefore, CS_2 was identified to be a more suitable raw material to be used in the formulation of NAR-CS NPs. Moreover, by using CS_2, which has a higher degree of deacetylation compared to CS_1 (90% vs. 75%), the developed drug-loaded NPs were predicted to have a higher %EE. As reported by Yang and Hon, with 3.5 mg of 5-FU (fluorouracil) loading into CS/TPP (tripolyphosphate sodium) NPs, CS with a DD of 75% gave a EE of 38.57 ± 0.69%, while a substantially higher %EE, 56.47% ± 0.81% could be seen for CS with 90% DD [554]. CS_2 was previously used in the preparation of CS NPs [145, 555]. For instance, using the ionic gelation method, Yan *et al.* developed puerarin-loaded CS NPs, which had a particle size of 126 ± 1 nm and a PDI value of 0.122 ± 0.001 [145]. Differences in CS MW and the degree of deacetylation (DD) were suggested to have an impact on the toxicity of the NPs [556]. A decrease in both factors resulted in lower NP toxicity [556].

A molar ratio of 1:2 for CS:SBE-ß-CD was employed in this study, which resulted in an opaque solution, indicating a successful formation of NAR-CS NPs. This phenomenon was also reported in previous works [144, 467, 505].The effect of SBE-ß-CD concentration in relation to CS for the formation of CS/SBE-ß-CD NPs was investigated by Mahmoud *et al.* [505] and Zhao *et al.* [144]. Both studies provided a similar observation. At a very low SBE-ß-CD concentration relative to CS (1:3 mass ratio), a clear colloidal solution was obtained which indicated that either the NPs could not be formed, or the quantity of the formed NPs was too low to be detected. On the other hand, when too high SBE-ß-CD concentration was used (e.g., the mass ratio 0.65:1 or below for CS/SBE-ß-CD) in the formulation of NPs, aggregates could be seen [144]. This was suggested to be due to an increase in the shielding of free positively charged groups of CS, which resulted in a reduction in the NPs positive zeta potential values [467, 505]. Consequently, this led to a decrease in repulsive forces between the NPs and cross-bridge formation between NPs (the hydroxyl groups on the surface of NPs), resulting in NP agglomeration [557].

In general, higher amounts of SBE-ß-CD relative to CS is preferable since this results in smaller sized NPs [144, 505]. For example, at 1.5:1 CS:SBE-ß-CD mass ratio, the NPs size was recorded to be around 800 nm, while a size of 465.9 nm was measured for NPs formed at 0.85:1 ratio [144].

A centrifugation technique has been used widely to wash and purify NPs in many previous studies [51, 136, 144, 543], where centrifugal force is used to increase the separation of nanomaterials due to the enhanced gravitational field [558]. According to Stoke's law, the particle diameter can be calculated from the difference in the sedimentation velocities (i.e., the complete particle size distribution) [559]. Based on Brownian motion, particles in the CS NP solution sediment and collide with each other at different rates, depending on size [560]. Centrifugation speeds of 14000 and 15000 rpm were previously used in the purification step of NPs [144, 283]. However, a higher speed of 18000-20000 rpm was also used in some studies in the formation of homogenously dispersed NPs [561, 562]. Thus, to study the effect of centrifugation speed on the formation of the NAR-CS NPs, specifically on their %yield, two centrifugation speeds were investigated in this study, 15000 and 18000 rpm (operational limit of the instrument). There was no statistical difference (p-value = 0.11) in NPs %yield formed under 18000 rpm (21.0 ± 0.4%) and 15000 rpm (20.3 ± 0.3%). Since 18000 rpm is the maximum speed of the instrument, excessive use at such high speed would in turn reduce the lifespan of the instrument. Hence, the centrifugation speed used in the formulation of NPs in this study was determined to be 15000 rpm. Following the centrifugation step, pellets were redispersed in 10 mL of ultrapure water and sonicated for 10 minutes. The effect of sonication on the formation of NPs was assessed by Pandit *et al.* [562], with the optimum sonication time proposed to be 10 minutes.

The final step in the formulation of NAR-CS NPs was freeze-drying, which has been known to give good long-term stability of colloidal NPs since it removes water/solvent by sublimation from the NPs [563]. A cryoprotectant, 2% trehalose, was used as part of this process in the NAR-CS nano-formulation, to remove excess moisture, protect and stabilize the colloidal system during the freeze-drying stages as extensively investigated by previous studies [283, 561, 564, 565].

Freeze-drying is based on removing of water or solvent from a frozen sample by sublimation (primary drying) and desorption (secondary drying) under vacuum [563, 566]. However, samples undergo various stresses throughout the lyophilization process as reviewed by Fonte *et al.* [567]. Such stresses include: ice formation which leads to solute exclusion, mechanical stress (from ice formation), surface dehydration and pH/ionic strength modifications [568], which in turn result in NP aggregation [569]. Aggregates can significantly hinder the re-dispersion of NPs and affect their sizes [570]. Cryoprotectant has been shown to stabilize and prevent a molecule from degrading during freeze-drying and storage [571]. The protection mechanism of cryoprotectants is due to their ability to remain in an amorphous form during the lyophilization process [572].

5.4.2 Physicochemical characterization of naringenin-loaded nanoparticles

5.4.2.1 Particle size, charge, and PDI of naringenin-loaded nanoparticles

DLS was the most commonly used sizing method by nanomedicine application (48%) from 1973 to 2015 [179]. DLS is also known as photon correlation spectroscopy and is based on elastic electromagnetic scattering of the dispersing particles [573-575]. As reviewed by Carvalho *et al.* [576], when the NP suspension is exposed to a light beam, the detection of the light scattered from the interaction with the particle provides information on the physical properties of the sample. DLS gives the average hydrodynamic radius (Z-average) of the particles [158, 505, 552]. The hydrodynamic radius is directly related to the diffusive motion of the particles [574, 577]. DLS can also provide a measurement of the zeta-potential of the particles. This value is measured at the slipping plane of a particle under an electrical field, which reflects the differences in potential between the electric double layer of electrophoretic mobile particles and the layer of dispersant around them [578].

The developed NAR-CS NPs had an average particle size of 333.3 ± 26.6 nm and a positive zeta potential of +22.0 ± 4.3 mV, while these values for unloaded CS NPs were 360.0 ± 9.9 nm and +38.6 ± 2.1 mV, respectively. Positively charged NPs (CS NPs) were reported to prolong precorneal retention time, leading to an increased in drug bioavailability since they can bind to negatively charged corneal mucin [144].

A moderate positive zeta potential value prevents particle aggregation while promoting electrostatic interaction between the NPs with the negatively charged mucus layer [144]. A similar observation was obtained in various studies on drug-loaded CS/SBE-ß-CD NPs [467, 505, 557]. In addition, zeta-potential data provided information on the stability of colloidal systems, a higher zeta potential value indicates a higher stable state of particles [579]. Typically, zeta potential values higher than +20 mV or lower than -20 mV indicate a stable suspension.

The polydispersity index (PDI) value describes the NP size distribution and was used as an indicator for NP stability and uniformity of formation [580]. The prepared blank CS NPs and NAR-CS NPs exhibited a narrow particle size distribution with PDI values of 0.0671 ± 0.0362 and 0.0777 ± 0.0580, respectively. These values suggested that the method used in the preparation of NAR-CS NPs produced homogenously dispersed NPs. To prepare monodisperse particles with a narrow range of average particle diameters, many studies have produced NPs with PDI values below 0.2 [580-582]. Values as high as 0.4 were considered acceptable in some studies [505, 583, 584].

As mentioned in Chapter 1 and reviewed by Hoshyar *et al.* [585], NPs should be small enough to escape the macrophages lodged in the reticuloendothelial system, while being big enough to prevent rapid leakage into blood capillaries. Hence, controlling the size of synthesized NPs for targeted drug delivery and sustained release was determined to be important [585]. NPs with sizes smaller than 200 nm could impact the isolation of the NPs from the suspension leading to a low recovery of the solid-state NPs [144].

5.4.2.2 TGA analysis of naringenin-loaded nanoparticles

DSC and TGA were used to characterize the thermal behaviour and stability of the drug and the NP-formulations, providing information on their hydration properties and their physical state [586, 587]. The TGA thermograms of raw materials CS, SBE-ß-CD, NAR, physical mixture, blank CS NPs, and NAR-CS NPs are presented in Figure 5.4.

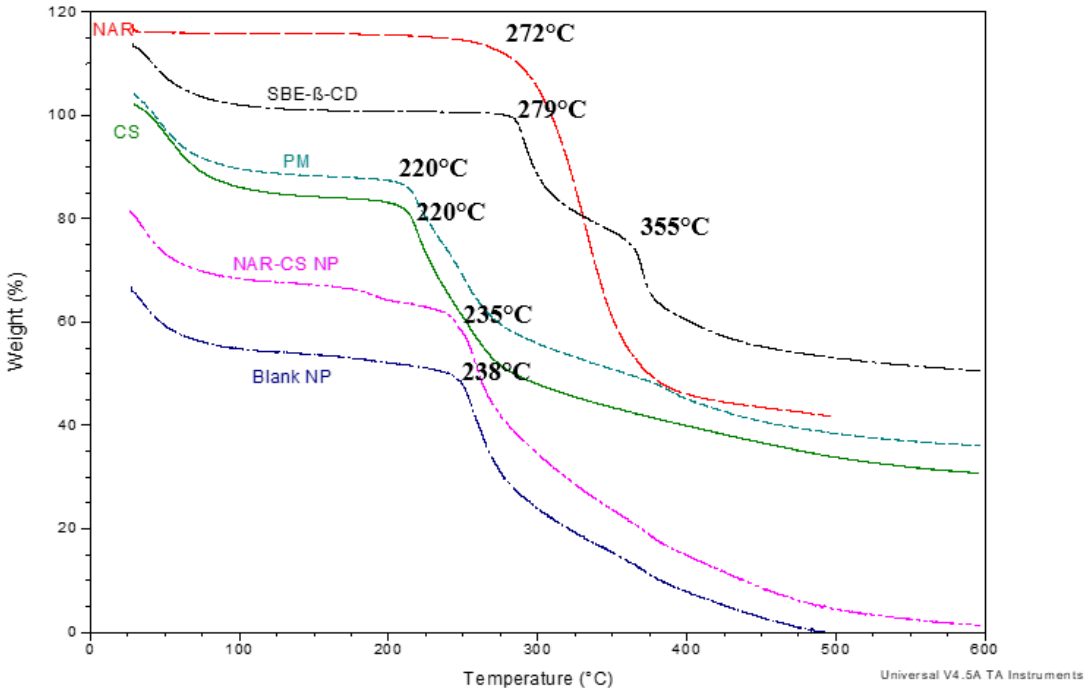

Figure 5.4: TGA thermograms of CS, SBE-ß-CD, NAR, physical mixture, blank CS NPs, and NAR-CS NPs. Degradation temperature (°C) of each material is reported (n = 3).

TGA analysis of NAR and SBE ß-CD is reported in Section 3.4.4.1 (Chapter 3), with NAR exhibiting a sharp melting peak at 272.1 ± 4.7 °C, while two endothermic peaks at 278.5 ± 9.7 °C and 355.3 ± 12.4 °C are noted for SBE-ß-CD. As could be observed in Figure 5.4, CS exhibited two stages of degradation. The first one was at 48.5 ± 3.5 °C, which was due to the evaporation of the residual water presented in the polymer sample, while the second one was at 220.1 ± 0.2 °C, which was assigned to the decomposition of CS. The observations of CS in this work agreed with previous studies on CS thermal behaviour [586-588]. As an example, two degradation points were also observed in the DSC analysis of CS, carried out by Kumar *et al.*, which were at 47 and 247 °C [589].

In the physical mixture thermogram, as expected due to the higher amount of CS presented, a degradation point started at the same temperature as the ones displayed in CS analysis, which was at 220.3 ± 0.4 °C. An increase in thermal stability of the formulated CS NPs in comparison to the CS itself was recorded. Blank CS NPs and NAR-CS NPs thermograms are comparable with each other with dehydration points at 34.9 ± 4.0 °C and 34.0 ± 3.3 °C, respectively, and a degradation temperature starting at 257.1 ± 0.9 °C and 257.2 ± 1.3 °C, respectively. Similar observations were reported in previous studies, in which the formed NPs exhibited enhanced thermal stability compared to the individual polymer (i.e., CS), which was suggested to be due to the interaction between CS and the crosslinker [7, 590]. For instance, Zhang *et al.* demonstrated that the %weight remaining of pure CS (2.78 ± 0.01%) was significantly higher in comparison to that of the formulated tea polyphenol-loaded CS NPs (40.93 ± 0.52%) in TGA analysis when the temperature was above 300 °C [591].

5.4.2.3 DSC analysis of naringenin-loaded nanoparticles

The DSC thermograms of raw materials CS, SBE-ß-CD, NAR, blank CS NPs, NAR-CS NPs, and the corresponding physical mixture are presented in Figure 5.5. In the CS thermogram, the peak appearing at around 92.1 ± 6.4 °C was quite broad, which indicated this could be due to the evaporation of the residual water in the sample [146, 467]. A second endothermic peak at 210.4 ± 0.1 °C was also observed, which corresponded to the decomposition of CS [146]. As analyzed in Section 3.4.5.1 (Chapter 3), the SBE-ß-CD thermogram included a broad endothermic peak at 96.0 ± 6.5 °C (liberation of crystal water) and double melting/decomposition peaks at 248.6 ± 0.8 and 260.9 ± 0.9 °C, while a sharp melting peak at 254.4 ± 0.3 °C was observed in the NAR thermogram. Physical mixture of CS and NAR:CD complex spectrum includes a broad endothermic peak at 87.8 ± 4.3 °C and another peak at 207.2 ± 0.8 °C, which is similar to those observed in the CS DSC thermogram.

The thermogram of blank CS NPs shows a broad peak at 86.5 ± 6.3 °C, which was corresponded to polymeric dehydration, and an endothermic peak at 232.4 ± 6.2 °C. A similar observation was seen in the NAR-CS NPs thermogram with two endothermic peaks at 84.9 ± 1.3 °C and 236.2 ± 2.9 °C. The observed thermal behaviors of the unloaded and loaded NPs indicated the intermolecular interactions between CS and SBE-ß-CD complex, including the combination of hydrogen bonds or van der Waals

forces, which agreed with previous studies [144, 467]. In a study carried out by Zhao *et al.*, a reduction in the melting temperature of SBE-ß-CD, from 263.3 °C to 238.3 °C and 241.3 °C was noted in the DSC thermogram of the formulated blank CS/SBE-ß-CD NPs and drug-loaded NPs, respectively [144].

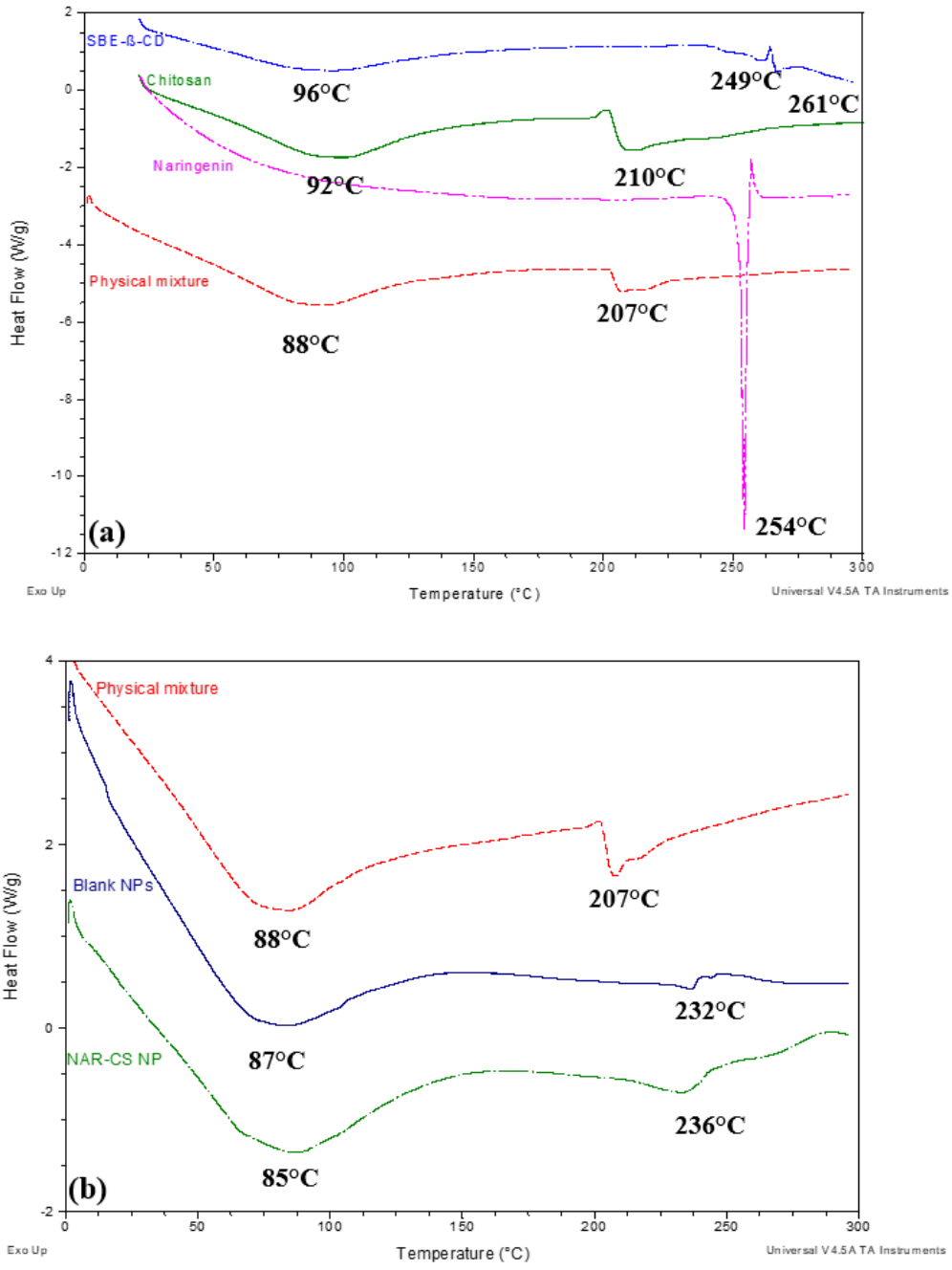

Figure 5.5: DSC thermograms (n = 3) of (a) raw materials CS, SBE-ß-CD, NAR, and physical mixture, and (b) physical mixture, blank CS NP, and NAR-CS NPs. T_g temperature (°C) of each material is reported.

5.4.2.4 FT-IR analysis of naringenin-loaded nanoparticles

Five samples were analyzed using FT-IR including: NAR, CS, SBE-ß-CD, unloaded and drug-loaded CS NPs. The comparative FT-IR spectra are shown in Figure 5.6. Table 5.2 lists the main characteristic peaks of CS, SBE-ß-CD, CS NP, and NAR-CS NP.

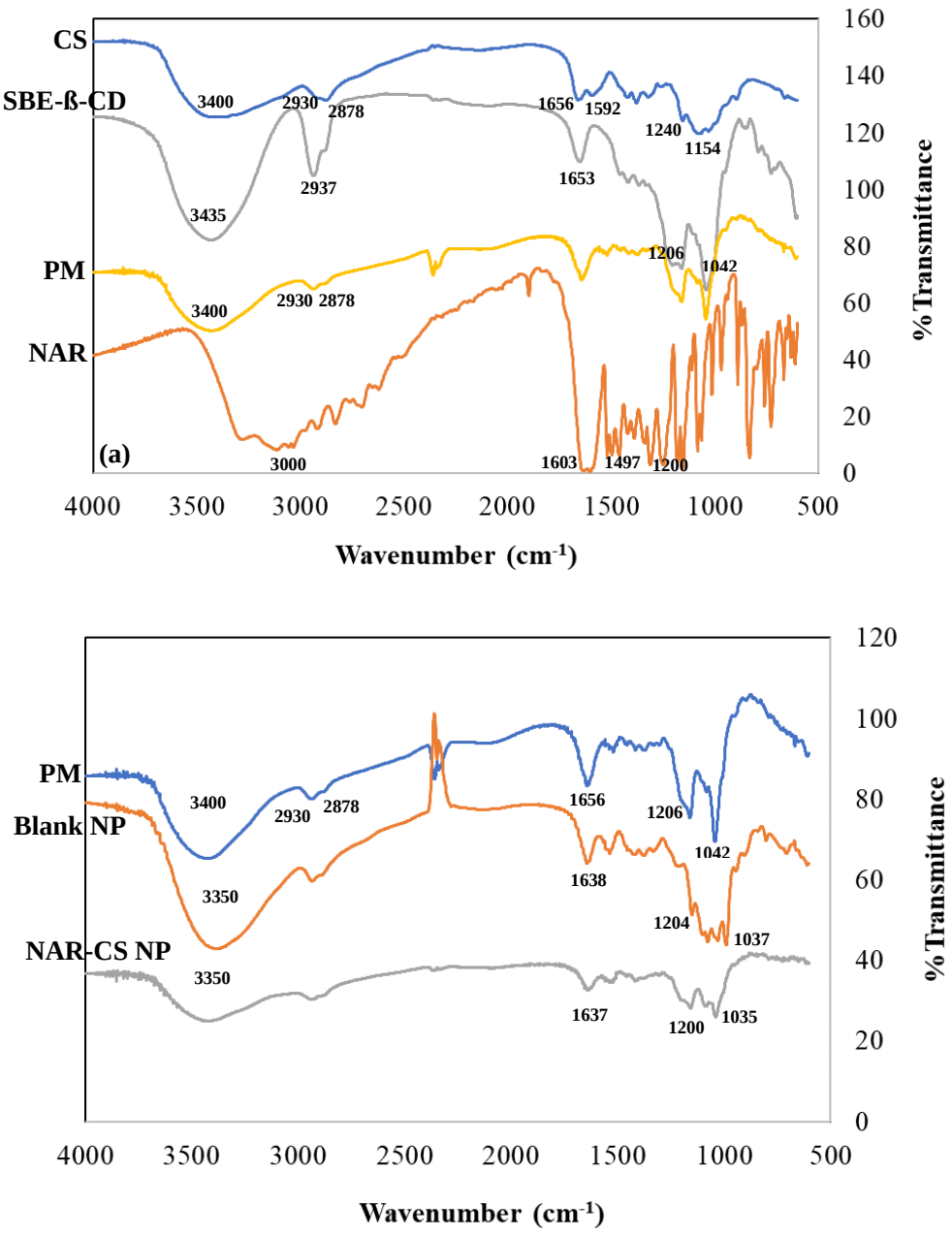

Figure 5.6: Representative FTIR spectra of (a) CS, SBE-ß-CD, NAR, and physical mixture, and (b) physical mixture, blank CS NPs, and NAR-CS NPs.

The IR spectrum of CS demonstrates a strong absorption peak at around 3400 cm^{-1} which corresponded to both O-H stretching and N-H stretching vibrations from intermolecular hydrogen bonding. –CH and $–CH_2$ stretching vibrations could be seen at 2930 and 2878 cm^{-1}. While peaks at 1656 cm^{-1} and 1592 cm^{-1} attributed to C=O stretching (amide) and N-H bending vibration of CS, respectively, peaks at 1240 cm^{-1}, 1154 cm^{-1} and 1075 cm^{-1} indicated $–O-SO_3^-$ stretching, C-O-C stretching and C-O stretching of SBE-ß-CD, respectively, which agreed with previous studies [143, 467, 592]. The FTIR spectrum of SBE-ß-CD was analyzed in Section 4.4.3.3 (Chapter 4). Briefly, the SBE-ß-CD spectrum was characterized by a broad and intense peak representing O-H stretching at 3430 cm^{-1}, C-H vibration at 2936 cm^{-1}, CH_2 vibration at 2810 cm^{-1}, and C-O stretching vibration at 1040 cm^{-1} [505, 535]. The physical mixture spectrum contained all the characteristic bands from both CS and NAR:CD complex, those such as 1656 cm^{-1} (C=O stretching, in CS) and 1653 cm^{-1} (C-H stretching, in SBE-ß-CD).

The unloaded and NAR-CS NPs spectra display a significant shift of the characteristic N-H bending (amide) peak of CS at 1656 cm^{-1} to 1638 and 1637 cm^{-1}, respectively. This might be caused by a different environment (i.e., H-bonding interaction between different components, CS, NAR and SBE-ß-CD) around this amide group [143, 593]. Furthermore, various shifts can be observed in the spectra of the developed NPs, which was caused by an addition of intermolecular interactions, potentially due to hydrogen-bonding and electrostatic interactions [594]. The peak at 1592 cm^{-1} in the CS spectrum and the peak at 1042 cm^{-1} in SBE-ß-CD spectrum moved to 1585 cm^{-1} and 1037 cm^{-1} in blank CS NPs spectrum, respectively. All these shifts indicated the formation of CS/SBE-ß-CD NPs through electrostatic interactions between the ammonium group of CS and the anionic sulfobutyl groups of SBE-ß-CD (Figure 5.6). Moreover, NAR characteristic peaks cannot be observed in the formed NAR-CS NPs, which confirms the successful encapsulation of NAR into the cavity of the NPs. These observations agreed with previous works [144, 467, 505, 595].

Table 5.2: Summary of FT-IR analysis of the NAR-CS NP, unloaded CS NP and their raw materials.

Ref. frequency (cm^{-1})	Functional group	Raw materials (cm^{-1})				Nanoparticles (cm^{-1})		Ref.
		SBE-ß-CD	CS	NAR	Physical mixture	Blank CS NP	NAR-CS NP	
3400	O-H stretching	3435	3400	-	3400	3350	3350	[146]
3100-2800	C-H stretching	2937-2892	2930-2878	3000	-	2932-2878	2930-2880	[505]
1650	C=O stretching (amide)	-	1656	-	-	1638	1637	[143]
1619	C=O stretching (amide II)	-	-	-	-	-	-	[587]
1644-1655	C-H (from aromatic ring)	1653	-	-	-	-	-	[535]
1604	C=C aromatic	-	-	1603	1603	-		
1589/1560	N-H bending vibrations	-	1592	-	-	1585	1588	[143, 592]
1500	C=C aromatic	-	-	1497	1497	-		
1240	-O-SO_3^- stretching	-	1240	-	-	-	-	[596]
1205	C-H stretching	1206	-	-	-	1204	1200	[535]
1200	O-H phenolic	-	-	1200	1200	1204	1200	
1149/1150	C-O-C stretching	-	1154	-	-	1152	1150	[143, 592]
1064/1026	C-O stretching	-	1075	-	-	1078	1076	[143, 592]
1040	Sulfoxide stretch	1042	-	-	-	1037	1035	[144, 596]

5.4.3 Naringenin encapsulation efficiency and loading capacity in naringenin-loaded nanoparticles

Drug encapsulation efficiency (%EE) studies have been widely used to determine the amount of drug present in the formulation that is successfully entrapped inside the NP [467]. The %EE is one of the most essential physicochemical properties of colloidal carrier loaded drugs [597]. Thus, it is important to accurately quantify the %EE of the synthesized NPs. Both indirect [51, 283, 562, 598, 599] and direct methods [136, 505, 586, 600-602] were previously used in the measurement of drug %EE. To ensure the %EE of drug was determined as accurately as possible, both of those approaches were used in this work (Table 5.3).

Table 5.3: Drug encapsulation efficiency and drug loading data on NAR-CS NPs (n = 3).

Indirect approach		
Sample	**%Encapsulation efficiency**	**%Drug loading**
Pellets: 3000 rpm Supernatant: 15000 rpm	33.4 ± 1.0	0.68 ± 0.03
Direct approach 1: MeOH		
Sample	**%Encapsulation efficiency**	**%Drug loading**
100 µL pellets:450 µL MeOH:450 µL water	12.0 ± 1.3	0.24 ± 0.06
Direct approach 2: DMSO		
Sample	**%Encapsulation efficiency**	**%Drug loading**
100 µL pellets:900 µL DMSO	13.9 ± 3.2	0.28 ± 0.08
Direct approach 3: 0.1M HCl		
Sample	**%Encapsulation efficiency**	**%Drug loading**
100 µL pellets:450 µL 0.1 M HCl:450 µL MeOH	34.5 ± 1.6	0.70 ± 0.04
Direct approach 4: Lysozyme		
Sample	**%Encapsulation efficiency**	**%Drug loading**
100 µL pellets:900 µL lysozyme solution	26.2 ± 0.5	0.54 ± 0.01
100 µL pellets:450 µL lysozyme solution:450 µL MeOH	37.4 ± 4.0	0.76 ± 0.09

As mentioned in Section 5.3.2, the work up of the formulated NAR-CS NPs included two centrifugation steps. The formulation was first centrifuged at 3000 rpm to remove unbound drug, which was followed by high-speed centrifugation at 15000 rpm to separate NAR-CS NPs from the aqueous solution that contained non-associated NAR.

Besides determining the free drug in the supernatant after high speed centrifugation [51, 283, 562, 598, 599], few studies have used low speed centrifugation to measure the amount of removed non-entrapped drug [603, 604]. A low speed centrifugation at 9100 rpm for 10 minutes was used to remove the unbound precipitated curcumin from exosomes [603]. By measuring the unbound curcumin from the precipitated pellet, its %EE was determined. Separation of non-entrapped dexamethasone from niosomes was also carried out using low speed centrifugation at 6000 rpm for 1 hour in a study carried out by Mavaddati *et al.* [604]. Therefore, to accurately determine NAR %EE using an indirect approach, the total amount of non-associated NAR from both centrifugation steps was measured. The %EE of NAR using this approach was measured to be 33.4 ± 1.0%, with 0.68 ± 0.03% loading capacity in the present study.

These values are lower than the previously quoted figures for the drug %EE of CS NPs, which were 61.8 ± 3.2% (ibrutinib-loaded CS/SBE-ß-CD NPs at 10 mg/mL SBE-ß-CD) [144] and 67.1 ± 0.3% (NAR-CS NPs) [467]. However, it should be noted that the complexation of NAR:SBE-ß-CD, which was reported in Chapter 4, was prepared differently through the implementation of lyophilisation of a monophasic solvent (TBA:water) approach, in comparison to forming an inclusion complex solely in water with filtration used in the works carried out by Zhang *et al.* and Zhao *et al.* [144, 467]. Thus, the encapsulation ability of the developed nano-formulation could be influenced due to different NP preparation methodologies. Additionally, the %EE of drug was shown to be influenced by the ratio of CS and SBE-ß-CD used in the formulation. In the study carried out by Fulop *et al.* [511], as the CS concentration increased in the formulation, the %EE of drug (hydrocortisone) decreased. The reason for this was postulated to be due to the changes in size of NPs, the larger the NPs, the more easily they released the drug. For instance, at 0.25 %wt. CS/SBE-ß-CD NPs, the %EE was found to be above 30%. However, when that concentration increased to 2%, the %EE of drug decreased to less than 10% [511].

A direct approach to determine the %EE was previously used in several studies as mentioned above. In this method, different solvent systems were used to break up the formed NAR-CS NPs to measure the actual drug amount inside the particles. A combination of MeOH and water solvent systems resulted in a %EE of 12.0 ± 1.3%, while a value of 13.9 ± 3.2% EE was recorded when using DMSO to break the formed

NPs. However, these %EE values are significantly smaller than ones obtained from the indirect method (i.e., 33.4 ± 1.0%). Based on a work reported by Mahmoud *et al*. [505], a co-solvent of 0.1 M HCl and lysozyme was also employed, with %EE was determined to be 34.5 ± 1.6% which agreed with the value from the indirect method.

To confirm the NAR %EE of the developed NPs, lysozyme was used to breakdown the NAR-CS NPs. CS can be degraded by enzymes that can hydrolyse linkages between glucosamine-glucosamine, glucosamine-N-acetyl-glucosamine, and N-acetyl -glucosamine-N-acetyl-glucosamine units, as cited by Loncarevic *et al.* [605]. Lysozyme, an enzyme that is available in the human body, was previously demonstrated to degrade CS through enzymatic hydrolysis reactions, by cleaving the 1,4-ß-glycosidic bond in the CS backbone [606]. In human tears, the lysozyme concentration was determined to be 2.13 mg/mL for adults [607]. Therefore, to ensure that the lysozyme concentration was sufficient to break up the formed NAR-CS NPs, 2.5 mg/mL lysozyme solution was prepared in PBS (pH 7.4). By mixing and incubating the nano-formulations in lysozyme solution for three days, the %EE of NAR in NAR-CS NPs in the present study was calculated to be 37.4 ± 4.0%.

It could be seen that by using 0.1M HCl:MeOH and lysozyme:MeOH to break up CS NPs, the quantified %EE of NAR from the developed NAR-CS NPs are comparable to the ones obtained from the indirect method. Following the determination of the optimum approach in measuring the %EE, the NAR loading capacity was calculated, which was in a range of 0.68 to 0.76% (i.e., 59.6 ± 7.8 µg NAR/mg CS NP) (Table 5.3).

5.4.4 In vitro release study of naringenin-loaded nanoparticles

Since NAR is sparingly soluble in water, the *in vitro* release study for NAR-loaded lens, which was detailed and discussed in Chapter 3, was carried out in PBS with 0.1% Tween® 80 to maintain adequate sink conditions. Through HPLC analysis, NAR was investigated to exhibit good stability for three months in the release medium at 37 °C. NAR concentration at Day 1 was 110 ± 2 µg/mL and remained stable at 109 ± 3 µg/mL after 3 months (p-value > 0.05).

The percentage cumulative drug release (%) profiles for a week (i.e., 168 hours) and a month (i.e., 720 hours) release from NAR-CS NPs in PBS with 0.1% Tween® 80 are shown in Figure 5.7(a) and Figure 5.7(b), respectively.

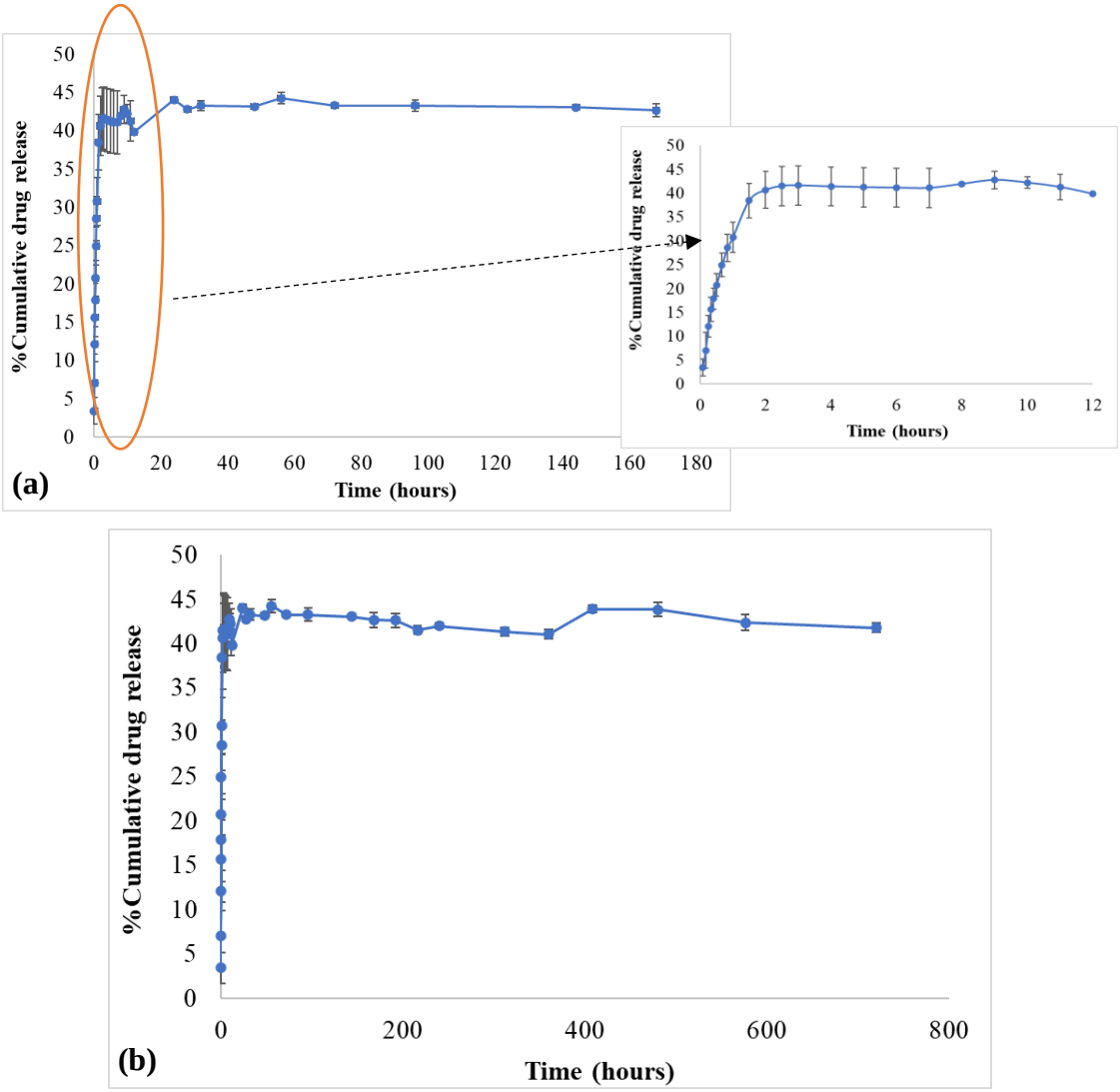

Figure 5.7: *In vitro* NAR release profiles of the developed NAR-CS NPs (n = 3) at (a) 1 week (i.e., 168 hours) and 12 hours, and (b) 30 days (i.e., 720 hours).

As can be observed in Figure 5.7, the formulated NPs exhibited a sustained release in the first 12 hours, followed by a controlled release from Day 2 to Day 30. The generated drug release profiles were postulated to be due to the burst release of the developed system due to the presence of free NAR as well as surface-binding NAR presented in the NP solution. These release patterns are similar to the previous investigations on drug-loaded CS/SBE-ß-CD NPs [144, 467, 505].

For example, econazole nitrate (ECO)-loaded CS/SBE-ß-CD NPs showed a prolonged drug release (in PBS at pH 7.4 at 37 °C) at approximately 50% rate over the first 8 hours [505]. The developed NPs had a particle size in a range of 90 to 673 nm, positively charged values of 22 to 33 mV, with a %EE of NAR ranging from 13 to 45% [505].

By applying various mathematical models: zero-order, first-order, Higuchi, and Korsmeyer-Peppas, the release mechanism of NAR-CS NPs in PBS with 0.1% Tween® 80 was investigated. The applicability of all the models was tested during the burst release phase (up to 2 hours). From the generated data, the correlation coefficient (R^2) values, along with the diffusion exponent (n), and rate parameter (k) were calculated to identify the best fit model to describe the release mechanism of the NAR-CS NPs (Table 5.4).

Table 5.4: Kinetic release data from the initial release phase obtained from zero order, first order, Higuchi, and Korsmeyer-Peppas mathematical models from the prepared NAR-CS NPs.

Mathematical model	NAR-CS NPs
Zero order	R^2: 0.8941
	k = 19.22 (M/s)
First order	R^2: 0.6427
	k = 0.44 (1/M)
Higuchi	R^2: 0.9800
	k = 34.82 ($M/s^{1/2}$)
Korsmeyer-Peppas	R^2: 0.9540
	n = 0.77

As can be observed from Table 5.4, based on the R^2 values generated from each of the mathematical models, the initial release of NAR (in the first 2 hours) from the formulated NAR-CS NPs in both release media indicated a good fit for the Higuchi and the Korsmeyer-Peppas models. The diffusion exponent values ‘n’ obtained from the Korsmeyer-Peppas model for the NPs released in PBS with Tween® 80 was higher than 0.5 (i.e., 0.77), indicating a non-Fickian release type. Thus, from the above observation, the mechanism of NAR release was postulated to be governed by diffusion, swelling, and dissolution. This observation agreed with previous work on a similar system [7, 283]. Behl *et al.* developed drug-loaded CS NPs (using dexamethasone sodium phosphate, DXP) by cross-linking with TPP, which resulted in NPs with a particle size of 132 ± 4 nm and 43.06 %EE of DXP.

The *in vitro* drug release of the developed NPs was carried out in PBS (pH 7.4, at 37 °C), which demonstrated a sustained and controlled drug release for 35 days. A diffusion-controlled drug release mechanism was proposed to represent the kinetics of DXP release from the developed CS NPs [283]. In addition, by applying all of the above release kinetic models, the quercetin release kinetic mechanisms from different ratios of fucoidan/CS (F/C) NPs were investigated by Barbosa *et al.* (Figure 5.8) [143]. The average particle sizes for 1F/1C, 3F/1C and 5F/1C were determined to be 427 ± 26 nm, 305 ± 10 nm and 355 ± 9 nm, respectively.

Mathematical Model	1F/1C	3F/1C	5F/1C
Zero-order	0.8658	0.9071	0.9600
First-order	0.7845	0.7773	0.8962
Hixson–Crowell	0.8139	0.8257	0.9221
Higuchi	0.9737	0.9762	0.9737
Korsmeyer–Peppas	0.9830	0.9790	0.9927
n-Value	0.4	0.6	0.5

Figure 5.8: Values of R^2 obtained from fits of different mathematical models for mechanisms of drug release to the 1F/1C, 3F/1C and 5F/1C NPs [143].

Results from Figure 5.8 indicated that the Korsmeyer-Peppas model best described the drug release kinetics in all the three ratios used in the formation of F/C NPs. This outcome indicated that drug release in that work was governed by a diffusion-controlled mechanism, described by the n-value. Since the n-values in 3F/1C and 5F/1C formulations were larger than 0.4, a non-Fickian diffusion of the drug was identified [143]. This can be described as a combination of the effects of diffusion and erosion of the polymeric structure, thus, resulting in a controlled drug release rate, as reviewed by J. Siepmann and F. Siepmann [608].

The outcome demonstrated that NAR was released from the formulated NAR-CS NPs at a rate of 10.9 µg/day, calculated at the end of the first 24 hours of release. However, this release rate was found to be lower than the estimated therapeutic concentrations as reported in Section 3.4 of Chapter 3, which should be in a range of 14.6 – 66.1 µg/day. This was potentially because of the low %EE of the developed NAR-CS NPs. As a result, further optimization on the developed NAR-CS NPs will be carried out in

future work to increase its encapsulation efficiency to ensure NAR is released within its therapeutically relevant concentrations.

5.5 Conclusions

In this chapter, NAR-CS NPs were successfully prepared by an ionic gelation technique. Ionically crosslinked CS NPs represent an interesting CS-based nanocarrier system for hydrophobic drugs to the ocular mucosa. Physicochemical characterization carried out by DLS, TGA, DSC, and FT-IR confirmed the formation of the NPs. The average diameters of blank CS NPs and NAR-CS NPs were measured to be 360.0 ± 9.9 nm and 333.3 ± 26.6 nm, respectively with zeta potential values of +38.6 ± 2.1 mV and +22.0 ± 4.3, respectively. PDI values indicated that the prepared NPs were homogenously redispersed with a narrow particle size distribution, with all the values below 0.2.

Thermal studies on raw materials and NPs through TGA and DSC demonstrated the thermal behaviour and stability of NAR and the NP, providing information on their hydration properties and their physical state. DSC thermograms of CS NP suggests interactions including a combination of hydrogen bonds or van der Waals force between CS and SBE-ß-CD, resulted in an increase in NP thermal stability in comparison to the individual components. FT-IR analysis of the shifts in frequency of functional groups in CS, NAR, and SBE-ß-CD before and after forming NP, was carried out. The formation of CS/SBE-ß-CD NP through electrostatic interactions between the ammonium group of CS and the CD anionic sulfobutyl groups was shown through the shifts in CS peaks (from 1656 and 1592 cm^{-1} in CS to 1638 and 1585 cm^{-1}) and in SBE-ß-CD peaks (from 1040 cm^{-1} to 1037 cm^{-1}).

To identify the best solvent system to break the developed NAR-CS NP to accurately determine the %EE of NAR, four solvent combinations were assessed including MeOH:water, DMSO, 0.1M HCl:MeOH and lysozyme:MeOH. The optimum solvent system was identified to be 0.1M HCL:MeOH, and lysozyme:MeOH, which indicated the highest amount of drug encapsulation efficiency, and had a comparable %EE of NAR to the indirect approach, which was in a range of 33.4-37.4%. Based on this finding, the NAR mass per mg of formulated NP was calculated to be 59.6 ± 7.8 µg NAR/mg NP.

In vitro release of the formulated NAR-CS NP was carried out in PBS with the presence of 0.1% Tween® 80 at 37 °C, which demonstrated a sustained and controlled drug release pattern at a rate of 10.9 µg/day. The *in vitro* release of the developed NAR-CS NPs followed a non-Fickian release type, which indicated that its release was mainly governed by diffusion and swelling. Due to the low %EE of NAR in the developed NAR-loaded CS NP, which resulted in a daily drug release concentration less than the estimated therapeutic concentration (14.6 – 66.1 µg/day), future study will be required to optimize and enhance the %EE of this nanocarrier.

The size and charge of the developed NAR-CS NP in conjunction with the biodegradable and biocompatible properties of this nanoparticulate system suggest it to be a promising approach in ocular drug delivery, which could improve patient comfort while reducing the need for intravitreal injections. Aiming to increase the controlled release and targeted delivery of NAR to develop a more effective drug delivery system to treat retinal diseases, the developed NPs were entrapped in the developed SCL (Chapter 2), which was discussed and reported in Chapter 6. To this end, the impact of loading such NP on lens' critical properties was studied and the NP-lens *in vitro* release behaviour was examined.

CHAPTER 6

FEASIBILITY OF INCORPORATING AN INCLUSION COMPLEX AND POLYMERIC NANOPARTICLE INTO SOFT HYDROGEL CONTACT LENS

6 FEASIBILITY OF INCORPORATING AN INCLUSION COMPLEX AND POLYMERIC NANOPARTICLE INTO SOFT HYDROGEL CONTACT LENS

6.1 Introduction

To develop an effective ocular drug delivery system (ODDS) that can provide targeted drug delivery, as well as a controlled and sustained drug release, incorporation of an inclusion complex and/or NP into SCL has been investigated [542, 609, 610]. These systems are favourable since they encompass all the beneficial properties of a CD, NP and SCL in the development of an ODDS. While the use of CD and NP can result in an enhancement in drug bioavailability and provide a controlled release profile [203, 204], SCL has been extensively studied to increase ocular retention time of a drug [611, 612].

Aiming to not only prolong the drug delivery of a therapeutic SCL, but also to improve the lens hydrophilicity to resist the deposition of tear proteins, Li *et al.* investigated the use of β-CD-HA impregnated pHEMA lens for the controlled release of diclofenac [610]. The optimum developed lens model showed comparable properties to commercial lens with >90% light transmission, 65% water content and a modulus of 1.8 MPa. A sustainable drug release was also recorded in rabbits for 72 hours through an *in vivo* study. In addition, *in vitro* cell viability experiment on the pHEMA/β-CD-crHA$_{10}$ hydrogel also was determined to be non-toxic to 3T3 mouse fibroblasts.

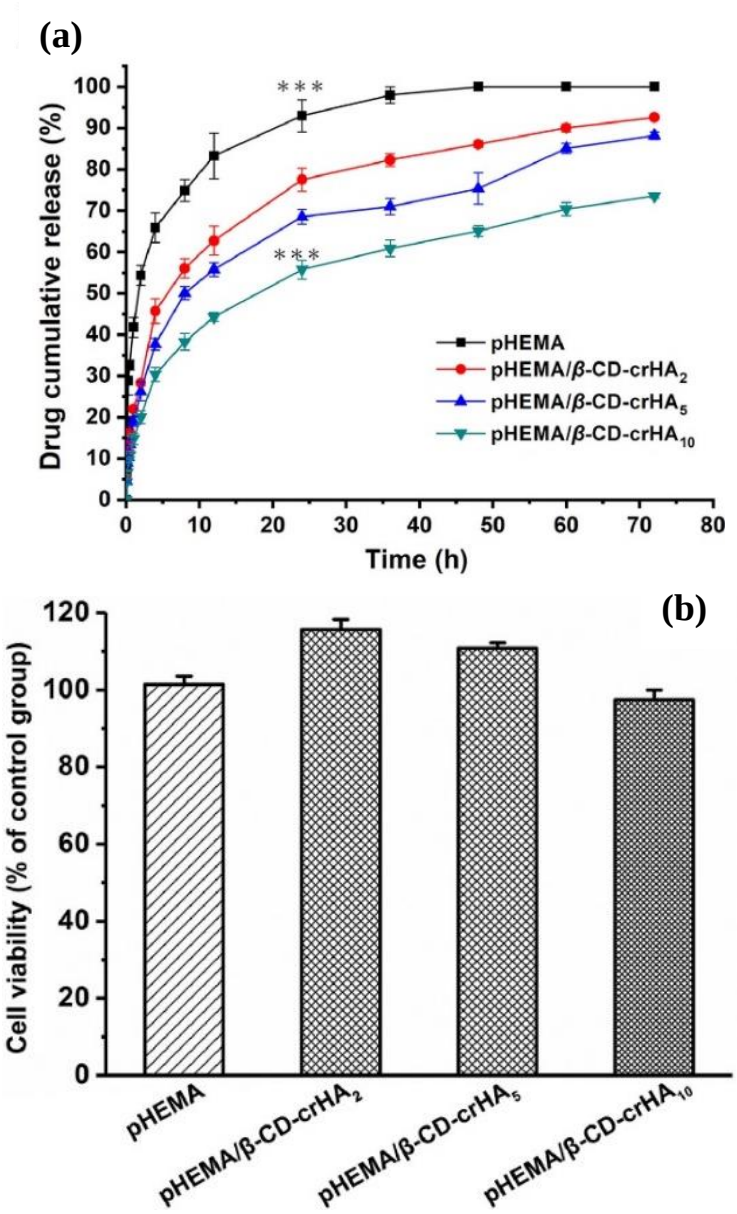

Figure 6.1: (a) Diclofenac %cumulative release profiles through pHEMA without and with the presence of β-CD-HA in PBS at 37 ºC (n = 3), and (b) viability of 3T3 fibroblast cells cultured in the extracts of various hydrogels for 72 h by MTT assay (n = 3) [610].

Following the successful formation of a NAR:sulfobutyl ether-ß-cyclodextrin (SBE-ß-CD) complex (Chapter 4), which was loaded into CS NPs (Chapter 5), these could lead to the development of an advantageous ODDS by impregnating them into the commercial-quality SCLs. The aim of this chapter was to investigate the feasibility of manufacturing complex- and NP-loaded SCLs, prepared by both direct entrapment and 'soak and release' approaches, to act as a therapeutic lens that has comparable properties to an unloaded commercial lens based on the relevant ISO standards.

6.2 Research Aims and Objectives

The aims and objectives of this chapter are:

- To manufacture NAR:SBE-ß-CD complex-loaded hydrogel SCLs by implementing direct entrapment and 'soak and release' approaches.
- To manufacture NAR-loaded CS NP impregnated hydrogel SCLs by implementing direct entrapment and 'soak and release' approaches.
- To fully characterize the developed complex- and NP-loaded SCLs for their physicochemical, mechanical, and dimensional properties.
- To evaluate the *in vitro* release behavior of the complex- and NP-loaded SCLs and identify the best fitted mathematical model for their release kinetics.
- To compare the lens' performance between direct entrapped complex- and NP-loaded SCLs versus NAR-loaded SCLs.
- To compare the lens' performance between complex- and NP-loaded SCLs versus NAR-loaded SCLs prepared by a 'soak and release' approach.

6.3 Experimental Methodology

6.3.1 Materials

As per Chapters 3 – 5.

6.3.2 Synthesis of complex- and NP-loaded lenses

NAR:SBE-ß-CD inclusion complex and NAR-loaded CS NPs were prepared using the methodologies outline in Section 4.3.3 (Chapter 4) and Section 5.3.2 (Chapter 5), respectively.

NAR:SBE-ß-CD inclusion complex and NAR-loaded CS NPs were entrapped in the SCL by adding either the complex or NP directly into the pre-polymerized monomer mixture. Six batches of complex- and six batches of NP-loaded lenses coding LC1-LC7, and LN1-LN7, respectively, were manufactured by adding 1-5, and 10 mg/mL of complex or NP in the pre-polymerized monomer mixture (Table 6.1).

NAR:SBE-ß-CD inclusion complex and NAR-loaded CS NPs were loaded into the SCL by soaking a lens in a complex solution and NP solution, respectively. Two batches of complex- and NP-loaded lenses coded LC3 and LN3, respectively, were manufactured by soaking each lens in 20.4 and 72.5 mg/3 mL of complex and NP solutions, respectively, in 0.1% Tween® 80 in PBS, pH 7.4 for 72 hours (Table 6.1).

The complex- and NP-loaded SCLs were prepared using the same procedure as described in Chapter 2, Section 2.3.

Table 6.1: Description of lenses used in this study.

Lens ID	Loading approach	Loaded complex (mg/mL)	Loaded NP (mg/mL)	NAR concentration (µg/lens)
CEP	Commercial Biotrue® ONEDay (nesofilcon A) lens.			
WM	Lens produced onsite using nesofilcon A pre-polymerized monomer mixture.			
LC1	Direct entrapment	1	-	0.93
LC2		2	-	1.86
LC3		3	-	2.79
LC4		4	-	3.72
LC5		5	-	4.65
LC6		10	-	9.30
LC7	Soak and Release		-	44.60 – 66.10
LN1	Direct entrapment	-	1	0.32
LN2		-	2	0.63
LN3		-	3	0.95
LN4		-	4	1.27
LN5		-	5	1.58
LN6		-	10	3.17
LN7	Soak and Release	-		44.60 – 66.10

6.3.3 Characterization of complex- and NP-loaded lenses

The following characterization techniques were carried out as per methodologies described in Section 3.3.4 (Chapter 3): thermogravimetric analysis (TGA), differential scanning calorimetry (DSC), Fourier-transform infrared spectroscopy (FT-IR), light transmission, equilibrium water content, refractive index, wettability, tensile strength, and lens dimensions (diameter, centre thickness, and sagittal depth).

The *in vitro* release studies of both soaked and directly entrapped complex- and NP-loaded SCLs (sterilized lenses stored in DI water) were performed using the same approach as described in Section 3.3.6 (Chapter 3).

The concentration of NAR was determined by HPLC, according to the procedure described in Section 3.3.3 (Chapter 3).

Statistical analysis was carried out as per Section 2.3.4 (Chapter 2).

6.4 Results and Discussion

6.4.1 Polymerization kinetics of complex- and nanoparticle-loaded lenses

A comparison of the polymerization kinetics, investigated by DSC, of four different lens systems, including blank, NAR-, complex- and NP-loaded SCLs, is presented in Figure 6.2 below. As mentioned in Chapter 2, a controlled and repeatable polymerisation process is essential to producing a commercial-quality lens. The potential impact the complex and NP had on the polymerization kinetics of the studied SCL was assessed in this study.

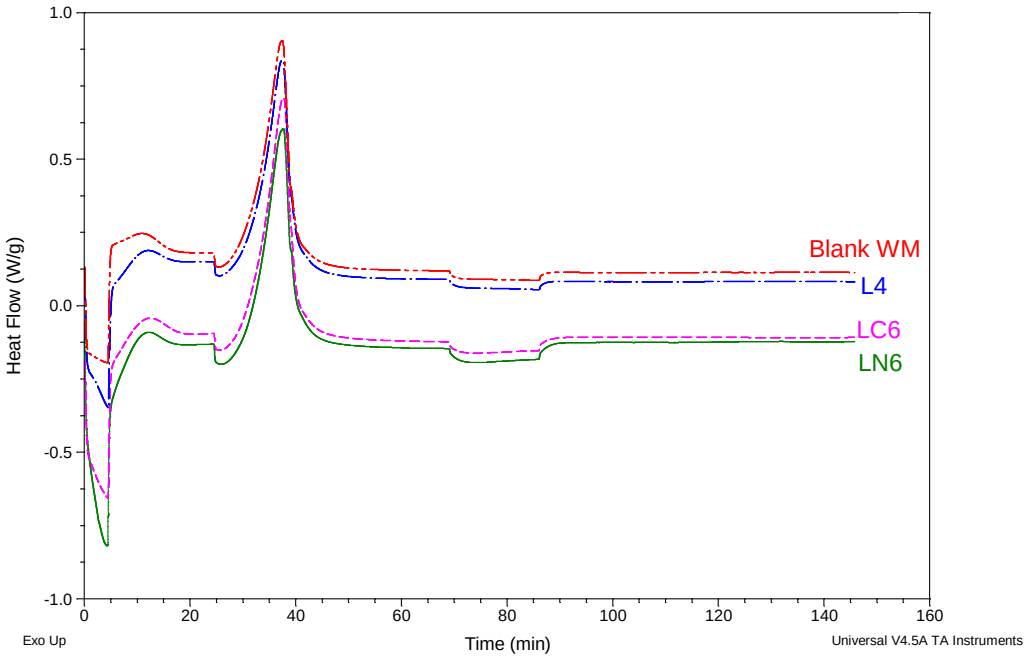

Figure 6.2: Polymerization kinetics of the pre-polymerization monomer mixture for blank, NAR- (L4), complex- and NP-loaded lenses as a function of time and temperature (n = 3).

As can be observed from Figure 6.2, the polymerization kinetics of complex- and NP-loaded SCLs resulted in a similar trend and curve to the blank and NAR-loaded lenses. The reaction enthalpy (J/g) at each of the two polymerization stages for CEP, NAR-, complex-, and NP-loaded SCLs was recorded in Table 6.2 below.

Table 6.2: Thermal data on peak temperatures and reaction enthalpy derived from the polymerization of pre-polymerized monomer mixture with and without the presence of NAR (n = 3, p-value > 0.05).

Sample	Peak 1		Peak 2	
	Temperature (°C)	**Reaction enthalpy (J/g)**	**Temperature (°C)**	**Reaction enthalpy (J/g)**
Nesofilcon A	63.99 ± 0.00	268.9 ± 17.1	90.16 ± 0.27	260.1 ± 4.9
L4	63.99 ± 0.00	284.2 ± 6.8	90.33 ± 0.04	245.7 ± 2.4
LC6	63.99 ± 0.25	277.6 ± 17.8	90.86 ± 0.43	249.9 ± 4.8
LN6	63.95 ± 0.06	383.6 ± 4.4	90.20 ± 0.16	248.9 ± 5.6

It can be seen from Table 6.2 that the polymerization kinetics of both LC6 and LN6 lenses encompassed two steps at comparable peak temperatures to CEP/Blank WM and L4 SCLs (p-value > 0.05). This indicated that the initiation process of this radical polymerization was not affected by the addition of either complex or NP. Comparing the reaction enthalpy generated from the CEP/Blank WM lens (268.9 ± 17.1 J/g), these values for LC6 and LN6 lenses were statistically higher which are 277.6 ± 17.8 J/g (p-value = 0.03) and 383.6 ± 4.4 J/g (p-value = 0.01), respectively.

This could be due to the presence of complex and NP that could hinder the chains' mobility within the polymeric matrix. On the other hand, reaction enthalpy values calculated in the second step of the polymerization for LC6 and LN6 SCLs showed no statistically significant difference in comparison to CEP/Blank WM lens (p-value > 0.05). In addition, when comparing the polymerization kinetics of these two systems to that of NAR-loaded lens, L4, while no statistical difference in the reaction enthalpies was observed for LC6 lens, the first initiated peak of LN6 lens gave a statistically higher value (p-value = 0.004). It was expected that a higher reaction enthalpy would have been obtained for LN7 lens due to the addition of NP into nesofilcon A polymerization mixture. Using DSC, Achilias investigated the impact of adding nano-compounds with different functional groups on polymerization kinetics of HEMA at 60 °C and 80 °C [413].

Although a lower activation energy was observed following the addition of the studied nanocomposite in Achilias's study, it was mentioned that a higher value would have been expected due to the extra barriers that the nano-compounds would add into the polymerization mixture [242, 613].

6.4.2 Physicochemical and mechanical analysis of complex- and NP-loaded SCLs

6.4.2.1 Thermal analysis of complex- and NP-loaded SCLs

Thermogravimetric analysis (TGA) was used to determine the degradation temperature of complex- and NP-loaded SCLs, with reference to the CEP, blank WM and NAR-loaded SCLs (i.e., L4), as well as NAR:CD inclusion complex and NAR-loaded CS NPs (Figure 6.3). All samples used in this analysis were in the dry state. For this part of the characterization, similarly to Section 6.4.1, only LC6 and LN6 (i.e., highest loading concentration) were used to investigate the effect of loading complex and NP on the lens' thermal properties.

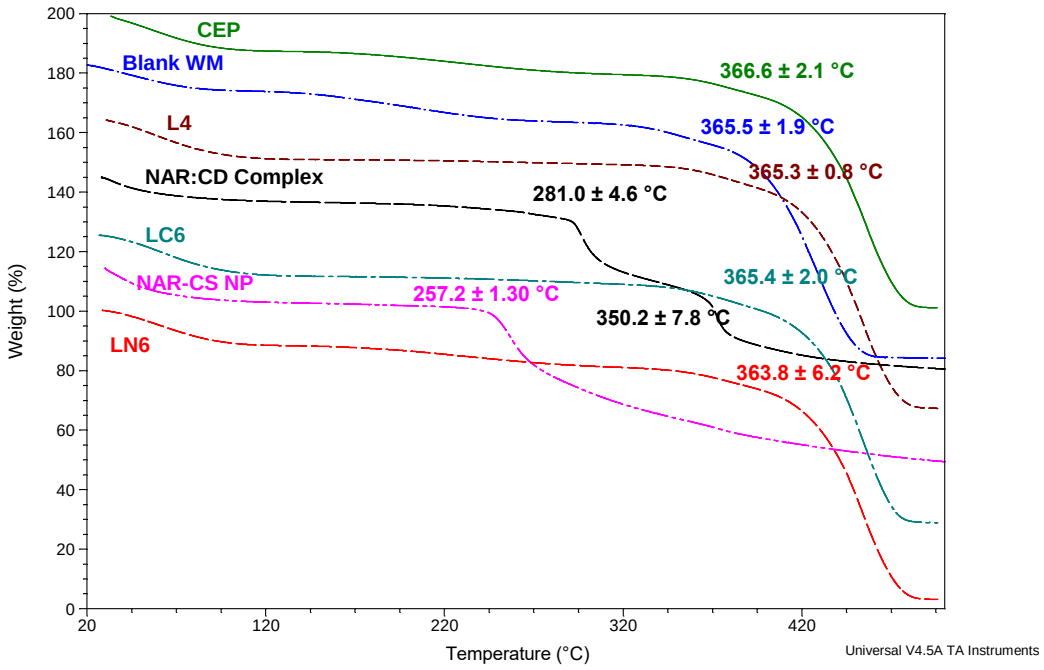

Figure 6.3: TGA thermograms of CEP, blank WM, L4, LC6, and LN6 lenses, as well as NAR:CD complex and NAR-CS NPs. All lenses were in the dry state and the instrumental value for degradation temperature was reported (n = 3).

Figure 6.3 demonstrates that all the five lens systems maintained over 80% of their weight up to 350 °C. Both LC6 and LN6 showed no statistically significant difference in the degradation temperature in comparison to both CEP, blank WM, and L4 SCLs (Table 6.5, p-value > 0.05). TGA analysis was previously used to confirm the thermal stability and thermoplasticity of a hydrogel material [477-479]. A similar observation was seen before in previous works on the development of NP-loaded hydrogel materials [614, 615]. Saygili *et al.* examined the influence of TGF-ß3 (transforming growth factor beta-3) PLGA NP on the thermal degradation of PAAm-Alg (polyacrylamide-alginate) hydrogel for cartilage repair and clinical application [616]. Following the incorporation of PLGA NP into the hydrogel matrix, no noteworthy differences were observed in the thermal properties of PAAM-Alg hydrogel (Figure 6.4).

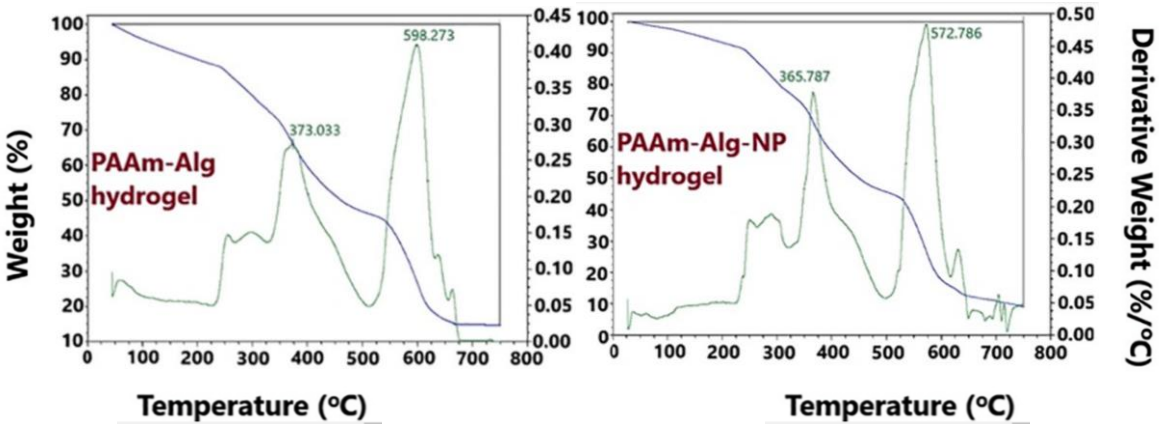

Figure 6.4: TGA thermograms of PAAM-Alg hydrogel and NP-loaded PAAM-Alg hydrogel [616].

To further study the stiffness and flexibility of the developed materials, the above SCLs were also analyzed using DSC to determine the lens's glass transition temperature (T_g, Figure 6.5) since it is determined by steric and electrostatic interactions [481].

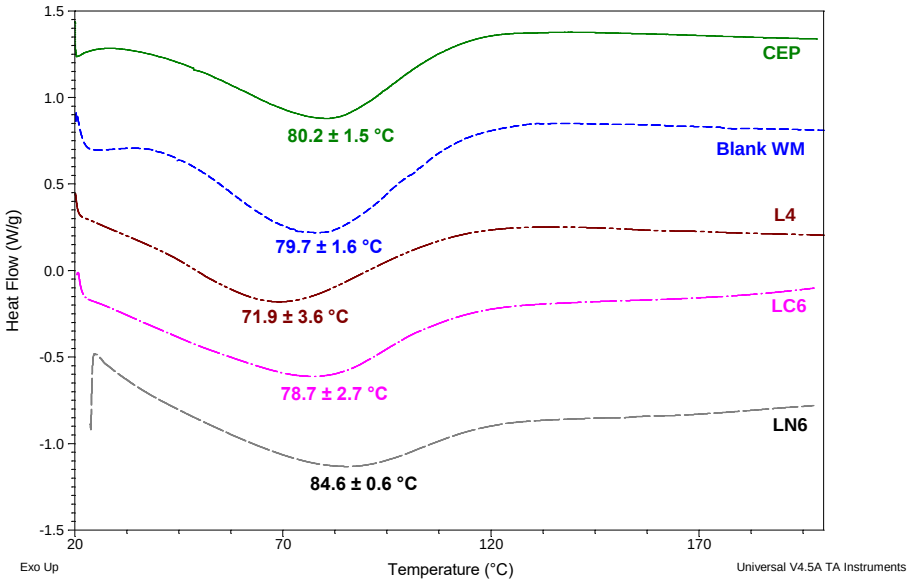

Figure 6.5: DSC thermograms of the CEP, blank WM, L4, LC6, and LN6 lenses. All lens' systems were in the dry state and the instrumental value for T_g was reported (n = 3).

A non-statistically significant difference in T_g between the referenced lens systems and LC6 lenses can be seen in Figure 6.5 (p-value > 0.05). A statistically higher T_g value was recorded for LN6 lens (78.7 ± 2.7 °C) in comparison to the remaining systems (Figure 6.5, Table 6.3). A similar trend was observed in a study carried out by Gaabour, which investigated the thermal behaviour of gold NP on PAM/CS hydrogel using DSC [615]. The first transition in the generated DSC thermograms in the aforementioned study was attributed to the T_g of the developed PAM/CS samples, measured to be in a range of 100-120 °C. This transition, also could be called as a relaxation process, was proposed to be due to the micro-Brownian motion of the main polymeric chain backbone in the hydrogel [615].

Table 6.3: Summary table of the fabricated lens' T_g and degradation temperature.

Lens sample	**T_g (°C)* (n = 3)**	**Degradation temperature (°C)* (n = 3)**
CEP	80.2 ± 1.5	366.6 ± 2.1
WM	79.7 ± 1.6	365.5 ± 1.9
L4	71.9 ± 3.6^{+}	365.3 ± 0.8
L6	N/A	N/A
LC6	78.7 ± 2.7	365.4 ± 2.0
LN6	84.6 ± 0.6^{+}	363.8 ± 6.2

$^{+}$: values exhibit a p-value < 0.05 in comparison to the CEP/blank WM lens.
*: measurement was carried out on samples in their dry state only.

As previously discussed in Section 3.4.4.1 (Chapter 3), T_g of a SCL is directly related to on-eye comfort. A higher T_g value suggests that there is more intermolecular constraint in the motion of the polymeric chain segment in the lens matrix, which results in a reduction in its water content (Table 6.4) and thus, an increase in its tensile strength (Table 6.5) [617]. This technique was used previously by Hao *et al.* to assess the T_g behaviour of a solid lipid NP (SLN) impregnated hydrogel (poloxamer-based) for the delivery of Resina Draconis to the eye [618]. An increase in T_g value following the incorporation of SLN into the hydrogel could be observed and the disappearance of a characteristic peak of the drug-loaded SLN can be noted in the generated thermograms illustrated in Figure 6.6 [618]. This observation agreed with the reported outcome on NP-laden SCL, LN6 lens, developed in the present work.

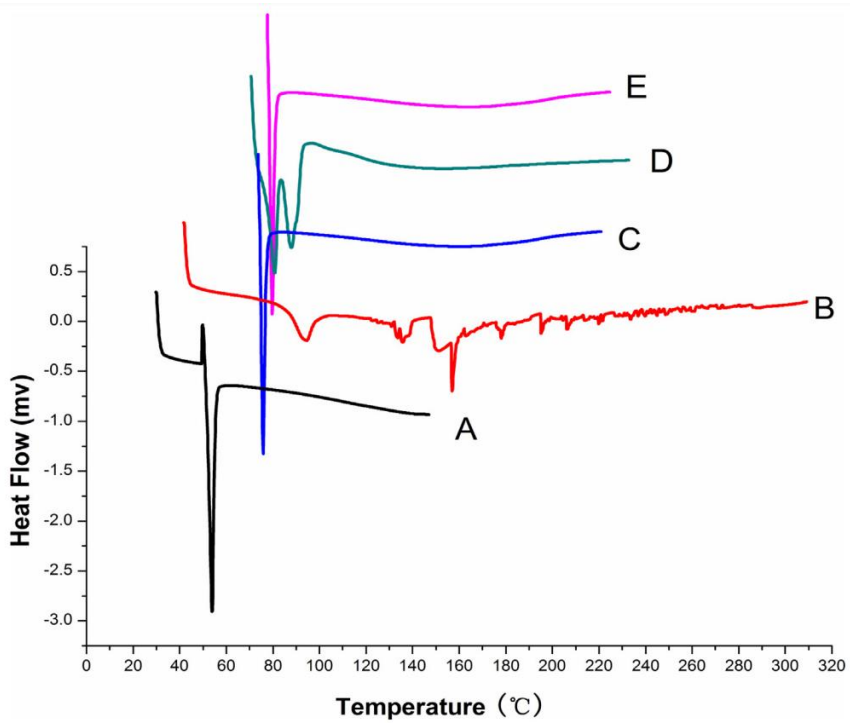

Figure 6.6: DSC thermograms of (A) lyophilized blank hydrogel; (B) Resina draconis; (C) lyophilized Resina draconis-loaded SLNs; (D) lyophilized SLNs-based hydrogel hybrid system; and (E) lyophilized blank SLN [618].

6.4.2.2 Equilibrium water content of complex- and NP-loaded SCLs

Equilibrium water content studies were performed to investigate the influence of the complex and NP on the swelling behaviours of the PVP SCLs (i.e., nesofilcon A). Each lens was fully hydrated in DI water at room temperature for 24 hours to induce

maximal swelling of the lens. Table 6.4 presents the %EWC and standard deviation for SCLs impregnated with complex and NP at various concentrations, with reference to CEP, blank WM, and NAR-loaded SCLs (i.e., L4 and L6 lenses). The data showed that the incorporation of both complex and NP resulted in a reduction in %EWC of the fabricated complex- and NP-loaded SCLs in comparison to blank WM lens (75.8 ± 0.2%, Table 6.3). Besides LC6 (72.5 ± 0.3%) and LN6 (71.2 ± 1.1%), which were the lenses with the highest amount of loading complex and NP, respectively, the remaining developed SCLs had a %EWC value within the ISO tolerance (i.e., ±2% of absolute value, which is 76.0% for CEP lens that was experimentally determined in Section 2.4.2.4).

Table 6.4: Summary table of the fabricated lens' light transmission, water content, and refractive index (n = 3).

Lens sample	%T	%EWC	Refractive index
CEP	98.1 ± 0.7	76.0 ± 0.5	1.373 ± 0.000
WM	98.2 ± 0.8	75.8 ± 0.2	1.373 ± 0.000
L4	97.6 ± 0.5	75.6 ± 0.6	1.373 ± 0.000
L6	98.2 ± 0.6	75.9 ± 1.0	1.373 ± 0.000
LC1	99.5 ± 0.1	73.9 ± 0.3^{+}	1.373 ± 0.002
LC2	98.7 ± 0.3	74.7 ± 0.1^{+}	1.373 ± 0.001
LC3	99.1 ± 0.2	74.3 ± 0.3	1.373 ± 0.002
LC4	98.4 ± 1.3	74.1 ± 0.3^{+}	1.374 ± 0.005^{+}
LC5	97.3 ± 0.6^{+}	74.3 ± 0.2^{+}	1.374 ± 0.004^{+}
LC6	90.6 ± 0.1^{+}	72.5 ± 0.3^{+}	1.375 ± 0.001^{+}
LC7	98.3 ± 0.2	73.5 ± 0.4^{+}	1.375 ± 0.001^{+}
LN1	98.6 ± 0.7	73.9 ± 0.2^{+}	1.373 ± 0.002
LN2	96.8 ± 1.4^{+}	74.5 ± 0.5	1.373 ± 0.001
LN3	97.7 ± 0.3	74.3 ± 0.5	1.373 ± 0.002
LN4	97.6 ± 0.6	74.3 ± 0.5	1.374 ± 0.003^{+}
LN5	97.9 ± 0.6	73.9 ± 0.1^{+}	1.374 ± 0.004^{+}
LN6	92.6 ± 1.1^{+}	71.2 ± 1.1^{+}	1.377 ± 0.002^{+}
LN7	98.2 ± 0.8^{+}	74.1 ± 0.4	1.375 ± 0.002^{+}
ISO tolerance [399]	± 5% absolute*	± 2% absolute*	± 0.005 absolute*

*: values from the CEP/blank WM lenses.
$^{+:}$ values exhibit a p-value < 0.05 in comparison to the CEP/blank WM lens.

The decrease in water content with an increase in the amount of complex loaded in the lens matrix in this study was opposite to what was previously observed in other studies. Li *et al.* cited that due to the hydrophilic nature of ß-CD-hyaluronan (crHA), when loaded in the hydrogel lens matrix, the fabricated lens had a water content of 65%

while a value of 50% was recorded for the unloaded lens [610]. In addition, an increase in the water content of the developed complex-loaded SCL (e.g., from 42% to 60%) was also observed in work carried out by Xu *et al.* [619]. The reason for this contradictory observation was postulated to be due to compatibility between the developed inclusion complex and the hydrogel matrix in this study. Although the NAR:CD complex is hydrophilic, its poor solubility in the pre-polymerized mixture could lead to precipitation within the matrix and thus, decreasing the swelling ability of the finished lens. Furthermore, the water content of the studied lens (nesofilcon A material) is significantly higher than those from the aforementioned studies (50% and 42%). Hence, an addition of either complex or NP would compete with the hydrophilic monomers in the pre-polymerized monomer mixture, resulting in a lower swelling ability of the lens.

A reduction in water content with an increase in loading amount of NP into the lens matrix as observed in this study agreed with previous works on NP-loaded lenses [51, 52, 378]. The average water content of developed pHEMA lens was measured to be 35.9 ± 0.4% as cited by Elshaer *et al.*, which significantly decreased to 30.4 ± 0.7% when the lens was loaded with 0.4 g PLGA NP [378]. This trend was suggested to be because of an increase in physical crosslinking between polymeric NPs and the hydrogel matrix which potentially hindered the swelling ability of the lens, which was demonstrated in Section 6.4.2.1.

6.4.2.3 Refractive index of complex- and NP-loaded SCLs

Table 6.4 shows that the RI values of both the complex- and NP-loaded lenses increased with an increase in their loading concentration. In both types, the RI of LC1-LC3 and LN1-LN3 lenses showed no statistically significant difference in comparison to blank WM and CEP lenses. However, when the loading concentration increased to 4 mg/mL, both complex- and NP-lenses exhibited a higher RI value (p-value < 0.05). This was postulated to be due to the higher loading concentration of complex and NP into the lens matrix, which leads to a reduction in water content of these lenses. As discussed in Section 1.4.6.4 (Chapter 1), RI of a lens is inversely related to its EWC. Nonetheless, all of the RI values obtained in the present study on both complex- and NP-loaded SCLs are comparable to the CEP lens when based on the ISO 18369-2 standard since these differences are within the tolerance limit (± 0.005) [399].

A range of commercial hydrogel SCLs, along with their water content and RI, was previously summarized by Gonzalez-Meijome *et al.* [301], where an increase in RI value was observed with a decrease in lens water content. For instance, an RI value of 1.38 was noted for Hilafilcon A lens that has 70% EWC, while for Alphafilcon A lens, which has a lower %EWC of 66% has an RI value of 1.39, this value further increases to 1.40 for etafilcon A lens with 58% water content.

A change in RI value between blank silicone hydrogel (SiHy) SCL (i.e., 1.417 ± 0.02) and lens after being coated with hyaluronic acid/poly(L-lysine) hydrobromide (1-ethyl-3-(3-dimethyl-amino-propyl) carbodiimide hydrochloride)+diclofenac sodium salt (i.e., 1.419 ± 0.02), which was also within the ISO tolerance, was previously observed in Silva *et al.* work [389]. Even though the RI is essential and one of the properties that commercial SCLs should be evaluated for according to the ISO 18369–1:2017 standard [433], this property has not been extensively investigated in therapeutic SCL research [218].

6.4.2.4 Light transmission of complex- and NP-loaded SCLs

From the generated data (Figure 6.7 and Table 6.4), it could be seen that the %light transmission of the complex- and NP-lenses prepared at a lower concentration than 5 mg/mL was above 96% and 93%, respectively. When compared to the blank WM lens, complex- and NP-lenses prepared at these concentrations showed a non-statistically significant difference in this property (p-value > 0.05). However, at the maximum loading concentrations, a statistically significant reduction in light transmission in both complex- and NP-lenses was observed (p-value > 0.05 in comparison to blank WM lens). For instance, in a range of visible light (400-800 nm), at 10 mg/mL loading concentration, an average of 90.6 ± 0.1 % light transmission was recorded for LC6 while a value of 92.6 ± 1.1 % was noted for LN6.

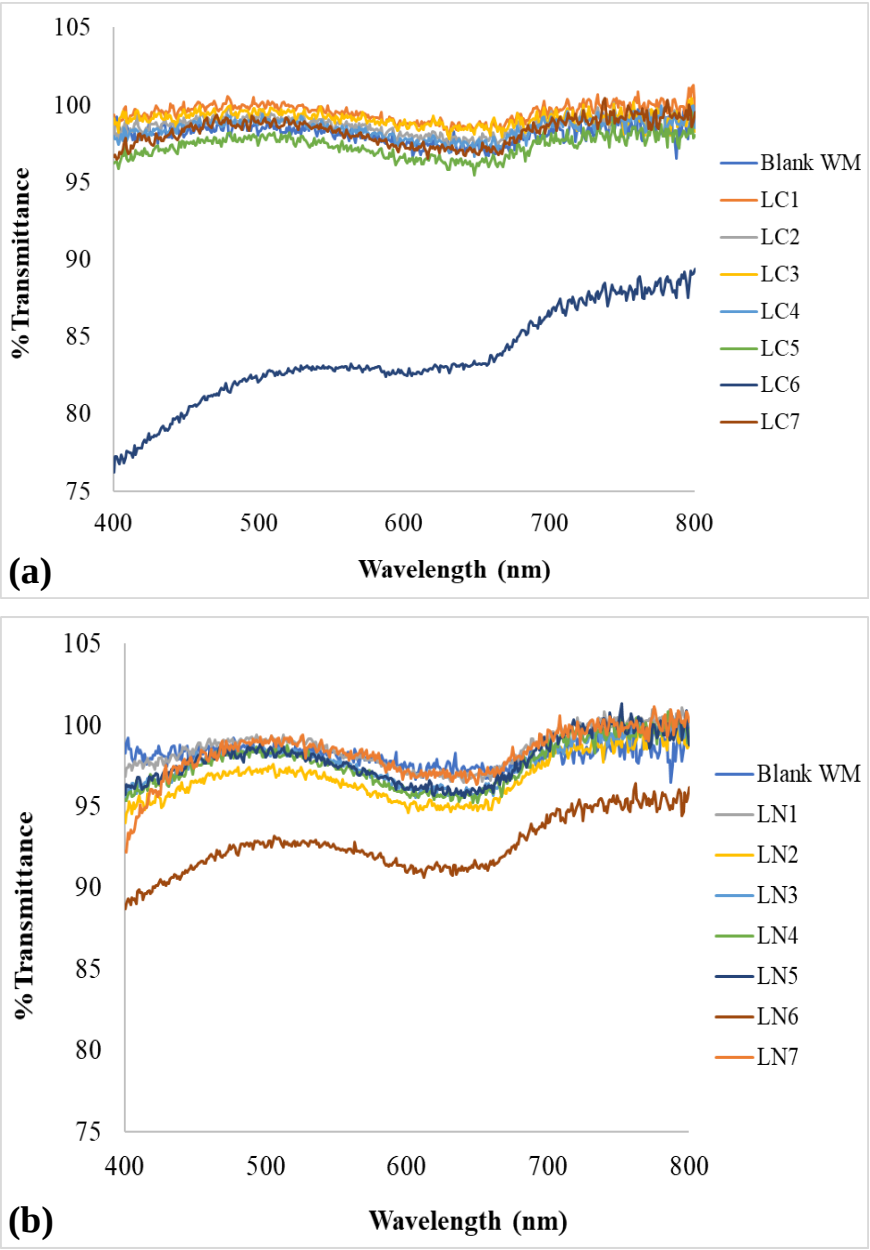

Figure 6.7: Spectral transmittance of (a) complex-lens and (b) NP-lens prepared by both direct entrapment and 'soak and release' approaches in a visible region (400-800 nm), with reference to blank WM lens.

The impact of NP on lens transmittance was widely reported and agree with the observation from this study. A reduction in light transmission of a therapeutic lens was previously noted in a study carried out by Elshaer *et al.* [378]. Their work developed a PLGA (poly(lactic-co-glycolic acid)) NP-loaded pHEMA lens for the delivery of prednisolone to reduce eye allergic reactions. The developed PLGA NPs had a size of 294.5 ± 1.8 nm and a positive charge of 5.6 ± 1.8 mV. Light transmission of NP-loaded lens, at 0.2 g loading concentration, resulted in an 86.2% optical clarity in comparison

to 94.5% for unloaded lens. This value decreased to 83.1% when the loading concentration increased to 0.4 g [378]. A similar trend was observed by Maulvi *et al.* through the incorporation of cyclosporine-loaded Eudragit S100 NPs into the pHEMA SCLs [51]. The light transmission of the developed NP-loaded SCLs decreased with an increase in the loaded concentration of NPs. For example, the transmittance of the unloaded pHEMA lens significantly decreased from 99.6 ± 0.5% to 91.6 ± 0.7% to as low as 56.7 ± 1.8% at 2.56 and 4.29 mg/mL NP loading concentrations, respectively. This was postulated to be due to the appearance of nano-cavities within the hydrogel matrix that triggered the precipitation of drug [51].

In the present work, 98% optical clarity was obtained for NP-lenses at a NP concentration of 5 mg/mL (LN5 lens, Figure 6.7). For complex-loaded SCLs, over 97% transmittance was recorded for LC1-LC5 lenses, which was statistically reduced to 90.6 ± 0.1% when the loading concentration was at 10 mg/mL (LC6). A similar observation was cited by Li *et al.*, which demonstrated that when 10 mg/mL of ß-CD-hyaluronic acid (HA) was loaded in the developed pHEMA lens, over 90% of light transmission was measured [610]. Nevertheless, as could be observed in Figure 6.8 below, eventhough LC6 exhibited >90% optical clarity, the lens was visibly opaque and so it was determined to be not suitable for use as commercial SCLs.

On the other hand, lenses prepared under ‘soak and release’ approach, which were at a higher loading concentration, exhibited a better light transmissibility in both cases (>98 %) and visibly clear as can be observed in Figure 6.8. This observation suggested that ‘soak and release’ could potentially be a better approach, in terms of light transmission, in comparison to direct entrapment for both complex- and NP-loaded SCLs due to the inclusion complex and the NP low solubility in the pre-polymerized monomer mixture in the present study.

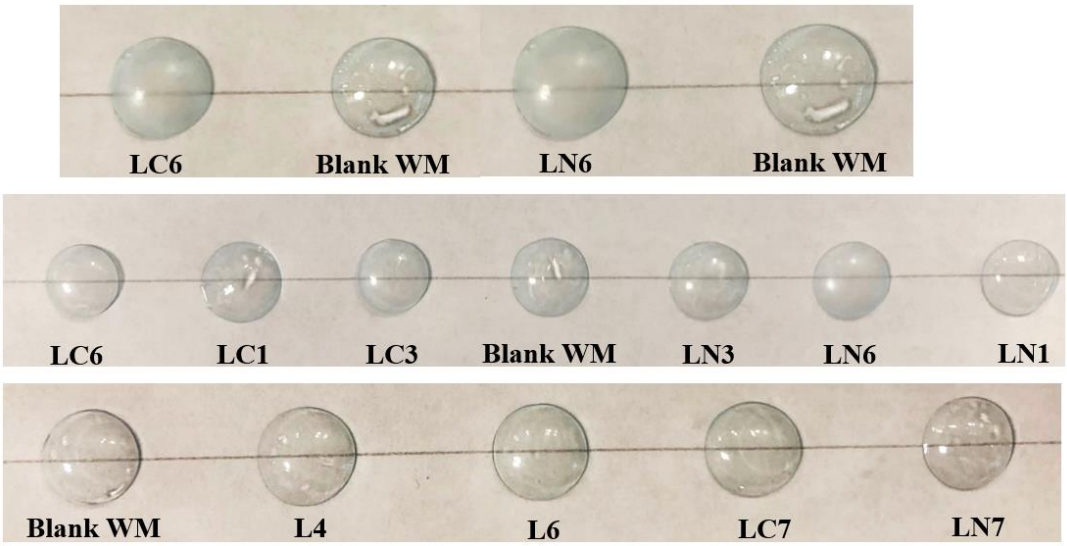

Figure 6.8: Images of blank lens (Blank WM) and lenses incorporated with NAR (L4 and L6), NAR:CD complex (LC3, LC6 and LC7), and NAR-CS NPs (LN3, LN6 and LN7), all lenses were in hydrated state.

6.4.2.5 Contact angle of complex- and NP-loaded SCLs

As discussed in Section 1.4 of Chapter 1, the hydrophilicity of a SCL has a significant influence on lens comfort, which can be characterized by CA measurement [218]. A CL that has a good wettability would maintain a normal and functional ocular surface. When comparing to blank WM lens (40.35 ± 0.66°), it was noted that the CA of both complex- and NP-loaded SCLs, prepared by either direct entrapment (41.48 ± 1.23° and 42.18 ± 1.01°, respectively) or 'soak and release' (42.37 ± 1.73° and 42.49 ± 1.33°, respectively) approaches, showed no statistical difference in comparison to blank WM lens (Table 6.5, p-value > 0.05). Hence, the outcome from this characterization implied that the incorporation of complex and NP into the hydrogel lens matrix did not alter its wettability.

This observation was in contrast for NAR-loaded SCLs, where an increase in loading NAR concentration resulted in an increase in lens' CA (e.g., L4: 45.76 ± 0.87°), and thus, a decrease in lens' hydrophilicity. The differences between the impact of NAR versus complex and NP had on the lens wettability were due to the hydrophobic nature of NAR and hydrophilic nature of complex and NP. An enhancement on water absorption of hydrogel SCLs following the incorporation of an inclusion complex and drug-loaded polymeric NPs was previously observed in different studies [378, 610].

For instance, Li *et al.*, using a sessile drop technique, demonstrated that by decorating the pHEMA lens by ß-CD-HA, the water contact angle noticeably reduced, from 90° to 55°, due to the distribution of hydrophilic CD on the hydrogel lens surface [610]. Using a similar methodology, Elshaer *et al.* also showed that by incorporating a PLGA NP into the hydrogel pHEMA lens matrix, CA values of the lens also decreased from 85° to 75°, which demonstrated an enhancement in lens wettability [378].

6.4.2.6 Tensile modulus of complex- and NP-loaded SCLs

The mechanical properties of the complex- and NP-loaded SCLs were characterized in reference to the CEP, blank WM and NAR-loaded lenses in this study (Table 6.5). Such values are essential to control in the development of a commercial-quality lens in order to optimise ease in handling and insertion onto the eye [218]. It was discussed previously in Section 1.4.6.8 (Chapter 1) that while a low Young's modulus would result in a lens that could be prone to breakage during handling, too high a Young's modulus would lead to an increase in lens stiffness, and hence, less comfort. This part of the characterisation included the analysis of LC6, LC7, LN6, and LN7 lenses to examine the impact of loading maximum concentration of complex and NP into the lens matrix. Furthermore, this study also investigated the possible effect of the different methods (i.e., direct entrapment and 'soak and release') on incorporating analytes into the lens on its mechanical properties.

Both complex- and NP-loaded SCLs, prepared by direct entrapment and 'soak and release' approaches, showed statistically significant higher values in the Young's moduli (0.72 – 0.83 MPa) in comparison to CEP, blank WM and L4 SCLs (0.53 – 0.54 MPa). Tensile modulus of complex- and NP-loaded SCLs was previously investigated in various works to study the impact on the lens mechanical properties [52, 378, 610, 619]. Xu *et al.* demonstrated an increase in lens modulus following the addition of 7.68 %wt and 15.24 %wt ß-CD into the pHEMA hydrogel, from 0.542 ± 0.139 MPa for pHEMA lens to 0.584 ± 0.098 MPa and 0.614 ± 0.253 MPa, respectively, for pHEMA/ß-CD lens [619]. The reason for such an outcome was postulated to be due to the presence of CD in the hydrogel matrix that could lead to a formation of interchain junctions, and thus, decreasing the flexibility of the polymer chain [620].

This trend was also observed in a case of NP-loaded hydrogel lens as cited by Nasr *et al.* [52]. An increase of lens modulus from 0.51 MPa for pHEMA hydrogel to 0.92 MPa for lens with 7.5% NP loading concentration. Similar to the proposed reason for complex-loaded lenses, the introduction of NP could potentially increase the crosslinking density of the hydrogel matrix, resulting in a higher lens modulus. Although both of the developed complex- and NP-loaded SCLs have higher moduli than CEP lens, those values are within the range of other hydrogel SCL materials with similar composition (0.1 – 1.9 MPa) [340, 435]. As a result, the developed loaded SCLs in this study can be considered to exhibit an appropriate mechanical property for commercialized hydrogel SCLs.

Table 6.5: Summary table of the fabricated lens' contact angle and Young's modulus.

Lens sample	Contact angle (°) (n = 10)	Tensile strength (MPa) (n = 10)
CEP	41.22 ± 0.57	0.53 ± 0.05
WM	40.35 ± 0.66	0.54 ± 0.06
L4	45.76 ± 0.87^{+}	0.53 ± 0.06
L6	44.47 ± 0.97^{+}	0.53 ± 0.07
LC6	41.48 ± 1.23	0.83 ± 0.19^{+}
LC7	42.37 ± 1.73	0.77 ± 0.10^{+}
LN6	42.18 ± 1.01	0.73 ± 0.11^{+}
LN7	42.49 ± 1.33	0.72 ± 0.11^{+}

$^{+:}$ values exhibit a p-value < 0.05 in comparison to the CEP/blank WM lenses.

6.4.2.7 Fourier transform infrared spectroscopic analysis of complex- and NP-loaded SCLs

The spectroscopic characterization of developed complex- and NP-loaded hydrogel SCLs was performed by Fourier-transform infrared spectroscopic analysis (FT-IR). To investigate the impact of loading complex (LC6) and NP (LN6) into the hydrogel matrix, the FT-IR spectra of blank WM, L4, NAR:CD complex and NAR-loaded CS NPs are also included in Figure 6.9.

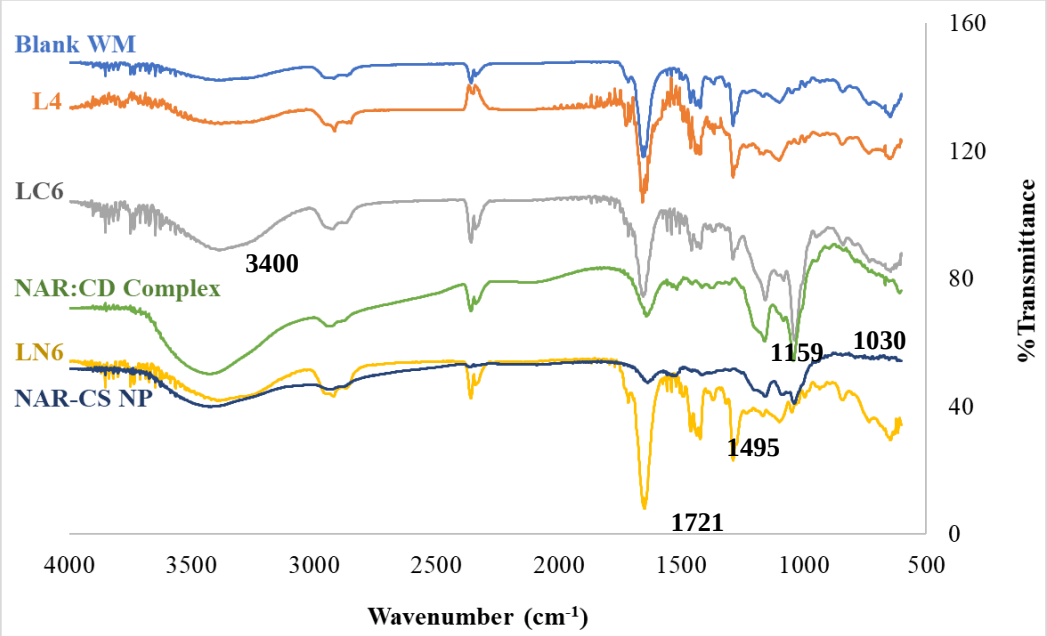

Figure 6.9: FT-IR spectra of blank WM, L4, LC6 and LN6 lenses (all were in dry state).

As mentioned in Chapter 2, NVP is the main component in the nesofilcon A monomer mixture, thus, it was expected that the FTIR spectra of the developed LC6 and LN6 lenses would exhibit the characteristic peaks of PVP (poly-vinylpyrrolidone Figure 2.22). Figure 6.9 shows that L4, LC6 and LN6 presented some different absorption peaks in comparison to the blank WM lens FT-IR spectrum as expected. While the main difference between L4 and blank WM spectra contributed to the additional peak at 1711 cm^{-1} indicated the presence of NAR, LC6 spectrum contained a strong absorption peak at 1159 cm^{-1} and 1030 cm^{-1} that could not be observed in either L4 or blank WM spectra. These peaks are at similar positions as the NAR:CD complex spectrum, which represented the HOC bending in NAR (1160 cm^{-1}) and C-O or sulfoxide stretching in SBE-ß-CD (1044 cm^{-1}) functional groups, respectively, as determined in Section 4.4.3.3 (Chapter 3). This observation confirms the presence of the inclusion complex within the hydrogel matrix. Using the same approach, Li *et al.* demonstrated the incorporation of ß-CD-HA into the developed pHEMA hydrogel through the appearance of additional peaks, representing HA, in the ß-CD-HA-loaded hydrogel FTIR spectrum [610].

For LN6, characteristic peaks of the NAR:CD complex at 1163 and 1045 cm^{-1} could also be observed but with less intensity, possibly due to the formation of NP through ionic cross-linking between the complex and CS. Moreover, a shift in wavenumbers

of a characteristic peak represented N-H bending vibration of CS (from 1588 to 1593 cm^{-1}), associated with NAR-NP, could also be seen in LN6 lens, which was not visible in other spectra in Figure 6.9. The outcome from this analysis indicated the successful formation of NP-loaded hydrogel lens. Similar observations were noted in the work carried out by Behl *et al.*, which investigated the potential microstructural changes and other potential interactions of dexamethasone-loaded CS NP-loaded hydrogel using FTIR analysis [283]. Their analysis demonstrated that the spectrum of the NP-loaded lens not only contained all the characteristic peaks of a pHEMA lens, but other main characteristic peaks of the developed drug-loaded CS NP could also be seen.

The above observations suggested that there were some intermolecular interactions (e.g., hydrogen bonding) between the complex/NP and the polymeric matrix. As discussed in Section 3.4.4.7, it was predicted that the drug release rate from the developed complex- and NP-loaded SCLs would be lower than that of NAR-loaded SCL due to such interaction.

6.4.3 In vitro naringenin release studies from complex- and nanoparticle-loaded SCLs

Due to the low NAR concentration in LC1-LC5 and LN1-LN5 lenses, which was below the HPLC limit of detection and quantification, these lenses were not studied using the *in vitro* release studies. Furthermore, as discussed in Section 6.4.2.4, LC6 and LN6 lenses did not exhibit commercial quality of a SCL (e.g., opaque lenses) and thus, these lens systems were not examined for their *in vitro* release behaviors.

This study was carried out using only LC7 and LN7 lenses in PBS+0.1% Tween® 80 at 37 °C. Figure 6.10 presents the percentage cumulative drug release (%) profiles for an initial daily release (24 hours) and a 7-day release (168 hours) for LC7 and LN7 lenses with reference to L4 lens and NAR-loaded CS NP release profiles.

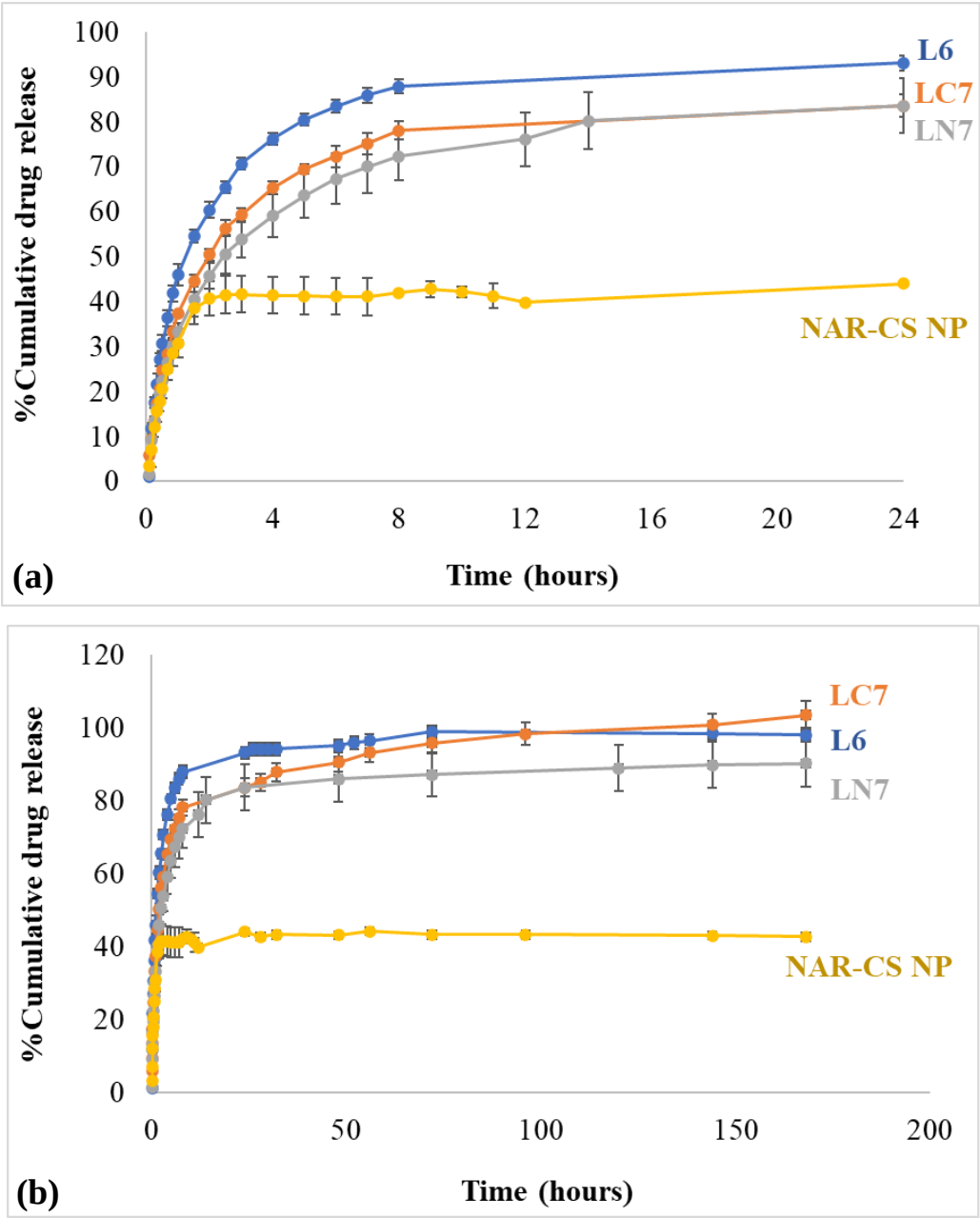

Figure 6.10: (a) 24-hour *in vitro* release profiles of LC7, LN7, L4 lenses, and NAR-loaded CS NP (n = 3); and (b) 7-day *in vitro* release profiles of LC7, LN7, L4 lenses, and NAR-loaded CS NP (n = 3).

As can be observed in Figure 6.10(a), a controlled and sustained NAR release took place in the first 24 hours was followed by a stabilized release of NAR over the next seven days (Figure 6.10(b)). The amount of NAR released from LC7 and LN7 was calculated at the end of the first 24 hours of release to be 45.95 ± 2.06 and 45.96 ± 5.18 µg/day, respectively. When comparing to the developed NAR-loaded lens prepared using the same methodology and NAR loading concentration (0.283 mg

NAR/mL/lens), L6 (54.42 µg/day), both LC7 and LN7 had statistically lower daily NAR released concentrations. However, the released amount of NAR of both LC7 and LN7 is still within the estimated therapeutic window of NAR as outlined in Section 3.4 (Chapter 3). Taking into consideration of the amount of NAR released during the initial burst phase (i.e., 8 hours), LN7 lens had the smallest amount (39.75 µg), followed by LC7 lens (42.93 µg), with L6 lens having the highest amount of NAR released, at 48.37 µg. This suggested that LC7 and LN7 provided a more controlled NAR release in comparison to L6, which was attributed to the formation of a NAR:CD inclusion complex and NAR-loaded CS NPs, respectively. The obtained release patterns are in agreement with the FTIR analysis in Section 6.4.2.7 regarding the impact of intermolecular interactions between the complex/NP and the polymeric matrix on *in vitro* release behavior of the complex- and NP-loaded SCLs. By loading NAR into the lens using a direct entrapment approach, a higher crosslinking was expected in comparison to those prepared using a 'soak and release approach'.

By applying a range of possible mathematical models: zero-order, first-order, Higuchi, and Korsmeyer-Peppas, the release mechanism of both the complex- and NP-loaded lenses was investigated. The model was determined based on the initial NAR release phase, i.e., 8 hours. From the generated *in* vitro release data, the correlation coefficient (R^2) values were calculated to identify the best fit model to describe the release mechanism of LC7 and LN7 lenses. The R^2 values, diffusion exponent (n), and rate parameter (k) values are listed in Table 6.6.

Table 6.6: Release kinetic data for initial release phase obtained from zero order, first order, Higuchi and Korsmeyer-Peppas mathematical models from the prepared therapeutic SCLs and NAR-loaded CS NPs.

Sample type	**Drug release during initial release**			
	Zero order (k unit: M/s)	**First order (k unit: 1/M)**	**Higuchi (k unit: $M/s^{1/2}$)**	**Korsmeyer-Peppas**
L6	$R^{2:}$ 0.7991 k = 0.1624	$R^{2:}$ 0.3920 k = 0.0019	$R^{2:}$ 0.9355 k = 4.2472	$R^{2:}$ 0.7727 n = 0.6759
NAR-loaded CS NP	R^2: 0.8941 k = 0.3203	R^2: 0.6427 k = 0.0073	R^2: 0.9804 k = 4.4959	R^2: 0.9540 n = 0.7745
LC7	R^2: 0.8445 k = 0.1459	R^2: 0.6125 k = 0.0017	R^2: 0.9618 k = 3.7628	R^2: 0.9613 n = 0.5487
LN7	R^2: 0.8397 k = 0.1389	R^2: 0.5962 k = 0.0017	R^2: 0.9596 k = 3.5889	R^2: 0.9534 n = 0.5553

As can be observed from Table 6.6, based on the R^2 values generated from each of the mathematical models, the Higuchi and the Korsmeyer-Peppas kinetic release models were determined to provide a good fit for both LC7 and LN7 SCLs. This observation suggested that the mechanism of NAR release in these developed SCLs is mainly governed by diffusion. The diffusion exponent values 'n' obtained from the Korsmeyer-Peppas model for LC7 and LN7 lenses were higher than 0.5 (i.e., 0.5487 and 0.5553, respectively), indicating a non-Fickian release type. Hence, the mechanism of NAR release in these developed SCLs is governed by both diffusion and swelling [496, 497]. The outcome from this *in vitro* release study agrees with previous investigations on *in vitro* release behaviours of complex- and NP-loaded hydrogel lenses [52, 378, 610, 612]. Therefore, it can be determined that the developed complex- and NP-loaded SCLs, prepared by 'soak and release' approach, in the current work exhibited an acceptable *in vitro* release behaviour.

6.4.4 Dimensional analysis of complex- and NP-loaded SCLs

As discussed in the previous Chapters, it is essential to assess the dimensional properties of the developed complex- and NP-loaded SCLs to evaluate the feasibility of commercialization of the developed lenses [218]. Diameter, sagittal depth, and centre thickness of the fabricated lenses are presented in Table 6.7.

Table 6.7: Diameter, sagittal depth, and centre thickness values of the control and developed lenses (n = 10).

Lens type	Diameter (mm)	Sagittal depth (mm)	Centre thickness (mm)
CEP	14.18 ± 0.10	3.82 ± 0.09	0.116 ± 0.008
Blank WM	14.15 ± 0.09	3.79 ± 0.06	0.117 ± 0.008
L4	14.08 ± 0.09	3.75 ± 0.14	0.128 ± 0.009^{+}
L6	14.13 ± 0.09	3.86 ± 0.12	0.124 ± 0.007^{+}
LC6	13.85 ± 0.13^{+}	3.75 ± 0.09	0.128 ± 0.004^{+}
LC7	13.94 ± 0.12^{+}	3.81 ± 0.10	0.110 ± 0.006^{+}
LN6	13.05 ± 0.20^{+}	3.79 ± 0.07	0.128 ± 0.004^{+}
LN7	13.52 ± 0.22^{+}	3.79 ± 0.11	0.116 ± 0.002
ISO tolerance limit [399]	± 0.20 absolute*	± 0.05 absolute*	± 0.010 absolute*

*: values from the CEP/blank WM lenses.
$^{+}$: values exhibit a p-value < 0.05 in comparison to the CEP/blank WM lens.

As can be seen in Table 6.7, the developed complex- and NP-loaded SCLs had statistically significant lower lens diameter in comparison to CEP, blank WM, as well as L4 lenses. The smallest lens diameter was measured for LN6 lens with an average of 13.05 ± 0.20 mm in comparison to 14.15 ± 0.09 mm for blank WM lens. This was postulated to be due to the presence of complex and NP inside the hydrogel matrix, which in turn affected the lens swelling ability. A non-statistical difference in lens sagittal depth and centre thickness was noted and are within the acceptance criteria when compared to those values in the CEP lenses, according to the ISO 18369-2:2017 (E) [399].

The published dimensions for nesofilcon A lens are: 14.20 mm in diameter, sagittal depth of 3.820 mm and centre thickness of 0.100 mm [398]. Additionally, it was previously reviewed by Jones *et al.* that the lens diameter of a commercialized lens is in a range of 13.8 to 14.5 mm [621]. It is essential for the lens to be able to fully cover the cornea throughout blinking to provide good lens fitting and thus, maintain in-eye comfort [218]. Although the produced complex- and NP- loaded SCLs did not have a suitable lens diameter, this can be resolved by using an alternative mould design, which is a common optimisation approach used in the manufacture of commercial SCLs. Hence, given that both LC7 and LN7 exhibited comparable physicochemical and mechanical properties to commercial lens of the same material, they can be considered as a promising ODDS to treat retinal diseases.

6.5 Conclusions

Following the successful formulation of NAR:CD inclusion complex and NAR-loaded CS NP in the previous Chapters 4 and 5, the purpose of this Chapter was to examine the feasibility of loading a complex and NP into the developed SCLs of commercial quality. The complex- and NP-loaded hydrogel SCLs were manufactured using the same approaches as described in Chapter 3, which are direct entrapment and ‘soak and release’. Complex- and NP-loaded SCLs at various loading concentrations were investigated to identify the optimum conditions where the developed lenses not only could provide a sustained drug delivery but also their lens critical properties were maintained. A total of 14 loading concentrations was investigated for both complex- and NP-loaded SCLs.

Based on the data from the light transmission experiment, it can be determined that both the developed complex and NP from the previous Chapters 4 and 5 are not compatible with the lens material. A statistically significant decrease in light transmission was observed as the amount of loading complex and NP increased, e.g., from 98.1 ± 0.7% in blank WM lens to 90.6 ± 0.1% and 92.6 ± 1.1% for LC6 and LN6, respectively. This was outside the accepted tolerance for light transmission of SCL as stated in the ISO standard (Table 1.2). Additionally, it was visually observed that the directly entrapped lens, with either complex or NP, was opaque (Figure 6.8). Although LC1-LC5 and LN1-LN5 SCLs produced good light transmittance with visibly clear lenses, the loaded amount was deemed to be too minimal to be used to assess the potential impacts of complex and NP on the lens thermal, physical, and mechanical properties. Despite that LC6 and LN6 lenses being opaque (lens with the highest possible amount of direct entrapped complex and NP in the hydrogel matrix, respectively, Figure 6.10), it is of scientific interest to assess their physical and mechanical properties to study the impact that complex and NP incorporation had on the lens properties. The polymerization kinetics of LC6 and LN6 was studied, which showed that the incorporation of either complex or NP did not significantly alter the lens DSC profiles. FTIR analysis evidenced the appearance of the complex and NP inside the lens matrix through the presence of additional characteristic peaks in their spectra, those not being observed in neither blank WM nor NAR-loaded lenses. LC6 and LN6 showed a non-statistically significant difference in both degradation temperature and wettability in comparison to CEP and blank WM lenses. The presence of complex and NP in the hydrogel matrix, which increased the formation of interchain junctions within the lens, an increase in the tensile modulus for both complex- and NP-loaded SCLs prepared by either ‘soak and release’, or direct entrapment approaches was observed.

Based on the results from all the chemical and physicochemical characterizations, as well as the amount of loaded complex and NP that provided NAR concentration within the estimated therapeutic window, it can be concluded that the ‘soak and release’ is an optimum methodology in the fabrication of complex- and NP- SCLs of nesofilcon A material. *In vitro* release studies under sink conditions showed that the loaded NAR in both LC7 and LN7 lenses could be released in a controlled manner for 24 hours within the estimated therapeutic window.

CHAPTER 7

FUTURE WORK

AND

THESIS CONCLUSION

7 FUTURE WORK AND THESIS CONCLUSION

As part of the investigation on developing a suitable NP as a drug carrier to be incorporated into the SCLs, a preliminary study on the formation of hyaluronic acid (HA)-coated CS NPs was carried out. The preparation and characterisation of the HA-coated CS NP are discussed within this section. Building on the work carried out in this thesis, the focus of this chapter is to detail the future work based on the successful development of the ODDSs including NAR-, complex-, and NP-eluting hydrogel soft contact lenses of commercial quality.

7.1 Drug-loaded HA-coated CS nanoparticles

HA, as discussed in Section 1.2.1, is known as a comfort enhancing agent when incorporated into CL since it can increase tear film stability, ocular hydration, and lubrication [382, 486]. HA can be found in the vitreous humour, the lacrimal gland, the conjunctiva, as well as corneal epithelium and tear film. HA's ability to specifically target CD44 receptors has increased its use as a drug carrier to improve drug delivery to effectively inhibit tumour growth [177]. HA, when using as drug-loaded NPs [544] or incorporating/immobilizing on lens surface [622], was shown to reduce the immunogenicity of the formed protein corona (i.e., protein adsorption).

Surface coating of CS/CD nanoparticles with HA was carried out in two parts:

1) 15 mg of HA (0.2-0.5 mDa) was dissolved in 5 mL of 0.1% acetic acid (pH 5) to make up a 0.15% HA solution. This was then added dropwise into the redispersed solution of CS NP prepared in Section 5.3.3 under continuous magnetic stirring for 3 hours.

Purification of the prepared nano-dispersion was carried out using two approaches:

- Centrifugation: the nano-dispersion was centrifuged at 16000 rpm for 20 minutes. Then, the pellets were redispersed in 10 mL of ultrapure water and washed with ultrapure water three times using centrifugation to remove the unbound CS and HA. The final pellets were redispersed in 10 mL of ultrapure water using vortex and sonicating probe for 10 minutes. After adding 2% trehalose into the solution, the HA-coated CS-CD NP was stored in -20 °C until frozen, which was then moved into the freeze dryer.

- Dialysis: the nano-dispersion was subjected to dialysis against ultrapure water (molecular weight cut-off (MWCO) 1000 kDa) for 72 hours, followed by freeze drying processes. In order to remove the salt from the dialysis bag stored in 0.025% sodium azide solution, it was placed in ultrapure water for at least 30 minutes prior to use.

2) The same HA concentration solution as Part 1 was used here, with dialysis only being used to purify the prepared HA-coated CS/CD NP in this part. The investigation into the optimized methodology for coating CS/CD NP with HA is depicted in Figure 7.1.

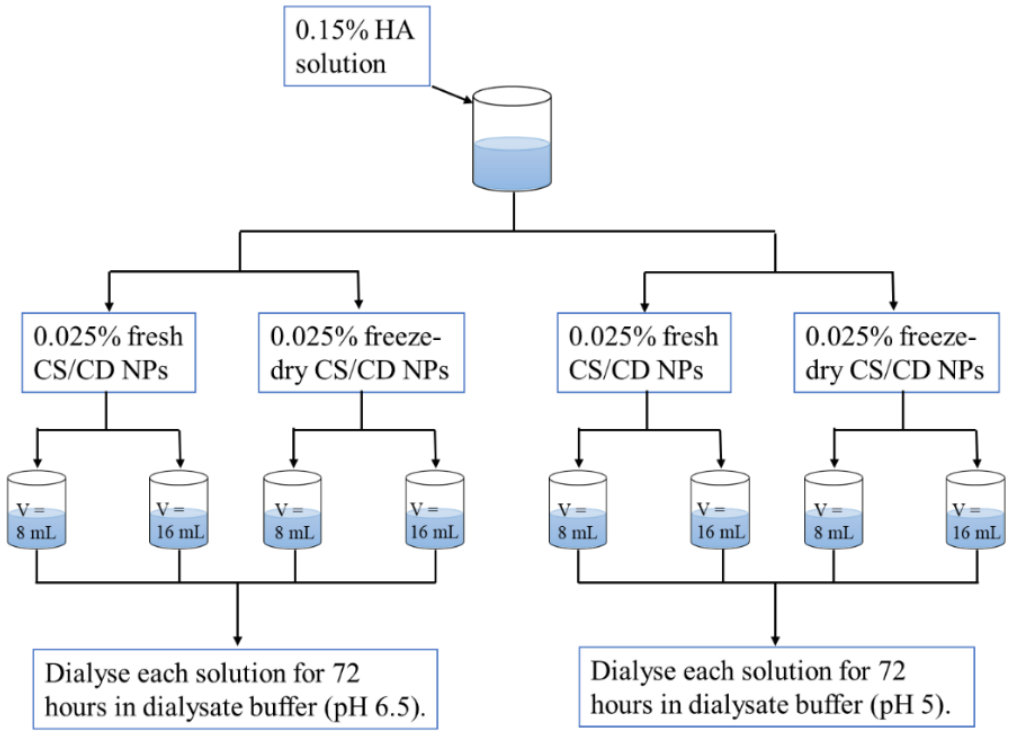

Figure 7.1: Schematic illustration of the optimization of the formation of HA-coated CS NP by a dialysis approach.

7.1.1 Formation of hyaluronic acid (HA)-coated chitosan nanoparticles

The critical step in HA surface absorption onto CS NPs is the inversion of the NPs zeta potential [552]. Hence, pH was said to play a vital role in the formation of HA-coated NP since agglomeration is likely to take place around the isoelectric point [552]. This could either be because of interactions between the positive CS and negative HA, or the absence of electrostatic stabilisation throughout the intermediate states of

adsorption [623]. The optimum pH was proposed to be 5, which could maximise both CS positive charge (amine protonation) and HA negative charge (deprotonation of carboxylic acid groups) [583].

In this study, both the CS NP solution and HA solution were controlled at pH 5. The coating process took place due to the interaction of ammonium ions of CS NPs and carboxylates of HA [552]. Figure 7.2 presents the formulation of HA-coated CS NPs process.

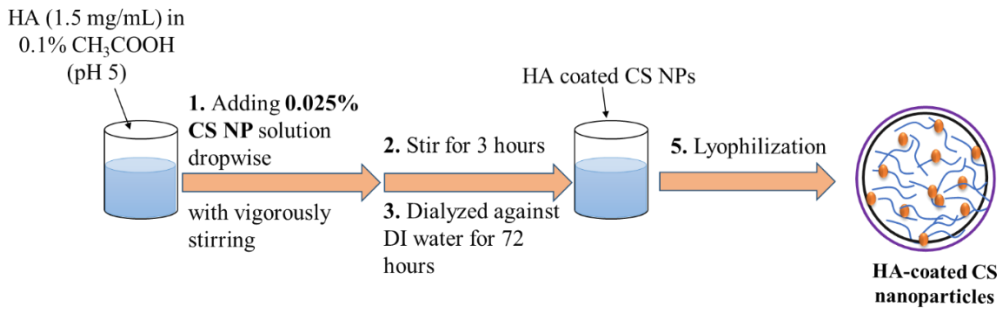

Figure 7.2: Schematic diagram illustrating the synthesis of HA-coated CS NPs.

In addition to pH, the formation mechanism of HA-coated CS NPs and their physicochemical properties are also influenced by the molecular weight of HA and its concentration [552]. The negative charge of HA provided by each macromolecule to the surface upon adsorption is postulated to be defined by its size/number of charges. Consequently, a high MW HA is required to invert the CS NP zeta potential. The same amount of adsorption from low MW HA (60 kDa) at a low concentration (0.1 mg/mL), on the other hand, could lead to the isoelectric point, thus, increasing the risk of agglomeration [552]. Higher HA concentration was proposed to decrease agglomeration since this factor also influenced the rate of adsorption and zeta potential inversion [552]. Nevertheless, very high MW HA (1000 kDa) was excluded due to its high viscosity that could lead to poor experimental reproducibility [624]. In addition, HA-coated NPs that formed using a HA MW of 1000 kDa was demonstrated to be agglomerated and flocculated regardless of the concentration used [624]. The optimum HA-coated CS NP formulation was proposed to be the combination of low MW CS (25 kDa) and high HA MW (360 kDa) and concentration (0.15% wt), which resulted in NPs with the lowest polydispersity and smallest size (e.g. 260 nm) [552, 623, 625].

High MW HA (200-500 kDa) with a concentration of 0.15 mg/mL was used to coat CS/SBE-ß-CD NPs. A freshly prepared CS NP solution after redispersing was used in the formation of HA-coated NPs. CS/SBE-ß-CD NP pellets were redispersed in 10 mL of 0.1% acetic acid (pH 5) at a concentration of 0.09 %wt, which was slowly added under stirring to 10 mL of 0.15 %wt HA solution (pH 5) for 3 hours. The final HA-coated NPs solution was then purified by either centrifugation at 16000 rpm for 20 minutes, 3 times [142] or dialysis (MWCO 1000 kDa) [552]. The NP suspension was dialyzed against ultrapure water (dialysate), and the volume of dialysate was at least 100 times greater than the volume of colloidal solution [626, 627], which resulted in an opalescent solution indicated the formation of NPs [144, 146].

As discussed in Section 5.4.1, in centrifugation, separation is achieved by forcing particles to sediment into a pellet under high centrifugal force over certain centrifugation times until the densities of the particle and surrounding medium are closely matched [559]. In the preparation of polymeric NPs, a dialysis technique was suggested to be a simple and effective approach that resulted in a narrow particle size distribution [626-628]. The molecular weight cut-off (MWCO) of dialysis membrane used in this study was chosen to be 1000 kDa [552] for the dialysis of high MW HA (360 kDa, which was in the range of HA MW used in this study: 200-500 kDa). The pore size of membranes used in dialysis has to be adequately large to allow diffusion of the dispersant through the pores [629]. Since the radius of gyration is much bigger for highly solvated polymer MWs compared to those of protein or dextran of the same MW, the MWCO of membranes is commonly given for protein or dextran sizes. Dialysis involves a change of the nanomaterial dispersant by means of submerging a dialysis bag filled with the nanomaterial dispersion in a receptor solution [630]. To achieve an osmotic equilibrium, the liquid diffuses through the membrane from the more concentrated environment (sample solution) to the less concentrated one (dialysate) [630]. The homogenous NPs suspension is subsequently formed by the displacement of solvent inside the membrane followed by progressive aggregation of polymer due to the loss of solubility [628].

Based on the data obtained from DLS measurement, the optimum purification approach for HA-coated NPs was proposed to be dialysis (MWCO 1000 kDa). Even after three washes using centrifugation at 16000 rpm, a poor PDI was recorded with a

value of 0.5392 ± 0.3722. Further, DLS data showed that there was only around 50 % of the total colloidal solution volume containing particles in the nano-sized range (317.4 ± 66.0 nm). Zeta potential value for this approach was also variable with a value of +10.7 ± 200.9 mV. For the dialysis approach, 100% of the NP solution was recorded to be in the nano-range (366.3 ± 27.7 nm), with a polydispersity index of 0.1212 ± 0.0216, and zeta potential of -28.6 ± 1.1 mV (Table 7.1). Following the coating of HA on CS NPs, the average size of NPs was measured to be 366.3 ± 27.7 nm, with a negative zeta potential of -28.6 ± 1.1 mV.

Table 7.1: Particle size, charge, and polydispersity index for developed NPs.

Samples (n = 3)	Average size (nm)	Zeta potential (mV)	Polydispersity index (PDI)
CS NP	360.0 ± 9.9	+38.6 ± 2.1	0.0671 ± 0.0362
Drug-loaded CS NP	333.3 ± 26.6	+22.0 ± 4.3	0.0777 ± 0.0580
HA-coated CS NP	366.3 ± 27.7	- 28.6 ± 1.1	0.1212 ± 0.0216

7.1.2 Preliminary characterisation of hyaluronic acid (HA)-coated chitosan nanoparticles

The TGA thermograms of raw materials CS, SBE-ß-CD, HA, and NAR are presented in Figure 7.3.

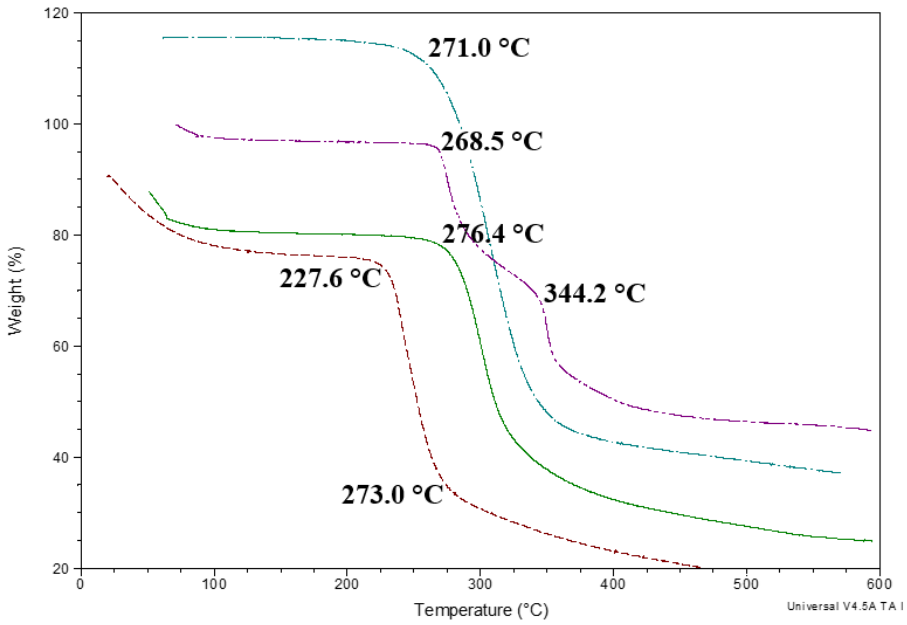

Figure 7.3: TGA thermograms of CS (green-solid line), HA (red-short dash), SBE-ß-CD (purple-broken double) and NAR (blue-dash dot) (n = 1).

Thermogravimetric analysis (TGA) was carried out to investigate the thermal stability of the raw materials from 20 °C to 600 °C at 10 °C/min heating rate. The TG curves in Figure 4.9 demonstrated that NAR decomposed at 271 °C [527], while two degradation points for SBE-ß-CD could be observed at 269 °C and 344 °C [528]. These observations were similar to work carried out in Section 3.4.4.1. Degradation temperatures of 276 °C and 228 °C were recorded for CS and HA, respectively, which were in agreement with previous studies [586-588]. TGA thermal profiles of HA was reported to consist of three degradation stages including: water evaporation (20-223 °C), and two-stage polysaccharide degradation at 223-269 °C and at 269-400 °C [586]. While the second stage was suggested to be due to a partial breakage of the molecular structure of HA, the third stage was due to the degradation of residues HA.

The DSC thermograms of raw materials CS, SBE-ß-CD and HA, HA-coated NP and the corresponding physical mixture are presented in Figure 7.4.

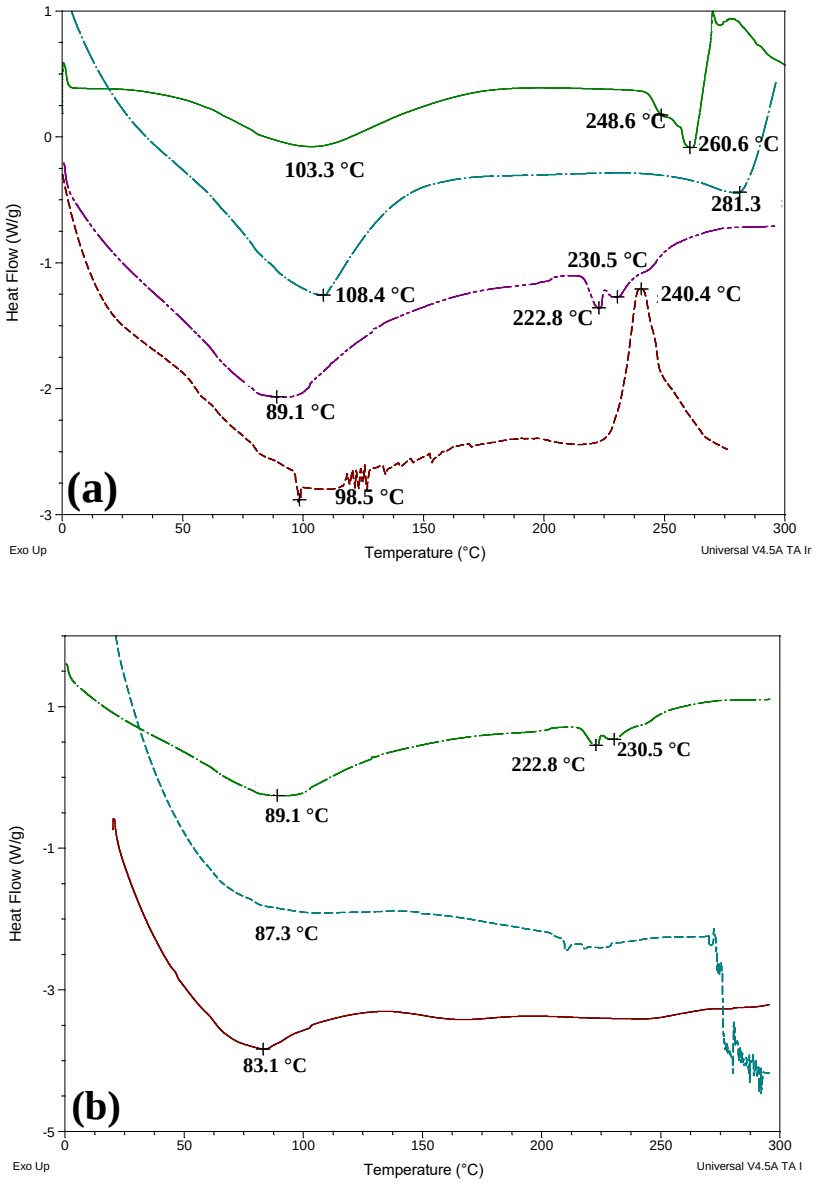

Figure 7.4: DSC thermograms of (a) raw materials CS (blue, dash dot line), SBE-ß-CD (green, solid line), HA (red, short dash line) and physical mixture (purple, broken double line), (b) HA-coated CS NP (blue, short dash line) with CS NP (red, solid line) and physical mixture (green, dash dot line).

The HA DSC thermogram demonstrated two representative peaks: a wide endothermic peak at 98.5 °C indicating a dehydration process, and an exothermic peak at 240.4 °C attributed to the degradation of the polysaccharide and formation of a carbonized residue [586, 587, 624, 631]. For the PM (CS, SBE-ß-CD and HA) thermogram, because of the ionic charge of the chitosan (cationic) and HA (anionic), these two compounds can potentially form a charge-transfer bond. As a result, this led to a shift

in degradation temperatures of SBE-ß-CD (from 248.6 and 260.6 °C to 222.8 and 230.5 °C) and the disappearance of the exothermic peak of HA and degradation peak of CS. The effect of HA coating on the thermal transitions of coated CS NPs was shown through the disappearance of CS peaks, shifts in HA peak from 98.5 °C to 87.3 °C, as well as flattening of the HA exothermic peak. Together with the disappearance of the distinctive degradation peaks of SBE-ß-CD, this outcome indicated the formation of HA-coated CS NPs. The DSC thermogram on HA-coated CS NPs (HA molecular weight 360 kDa) in a study carried out by Hashad *et al.* also had a similar observation [624]. As such, upon coating with HA, a shift in HA peak from 73 °C to 92 °C accompanied by a disappearance of both CS and drug peaks were obtained.

A total of four samples were analyzed using FT-IR including CS, SBE-ß-CD, HA, and HA-coated CS NP. The comparative FT-IR spectra are presented in Figure 7.5.

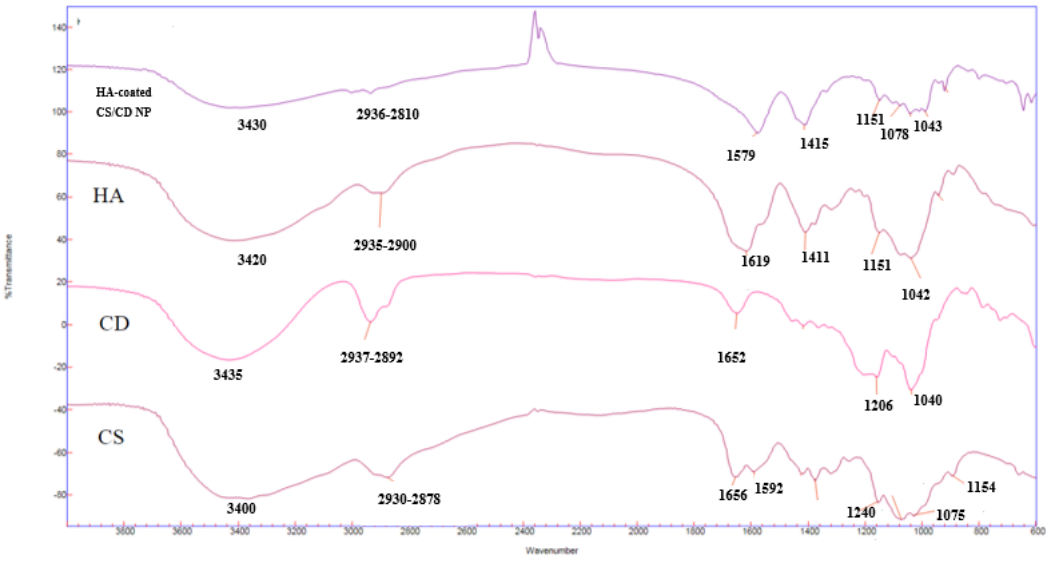

Figure 7.5: Representative FTIR spectra of HA-coated CS NP with CS, SBE-ß-CD and HA.

Analysis of the HA spectrum showed several characteristic peaks related to its glycosoaminoglycan structure [624]. A band at 3420 cm^{-1} corresponded to O-H and N-H stretching region (which is similar to CS). Stretching vibration of C-H could be seen at 2935-2900 cm^{-1}. A peak at 1619 cm^{-1} was attributed to the amide carbonyl (C=O stretching), while the band at 1411 cm^{-1} is associated with the stretching of COO^- (acidic group of HA). The saccharidic unit was shown through a broad band in the region of 1151-1042 cm^{-1} [632].

The construction of HA-coated CS NPs was investigated using FT-IR spectroscopy (Figure 5.6). The FT-IR spectrum showed a peak at 1579 cm^{-1}, which could correlate to the amide bands in either CS and HA (1656 cm^{-1} in CS spectrum or 1619 cm^{-1} in HA spectrum). Along with a shift in the HA related peak in the NP spectrum (e.g., 1411 cm^{-1} to 1415 cm^{-1}), the presence of this peak indicated the successful amide bonding between the carboxylic and amino groups on the coated-layer and surface of the NPs. This observation suggested the formation of HA-coated CS NPs was achieved in this study and was in agreement with previous study [624]. The success of the HA surface functionalization step was shown through a shift in the amide bands and the intensification of HA characteristic peaks.

7.1.3 Further potential optimisation on the developed drug-loaded NPs

Incorporation of NPs could influence the lens' ability to transmit light significantly because the nanosized particles could diffract and scatter incident light. Several studies indicated that the transparency of CLs was not affected when the NP size was below 180 nm [283, 284, 390]. However, NPs of size greater than 200 nm resulted in a reduction in lens optical clarity. For example, the incorporation of drug-loaded NPs of size 294.5 ± 1.8 nm decreased the pHEMA hydrogels transmission from 94.5% to 86.2% [378]. As a result, further study on the formation of CS/SBE-ß-CD NPs is expected to be carried out to potentially reduce the particle size by altering CS/SBE-ß-CD mass ratio, pH and initial CS concentration, in a manner similar to that of Zhao *et al.* [144]. Their study postulated that the optimum drug-loaded CS/SBE-ß-CD NPs of size 278 nm, zeta potential 19 mV and PDI value 0.09 were produced with a mass ratio of 0.85/1, CS solution of pH 4.5 and a CS initial concentration of 0.5 mg/mL. In addition, Zhao *et al.* demonstrated the influence of SBE-ß-CD concentration (5-30 mg/mL) on the drug loading capacity and encapsulation efficiency of ibrutinib. NPs cannot be formed (i.e., clear nano-formulation) when the SBE-ß-CD concentration is too low (e.g., 3 CS: 1 SBE-ß-CD, mass ratio), whereas an increase in SBE-ß-CD concentration resulted in a reduction in particle size (e.g., 620 and 420 nm for CS/SBE-ß-CD NPs formed at a mass ratio of 1:1 and 0.85:1, respectively). While higher SBE-ß-CD concentration increased the %EE from 48.5% at 5 mg/mL to 76.9% at 20 mg/mL, excessive SBE-ß-CD (over 30 mg/mL) resulted in a reduction of %EE (72.4% at 30 mg/mL) [144].

In addition to stability of NPs under various pH conditions, it is expected that the stability of both uncoated and HA-coated NPs under saline conditions (presence of calcium [146] and sodium ions [633]) will also be carried out. It was observed that under NaCl condition, CS NPs with CS that have a DD-value of 91-95% were stable against both aggregation and dissolution up to 150 mM (0.88 %wt) NaCl [633]. This observation was relevant to this study since high %DD CS (>90%) was used in the formulation of CS NPs. However, NPs prepared using CS with lower %DD (82%, 72% and 61-63%) were shown to be dissociated in 50 mM NaCl [633]. In a different study, CS/TPP NPs was shown to be immediately and completely dissolved in $CaCl_2$ solution regardless of concentration [146]. This was postulated to be because Ca ions have an ability to form stable chelates with phosphate ions, thus, prevent phosphate from being electrostatically complexed to CS [634]. The observations from these studies postulated that NPs were stable under saline conditions with the presence of sodium ions but not calcium ions. Nevertheless, since the contact lens storage solution (BBS – borate buffered saline) used in this study contained several different components (e.g., NaCl, sodium borate, etc.), future work should include the stability study of the synthesized NPs in these solutions.

7.2 Characterisation of soft contact lens laden with drug-loaded nanoparticles

Along with several SCL characterisation methodologies reported in Chapter 2, there is potential to develop further analytical techniques to examine the effects of drug-loaded NPs on the formation of SCLs. The techniques that will potentially be investigated in the future study include scanning electron microscopy (SEM), atomic force microscopy (AFM), and/or transmission electron microscopy (TEM). Morphology assessment of the NPs and the SCLs was assessed by several techniques including SEM [140], AFM [389], and TEM [144].

7.2.1 In vitro drug release study

Even though *in vitro* released models do not represent the actual ocular environment, they add valuable information and knowledge on the developed ODDS with regard to the robustness and reproducibility of the system. Being a cost-effective approach, *in vitro* study also aids in the identification of critical elements of a drug-carrier that are essential for *ex vivo* and *in vivo* performances. Drug release from nanoparticulate or polymeric platforms (e.g. SCLs) are commonly assessed using either the conventional [358, 378] or dialysis approaches [283, 467].

Microfluidic and 3D (i.e., blinking-mimic) devices have been explored to better reproduce the actual ocular environment in comparison to other techniques in *in vitro* testing of an OODS [635-637]. Pimenta *et al.* developed a novel *in vitro* eye model to facilitate the release study of a drug from hydrogel SCLs [635]. The model has an inner volume chamber of 45 µL (which would be one of the closest *in vitro* models to represent the tear film volume in the eye) and 8 outlets that meet in a common collector (Figure 7.6). The release profiles of diclofenac from pHEMA hydrogel SCL used this technology were determined to be significantly slower than using a conventional approach (e.g., direct entrapment, 'soak and release').

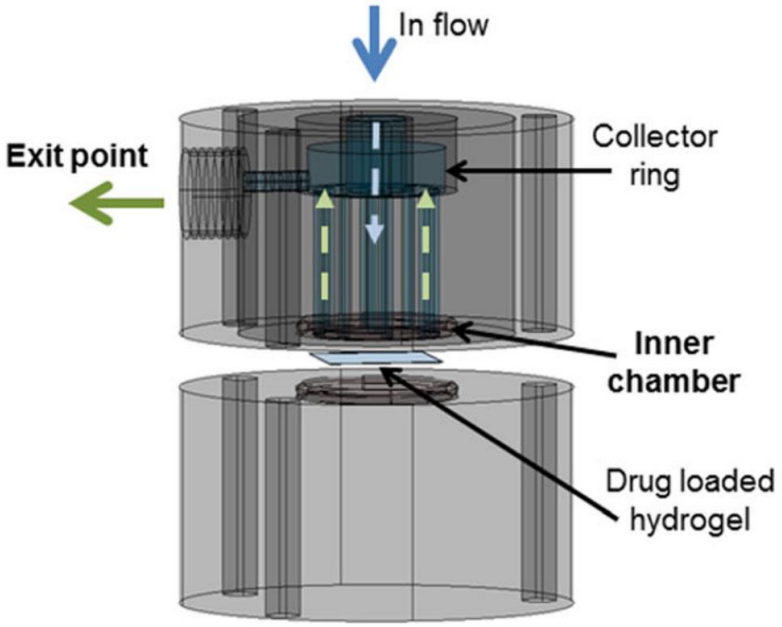

Figure 7.6: Schematic illustration of microfluidic device for *in vitro* release study [635].

7.2.2 Cytotoxicity study of pharmaceutical-loaded SCLs

In vitro cytotoxicity testing of polymeric biomaterials is an essential part of the development of drug delivery systems and was previously examined in various studies [52, 311, 386]. This will be carried out using the developed MTT assay technique in the lab to investigate both the NAR-loaded NP and NP-loaded SCL cytotoxicity on the Human Corneal Epithelial Cells (HCEC).

The MTT (3-(4,5-dimethylthiazol-2-yl)-2,5-diphenyltetrazolium bromide) test was used to evaluate the effects of surface modification of pHEMA discs with HA on the metabolic activity of immortalized human corneal epithelial cells (HCECs) [386]. This was achieved through the conversion of soluble yellow chromogen MTT into the water-soluble formazan salt via the dehydrogenases present in viable cells. The detailed method for this test is described in the study carried out by Korogiannaki *et al.* [386]. Immortalized HCECs were investigated to be appropriate as an *in vitro* model of human ocular surface in toxicity and inflammation studies for the biomaterial applications to the front-of-the eye such as SCLs [638, 639].

7.2.3 Ex vivo studies on the pharmaceutical-loaded SCLs

To gain a better insight on a performance of an ODDS, quantifying the rate and amount of drug permeation through a biological membrane plays a vital role. Moreover, due to the fact that *in vitro* testing cannot mimic biological tissue, it is imperative to conduct *ex vivo* testing in order to investigate the absorption and distribution of the released therapeutic agent within the ocular environment [640, 641]. Using the corneal layer extracted from bovine eyes, *ex vivo* study on timolol maleate (TM) eluting SCLs (PVP-based) to treat glaucoma through diffusion cells was cited by Mehta *et al*. [641]. A controlled release of TM permeated through the bovine cornea was observed over 24 hours. This study also reported that the addition of permeation enhancer such as benzalkonium chloride and Brij 78 resulted in an enhancement of TM permeation through the corneal tissue.

7.2.4 In vivo studies on the pharmaceutical-loaded SCLs

Development of a novel ODDS to deliver therapeutics to the eye has always received a substantial interest to effectively treat and prevent various ocular diseases such as AMD, infection, DED, glaucoma. As discussed in Section 1.1, the eyes, although being highly accessible, there are numerous challenges to deliver drugs into the targeted tissue due to their sophisticated anatomy. Hence, in addition to the listed characterisation techniques throughout this thesis, *in vivo* performance of the developed technologies should be evaluated to investigate their safety and efficacy, which ultimately demonstrate the feasibility of medical device for commercialisation [611, 642, 643]. Minami *et al.* analyzed and compared the *in vitro* and *in vivo* performances of epinastine hydrochloride (EH)-loaded pHEMA SCLs for the treatment of allergic conjunctivitis [611]. I*n vivo* studies were carried out on 30 guinea pigs. The amount of released EH *in vivo* was found to be larger than that recorded in the *in vitro* study during the 6-12 hours period, which was postulated to be due to the difference in the tested environment between the 2 methodologies, which was expected.

7.3 Final Discussion and Conclusion

An ability to provide a controlled, prolonged, and sustained release of a therapeutic agent from an ocular drug delivery system (ODDS) has received considerable attention from the scientific world as an innovative and effective strategy for treating various ocular pathologies. Moreover, such developed technology should also be able to overcome the limitations of the current ODDSs such as low ocular bioavailability, infections, retinal detachment. The present PhD work focused on the development and characterization of pharmaceutical-loaded hydrogel SCL for the treatment of ocular diseases, those that affect anterior as well as posterior segments of the eye.

Chapter 1 of this thesis provides not only an overview on the eye anatomy and the common ocular diseases, but also compares and reviews the conventional and novel ODDSs for the treatment of various disorders that affect both anterior and posterior segments. As a result, from this literature review, a gap in scientific knowledge was identified, which was on the physicochemical, mechanical, and dimensional characterization of therapeutic lens for commercialization purposes. Based on this finding, a review article was successfully published on Contact Lens & Anterior Eye journal, titled "Pharmaceutical-loaded contact lenses as an ocular drug delivery system: A review of critical lens characterization methodologies with reference to ISO standards", on the 02th August 2021 (DOI: https://doi.org/10.1016/ j.clae.2021.101487).

Chapter 2 explored a commercial-standard process in the manufacturing of a SCL (nesofilcon A materials) which was employed to ensure the developed lens in this work exhibited all the critical commercialized lens properties. Following the successful manufacturing of hydrogel SCLs of commercial quality, the research was continued with the development and optimization of NAR-loaded hydrogel SCLs as an alternative ODDS to potentially prevent retinal diseases. The outcome from Chapter 3 demonstrates the ability of sustained and controlled released of NAR from the developed SCLs (nesofilcon A) within the estimated therapeutic window, while maintaining their commercial lens qualities. A research article was successfully published as a result of this work, titled "Controlled release of naringenin from soft hydrogel contact lens: An investigation into lens critical properties and *in vitro*

release". This paper was published on the International Journal of Pharmaceutics on the 10th June 2022 (DOI: https://doi.org/10.1016/ j.ijpharm.2022.121793).

Aiming to improve the ocular bioavailability of NAR, which is significantly hindered by its low aqueous solubility, Chapter 4 of this work focused on the development and optimization of a NAR:CD (sulfobutyl ether-ß-cyclodextrin) inclusion complex. The developed complex was fully characterized, which resulted in a substantial increase in NAR aqueous solubility of up to 6000-fold. With the increasing interest in the implementation of nanotechnology in ODD, experimental work in Chapter 5 concentrated on the formulation of NAR-loaded CS NPs through an ionic gelation methodology. This was carried out by cross-linking between the cationic group in CS and anionic group in the NAR:CD complex. The developed NPs exhibited a positive charge with an average size of 333.3 ± 26.6 nm and a positive zeta potential of +22.0 ± 4.3 mV, while providing a sustained NAR release for 30 days, and thus, are deemed to be suitable to be used in ODD.

Based on the successful preparation of NAR:CD complex and NAR-loaded CS NPs, Chapter 6 investigated the feasibility of loading these analytes inside the developed SCLs of commercial quality. It was identified that the developed complex and NP were not compatible with the lens materials and therefore, neither of them could be fully re-dispersed within the pre-polymerized monomer without impacting the lens light transmission. Consequently, 'soak and release' was determined to be a more suitable approach over direct entrapment in the preparation of complex- and NP-loaded lenses, which resulted in lenses with comparable properties to the unloaded WM lens, while providing a sufficient NAR loading within the estimated therapeutic concentration.

In conclusion, this present research has contributed to the current scientific knowledge on the feasibility of manufacturing pharmaceutical-loaded hydrogel SCLs for commercialization, those that not only can provide a more sustained and targeted drug delivery for treatment of ocular diseases, but also can improve on eye comfort.

REFERENCES

[1] W. H. Organization. "Blindness and vision impairment." https://www.who.int/news-room/fact-sheets/detail/blindness-and-visual-impairment (accessed 17 November, 2019).

[2] K. Nayak, M. V. Choudhari, S. Bagul, T. A. Chavan, and M. Misra, "Chapter 24 - Ocular drug delivery systems," in *Drug Delivery Devices and Therapeutic Systems*, E. Chappel Ed.: Academic Press, 2021, pp. 515-566.

[3] Y. Weng, J. Liu, S. Jinb, W. Guo, X. Liang, and Z. Hu, "Nanotechnology-based strategies for treatment of ocular diseases," *Acta Pharmaceutica Sinica B*, vol. 7, no. 3, pp. 281-291, 2017.

[4] V. A. de Vries, F. L. Bassil, and W. D. Ramdas, "The effects of intravitreal injections on intraocular pressure and retinal nerve fiber layer: a systematic review and meta-analysis," *Scientific Reports*, vol. 10, no. 1, p. 13248, 2020/08/06 2020, doi: 10.1038/s41598-020-70269-7.

[5] K. R. Brown *et al.*, "Rhegmatogenous Retinal Detachment after Intravitreal Injection," *Ophthalmology Retina*, vol. 5, no. 2, pp. 178-183, 2021/02/01/ 2021, doi: https://doi.org/10.1016/j.oret.2020.07.007.

[6] M. Morioka *et al.*, "Incidence of endophthalmitis after intravitreal injection of an anti-VEGF agent with or without topical antibiotics," *Scientific Reports*, vol. 10, no. 1, p. 22122, 2020/12/17 2020, doi: 10.1038/s41598-020-79377-w.

[7] M. Dandamudi *et al.*, "Chitosan-Coated PLGA Nanoparticles Encapsulating Triamcinolone Acetonide as a Potential Candidate for Sustained Ocular Drug Delivery," *Pharmaceutics*, vol. 13, no. 10, p. 1590, 2021. [Online]. Available: https://www.mdpi.com/1999-4923/13/10/1590.

[8] S. Swetledge, R. Carter, R. Stout, C. E. Astete, J. P. Jung, and C. M. Sabliov, "Stability and ocular biodistribution of topically administered PLGA nanoparticles," *Scientific Reports*, vol. 11, no. 1, p. 12270, 2021/06/10 2021, doi: 10.1038/s41598-021-90792-5.

[9] Y. Wei, Y. Hu, X. Shen, X. Zhang, J. Guan, and S. Mao, "Design of circular-ring film embedded contact lens for improved compatibility and sustained ocular drug delivery," *European Journal of Pharmaceutics and Biopharmaceutics*, vol. 157, pp. 28-37, 2020/12/01/ 2020, doi: https://doi.org/10.1016/j.ejpb.2020.09.010.

[10] C.-C. Peng, J. Kim, and A. Chauhan, "Extended delivery of hydrophilic drugs from silicone-hydrogel contact lenses containing Vitamin E diffusion barriers," *Biomaterials*, vol. 31, no. 14, pp. 4032-4047, 2010, doi: https://doi.org/10.1016/j.biomaterials.2010.01.113.

[11] C.-C. Li and A. Chauhan, "Modeling Ophthalmic Drug Delivery by Soaked Contact Lenses," *Industrial & Engineering Chemistry Research*, vol. 45, no. 10, pp. 3718-3734, 2006, doi: 10.1021/ie0507934.

[12] J. J. Inc. "Acuvue Theravision with Ketotifen." https://www.jnjvisionpro.ca/products/acuvue-theravision (accessed 2022).

[13] Q. Xu, S. P. Kambhampati, and R. M. Kannan, "Nanotechnology approaches for ocular drug delivery," *Middle East Afr J Ophthalmol*, vol. 20, no. 1, pp. 26-37, 2013, doi: 10.4103/0974-9233.106384.

[14] Y. Hamdi, F. Lallemand, and S. Benita, "Drug-loaded nanocarriers for back-of-the-eye diseases- formulation limitations," *Journal of Drug Delivery*

Science and Technology, vol. 30, pp. 331-341, 2015, doi: 10.1016/j.jddst.2015.09.010.
[15] F. J. Romero, B. Nicolaissen, and C. Peris-Martinez, "New trends in anterior segment diseases of the eye," *J Ophthalmol*, vol. 2014, p. 393040, 2014, doi: 10.1155/2014/393040.
[16] K. Cholkar, S. R. Dasari, D. Pal, and A. K. Mitra, "Eye: anatomy, physiology and barriers to drug delivery," pp. 1-36, 2013, doi: 10.1533/9781908818317.1.
[17] T. W. Todd, H. Beecher, G. H. Williams, and A. W. Todd, "The weight and growth of the human eyeball," *Human Biology*, vol. 12, no. 1, pp. 1-20, 1940. [Online]. Available: http://www.jstor.org/stable/41447437.
[18] K. Cholkar, A. D. Vadlapudi, S. Reddy Dasari, and A. Mitra, *Ocular Drug Delivery*. 2014, pp. 219-263.
[19] V. Delplace, S. Payne, and M. Shoichet, "Delivery strategies for treatment of age-related ocular diseases: From a biological understanding to biomaterial solutions," *J Control Release*, vol. 219, pp. 652-668, 2015, doi: 10.1016/j.jconrel.2015.09.065.
[20] R. R. Hodges and D. A. Dartt, "Tear film mucins: front line defenders of the ocular surface; comparison with airway and gastrointestinal tract mucins," *Exp Eye Res*, vol. 117, pp. 62-78, 2013, doi: 10.1016/j.exer.2013.07.027.
[21] L. Cwiklik, "Tear film lipid layer: A molecular level view," *Biochim Biophys Acta*, vol. 1858, no. 10, pp. 2421-2430, 2016, doi: 10.1016/j.bbamem.2016.02.020.
[22] H. S. Dua, L. A. Faraj, and D. G. Said, "Dua's layer: discovery, characteristics, clinical applications, controversy and potential relevance to glaucoma," *Expert Review of Ophthalmology*, vol. 10, no. 6, pp. 531-547, 2015, doi: 10.1586/17469899.2015.1103180.
[23] D. A. Dartt and M. D. Willcox, "Complexity of the tear film: importance in homeostasis and dysfunction during disease," *Exp Eye Res*, vol. 117, pp. 1-3, 2013, doi: 10.1016/j.exer.2013.10.008.
[24] A. D. Pucker and K. M. Haworth, "The presence and significance of polar meibum and tear lipids," *Ocul Surf*, vol. 13, no. 1, pp. 26-42, 2015, doi: 10.1016/j.jtos.2014.06.002.
[25] P. Kulovesi, A. H. Rantamaki, and J. M. Holopainen, "Surface properties of artificial tear film lipid layers: effects of wax esters," *Invest Ophthalmol Vis Sci*, vol. 55, no. 7, pp. 4448-54, 2014, doi: 10.1167/iovs.14-14122.
[26] D. A. Dartt, "Tear Lipocalin: Structure and Function," *The ocular surface*, vol. 9, no. 3, pp. 126-138, 2011. [Online]. Available: http://www.ncbi.nlm.nih.gov/pmc/articles/PMC4209957/.
[27] J. Wiesner and A. Vilcinskas, "Antimicrobial peptides: the ancient arm of the human immune system," *Virulence*, vol. 1, no. 5, pp. 440-64, 2010, doi: 10.4161/viru.1.5.12983.
[28] I. K. Gipson and T. Inatomi, "Mucin genes expressed by the ocular surface Epithelium," *Progress in Retinal and Eye Research*, vol. 16, no. 1, pp. 81-98, 1997, doi: https://doi.org/10.1016/S1350-9462(96)00022-5.
[29] O. A. Candia, L. J. Alvarez, and D. A. Dartt, "Overview of Electrolyte and Fluid Transport Across the Conjunctiva ☆," in *Reference Module in Neuroscience and Biobehavioral Psychology*: Elsevier, 2017.
[30] R. Varela-Fernández *et al.*, "Drug Delivery to the Posterior Segment of the Eye: Biopharmaceutic and Pharmacokinetic Considerations," (in eng),

Pharmaceutics, vol. 12, no. 3, p. 269, 2020, doi: 10.3390/pharmaceutics12030269.

[31] E. A. Kimbrel and R. Lanza, "Current status of pluripotent stem cells: moving the first therapies to the clinic," *Nat Rev Drug Discov*, vol. 14, no. 10, pp. 681-92, 2015, doi: 10.1038/nrd4738.

[32] Riordan-Eva P and C. E, "Anatomy & Embryology of the Eye," in *Vaughan & Asbury's General Ophthalmology*, 18th ed.: McGraw Hill.

[33] J. R. Sparrow, D. Hicks, and C. P. Hamel, "The retinal pigment epithelium in health and disease," (in eng), *Curr Mol Med*, vol. 10, no. 9, pp. 802-823, 2010, doi: 10.2174/156652410793937813.

[34] O. Strauss, "The Retinal Pigment Epithelium in Visual Function," *Physiological Reviews*, vol. 85, no. 3, pp. 845-881, 2005, doi: 10.1152/physrev.00021.2004.

[35] N. M. Bressler, J. C. Silva, S. B. Bressler, S. L. Fine, and W. R. Green, "Clinicopathologic correlation of drusen and retinal pigment epithelial abnormalities in age-related macular degeneration," *RETINA*, vol. 14, no. 2, pp. 130-142, 1994. [Online]. Available: https://journals.lww.com/retinajournal/Fulltext/1994/14020/CLINICOPATHOLOGIC_CORRELATION_OF_DRUSEN_AND.6.aspx.

[36] M. Istrate, B. Vlaicu, M. Poenaru, M. Hasbei-Popa, M. Salavat, and D. Iliescu, "Photoprotection role of melanin in the human retinal pigment epithelium. Imaging techniques for retinal melanin," *romanian journal of ophthalmology*, vol. 64, pp. 100-104, 06/24 2020, doi: 10.22336/rjo.2020.20.

[37] S. Yang, J. Zhou, and D. Li, "Functions and Diseases of the Retinal Pigment Epithelium," *Front Pharmacol*, Mini Review vol. 12, 2021. [Online]. Available: https://www.frontiersin.org/articles/10.3389/fphar.2021.727870.

[38] R. Nagymihály *et al.*, "Chapter Four - The retinal pigment epithelium: at the forefront of the blood-retinal barrier in physiology and disease," in *Tissue Barriers in Disease, Injury and Regeneration*, N. V. Gorbunov Ed.: Elsevier, 2021, pp. 115-146.

[39] L. Hong, J. D. Simon, and T. Sarna, "Melanin structure and the potential functions of uveal melanosomes," *Pigment Cell Research*, https://doi.org/10.1111/j.1600-0749.2006.00330.x vol. 19, no. 5, pp. 465-466, 2006/10/01 2006, doi: https://doi.org/10.1111/j.1600-0749.2006.00330.x.

[40] A.-K. Rimpelä *et al.*, "Implications of melanin binding in ocular drug delivery," *Advanced Drug Delivery Reviews*, vol. 126, pp. 23-43, 2018/02/15/ 2018, doi: https://doi.org/10.1016/j.addr.2017.12.008.

[41] S. Bahrpeyma, A.-K. Rimpelä, M. Hagström, and A. Urtti, "Ocular melanin binding of drugs: in vitro binding studies," *Acta Ophthalmologica*, https://doi.org/10.1111/j.1755-3768.2019.5366 vol. 97, no. S263, 2019/12/01 2019, doi: https://doi.org/10.1111/j.1755-3768.2019.5366.

[42] P. Jakubiak, C. Cantrill, A. Urtti, and R. Alvarez-Sánchez, "Establishment of an In Vitro–In Vivo Correlation for Melanin Binding and the Extension of the Ocular Half-Life of Small-Molecule Drugs," *Molecular Pharmaceutics*, vol. 16, no. 12, pp. 4890-4901, 2019/12/02 2019, doi: 10.1021/acs.molpharmaceut.9b00769.

[43] T. L. Ponsioen *et al.*, "Mature enzymatic collagen cross-links, hydroxylysylpyridinoline and lysylpyridinoline, in the aging human vitreous," *Invest Ophthalmol Vis Sci*, vol. 50, no. 3, pp. 1041-6, 2009, doi: 10.1167/iovs.08-1714.

[44] L. A. Remington, "Aqueous and Vitreous Humors," pp. 109-122, 2012, doi: 10.1016/b978-1-4377-1926-0.10006-2.
[45] S. Sudesh and P. R. Laibson, "The impact of the Herpetic Eye Disease Studies on the management of herpes simplex virus ocular infections," *Current Opinion in Ophthalmology*, vol. 10, no. 4, 1999. [Online]. Available: https://journals.lww.com/co-ophthalmology/Fulltext/1999/08000/The_impact_of_the_Herpetic_Eye_Disease_Studies_on.2.aspx.
[46] W. Stevenson, S. K. Chauhan, and R. Dana, "Dry eye disease: an immune-mediated ocular surface disorder," (in eng), *Arch Ophthalmol*, vol. 130, no. 1, pp. 90-100, 2012, doi: 10.1001/archophthalmol.2011.364.
[47] E. B. Papas, "The global prevalence of dry eye disease: A Bayesian view," *Ophthalmic and Physiological Optics*, vol. 41, no. 6, pp. 1254-1266, 2021, doi: https://doi.org/10.1111/opo.12888.
[48] S. P. Phadatare, M. Momin, P. Nighojkar, S. Askarkar, and K. K. Singh, "A Comprehensive Review on Dry Eye Disease: Diagnosis, Medical Management, Recent Developments, and Future Challenges," *Advances in Pharmaceutics*, vol. 2015, pp. 1-12, 2015, doi: 10.1155/2015/704946.
[49] L. A. Vickers and P. K. Gupta, "The Future of Dry Eye Treatment: A Glance into the Therapeutic Pipeline," *Ophthalmol Ther*, vol. 4, no. 2, pp. 69-78, 2015, doi: 10.1007/s40123-015-0038-y.
[50] C.-M. Phan, L. N. Subbaraman, and L. Jones, "In Vitro Uptake and Release of Natamycin From Conventional and Silicone Hydrogel Contact Lens Materials," *Eye & Contact Lens*, vol. 39, no. 2, pp. 162-168, 2013, doi: 10.1097/ICL.0b013e31827a7a07.
[51] F. A. Maulvi *et al.*, "pH triggered controlled drug delivery from contact lenses: Addressing the challenges of drug leaching during sterilization and storage," *Colloids and Surfaces B: Biointerfaces*, vol. 157, pp. 72-82, 2017, doi: https://doi.org/10.1016/j.colsurfb.2017.05.064.
[52] F. H. Nasr, S. Khoee, M. M. Dehghan, S. S. Chaleshtori, and A. Shafiee, "Preparation and Evaluation of Contact Lenses Embedded with Polycaprolactone-Based Nanoparticles for Ocular Drug Delivery," *Biomacromolecules*, vol. 17, no. 2, pp. 485-95, 2016, doi: 10.1021/acs.biomac.5b01387.
[53] I. P. Kaur and S. Kakkar, "Nanotherapy for posterior eye diseases," *J Control Release*, vol. 193, pp. 100-12, 2014, doi: 10.1016/j.jconrel.2014.05.031.
[54] V. Saunier *et al.*, "Incidence of and Risk Factors Associated With Age-Related Macular Degeneration: Four-Year Follow-up From the ALIENOR Study," *JAMA Ophthalmology*, vol. 136, no. 5, pp. 473-481, 2018, doi: 10.1001/jamaophthalmol.2018.0504.
[55] S. Bahadorani and M. Singer, "Recent advances in the management and understanding of macular degeneration," *F1000Research*, vol. 6, p. 519, 2017, doi: 10.12688/f1000research.10998.1.
[56] W. M. Al-Zamil and S. A. Yassin, "Recent developments in age-related macular degeneration: a review," *Clinical Interventions in Aging*, vol. 12, pp. 1313-1330, 2017, doi: 10.2147/CIA.S143508.
[57] A. Gheorghe, L. Mahdi, and O. Musat, "Age-related macular degeneration," *Romanian Journal of Ophthalmology*, vol. 59, no. 2, pp. 74-77, 2015. [Online]. Available: http://www.ncbi.nlm.nih.gov/pmc/articles/PMC5712933/.

[58] I. Bhutto and G. Lutty, "Understanding age-related macular degeneration (AMD): Relationships between the photoreceptor/retinal pigment epithelium/Bruch's membrane/choriocapillaris complex," *Molecular Aspects of Medicine,* vol. 33, no. 4, pp. 295-317, 2012, doi: 10.1016/j.mam.2012.04.005.

[59] F. Horner *et al.*, "Comparing Effectiveness of Three Different Anti-VEGF Treatment Regimens for Neovascular Age-Related Macular Degeneration: Two Years' Real-World Clinical Outcomes," (in eng), *Clinical ophthalmology (Auckland, N.Z.),* vol. 15, pp. 1703-1713, 2021, doi: 10.2147/OPTH.S305141.

[60] Y. Gao, Y. C. K. Teo, R. W. Beuerman, T. Y. Wong, L. Zhou, and C. M. G. Cheung, "A serum metabolomics study of patients with nAMD in response to anti-VEGF therapy," *Scientific Reports,* vol. 10, no. 1, p. 1341, 2020/01/28 2020, doi: 10.1038/s41598-020-58346-3.

[61] H. M. Kim and S. J. Woo, "Ocular Drug Delivery to the Retina: Current Innovations and Future Perspectives," (in eng), *Pharmaceutics,* vol. 13, no. 1, p. 108, 2021, doi: 10.3390/pharmaceutics13010108.

[62] A. G. Marneros *et al.*, "Vascular endothelial growth factor expression in the retinal pigment epithelium is essential for choriocapillaris development and visual function," (in eng), *Am J Pathol,* vol. 167, no. 5, pp. 1451-1459, 2005, doi: 10.1016/S0002-9440(10)61231-X.

[63] K. Nishijima *et al.*, "Vascular endothelial growth factor-A is a survival factor for retinal neurons and a critical neuroprotectant during the adaptive response to ischemic injury," (in eng), *Am J Pathol,* vol. 171, no. 1, pp. 53-67, 2007, doi: 10.2353/ajpath.2007.061237.

[64] L. J. Singerman *et al.*, "Pegaptanib sodium for neovascular age-related macular degeneration: third-year safety results of the VEGF Inhibition Study in Ocular Neovascularisation (VISION) trial," (in eng), *The British journal of ophthalmology,* vol. 92, no. 12, pp. 1606-1611, 2008, doi: 10.1136/bjo.2007.132597.

[65] M. Zhu *et al.*, "Intravitreal Ranibizumab for neovascular Age-related macular degeneration in clinical practice: five-year treatment outcomes," *Graefe's Archive for Clinical and Experimental Ophthalmology,* vol. 253, no. 8, pp. 1217-1225, 2015, doi: 10.1007/s00417-014-2799-8.

[66] C. L. Nguyen, L. J. Oh, E. Wong, J. Wei, and M. Chilov, "Anti-vascular endothelial growth factor for neovascular age-related macular degeneration: a meta-analysis of randomized controlled trials," *BMC Ophthalmology,* vol. 18, no. 1, p. 130, 2018, doi: 10.1186/s12886-018-0785-3.

[67] R. H. F. Lim, B. Gupta, and P. Simcock, "Intravitreal aflibercept in neovascular age-related macular degeneration previously treated with ranibizumab," (in eng), *Int J Ophthalmol,* vol. 10, no. 3, pp. 423-426, 2017, doi: 10.18240/ijo.2017.03.15.

[68] B.-H. Wu, B. Wang, H.-Q. Wu, Q. Chang, and H.-Q. Lu, "Intravitreal conbercept injection for neovascular age-related macular degeneration," (in eng), *Int J Ophthalmol,* vol. 12, no. 2, pp. 252-257, 2019, doi: 10.18240/ijo.2019.02.11.

[69] D. Wyględowska-Promieńska, A. Piotrowska-Gwóźdź, A. Piotrowska-Seweryn, and G. Mazur-Piotrowska, "Combination of Aflibercept and Bromfenac Therapy in Age-Related Macular Degeneration: A Pilot Study Aflibercept and Bromfenac in AMD," (in eng), *Med Sci Monit,* vol. 21, pp. 3906-3912, 2015, doi: 10.12659/msm.895977.

[70] Y. Shen, W.-Y. Zhang, and G. C. Y. Chiou, "Effect of naringenin on NaIO(3)-induced retinal pigment epithelium degeneration and laser-induced choroidal neovascularization in rats," (in eng), *Int J Ophthalmol,* vol. 3, no. 1, pp. 5-8, 2010, doi: 10.3980/j.issn.2222-3959.2010.01.02.

[71] P. Narvekar, P. Bhatt, G. Fnu, and V. Sutariya, "Axitinib-Loaded Poly(Lactic-Co-Glycolic Acid) Nanoparticles for Age-Related Macular Degeneration: Formulation Development and In Vitro Characterization," *ASSAY and Drug Development Technologies,* vol. 17, no. 4, pp. 167-177, 2019, doi: 10.1089/adt.2019.920.

[72] D. Huang, Y.-S. Chen, and I. D. Rupenthal, "Hyaluronic Acid Coated Albumin Nanoparticles for Targeted Peptide Delivery to the Retina," *Molecular Pharmaceutics,* vol. 14, no. 2, pp. 533-545, 2017, doi: 10.1021/acs.molpharmaceut.6b01029.

[73] A. P. M. T. Oguido *et al.*, "Naringenin Eye Drops Inhibit Corneal Neovascularization by Anti-Inflammatory and Antioxidant Mechanisms," *Investigative Ophthalmology & Visual Science,* vol. 58, no. 13, pp. 5764-5776, 2017, doi: 10.1167/iovs.16-19702.

[74] N. H. Zaidun, Z. C. Thent, and A. A. Latiff, "Combating oxidative stress disorders with citrus flavonoid: Naringenin," *Life Sciences,* vol. 208, pp. 111-122, 2018, doi: https://doi.org/10.1016/j.lfs.2018.07.017.

[75] A. Hanneken, F.-F. Lin, J. Johnson, and P. Maher, "Flavonoids Protect Human Retinal Pigment Epithelial Cells from Oxidative-Stress–Induced Death," *Investigative Ophthalmology & Visual Science,* vol. 47, no. 7, pp. 3164-3177, 2006, doi: 10.1167/iovs.04-1369.

[76] S. Sharma, S. L. Ball, and N. S. Peachey, "Pharmacological studies of the mouse cone electroretinogram," *Visual Neuroscience,* vol. 22, no. 5, pp. 631-636, 2005, doi: 10.1017/S0952523805225129.

[77] A. R. Shah and T. W. Gardner, "Diabetic retinopathy: research to clinical practice," *Clinical Diabetes and Endocrinology,* vol. 3, p. 9, 2017, doi: 10.1186/s40842-017-0047-y.

[78] J. W. Y. Yau *et al.*, "Global Prevalence and Major Risk Factors of Diabetic Retinopathy," *Diabetes Care,* vol. 35, no. 3, pp. 556-564, 2012, doi: 10.2337/dc11-1909.

[79] T. W. Gardne and E. Y. Chew, "Future Opportunities in Diabetic Retinopathy Research," *Current opinion in endocrinology, diabetes, and obesity,* vol. 23, no. 2, pp. 91-96, 2016, doi: 10.1097/MED.0000000000000238.

[80] A.-A. Szigiato, D. W. Podbielski, and I. I. K. Ahmed, "Sustained drug delivery for the management of glaucoma," *Expert Review of Ophthalmology,* vol. 12, no. 2, pp. 173-186, 2017, doi: 10.1080/17469899.2017.1280393.

[81] N. Gooch *et al.*, "Ocular Drug Delivery for Glaucoma Management," *Pharmaceutics,* vol. 4, no. 1, pp. 197-211, 2012, doi: 10.3390/pharmaceutics4010197.

[82] C. Durairaj, "Ocular Pharmacokinetics," *Handb Exp Pharmacol,* vol. 242, pp. 31-55, 2017, doi: 10.1007/164_2016_32.

[83] J. A. Last, S. J. Liliensiek, P. F. Nealey, and C. J. Murphy, "Determining the mechanical properties of human corneal basement membranes with atomic force microscopy," (in eng), *J Struct Biol,* vol. 167, no. 1, pp. 19-24, 2009, doi: 10.1016/j.jsb.2009.03.012.

[84] V. H. L. Lee, "Mechanisms and facilitation of corneal drug penetration," *Journal of Controlled Release*, vol. 11, no. 1, pp. 79-90, 1990, doi: https://doi.org/10.1016/0168-3659(90)90122-A.
[85] H. J. Gukasyan, B. R. Yerxa, W. Pendergast, and V. H. L. Lee, "Metabolism and Transport of Purinergic Receptor Agonists in Rabbit Conjunctival Epithelial Cells," in *Lacrimal Gland, Tear Film, and Dry Eye Syndromes 3: Basic Science and Clinical Relevance Part A and B*, D. A. Sullivan, M. E. Stern, K. Tsubota, D. A. Dartt, R. M. Sullivan, and B. B. Bromberg Eds. Boston, MA: Springer US, 2002, pp. 255-259.
[86] K. Peynshaert, J. Devoldere, S. C. De Smedt, and K. Remaut, "In vitro and ex vivo models to study drug delivery barriers in the posterior segment of the eye," *Advanced Drug Delivery Reviews*, vol. 126, pp. 44-57, 2018/02/15/ 2018, doi: https://doi.org/10.1016/j.addr.2017.09.007.
[87] D. Huang, Y.-S. Chen, and I. D. Rupenthal, "Overcoming ocular drug delivery barriers through the use of physical forces," *Advanced Drug Delivery Reviews*, vol. 126, pp. 96-112, 2018/02/15/ 2018, doi: https://doi.org/10.1016/j.addr.2017.09.008.
[88] N. P. Cheruvu and U. B. Kompella, "Bovine and porcine transscleral solute transport: influence of lipophilicity and the Choroid-Bruch's layer," *Invest Ophthalmol Vis Sci*, vol. 47, no. 10, pp. 4513-22, 2006, doi: 10.1167/iovs.06-0404.
[89] R. Gaudana, H. K. Ananthula, A. Parenky, and A. K. Mitra, "Ocular drug delivery," *AAPS J*, vol. 12, no. 3, pp. 348-60, 2010, doi: 10.1208/s12248-010-9183-3.
[90] S. P. Chaplot and I. D. Rupenthal, "Dendrimers for gene delivery--a potential approach for ocular therapy?," *J Pharm Pharmacol*, vol. 66, no. 4, pp. 542-56, 2014, doi: 10.1111/jphp.12104.
[91] N. Toffoletto, M. Salema-Oom, S. Anguiano Igea, C. Alvarez-Lorenzo, B. Saramago, and A. P. Serro, "Drug-Loaded Hydrogels for Intraocular Lenses with Prophylactic Action against Pseudophakic Cystoid Macular Edema," *Pharmaceutics*, vol. 13, no. 7, 2021, doi: 10.3390/pharmaceutics13070976.
[92] G. Begum *et al.*, "Rapid assessment of ocular drug delivery in a novel ex vivo corneal model," *Scientific Reports*, vol. 10, no. 1, p. 11754, 2020/07/16 2020, doi: 10.1038/s41598-020-68254-1.
[93] P. Dixon, R. C. Fentzke, A. Bhattacharya, A. Konar, S. Hazra, and A. Chauhan, "In vitro drug release and in vivo safety of vitamin E and cysteamine loaded contact lenses," *International Journal of Pharmaceutics*, vol. 544, no. 2, pp. 380-391, 2018/06/15/ 2018, doi: https://doi.org/10.1016/j.ijpharm.2017.11.059.
[94] R. Urban-Chmiel *et al.*, "The in vitro efficacy of eye drops containing a bacteriophage solution specific for Staphylococcus spp. isolated from dogs with bacterial conjunctivitis," *Irish Veterinary Journal*, vol. 73, no. 1, p. 21, 2020/11/04 2020, doi: 10.1186/s13620-020-00175-x.
[95] C. Sotozono *et al.*, "Vancomycin Ophthalmic Ointment 1% for methicillin-resistant Staphylococcus aureus or methicillin-resistant Staphylococcus epidermidis infections: a case series," *BMJ Open*, vol. 3, no. 1, p. e001206, 2013, doi: 10.1136/bmjopen-2012-001206.
[96] R. Jin, Y. Li, L. Li, J. Kim, H. J. Yoon, and K. C. Yoon, "Comparative analysis of 0.1% cyclosporin A cationic emulsion and 0.05% cyclosporin A emulsion

in murine dry eye cases with different severities," (in eng), *Exp Ther Med,* vol. 22, no. 6, pp. 1363-1363, 2021, doi: 10.3892/etm.2021.10797.

[97] S. Pandey and T. Kunsel, "Eye Drops and Lubricants Market by Type (Antibiotics, Hormones, Artificial Tears, and Others) and Application (Eye Diseases, Eye Care, and Others): Global Opportunity Analysis and Industry Forecast, 2018 - 2025," Allied MArket Research, 2019. [Online]. Available: https://www.alliedmarketresearch.com/eye-drop-and-lubricants-market

[98] M. Ayaki, A. Iwasawa, S. Yaguchi, and R. Koide, "Preserved and unpreserved 12 anti-allergic ophthalmic solutions and ocular surface toxicity: in vitro assessment in four cultured corneal and conjunctival epithelial cell lines," *Biocontrol Science,* vol. 15, no. 4, pp. 143-148, 2010, doi: 10.4265/bio.15.143.

[99] M. Ayaki, S. Yaguchi, A. Iwasawa, and R. Koide, "Cytotoxicity of ophthalmic solutions with and without preservatives to human corneal endothelial cells, epithelial cells and conjunctival epithelial cells," *Clin Exp Ophthalmol,* vol. 36, no. 6, pp. 553-9, 2008, doi: 10.1111/j.1442-9071.2008.01803.x.

[100] D. H. Shastri, P. K. Shelat, A. K. Shukla, and P. B. Patel, "Ophthalmic drug delivery system: Challenges and approaches," *Systematic Reviews in Pharmacy,* vol. 1, no. 2, p. 113, 2010, doi: 10.4103/0975-8453.75042.

[101] S. Mishima, A. Gasset, S. D. Klyce, Jr., and J. L. Baum, "Determination of Tear Volume and Tear Flow," *Investigative Ophthalmology & Visual Science,* vol. 5, no. 3, pp. 264-276, 1966.

[102] W. A. Gahl, E. M. Kuehl, F. Iwata, A. Lindblad, and M. I. Kaiser-Kupfer, "Corneal crystals in nephropathic cystinosis: natural history and treatment with cysteamine eyedrops," *Mol Genet Metab,* vol. 71, no. 1-2, pp. 100-20, 2000, doi: 10.1006/mgme.2000.3062.

[103] University of Illinois at Chicago. New treatment for severe dry eye disease promising in early clinical trials [Online] Available: sciencedaily.com/releases/2019/05/190507121435.htm

[104] D. T. H. Tan, S.-P. Chee, L. Lim, and A. S. M. Lim, "Randomized clinical trial of a new dexamethasone delivery system (surodex) for treatment of post-cataract surgery inflammation¹," *Ophthalmology,* vol. 106, no. 2, pp. 223-231, 1999, doi: 10.1016/S0161-6420(99)90060-X.

[105] G. P. Mishra, M. Bagui, V. Tamboli, and A. K. Mitra, "Recent applications of liposomes in ophthalmic drug delivery," *J Drug Deliv,* vol. 2011, p. 863734, 2011, doi: 10.1155/2011/863734.

[106] S. P. Thornion and E. Troyer, "Treatment for dry eye syndrome (US20060088600A1)," 2006.

[107] I. Avni *et al.*, "Treatment of dry eye syndrome with orally administered CF101: data from a phase 2 clinical trial," (in eng), *Ophthalmology,* vol. 117, no. 7, pp. 1287-1293, 2010, doi: 10.1016/j.ophtha.2009.11.029.

[108] J.-Y. Huang, P.-T. Yeh, and Y.-C. Hou, "A randomized, double-blind, placebo-controlled study of oral antioxidant supplement therapy in patients with dry eye syndrome," (in eng), *Clinical ophthalmology (Auckland, N.Z.),* vol. 10, pp. 813-820, 2016, doi: 10.2147/OPTH.S106455.

[109] Y. Kim, C. H. Moon, B.-Y. Kim, and S. Y. Jang, "Oral Hyaluronic Acid Supplementation for the Treatment of Dry Eye Disease: A Pilot Study," *Journal of Ophthalmology,* vol. 2019, p. 5491626, 2019, doi: 10.1155/2019/5491626.

[110] Y. Shirasaki, "Molecular design for enhancement of ocular penetration," *J Pharm Sci,* vol. 97, no. 7, pp. 2462-96, 2008, doi: 10.1002/jps.21200.

[111] A. Urtti, "Challenges and obstacles of ocular pharmacokinetics and drug delivery," *Adv Drug Deliv Rev*, vol. 58, no. 11, pp. 1131-5, 2006, doi: 10.1016/j.addr.2006.07.027.
[112] K. Hosseini *et al.*, "Pharmacokinetic study of dexamethasone disodium phosphate using intravitreal, subconjunctival, and intravenous delivery routes in rabbits," *J Ocul Pharmacol Ther*, vol. 24, no. 3, pp. 301-8, 2008, doi: 10.1089/jop.2007.0117.
[113] S. H. Kim, K. G. Csaky, N. S. Wang, and R. J. Lutz, "Drug elimination kinetics following subconjunctival injection using dynamic contrast-enhanced magnetic resonance imaging," *Pharm Res*, vol. 25, no. 3, pp. 512-20, 2008, doi: 10.1007/s11095-007-9408-z.
[114] D. F. Martin *et al.*, "Ranibizumab and Bevacizumab for Treatment of Neovascular Age-Related Macular Degeneration: 2-Year Results: Comparison of Age-related Macular Degeneration Treatments Trials (CATT) Research Group," *Ophthalmology*, vol. 119, no. 7, pp. 1388-1398, 2012, doi: 10.1016/j.ophtha.2012.03.053.
[115] J. S. Heier *et al.*, "Intravitreal Aflibercept (VEGF Trap-Eye) in Wet Age-related Macular Degeneration," *Ophthalmology*, vol. 119, no. 12, pp. 2537-2548, 2012, doi: 10.1016/j.ophtha.2012.09.006.
[116] E. M. Del Amo *et al.*, "Pharmacokinetic aspects of retinal drug delivery," *Prog Retin Eye Res*, vol. 57, pp. 134-185, 2017, doi: 10.1016/j.preteyeres.2016.12.001.
[117] H. Kim, S. B. Robinson, and K. G. Csaky, "Investigating the movement of intravitreal human serum albumin nanoparticles in the vitreous and retina," *Pharm Res*, vol. 26, no. 2, pp. 329-37, 2009, doi: 10.1007/s11095-008-9745-6.
[118] C. H. Meyer *et al.*, "Incidence of rhegmatogenous retinal detachments after intravitreal antivascular endothelial factor injections," *Acta Ophthalmologica*, vol. 89, no. 1, pp. 70-75, 2011, doi: 10.1111/j.1755-3768.2010.02064.x.
[119] T. Diago, C. A. McCannel, S. J. Bakri, J. S. Pulido, A. O. Edwards, and J. M. Pach, "Infectious endophthalmitis after intravitreal injection of antiangiogenic agents," *RETINA*, vol. 29, no. 5, 2009. [Online]. Available: https://journals.lww.com/retinajournal/Fulltext/2009/05000/INFECTIOUS_ENDOPHTHALMITIS_AFTER_INTRAVITREAL.6.aspx.
[120] X. Gao *et al.*, "Loss to Follow-up After Intravitreal Anti–Vascular Endothelial Growth Factor Injections in Patients with Diabetic Macular Edema," *Ophthalmology Retina*, vol. 3, no. 3, pp. 230-236, 2019/03/01/ 2019, doi: https://doi.org/10.1016/j.oret.2018.11.002.
[121] T. R. Thrimawithana, S. Young, C. R. Bunt, C. R. Green, and R. G. Alany, "Drug Delivery to the Posterior Segment of the Eye: Challenges and Opportunities," *Drug Delivery Letters*, vol. 1, no. 1, pp. 40-44, 2011, doi: http://dx.doi.org/10.2174/2210304x11101010040.
[122] D. R. Janagam, L. Wu, and T. L. Lowe, "Nanoparticles for drug delivery to the anterior segment of the eye," *Adv Drug Deliv Rev*, vol. 122, pp. 31-64, 2017, doi: 10.1016/j.addr.2017.04.001.
[123] J. Alvarez-Trabado, Y. Diebold, and A. Sanchez, "Designing lipid nanoparticles for topical ocular drug delivery," *Int J Pharm*, vol. 532, no. 1, pp. 204-217, 2017, doi: 10.1016/j.ijpharm.2017.09.017.
[124] S. Manchanda and P. K. Sahoo, "Topical delivery of acetazolamide by encapsulating in mucoadhesive nanoparticles," *Asian Journal of*

Pharmaceutical Sciences, vol. 12, no. 6, pp. 550-557, 2017, doi: https://doi.org/10.1016/j.ajps.2017.04.005.

[125] B. Srinivasan, A. R. Kolli, M. B. Esch, H. E. Abaci, M. L. Shuler, and J. J. Hickman, "TEER measurement techniques for in vitro barrier model systems," *J Lab Autom*, vol. 20, no. 2, pp. 107-26, 2015, doi: 10.1177/2211068214561025.

[126] K. M. Hämäläinen, K. Kananen, S. Auriola, K. Kontturi, and A. Urtti, "Characterization of paracellular and aqueous penetration routes in cornea, conjunctiva, and sclera," *Investigative Ophthalmology & Visual Science*, vol. 38, no. 3, pp. 627-634, 1997. [Online]. Available: http://dx.doi.org/.

[127] M. L. Occhiutto, F. R. Freitas, R. C. Maranhao, and V. P. Costa, "Breakdown of the blood-ocular barrier as a strategy for the systemic use of nanosystems," *Pharmaceutics*, vol. 4, no. 2, pp. 252-75, 2012, doi: 10.3390/pharmaceutics4020252.

[128] S. H. Kim, R. J. Lutz, N. S. Wang, and M. R. Robinson, "Transport barriers in transscleral drug delivery for retinal diseases," *Ophthalmic Res*, vol. 39, no. 5, pp. 244-54, 2007, doi: 10.1159/000108117.

[129] J. Ambati *et al.*, "Diffusion of High Molecular Weight Compounds through Sclera," *Investigative Ophthalmology & Visual Science*, vol. 41, no. 5, pp. 1181-1185, 2000. [Online]. Available: http://dx.doi.org/.

[130] L. Pitkanen, V. P. Ranta, H. Moilanen, and A. Urtti, "Permeability of retinal pigment epithelium: effects of permeant molecular weight and lipophilicity," *Invest Ophthalmol Vis Sci*, vol. 46, no. 2, pp. 641-6, 2005, doi: 10.1167/iovs.04-1051.

[131] D. Ghate, W. Brooks, B. E. McCarey, and H. F. Edelhauser, "Pharmacokinetics of intraocular drug delivery by periocular injections using ocular fluorophotometry," *Invest Ophthalmol Vis Sci*, vol. 48, no. 5, pp. 2230-7, 2007, doi: 10.1167/iovs.06-0954.

[132] M. A. Kalam, "The potential application of hyaluronic acid coated chitosan nanoparticles in ocular delivery of dexamethasone," *International Journal of Biological Macromolecules*, vol. 89, pp. 559-568, 2016/08/01/ 2016, doi: https://doi.org/10.1016/j.ijbiomac.2016.05.016.

[133] H. Chen *et al.*, "The potential use of novel chitosan-coated deformable liposomes in an ocular drug delivery system," *Colloids and Surfaces B: Biointerfaces*, vol. 143, pp. 455-462, 2016/07/01/ 2016, doi: https://doi.org/10.1016/j.colsurfb.2016.03.061.

[134] M. M. Silva, R. Calado, J. Marto, A. Bettencourt, A. J. Almeida, and L. M. D. Gonçalves, "Chitosan Nanoparticles as a Mucoadhesive Drug Delivery System for Ocular Administration," (in eng), *Mar Drugs*, vol. 15, no. 12, p. 370, 2017, doi: 10.3390/md15120370.

[135] Y. Wang, X. Xu, Y. Gu, Y. Cheng, and F. Cao, "Recent advance of nanoparticle-based topical drug delivery to the posterior segment of the eye," *Expert Opinion on Drug Delivery*, vol. 15, no. 7, pp. 687-701, 2018, doi: 10.1080/17425247.2018.1496080.

[136] I. Luis de Redín *et al.*, "Human serum albumin nanoparticles for ocular delivery of bevacizumab," *International Journal of Pharmaceutics*, vol. 541, no. 1, pp. 214-223, 2018, doi: https://doi.org/10.1016/j.ijpharm.2018.02.003.

[137] J. Mun, J. w. Mok, S. Jeong, S. Cho, C.-K. Joo, and S. K. Hahn, "Drug-eluting contact lens containing cyclosporine-loaded cholesterol-hyaluronate micelles

for dry eye syndrome," *RSC Advances*, 10.1039/C9RA02858G vol. 9, no. 29, pp. 16578-16585, 2019, doi: 10.1039/C9RA02858G.
[138] C.-L. Savin, M. Popa, C. Delaite, M. Costuleanu, D. Costin, and C. A. Peptu, "Chitosan grafted-poly(ethylene glycol) methacrylate nanoparticles as carrier for controlled release of bevacizumab," *Materials Science and Engineering: C*, vol. 98, pp. 843-860, 2019, doi: https://doi.org/10.1016/j.msec.2019.01.036.
[139] J. Ali, M. Fazil, M. Qumbar, N. Khan, and A. Ali, "Colloidal drug delivery system: amplify the ocular delivery," *Drug Deliv*, vol. 23, no. 3, pp. 710-26, 2016, doi: 10.3109/10717544.2014.923065.
[140] H. Thai *et al.*, "Characterization of chitosan/alginate/lovastatin nanoparticles and investigation of their toxic effects in vitro and in vivo," (in eng), *Scientific reports*, vol. 10, no. 1, p. 909, 2020, doi: 10.1038/s41598-020-57666-8.
[141] D. Bennet and S. Kim, "Polymer Nanoparticles for Smart Drug Delivery," 2014, doi: 10.5772/58422.
[142] T. Wang, J. Hou, C. Su, L. Zhao, and Y. Shi, "Hyaluronic acid-coated chitosan nanoparticles induce ROS-mediated tumor cell apoptosis and enhance antitumor efficiency by targeted drug delivery via CD44," (in eng), *J Nanobiotechnology*, vol. 15, no. 7, pp. 1-12, 2017, doi: 10.1186/s12951-016-0245-2.
[143] A. I. Barbosa, S. A. Costa Lima, and S. Reis, "Application of pH-Responsive Fucoidan/Chitosan Nanoparticles to Improve Oral Quercetin Delivery," (in eng), *Molecules*, vol. 24, no. 2, pp. 346-360, 2019, doi: 10.3390/molecules24020346.
[144] L. Zhao *et al.*, "Chitosan/Sulfobutylether-β-Cyclodextrin Nanoparticles for Ibrutinib Delivery: A Potential Nanoformulation of Novel Kinase Inhibitor," *Journal of Pharmaceutical Sciences*, vol. 109, no. 2, pp. 1136-1144, 2020, doi: https://doi.org/10.1016/j.xphs.2019.10.007.
[145] J. Yan *et al.*, "Preparation of Puerarin Chitosan Oral Nanoparticles by Ionic Gelation Method and Its Related Kinetics," *Pharmaceutics*, vol. 12, p. 216, 2020, doi: 10.3390/pharmaceutics12030216.
[146] R. M. Saeed, I. Dmour, and M. O. Taha, "Stable Chitosan-Based Nanoparticles Using Polyphosphoric Acid or Hexametaphosphate for Tandem Ionotropic/Covalent Crosslinking and Subsequent Investigation as Novel Vehicles for Drug Delivery," (in English), *Frontiers in Bioengineering and Biotechnology*, Original Research vol. 8, no. 4, 2020, doi: 10.3389/fbioe.2020.00004.
[147] Y. Ciro, J. Rojas, M. J. Alhajj, G. A. Carabali, and C. H. Salamanca, "Production and Characterization of Chitosan-Polyanion Nanoparticles by Polyelectrolyte Complexation Assisted by High-Intensity Sonication for the Modified Release of Methotrexate," (in eng), *Pharmaceuticals (Basel)*, vol. 13, no. 1, p. 11, 2020, doi: 10.3390/ph13010011.
[148] S. Katiyar *et al.*, "In situ gelling dorzolamide loaded chitosan nanoparticles for the treatment of glaucoma," *Carbohydrate Polymers*, vol. 102, pp. 117-124, 2014, doi: https://doi.org/10.1016/j.carbpol.2013.10.079.
[149] L. Widjaja, M. Bora, P. Chan, V. Lipik, T. Wong, and S. Venkatraman, "Hyaluronic acid-based nanocomposite hydrogels for ocular drug delivery applications," *Journal of biomedical materials research. Part A*, vol. 102, 2014, doi: 10.1002/jbm.a.34976.
[150] V. Nayak, M. S. Jyothi, R. G. Balakrishna, M. Padaki, and A. F. Ismail, "Preparation and Characterization of Chitosan Thin Films on Mixed-Matrix

Membranes for Complete Removal of Chromium," *ChemistryOpen*, vol. 4, no. 3, pp. 278-287, 2015, doi: 10.1002/open.201402133.
[151] M.-M. Lou *et al.*, "Antibacterial activity and mechanism of action of chitosan solutions against apricot fruit rot pathogen Burkholderia seminalis," *Carbohydrate Research*, vol. 346, no. 11, pp. 1294-1301, 2011, doi: https://doi.org/10.1016/j.carres.2011.04.042.
[152] D. Tzaneva, M. Dzhivoderova, N. Petkova, P. Denev, D. Hadzhikinov, and A. Stoyanova, "Rheological Properties of the Cosmetic Gel Including Carboxymethyl Chitosan," *Journal of Pharmaceutical Sciences and Research*, vol. 9, pp. 1383-1387, 2017.
[153] O. M. Dragostin *et al.*, "New antimicrobial chitosan derivatives for wound dressing applications," *Carbohydrate Polymers*, vol. 141, pp. 28-40, 2016, doi: https://doi.org/10.1016/j.carbpol.2015.12.078.
[154] G. Galed, B. Miralles, I. Paños, A. Santiago, and Á. Heras, "N-Deacetylation and depolymerization reactions of chitin/chitosan: Influence of the source of chitin," *Carbohydrate Polymers*, vol. 62, no. 4, pp. 316-320, 2005, doi: https://doi.org/10.1016/j.carbpol.2005.03.019.
[155] I. Younes and M. Rinaudo, "Chitin and chitosan preparation from marine sources. Structure, properties and applications," (in eng), *Mar Drugs*, vol. 13, no. 3, pp. 1133-1174, 2015, doi: 10.3390/md13031133.
[156] R. S. C. M. de Queiroz Antonino *et al.*, "Preparation and Characterization of Chitosan Obtained from Shells of Shrimp (Litopenaeus vannamei Boone)," (in eng), *Mar Drugs*, vol. 15, no. 5, p. 141, 2017, doi: 10.3390/md15050141.
[157] M. Jahan, N. F, M. Sm, A. M, R. Sk, and H. Mm, "A process of preparation of chitin and chitosan from prawn shell waste," *Bangladesh Journal of Scientific and Industrial Research*, vol. 45, pp. 323-330, 01/01 2010, doi: 10.3329/bjsir.v45i4.7330.
[158] R. Esquivel, J. Juárez, M. Almada, J. Ibarra-Hurtado, and M. Valdez, "Synthesis and Characterization of New Thiolated Chitosan Nanoparticles Obtained by Ionic Gelation Method," *International Journal of Polymer Science*, vol. 2015, pp. 1-18, 2015, doi: 10.1155/2015/502058.
[159] J.-W. Park, K.-H. Choi, and K.-h. Park, "Acid-Base Equilibria and Related Properites of Chitosan," *Bulletin of the Korean Chemical Society*, vol. 4, 1983.
[160] N. Kubota and Y. Eguchi, "Facile Preparation of Water-Soluble N-Acetylated Chitosan and Molecular Weight Dependence of Its Water-Solubility," *Polymer Journal*, vol. 29, no. 2, pp. 123-127, 1997, doi: 10.1295/polymj.29.123.
[161] J. Cui, Z. Yu, and D. Lau, "Effect of Acetyl Group on Mechanical Properties of Chitin/Chitosan Nanocrystal: A Molecular Dynamics Study," (in eng), *Int J Mol Sci*, vol. 17, no. 1, p. 61, 2016, doi: 10.3390/ijms17010061.
[162] R. Paliwal, S. R. Paliwal, K. Sulakhiya, B. D. Kurmi, R. Kenwat, and A. Mamgain, "4 - Chitosan-based nanocarriers for ophthalmic applications," in *Polysaccharide Carriers for Drug Delivery*, S. Maiti and S. Jana Eds.: Woodhead Publishing, 2019, pp. 79-104.
[163] G. A. Morris, S. M. Kök, S. E. Harding, and G. G. Adams, "Polysaccharide drug delivery systems based on pectin and chitosan," *Biotechnology and Genetic Engineering Reviews*, vol. 27, no. 1, pp. 257-284, 2010, doi: 10.1080/02648725.2010.10648153.
[164] M. Badawy and E. Rabea, "A Biopolymer Chitosan and Its Derivatives as Promising Antimicrobial Agents against Plant Pathogens and Their Applications in Crop Protection," *Hindawi Publishing Corporation*

International Journal of Carbohydrate Chemistry Article ID, vol. 460381, 2011, doi: 10.1155/2011/460381.

[165] S. E. Harding, S. S. B. Davis, M. P. Deacon, and I. Fiebrig, "Biopolymer Mucoadhesives," *Biotechnology and Genetic Engineering Reviews*, vol. 16, no. 1, pp. 41-86, 1999, doi: 10.1080/02648725.1999.10647971.

[166] H. Takeuchi, J. Thongborisute, Y. Matsui, H. Sugihara, H. Yamamoto, and Y. Kawashima, "Novel mucoadhesion tests for polymers and polymer-coated particles to design optimal mucoadhesive drug delivery systems," *Advanced Drug Delivery Reviews*, vol. 57, no. 11, pp. 1583-1594, 2005, doi: https://doi.org/10.1016/j.addr.2005.07.008.

[167] I. A. Sogias, A. C. Williams, and V. V. Khutoryanskiy, "Why is Chitosan Mucoadhesive?," *Biomacromolecules*, vol. 9, no. 7, pp. 1837-1842, 2008, doi: 10.1021/bm800276d.

[168] X. Xu, L. Sun, L. Zhou, Y. Cheng, and F. Cao, "Functional chitosan oligosaccharide nanomicelles for topical ocular drug delivery of dexamethasone," *Carbohydrate Polymers*, vol. 227, p. 115356, 2020, doi: https://doi.org/10.1016/j.carbpol.2019.115356.

[169] J. R. E. Fraser, T. C. Laurent, and U. B. G. Laurent, "Hyaluronan: its nature, distribution, functions and turnover," *Journal of Internal Medicine*, vol. 242, no. 1, pp. 27-33, 1997, doi: 10.1046/j.1365-2796.1997.00170.x.

[170] J. E. Scott and F. Heatley, "Hyaluronan forms specific stable tertiary structures in aqueous solution: a 13C NMR study," (in eng), *Proc Natl Acad Sci U S A*, vol. 96, no. 9, pp. 4850-4855, 1999, doi: 10.1073/pnas.96.9.4850.

[171] M. Brown and S. Jones, "Hyaluronic acid: A unique topical vehicle for the localized delivery of drugs to the skin," *Journal of the European Academy of Dermatology and Venereology : JEADV*, vol. 19, pp. 308-18, 2005, doi: 10.1111/j.1468-3083.2004.01180.x.

[172] E. A. Balazs, D. Watson, I. F. Duff, and S. Roseman, "Hyaluronic acid in synovial fluid. I. Molecular parameters of hyaluronic acid in normal and arthritic human fluids," *Arthritis & Rheumatism*, vol. 10, no. 4, pp. 357-376, 1967, doi: 10.1002/art.1780100407.

[173] K. Meyer and J. W. Palmer, "The polysaccharide of the vitreous humor," *Journal of Biological Chemistry*, vol. 107, no. 3, pp. 629-634, 1934. [Online]. Available: http://www.jbc.org/content/107/3/629.short.

[174] S. M. Jegasothy, V. Zabolotniaia, and S. Bielfeldt, "Efficacy of a New Topical Nano-hyaluronic Acid in Humans," (in eng), *J Clin Aesthet Dermatol*, vol. 7, no. 3, pp. 27-29, 2014. [Online]. Available: https://pubmed.ncbi.nlm.nih.gov/24688623.

[175] J. B. Leach, K. A. Bivens, C. N. Collins, and C. E. Schmidt, "Development of photocrosslinkable hyaluronic acid-polyethylene glycol-peptide composite hydrogels for soft tissue engineering," *Journal of Biomedical Materials Research Part A*, vol. 70A, no. 1, pp. 74-82, 2004, doi: 10.1002/jbm.a.30063.

[176] G. S. Jensen, V. L. Attridge, M. R. Lenninger, and K. F. Benson, "Oral intake of a liquid high-molecular-weight hyaluronan associated with relief of chronic pain and reduced use of pain medication: results of a randomized, placebo-controlled double-blind pilot study," (in eng), *J Med Food*, vol. 18, no. 1, pp. 95-101, 2015, doi: 10.1089/jmf.2013.0174.

[177] X. Fan, X. Zhao, X. Qu, and J. Fang, "pH sensitive polymeric complex of cisplatin with hyaluronic acid exhibits tumor-targeted delivery and improved

in vivo antitumor effect," *International Journal of Pharmaceutics,* vol. 496, no. 2, pp. 644-653, 2015, doi: https://doi.org/10.1016/j.ijpharm.2015.10.066.
[178] B. Silva, L. M. Gonçalves, B. S. Braz, and E. Delgado, "Chitosan and Hyaluronic Acid Nanoparticles as Vehicles of Epoetin Beta for Subconjunctival Ocular Delivery," *Mar Drugs,* vol. 20, no. 2, doi: 10.3390/md20020151.
[179] S. R. D'Mello, C. N. Cruz, M.-L. Chen, M. Kapoor, S. L. Lee, and K. M. Tyner, "The evolving landscape of drug products containing nanomaterials in the United States," *Nature Nanotechnology,* vol. 12, no. 6, pp. 523-529, 2017, doi: 10.1038/nnano.2017.67.
[180] J.-B. Coty and C. Vauthier, "Characterization of nanomedicines: A reflection on a field under construction needed for clinical translation success," *Journal of Controlled Release,* vol. 275, pp. 254-268, 2018, doi: https://doi.org/10.1016/j.jconrel.2018.02.013.
[181] S. Gioria *et al.*, "Are existing standard methods suitable for the evaluation of nanomedicines: some case studies," *Nanomedicine,* vol. 13, no. 5, pp. 539-554, 2018, doi: 10.2217/nnm-2017-0338.
[182] S. Bremer-Hoffmann, B. Halamoda-Kenzaoui, and S. E. Borgos, "Identification of regulatory needs for nanomedicines," *Journal of Interdisciplinary Nanomedicine,* vol. 3, no. 1, pp. 4-15, 2018, doi: 10.1002/jin2.34.
[183] *Drug Products, Including Biological Products, that Contain Nanomaterials,* U. S. D. o. H. a. H. Services, F. a. D. Administration, C. f. D. E. a. R. (CDER), and C. f. B. E. a. R. (CBER), 2017.
[184] *Joint MHLW/EMA reflection paper on the development of block copolymer micelle medicinal products,* E. M. Agency EMA/CHMP/13099/2013, 2014.
[185] *Reflection paper on the data requirements for intravenous liposomal products developed with reference to an innovator liposomal product,* E. M. Agency EMA/CHMP/806058/2009/Rev. 02, 2013.
[186] *Reflection paper on the data requirements for intravenous iron-based nano-colloidal products developed with reference to an innovator medicinal product,* E. M. Agency EMA/CHMP/SWP/620008/2012, 2015.
[187] *Liposome Drug Products: Chemistry, Manufacturing, and Controls; Human Pharmacokinetics and Bioavailability; and Labeling Documentation,* FDA Guidance for Industry, 2018.
[188] A. Shvedova, A. Pietroiusti, and V. Kagan, "Nanotoxicology ten years later: Lights and shadows," *Toxicol Appl Pharmacol,* vol. 299, pp. 1-2, 2016, doi: 10.1016/j.taap.2016.02.014.
[189] H. A. Khan and R. Shanker, "Toxicity of Nanomaterials," *Biomed Res Int,* vol. 2015, p. 521014, 2015, doi: 10.1155/2015/521014.
[190] S. Bamrungsap *et al.*, "Nanotechnology in therapeutics: a focus on nanoparticles as a drug delivery system," *Nanomedicine,* vol. 7, no. 8, pp. 1253-1271, 2012, doi: 10.2217/nnm.12.87.
[191] A. A. Shvedova *et al.*, "Exposure to carbon nanotube material: assessment of nanotube cytotoxicity using human keratinocyte cells," *J Toxicol Environ Health A,* vol. 66, no. 20, pp. 1909-26, 2003, doi: 10.1080/713853956.
[192] G. Oberdörster, E. Oberdörster, and J. Oberdörster, "Nanotoxicology: An Emerging Discipline Evolving from Studies of Ultrafine Particles," *Environmental Health Perspectives,* vol. 113, no. 7, pp. 823-839, 2005, doi: 10.1289/ehp.7339.

[193] L. Thrall, N. Lubick, K. Betts, C. M. Cooney, M. Burke, and R. Renner, "Study links TiO2 nanoparticles with potential for brain-cell damage," *Environmental Science & Technology*, vol. 40, no. 14, pp. 4326-4334, 2006, doi: 10.1021/es062989g.

[194] W. H. De Jong and P. J. A. Borm, "Drug delivery and nanoparticles: Applications and hazards," *International Journal of Nanomedicine*, vol. 3, no. 2, pp. 133-149, 2008. [Online]. Available: http://www.ncbi.nlm.nih.gov/pmc/articles/PMC2527668/.

[195] *Regulation (EU) 2017/745 of the european parliament and of the council*, T. E. P. A. T. C. O. T. E. UNION on medical devices, amending Directive 2001/83/EC, Regulation (EC) No 178/2002 and Regulation (EC) No 1223/2009 and repealing Council Directives 90/385/EEC and 93/42/EEC, 2017.

[196] A. Fahr and X. Liu, "Drug delivery strategies for poorly water-soluble drugs," *Expert Opinion on Drug Delivery*, vol. 4, no. 4, pp. 403-416, 2007, doi: 10.1517/17425247.4.4.403.

[197] R. Neslihan Gursoy and S. Benita, "Self-emulsifying drug delivery systems (SEDDS) for improved oral delivery of lipophilic drugs," *Biomedicine & Pharmacotherapy*, vol. 58, no. 3, pp. 173-182, 2004, doi: https://doi.org/10.1016/j.biopha.2004.02.001.

[198] A. Scholz *et al.*, "Influence of Hydrodynamics and Particle Size on the Absorption of Felodipine in Labradors," *Pharmaceutical Research*, vol. 19, no. 1, pp. 42-46, 2002, doi: 10.1023/A:1013651215061.

[199] K. T. Jensen *et al.*, "Preparation and characterization of spray-dried co-amorphous drug–amino acid salts," *Journal of Pharmacy and Pharmacology*, vol. 68, no. 5, pp. 615-624, 2016, doi: 10.1111/jphp.12458.

[200] A. S. Tatavarti and S. W. Hoag, "Microenvironmental pH Modulation Based Release Enhancement of a Weakly Basic Drug from Hydrophilic Matrices *," *Journal of Pharmaceutical Sciences*, vol. 95, no. 7, pp. 1459-1468, 2006, doi: 10.1002/jps.20612.

[201] A. D. Kulkarni and V. S. Belgamwar, "Inclusion complex of chrysin with sulfobutyl ether-β-cyclodextrin (Captisol®): Preparation, characterization, molecular modelling and in vitro anticancer activity," *Journal of Molecular Structure*, vol. 1128, pp. 563-571, 2017, doi: https://doi.org/10.1016/j.molstruc.2016.09.025.

[202] T. Bíró *et al.*, "New Approach in Ocular Drug Delivery: In vitro and ex vivo Investigation of Cyclodextrin-Containing, Mucoadhesive Eye Drop Formulations," (in eng), *Drug Des Devel Ther*, vol. 15, pp. 351-360, 2021, doi: 10.2147/DDDT.S264745.

[203] T. Loftsson and E. Stefánsson, "Aqueous eye drops containing drug/cyclodextrin nanoparticles deliver therapeutic drug concentrations to both anterior and posterior segment," *Acta Ophthalmologica*, vol. 100, no. 1, pp. 7-25, 2022/02/01 2022, doi: https://doi.org/10.1111/aos.14861.

[204] F. Ricci *et al.*, "Chitosan/sulfobutylether-β-cyclodextrin based nanoparticles coated with thiolated hyaluronic acid for indomethacin ophthalmic delivery," *International Journal of Pharmaceutics*, vol. 622, p. 121905, 2022/06/25/ 2022, doi: https://doi.org/10.1016/j.ijpharm.2022.121905.

[205] E. M. M. Del Valle, "Cyclodextrins and their uses: a review," *Process Biochemistry*, vol. 39, no. 9, pp. 1033-1046, 2004, doi: https://doi.org/10.1016/S0032-9592(03)00258-9.

[206] T. Loftsson and E. Stefánsson, "Cyclodextrins in ocular drug delivery: theoretical basis with dexamethasone as a sample drug," *Journal of Drug Delivery Science and Technology*, vol. 17, no. 1, pp. 3-9, 2007, doi: https://doi.org/10.1016/S1773-2247(07)50001-8.
[207] S. Anand and V. M. L. Braga, "Cyclodextrins in Ocular Drug Delivery," in *Nano-Biomaterials For Ophthalmic Drug Delivery*, Y. Pathak, V. Sutariya, and A. A. Hirani Eds. Cham: Springer International Publishing, 2016, pp. 243-252.
[208] T. Loftsson and E. Stefánsson, "Effect of Cyclodextrins on Topical Drug Delivery to the Eye," *Drug Development and Industrial Pharmacy*, vol. 23, pp. 473-481, 2008, doi: 10.3109/03639049709148496.
[209] S. Y. Vafaei, R. Dinarvand, M. Esmaeili, R. Mahjub, and T. Toliyat, "Controlled-release drug delivery system based on fluocinolone acetonide–cyclodextrin inclusion complex incorporated in multivesicular liposomes," *Pharmaceutical Development and Technology*, vol. 20, no. 7, pp. 775-781, 2015, doi: 10.3109/10837450.2014.920358.
[210] X. Sun, Z. Yu, Z. Cai, L. Yu, and Y. Lv, "Voriconazole Composited Polyvinyl Alcohol/Hydroxypropyl-β-Cyclodextrin Nanofibers for Ophthalmic Delivery," (in eng), *PLoS One*, vol. 11, no. 12, 2016, doi: 10.1371/journal.pone.0167961.
[211] A. Ohira *et al.*, "Topical dexamethasone γ-cyclodextrin nanoparticle eye drops increase visual acuity and decrease macular thickness in diabetic macular oedema," *Acta Ophthalmologica*, vol. 93, no. 7, pp. 610-615, 2015, doi: 10.1111/aos.12803.
[212] Z. Wang, Y. Deng, S. Sun, and X. Zhang, "Preparation of Hydrophobic Drugs Cyclodextrin Complex by Lyophilization Monophase Solution," *Drug Development and Industrial Pharmacy*, vol. 32, no. 1, pp. 73-83, 2006, doi: 10.1080/03639040500388359.
[213] R. Stancanelli *et al.*, "Isoflavone aglycons-sulfobutyl ether-β-cyclodextrin inclusion complexes: In solution and solid state studies," *Journal of Inclusion Phenomena and Macrocyclic Chemistry*, vol. 83, 2015, doi: 10.1007/s10847-015-0535-6.
[214] T. Higuchi and A. K. Connors, "Phase-solubility techniques," in *Adv. Anal. Chem. Instrum*, 1965, ch. 4, pp. 117-212.
[215] P. K. Soni and T. R. Saini, "Development and evaluation of hp-β-cd complexation based novel ophthalmic gel formulation of nepafenac," *Int. J. Pharm. Sci. Res.*, vol. 10, no. 12, pp. 5707-5714, 2019.
[216] U. A. Shinde, P. N. Joshi, D. D. Jain, and K. Singh, "Preparation and Evaluation of N-Trimethyl Chitosan Nanoparticles of Flurbiprofen for Ocular Delivery," *Current Eye Research*, vol. 44, no. 5, pp. 575-582, 2019, doi: 10.1080/02713683.2019.1567793.
[217] A. Nanda *et al.*, "Drug-in-mucoadhesive type film for ocular anti-inflammatory potential of amlodipine: Effect of sulphobutyl-ether-beta-cyclodextrin on permeation and molecular docking characterization," *Colloids and Surfaces B: Biointerfaces*, vol. 172, pp. 555-564, 2018, doi: https://doi.org/10.1016/j.colsurfb.2018.09.011.
[218] D. C. T. Nguyen, J. Dowling, R. Ryan, P. McLoughlin, and L. Fitzhenry, "Pharmaceutical-loaded contact lenses as an ocular drug delivery system: A review of critical lens characterization methodologies with reference to ISO

standards," *Contact Lens and Anterior Eye*, p. 101487, 2021/08/03/ 2021, doi: https://doi.org/10.1016/j.clae.2021.101487.
[219] L. C. Bengani, K.-H. Hsu, S. Gause, and A. Chauhan, "Contact lenses as a platform for ocular drug delivery," *Expert Opinion on Drug Delivery*, vol. 10, no. 11, pp. 1483-1496, 2013, doi: 10.1517/17425247.2013.821462.
[220] P. Dixon, C. Shafor, S. Gause, K.-H. Hsu, K. C. Powell, and A. Chauhan, "Therapeutic contact lenses: a patent review," *Expert Opinion on Therapeutic Patents*, vol. 25, no. 10, pp. 1117-1129, 2015, doi: 10.1517/13543776.2015.1057501.
[221] C. Maldonado-Codina, "4 - Soft Lens Materials," in *Contact Lens Practice (Third Edition)*, N. Efron Ed.: Elsevier, 2018, pp. 45-60.e1.
[222] R. Moreddu, D. Vigolo, and A. K. Yetisen, "Contact Lens Technology: From Fundamentals to Applications," *Advanced Healthcare Materials*, vol. 8, no. 15, p. 1900368, 2019, doi: 10.1002/adhm.201900368.
[223] J. J. S. Nichols, L., "Contact lenses 2019: A most quiet year of steady growth ended with and FDA decision that could prove to be the tipping point in how practitioners manage young progressive myopes.," in *Contact Lens Spectrum* vol. January 2020, ed.
[224] J. Stern, R. Wong, T. j. Naduvilath, S. Stretton, B. a. Holden, and D. f. Sweeney, "Comparison of the Performance of 6- or 30-night Extended Wear Schedules with Silicone Hydrogel Lenses over 3 Years," *Optometry and Vision Science*, vol. 81, no. 6, pp. 398-406, 2004, doi: 10.1097/01.opx.0000135092.69383.fd.
[225] D. Fonn, D. Sweeney, B. A. Holden, and D. Cavanagh, "Corneal Oxygen Deficiency," *Eye & Contact Lens*, vol. 31, no. 1, pp. 23-27, 2005, doi: 10.1097/01.icl.0000151949.30730.9d.
[226] J. J. Kang-Mieler and W. F. Mieler, "Thermo-Responsive Hydrogels for Ocular Drug Delivery," in *Retinal Pharmacotherapeutics*, vol. 55, Q. D. Nguyen, E. B. Rodrigues, M. E. Farah, W. F. Mieler, and D. V. Do Eds., (Dev Ophthalmol. Basel: Karger, 2016, pp. 104-111.
[227] M. Fathi, J. Barar, A. Aghanejad, and Y. Omidi, "Hydrogels for ocular drug delivery and tissue engineering," *BioImpacts : BI*, vol. 5, no. 4, pp. 159-164, 2015, doi: 10.15171/bi.2015.31.
[228] S. Kirchhof, A. M. Goepferich, and F. P. Brandl, "Hydrogels in ophthalmic applications," *European Journal of Pharmaceutics and Biopharmaceutics*, vol. 95, pp. 227-238, 2015, doi: https://doi.org/10.1016/j.ejpb.2015.05.016.
[229] S. J. Buwalda, K. W. M. Boere, P. J. Dijkstra, J. Feijen, T. Vermonden, and W. E. Hennink, "Hydrogels in a historical perspective: From simple networks to smart materials," *Journal of Controlled Release*, vol. 190, pp. 254-273, 2014, doi: https://doi.org/10.1016/j.jconrel.2014.03.052.
[230] R. Galante *et al.*, *Sterilization of silicone-based hydrogels for biomedical application using ozone gas: Comparison with conventional techniques*. 2017.
[231] C. C. S. Karlgard, N. S. Wong, L. W. Jones, and C. Moresoli, "In vitro uptake and release studies of ocular pharmaceutical agents by silicon-containing and p-HEMA hydrogel contact lens materials," *International Journal of Pharmaceutics*, vol. 257, no. 1, pp. 141-151, 2003, doi: https://doi.org/10.1016/S0378-5173(03)00124-8.
[232] S. Mukherjee, M. R Hill, and B. Sumerlin, *Self-healing hydrogels containing reversible oxime crosslinks*. 2015.

[233] D. L. Alge, M. A. Azagarsamy, D. F. Donohue, and K. S. Anseth, "Synthetically tractable click hydrogels for three-dimensional cell culture formed using tetrazine-norbornene chemistry," (in eng), *Biomacromolecules,* vol. 14, no. 4, pp. 949-953, 2013, doi: 10.1021/bm4000508.
[234] G. A. Hirani A, Lee YW, Pathak Y, Sutariya V, "Polymer-based Therapies for Posterior Segment Ocular Disease," *J Biomol Res Ther,* vol. 3, no. 1, pp. 1-2, 2013, doi: 10.4172/2167-7956.1000e122.
[235] C. S. A. Musgrave and F. Fang, "Contact Lens Materials: A Materials Science Perspective," (in eng), *Materials (Basel),* vol. 12, no. 2, p. 261, 2019, doi: 10.3390/ma12020261.
[236] B. Tighe, "A Decade of Silicone Hydrogel Development: Surface Properties, Mechanical Properties, and Ocular Compatibility," *Eye & contact lens,* vol. 39, pp. 3-11, 2013, doi: 10.1097/ICL.0b013e318275452b.
[237] K. D. Brown *et al.*, "Plasma polymer-coated contact lenses for the culture and transfer of corneal epithelial cells in the treatment of limbal stem cell deficiency," (in eng), *Tissue Eng Part A,* vol. 20, no. 3-4, pp. 646-655, 2014, doi: 10.1089/ten.TEA.2013.0089.
[238] J. G. L. G. M. A. Paul L. Valint, Jr.Michael J. Moorehead, "Plasma surface treatment of silicone hydrogel contact lenses," USA, 2001.
[239] A. Weeks, D. Morrison, J. G. Alauzun, M. A. Brook, L. Jones, and H. Sheardown, "Photocrosslinkable hyaluronic acid as an internal wetting agent in model conventional and silicone hydrogel contact lenses," *Journal of Biomedical Materials Research Part A,* vol. 100A, no. 8, pp. 1972-1982, 2012, doi: 10.1002/jbm.a.33269.
[240] A. Weeks, D. Luensmann, A. Boone, L. Jones, and H. Sheardown, "Hyaluronic acid as an internal wetting agent in model DMAA/TRIS contact lenses," *Journal of Biomaterials Applications,* vol. 27, no. 4, pp. 423-432, 2011, doi: 10.1177/0885328211410999.
[241] L. Jones, L. Subbaraman, R. Rogers, and K. Dumbleton, "Surface treatment, wetting and modulus of silicone hydrogels," *Optician,* vol. 232, pp. 28-34, 2006.
[242] S. D. Achilias and I. P. Siafaka, "Polymerization Kinetics of Poly(2-Hydroxyethyl Methacrylate) Hydrogels and Nanocomposite Materials," *Processes,* vol. 5, no. 2, 2017, doi: 10.3390/pr5020021.
[243] C.-W. Huang, Y.-M. Sun, and W.-F. Huang, "Curing kinetics of the synthesis of poly(2-hydroxyethyl methacrylate) (PHEMA) with ethylene glycol dimethacrylate (EGDMA) as a crosslinking agent," *Journal of Polymer Science Part A: Polymer Chemistry,* vol. 35, no. 10, pp. 1873-1889, 1997, doi: 10.1002/(SICI)1099-0518(19970730)35:10<1873::AID-POLA2>3.0.CO;2-P.
[244] G. Moad, "Radical Polymerization," in *Reference Module in Materials Science and Materials Engineering*: Elsevier, 2016.
[245] F. Redaelli, M. Sorbona, and F. Rossi, "10 - Synthesis and processing of hydrogels for medical applications," in *Bioresorbable Polymers for Biomedical Applications,* G. Perale and J. Hilborn Eds.: Woodhead Publishing, 2017, pp. 205-228.
[246] S. Edmondson and M. Gilbert, "Chapter 2 - The Chemical Nature of Plastics Polymerization," in *Brydson's Plastics Materials (Eighth Edition),* M. Gilbert Ed.: Butterworth-Heinemann, 2017, pp. 19-37.

[247] J. Xu *et al.*, "A comprehensive review on contact lens for ophthalmic drug delivery," *Journal of Controlled Release*, vol. 281, pp. 97-118, 2018, doi: https://doi.org/10.1016/j.jconrel.2018.05.020.
[248] Ş. Ţălu, M. Ţălu, S. Giovanzana, and R. D. Shah, "A brief history of contact lenses," *HVM Bioflux*, vol. 3, no. 1, pp. 33-37, 2011.
[249] L. B. Szczotka-Flynn, "A Brief History of Contact Lens Materials," *Contact Lens Spectrum* 2006.
[250] *Ophhalmic optics - Contact lenses*, S. S. Institute, 2017.
[251] A. Alli; and A. Guzman, "Silicone hydrogels comprising polyamides (US20180011222)," 2019. [Online]. Available: https://patents.justia.com/patent/10371865
[252] D. C. Turner, R. B. Steffen, C. Wildsmith, and T. A. Matiacio, "Method for manufacturing a contact lens (US007422710B2)," 2008.
[253] P. Chandra, J. J. Yoo, and S. J. Lee, "Chapter 13 - Biomaterials in Regenerative Medicine: Challenges in Technology Transfer from Science to Process Development," in *Translational Regenerative Medicine*, A. Atala and J. G. Allickson Eds. Boston: Academic Press, 2015, pp. 151-167.
[254] S. S. Karajanagi *et al.*, "Application of a dense gas technique for sterilizing soft biomaterials," *Biotechnology and Bioengineering*, vol. 108, no. 7, pp. 1716-1725, 2011, doi: 10.1002/bit.23105.
[255] K. A. Murray *et al.*, "Effects of gamma ray and electron beam irradiation on the mechanical, thermal, structural and physicochemical properties of poly (ether-block-amide) thermoplastic elastomers," *Journal of the Mechanical Behavior of Biomedical Materials*, vol. 17, pp. 252-268, 2013, doi: https://doi.org/10.1016/j.jmbbm.2012.09.011.
[256] E. Phillip *et al.*, "Ethylene oxide's role as a reactive agent during sterilization: Effects of polymer composition and device architecture," *Journal of Biomedical Materials Research Part B: Applied Biomaterials*, vol. 101B, no. 4, pp. 532-540, 2013, doi: 10.1002/jbm.b.32853.
[257] M. Ahmed, G. Punshon, A. Darbyshire, and A. M. Seifalian, "Effects of sterilization treatments on bulk and surface properties of nanocomposite biomaterials," *Journal of Biomedical Materials Research Part B: Applied Biomaterials*, vol. 101, no. 7, pp. 1182-1190, 2013, doi: 10.1002/jbm.b.32928.
[258] R. Galante, T. J. A. Pinto, R. Colaço, and A. P. Serro, "Sterilization of hydrogels for biomedical applications: A review," *Journal of Biomedical Materials Research Part B: Applied Biomaterials*, vol. 106, no. 6, pp. 2472-2492, 2018, doi: doi:10.1002/jbm.b.34048.
[259] W. J. Rogers, "Steam and dry heat sterilization of biomaterials and medical devices," 2012, pp. 20-55.
[260] W. A. Rutala and D. J. Weber, "Disinfection, sterilization, and antisepsis: An overview," *American Journal of Infection Control*, vol. 44, no. 5, pp. 1-6, 2016, doi: 10.1016/j.ajic.2015.10.038.
[261] R. Singh, D. Singh, and A. Singh, "Radiation sterilization of tissue allografts: A review," *World journal of radiology*, vol. 8, no. 4, pp. 355-369, 2016, doi: 10.4329/wjr.v8.i4.355.
[262] J. Marmo and J. Browning, "Methods for sterilizing silicone hydrogel contact lenses (US 2007/0104611 A1)," US, 2007. [Online]. Available: https://patents.google.com/patent/US20070104611A1/en

[263] M. Silindir Gunay and Y. Ozer, "Sterilization methods and the comparison of E-Beam sterilization with gamma radiation sterilization," *FABAD J Pharm Sci*, vol. 34, pp. 43-53, 2009.
[264] G. McDonnell and A. D. Russell, "Antiseptics and disinfectants: activity, action, and resistance," *Clinical microbiology reviews*, vol. 12, no. 1, pp. 147-179, 1999. [Online]. Available: https://www.ncbi.nlm.nih.gov/pubmed/9880479.
[265] D. Gritz, T. Lee, P. McDonnell, K. Shih, and N. Baron, "Ultraviolet radiation for the sterilisation of contact lenses," *The CLAO journal : official publication of the Contact Lens Association of Ophthalmologists, Inc*, vol. 16, pp. 294-298, 1990.
[266] R. Galante *et al.*, "Drug-eluting silicone hydrogel for therapeutic contact lenses: Impact of sterilization methods on the system performance," *Colloids and Surfaces B: Biointerfaces*, vol. 161, pp. 537-546, 2018, doi: https://doi.org/10.1016/j.colsurfb.2017.11.021.
[267] *Ophthalmic optics – Contact lenses – Part 2: Tolerances (ISO 18369-2:2017)*, S. S. Institute, 2017.
[268] *Ophthalmic optics – Contact lenses – Part 1: Vocalbulary, classification system and recommendations or labelling specifications (ISO 18369-1:2017)*, S. S. Institute, 2017.
[269] *Ophthalmic optics - Contact lenses - Part 3: Measurement methods (ISO 18369-3:2017)*, S. S. Institute, 2017.
[270] *Ophthalmic optics - Contact lenses - Part 4: Physicochemical properties of contact lens materials (ISO 18369-4:2017)*, S. S. Institute, 2017.
[271] A. Ashraf. *Thermal Analysis of Polymers (LDPE, HDPE) by Differential Scanning Calorimetry Technique*, doi: 10.13140/2.1.1558.0963.
[272] T. V. G. Alves *et al.*, "Thermal analysis characterization of PAAm-co-MC hydrogels," *Journal of Thermal Analysis and Calorimetry*, vol. 106, no. 3, pp. 717-724, 2011, doi: 10.1007/s10973-011-1572-z.
[273] N. A. Peppas, Y. Huang, M. Torres-Lugo, J. H. Ward, and J. Zhang, "Physicochemical Foundations and Structural Design of Hydrogels in Medicine and Biology," *Annual Review of Biomedical Engineering*, vol. 2, no. 1, pp. 9-29, 2000, doi: 10.1146/annurev.bioeng.2.1.9.
[274] S. Bennour and F. Louzri, "Study of Swelling Properties and Thermal Behavior of Poly(N,N-Dimethylacrylamide-co-Maleic Acid) Based Hydrogels," *Advances in Chemistry*, vol. 2014, p. 10, 2014, Art no. 147398, doi: 10.1155/2014/147398.
[275] C. A. Gracia-Fernández, S. Gómez-Barreiro, J. López-Beceiro, J. Tarrío Saavedra, S. Naya, and R. Artiaga, "Comparative study of the dynamic glass transition temperature by DMA and TMDSC," *Polymer Testing*, vol. 29, no. 8, pp. 1002-1006, 2010, doi: https://doi.org/10.1016/j.polymertesting.2010.09.005.
[276] J. M. Hutchinson, "Determination of the glass transition temperature," *Journal of Thermal Analysis and Calorimetry*, vol. 98, no. 3, p. 579, 2009/08/28 2009, doi: 10.1007/s10973-009-0268-0.
[277] A. Panagopoulou *et al.*, "Glass Transition and Water Dynamics in Hyaluronic Acid Hydrogels," *Food Biophysics*, vol. 8, no. 3, pp. 192-202, 2013, doi: 10.1007/s11483-013-9295-2.

[278] M. F. Passos *et al.*, "pHEMA hydrogels," *Journal of Thermal Analysis and Calorimetry*, vol. 125, no. 1, pp. 361-368, 2016, doi: 10.1007/s10973-016-5329-6.
[279] L. Ning, N. Xu, C. Xiao, R. Wang, and Y. Liu, "Analysis for the Reaction of Hydroxyethyl Methacrylate/Benzoyl Peroxide/Polymethacrylate Through DSC and Viscosity Changing and Their Resultants as Oil Absorbent," *Journal of Macromolecular Science, Part A*, vol. 52, no. 12, pp. 1017-1027, 2015, doi: 10.1080/10601325.2015.1095605.
[280] C.-W. Huang, Y.-M. Sun, and W.-F. Huang, "Curing kinetics of the synthesis of poly(2-hydroxyethyl methacrylate) (PHEMA) with ethylene glycol dimethacrylate (EGDMA) as a crosslinking agent," *Journal of Polymer Science Part A: Polymer Chemistry*, vol. 35, no. 10, pp. 1873-1889, 2000, doi: 10.1002/(SICI)1099-0518(19970730)35:10<1873::AID-POLA2>3.0.CO;2-P.
[281] A. G. Mikos and N. A. Peppas, "A model for prediction of the structural characteristics of egdma-crosslinked phema microparticles produced by suspension copolymerization/crosslinking," *Journal of Controlled Release*, vol. 5, no. 1, pp. 53-62, 1987, doi: https://doi.org/10.1016/0168-3659(87)90037-X.
[282] M. D. Goodner, H. R. Lee, and C. N. Bowman, "Method for Determining the Kinetic Parameters in Diffusion-Controlled Free-Radical Homopolymerizations," *Industrial & Engineering Chemistry Research*, vol. 36, no. 4, pp. 1247-1252, 1997, doi: 10.1021/ie9605387.
[283] G. Behl, J. Iqbal, N. J. O'Reilly, P. McLoughlin, and L. Fitzhenry, "Synthesis and Characterization of Poly(2-hydroxyethylmethacrylate) Contact Lenses Containing Chitosan Nanoparticles as an Ocular Delivery System for Dexamethasone Sodium Phosphate," *Pharmaceutical Research*, vol. 33, no. 7, pp. 1638-1648, 2016, doi: 10.1007/s11095-016-1903-7.
[284] P. Paradiso, R. Colaço, J. L. G. Mata, R. Krastev, B. Saramago, and A. P. Serro, "Drug release from liposome coated hydrogels for soft contact lenses: the blinking and temperature effect," *Journal of Biomedical Materials Research Part B: Applied Biomaterials*, vol. 105, no. 7, pp. 1799-1807, 2017, doi: 10.1002/jbm.b.33715.
[285] R. Fuentes, E. Fernández, I. Pascual, and C. García, *UV-Visible Transmittance of Silicone-Hydrogel Contact Lenses measured with a fiber optic spectrometer*. 2013.
[286] Y. Kapoor, P. Dixon, P. Sekar, and A. Chauhan, "Incorporation of drug particles for extended release of Cyclosporine A from poly-hydroxyethyl methacrylate hydrogels," *European Journal of Pharmaceutics and Biopharmaceutics*, vol. 120, pp. 73-79, 2017, doi: https://doi.org/10.1016/j.ejpb.2017.08.007.
[287] E. Insua Pereira and M. Lira, "Comfort, Ocular Dryness, and Equilibrium Water Content Changes of Daily Disposable Contact Lenses," *Eye & Contact Lens*, vol. 44, pp. S233-S240, 2018, doi: 10.1097/icl.0000000000000441.
[288] A. Guzman-Aranguez, B. Colligris, and J. Pintor, "Contact lenses: promising devices for ocular drug delivery," *J Ocul Pharmacol Ther*, vol. 29, no. 2, pp. 189-99, 2013, doi: 10.1089/jop.2012.0212.
[289] G. Young, J. Veys, N. Pritchard, and S. Coleman, "A multi-centre study of lapsed contact lens wearers," *Ophthalmic and Physiological Optics*, vol. 22, no. 6, pp. 516-527, 2002, doi: 10.1046/j.1475-1313.2002.00066.x.

[290] N. Pritchard, D. Fonn, and D. Brazeau, "Discontinuation of contact lens wear: a survey," *International Contact Lens Clinic*, vol. 26, no. 6, pp. 157-162, 1999, doi: https://doi.org/10.1016/S0892-8967(01)00040-2.
[291] N. Pritchard and D. Fonn, "Dehydration, lens movement and dryness ratings of hydrogel contact lenses," *Ophthalmic and Physiological Optics*, vol. 15, no. 4, pp. 281-286, 1995, doi: 10.1046/j.1475-1313.1995.9500004w.x.
[292] S. A. Little and A. S. Bruce, "Environmental influences on hydrogel lens dehydration and the postlens tear film," *International Contact Lens Clinic*, vol. 22, no. 7, pp. 148-155, 1995, doi: 10.1016/0892-8967(95)00049-Z.
[293] B. Fink and R. M. Hill, "Corneal oxygen uptake: A review of polarographic techniques, applications, and variables," *Contact Lens and Anterior Eye*, vol. 29, no. 5, pp. 221-229, 2006, doi: https://doi.org/10.1016/j.clae.2006.09.005.
[294] J. M. Chi, B. A. Fink, R. M. Hill, and G. L. Mitchell, "Factors influencing the measurement of oxygen shortfall of the human cornea: Sequencing of test conditions," *Contact Lens and Anterior Eye*, vol. 30, no. 1, pp. 17-21, 2007, doi: https://doi.org/10.1016/j.clae.2006.10.002.
[295] P. Ramamoorthy, L. T. Sinnott, and J. J. Nichols, "Contact lens material characteristics associated with hydrogel lens dehydration," *Ophthalmic and Physiological Optics*, vol. 30, no. 2, pp. 160-166, 2010, doi: 10.1111/j.1475-1313.2009.00705.x.
[296] J. Gispets, R. Solá, and C. Varón, "The influence of water content of hydrogel contact lenses when fitting patients with 'tear film deficiency'," *Contact Lens and Anterior Eye*, vol. 23, no. 1, pp. 16-21, 2000, doi: https://doi.org/10.1016/S1367-0484(00)80036-3.
[297] D. Fonn, P. Situ, and T. Simpson, *Hydrogel Lens Dehydration and Subjective Comfort and Dryness Ratings in Symptomatic and Asymptomatic Contact Lens Wearers*. 1999, pp. 700-4.
[298] P. B. Morgan, N. Efron, S. L. Morgan, and S. A. Little, "Hydrogel Contact Lens Dehydration in Controlled Environmental Conditions," *Eye & Contact Lens*, vol. 30, no. 2, pp. 99-102, 2004, doi: 10.1097/01.icl.00000118532.90284.09.
[299] P. B. Morgan and N. Efron, "In Vivo Dehydration of Silicone Hydrogel Contact Lenses," *Eye & Contact Lens*, vol. 29, no. 3, pp. 173-176, 2003, doi: 10.1097/01.icl.0000072825.23491.59.
[300] A. López-Alemany and M. F Refojo, *Comparative study of the hydration of hydrophilic contact lenses by refractive index and gravimetry*. 2000, pp. 200-3.
[301] J. M. González-Méijome, A. López-Alemany, M. Lira, J. B. Almeida, M. E. C. D. R. Oliveira, and M. A. Parafita, "Equivalences between refractive index and equilibrium water content of conventional and silicone hydrogel soft contact lenses from automated and manual refractometry," *Journal of Biomedical Materials Research Part B: Applied Biomaterials*, vol. 80B, no. 1, pp. 184-191, 2007, doi: 10.1002/jbm.b.30583.
[302] J. M. González-Méijome, M. Lira, A. López-Alemany, J. B. Almeida, M. A. Parafita, and M. F. Refojo, "Refractive index and equilibrium water content of conventional and silicone hydrogel contact lenses," *Ophthalmic and Physiological Optics*, vol. 26, no. 1, pp. 57-64, 2006, doi: 10.1111/j.1475-1313.2005.00342.x.
[303] F. H. Nasr, S. Khoee, M. M. Dehghan, S. S. Chaleshtori, and A. Shafiee, "Preparation and Evaluation of Contact Lenses Embedded with

Polycaprolactone-Based Nanoparticles for Ocular Drug Delivery," *Biomacromolecules,* vol. 17, no. 2, pp. 485-495, 2016, doi: 10.1021/acs.biomac.5b01387.
[304] I. Tranoudis and N. Efron, "Refractive index of rigid contact lens materials," *Contact Lens and Anterior Eye,* vol. 21, no. 1, pp. 15-18, 1998, doi: 10.1016/S1367-0484(98)80019-2.
[305] J. Varikooty, N. Keir, C. A. Woods, and D. Fonn, "Measurement of the Refractive Index of Soft Contact Lenses During Wear," *Eye & Contact Lens,* vol. 36, no. 1, pp. 2-5, 2010, doi: 10.1097/ICL.0b013e3181c8135f.
[306] M. Lira, L. Santos, J. Azeredo, E. Yebra-Pimentel, and M. E. C. D. Real Oliveira, "The effect of lens wear on refractive index of conventional hydrogel and silicone-hydrogel contact lenses: A comparative study," *Contact Lens and Anterior Eye,* vol. 31, no. 2, pp. 89-94, 2008, doi: 10.1016/j.clae.2007.09.001.
[307] *Ophthalmic optics - Contact lenses,* S. S. Institute, 2017.
[308] J. Pozuelo, V. Compañ, J. M. González-Méijome, M. González, and S. Mollá, "Oxygen and ionic transport in hydrogel and silicone-hydrogel contact lens materials: An experimental and theoretical study," *Journal of Membrane Science,* vol. 452, pp. 62-72, 2014, doi: https://doi.org/10.1016/j.memsci.2013.10.010.
[309] D. Austin and R. V. Kumar, "Ionic conductivity in hydrogels for contact lens applications," *Ionics,* vol. 11, no. 3, pp. 262-268, 2005, doi: 10.1007/BF02430387.
[310] N. Efron and C. Maldonado-Codina, "6.633 - Development of Contact Lenses from a Biomaterial Point of View – Materials, Manufacture, and Clinical Application," in *Comprehensive Biomaterials*, P. Ducheyne Ed. Oxford: Elsevier, 2011, pp. 517-541.
[311] D. F. Maulvi, T. Soni, and D. Shah, "Extended release of hyaluronic acid from hydrogel contact lenses for dry eye syndrome," *Journal of biomaterials science. Polymer edition,* vol. 26, pp. 1-26, 07/15 2015, doi: 10.1080/09205063.2015.1072902.
[312] D. Silva *et al.*, "Antibacterial layer-by-layer coatings to control drug release from soft contact lenses material," *International Journal of Pharmaceutics,* vol. 553, 2018, doi: 10.1016/j.ijpharm.2018.10.041.
[313] C.-C. Peng and A. Chauhan, "Ion transport in silicone hydrogel contact lenses," *Journal of Membrane Science,* vol. 399-400, pp. 95-105, 2012, doi: https://doi.org/10.1016/j.memsci.2012.01.039.
[314] F. A. Maulvi *et al.*, "In vitro and in vivo evaluation of novel implantation technology in hydrogel contact lenses for controlled drug delivery," *Journal of Controlled Release,* vol. 226, pp. 47-56, 2016, doi: https://doi.org/10.1016/j.jconrel.2016.02.012.
[315] P. Paradiso *et al.*, "Comparison of two hydrogel formulations for drug release in ophthalmic lenses," *Journal of Biomedical Materials Research Part B: Applied Biomaterials,* vol. 102, no. 6, pp. 1170-1180, 2014, doi: 10.1002/jbm.b.33099.
[316] P. Sekar and A. Chauhan, "Effect of vitamin-E integration on delivery of prostaglandin analogs from therapeutic lenses," *Journal of Colloid and Interface Science,* vol. 539, pp. 457-467, 2019, doi: https://doi.org/10.1016/j.jcis.2018.12.036.
[317] R. Gavara and V. Compañ, "Oxygen, water, and sodium chloride transport in soft contact lenses materials," *Journal of Biomedical Materials Research Part*

B: Applied Biomaterials, vol. 105, no. 8, pp. 2218-2231, 2017, doi: 10.1002/jbm.b.33762.

[318] S. E. Lee, S. R. Kim, and M. Park, "Oxygen permeability of soft contact lenses in different pH, osmolality and buffering solution," (in eng), *Int J Ophthalmol*, vol. 8, no. 5, pp. 1037-1042, 2015, doi: 10.3980/j.issn.2222-3959.2015.05.33.

[319] K. A. Lebow and D. Campbell-Burns, "Understanding the Values that Describe Oxygen Flux Through a Contact Lens," *Contact lens spectrum*, no. Jan 1998, 1998. [Online]. Available: https://www.clspectrum.com/issues/1998/january-1998/understanding-the-values-that-describe-oxygen-flux.

[320] B. A. Holden and G. W. Mertz, "Critical oxygen levels to avoid corneal edema for daily and extended wear contact lenses," *Investigative Ophthalmology & Visual Science*, vol. 25, no. 10, pp. 1161-1167, 1984.

[321] M. D. Young and W. J. Benjamin, "Calibrated Oxygen Permeability of 35 Conventional Hydrogel Materials and Correlation with Water Content," *Eye & Contact Lens*, vol. 29, no. 2, pp. 126-133, 2003, doi: 10.1097/01.icl.0000062463.64717.86.

[322] N. Efron, P. B. Morgan, I. D. Cameron, N. A. Brennan, and M. Goodwin, "Oxygen Permeability and Water Content of Silicone Hydrogel Contact Lens Materials," *Optometry and Vision Science*, vol. 84, no. 4, 2007. [Online]. Available: https://journals.lww.com/optvissci/Fulltext/2007/04000/Oxygen_Permeability_and_Water_Content_of_Silicone.16.aspx.

[323] C. González-Chomón, M. Silva, A. Concheiro, and C. Alvarez-Lorenzo, "Biomimetic contact lenses eluting olopatadine for allergic conjunctivitis," *Acta Biomaterialia*, vol. 41, pp. 302-311, 2016, doi: https://doi.org/10.1016/j.actbio.2016.05.032.

[324] J. R. Larke, S. T. Parrish, and C. G. Wigham, "Apparent Human Corneal Oxygen Uptake Rate," *Optometry and Vision Science*, vol. 58, no. 10, pp. 803-805, 1981. [Online]. Available: https://journals.lww.com/optvissci/Fulltext/1981/10000/Apparent_Human_Corneal_Oxygen_Uptake_Rate.4.aspx.

[325] I. Fatt, "Comparison of the single-chamber polarographic and the coulometric carrier gas procedures for measuring oxygen permeability," *International Contact Lens Clinic*, vol. 16, no. 7, pp. 226-231, 1989, doi: https://doi.org/10.1016/0892-8967(89)90037-0.

[326] I. Fatt, "Measurement of oxygen flux into the cornea by pressing a sensor onto a soft contact lens on the eye," (in eng), *Am J Optom Physiol Opt*, vol. 55, no. 5, pp. 294-301, 1978, doi: 10.1097/00006324-197805000-00002.

[327] T. G. Quinn and J. P. Schoessler, "Solubility effects on corneal oxygen measurement," (in eng), *Am J Optom Physiol Opt*, vol. 60, no. 5, pp. 360-363, 1983, doi: 10.1097/00006324-198305000-00003.

[328] A. Barber, B. A. Fink, and R. M. Hill, "(CL-163)human cornea: Its rapid response to anoxia—the first 540 seconds: Poster # 59," *Optometry and Vision Science*, vol. 77, no. 12, p. 170, 2000. [Online]. Available: https://journals.lww.com/optvissci/Fulltext/2000/12001/_CL_163_HUMAN_CORNEA__ITS_RAPID_RESPONSE_TO.278.aspx.

[329] B. A. Holden, D. F. Sweeney, A. Vannas, K. T. Nilsson, and N. Efron, "Effects of long-term extended contact lens wear on the human cornea," *Investigative Ophthalmology & Visual Science*, vol. 26, no. 11, pp. 1489-1501, 1985.

[330] M. J. Jauregui and I. Fatt, "Estimation of oxygen tension under a contact lens*," *Optometry and Vision Science*, vol. 48, no. 3, pp. 210-218, 1971. [Online]. Available: https://journals.lww.com/optvissci/Fulltext/1971/03000/ESTIMATION_OF_OXYGEN_TENSION_UNDER_A_CONTACT_LENS_.4.aspx.
[331] W. J. Benjamin and R. M. Hill, "Closed-lid factors influencing human corneal oxygen demand," *Acta Ophthalmologica*, vol. 64, no. 6, pp. 644-648, 1986, doi: 10.1111/j.1755-3768.1986.tb00681.x.
[332] W. J. Benjamin and R. M. Hill, "Human cornea: Oxygen uptake immediately following graded deprivation," *Graefe's Archive for Clinical and Experimental Ophthalmology*, vol. 223, no. 1, pp. 47-49, 1985, doi: 10.1007/BF02150573.
[333] N. Efron and J. P. Fitzgerald, "Distribution of oxygen across the surface of the human cornea during soft contact lens wear," (in eng), *Optom Vis Sci*, vol. 73, no. 10, pp. 659-665, 1996, doi: 10.1097/00006324-199610000-00005.
[334] R. M. Hill and G. E. Lowther, "Oxygen flux across the tear-epithelial interface as an index of corneal wound repair*," *Optometry and Vision Science*, vol. 44, no. 5, pp. 267-275, 1967. [Online]. Available: https://journals.lww.com/optvissci/Fulltext/1967/05000/OXYGEN_FLUX_ACROSS_THE_TEAR_EPITHELIAL_INTERFACE.1.aspx.
[335] N. Malakooti, C. Alexander, and C. Alvarez-Lorenzo, "Imprinted Contact Lenses for Sustained Release of Polymyxin B and Related Antimicrobial Peptides," *Journal of Pharmaceutical Sciences*, vol. 104, no. 10, pp. 3386-3394, 2015, doi: https://doi.org/10.1002/jps.24537.
[336] E. B. Papas, "The significance of oxygen during contact lens wear," *Contact Lens and Anterior Eye*, vol. 37, no. 6, pp. 394-404, 2014, doi: https://doi.org/10.1016/j.clae.2014.07.012.
[337] D. Campbell, S. M. Carnell, and R. J. Eden, "Applicability of Contact Angle Techniques Used in the Analysis of Contact Lenses, Part 1: Comparative Methodologies," *Eye & Contact Lens*, vol. 39, no. 3, pp. 254-262, 2013, doi: 10.1097/ICL.0b013e31828ca174.
[338] M. C. Lin and T. F. Svitova, "Contact lenses wettability in vitro: effect of surface-active ingredients," (in eng), *Optom Vis Sci*, vol. 87, no. 6, pp. 440-447, 2010, doi: 10.1097/OPX.0b013e3181dc9a1a.
[339] C. Maldonado-Codina and N. Efron, "Dynamic wettability of pHEMA-based hydrogel contact lenses," *Ophthalmic and Physiological Optics*, vol. 26, no. 4, pp. 408-418, 2006, doi: 10.1111/j.1475-1313.2006.00394.x.
[340] T. S. Bhamra and B. J. Tighe, "Mechanical properties of contact lenses: The contribution of measurement techniques and clinical feedback to 50 years of materials development," *Contact Lens and Anterior Eye*, vol. 40, no. 2, pp. 70-81, 2017, doi: 10.1016/j.clae.2016.11.005.
[341] I. Tranoudis and N. Efron, "Tensile properties of soft contact lens materials," *Contact Lens and Anterior Eye*, vol. 27, no. 4, pp. 177-191, 2004, doi: 10.1016/j.clae.2004.08.002.
[342] N. Efron, "Unravelling Contact Lens Specifications*," *The Australian Journal of Optometry*, vol. 63, no. 6, pp. 273-279, 1980, doi: 10.1111/j.1444-0938.1980.tb02946.x.
[343] B. J. Tighe, *The design of polymers for contact lens applications*. 1976, pp. 71-77.
[344] O. Sterner *et al.*, "Friction Measurements on Contact Lenses in a Physiologically Relevant Environment: Effect of Testing Conditions on

FrictionFriction Measurements on Contact Lenses," *Investigative Ophthalmology & Visual Science*, vol. 57, no. 13, pp. 5383-5392, 2016, doi: 10.1167/iovs.16-19713.
[345] A. C. Rennie, P. L. Dickrell, and W. G. Sawyer, "Friction coefficient of soft contact lenses: measurements and modeling," *Tribology Letters*, vol. 18, no. 4, pp. 499-504, 2005, doi: 10.1007/s11249-005-3610-0.
[346] J. Nairn and T. Jiang, *Measurement of the friction and lubricity properties of contact lenses*. 1995, pp. 1-5.
[347] M. D. Pascovici and T. Cicone, "Squeeze-film of unconformal, compliant and layered contacts," *Tribology International*, vol. 36, no. 11, pp. 791-799, 2003, doi: https://doi.org/10.1016/S0301-679X(03)00095-1.
[348] M. E. Freeman, M. J. Furey, B. J. Love, and J. M. Hampton, "Friction, wear, and lubrication of hydrogels as synthetic articular cartilage," *Wear*, vol. 241, no. 2, pp. 129-135, 2000, doi: https://doi.org/10.1016/S0043-1648(00)00387-2.
[349] C. Alvarez-Lorenzo, H. Hiratani, J. L. Gómez-Amoza, R. Martínez‐Pacheco, C. Souto, and A. Concheiro, "Soft Contact Lenses Capable of Sustained Delivery of Timolol," *Journal of Pharmaceutical Sciences*, vol. 91, no. 10, pp. 2182-2192, 2002, doi: 10.1002/jps.10209.
[350] H. Hiratani and C. Alvarez-Lorenzo, "Timolol uptake and release by imprinted soft contact lenses made of N,N-diethylacrylamide and methacrylic acid," *Journal of Controlled Release*, vol. 83, no. 2, pp. 223-230, 2002, doi: https://doi.org/10.1016/S0168-3659(02)00213-4.
[351] C. J. White, A. Tieppo, and M. E. Byrne, "Controlled drug release from contact lenses: a comprehensive review from 1965-present," *Journal of Drug Delivery Science and Technology*, vol. 21, no. 5, pp. 369-384, 2011, doi: https://doi.org/10.1016/S1773-2247(11)50062-0.
[352] K. Kakisu, T. Matsunaga, S. Kobayakawa, T. Sato, and T. Tochikubo, "Development and Efficacy of a Drug-Releasing Soft Contact Lens," *Investigative Ophthalmology & Visual Science*, vol. 54, no. 4, pp. 2551-2561, 2013, doi: 10.1167/iovs.12-10614.
[353] C. C. Li and A. Chauhan, "Ocular transport model for ophthalmic delivery of timolol through p-HEMA contact lenses," *Journal of Drug Delivery Science and Technology*, vol. 17, no. 1, pp. 69-79, 2007, doi: https://doi.org/10.1016/S1773-2247(07)50010-9.
[354] J. Kim and A. Chauhan, "Dexamethasone transport and ocular delivery from poly(hydroxyethyl methacrylate) gels," *International Journal of Pharmaceutics*, vol. 353, no. 1, pp. 205-222, 2008, doi: https://doi.org/10.1016/j.ijpharm.2007.11.049.
[355] M. Ruben and R. Watkins, "Pilocarpine dispensation for the soft hydrophilic contact lens," *The British journal of ophthalmology*, vol. 59, no. 8, pp. 455-458, 1975. [Online]. Available: arez.
[356] M. Yang *et al.*, "Experimental studies on soft contact lenses for controlled ocular delivery of pirfinedone: in vitro and in vivo," *Drug Delivery*, vol. 23, no. 9, pp. 3538-3543, 2016, doi: 10.1080/10717544.2016.1204570.
[357] E. M Hehl, R. Beck, K. Luthard, R. Guthoff, and B. Drewelow, *Improved penetration of aminoglycosides and fluoroquinolones into the aqueous humour of patients by means of Acuvue contact lenses*. 1999, pp. 317-23.
[358] Q. Zhu, H. Cheng, Y. Huo, and S. Mao, "Sustained ophthalmic delivery of highly soluble drug using pH-triggered inner layer-embedded contact lens,"

International Journal of Pharmaceutics, vol. 544, no. 1, pp. 100-111, 2018, doi: https://doi.org/10.1016/j.ijpharm.2018.04.004.

[359] C.-C. Peng, M. T. Burke, and A. Chauhan, "Transport of Topical Anesthetics in Vitamin E Loaded Silicone Hydrogel Contact Lenses," *Langmuir*, vol. 28, no. 2, pp. 1478-1487, 2012, doi: 10.1021/la203606z.

[360] M. S. Rad, S. A. Sajadi Tabassi, M. H. Moghadam, and S. A. Mohajeri, "Controlled release of betamethasone from vitamin E-loaded silicone-based soft contact lenses," *Pharmaceutical Development and Technology*, vol. 21, no. 7, pp. 894-899, 2016, doi: 10.3109/10837450.2015.1078355.

[361] F. A. Maulvi, T. G. Soni, and D. O. Shah, "A review on therapeutic contact lenses for ocular drug delivery," *Drug Delivery*, vol. 23, no. 8, pp. 3017-3026, 2016, doi: 10.3109/10717544.2016.1138342.

[362] G. Wulff, "Molecular Imprinting in Cross-Linked Materials with the Aid of Molecular Templates— A Way towards Artificial Antibodies," *Angewandte Chemie International Edition in English*, vol. 34, no. 17, pp. 1812-1832, 1995, doi: 10.1002/anie.199518121.

[363] C. J. White and M. E. Byrne, "Molecularly imprinted therapeutic contact lenses," *Expert Opinion on Drug Delivery*, vol. 7, no. 6, pp. 765-780, 2010, doi: 10.1517/17425241003770098.

[364] H. Hiratani, Y. Mizutani, and C. Alvarez-Lorenzo, "Controlling Drug Release from Imprinted Hydrogels by Modifying the Characteristics of the Imprinted Cavities," *Macromolecular Bioscience*, vol. 5, no. 8, pp. 728-733, 2005, doi: 10.1002/mabi.200500065.

[365] C. Alvarez-Lorenzo, F. Yañez, R. Barreiro-Iglesias, and A. Concheiro, "Imprinted soft contact lenses as norfloxacin delivery systems," *Journal of Controlled Release*, vol. 113, no. 3, pp. 236-244, 2006, doi: https://doi.org/10.1016/j.jconrel.2006.05.003.

[366] M. Ali, S. Horikawa, S. Venkatesh, J. Saha, J. W. Hong, and M. E. Byrne, "Zero-order therapeutic release from imprinted hydrogel contact lenses within in vitro physiological ocular tear flow," *Journal of Controlled Release*, vol. 124, no. 3, pp. 154-162, 2007, doi: https://doi.org/10.1016/j.jconrel.2007.09.006.

[367] M. Ali and M. E. Byrne, "Controlled Release of High Molecular Weight Hyaluronic Acid from Molecularly Imprinted Hydrogel Contact Lenses," *Pharmaceutical Research*, vol. 26, no. 3, pp. 714-726, 2009, doi: 10.1007/s11095-008-9818-6.

[368] F. Yañez, A. Chauhan, A. Concheiro, and C. Alvarez-Lorenzo, "Timolol-imprinted soft contact lenses: Influence of the template: Functional monomer ratio and the hydrogel thickness," *Journal of Applied Polymer Science*, vol. 122, no. 2, pp. 1333-1340, 2011, doi: 10.1002/app.34022.

[369] C. J. White, M. K. McBride, K. M. Pate, A. Tieppo, and M. E. Byrne, "Extended release of high molecular weight hydroxypropyl methylcellulose from molecularly imprinted, extended wear silicone hydrogel contact lenses," *Biomaterials*, vol. 32, no. 24, pp. 5698-5705, 2011, doi: https://doi.org/10.1016/j.biomaterials.2011.04.044.

[370] B. Malaekeh-nikouei, F. Ghaeni, V. Sadat Motamedshariaty, and S. Mohajeri, *Controlled release of prednisolone acetate from molecularly imprinted hydrogel contact lenses*. 2012.

[371] H. Omranipour, S. Tabassi, R. Kowsari, M. Rad, and S. Mohajeri, "Brimonidine Imprinted Hydrogels and Evaluation of Their Binding and

Releasing Properties as New Ocular Drug Delivery Systems," *Current drug delivery*, vol. 12, 2015, doi: 10.2174/1567201812666150316110838.

[372] S. Kioomars, S. Heidari, B. Malaekeh-Nikouei, M. Shayani Rad, B. Khameneh, and S. A. Mohajeri, "Ciprofloxacin-imprinted hydrogels for drug sustained release in aqueous media," *Pharmaceutical Development and Technology*, vol. 22, no. 1, pp. 122-129, 2017, doi: 10.1080/10837450.2016.1230131.

[373] A. Tieppo, K. M. Pate, and M. E. Byrne, "In vitro controlled release of an anti-inflammatory from daily disposable therapeutic contact lenses under physiological ocular tear flow," *European Journal of Pharmaceutics and Biopharmaceutics*, vol. 81, no. 1, pp. 170-177, 2012, doi: https://doi.org/10.1016/j.ejpb.2012.01.015.

[374] A. F. Pereira-da-Mota, M. Vivero-Lopez, A. Topete, A. P. Serro, A. Concheiro, and C. Alvarez-Lorenzo, "Atorvastatin-Eluting Contact Lenses: Effects of Molecular Imprinting and Sterilization on Drug Loading and Release," *Pharmaceutics*, vol. 13, no. 5, p. 606, 2021. [Online]. Available: https://www.mdpi.com/1999-4923/13/5/606.

[375] S. DiPasquale, B. Uricoli, M. DiCerbo, T. Brown, and M. Byrne, "Controlled Release of Multiple Therapeutics From Silicone Hydrogel Contact Lenses for Post-Cataract/Post-Refractive Surgery and Uveitis Treatment," *Translational Vision Science & Technology*, vol. 10, p. 5, 12/06 2021, doi: 10.1167/tvst.10.14.5.

[376] S. Liu, L. Jones, and F. X. Gu, "Nanomaterials for ocular drug delivery," *Macromol Biosci*, vol. 12, no. 5, pp. 608-20, 2012, doi: 10.1002/mabi.201100419.

[377] M. M. Mehanna, H. A. Elmaradny, and M. W. Samaha, "Mucoadhesive liposomes as ocular delivery system: physical, microbiological, and in vivo assessment," *Drug Development and Industrial Pharmacy*, vol. 36, no. 1, pp. 108-118, 2010, doi: 10.3109/03639040903099751.

[378] A. ElShaer, S. Mustafa, M. Kasar, S. Thapa, B. Ghatora, and R. G. Alany, "Nanoparticle-Laden Contact Lens for Controlled Ocular Delivery of Prednisolone: Formulation Optimization Using Statistical Experimental Design," (in eng), *Pharmaceutics*, vol. 8, no. 2, p. 14, 2016, doi: 10.3390/pharmaceutics8020014.

[379] H. J. Jung and A. Chauhan, "Temperature sensitive contact lenses for triggered ophthalmic drug delivery," *Biomaterials*, vol. 33, no. 7, pp. 2289-2300, 2012, doi: https://doi.org/10.1016/j.biomaterials.2011.10.076.

[380] Y. Kapoor, J. C. Thomas, G. Tan, V. T. John, and A. Chauhan, "Surfactant-laden soft contact lenses for extended delivery of ophthalmic drugs," *Biomaterials*, vol. 30, no. 5, pp. 867-878, 2009, doi: https://doi.org/10.1016/j.biomaterials.2008.10.032.

[381] A. Danion, H. Brochu, Y. Martin, and P. Vermette, "Fabrication and characterization of contact lenses bearing surface-immobilized layers of intact liposomes," *Journal of biomedical materials research. Part A*, vol. 82, pp. 41-51, 2007, doi: 10.1002/jbm.a.31147.

[382] M. Korogiannaki, L. Jones, and H. Sheardown, "Impact of a Hyaluronic Acid-Grafted Layer on the Surface Properties of Model Silicone Hydrogel Contact Lenses," *Langmuir*, vol. 35, no. 4, pp. 950-961, 2019, doi: 10.1021/acs.langmuir.8b01693.

[383] A. Singh, P. Li, V. Beachley, P. McDonnell, and J. H. Elisseeff, "A hyaluronic acid-binding contact lens with enhanced water retention," *Contact Lens and Anterior Eye*, vol. 38, no. 2, pp. 79-84, 2015, doi: 10.1016/j.clae.2014.09.002.
[384] C.-H. Lin, H.-L. Cho, Y.-H. Yeh, and M.-C. Yang, "Improvement of the surface wettability of silicone hydrogel contact lenses via layer-by-layer self-assembly technique," *Colloids and Surfaces B: Biointerfaces*, vol. 136, pp. 735-743, 2015, doi: https://doi.org/10.1016/j.colsurfb.2015.10.006.
[385] S. Guo, X. Zhu, and X. J. Loh, "Controlling cell adhesion using layer-by-layer approaches for biomedical applications," *Materials Science and Engineering: C*, vol. 70, pp. 1163-1175, 2017, doi: https://doi.org/10.1016/j.msec.2016.03.074.
[386] M. Korogiannaki, J. Zhang, and H. Sheardown, "Surface modification of model hydrogel contact lenses with hyaluronic acid via thiol-ene “click” chemistry for enhancing surface characteristics," *Journal of Biomaterials Applications*, vol. 32, no. 4, pp. 446-462, 2017, doi: 10.1177/0885328217733443.
[387] J. W. Chan, C. E. Hoyle, A. B. Lowe, and M. Bowman, "Nucleophile-Initiated Thiol-Michael Reactions: Effect of Organocatalyst, Thiol, and Ene," *Macromolecules*, vol. 43, no. 15, pp. 6381-6388, 2010, doi: 10.1021/ma101069c.
[388] S. Kumari, B. Malvi, A. K. Ganai, V. K. Pillai, and S. Sen Gupta, "Functionalization of SBA-15 Mesoporous Materials using “Thiol–Ene Click” Michael Addition Reaction," *The Journal of Physical Chemistry C*, vol. 115, no. 36, pp. 17774-17781, 2011, doi: 10.1021/jp2056442.
[389] D. Silva *et al.*, "Antibacterial layer-by-layer coatings to control drug release from soft contact lenses material," *International Journal of Pharmaceutics*, vol. 553, no. 1, pp. 186-200, 2018, doi: https://doi.org/10.1016/j.ijpharm.2018.10.041.
[390] F. A. Maulvi *et al.*, "Extended release of ketotifen from silica shell nanoparticle-laden hydrogel contact lenses: in vitro and in vivo evaluation," *Journal of Materials Science: Materials in Medicine*, vol. 27, no. 6, p. 113, 2016, doi: 10.1007/s10856-016-5724-3.
[391] D. Gulsen and A. Chauhan, "Dispersion of microemulsion drops in HEMA hydrogel: a potential ophthalmic drug delivery vehicle," *International Journal of Pharmaceutics*, vol. 292, no. 1, pp. 95-117, 2005, doi: https://doi.org/10.1016/j.ijpharm.2004.11.033.
[392] D. Gulsen, C.-C. Li, and A. Chauhan, "Dispersion of DMPC Liposomes in Contact Lenses for Ophthalmic Drug Delivery," *Current Eye Research*, vol. 30, no. 12, pp. 1071-1080, 2005, doi: 10.1080/02713680500346633.
[393] H. J. Jung, M. Abou-Jaoude, B. E. Carbia, C. Plummer, and A. Chauhan, "Glaucoma therapy by extended release of timolol from nanoparticle loaded silicone-hydrogel contact lenses," *Journal of Controlled Release*, vol. 165, no. 1, pp. 82-89, 2013, doi: https://doi.org/10.1016/j.jconrel.2012.10.010.
[394] M.-J. Lee, S.-Y. Park, and A. Y. Sung, "Characterization of Biocompatible Hydrogel Lenses Using Methacrylic Acid with Neodymium Oxide Nanoparticles," (in eng), *Polymers*, vol. 13, no. 10, p. 1575, 2021, doi: 10.3390/polym13101575.
[395] W. Yang, Y. Tan, C. Li, Y. Liu, and G. Lu, "Observation of curative effect of intravitreal injection of conbercept in wet age-related macular degeneration:

Optical coherence tomography analysis after injection," *Microscopy Research and Technique*, vol. 81, no. 4, pp. 384-388, 2018, doi: 10.1002/jemt.22989.
[396] K. G. Falavarjani and Q. D. Nguyen, "Adverse events and complications associated with intravitreal injection of anti-VEGF agents: a review of literature," (in eng), *Eye (Lond)*, vol. 27, no. 7, pp. 787-794, 2013, doi: 10.1038/eye.2013.107.
[397] I. Tranoudis and N. Efron, "Water properties of soft contact lens materials," *Contact Lens and Anterior Eye*, vol. 27, no. 4, pp. 193-208, 2004, doi: https://doi.org/10.1016/j.clae.2004.08.003.
[398] B. L. Incorporated. "Biotrue ONEDay Contact Lenses." https://www.bausch.com/ecp/our-products/contact-lenses/myopia-hyperopia/biotrue-oneday-contact-lenses (accessed 2021).
[399] *ISO18369-2:2017: Ophthalmic optics-Contact lenses*, S. S. Institute, CEN-CENELEC Management Centre: Avenue Marnix 17, B-1000 Brussels, 2017. [Online]. Available: https://www.iso.org/obp/ui/#iso:std:iso:18369:-2:ed-3:v1:en
[400] *ISO18369-4:2017: Ophthalmic optics-Contact lenses*, S. S. Institute, CEN-CENELEC Management Centre: Avenue Marnix 17, B-1000 Brussels, 2017. [Online]. Available: https://www.iso.org/obp/ui/#iso:std:iso:18369:-4:ed-2:v2:en
[401] C. C. Ferreira, K. A. d. S. Aquino, and E. S. Araujo, "Effects of gamma irradiation on optical properties of polycarbonate: different formulations with commercial stabilizers," in *INAC 2009: International nuclear atlantic conference Innovations in nuclear technology for a sustainable future*, Brazil, 2009. [Online]. Available: http://inis.iaea.org/search/search.aspx?orig_q=RN:41097048. [Online]. Available: http://inis.iaea.org/search/search.aspx?orig_q=RN:41097048
[402] A. Topete, A. S. Oliveira, A. Fernandes, T. G. Nunes, A. P. Serro, and B. Saramago, "Improving sustained drug delivery from ophthalmic lens materials through the control of temperature and time of loading," *European Journal of Pharmaceutical Sciences*, vol. 117, pp. 107-117, 2018, doi: https://doi.org/10.1016/j.ejps.2018.02.017.
[403] E. Kim, M. Saha, and K. Ehrmann, "Mechanical Properties of Contact Lens Materials," *Eye & Contact Lens*, vol. 44, 2018. [Online]. Available: https://journals.lww.com/claojournal/Fulltext/2018/11002/Mechanical_Properties_of_Contact_Lens_Materials.26.aspx.
[404] Y. Li, Z. Zhang, X. Hao, and W. Yin, "A Measurement System for Time Constant of Thermocouple Sensor Based on High Temperature Furnace," *Applied Sciences*, vol. 8, p. 2585, 2018, doi: 10.3390/app8122585.
[405] F. Hamze, S. A. Ganjalikhan Nasab, A. Eskandarizadeh, A. Shahravan, F. Akhavan Fard, and N. Sinaee, "Thermal Scanning of Dental Pulp Chamber by Thermocouple System and Infrared Camera during Photo Curing of Resin Composites," (in eng), *Iran Endod J*, vol. 13, no. 2, pp. 195-199, 2018, doi: 10.22037/iej.v13i2.18756.
[406] M. Alkurt, Z. Y. Duymus, M. Gundogdu, and M. Karadas, "Comparison of temperature change among different adhesive resin cement during polymerization process," (in eng), *J Indian Prosthodont Soc*, vol. 17, no. 2, pp. 183-188, 2017, doi: 10.4103/jips.jips_327_16.
[407] O. Karatas, V. Turel, and Y. Z. Bayindir, "Temperature rise during polymerization of different cavity liners and composite resins," (in eng), *J*

Conserv Dent, vol. 18, no. 6, pp. 431-435, 2015, doi: 10.4103/0972-0707.168795.
[408] N. O. Ilday, O. Sagsoz, O. Karatas, Y. Z. Bayindir, and N. Çelik, "Temperature changes caused by light curing of fiber-reinforced composite resins," (in eng), *J Conserv Dent,* vol. 18, no. 3, pp. 223-226, 2015, doi: 10.4103/0972-0707.157258.
[409] G. Li *et al.*, "Real-Time Two-Dimensional Mapping of Relative Local Surface Temperatures with a Thin-Film Sensor Array," (in eng), *Sensors (Basel),* vol. 16, no. 7, p. 977, 2016, doi: 10.3390/s16070977.
[410] C. Kousiatza, N. Chatzidai, and D. Karalekas, "Temperature Mapping of 3D Printed Polymer Plates: Experimental and Numerical Study," (in eng), *Sensors (Basel),* vol. 17, no. 3, p. 456, 2017, doi: 10.3390/s17030456.
[411] S. Imafuku, "Silicone hydrogel soft contact lens having wettable surface (EP2840431B1)," 2016.
[412] S. Barton, P. J. S. Foot, P. Tate, M. Kishi, and B. Ghatora, "The Effects of Gamma Irradiation on Medical Grade Poly(Methyl Methacrylate)," *Polymers and Polymer Composites,* vol. 21, pp. 1-8, 2013, doi: 10.1177/096739111302100101.
[413] D. S. Achilias, "Investigation of the radical polymerization kinetics using DSC and mechanistic or isoconversional methods," *Journal of Thermal Analysis and Calorimetry,* vol. 116, no. 3, pp. 1379-1386, 2014, doi: 10.1007/s10973-013-3633-y.
[414] D. W. Koetsier, Y. Y. Tan, and G. Challa, "Radical polymerization of N-vinylpyrrolidone in the presence of syndiotactic poly(methacrylic acid) templates," *Journal of Polymer Science: Polymer Chemistry Edition,* vol. 18, no. 6, pp. 1933-1943, 1980, doi: 10.1002/pol.1980.170180629.
[415] D. Wan, K. Satoh, M. Kamigaito, and Y. Okamoto, "Xanthate-Mediated Radical Polymerization of N-Vinylpyrrolidone in Fluoroalcohols for Simultaneous Control of Molecular Weight and Tacticity," *Macromolecules,* vol. 38, no. 25, pp. 10397-10405, 2005, doi: 10.1021/ma0515230.
[416] R. Devasia, B. Raveendra, R. Borsali, N. Mougin, and Y. Gnanou, "Controlled Radical Polymerization ofN-Vinylpyrrolidone by Reversible Addition-Fragmentation Chain Transfer Process," *Macromolecular Symposia,* vol. 229, pp. 8-17, 2005, doi: 10.1002/masy.200551102.
[417] D. Phelan, "Designing novel smart hydrogel formulations for the controlled delivery of ocular therapies in contact lens devices," Doctor of Philosophy, Science, Waterford Institute of Technology, Ireland, 2015.
[418] V. Rao, P. Latha, P. V. Ashokan, and M. H. Shridhar, "Thermal Degradation of Poly(N-vinylpyrrolidone)–Poly(vinyl alcohol) Blends," *Polymer Journal,* vol. 31, no. 10, pp. 887-889, 1999, doi: 10.1295/polymj.31.887.
[419] Y. Du, P. Yang, Z. Mou, N. Hua, and L. Jiang, "Thermal decomposition behaviors of PVP coated on platinum nanoparticles," *J Appl Polym Sci,* vol. 99, pp. 23-26, 2006, doi: 10.1002/app.21886.
[420] D. Silva, A. C. Fernandes, T. G. Nunes, R. Colaço, and A. P. Serro, "The effect of albumin and cholesterol on the biotribological behavior of hydrogels for contact lenses," *Acta Biomaterialia,* vol. 26, pp. 184-194, 2015, doi: https://doi.org/10.1016/j.actbio.2015.08.011.
[421] M. d. P. Buera, G. Levi, and M. Karel, "Glass transition in poly(vinylpyrrolidone): effect of molecular weight and diluents,"

Biotechnology Progress, vol. 8, no. 2, pp. 144-148, 1992, doi: 10.1021/bp00014a008.
[422] T. Caykara, C. Özyürek, and O. Kantoğlu, "Investigation of thermal behavior of Poly (2-hydroxyethyl methacrylate-co-itaconic acid) networks," *J Appl Polym Sci*, vol. 103, pp. 1602-1607, 2007, doi: 10.1002/app.24522.
[423] L. Guan, H. Xu, and D. Huang, "The investigation on states of water in different hydrophilic polymers by DSC and FTIR," *Journal of Polymer Research*, vol. 18, pp. 681-689, 2011, doi: 10.1007/s10965-010-9464-7.
[424] I. Tranoudis and N. Efron, "Parameter stability of soft contact lenses made from different materials," *Contact Lens and Anterior Eye*, vol. 27, no. 3, pp. 115-131, 2004, doi: https://doi.org/10.1016/j.clae.2004.03.001.
[425] D. Mirejovsky, A. S. Patel, and G. Young, "Water properties of hydrogel contact lens materials: a possible predictive model for corneal desiccation staining," *Biomaterials*, vol. 14, no. 14, pp. 1080-1088, 1993/11/01/ 1993, doi: https://doi.org/10.1016/0142-9612(93)90209-K.
[426] N. Efron and N. A. Brennan, "The clinical relevance ofhydrogel lens water content," *Journal of The British Contact Lens Association*, vol. 10, pp. 9-14, 1987, doi: https://doi.org/10.1016/S0141-7037(87)80040-X.
[427] R. E. Gundel and C. Hi, "Soft Lens Dehydration: Thin Low Water vs. Thick High Water Lenses," *Eyecare*, vol. 2, 1986.
[428] M. R. Lattimore, T. H. Harding, and S. T. Williams, "Hydrogel Contact Lens Water Content is Dependent on Tearfilm pH," *Military Medicine*, vol. 183, no. suppl_1, pp. 224-230, 2018, doi: 10.1093/milmed/usx233.
[429] G. HØVDING, "The fluid content of hydrophilic contact lenses on the eye," *Acta Ophthalmologica*, vol. 61, no. 5, pp. 889-897, 1983, doi: 10.1111/j.1755-3768.1983.tb01471.x.
[430] I. Thormählen, J. Straub, and U. Grigull, "Refractive Index of Water and Its Dependence on Wavelength, Temperature, and Density," *Journal of Physical and Chemical Reference Data*, vol. 14, no. 4, pp. 933-945, 1985, doi: 10.1063/1.555743.
[431] E. Kim and K. Ehrmann, "Refractive index of soft contact lens materials measured in packaging solution and standard phosphate buffered saline and the effect on back vertex power calculation," *Contact Lens and Anterior Eye*, vol. 43, no. 2, pp. 123-129, 2020, doi: https://doi.org/10.1016/j.clae.2019.12.005.
[432] R. Fuentes, E. Fernández, I. Pascual, and C. García, "UV-Visible Transmittance of Silicone-Hydrogel Contact Lenses measured with a fiber optic spectrometer," *Proc SPIE*, vol. 8785, 2013, doi: 10.1117/12.2025710.
[433] *ISO18369-1:2017: Ophthalmic optics-Contact lenses*, S. S. Institute, CEN-CENELEC Management Centre: Avenue Marnix 17, B-1000 Brussels, 2017. [Online]. Available: https://www.iso.org/obp/ui/#iso:std:iso:18369:-1:ed-2:v2:en:sec:3.1.6.1
[434] C. Snyder, "Modulus and its Effect on Contact Lens Fit: Higher lens modulus and lens design characteristics may impact fitting success for some patients.," in *Contact Lens Spectrum*, ed, 2007.
[435] *Materials Data Book, Cambridge University Engineering Department*, 2003 ed. Cambridge, UK: Cambridge University Engineering Department, 2003. [Online]. Available: http://www-mdp.eng.cam.ac.uk/web/library/enginfo/cueddatabooks/materials.pdf. Accessed on: 15 April, 2019.

[436] E. Kim, M. Saha, and K. Ehrmann, "Mechanical Properties of Contact Lens Materials," *Eye & Contact Lens*, vol. 44, pp. S148-S156, 2018, doi: 10.1097/icl.0000000000000442.
[437] C.-F. Lai, J.-S. Li, Y.-T. Fang, C.-J. Chien, and C.-H. Lee, "UV and blue-light anti-reflective structurally colored contact lenses based on a copolymer hydrogel with amorphous array nanostructures," *RSC Advances*, vol. 8, pp. 4006-4013, 2018, doi: 10.1039/C7RA12753G.
[438] I. A. Safo, M. Werheid, C. Dosche, and M. Oezaslan, "The role of polyvinylpyrrolidone (PVP) as a capping and structure-directing agent in the formation of Pt nanocubes," *Nanoscale Advances*, vol. 1, no. 8, pp. 3095-3106, 2019, doi: 10.1039/C9NA00186G.
[439] M. Loría-Bastarrachea, W. Herrera, J. Cauich, H. Vázquez, A. Avila‐Ortega, and M. Cervantes, "A TG/FTIR study on the thermal degradation of poly(vinyl pyrrolidone)," *J Therm Anal Calorim*, vol. 104, pp. 737-742, 2011, doi: 10.1007/s10973-010-1061-9.
[440] R. W. Bobst, B. J. Garner, and F. W. Jacob, "Degassing process for removing unpolymerized monomers from olefin polymers (US4,372,758)," 1983.
[441] A. S. Rhee and D.-F. Wang, "Process for post reactor purging of residual monomers from solid polymer resins (US005478922A)," 1995.
[442] C. Extrand, J. Schafbuch, and M. W. Johnson, "The influence of polymer processing on extractables and leachables," *BioProcess International*, vol. 11, pp. 36-39, 04/01 2013.
[443] C. L. Stults, J. M. Ansell, A. J. Shaw, and L. M. Nagao, "Evaluation of extractables in processed and unprocessed polymer materials used for pharmaceutical applications," (in eng), *AAPS PharmSciTech*, vol. 16, no. 1, pp. 150-64, Feb 2015, doi: 10.1208/s12249-014-0188-6.
[444] S. Majumdar and R. Srirangam, "Potential of the bioflavonoids in the prevention/treatment of ocular disorders," (in eng), *The Journal of pharmacy and pharmacology*, vol. 62, no. 8, pp. 951-965, 2010, doi: 10.1211/jpp.62.08.0001.
[445] R. Joshi, Y. A. Kulkarni, and S. Wairkar, "Pharmacokinetic, pharmacodynamic and formulations aspects of Naringenin: An update," *Life Sciences*, vol. 215, pp. 43-56, 2018, doi: https://doi.org/10.1016/j.lfs.2018.10.066.
[446] Y. A. Kulkarni, M. S. Garud, M. J. Oza, K. H. Barve, and A. B. Gaikwad, "Chapter 5 - Diabetes, diabetic complications, and flavonoids," in *Fruits, Vegetables, and Herbs*, R. R. Watson and V. R. Preedy Eds.: Academic Press, 2016, pp. 77-104.
[447] T. Iwashina, "The Structure and Distribution of the Flavonoids in Plants," *Journal of Plant Research*, vol. 113, no. 3, pp. 287-299, 2000, doi: 10.1007/PL00013940.
[448] A. N. Panche, A. D. Diwan, and S. R. Chandra, "Flavonoids: an overview," (in eng), *J Nutr Sci*, vol. 5, p. 47, 2016, doi: 10.1017/jns.2016.41.
[449] S. Kumar and A. K. Pandey, "Chemistry and biological activities of flavonoids: an overview," (in eng), *ScientificWorldJournal*, vol. 2013, pp. 162750-162750, 2013, doi: 10.1155/2013/162750.
[450] T. J. Mabry, K. R. Markham, and M. B. Thomas, "The Ultraviolet Spectra of Isoflavones, Flavanones and Dihydroflavonols," in *The Systematic Identification of Flavonoids*, T. J. Mabry, K. R. Markham, and M. B. Thomas Eds. Berlin, Heidelberg: Springer Berlin Heidelberg, 1970, pp. 165-226.

[451] Y. Nogata, K. Sakamoto, H. Shiratsuchi, T. Ishii, M. Yano, and H. Ohta, "Flavonoid Composition of Fruit Tissues of Citrus Species," *Bioscience, Biotechnology, and Biochemistry,* vol. 70, no. 1, pp. 178-192, 2006, doi: 10.1271/bbb.70.178.
[452] M. A. Alam, N. Subhan, M. M. Rahman, S. J. Uddin, H. M. Reza, and S. D. Sarker, "Effect of citrus flavonoids, naringin and naringenin, on metabolic syndrome and their mechanisms of action," (in eng), *Adv Nutr,* vol. 5, no. 4, pp. 404-417, 2014, doi: 10.3945/an.113.005603.
[453] M. F. Ruh, T. Zacharewski, K. Connor, J. Howell, I. Chen, and S. Safe, "Naringenin: A weakly estrogenic bioflavonoid that exhibits antiestrogenic activity," *Biochemical Pharmacology,* vol. 50, no. 9, pp. 1485-1493, 1995, doi: https://doi.org/10.1016/0006-2952(95)02061-6.
[454] R. M. Martinez *et al.*, "Naringenin Inhibits UVB Irradiation-Induced Inflammation and Oxidative Stress in the Skin of Hairless Mice," *Journal of Natural Products,* vol. 78, no. 7, pp. 1647-1655, 2015, doi: 10.1021/acs.jnatprod.5b00198.
[455] M. F. Manchope *et al.*, "Naringenin Inhibits Superoxide Anion-Induced Inflammatory Pain: Role of Oxidative Stress, Cytokines, Nrf-2 and the NO-cGMP-PKG-KATP Channel Signaling Pathway," (in eng), *PLoS One,* vol. 11, no. 4, 2016, doi: 10.1371/journal.pone.0153015.
[456] T. Ramprasath, M. Senthamizharasi, V. Vasudevan, S. Sasikumar, S. Yuvaraj, and G. S. Selvam, "Naringenin confers protection against oxidative stress through upregulation of Nrf2 target genes in cardiomyoblast cells," *Journal of Physiology and Biochemistry,* vol. 70, no. 2, pp. 407-415, 2014, doi: 10.1007/s13105-014-0318-3.
[457] R. Rashmi, S. Bojan Magesh, K. Mohanram Ramkumar, S. Suryanarayanan, and M. Venkata SubbaRao, "Antioxidant Potential of Naringenin Helps to Protect Liver Tissue from Streptozotocin-Induced Damage," (in eng), *Rep Biochem Mol Biol,* vol. 7, no. 1, pp. 76-84, 2018. [Online]. Available: https://pubmed.ncbi.nlm.nih.gov/30324121.
[458] H. Wang *et al.*, "Nanocomplexes based polyvinylpyrrolidone K-17PF for ocular drug delivery of naringenin," *International Journal of Pharmaceutics,* vol. 578, p. 119133, 2020/03/30/ 2020, doi: https://doi.org/10.1016/j.ijpharm.2020.119133.
[459] Y. Ma *et al.*, "Development of a naringenin microemulsion as a prospective ophthalmic delivery system for the treatment of corneal neovascularization: in vitro and in vivo evaluation," *Drug Delivery,* vol. 29, no. 1, pp. 111-127, 2022/12/31 2022, doi: 10.1080/10717544.2021.2021323.
[460] F. A. Maulvi, "Effect of Timolol Maleate Concentration on Uptake and Release from Hydrogel Contact Lenses using Soaking Method," *Journal of Pharmacy and Applied Sciences,* vol. 1, pp. 16-22, 2014.
[461] Z. Wang *et al.*, "Novel Contact Lenses Embedded with Drug-Loaded Zwitterionic Nanogels for Extended Ophthalmic Drug Delivery," (in eng), *Nanomaterials (Basel),* vol. 11, no. 9, p. 2328, 2021, doi: 10.3390/nano11092328.
[462] F. Alvarez-Rivera *et al.*, "Controlled Release of rAAV Vectors from APMA-Functionalized Contact Lenses for Corneal Gene Therapy," *Pharmaceutics,* vol. 12, no. 4, doi: 10.3390/pharmaceutics12040335.
[463] C. Torres-Luna *et al.*, "Extended delivery of cationic drugs from contact lenses loaded with unsaturated fatty acids," *European Journal of Pharmaceutics and*

Biopharmaceutics, vol. 155, pp. 1-11, 2020/10/01/ 2020, doi: https://doi.org/10.1016/j.ejpb.2020.07.033.

[464] D. Silva *et al.*, "Diclofenac sustained release from sterilised soft contact lens materials using an optimised layer-by-layer coating," *International Journal of Pharmaceutics*, vol. 585, p. 119506, 2020/07/30/ 2020, doi: https://doi.org/10.1016/j.ijpharm.2020.119506.

[465] A. Pulliero, A. Profumo, C. Rosano, A. Izzotti, and S. C. Saccà, "Therapeutic Hydrogel Lenses and the Antibacterial and Antibiotic Drugs Release," *Applied Sciences*, vol. 11, no. 4, 2021, doi: 10.3390/app11041931.

[466] O. Ford, "J&J's 'Limit-Breaking' Contact Lens Win FDA Nod," *The company's drug-eluting product treats allergic eye itch for contact lens wearers and reduces the need for eyedrops.*, March 02,2022, doi: https://www.mddionline.com/technologies/jjs-limit-breaking-contact-lens-win-fda-nod?ADTRK=InformaMarkets&elq_mid=21119&elq_cid=882233.

[467] P. Zhang, X. Liu, W. Hu, Y. Bai, and L. Zhang, "Preparation and evaluation of naringenin-loaded sulfobutylether-β-cyclodextrin/chitosan nanoparticles for ocular drug delivery," *Carbohydrate Polymers*, vol. 149, pp. 224-230, 2016, doi: https://doi.org/10.1016/j.carbpol.2016.04.115.

[468] B. Q. Lin and G. Chiou, "Antioxidant activity of naringenin on various oxidants induced damages in ARPE-19 cells and HUVEC," *Int J Ophthalmol*, vol. 8, pp. 1963-1967, 10/25 2008.

[469] J. Lin *et al.*, "Ocular pharmacokinetics of naringenin eye drops following topical administration to rabbits," (in eng), *Journal of ocular pharmacology and therapeutics : the official journal of the Association for Ocular Pharmacology and Therapeutics*, vol. 31, no. 1, pp. 51-56, 2015, doi: 10.1089/jop.2014.0047.

[470] D. A. Armbruster and T. Pry, "Limit of blank, limit of detection and limit of quantitation," (in eng), *Clin Biochem Rev*, vol. 29 Suppl 1, no. Suppl 1, pp. S49-S52, 2008. [Online]. Available: https://pubmed.ncbi.nlm.nih.gov/18852857.

[471] K. Uney, F. Altan, and M. Elmas, "Development and validation of a high-performance liquid chromatography method for determination of cefquinome concentrations in sheep plasma and its application to pharmacokinetic studies," (in eng), *Antimicrob Agents Chemother*, vol. 55, no. 2, pp. 854-859, 2011, doi: 10.1128/AAC.01126-10.

[472] M. Latos-Brozio, A. Masek, and M. Piotrowska, "Novel Polymeric Biomaterial Based on Naringenin," *Materials*, vol. 14, no. 9, p. 2142, 2021. [Online]. Available: https://www.mdpi.com/1996-1944/14/9/2142.

[473] E. B. Manaia, M. P. Abuçafy, B. G. Chiari-Andréo, B. L. Silva, J. A. Oshiro Junior, and L. A. Chiavacci, "Physicochemical characterization of drug nanocarriers," (in eng), *International journal of nanomedicine*, vol. 12, pp. 4991-5011, 2017, doi: 10.2147/IJN.S133832.

[474] J. Wu, Q. Shen, and L. Fang, "Sulfobutylether-β-cyclodextrin/chitosan nanoparticles enhance the oral permeability and bioavailability of docetaxel," *Drug Development and Industrial Pharmacy*, vol. 39, no. 7, pp. 1010-1019, 2013, doi: 10.3109/03639045.2012.694588.

[475] M. Guan *et al.*, "Characterization, in Vitro and in Vivo Evaluation of Naringenin-Hydroxypropyl-β-Cyclodextrin Inclusion for Pulmonary Delivery," *Molecules*, vol. 25, no. 3, p. 554, 2020. [Online]. Available: https://www.mdpi.com/1420-3049/25/3/554.

[476] C. Lucas-Abellán *et al.*, "Effect of temperature, pH, β- and HP-β-cds on the solubility and stability of flavanones: Naringenin and hesperetin," *LWT*, vol. 108, pp. 233-239, 2019/07/01/ 2019, doi: https://doi.org/10.1016/j.lwt.2019.03.059.
[477] K. E. Smith, S. Sawicki, M. A. Hyjek, S. Downey, and K. Gall, "The effect of the glass transition temperature on the toughness of photopolymerizable (meth)acrylate networks under physiological conditions," (in eng), *Polymer*, vol. 50, no. 21, pp. 5112-5123, 2009, doi: 10.1016/j.polymer.2009.08.040.
[478] L. Zhao, H. Wang, C. Feng, F. Song, and X. Du, "Preparation and Evaluation of Starch Hydrogel/Contact Lens Composites as Epigallocatechin Gallate Delivery Systems for Inhibition of Bacterial Adhesion," (in English), *Frontiers in Bioengineering and Biotechnology*, Original Research vol. 9, 2021-November-16 2021, doi: 10.3389/fbioe.2021.759303.
[479] L. Zhao, X. Qi, T. Cai, Z. Fan, H. Wang, and X. Du, "Gelatin hydrogel/contact lens composites as rutin delivery systems for promoting corneal wound healing," *Drug Delivery*, vol. 28, pp. 1951-1961, 12/01 2021, doi: 10.1080/10717544.2021.1979126.
[480] M. Y. Efremov, E. A. Olson, M. Zhang, Z. Zhang, and L. H. Allen, "Probing Glass Transition of Ultrathin Polymer Films at a Time Scale of Seconds Using Fast Differential Scanning Calorimetry," *Macromolecules*, vol. 37, no. 12, pp. 4607-4616, 2004, doi: 10.1021/ma035909r.
[481] M. Klähn, R. Krishnan, J. M. Phang, F. C. H. Lim, A. M. van Herk, and S. Jana, "Effect of external and internal plasticization on the glass transition temperature of (Meth)acrylate polymers studied with molecular dynamics simulations and calorimetry," *Polymer*, vol. 179, p. 121635, 2019/09/28/ 2019, doi: https://doi.org/10.1016/j.polymer.2019.121635.
[482] B. C. Hancock and G. Zografi, "The Relationship Between the Glass Transition Temperature and the Water Content of Amorphous Pharmaceutical Solids," *Pharmaceutical Research*, vol. 11, no. 4, pp. 471-477, 1994/04/01 1994, doi: 10.1023/A:1018941810744.
[483] F. Fornasiero, M. Ung, C. J. Radke, and J. M. Prausnitz, "Glass-transition temperatures for soft-contact-lens materials. Dependence on water content," *Polymer*, vol. 46, no. 13, pp. 4845-4852, 2005/06/17/ 2005, doi: https://doi.org/10.1016/j.polymer.2005.03.084.
[484] M. Lira, C. Lourenço, M. Silva, and G. Botelho, "Physicochemical stability of contact lenses materials for biomedical applications," (in eng), *J Optom*, vol. 13, no. 2, pp. 120-127, Apr-Jun 2020, doi: 10.1016/j.optom.2019.10.002.
[485] K. Tompa, P. Bánki, M. Bokor, P. Kamasa, P. Rácz, and P. Tompa, "Hydration water/interfacial water in crystalline lens," *Experimental Eye Research*, vol. 91, no. 1, pp. 76-84, 2010/07/01/ 2010, doi: https://doi.org/10.1016/j.exer.2010.04.005.
[486] A. Desai *et al.*, "Co-delivery of timolol and hyaluronic acid from semi-circular ring-implanted contact lenses for the treatment of glaucoma:: In vitro and in vivo evaluation," *Biomaterials Science*, vol. 6, 04/16 2018, doi: 10.1039/C8BM00212F.
[487] A. Topete, A. P. Serro, and B. Saramago, "Dual drug delivery from intraocular lens material for prophylaxis of endophthalmitis in cataract surgery," *International Journal of Pharmaceutics*, vol. 558, pp. 43-52, 2019/03/10/ 2019, doi: https://doi.org/10.1016/j.ijpharm.2018.12.028.

[488] P. Paradiso, A. P. Serro, B. Saramago, R. Colaço, and A. Chauhan, "Controlled Release of Antibiotics From Vitamin E–Loaded Silicone-Hydrogel Contact Lenses," *Journal of Pharmaceutical Sciences*, vol. 105, no. 3, pp. 1164-1172, 2016/03/01/ 2016, doi: https://doi.org/10.1016/S0022-3549(15)00193-8.

[489] O. ÜNsalan and M. Gulluoglu, "FT ‐ Raman and FT ‐ IR spectral and quantum chemical studies on some flavonoid derivatives: Baicalein and Naringenin," *Journal of Raman Spectroscopy*, vol. 40, pp. 562-570, 2009, doi: 10.1002/jrs.2166.

[490] K. Wang *et al.*, "Preparation and in vitro release of buccal tablets of naringenin-loaded MPEG-PCL nanoparticles," *RSC Adv.*, vol. 4, 2014, doi: 10.1039/C4RA04920A.

[491] J. Long, A. V. Nand, C. Bunt, and A. Seyfoddin, "Controlled release of dexamethasone from poly(vinyl alcohol) hydrogel," (in eng), *Pharm Dev Technol*, vol. 24, no. 7, pp. 839-848, Sep 2019, doi: 10.1080/10837450.2019.1602632.

[492] J.-S. Garrigue, M. Amrane, M.-O. Faure, J. M. Holopainen, and L. Tong, "Relevance of Lipid-Based Products in the Management of Dry Eye Disease," (in eng), *Journal of ocular pharmacology and therapeutics : the official journal of the Association for Ocular Pharmacology and Therapeutics*, vol. 33, no. 9, pp. 647-661, 2017, doi: 10.1089/jop.2017.0052.

[493] S. A. Abouelmagd, B. Sun, A. C. Chang, Y. J. Ku, and Y. Yeo, "Release Kinetics Study of Poorly Water-Soluble Drugs from Nanoparticles: Are We Doing It Right?," *Molecular Pharmaceutics*, vol. 12, no. 3, pp. 997-1003, 2015/03/02 2015, doi: 10.1021/mp500817h.

[494] J. Telenius, A. Koivuniemi, P. Kulovesi, J. M. Holopainen, and I. Vattulainen, "Role of Neutral Lipids in Tear Fluid Lipid Layer: Coarse-Grained Simulation Study," *Langmuir*, vol. 28, no. 49, pp. 17092-17100, 2012/12/11 2012, doi: 10.1021/la304366d.

[495] G. Kwak, H. Kim, W.-D. Jang, G.-C. Ryu, and I.-S. Kim, "Antibacterial Effect of Naringin-containing Soft Contact Lens," *Bulletin of the Korean Chemical Society*, vol. 42, no. 10, pp. 1345-1350, 2021, doi: https://doi.org/10.1002/bkcs.12375.

[496] "5 - Mathematical models of drug release," in *Strategies to Modify the Drug Release from Pharmaceutical Systems*, M. L. Bruschi Ed.: Woodhead Publishing, 2015, pp. 63-86.

[497] M. Vigata, C. Meinert, D. W. Hutmacher, and N. Bock, "Hydrogels as Drug Delivery Systems: A Review of Current Characterization and Evaluation Techniques," *Pharmaceutics*, vol. 12, no. 12, p. 1188, 2020. [Online]. Available: https://www.mdpi.com/1999-4923/12/12/1188.

[498] R. Jeencham, M. Sutheerawattananonda, S. Rungchang, and W. Tiyaboonchai, "Novel daily disposable therapeutic contact lenses based on chitosan and regenerated silk fibroin for the ophthalmic delivery of diclofenac sodium," *Drug Delivery*, vol. 27, no. 1, pp. 782-790, 2020/01/01 2020, doi: 10.1080/10717544.2020.1765432.

[499] O. L. Lanier, M. Manfre, S. Kulkarni, C. Bailey, and A. Chauhan, "Combining modeling of drug uptake and release of cyclosporine in contact lenses to determine partition coefficient and diffusivity," *European Journal of Pharmaceutical Sciences*, vol. 164, p. 105891, 2021/09/01/ 2021, doi: https://doi.org/10.1016/j.ejps.2021.105891.

[500] S. K. Gade, J. Nirmal, P. Garg, and V. V. K. Venuganti, "Corneal delivery of moxifloxacin and dexamethasone combination using drug-eluting mucoadhesive contact lens to treat ocular infections," *International Journal of Pharmaceutics*, vol. 591, p. 120023, 2020/12/15/ 2020, doi: https://doi.org/10.1016/j.ijpharm.2020.120023.

[501] P. Zhang, R. Lin, G. Yang, J. Zhang, L. Zhou, and T. Liu, "Solubility of Naringenin in Ethanol and Water Mixtures," *Journal of Chemical & Engineering Data*, vol. 58, no. 9, pp. 2402-2404, 2013, doi: 10.1021/je4000718.

[502] S.-L. Hsiu, T.-Y. Huang, Y.-C. Hou, D.-H. Chin, and P.-D. L. Chao, "Comparison of metabolic pharmacokinetics of naringin and naringenin in rabbits," *Life Sciences*, vol. 70, no. 13, pp. 1481-1489, 2002, doi: https://doi.org/10.1016/S0024-3205(01)01491-6.

[503] F.-L. Yen, T.-H. Wu, L.-T. Lin, T.-M. Cham, and C.-C. Lin, "Naringenin-Loaded Nanoparticles Improve the Physicochemical Properties and the Hepatoprotective Effects of Naringenin in Orally-Administered Rats with CCl4-Induced Acute Liver Failure," *Pharmaceutical Research*, vol. 26, no. 4, pp. 893-902, 2009, doi: 10.1007/s11095-008-9791-0.

[504] H. J. Vila Real, A. J. Alfaia, A. R. T. Calado, and M. H. L. Ribeiro, "High pressure-temperature effects on enzymatic activity: Naringin bioconversion," *Food Chemistry*, vol. 102, no. 3, pp. 565-570, 2007, doi: https://doi.org/10.1016/j.foodchem.2006.05.033.

[505] A. A. Mahmoud, G. S. El-Feky, R. Kamel, and G. E. A. Awad, "Chitosan/sulfobutylether-β-cyclodextrin nanoparticles as a potential approach for ocular drug delivery," *International Journal of Pharmaceutics*, vol. 413, no. 1, pp. 229-236, 2011, doi: https://doi.org/10.1016/j.ijpharm.2011.04.031.

[506] L.-J. Yang *et al.*, "Preparation and characterization of inclusion complexes of naringenin with β-cyclodextrin or its derivative," *Carbohydrate Polymers*, vol. 98, no. 1, pp. 861-869, 2013, doi: https://doi.org/10.1016/j.carbpol.2013.07.010.

[507] A. Vyas, S. Saraf, and S. Saraf, "Encapsulation of cyclodextrin complexed simvastatin in chitosan nanocarriers: A novel technique for oral delivery," *Journal of Inclusion Phenomena and Macrocyclic Chemistry*, vol. 66, no. 3, pp. 251-259, 2010, doi: 10.1007/s10847-009-9605-y.

[508] E. A. Luna, E. R. Bornancini, D. O. Thompson, R. A. Rajewski, and V. J. Stella, "Characterization of Sulfobutyl Ether β-Cyclodextrin Mixtures," in *Proceedings of the Eighth International Symposium on Cyclodextrins*, Dordrecht, J. Szejtli and L. Szente, Eds., 1996// 1996: Springer Netherlands, pp. 133-136.

[509] Y. Xu *et al.*, "Chloramphenicol/sulfobutyl ether-β-cyclodextrin complexes in an ophthalmic delivery system: prolonged residence time and enhanced bioavailability in the conjunctival sac," *Expert Opinion on Drug Delivery*, vol. 16, no. 6, pp. 657-666, 2019, doi: 10.1080/17425247.2019.1609447.

[510] T. Loftsson, D. Hreinsdóttir, and M. Másson, "The complexation efficiency," *Journal of Inclusion Phenomena and Macrocyclic Chemistry*, vol. 57, no. 1, pp. 545-552, 2007, doi: 10.1007/s10847-006-9247-2.

[511] Z. Fülöp, P. Saokham, and T. Loftsson, "Sulfobutylether-β-cyclodextrin/chitosan nano- and microparticles and their physicochemical characteristics," *International Journal of Pharmaceutics*, vol. 472, no. 1, pp. 282-287, 2014, doi: https://doi.org/10.1016/j.ijpharm.2014.06.039.

[512] M. Shulman *et al.*, "Enhancement of naringenin bioavailability by complexation with hydroxypropyl-β-cyclodextrin. [corrected]," (in eng), *PLoS One*, vol. 6, no. 4, pp. 18033-18033, 2011, doi: 10.1371/journal.pone.0018033.
[513] H. F. Tooski, M. Jabbari, and A. Farajtabar, "Solubility and Preferential Solvation of the Flavonoid Naringenin in Some Aqueous/Organic Solvent Mixtures," *Journal of Solution Chemistry*, vol. 45, no. 12, pp. 1701-1714, 2016, doi: 10.1007/s10953-016-0526-2.
[514] W. Sangpheak *et al.*, "Physical properties and biological activities of hesperetin and naringenin in complex with methylated β-cyclodextrin," (in eng), *Beilstein J Org Chem*, vol. 11, pp. 2763-2773, 2015, doi: 10.3762/bjoc.11.297.
[515] T. Loftsson, P. Saokham, and A. R. Sá Couto, "Self-association of cyclodextrins and cyclodextrin complexes in aqueous solutions," *International Journal of Pharmaceutics*, vol. 560, pp. 228-234, 2019, doi: https://doi.org/10.1016/j.ijpharm.2019.02.004.
[516] A. Magnusdottir, M. Másson, and T. Loftsson, "Self Association and Cyclodextrin Solubilization of NSAIDs," *Journal of inclusion phenomena and macrocyclic chemistry*, vol. 44, no. 1, pp. 213-218, 2002, doi: 10.1023/A:1023079322024.
[517] M. S. Duan, N. Zhao, Í. B. Össurardóttir, T. Thorsteinsson, and T. Loftsson, "Cyclodextrin solubilization of the antibacterial agents triclosan and triclocarban: Formation of aggregates and higher-order complexes," *International Journal of Pharmaceutics*, vol. 297, no. 1, pp. 213-222, 2005, doi: https://doi.org/10.1016/j.ijpharm.2005.04.007.
[518] T. Loftsson, D. Hreinsdóttir, and M. Másson, "Evaluation of cyclodextrin solubilization of drugs," *International Journal of Pharmaceutics*, vol. 302, no. 1, pp. 18-28, 2005, doi: https://doi.org/10.1016/j.ijpharm.2005.05.042.
[519] C. Yang, L. Liu, T.-W. Mu, and Q.-X. Guo, "The Performance of the Benesi-Hildebrand Method in Measuring the Binding Constants of the Cyclodextrin Complexation," *Analytical Sciences - ANAL SCI*, vol. 16, pp. 537-539, 2000, doi: 10.2116/analsci.16.537.
[520] J. Patil, "Inclusion complex system; a novel technique to improve the solubility and bioavailability of poorly soluble drugs: A review," *Int J Pharm Sci Rev Res.*, vol. 2, no. 2, pp. 29-34, 2010.
[521] A. R. Hedges, "Industrial Applications of Cyclodextrins," *Chemical Reviews*, vol. 98, no. 5, pp. 2035-2044, 1998, doi: 10.1021/cr970014w.
[522] T. Loftsson and D. Hreinsdôttir, "Determination of aqueous solubility by heating and equilibration: A technical note," *AAPS PharmSciTech*, vol. 7, no. 1, pp. E29-E32, 2006, doi: 10.1208/pt070104.
[523] J. Y. Oh, J. M. Yu, and J. H. Ko, "Analysis of Ethanol Effects on Corneal Epithelium," *Investigative Ophthalmology & Visual Science*, vol. 54, no. 6, pp. 3852-3856, 2013, doi: 10.1167/iovs.13-11717.
[524] D. L. Teagarden and D. S. Baker, "Practical aspects of lyophilization using non-aqueous co-solvent systems," *European Journal of Pharmaceutical Sciences*, vol. 15, no. 2, pp. 115-133, 2002, doi: https://doi.org/10.1016/S0928-0987(01)00221-4.
[525] K. Kasraian and P. P. DeLuca, "The Effect of Tertiary Butyl Alcohol on the Resistance of the Dry Product Layer During Primary Drying," *Pharmaceutical Research*, vol. 12, no. 4, pp. 491-495, 1995, doi: 10.1023/A:1016285425670.

[526] L. Leclercq, "Interactions between cyclodextrins and cellular components: Towards greener medical applications?," (in eng), *Beilstein J Org Chem,* vol. 12, pp. 2644-2662, 2016, doi: 10.3762/bjoc.12.261.
[527] L. Ferreira, M. Kobelnik, L. Regasini, L. Dutra, V. Bolzani, and C. Ribeiro, "Synthesis and evaluation of the thermal behavior of flavonoids: Thermal decomposition of flavanone and 6-hydroxyflavanone," *Journal of Thermal Analysis and Calorimetry,* 2016, doi: 10.1007/s10973-016-5896-6.
[528] G. P. Bettinetti, M. Sorrenti, S. Rossi, F. Ferrari, P. Mura, and M. T. Faucci, "Assessment of solid-state interactions of naproxen with amorphous cyclodextrin derivatives by DSC," *Journal of Pharmaceutical and Biomedical Analysis,* vol. 30, no. 4, pp. 1173-1179, 2002, doi: https://doi.org/10.1016/S0731-7085(02)00421-1.
[529] L. Ai, J. Hu, X. Ji, and H. Zhao, "Structure confirmation and thermal kinetics of the inclusion of cis -jasmone in β-cyclodextrin," *RSC Advances,* vol. 9, pp. 26224-26229, 2019, doi: 10.1039/C9RA03343B.
[530] Y.-l. Shen, S.-h. Yang, L.-m. Wu, and X.-y. Ma, "Study on structure and characterization of inclusion complex of gossypol/beta cyclodextrin," *Spectrochimica Acta Part A: Molecular and Biomolecular Spectroscopy,* vol. 61, no. 6, pp. 1025-1028, 2005, doi: https://doi.org/10.1016/j.saa.2004.04.024.
[531] C. Xu *et al.*, "Investigation of inclusion complex of honokiol with sulfobutyl ether-β-cyclodextrin," *Carbohydrate Polymers,* vol. 113, pp. 9-15, 2014, doi: https://doi.org/10.1016/j.carbpol.2014.06.059.
[532] R. Ficarra *et al.*, "Study of flavonoids/β-cyclodextrins inclusion complexes by NMR, FT-IR, DSC, X-ray investigation," *Journal of Pharmaceutical and Biomedical Analysis,* vol. 29, no. 6, pp. 1005-1014, 2002, doi: https://doi.org/10.1016/S0731-7085(02)00141-3.
[533] F. Semcheddine, N. E. I. Guissi, X. Liu, Z. Wu, and B. Wang, "Effects of the Preparation Method on the Formation of True Nimodipine SBE-β-CD/HP-β-CD Inclusion Complexes and Their Dissolution Rates Enhancement," (in eng), *AAPS PharmSciTech,* vol. 16, no. 3, pp. 704-715, 2015, doi: 10.1208/s12249-014-0257-x.
[534] V. Venuti *et al.*, "Solute–Solvent Interactions in Aqueous Solutions of Sulfobutyl Ether-β-cyclodextrin As Probed by UV-Raman and FTIR-ATR Analysis," *The Journal of Physical Chemistry B,* vol. 120, no. 15, pp. 3746-3753, 2016, doi: 10.1021/acs.jpcb.6b02261.
[535] C. cannavà *et al.*, "Phase solubility and FTIR-ATR studies of idebenone/sulfobutyl ether β-cyclodextrin inclusion complex," *Journal of Inclusion Phenomena and Macrocyclic Chemistry,* vol. 75, 2012, doi: 10.1007/s10847-012-0110-3.
[536] B. Vaidya *et al.*, "Nintedanib-Cyclodextrin Complex to Improve Bio-Activity and Intestinal Permeability," *Carbohydrate Polymers,* vol. 204, 2018, doi: 10.1016/j.carbpol.2018.09.080.
[537] V. Venuti *et al.*, "A characterization study of resveratrol/sulfobutyl ether-β-cyclodextrin inclusion complex and in vitro anticancer activity," *Colloids and Surfaces B: Biointerfaces,* vol. 115, pp. 22-28, 2014, doi: https://doi.org/10.1016/j.colsurfb.2013.11.025.
[538] N. M. Dimitriou, A. Pavlopoulou, I. Tremi, V. Kouloulias, G. Tsigaridas, and A. G. Georgakilas, "Prediction of Gold Nanoparticle and Microwave-Induced Hyperthermia Effects on Tumor Control via a Simulation Approach," (in eng), *Nanomaterials (Basel),* vol. 9, no. 2, p. 167, 2019, doi: 10.3390/nano9020167.

[539] C. Yu *et al.*, "Hyaluronic Acid Coated Acid-Sensitive Nanoparticles for Targeted Therapy of Adjuvant-Induced Arthritis in Rats," (in eng), *Molecules*, vol. 24, no. 1, p. 146, 2019, doi: 10.3390/molecules24010146.
[540] S. Pandey *et al.*, "Co-Delivery of Teriflunomide and Methotrexate from Hydroxyapatite Nanoparticles for the Treatment of Rheumatoid Arthritis: In Vitro Characterization, Pharmacodynamic and Biochemical Investigations," *Pharmaceutical Research*, vol. 35, no. 11, p. 201, 2018, doi: 10.1007/s11095-018-2478-2.
[541] A. Romeo *et al.*, "Ferulic Acid-Loaded Polymeric Nanoparticles for Potential Ocular Delivery," *Pharmaceutics*, vol. 13, no. 5, doi: 10.3390/pharmaceutics13050687.
[542] N.-P.-D. Tran and M.-C. Yang, "The Ophthalmic Performance of Hydrogel Contact Lenses Loaded with Silicone Nanoparticles," *Polymers*, vol. 12, no. 5, doi: 10.3390/polym12051128.
[543] E. Chiesa *et al.*, "Hyaluronic Acid-Decorated Chitosan Nanoparticles for CD44-Targeted Delivery of Everolimus," (in eng), *Int J Mol Sci*, vol. 19, no. 8, pp. 1-26, 2018, doi: 10.3390/ijms19082310.
[544] T. A. Jacinto, B. Oliveira, S. P. Miguel, M. P. Ribeiro, and P. Coutinho, "Ciprofloxacin-Loaded Zein/Hyaluronic Acid Nanoparticles for Ocular Mucosa Delivery," *Pharmaceutics*, vol. 14, no. 8, doi: 10.3390/pharmaceutics14081557.
[545] C.-S. Wu, Y.-C. Hsu, H.-T. Liao, and Y.-X. Cai, "Antibacterial activity and in vitro evaluation of the biocompatibility of chitosan-based polysaccharide/polyester membranes," *Carbohydrate Polymers*, vol. 134, pp. 438-447, 2015, doi: https://doi.org/10.1016/j.carbpol.2015.08.021.
[546] M. Rajan, M. Murugan, D. Ponnamma, K. K. Sadasivuni, and M. A. Munusamy, "Poly-carboxylic acids functionalized chitosan nanocarriers for controlled and targeted anti-cancer drug delivery," *Biomedicine & Pharmacotherapy*, vol. 83, pp. 201-211, 2016, doi: https://doi.org/10.1016/j.biopha.2016.06.026.
[547] R. Saud, S. Pokhrel, and P. N. Yadav, "Synthesis, characterization and antimicrobial activity of maltol functionalized chitosan derivatives," *Journal of Macromolecular Science, Part A*, vol. 56, no. 4, pp. 375-383, 2019, doi: 10.1080/10601325.2019.1578616.
[548] N. Mittal Garg and G. Kaur, "Investigations on Polymeric Nanoparticles for Ocular Delivery," *Advances in Polymer Technology*, vol. 2019, pp. 1-14, 2019, doi: 10.1155/2019/1316249.
[549] M. Collado-González, Y. González Espinosa, and F. M. Goycoolea, "Interaction Between Chitosan and Mucin: Fundamentals and Applications," (in eng), *Biomimetics (Basel)*, vol. 4, no. 2, p. 32, 2019, doi: 10.3390/biomimetics4020032.
[550] M. M. Ibrahim, A.-E. H. Abd-Elgawad, O. A.-E. Soliman, and M. M. Jablonski, "Stability and Ocular Pharmacokinetics of Celecoxib-Loaded Nanoparticles Topical Ophthalmic Formulations," *Journal of Pharmaceutical Sciences*, vol. 105, no. 12, pp. 3691-3701, 2016, doi: 10.1016/j.xphs.2016.09.019.
[551] N. H. Hoang *et al.*, "Chitosan Nanoparticles-Based Ionic Gelation Method: A Promising Candidate for Plant Disease Management," *Polymers*, vol. 14, no. 4, doi: 10.3390/polym14040662.

[552] A. Almalik, R. Donno, C. J. Cadman, F. Cellesi, P. J. Day, and N. Tirelli, "Hyaluronic acid-coated chitosan nanoparticles: Molecular weight-dependent effects on morphology and hyaluronic acid presentation," *Journal of Controlled Release,* vol. 172, no. 3, pp. 1142-1150, 2013, doi: https://doi.org/10.1016/j.jconrel.2013.09.032.

[553] A. Gennari *et al.*, "The different ways to chitosan/hyaluronic acid nanoparticles: templated vs direct complexation. Influence of particle preparation on morphology, cell uptake and silencing efficiency," *Beilstein Journal of Nanotechnology,* vol. 10, pp. 2594-2608, 2019, doi: 10.3762/bjnano.10.250.

[554] H.-C. Yang and M.-H. Hon, "The Effect of the Degree of Deacetylation of Chitosan Nanoparticles and its Characterization and Encapsulation Efficiency on Drug Delivery," *Polym-Plast Technol Eng,* vol. 49, pp. 1292-1296, 2010, doi: 10.1080/03602559.2010.482076.

[555] A. Dey, U. Koli, P. Dandekar, and R. Jain, "Investigating behaviour of polymers in nanoparticles of Chitosan Oligosaccharides coated with Hyaluronic Acid," *Polymer,* vol. 93, pp. 44-52, 2016, doi: https://doi.org/10.1016/j.polymer.2016.04.027.

[556] M. Huang, E. Khor, and L.-Y. Lim, "Uptake and Cytotoxicity of Chitosan Molecules and Nanoparticles: Effects of Molecular Weight and Degree of Deacetylation," *Pharmaceutical Research,* vol. 21, no. 2, pp. 344-353, 2004, doi: 10.1023/B:PHAM.0000016249.52831.a5.

[557] F. A. Oyarzun-Ampuero, J. Brea, M. I. Loza, D. Torres, and M. J. Alonso, "Chitosan–hyaluronic acid nanoparticles loaded with heparin for the treatment of asthma," *International Journal of Pharmaceutics,* vol. 381, no. 2, pp. 122-129, 2009, doi: https://doi.org/10.1016/j.ijpharm.2009.04.009.

[558] J. Li, K. D. Caldwell, and W. Mächtle, "Particle characterization in centrifugal fields: Comparison between ultracentrifugation and sedimentation field-flow fractionation," *Journal of Chromatography A,* vol. 517, pp. 361-376, 1990, doi: https://doi.org/10.1016/S0021-9673(01)95734-6.

[559] W. Mächtle, "Centrifugation in Particle Size Analysis," in *Encyclopedia of Analytical Chemistry*, Walter Mächtle ed.: John Wiley & Sons, Ltd., 2006.

[560] X. Zhang and R. H. Davis, "The rate of collisions due to Brownian or gravitational motion of small drops," *Journal of Fluid Mechanics,* vol. 230, pp. 479-504, 1991, doi: 10.1017/S0022112091000861.

[561] K. Tahara, K. Karasawa, R. Onodera, and H. Takeuchi, "Feasibility of drug delivery to the eye's posterior segment by topical instillation of PLGA nanoparticles," *Asian Journal of Pharmaceutical Sciences,* vol. 12, no. 4, pp. 394-399, 2017, doi: https://doi.org/10.1016/j.ajps.2017.03.002.

[562] J. Pandit, Y. Sultana, and M. Aqil, "Chitosan-coated PLGA nanoparticles of bevacizumab as novel drug delivery to target retina: optimization, characterization, and in vitro toxicity evaluation," *Artificial Cells, Nanomedicine, and Biotechnology,* vol. 45, no. 7, pp. 1397-1407, 2017, doi: 10.1080/21691401.2016.1243545.

[563] S. Bozdag, K. Dillen, J. Vandervoort, and A. Ludwig, "The effect of freeze-drying with different cryoprotectants and gamma-irradiation sterilization on the characteristics of ciprofloxacin HCl-loaded poly(D,L-lactide-glycolide) nanoparticles," *Journal of Pharmacy and Pharmacology,* vol. 57, no. 6, pp. 699-707, 2005, doi: 10.1211/0022357056145.

[564] L. Wang *et al.*, "Cryoprotectant choice and analyses of freeze-drying drug suspension of nanoparticles with functional stabilisers," *Journal of Microencapsulation,* vol. 35, no. 3, pp. 241-248, 2018, doi: 10.1080/02652048.2018.1462416.
[565] L. Niu and J. Panyam, "Freeze concentration-induced PLGA and polystyrene nanoparticle aggregation: Imaging and rational design of lyoprotection," *Journal of Controlled Release,* vol. 248, pp. 125-132, 2017, doi: https://doi.org/10.1016/j.jconrel.2017.01.019.
[566] N.-O. Chung, M. K. Lee, and J. Lee, "Mechanism of freeze-drying drug nanosuspensions," *International Journal of Pharmaceutics,* vol. 437, no. 1, pp. 42-50, 2012, doi: https://doi.org/10.1016/j.ijpharm.2012.07.068.
[567] P. Fonte, S. Reis, and B. Sarmento, "Facts and evidences on the lyophilization of polymeric nanoparticles for drug delivery," *Journal of Controlled Release,* vol. 225, pp. 75-86, 2016, doi: https://doi.org/10.1016/j.jconrel.2016.01.034.
[568] P. Fonte *et al.*, "Stability Study Perspective of the Effect of Freeze-Drying Using Cryoprotectants on the Structure of Insulin Loaded into PLGA Nanoparticles," *Biomacromolecules,* vol. 15, no. 10, pp. 3753-3765, 2014, doi: 10.1021/bm5010383.
[569] W. Abdelwahed, G. Degobert, and H. Fessi, "A pilot study of freeze drying of poly(epsilon-caprolactone) nanocapsules stabilized by poly(vinyl alcohol): Formulation and process optimization," *International Journal of Pharmaceutics,* vol. 309, no. 1, pp. 178-188, 2006, doi: https://doi.org/10.1016/j.ijpharm.2005.10.003.
[570] A. Fàbregas *et al.*, "Impact of physical parameters on particle size and reaction yield when using the ionic gelation method to obtain cationic polymeric chitosan–tripolyphosphate nanoparticles," *International Journal of Pharmaceutics,* vol. 446, no. 1, pp. 199-204, 2013, doi: https://doi.org/10.1016/j.ijpharm.2013.02.015.
[571] A. Almalik, I. Alradwan, M. A. Kalam, and A. Alshamsan, "Effect of cryoprotection on particle size stability and preservation of chitosan nanoparticles with and without hyaluronate or alginate coating," (in eng), *Saudi Pharm J,* vol. 25, no. 6, pp. 861-867, 2017, doi: 10.1016/j.jsps.2016.12.008.
[572] A. Rampino, M. Borgogna, P. Blasi, B. Bellich, and A. Cesàro, "Chitosan nanoparticles: Preparation, size evolution and stability," *International Journal of Pharmaceutics,* vol. 455, no. 1, pp. 219-228, 2013, doi: https://doi.org/10.1016/j.ijpharm.2013.07.034.
[573] J. Stetefeld, S. A. McKenna, and T. R. Patel, "Dynamic light scattering: a practical guide and applications in biomedical sciences," (in eng), *Biophys Rev,* vol. 8, no. 4, pp. 409-427, 2016, doi: 10.1007/s12551-016-0218-6.
[574] J. Lim, S. P. Yeap, H. X. Che, and S. C. Low, "Characterization of magnetic nanoparticle by dynamic light scattering," (in eng), *Nanoscale Res Lett,* vol. 8, no. 1, pp. 381-381, 2013, doi: 10.1186/1556-276X-8-381.
[575] S. Falke and C. Betzel, "Dynamic Light Scattering (DLS): Principles, Perspectives, Applications to Biological Samples," (in eng), *Radiation in Bioanalysis,* vol. 8, pp. 173-193, 2019, doi: 10.1007/978-3-030-28247-9_6.
[576] P. M. Carvalho, M. R. Felício, N. C. Santos, S. Gonçalves, and M. M. Domingues, "Application of Light Scattering Techniques to Nanoparticle Characterization and Development," (in eng), *Front Chem,* vol. 6, pp. 237-237, 2018, doi: 10.3389/fchem.2018.00237.

[577] Z. Adamczyk, K. Sadlej, E. Wajnryb, M. L. Ekiel-Jeżewska, and P. Warszyński, "Hydrodynamic radii and diffusion coefficients of particle aggregates derived from the bead model," *Journal of Colloid and Interface Science*, vol. 347, no. 2, pp. 192-201, 2010, doi: https://doi.org/10.1016/j.jcis.2010.03.066.

[578] F. Ruiz-Cabello, G. Trefalt, P. Maroni, and M. Borkovec, "Electric double-layer potentials and surface regulation properties measured by colloidal-probe atomic force microscopy," *Physical Review E*, vol. 90, p. 012301, 2014, doi: 10.1103/PhysRevE.90.012301.

[579] E. Cruz, Y. Zheng, E. Torres, W. Li, W. Song, and K. Burugapalli, "Zeta Potential of Modified Multi-walled Carbon Nanotubes in Presence of poly(vinyl alcohol) Hydrogel," *International journal of electrochemical science*, vol. 7, pp. 3577-3590, 2012.

[580] M. J. Masarudin, S. M. Cutts, B. J. Evison, D. R. Phillips, and P. J. Pigram, "Factors determining the stability, size distribution, and cellular accumulation of small, monodisperse chitosan nanoparticles as candidate vectors for anticancer drug delivery: application to the passive encapsulation of [(14)C]-doxorubicin," (in eng), *Nanotechnol Sci Appl*, vol. 8, pp. 67-80, 2015, doi: 10.2147/NSA.S91785.

[581] N. Sawtarie, Y. Cai, and Y. Lapitsky, "Preparation of chitosan/tripolyphosphate nanoparticles with highly tunable size and low polydispersity," *Colloids and Surfaces B: Biointerfaces*, vol. 157, pp. 110-117, 2017, doi: https://doi.org/10.1016/j.colsurfb.2017.05.055.

[582] L. Bugnicourt, P. Alcouffe, and C. Ladavière, "Elaboration of chitosan nanoparticles: Favorable impact of a mild thermal treatment to obtain finely divided, spherical, and colloidally stable objects," *Colloids and Surfaces A: Physicochemical and Engineering Aspects*, vol. 457, pp. 476-486, 2014, doi: https://doi.org/10.1016/j.colsurfa.2014.06.029.

[583] A. Almalik *et al.*, "Hyaluronic Acid Coated Chitosan Nanoparticles Reduced the Immunogenicity of the Formed Protein Corona," *Scientific Reports*, vol. 7, no. 1, p. 10542, 2017, doi: 10.1038/s41598-017-10836-7.

[584] S. Sreekumar, F. M. Goycoolea, B. M. Moerschbacher, and G. R. Rivera-Rodriguez, "Parameters influencing the size of chitosan-TPP nano- and microparticles," (in eng), *Scientific reports*, vol. 8, no. 1, pp. 4695-4695, 2018, doi: 10.1038/s41598-018-23064-4.

[585] N. Hoshyar, S. Gray, H. Han, and G. Bao, "The effect of nanoparticle size on in vivo pharmacokinetics and cellular interaction," (in eng), *Nanomedicine (Lond)*, vol. 11, no. 6, pp. 673-692, 2016, doi: 10.2217/nnm.16.5.

[586] A. Fallacara *et al.*, "Formulation and Characterization of Native and Crosslinked Hyaluronic Acid Microspheres for Dermal Delivery of Sodium Ascorbyl Phosphate: A Comparative Study," (in eng), *Pharmaceutics*, vol. 10, no. 4, pp. 254-275, 2018, doi: 10.3390/pharmaceutics10040254.

[587] D. Sgorla, A. Almeida, C. Azevedo, ÿ. J. Bunhak, B. Sarmento, and O. A. Cavalcanti, "Development and characterization of crosslinked hyaluronic acid polymeric films for use in coating processes," *International Journal of Pharmaceutics*, vol. 511, no. 1, pp. 380-389, 2016, doi: https://doi.org/10.1016/j.ijpharm.2016.07.033.

[588] P.-Z. Hong, S.-D. Li, C.-Y. Ou, C.-P. Li, L. Yang, and C.-H. Zhang, "Thermogravimetric analysis of chitosan," *Journal of Applied Polymer Science*, vol. 105, no. 2, pp. 547-551, 2007, doi: 10.1002/app.25920.

[589] S. Kumar and J. Koh, "Physiochemical, Optical and Biological Activity of Chitosan-Chromone Derivative for Biomedical Applications," *Int J Mol Sci*, vol. 13, pp. 6102-16, 05/01 2012, doi: 10.3390/ijms13056102.
[590] F. Hu, W. Liu, L. Yan, F. Kong, and K. Wei, "Optimization and characterization of poly(lactic-co-glycolic acid) nanoparticles loaded with astaxanthin and evaluation of anti-photodamage effect in vitro," (in eng), *R Soc Open Sci*, vol. 6, no. 10, pp. 191184-191184, 2019, doi: 10.1098/rsos.191184.
[591] H. Zhang and Y. Zhao, "Preparation, characterization and evaluation of tea polyphenol–Zn complex loaded β-chitosan nanoparticles," *Food Hydrocolloids*, vol. 48, 06/30 2015, doi: 10.1016/j.foodhyd.2015.02.015.
[592] S. Kalliola, E. Repo, M. Sillanpää, J. Singh Arora, J. He, and V. T. John, "The stability of green nanoparticles in increased pH and salinity for applications in oil spill-treatment," *Colloids and Surfaces A: Physicochemical and Engineering Aspects*, vol. 493, pp. 99-107, 2016, doi: https://doi.org/10.1016/j.colsurfa.2016.01.011.
[593] Y.-C. Huang and T.-H. Kuo, "O-carboxymethyl chitosan/fucoidan nanoparticles increase cellular curcumin uptake," *Food Hydrocolloids*, vol. 53, pp. 261-269, 2016, doi: https://doi.org/10.1016/j.foodhyd.2015.02.006.
[594] B. Nie, J. Stutzman, and A. Xie, "A Vibrational Spectral Maker for Probing the Hydrogen-Bonding Status of Protonated Asp and Glu Residues," *Biophysical Journal*, vol. 88, no. 4, pp. 2833-2847, 2005, doi: https://doi.org/10.1529/biophysj.104.047639.
[595] M. Samy, S. H. Abd El-Alim, A. E. G. Rabia, A. Amin, and M. M. H. Ayoub, "Formulation, characterization and in vitro release study of 5-fluorouracil loaded chitosan nanoparticles," *International Journal of Biological Macromolecules*, vol. 156, pp. 783-791, 2020/08/01/ 2020, doi: https://doi.org/10.1016/j.ijbiomac.2020.04.112.
[596] R. Servaty, J. Schiller, H. Binder, and K. Arnold, "Hydration of polymeric components of cartilage — an infrared spectroscopic study on hyaluronic acid and chondroitin sulfate," *International Journal of Biological Macromolecules*, vol. 28, no. 2, pp. 121-127, 2001, doi: https://doi.org/10.1016/S0141-8130(00)00161-6.
[597] X. Liu, Y. Zhang, X. Tang, and H. Zhang, "Determination of entrapment efficiency and drug phase distribution of submicron emulsions loaded silybin," *Journal of Microencapsulation*, vol. 26, no. 2, pp. 180-186, 2009, doi: 10.1080/02652040802211741.
[598] N. Ahmad, M. A. Alam, R. Ahmad, A. A. Naqvi, and F. J. Ahmad, "Preparation and characterization of surface-modified PLGA-polymeric nanoparticles used to target treatment of intestinal cancer," *Artificial Cells, Nanomedicine, and Biotechnology*, vol. 46, no. 2, pp. 432-446, 2018, doi: 10.1080/21691401.2017.1324466.
[599] M. M. Badran, A. H. Alomrani, G. I. Harisa, A. E. Ashour, A. Kumar, and A. E. Yassin, "Novel docetaxel chitosan-coated PLGA/PCL nanoparticles with magnified cytotoxicity and bioavailability," *Biomedicine & Pharmacotherapy*, vol. 106, pp. 1461-1468, 2018, doi: https://doi.org/10.1016/j.biopha.2018.07.102.
[600] L. Chronopoulou *et al.*, "Chitosan-coated PLGA nanoparticles: A sustained drug release strategy for cell cultures," *Colloids and Surfaces B: Biointerfaces*, vol. 103, pp. 310-317, 2013, doi: https://doi.org/10.1016/j.colsurfb.2012.10.063.

[601] D. L. Cooper and S. Harirforoosh, "Design and Optimization of PLGA-Based Diclofenac Loaded Nanoparticles," *PLoS One*, vol. 9, no. 1, p. e87326, 2014, doi: 10.1371/journal.pone.0087326.
[602] N. Sharma, P. Madan, and S. Lin, "Effect of process and formulation variables on the preparation of parenteral paclitaxel-loaded biodegradable polymeric nanoparticles: A co-surfactant study," *Asian Journal of Pharmaceutical Sciences*, vol. 11, no. 3, pp. 404-416, 2016, doi: https://doi.org/10.1016/j.ajps.2015.09.004.
[603] F. Aqil, R. Munagala, J. Jeyabalan, A. K. Agrawal, and R. Gupta, "Exosomes for the Enhanced Tissue Bioavailability and Efficacy of Curcumin," *The AAPS Journal*, vol. 19, no. 6, pp. 1691-1702, 2017, doi: 10.1208/s12248-017-0154-9.
[604] M. A. Mavaddati, F. Moztarzadeh, and F. Baghbani, "Effect of Formulation and Processing Variables on Dexamethasone Entrapment and Release of Niosomes," *Journal of Cluster Science*, vol. 26, no. 6, pp. 2065-2078, 2015, doi: 10.1007/s10876-015-0908-4.
[605] L. Andrea, I. Marica, and R. Anamarija, "Lysozyme-Induced Degradation of Chitosan: The Characterisation of Degraded Chitosan Scaffolds," *Journal of Tissue Repair and Regeneration*, vol. 1, no. 1, pp. 12-22, 1// 2017, doi: https://doi.org/10.14302/issn.2640-6403.jtrr-17-1840.
[606] S. Kim, Z.-K. Cui, B. Koo, J. Zheng, T. Aghaloo, and M. Lee, "Chitosan–Lysozyme Conjugates for Enzyme-Triggered Hydrogel Degradation in Tissue Engineering Applications," *ACS Applied Materials & Interfaces*, vol. 10, no. 48, pp. 41138-41145, 2018/12/05 2018, doi: 10.1021/acsami.8b15591.
[607] M. Zahoor, H. Bahadar, M. Ayaz, A. Khan, and M. Shah, "In vitro Study on the Antimicrobial Activity of Human Tears with Respect to Age," *The Korean Journal of Clinical Laboratory Science*, vol. 50, pp. 93-99, 06/30 2018, doi: 10.15324/kjcls.2018.50.2.93.
[608] J. Siepmann and F. Siepmann, "Mathematical modeling of drug dissolution," *International Journal of Pharmaceutics*, vol. 453, no. 1, pp. 12-24, 2013, doi: https://doi.org/10.1016/j.ijpharm.2013.04.044.
[609] Z. Yang, J. Liu, and Y. Lu, "Doxorubicin and CD-CUR inclusion complex co-loaded in thermosensitive hydrogel PLGA-PEG-PLGA localized administration for osteosarcoma," *Int J Oncol*, vol. 57, no. 2, pp. 433-444, 2020/08/01 2020, doi: 10.3892/ijo.2020.5067.
[610] R. Li *et al.*, "Poly(2-hydroxyethyl methacrylate)/β-cyclodextrin-hyaluronan contact lens with tear protein adsorption resistance and sustained drug delivery for ophthalmic diseases," *Acta Biomaterialia*, vol. 110, pp. 105-118, 2020/07/01/ 2020, doi: https://doi.org/10.1016/j.actbio.2020.04.002.
[611] T. Minami *et al.*, "In vitro and in vivo performance of epinastine hydrochloride-releasing contact lenses," (in eng), *PLoS One*, vol. 14, no. 1, pp. e0210362-e0210362, 2019, doi: 10.1371/journal.pone.0210362.
[612] M. G. Hewitt *et al.*, "In Vitro Topical Delivery of Chlorhexidine to the Cornea: Enhancement Using Drug-Loaded Contact Lenses and β-Cyclodextrin Complexation, and the Importance of Simulating Tear Irrigation," *Molecular Pharmaceutics*, vol. 17, no. 4, pp. 1428-1441, 2020/04/06 2020, doi: 10.1021/acs.molpharmaceut.0c00140.
[613] O. Zabihi, A. Omrani, and A. A. Rostami, "Thermo-oxidative degradation kinetics and mechanism of the system epoxy nanocomposite reinforced with

nano-Al2O3," *Journal of Thermal Analysis and Calorimetry*, vol. 108, no. 3, pp. 1251-1260, 2012/06/01 2012, doi: 10.1007/s10973-011-1945-3.
[614] P. Ramasubba Reddy, M. R. Kummara, K. S. V. Krishna Rao, Y. Shchipunov, and C.-S. Ha, "Synthesis of alginate based silver nanocomposite hydrogels for biomedical applications," *Macromolecular Research*, vol. 22, pp. 832-842, 08/31 2014, doi: 10.1007/s13233-014-2117-7.
[615] L. H. Gaabour, "Spectroscopic and thermal analysis of polyacrylamide/chitosan (PAM/CS) blend loaded by gold nanoparticles," *Results in Physics*, vol. 7, pp. 2153-2158, 2017/01/01/ 2017, doi: https://doi.org/10.1016/j.rinp.2017.06.027.
[616] E. Saygili *et al.*, "An alginate-poly(acrylamide) hydrogel with TGF-β3 loaded nanoparticles for cartilage repair: Biodegradability, biocompatibility and protein adsorption," *International Journal of Biological Macromolecules*, vol. 172, pp. 381-393, 2021/03/01/ 2021, doi: https://doi.org/10.1016/j.ijbiomac.2021.01.069.
[617] D. Nguyen, J. Dowling, R. Ryan, P. McLoughlin, and L. Fitzhenry, "Controlled release of naringenin from soft hydrogel contact lens: An investigation into lens critical properties and in vitro release," *International Journal of Pharmaceutics*, vol. 621, p. 121793, 2022/06/10/ 2022, doi: https://doi.org/10.1016/j.ijpharm.2022.121793.
[618] J. Hao *et al.*, "Fabrication of a composite system combining solid lipid nanoparticles and thermosensitive hydrogel for challenging ophthalmic drug delivery," *Colloids and Surfaces B: Biointerfaces*, vol. 114, pp. 111-120, 2014/02/01/ 2014, doi: https://doi.org/10.1016/j.colsurfb.2013.09.059.
[619] J. Xu, X. Li, and F. Sun, "Cyclodextrin-containing hydrogels for contact lenses as a platform for drug incorporation and release," *Acta Biomaterialia*, vol. 6, no. 2, pp. 486-493, 2010/02/01/ 2010, doi: https://doi.org/10.1016/j.actbio.2009.07.021.
[620] C. G. Gomez, G. Chambat, A. Heyraud, M. Villar, and R. Auzély-Velty, "Synthesis and characterization of a β-CD-alginate conjugate," *Polymer*, vol. 47, no. 26, pp. 8509-8516, 2006/12/08/ 2006, doi: https://doi.org/10.1016/j.polymer.2006.10.011.
[621] L. Jones and K. Dumbleton, "10 - Soft Contact Lens Fitting," in *Contact Lenses (Sixth Edition)*, A. J. Phillips and L. Speedwell Eds. London: Elsevier, 2019, pp. 207-222.
[622] M. Van Beek, L. Jones, and H. Sheardown, "Hyaluronic acid containing hydrogels for the reduction of protein adsorption," *Biomaterials*, vol. 29, no. 7, pp. 780-789, 2008, doi: https://doi.org/10.1016/j.biomaterials.2007.10.039.
[623] A. Nasti *et al.*, "Chitosan/TPP and Chitosan/TPP-hyaluronic Acid Nanoparticles: Systematic Optimisation of the Preparative Process and Preliminary Biological Evaluation," *Pharmaceutical Research*, vol. 26, no. 8, pp. 1918-1930, 2009, doi: 10.1007/s11095-009-9908-0.
[624] R. Hashad, R. Ishak, A. Geneidi, and S. Mansour, "Surface Functionalization of Methotrexate-loaded Chitosan Nanoparticles with Hyaluronic acid/Human serum albumin: Comparative characterization and in vitro cytotoxicity," *International Journal of Pharmaceutics*, vol. 522, 2017, doi: 10.1016/j.ijpharm.2017.03.008.
[625] N. M. Zaki, A. Nasti, and N. Tirelli, "Nanocarriers for Cytoplasmic Delivery: Cellular Uptake and Intracellular Fate of Chitosan and Hyaluronic Acid-Coated Chitosan Nanoparticles in a Phagocytic Cell Model," *Macromolecular*

Bioscience, vol. 11, no. 12, pp. 1747-1760, 2011, doi: 10.1002/mabi.201100156.

[626] Y.-I. Jeong *et al.*, "Preparation of poly(DL-lactide-co-glycolide) nanoparticles without surfactant," *Journal of Applied Polymer Science*, vol. 80, no. 12, pp. 2228-2236, 2001, doi: 10.1002/app.1326.

[627] J.-W. Nah *et al.*, "Clonazepam release from poly(DL-lactide-co-glycolide) nanoparticles prepared by dialysis method," *Archives of Pharmacal Research*, vol. 21, no. 4, pp. 418-422, 1998, doi: 10.1007/BF02974636.

[628] K. Krishnamoorthy and M. Mahalingam, "Selection of a suitable method for the preparation of polymeric nanoparticles: multi-criteria decision making approach," (in eng), *Adv Pharm Bull*, vol. 5, no. 1, pp. 57-67, 2015, doi: 10.5681/apb.2015.008.

[629] A. Lassenberger, O. Bixner, T. Gruenewald, H. Lichtenegger, R. Zirbs, and E. Reimhult, "Evaluation of High-Yield Purification Methods on Monodisperse PEG-Grafted Iron Oxide Nanoparticles," (in eng), *Langmuir : the ACS journal of surfaces and colloids*, vol. 32, no. 17, pp. 4259-4269, 2016, doi: 10.1021/acs.langmuir.6b00919.

[630] K. E. Sapsford, K. M. Tyner, B. J. Dair, J. R. Deschamps, and I. L. Medintz, "Analyzing Nanomaterial Bioconjugates: A Review of Current and Emerging Purification and Characterization Techniques," *Analytical Chemistry*, vol. 83, no. 12, pp. 4453-4488, 2011, doi: 10.1021/ac200853a.

[631] M. N. Collins and C. Birkinshaw, "Comparison of the effectiveness of four different crosslinking agents with hyaluronic acid hydrogel films for tissue-culture applications," *Journal of Applied Polymer Science*, vol. 104, no. 5, pp. 3183-3191, 2007, doi: 10.1002/app.25993.

[632] G. Leone, M. Consumi, S. Lamponi, and A. Magnani, "New hyaluroran derivative with prolonged half-life for ophthalmogical formulation," *Carbohydrate Polymers*, vol. 88, no. 3, pp. 799-808, 2012, doi: https://doi.org/10.1016/j.carbpol.2011.12.047.

[633] Y. Huang, Y. Cai, and Y. Lapitsky, "Factors affecting the stability of chitosan/tripolyphosphate micro- and nanogels: resolving the opposing findings," *Journal of Materials Chemistry B*, 10.1039/C5TB00431D vol. 3, no. 29, pp. 5957-5970, 2015, doi: 10.1039/C5TB00431D.

[634] S. J. Rehfeld, H. F. Loken, and D. J. Eatough, "Interaction of calcium ion with sodium triphosphate determined by potentiometric and calorimetric techniques," *Thermochimica Acta*, vol. 18, no. 3, pp. 265-271, 1977, doi: https://doi.org/10.1016/0040-6031(77)85060-0.

[635] A. Pimenta *et al.*, "Simulation of the hydrodynamic conditions of the eye to better reproduce the drug release from hydrogel contact lenses: experiments and modeling," *Drug Delivery and Translational Research*, vol. 6, 2016, doi: 10.1007/s13346-016-0303-1.

[636] C. M. Phan, M. Bajgrowicz, H. Gao, L. N. Subbaraman, and L. W. Jones, "Release of Fluconazole from Contact Lenses Using a Novel In Vitro Eye Model," (in eng), *Optom Vis Sci*, vol. 93, no. 4, pp. 387-94, Apr 2016, doi: 10.1097/opx.0000000000000760.

[637] C.-M. Phan, H. Walther, H. Qiao, R. Shinde, and L. Jones, "Development of an Eye Model With a Physiological Blink Mechanism," *Translational Vision Science & Technology*, vol. 8, no. 5, pp. 1-1, 2019, doi: 10.1167/tvst.8.5.1.

[638] J. Bednarz, M. Teifel, P. Friedl, and K. Engelmann, "Immortalization of human corneal endothelial cells using electroporation protocol optimized for human

corneal endothelial and human retinal pigment epithelial cells," *Acta ophthalmologica Scandinavica*, vol. 78, pp. 130-6, 2000, doi: 10.1034/j.1600-0420.2000.078002130.x.

[639] T. Schmedt, Y. Chen, T. T. Nguyen, S. Li, J. A. Bonanno, and U. V. Jurkunas, "Telomerase immortalization of human corneal endothelial cells yields functional hexagonal monolayers," (in eng), *PLoS One*, vol. 7, no. 12, p. 51427, 2012, doi: 10.1371/journal.pone.0051427.

[640] U. Ubani-Ukoma, D. Gibson, G. Schultz, B. O. Silva, and A. Chauhan, "Evaluating the potential of drug eluting contact lenses for treatment of bacterial keratitis using an ex vivo corneal model," *International Journal of Pharmaceutics*, vol. 565, pp. 499-508, 2019/06/30/ 2019, doi: https://doi.org/10.1016/j.ijpharm.2019.05.031.

[641] P. Mehta *et al.*, "Assessing the ex vivo permeation behaviour of functionalised contact lens coatings engineered using an electrohydrodynamic technique," *Journal of Physics: Materials*, vol. 2, no. 1, p. 014002, 2018/12/14 2019, doi: 10.1088/2515-7639/aaf263.

[642] L. D. Wuchte, S. A. DiPasquale, and M. E. Byrne, "In vivo drug delivery via contact lenses: The current state of the field from origins to present," (in eng), *J Drug Deliv Sci Technol*, vol. 63, Jun 2021, doi: 10.1016/j.jddst.2021.102413.

[643] S. A. DiPasquale, L. D. Wuchte, R. J. Mosley, R. M. Demarest, M. L. Voyles, and M. E. Byrne, "One Week Sustained In Vivo Therapeutic Release and Safety of Novel Extended-Wear Silicone Hydrogel Contact Lenses," *Advanced Healthcare Materials*, vol. 11, no. 7, p. 2101263, 2022/04/01 2022.

APPENDIX 1

RESEARCH OUTPUTS

Appendix 1.1: Review Article

Contact Lens and Anterior Eye 44 (2021) 101487

Contents lists available at ScienceDirect

Contact Lens and Anterior Eye

journal homepage: www.elsevier.com/locate/clae

Review article

Pharmaceutical-loaded contact lenses as an ocular drug delivery system: A review of critical lens characterization methodologies with reference to ISO standards

Dan Chau Thuy Nguyen [a,*], Joseph Dowling [b], Richie Ryan [a], Peter McLoughlin [a], Laurence Fitzhenry [a]

[a] Ocular Therapeutics Research Group (OTRG), Pharmaceutical & Molecular Biotechnology Research Centre (PMBRC), Waterford Institute of Technology, Waterford City, County Waterford X91 K0EK, Ireland
[b] Research and Development Department, Bausch + Lomb Ireland Ltd., Waterford City, County Waterford X91 V383, Ireland

ARTICLE INFO

Keywords:
Ocular drug delivery
Therapeutic contact lens
Characterization techniques
Physical properties
Chemical properties
ISO standards

ABSTRACT

Therapeutic contact lenses for ocular drug delivery have received considerable interest as they can potentially enhance ocular bioavailability, increase patient compliance, and reduce side effects. Along with the successful *in vitro* and *in vivo* studies on sustained drug delivery through contact lenses, lens critical properties such as water content, optical transparency and modulus have also been investigated. Aside from issues such as drug stability or burst release, the potential for the commercialization of pharmaceutical-loaded lenses can be limited by the alteration of lens physical and chemical properties upon the incorporation of therapeutic or non-therapeutic components.

This review outlines advances in the use of pharmaceutical-loaded contact lenses and their relevant characterization methodologies as a potential ocular drug delivery system from 2010 to 2020, while summarizing current gaps and challenges in this field. A key reference point for this review is the relevant ISO standards on contact lenses, relating to the associated characterization methodologies. The content of this review is categorized based on the chemical, physical and mechanical properties of the loaded lens with the shortcomings of such analytical technologies examined.

1. Introduction

In 2020, the World Health Organization (WHO) reported that there are at least 1 billion people worldwide with either vision impairment diseases or blindness [1]. The fact that the eye is such a sophisticated organ, with a high level of protection afforded by various biological barriers, along with limitations from the blinking reflex and the renewal rate of the lachrymal fluid, has meant that controlled ocular drug delivery (ODD) has always been a significant challenge for scientists [2]. Overcoming such challenges is imperative for effective treatment of various vision threatening disorders, such as age-related macular degeneration (AMD), diabetic retinopathy (DR), as well as conditions related to vision quality, such as dry-eye disease (DED).

Treatment of ocular disorders have often relied upon a topical delivery strategy which accounts for 90% of the marketed ophthalmic formulations [3,4]. Such figures are evident in a notable increase in the global eye drops and lubricants market size, which was $15,587 million in 2017 and is expected to reach over $22,625 million in 2025 [5]. However, this approach is often associated with low drug bioavailability [2,6,7]. Where relevant, intravitreal, or periocular routes have been employed [8-10], which, while improving therapeutic bioavailability, can result in a higher number of systemic adverse effects and devastating ocular complications. These were extensively reviewed through the work of Falavarjani and Nguyen [11].

The increased emergence of nanotechnology and nanoscience methods in biopharmaceutical applications has resulted in several investigations into a number of different novel, safe, patient-friendly formulations and drug delivery carriers/techniques [12-16]. Such methods may enhance the efficacy of the ocular drug delivery system (ODDS) while possessing lower toxicity compared to conventional approaches. Extensive reviews have been completed on the use of nanoparticle-drug loaded soft contact lenses (SCLs) in relation to the anatomy of the eye,

* Corresponding author.
E-mail address: danchauthuy.nguyen@postgrad.wit.ie (D.C.T. Nguyen).

https://doi.org/10.1016/j.clae.2021.101487
Received 12 April 2021; Received in revised form 28 June 2021; Accepted 4 July 2021
Available online 3 August 2021

routes of administration and ocular barriers/challenges for the delivery of drugs to anterior and posterior segments, together with various nanocarrier systems for ODD [16-19]. In addition, safety and regulatory considerations [17] for such systems have also been assessed. As such, these aspects are not within the scope of this review.

Controlled and sustained delivery using CLs have been extensively investigated through various *in vitro* [20-22], *in vivo* [23,24], cell viability (e.g. cytotoxicity) [25,26], and *ex vivo* studies [27]. To ensure the performance of the fabricated pharmaceutical-loaded lens, their critical chemical, physical and mechanical properties were examined. These include but not limited to swelling [28], optical transparency [29], ionic permeability [30], modulus [31], refractive index [32], wettability [33], and morphological characterizations [34]. To the best of our knowledge, there are currently no reviews on different characterization methodologies and comparing them to the ISO standards for SCLs. This review provides an insight into various characterization methodologies used in the development of SCLs as an ODD platform. The main reference point of this review centres on the relevant ISO standards [35–38] in the manufacturing of SCLs, while highlighting other critical characterization techniques that currently have no standardised measurement methodologies.

2. Soft contact lens in ocular drug Delivery1

2.1. Classifications of soft contact lens

The type of lens materials, hydrogel and silicone hydrogel (SiHy), not only influence corneal physiology [39], but can also affect the drug loading and release properties [40,41] of the formulated CLs. Therefore, when developed SCL as an ocular drug delivery system (ODDS), choosing an appropriate SCL material to use as a drug delivery vehicle in a specific clinical application is essential.

2.1.1. Hydrogel soft contact lens

Hydrogels are a three-dimensional, hydrophilic, and cross-linked polymeric network [42,43]. They can absorb and retain water or biological fluids, which in turn increases their original mass [44–46]. Hydrogels hold great potential as sustained ocular drug delivery systems (ODDSs). This is mainly due to their ability to swell in an aqueous solvent platform, thus, retaining solvents within a cross-linked gel network, along with other hydrophobic and hydrophilic agents, small molecules and macromolecules [42]. They can also combine with micro- or nanomaterials to enhance ODD, regardless of their solubility characteristics [47].

2.1.2. Silicone hydrogel soft contact lens

According to Nichols and Fisher [48], silicone based hydrogel (SiHy) SCLs occupy the largest sector in the CL market. Silicone-based hydrogels encompass silicone, siloxanes, fluorosiloxanes and their derivative materials [49]. SiHy CLs exhibit almost identical comfort compared to hydrogel materials, while providing substantially higher oxygen and ionic permeability. In addition, SiHy CLs are also known to offer easier handling, reduce conjunctival redness [50], and also exhibit less protein deposition on the lens surface [51].

2.2. Approaches used for the development of pharmaceutical-loaded soft contact lens

Many published studies on pharmaceutical-loaded SCL use SCL-like materials such as hydrogels and SiHy thin films, including the development of novel lens materials, in addition to commercial SCLs available in the market. In order to assess the potential of pharmaceutical-loaded SCLs, various approaches to drug loading into SCLs have been extensively investigated.

2.2.1. Soak and release

A majority of early studies on the incorporation of drugs into SCLs focused on soaking the lenses in drug solution, followed by insertion of the lenses in the eye [52–55]. This approach is widely known as the "soak and release" method, and is the simplest and the cheapest approach to loading pharmaceutical actives into CLs (Fig. 1) [17].

The 'soak and release' approach has been applied successfully in loading ophthalmic drugs, both hydrophilic and hydrophobic, such as moxifloxacin, diclofenac and ketorolac [56], levofloxacin, chlorhexidine and timolol [57], timolol maleate [58], hyaluronic acid [22], vancomycin HCl and polymyxin B sulfate [59].

2.2.2. Molecular imprinting

The concept of molecular imprinting (MI) through the imprinting of organic polymers was first introduced by Wulff's research group in 1972 [60]. Its concept involves the complexation of functional groups on a monomer in a pre-polymerization solution to a suitable template molecule, which is then copolymerized, resulting in highly cross-linked polymers with a defined and fixed arrangement of polymer chains. This is followed by the removal of template molecules to obtain polymers with well-defined cavities, complementary to, and having an affinity for the original target molecule [61] (Fig. 2).

MI technology has been successfully investigated by researchers to increase the drug loading and the drug release time from hydrogel matrices [59,62–64]. There are several factors that can cause the increase in partitioning due to imprinting, including but not limited to temperature, pressure, polarity of polymerization solvent, initiator concentration and degree of crosslinking [65,66]. The importance of the functional monomer to template (M/T) ratio in the optimization of imprinted CLs design was assessed [67–69]. A slower *in vitro* release with 50% timolol being released in three days (2-fold increase in release duration) was observed with an increase in M/T ratios (1:16 to 1:32) for MAA-based systems [67]. A similar study by Alvarez-Lorenzo *et al.* [68] showed imprinted hydrogels prepared with a high M/T (acrylic acid/drug) ratio (1:2 to 1:16) gave controlled release of the antibiotic norfloxacin (2–5 days release duration). Tieppo *et al.* [69] illustrated a dramatic decrease in the release rate of sodium diclofenac (from 11.72 μg/h to 6.75 μg/h during the first 48 h) from imprinted CLs by increasing M/T ratio up to 10.5, where zero-order release was achieved. This strategy was applied in the treatment of DED (dry eye diseases) using 120 kDa hydroxypropyl methylcellulose (HPMC). The release duration was extended up to 60 days with a rate of 16 μg/day, and was found to depend essentially on the M/T ratio [70].

2.2.3. Nanoparticle-laden contact lens

Nanoparticle-loaded SCLs were studied as nanocarriers to extend drug release in the eye [28,32,71–73]. This technique is based on the ability of NPs (e.g., polymeric NPs [74], lipid NPs, liposomes [75], etc.) to encapsulate or entrap drug and control its release rate from CLs. In this delivery system, the drug may first diffuse through the NPs to reach the CL matrix, and consequently, it moves through the hydrogel matrix to reach the tissue as illustrated in Fig. 3 [31].

One of the commonly used techniques is direct-entrapment of drug-loaded NPs into the lens matrix [22,71,76]. After the preparation of drug-loaded NPs, they are dispersed into the monomer mixture followed by polymerization to form a NP-loaded CL [31,77]. To load the prepared NPs by this method, a specified mass fraction of NPs was added to the pre-polymerized monomer mixture before the polymerization process. As an example, dexamethasone sodium phosphate (DXP)-loaded chitosan (CS) NPs laden pHEMA lenses were successfully prepared using this technique [71]. Similar lens diameters of around 10 mm and lens centre thickness of 50 μm were obtained for both types of pHEMA lenses. The addition of drug-loaded CS NPs did not significantly affect the optical transparency of the lenses (95–98% transmittance relative to the unloaded CLs). The surfaces of unloaded and NP-loaded CLs were assessed by SEM to have a similar morphology to each other [71].

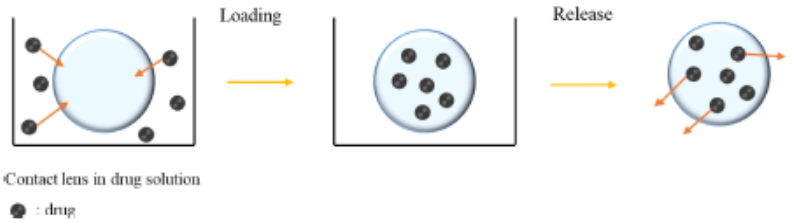

Fig. 1. Schematic representation of the "soak and release" method of integrating drug into a contact lens.

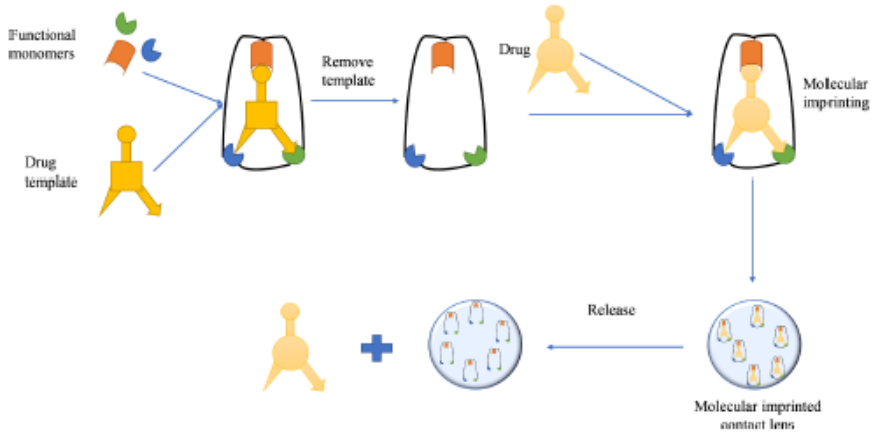

Fig. 2. Schematic illustration of molecular imprinting contact lens.

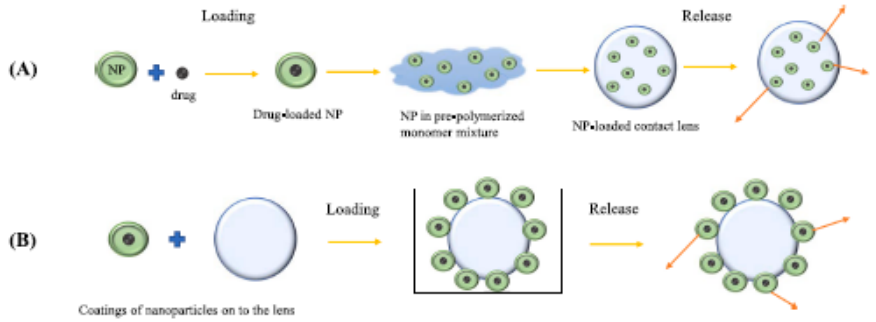

Fig. 3. Schematic diagram of drug release from nanoparticle-laden contact lens by (A) direct incorporation of nanoparticles in lens pre-polymerization mixture, and (B) coating nanoparticles onto the lens.

Alternatively, a different approach was previously used in a NP-laden SCLs study including the addition of both surfactant and drugs into the monomer mixture to create micelles throughout polymerization [73,78]. In order to overcome the burst release of drugs and the limited drug loading capacity, Mun *et al.* [73] investigated a cholesterol-hyaluronate (C-HA) micelle-loaded hydrogel CL (pHEMA) for the delivery of cyclosporine. The diameter of C-HA micelle was determined to be 290 ± 35.95 nm with a negative charge of −17.4 ± 3 mV. The drug-loaded C-HA micelle was then incorporated into the CL mixture prior to curing. The developed formulation provided a slight decrease in light transmittance (95% vs 90% for non-loaded- and loaded-micelle lenses, respectively), and an increase in equilibrium water content (39% vs 43% for non-loaded- and loaded-micelle lenses, respectively). A significant improvement in lens wettability (48.07° vs 39.6° for non-loaded and loaded-micelle lenses, respectively) and mechanical strength (C-HA micelle-loaded pHEMA lens was more stretchable than blank pHEMA lens) for the drug-loaded micelle lens was obtained. Cyclosporine was shown to be released in a controlled manner, with 50% of drug released from the lens over 12 days through *in vitro* study in this particular model [73].

2.3. ISO requirements for pharmaceutical-loaded contact lenses

In order for particular SCLs to be feasible and acceptable in the commercial market, they must meet several important requirements in line with ISO-18369:2017 standards (4 parts) [35–38]. The requirements/tolerances for some of lens' critical properties of a commercial SCL from the ISO standards are summarized in Table 1.

Table 2 below summarizes several types of lenses used in the study of ODD of therapeutic lenses and the characterization methodologies used in each study compared to those standards illustrated in Table 1. It should be noted that only the characterization methodologies within the scope of this review are mentioned in this table.

3. Characterization of pharmaceutical-laden soft contact lens

3.1. Chemical characterization of pharmaceutical-laden soft contact lens

3.1.1. Optical transparency

One of the most essential parameters in SCLs is their optical transparency. This spectral transmittance property is especially significant for visual performance [85]. This property is generally expressed as the percentage transmission of the visible electromagnetic spectrum. As extensively reviewed by Efron and Maldonado-Codina on the development of contact lenses [86], in order for a hydrogel material to be useful as a CL material, it must be able to transmit over 90% of light in the visible spectrum. Due to the importance of this property, almost all research work carried out in the area of drug delivery CLs includes this parameter.

Drug-loaded NPs loaded into SCLs have generally been shown to be able to release drug at an extended rate by tailoring the drug concentration [29]. However, the particles could potentially reduce the transparent behavior of the lens, making it one of the main limitations for particle loaded SCLs. The optical clarity of the NP-loaded SCLs was generally determined by measuring transmittance spectra in the range from 200 to 700 nm and scanned at 1 nm intervals, as extensively carried out in several studies [28,29,32,56,57,87–89].

Kapoor *et al.* [29] investigated the effect of drug (cyclosporine A) concentration on the transparency of 200 μm thick pHEMA hydrogels. The results indicated that the optical clarity was maintained (>95%) if the drug loading was<0.4% (close to the limit of drug solubility in pHEMA). As the drug concentration increased, it could be observed that the gels turned hazy and almost opaque [29], resulting in a reduction in lens light transmission. A study carried out by Paradiso *et al.* [90] showed that a liposome coating layer (DMPC and DPMC + CHOL, where DMPC is 1,2-dimyristol-*sn*-glycero-3-phosphocholine and CHOL is cholesterol) on top of a hydrogel, did not substantially alter their optical transparency (values were all above 95%). This was due to the small size of liposomes, with an average size of 103 ± 8 nm. The incorporation of NPs could influence the lens' ability to transmit light significantly because the nanosized particles could diffract and scatter the incident light. Several studies indicated that the transparency of the CLs was not affected when the NP size was below 180 nm [71,90,91]. However, NPs of size around 300 nm were shown to reduce the lens optical clarity. For example, the incorporation of 0.2 g and 0.4 g of drug-loaded NPs of size 294.5 ± 1.8 nm decreased the pHEMA hydrogels transmission from 94.5% to 86.2% and 83.1%, respectively [31]. As stated in Table 1, ISO tolerance for light transmission is ± 5% absolute value, which is 94.5% in this case, hence, the incorporation of drug-loaded NPs at those concentrations resulted in an unacceptable lens optical clarity.

Table 1
Tolerances for some of lens' critical properties from the relevant ISO standard [36].

ISO standard number: 18369-2:2017 Lens' property	Requirements/Tolerance
Back optic zone radius/base curve equivalent/ equivalent posterior radius of curvature	± 0.20 mm
Sagittal depth	± 0.05 mm absolute (control value)
Total diameter	± 0.20 mm absolute (control value)
Centre thickness (t_C)	Thickness > 0.10 mm: ±(0.015 mm + 0.05t_C)Thickness ≤ 0.10 mm: ±(0.010 mm + 0.10t_C)
Spherical Power	Power ≤ 10.00 D: ± 0.25 D10.00 D < Power < 20.00 D: ± 0.50 DPower > 20.00 D: ± 1.00 D
Spectral transmittance in the visible region	± 5% absolute (control value)
Refractive index	± 0.005 absolute (control value)
Water content	± 2% absolute (control value)
Oxygen permeability	± 20% absolute (control value)

3.1.2. Equilibrium water content

The ability of the hydrogel or SiHy to bind water in its equilibrium state is called the equilibrium water content (EWC) [92]. Water content is defined by ISO 18369–4:2017 standard as the mass fraction present in a hydrated material, which has been fully equilibrated at room temperature [37]. This value indicates the comfort of SCLs and is also closely related to their dehydration [93]. SCL dehydration can lead to several problems, such as: changes in lens parameters (e.g., diameter, sagittal depth and base curve) [94,95], and changes in oxygen [96,97] and ionic permeability [98]. The amount of dehydration and the time to reach equilibrium are influenced by several elements, including: the maximum water content of the polymer [99,100], the lens thickness [94,98,99,101], the temperature and relative humidity [95], and also the volume and tonicity (i.e. salt-uptake ability of a solution) of the wearers' tears [102,103].

The standard method for determining the water content of tested specimens is a gravimetric method utilizing loss on drying using an oven [38,104]. Another approach to measuring this property is refractometry, which was also used in a number of studies [92,105,106].

The gravimetric method is based on the weight difference between the dry lens after removing from the mold versus the lens after hydration in a specified aqueous solution for a specific time. This appears to be the most commonly used method for the determination of EWC in work done in ocular drug delivery with the use of SCLs [28,56,76]. As illustrated in Maulvi *et al.* [58], dry hydrogel samples (composed of HEMA, NVP, EGDMA, TRIS, DMA and Irgacure®) were weighed at the beginning (W_D). They were then immersed in a chosen aqueous medium in individual containers at a controlled temperature. At a specified time, the samples were removed from the medium and carefully blotted with absorbent paper and immediately weighed (W_W). The EWC value can then be calculated according to Equation 3.1:

$$\%\mathrm{EWC} = \frac{W_w - W_D}{W_w} \mathrm{x}\, 100$$

Although there are numerous studies on lens equilibrium water content using this technique, it is worth noting that there are limitations associated to this technique. Weighing dry lenses after removing from the mould can lead to the risk of ignoring uncured material that will be extracted as the lens is hydrated, extracted, and sterilized (as in real manufacturing processes). Furthermore, the term "carefully blotted" used in this technique would also introduce significant human error.

For the treatment of glaucoma, Dessi *et al.* [28] investigated the co-delivery of timolol and hyaluronic acid (HA) from semi-circular ring-implanted CLs (i.e. the drug-loaded rings were implanted separately within the periphery of the lenses), which were made of 66.9% HEMA, 0.05% EGDMA, 31% DMA, 0.01% TRIS, 0.1% NVP and 0.05% Irgacure D. The lens was soaked in a simulated tear fluid for 24 h prior to the test. An insignificant reduction in the percentage of equilibrium water content between the soaked timolol and HA lens (92.54% ± 3.54%), and the control lens (92.45% ± 3.76%) was observed. This observation suggested that both the soaked timolol base and HA did not make an impact

Table 2
Various drug loading methodologies for therapeutic contact lens and the associated physical and chemical lens characterization methodologies in comparison to the relevant ISO standards[1].

Lens type	Principal monomers	Therapeutic agent	Lens physical, chemical, and mechanical characterization	In-line with ISO standard?	Drug loading approach	Ref.
11 types of hydrogel and SiHy commercial lenses	N/A	Pirfinedone	No physical, chemical, and mechanical tests were carried out	Not demonstrated	Soak and release	[24]
SiHy	HEMA and MPTS	Gatifloxacin and Moxifloxacin	No physical, chemical, and mechanical tests were carried out	Not demonstrated		[79]
Intraocular lens (CI26Y), SiHy (Definitive 50)	HEMA and MMA (CI26Y) Definitive 50: Contamac proprietary SiHy	Moxifloxacin, diclofenac and ketorolac	Water content, optical transparency, tensile strength	Yes: water content and optical clarity properties.		[56]
SiHy (ACUVUE OASYS and ACUVUE TruEye) lenses (Diopter −3.50)	HEMA, DMA, PDMS, PEG and PVP	Bimatoprost and latanoprostVitamin E	Water content, optical transparency, and ion permeability	Yes: water content and optical clarity properties.		[80]
Hydrogel	HEMA	Vancomycin HCl and polymyxin B sulfate	Water content, optical transparency, and oxygen permeability	Yes: water content, optical clarity and oxygen permeability properties.		[59]
Hydrogel	HEMA	Triamcinolone acetonide	Optical transparency, water content, morphology	Yes: water content and optical clarity properties.		[34]
SiHy	HEMA, NVP, and TRIS	Betaxolol hydrochloride	Water content, optical transparency, ionic and oxygen permeability	Yes: water content, optical clarity and oxygen permeability properties.		[72]
Hydrogel	HEMA	Dexametha-sone 21-phosphate disodium salt	Water content, optical transparency, morphology	Yes: water content and optical clarity properties.	Nano-particle-loaded contact lens	[71]
Hydrogel	HEMA	Cyclosporine	Water content, optical transparency	Yes: water content and optical clarity properties.		[81]
Implant pHEMA lens	HEMA, MAA, NVP, DMA and TRIS	Timolol maleate and HA	Optical transparency, water content, morphology	Yes: water content and optical clarity properties.		[28]
Hydrogel	HEMA, PEG-DA and NVP	Loteprednol etabonate	Water content, optical transparency, ionic and oxygen permeability, tensile strength	Yes: water content, optical clarity and oxygen permeability properties.		[76]
Hydrogel	HEMA and MAA	Prednisolone	Water content, wettability, optical transparency, tensile strength	Yes: water content and optical clarity properties.		[31]
Hydrogel	HPMC	Norfloxacin	No physical, chemical and mechanical tests were carried out	Not demonstrated		[82]
Hydrogel	HEMA and MAA	Timolol maleate	Water content, wettability, optical transparency, tensile strength, oxygen permeability	Yes: water content, optical clarity and oxygen permeability properties.	Molecular imprinting	[83]
Hydrogel	HEMA, DEAEM and PEG200DMA	Diclofenac sodium	Water content, optical transparency, tensile strength	Yes: water content and optical clarity properties.		[69]
SiHy (Lotrafilcon B)	TRIS and DMA	Hydroxypropyl methylcellulose	Optical transparency, water content, tensile strength	Yes: water content and optical clarity properties.		[70]
SiHy	HEMA, TRIS, EGDMA, acrylic acid, and PVP	Ciprofloxacin-HCl	Water content, optical transparency, center thickness and surface wettability	Yes: water content, optical clarity properties and center thickness.		[84]

[1] MA: methacrylic acid, MMA: methyl methacrylate, MAA: allyl methacrylate, DMA: N,N-dimethylacrylamide, PDMS: polydimethylsiloxane, TPVC: tris-(trimethylsiloxysilyl) propylvinyl carbamate, MPTS: 3-methacryloxypropyltris-(trimethylsiloxy)silane, PEG: polyethylene glycol, PEG-DA: polyethylene glycol diacrylate, DEAEM: diethylaminoethyl methacrylate, PEG200DMA: polyethylene glycol 200 dimethacrylate.

on the swelling behavior of the lens. On the other hand, an increase in swelling was observed in the case of HA-loaded implants (95.49% ± 6.78%) due to the hydrophilic nature of HA [28]. However, with the high standard deviations in the water content values in all cases, the modified lenses in this study exhibited swelling behaviour within the tolerance stated in the ISO standard (Table 1). Topete *et al.* [56] also studied this perspective of hydrogels to examine the impact of the temperature (4 and 60 °C) on the material in the absence of drug. Two types of lenses were used in this study, including CI26Y (a hydrophilic materials composed of hydroxyethyl methacrylate and methyl methacrylate) and Definitive 50 (a SiHy lens). The data revealed a decline in swelling capacity with an increase in temperature, although all samples showed a light transmittance of above 90%. This phenomenon can be explained by unfavorable hydrogen bonding between the water and the polymer compared to polymer–polymer interactions at higher temperature, and is commonly known as a property of negative thermosensitive hydrogels, as reviewed by Ruel-Gariepy *et al.* [107].

The impact of surfactant chain length (sodium caprylate C_8 (SC), Tween 20 and Tween 80) and the molecular weight of block copolymers (Pluronic F68 and Pluronic F127) was examined to study their effect on release kinetics from cyclosporine-loaded microemulsion-laden hydrogel lens (composed of HEMA, EGDMA, MAA and Darocur®) [81]. Upon direct loading of cyclosporine into CL, the %EWC was substantially decreased, from 38.9% ± 2.6% (control lens) to 72.9% ± 4.1%, and hence, is outside the ISO tolerance for SCL water content (Table 1), which was attributed to the hydrophobic nature of the drug. Moreover, the CL also lost their transparent behavior and appeared opaque due to the precipitation of the drug. Upon the incorporation of microemulsion, it could be observed that the longer chain surfactant Tween 80 gave a significantly higher %swelling when compared to the shorter ones (Tween 20 and SC), which were 75%, 90% and 110% for PL127-SC, -T20 and −T80, respectively. This study also showed that the microemulsion using PL127 provided a higher stability, hence, higher %EWC comparing to PL68 (e.g., 77% vs 90%, corresponded to PL68-T20 and PL127-T20) [81]. No significant effects on the swelling property of the SCLs was observed with the presence of hydrophilic drugs (moxifloxacin HCl and HA) [108]. Also, the HA loaded SCL also gave a similar %EWC in comparison to the control lens. However, a noticeable reduction in this value was seen for moxifloxacin HCl loaded implants [108]. It was suggested that the monomer composition should be modified in order to increase the %EWC of the implant CLs.

3.1.3. Refractive index

Besides optical transparency, ideal hydrogel materials used in the manufacturing of SLCs must provide a refractive index (RI) or index of refraction that is similar to that of the cornea (i.e. a RI of ~ 1.37) [86]. ISO 18369–1:2017 [35] states that RI is a "ratio of the speed of light in a vacuum to the speed of that same light in a material". A higher RI material can allow for a decrease in lens thickness and thus, improve wearing comfort [109]. Not only is it important from the optical point of view, but it is also an essential parameter from a physiological perspective. This is due to the fact that RI is a measurable value that reflects the alterations in the EWC of polymers [105]. The quoted reference values for RI for commercial hydrogel and SiHy CLs, which were determined in Varikooty *et al.* [109] and Lira *et al.* [110], were determined to be in the range of 1.40 to 1.43.

According to ISO 18369-4:2017 [38], the RI of the CL material should be measured at either 589 nm (sodium D-line) or at 546.1 nm (mercury E-line). There are many methodologies involved in the determination of RI based on the lens shape and measuring conditions (dry, blotted, or immersed). The technique of determining the RI of the hydrogel materials is also noted under this ISO standard, which uses the calibrated Abbe refractometer or an equivalent instrument at room temperature.

The RI of the blank silicone-based TRIS/NVP/HEMA hydrogel versus coated silicone-based hydrogel used in diclofenac sodium salt-loaded SCLs was investigated using an Abbe refractometer by Silva *et al* [32]. Three types of coatings, including ALG (sodium alginate), PLL (polylysine) hydrobromide), EDC (1-ethyl-3-(3-dimethylaminopropyl) carbodiimide hydrochloride), and HA (hyaluronic acid), were deposited on the surface of the silicone-based hydrogel in this study. The RI values of uncoated (1.417 ± 0.020) and coated samples (1.411 ± 0.003 – 1.418 ± 0.001) showed no statistically significant differences. However, the test was carried out at 37 °C (body temperature) instead of room temperature.

Even though the RI is essential and one of the properties that commercial SCLs should be evaluated for according to the ISO 18369–1:2017 standard [35], to the best of the authors' knowledge, this property has not been investigated in therapeutic-loaded lens research in the last 10 years.

3.1.4. Oxygen permeability

Most cornea oxygen is derived from the atmosphere. Therefore, in order to sustain corneal integrity and provide sufficient defense against infection [76], SCL materials are generally oxygen permeable (D_k) due to their high water content, which is a key factor in governing the clinical success of such materials [111,112]. As stated in ISO 18369–1:2017 oxygen permeability (D_k) is defined as the "oxygen flux (j) under specified conditions through contact lens material of unit thickness when subjected to unit pressure difference". The ISO unit of D_k is 10^{-11} (cm^2/s)[$mlO_2/(ml \times hPa)$], and is called the "D_k unit" [35]. "D" is the diffusion coefficient of the material, whereas "k" represents the solubility coefficient. D_k is an intrinsic physical property of a material, which demonstrates the rate of oxygen flow through that material, as defined by Lebow and Campbell-Burns [113]. The D_k value of a material is directly dependent on its water content. As an example, a D_k value of 8 D_k was recorded for Softlens 04 (38.6% water content), while for a Duragel 75 lens that has 75% water content, the oxygen permeability value was determined to be 40 D_k [114]. This observation was also in agreement with a study carried out by Young and Benjamin [115]. Their work investigated the relationship between material water content and D_k of 35 conventional hydrogel materials based on the general format of ANSI Z80.20:1998 and ISO 9913–1:1996. Silicone hydrogel CLs (SiHys), on the other hand, were noted to have an inverse relationship between water content and D_k (at 35 °C) as cited by Efron *et al.* [116]. Focus Night and Day SiHys of water content 23 ± 3.2% provided 162.0 ± 9.8 D_k. A D_k value of 75.2 ± 9.8 D_k was recorded for Acuvue Advance SiHys that had 46.5 ± 1.1% water content.

According to ISO 18369-4:2017 [38], the two main methodologies for determining the D_k value are the polarographic method [117] and the coulometric method. The oxygen permeability of olopatadine-loaded (used in the treatment of the allergic conjunctivitis) biomimetic acrylic hydrogels was investigated by immersing the discs in 0.9% NaCl solution for 48 h [117]. The oxygen permeability was measured using a Createch Permeometer model 210 T (Redher Development Co., Castro Valley, CA, USA) at 100% humidity at room temperature. Biomimetic acrylic hydrogel CL, a lens designed to mimic the active site of the H_1-receptor (for which olopatadine acts as a selective antagonist), was synthesized by combining the selected monomers and applying a molecular imprinting technique. In comparison to the control hydrogel materials, non-imprinted and imprinted biomimetic olopatadine-eluted CLs showed no significant difference with lenses all within the typical values of HEMA-based lenses (45–56 D_k) [117].

There are various parameters associated with the successful measurement of this property after the insertion of CLs for a short period of time. Such parameters include the reservoir of oxygen in the polarographic electrode [118,119]; the material and thickness of the membrane [118,120,121]; the duration of exposure leading to the reduction of oxygen tension (i.e. the partial pressure of the dissolved oxygen) [122,123]; the time between exposure and measurement [118,124]; the surrounding corneal environment (temperature [125] and oxygen tension [126]); pH, osmolarity and buffering condition of tear [112]; corneal conditions (location [127], thickness [118,127] and health [128]). The acceptable values for oxygen transmissivity of SCLs are around 25 D_k units for open eyes and 75 up to 200 D_k units for closed eyes, even though the results may vary slightly depending on the measurement approach [59,76,115,129]. These are recommended figures to prevent corneal edema while providing sufficient oxygen to the cornea.

Nasr *et al.* [76] measured the D_k of hydrogels with and without drug-loading. The concentration of oxygen was measured using an OX-TRAN® Model 2/21 from Mocon. At a 200 μm thickness, the hydrogel with 7.5% drug loading gave a D_k of 28.3 ± 1.3 [(10^{-11} (cm^2/s).(ml O_2/(ml mm Hg)] comparing to 27.4 ± 2.2 [(10^{-11} (cm^2/s).(ml O_2/(ml mm Hg)] for the control lens[76]. As outlined in Table 1, the ISO tolerance for oxygen permeability is within 20% of the control value, hence, the Dk value of drug-loaded hydrogel in this study was in an acceptable range.

The oxygen permeability (D_k) of various hydrogel materials swollen in 0.9% NaCl solution were studied by Malakooti *et al.* [59]. They utilized a Createch permeometer (201 T, Redher Development Co., USA) fitted with a flat polarographic cell, which was in 100% relative humidity condition, to measure D_k values of the different hydrogels [112,130]. Three different hydrogels within this study had the D_k values in the range of 65 to 80 Barrer [59]. The oxygen permeability of multilayered SCLs versus the control lens were investigated by Zhu *et al.* [72]. Using a polarographic dissolved oxygen sensor (Hanna Instruments, HI 9143, Temse, Belgium), the experiment was carried out using a horizontal diffusion cell [40,76] and the amount of oxygen in a receiver chamber was recorded every 60 s *in situ*. The calculated D_k of the inner layer embedded CLs declined noticeably when compared to the pure CLs (~24 vs. ~ 40 Barrer). This difference is significant since it exceeds 20% tolerance in comparison to the control lens as stated in ISO standard. Hence, for further development, materials with higher OP would be a better choice.

Oxygen transmissibility (D_k/t) defines the oxygen permeability (D_k) of a material since it relates to a specific lens design, which has a thickness (t) [113]. Based on the study of Holden and Mertz, physiologically and ideally, the SCL when worn daily should not cause corneal swelling which results in lens discomfort [114]. As such, to minimize SCL's impact on the cornea, the oxygen transmissibility of a SCL should be at 24.1 ± 2.7 × 10^{-9} units.

3.1.5. Fluid and ionic permeability

It is essential to obtain an adequate ion permeability (D_{ion}) in SCLs to

ensure the formation of a fluid hydrodynamic boundary layer, which in turn, decreases the direct abrasion between the lens and the eye [76]. Adequate lens movement can only be maintained when there is a minimum level of ionic permeability. The permeation of ions in polymeric membranes encompasses the dissociation of ion from salt. As such, it includes the movement of anion and cation to the aqueous medium, and eventually, spreading of the ions in the confined water within the polymer matrix [131]. This property is vital since it allows the post lens tear film (PLTF) to reform between blinks, and for metabolic waste removal [132], hence, reducing the possibility of the elastic SCLs from binding to the cornea [86]. A major part of the tear film is known to contain sodium ions. As cited by Pozuelo *et al.* [131], for extended wear SCLs, the effective ion diffusivity (D_{ion}) should be $>1.5 \times 10^{-6}$ mm^2/min to ensure homeostasis of ion concentration between the lens and cornea. As such, the lens would be free from abrasion and friction [131].

Ionic permeability of SCLs were generally measured using a modified conductivity meter in several studies [22,32,131,133]. As an example, the hydrated lens was attached to the bottom of the donor tube, which was filled with 24 mL of saline solution (130 mM). This was then placed on top of an acceptor compartment that had 32 mL of deionized water. After securing the position of the two cells, they were placed horizontally. The conductivity probe was placed inside the acceptor part to measure the conductivity over a specified time. This whole set-up (except for the conductivity meter) was placed in an oven at 36 °C [32]. The data was then calculated to give the D_{ion} based on the concentration of Na^+ ions that had travelled through the lens into the water in a specific time interval [22,131].

Based on the methodology cited by Peng *et al.* [133], work done by Maulvi *et al.* [30] demonstrated a noticeable reduction in D_{ion} with the NP-laden ring implant in hydrogel CLs and also with the increase in ratios of timolol to ethyl cellulose. This could be explained by the presence of hydrophobic ethyl cellulose NPs. In addition, it also pointed out that the ion flux diffusion coefficients would decrease in the presence of NPs. However, since the D_{ion} value was still higher than $1.5x10^{-6}$ mm^2/min, the developed modified lens would be still fit for use [30]. Nasr *et al.* also studied the impact on ionic permeability of drug-loaded NPs loaded hydrogel [76]. The D_{ion} values for blank CLs and CLs with 7.5% NPs loaded were calculated to be 1.71×10^{-3} and 2.83×10^{-3} mm^2/min, which were both larger than the critical value as mentioned above. Their study also stated that following an increase in water uptake, the salt diffusion coefficient would also increase. Ionic permeability of two hydrogels for drug release was studied by Paradiso *et al.* [88]. Due to higher swelling capacity, the TRIS/NVP/HEMA hydrogel had a higher ionic permeability than HEMA/PVP hydrogel (5×10^{-7} vs. $8 \times 10^{-8} \pm 2 \times 10^{-8}$ cm^2/s). The impact on lens (ACUVUE® OASYS®) ion permeability post-vitamin E and drug loading was investigated in a work carried out by Sekar *et al.* [80]. Upon the incorporation of vitamin E, a minor decrease in this value was observed in experiments (e.g., 0.65 ± 0.04 vs $0.50 \pm 0.1 \times 10^{-4}$ mm^2/min for control lens and lens with 10% vitamin E loading, respectively).

While ionic permeability is an important parameter of CL that directly correlated to comfort and was quoted in several studies in the development of pharmaceutical-loaded CLs, there are currently no ISO standards on both the measurement method and tolerance of this property.

3.2. Physical characterisation of pharmaceutical-laden soft contact lens

3.2.1. Wettability

The most commonly used methodology to gauge the wettability of a solid surface is to determine the contact angle (CA). By assessing the CA, the performance of the CL *in vivo* can be predicted [134]. As such, the lower the CA, the better the wetting ability of the material over a substrate, and hence, the higher the stability of the tear film spread over the lens surface [134,135]. CA is calculated by Young's equation as shown Equation 3.2 [136,137]:

$$\cos\theta_c = \frac{\gamma_{sv} - \gamma_{sl}}{\gamma_{lv}}$$

where θ_c is the equilibrium CA, γ is the interfacial tension/energy between the two respective phases (s = solid, l = liquid, v = vapor). The expression in parenthesis characterizes the propensity of a liquid attraction toward a solid, and is known as the adhesion tension/energy [136]. CAs may be categorized as advancing or receding, and static or dynamic [136].

As defined in ISO 18369-1:2017 [35]: "Contact angle (CA) formed by an intersection of the tangents at the solid–liquid-gaseous interface comprised of a contact lens material, a known liquid, and air, under specified conditions". While advancing CA is "created when the liquid has been moving along a solid surface", receding CA "formed when the liquid has been moving away from an area of the solid surface which was previously wet".

Wettability of the ocular surface is said to be the main influence for the viability of ocular tissues [138]. In the case of CLs, it refers to the lens surface wetting behavior [139,140]. As cited by Lin *et al.* [134], wettability is defined by a phenomenon that leads to a formation of an adhesive force between a solid and a liquid, when a liquid covers a solid surface. It can also be described as the ability of the solid to cause the liquid on it to spread, while maintaining a stable liquid film. In addition, Cheng *et al.* [140] noted that the wettability of CLs can be referred to as the competition between two fluid phases to reside adjacent to the solid surface. Wettability is a crucial characteristic since it infers the spreading ability of the tear film along the material surface, which can affect the tribology of the SCLs [135]. The tribology property of the SCLs will be defined and discussed in Section 3.2.4. Since this property is fundamentally linked to comfort and performance throughout CL wear, the CL industry and scientists have paid considerable attention and effort to developing a highly wettable SCL surface in an ocular environment. CL wettability has been measured in many ways: sessile drop [33], captive bubble [88], Wilhelmy plate [141], with variations of the above approaches also reported.

The sessile drop (SD) technique is one of the most commonly used methods to determine lens wettability (Fig. 4) [33,87,142]. It is an optical-based tensiometry technique that involves the placement of a liquid droplet onto a substrate of interest (e.g., CL). The droplet can be formed by using a computer-controlled syringe, which will give a reproducible chosen test volume. A test specimen is placed on a movable stage that is directly below the syringe. Images or videos of the experiment are recorded simultaneously by a camera focused on the stage over specified periods from which the CA can be established. The sample must be dried in order to be tested using this approach [139].

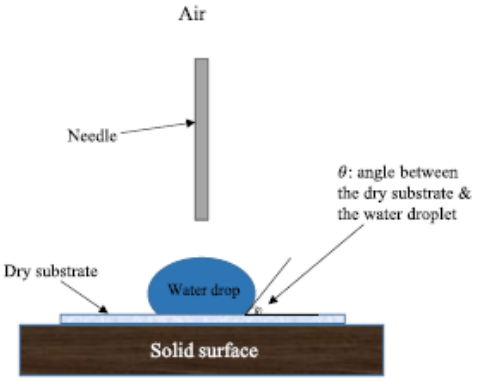

Fig. 4. Schematic diagram illustrating the sessile drop method for measuring CA.

A different work of Silva *et al.* [87] confirmed the high hydrophobicity of dry silicone-based hydrogels composed of TRIS, NVP and HEMA (θ_{water} close to 90°). θ_{water} is the angle between the dry substrate and the water droplet as illustrated in Fig. 4. This behaviour of the hydrogel is reversed to become more hydrophilic in the hydrated state due to the presence of water in the structure (θ_{water} close to 40°). In addition, this study also demonstrated that when compared to a HEMA/PVP hydrogel (72.7° ± 0.5°), TRIS/NVP/HEMA SiHy (87.5° ± 0.4°) showed a more noticeable hydrophilicity [87]. This is because of the structural arrangements of the silicon hydrophobic groups to an innermost position, allowing the hydrophilic groups to be arranged on the surface of the SiHys [142]. The advancing contact angle of ciprofloxacin-HCl laden SiHy lens through molecular imprinting approach was investigated by Hui *et al.* [84]. A reduction in CA values of imprinted lenses in comparison to control lens was observed. As an example, the CA for the control lens was 94.6 ± 1.5°, while a value of 77.4 ± 2.0° was measured for 4:1 imprinted lens (4:1 mol of acrylic acid: ciprofloxacin HCl). However, it should be noted that these values are all in line with other non-surface treated SiHys that incorporate an internal wetting agent.

The use of chitosan to create a nanocoating layer on a CL was investigated by Mehta *et al.* [33]. Using a Thetalite TL100 CA goniometer, and OneAttention software, the wettability of this type of lens was quantitatively analysed. The introduction of a hydrophilic excipient, borneal acted as a surface active agent, which lowered the contact angle (126.27° to 71.5°) while improving the spreadability of the liquid droplet. Mehta *et al.* [33] noted that upon the incorporation of solid particles of chitosan, the CA of the tested materials increased (from 71.5° to around 91°- 96°). The increase in CA value was postulated to be due to the incorporation of CS, which potentially acted as an additional barrier. This would fill pores between the polymeric matrix and CS. Hence, the water molecules have to penetrate through both lens polymeric matrix and CS, resulting in an increase in lens CA values.

The SD approach is not ideal for hydrogel materials as the sample needs to be blotted and the approach suffers from dehydration issues and lack of reproducibility [139]. With minimal preparation required and minimal evaporation effects, while providing dynamic contact angle data, the captive bubble (CB) technique, is more advantageous when it comes to hydrogels especially [139] (Fig. 5).

The captive bubble approach can also be referred to as an inverted sessile drop technique. With this method, the tested material is immersed in a probe fluid (generally water), and air or other immiscible liquid is dosed from a needle to form the droplet. As the air bubble comes into contact with the surface of the tested object, a solid–liquid interface is created. By placing an air bubble onto the lens surface immersed in water using a curved needle/syringe, the CA of each sample is measured. Similar to the SD technique, images of the formed CA at this interface can be captured and measured using similar instrumentation and software.

The aforementioned work carried out by Silva *et al.* [32] in Section 3.1.3, on antibacterial layer-by-layer coated SCLs, investigated the wettability of the coated and uncoated samples, drug-loaded and control lens. Due to the rearrangement of the hydrophilic groups of HEMA and NVP, the uncoated TRIS/NVP/HEMA sample had a lower CA [88]. There were no substantial effects on the CA of drug-loaded samples. The study indicated the influences of the coated layers, which showed that the lowest CA on drug-loaded samples was for those coated with ALG/PLL (EDC)//HA, with θ_{water} around 30° [32]. The wettability of the hydrated unloaded and drug-loaded CL (levofloxacin and chlorhexidine), with and without the addition of vitamin E (20%) was studied through the work of Paradiso *et al.* [89]. There was no considerable effect on the CA of the lens before and after the incorporation of drugs and/or vitamin E, with θ_{water} in a range between 30° and 40° [89].

In the Wilhelmy plate technique [141,143], contact angle of the lens is assessed by alternatively immersing and withdrawing the sample from the test liquid. A micro-balance is used to determine the weight of the sample as it is moving in and out of the liquid (Fig. 6). In order to use this technique in studying hydrogel materials, some studies have attached a small weight to the hydrogel [144] or mounted the sample on the force sensor [145,146] before testing to increase dimensional stability of intact hydrogel lens upon immersion into a fluid.

Due to the complexity of this method in measuring the contact angle of materials, to the best of the authors' knowledge, within the last 10 years, there are no studies on the wettability of the therapeutic lens using this technique.

As mentioned earlier in this section, CL wettability represents CL surface properties and is a critical factor that can influence the comfort of the lens. A good wetting surface is needed to prevent changes to the under surface of the eyelid as it blinks over the CL. Further, wettability also has an impact on lens deposition [147]. Hence, it is essential to accurately determine the contact angle of the lens, both unmodified and modified lenses, in order to further study the impact of the loaded materials on lens properties.

Although CAs are quoted in the literature of CL manufacturers and research journals, there is currently no accepted ISO standard for this characteristic [134]. This could be due to two main reasons: unless the exact measurement conditions (the liquid used, the tested temperature and also the employed method) are known with comparative data, the values are said to be meaningless [139]; since this technique relies mainly on image processing, it possesses inherent errors due to optical limitations, which results in uncertainties in the determination of the baseline that can lead to errors in the measured CA [140]. No available standardised methodology for the measurement of CA of the lens has contributed to several different published data sets on a specific material that are not easily comparable between studies as reviewed by Campbell *et al.* [135]. Therefore, for the data from this test to be valid and quoted in future studies, further work is required to establish a standard method for the measurement of lens wettability.

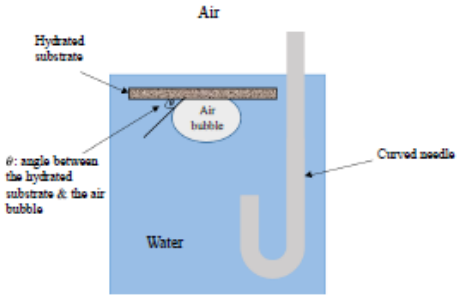

Fig. 5. Schematic diagram illustrating the captive bubble method to measure CA.

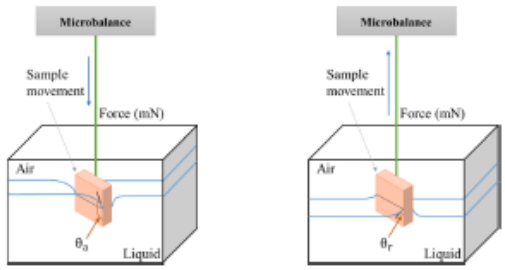

Fig. 6. Schematic representation of the Wilhelmy plate technique (where: θ_a and θ_r are the advancing and receding contact angles, respectively).

3.2.2. Morphological characterisation

As mentioned by Dumbleton *et al.* [149], roughly 50% of 140 million CL wearers worldwide have reported having adverse ocular dryness, which is the main cause of CL discomfort. There are several properties related to SCL comfort, such as water content, oxygen permeability, lubricity, and surface roughness. In several studies, the surface of the lens after the incorporation of drug-loaded NPs was investigated using various microscopic techniques including scanning electron microscopy (SEM), transmission electron microscopy (TEM) and atomic force microscopy (AFM) [57,87,88].

To observe the changes on the SCLs' surface upon the incorporation of water into the monomer mixture, SEM images of both dry lens (prepared by thermal and photochemical polymerization) with and without different amounts of water were analysed by Garcia-Millan *et al.* [34]. It could be seen that samples, which contained 20% and 40% water showed pores on their surfaces compared to smooth surfaces on those without water incorporation. The formation of pores was attributed to the formation of water drops, which led to microphase separation throughout the polymerization.

The surface morphology of NPs, hydrogel and NP-loaded hydrogel was investigated using both SEM and TEM in order to further characterize a polycaprolactone-based NP loaded hydrogel, composed of HEMA, NVP and PEG-DA [76]. The drug-loaded nanoparticles were prepared using an oil-in-water surfactant free mini-emulsion approach, which comprised of a PEG hydrophilic outer shell, pHEMA hydrophobic inner shell and PCL hydrophobic core, with a particle size of 83.4 nm. A smooth and non-porous surface of a hydrogel could be observed through its SEM image. NPs that are entrapped inside the hydrogel matrix were shown through the SEM image of an NP-loaded hydrogel. TEM micrographs demonstrated that the prepared polymeric NPs were spherical and uniform in shape [76]. Shape and size of the developed drug (dexamethasone-21-disodium phosphate)-loaded chitosan NP from chitosan NP-loaded hydrogel lens (unhydrated state) were identified and estimated using both SEM and AFM in work carried out by Behl *et al.* [71]. The spherical shape of chitosan NP was observed with an estimated size of 50 nm. When measuring the particle size of the developed NP using a different technique called Dynamic Light Scattering, the NP size was determined to be 105 ± 11 nm instead of ~ 50 nm estimated from SEM and AFM. It was proposed that this difference in size was attributed to the swelling capacities of the NP in water [71].

Besides characterizing the shape and estimating the particle size of the developed NP-loaded SCL, AFM has also been used to study the surface roughness of both unmodified and modified lenses. The surface roughness of several commercial CLs were determined to be in a range of 0.7–18.8 nm by Guryca *et al.* [150], while a value range of 2.34–12.99 nm was cited by Giraldez *et al.* [151].

The impact of hydrating HEMA-based hydrogels in the biomolecule solution (e.g., albumin and cholesterol) on lens surface roughness was investigated using AFM topographic images in the aforementioned study carried out by Silva *et al.* [87] in Section 3.2.1. No significant changes in the surface roughness of lenses hydrated in water and those hydrated in cholesterol solution, 3.6 ± 1.0 nm and 3.5 ± 0.3 nm, respectively, were observed. On the other hand, SiHy TRIS/NVP/HEMA, when hydrated in albumin solution showed a reduction in lens surface roughness (2.7 ± 0.5 nm) in comparison to a senofilcon A lens (i.e. a SiHy lens, 3.3 ± 0.3 nm). This observation was postulated to be because albumin is a globular protein with a much higher molecular weight compared to cholesterol (66000 Da and 386 Da, respectively). However, it should be noted that, in all cases, the surface roughness values of the lenses hydrated in either water, cholesterol or albumin were within the range of the commercial lenses.

There are many studies on the investigation of a pharmaceutical-loaded lens utilizing the use of SEM, AFM or TEM to examine the lens' morphology and surface roughness. However, according to the ISO standard [36], this part of lens characterization can also be investigated through edge profiles and a comparator with a required magnification as mentioned in Section 4.3.

3.2.3. Tensile strength

Fluid as well as mechanical transport characteristics of SCLs have received special attention in the design and quality control assessment of lenses [152]. Stresses on lens materials can be caused by various factors, e.g., repeated application, removal of lens or eye movement [153]. This can impact on clinical performance, such as on-eye movement, wettability and fitting [154,155], hence, customers' comfort [153], and potentially leading to ocular lesions [155]. Modulus is a parameter commonly used to express CL mechanical properties, which demonstrates the material's elasticity [156]. The SI unit for this property is Mega Pascal (MPa):

$$\text{MPa} = 10^6 \text{N/m}^2 = 145.04 \text{ psi} = 10^7 \text{ dynes/cm}^2$$

Tension, also well-known as tensile strength, has been the most commonly quoted in the assessment of SCL mechanical properties [157]. Upon the breakage of the sample, a stress–strain curve is generated, of which the values for mechanical behaviours of a specimen will be calculated. A typical tensile strength test should give three outcomes including: tensile modulus (Young's modulus), tensile strength and elongation to break [156]. Young's modulus (E) can be calculated according to the following equation (Equation 3.3):

$$\text{Modulus} = \frac{\text{Stress}}{\text{Strain}}$$

A schematic of this technique and the processes involved is shown in Fig. 7 below.

The mechanical property of several commercial SCLs have been widely studied to investigate the differences in tensile strength between various hydrogel vs. SiHy materials [157–159], and the effect of SCL care product on this property [160]. However, there are currently no standard lens material available, and also no ISO standardized

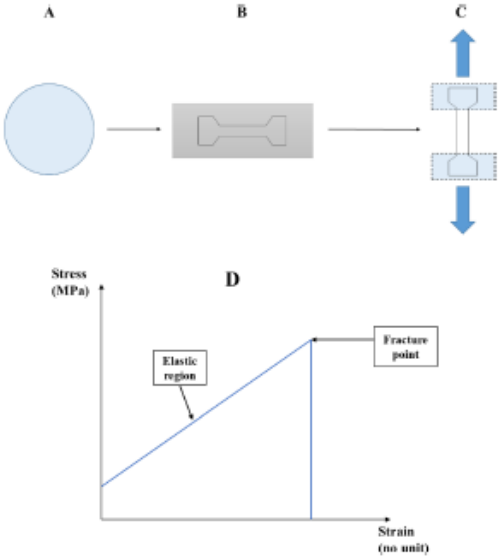

Fig. 7. Schematic illustrating a method used for tensile testing, where (A) lens sample, (B) dog-bone cutter, (C) lens strip after cutting and attached onto the texture analyser (i.e., instrument used to measure tensile strength of the lens), and (D) an example of tensile stress vs. strain diagram of a material with ideal elastic behaviour (e.g., soft contact lens).

measurement techniques for SCLs, and therefore validation and accuracy of such measurements are hard to achieve. Some of the Young's modulus values of various hydrogel lenses [156] and SiHy lenses [159] from different manufacturers are shown in the Table 3below.

The impact on tensile strength of the hydrated samples after and before drug-loading and sterilisation under different conditions (e.g., steam heat, gamma irradiation and ozonation) was investigated by Galante *et al.* [57]. Firstly, the samples were cut into strips, by applying a 5 mN trigger force and a speed of 0.3 mm/second. A texture analyser was used to measure the mechanical properties. The Young's modulus (E) was calculated after obtaining the data from Exponent Stable Micro Systems machine, which was based on the slope of the initial linear portion of the stress–strain curve. It could be seen that loading drugs caused a significant influence on the E values of the materials ($p < 0.0005$). The drug-loaded SCLs in all cases provided a higher E value compared to the control lens. This trend illustrated the presence of drug-polymer interactions [57]. Because of different sterilisation approaches, some degradation/changes in the SiHy materials' characteristics could be observed. Nevertheless, in all cases, the Young's modulus values were within the expected order of magnitude of the lens material, ranging from 2.2 to 9.0 MPa [153,161]. Similar mechanical properties of drug-loaded intra-ocular lens (CI26Y, a hydrophilic materials composed of hydroxyethyl methacrylate and methyl methacrylate) were shown by Topete *et al.* [56]. The Young's modulus values obtained for lenses hydrated in PBS and loaded with drugs (moxifloxacin, diclofenac, and ketorolac) at 4 °C and 60 °C were in a range of 1.5–2.5 MPa.

Using a similar method, Elshaer *et al.* [31] examined the Young's modulus and tensile strength of SCLs before and after prednisolone-loaded PLGA (poly D,L-lactic-co-glycolic acid) NPs. When compared with the control lens, lenses with 0.2 g and 0.4 g drug-loaded NPs, the elasticity given by Young's modulus did not change significantly (0.0163 ± 0.002 MPa, 0.0156 ± 0.001 MPa, and 0.0135 ± 0.003 MPa, respectively). Moreover, this study also mentioned that by combining HEMA and MAA in SCL formulations, not only the hydrophilicity of lenses can improve, which in turn leads to an increase in water content, but it can also maintain the mechanical strength of the material [162]. Anirudhan *et al.* [83] used an Instron 5533 instrument (model: ASTM D 7137 M−05) to test the material's tensile strength from a rectangular specimen of the prepared pHEMA thin film (composed of Chitosan, HEMA, acrylamide, methacrylic acid EGDMA). The Young's modulus (E) values of the materials were calculated by taking data from the initial 5% slope from the stress–strain curve. The developed therapeutic CL was shown to have a higher E value when compared to pristine pHEMA by a magnitude of 0.04 MPa. Furthermore, this behaviour of fabricated CLs remained the same after three cycles of timolol loading and release. Additionally, the increase in E value was also observed when the molecular-imprinted polymer was loaded into a pHEMA lens (0.14 MPa for blank pHEMA lens and 0.17 MPa for molecular-imprinted lens).

It is worth noting that there is a general correlation between modulus, water content and oxygen permeability, as cited by Jones *et al.* [163], although this correlation is different between conventional hydrogel and SiHy materials. For hydrogels, as the modulus and water content increases, the oxygen permeability increases [164]. However, for SiHy materials, due to the fact that oxygen is primarily diffused through the lens by silicone and not water, the relationship between water and oxygen permeability is inverted in comparison to those in conventional hydrogels [165,166].

3.2.4. *Tribological property*

CL discomfort has found to be related to several factors encompassing dryness, protein adsorption, physiological factors and friction generated during the blinking process [167–170]. To gain a better understanding and improve comfort of different lens materials and ophthalmic solutions, several clinical evaluations have taken place [171–177], including incorporation of wetting agents into SCLs [170]. The main comfort component in relation to the blinking cycle of the eye is low frictional losses which the eyelid experiences as it moves back and forth across the cornea [178]. The natural function of the tear film is interrupted due to the insertion of SCLs between the cornea and the eyelid [178]. Consequently, this leads to an alteration in the tear-exchange rate, and in the stability and activity of both lipids and proteins in the lubricant as they come in contact with the lens surface [179,180]. To access the tribological behavior of a material, its coefficient of friction (CoF) is determined (Fig. 8).

The CoF is defined as the ratio of the frictional and normal forces between the two surfaces [181]. CoF is dependent not only on the

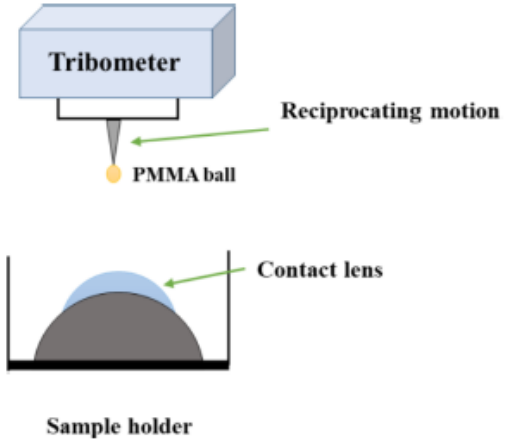

Fig. 8. Schematic of a typical tribological test experimental set-up: friction coefficient measurements are performed in lubricated conditions using a PMMA (polymethyl methacrylate) ball as a counter body which runs in a reciprocating movement over the sample.

Table3
Young's modulus values of various lens materials[2].

Lens type	Trade name	Principal monomer	Water content (%)	Young's modulus (MPa)
Hydrogel	Optima 38	HEMA	38	0.6
	Acuvue	HEMA/MA	58	0.2
	Softlens 03	HEMA	38	0.3
	Omniflex	MMA/NVP	70	0.3
	Vistagel 42 HC	HEMA/NVP	40	0.7
	Vistagel 70 MA	HEMA/MAA	70	0.8
Silicone-hydrogel	Galyfilcon A	mPDMS, DMA, EGDMA, HEMA, siloxane macromer, PVP	47	0.4
	Lotrafilcon B	DMA, TRIS, siloxane macromer	33	1.0
	Balafilcon A	NVP, TPVC, NCVE, PBVC	36	1.1

[2] MA: methacrylic acid, MMA: methyl methacrylate, MAA: allyl methacrylate, DMA: N,N-dimethylacrylamide, mPDMS: polydimethylsiloxane, TPVC: tris-(trimethylsiloxysilyl) propylvinyl carbamate, NCVE: N-carboxyvinyl ester, PBVC: poly(dimethysiloxy)-di(silylbutanol)-bis(vinyl carbamate).

inherent properties of the materials, but also on the experimental conditions [182]. Due to resolution limits of the used micro-tribometer and also the complication of performing the tribology test, there are several practical difficulties in achieving adequate tribological properties of SCLs materials [183]. Hence, most of the tribological studies have been based on the reported values for the contact pressures, which are within the range of 3–5 kPa, with the sliding speed being around 12 cm/s, through the work of Conway *et al.* [184] and Alyra *et al.* [185]. Based on the correlation between SCL comfort and their frictional properties, and the potential of predicting the performance of SCLs, there have been numerous studies exploring the tribological properties of SCLs [167,168,186–188]. The tribology between glass and a CL with and without an addition of lubricant [167,168], the friction for both anterior and posterior sides of the hydrogels with an addition of lubricant [189], as well as the friction between the anterior side of a lens and corneal epithelial cells [169] were carried out by various research groups. These studies used various methodologies to determine CoF in CLs. Therefore, the reported CoF values in each study should only be considered in the context of the experiments carried out under the same conditions and with similar instruments. However, in many of cases, the physiological conditions of the eye (the properties of tear film, the temperature of the ocular tissues), surface properties of the human eyelid and SCLs, as well as how the materials respond at such temperature have not been taken into consideration, though these are imperative to clinical relevance [183,190].

Sterner *et al.* [178] developed an alternative approach to analyse the tribological behavior of SCL materials that takes the physiological environment into consideration, and also aims to overcome the low moduli limitation of SCLs. It was designed to mimic the *in vivo* performance from *in vitro* data. Using this technique, Lau *et al.* [190] examined and compared the lubricity of five commercial cosmetic SCLs, including etafilcon A 58% (lens A), hilafilcon B 59% (lens B), 2-HEMA EGDMA 38% (lens C), hefilcon A 42% (lens D) and hefilcon A (lens E). While lens A has a polymer layer with the pigment in between, the other four have varying amount of polymer encasing the pigment. CoF measurement for each lens was performed on two locations: central and peripheral. When comparing the CoF values between pigmented and clear regions, lens A (e.g., −0.014 and −0.002) showed no statistically significant difference in comparison to the clear region. The other four showed a statistically significantly higher CoF in the pigmented regions, compared with the clear regions (lens B: 0.017 and 0.055, lens C: 0.077 and 0.286, lens D: 0.400 and 0.505, and lens E: 0.407 and 0.518, respectively).

The effects of various sterilization methods on lens materials was demonstrated through the work of Galante *et al.*[46]. Following an increase in dosage, materials sterilized using gamma radiation gave a higher CoF value. At the highest dose (25 kGy), this value was significantly higher, which indicated the degradation/ modification of the material's surface (CoF: 1.00). As for ozone sterilization, similar outcomes were observed for the materials sterilized under the highest ozonation pulse, 10 pulses (CoF: 0.90). However, the CoF values reported in this study for non-sterilized (CoF: 0.25), autoclaved (CoF: 0.05), ozonized at 8 pulses (CoF: 0.10), and gamma radiation at 5 kGy (CoF: 0.20) samples were in agreement with the previously reported figures for similar materials [87].

The CoF has been shown to correlate with the *in vivo* comfort of the SCL, allowing the lens comfort to be predicted from *in vitro* tribological data [181]. This has made the measurement of lens CoF value essential to the development and screening of new lens materials [191]. Despite the importance of determining the tribological properties of SCLs, to the best of the authors' knowledge, within the last 10 years, there are no studies on therapeutic lenses which investigated tribological behavior. Additionally, there is currently no ISO standard on the measurement of CL tribological property.

4. Feasibility of using Pharmaceutical-loaded lenses as an ocular drug delivery system

Even though a large amount of work has been carried out in the development of hydrogel and SiHy SCLs as an ODDS for therapeutic applications, it is worth paying great attention to the fact that a vast majority of these studies were executed using the SCLs model (flat thin film of hydrogel/SiHy polymers) instead of actual SCLs on the commercial market [28,31,56,76,91]. Following the extensive review presented, it is noteworthy that due to the non-commercial models utilised, several important SCLs characteristics have been missing, those that would potentially influence the feasibility of the concept of using SCLs for therapeutic purposes. Such tests, according to the recent ISO 18369:2017 standards [35–38], are listed below:

- Dimensional test (diameter, center thickness, sagittal depth, base curve, roundness).
- Lens power.
- Edge profiles and surface imperfections.
- Extractable profiles of therapeutic SCLs.

4.1. Dimensional parameters and lens power

As described under ISO 18369–2:2017 [36], dimensional parameters included in the tolerance table for SCLs include: base curve equivalent/ back optic zone radius/equivalent posterior radius of curvature, sagittal depth, total diameter, centre thickness, label back vertex power, and cylinder power. This standard also cited that, unless there are clinical data and risk assessment to support the product's safety and performance, a manufacturer of SCLs must follow one or more specified tolerance limits given within this document. The definitions for each term are defined within the ISO 18369–1:2017 standard [35], while measurement methodologies for SCL dimension are specified under the ISO 18369–3:2017 standard [37].

The lens should provide full corneal coverage in all directions of gaze and throughout blinking. Generally, the diameter for SCLs is in a range of 13.8 to 14.5 mm [192]. The impacts of lens diameter on lens performance and initial comfort were also investigated by Sorbara and Mueller [193]. Their study indicated that this parameter influenced wearer's comfort and centration. While in primary gaze, centration of the CL can be determined by measuring the distance between CL edge and the limbus at the superior, inferior, nasal and temporal location of the CL [194]. It is unacceptable if the lens is smaller than the cornea as it cannot fully cover the cornea. On the other hand, lens fitting will not be possible if the lens becomes too big for the cornea.

Lens central and edge thickness was studied to have an impact on lens movement [195,196]. As cited by Jones and Dumbleton, positive power lens have a higher thickness compared to negative power lens [192]. Lens thickness also influences oxygen permeability of the lens. As such, comparing a thinner lens of the same material and water content, the thicker lens is said to transmit less oxygen [192]. Hui *et al.* investigated SiHy lens center thickness before and after the incorporation of ciprofloxacin HCl, which showed no statistically significant difference with an average value in a range of 61–64 μm [84].

Label back vertex power of a lens is defined as the dioptric power measured by focimeter either in air or in saline solution (Moire deflectometer or Hartmann methods), according to the current international standard [37]. Tolerance for such measurement is given in the ISO 18369–2:2017 standard [36]. Pearson and Evans [197] work demonstrated that focimeter measurement in saline generated a slightly more reliable outcome compared to the in-air approach, although in both cases, the mean errors were smaller than 0.05 D and 0.07 D for hydrogels and SiHys, respectively. There are also several studies which have used this technique to measure the vertex powers of rigid lens [198], hydrogel lens [199] and progressive addition lens [200].

If the lens power alters upon the incorporation of NPs, further adjustments in lens design would be required, otherwise the lens would be inappropriate for commercial use. Despite the significance of these lens properties, they do not receive enough attention and are often left out of studies of SCLs as a potential ODDS.

4.2. Extractable profiles

As per ISO 18369-4:2017 [38], it is vital to identify and characterize the extractable substances from the lens to study new lens materials and determine the subsequent pre-clinical examination programme. The standard method for quantitatively determining extractables from SCLs is Soxhlet extraction according to this ISO standard.

Lens extractable profiles have been studied as a potential way to provide a more direct methodology to quantify the drug uptake in the therapeutic SCLs [79,201]. The drug uptake (natamycin, moxifloxacin, timolol maleate and ketotifen fumarate) of four conventional hydrogel and four SiHy SCLs was studied using this methodology [201]. Three extraction cycles were carried out with three lenses of each type extracted in 2 mL of methanol for two hours in each cycle. The data indicated that after the first cycle the majority of drugs were extracted in all cases [201]. This approach was previously used by Kakisu *et al.* [79] in his study to evaluate the drug uptake of antibiotics (gatifloxacin and moxifloxacin) from three types of hydrogel SCLs. Extractable tests were also applied to analyze residual solvent released from CLs as cited by the work of Ciolino *et al.* [202]. This test is used to further characterise the lenses more thoroughly and the potential impact of any loaded materials (drugs, NPs or supplements) on the lens.

In addition, it was previously investigated that hydration, extraction and sterilization steps in the process of manufacturing CLs would significantly reduce residue when comparing the extractable profiles between dry lens after curing vs. lens that go through all such steps [203,204]. As such, for the lens with loaded materials (e.g., drug or supplement), these materials could potentially be lost through these steps that in turn affect the final extractable values reported. Therefore, it is important to record the extractable profiles of both unmodified and modified lenses at every step of the lens manufacturing processes in order to obtain the most accurate lens extractable profile.

Generally, the drug uptake into the lens can be measured by quantifying the drug-loading solution concentration at the beginning and the end of the process [34,205]. Nevertheless, this method could lead to a non-representative result for drug uptake since the drug might precipitate out of the solution and settle at the bottom or side of the tested vials over time. In addition, several studies have also shown that the amounts of actual absorbed drug are much smaller than the concentration of drug-loading solutions. Hence, there would be very high associated errors within this measurement.

4.3. Edge profiles and surface imperfections

Another essential parameter that must be assessed for a finished lens in order to meet the commercial standard, which also has an impact on lens comfort, [37] is its edge profile/thickness and its surface. The lens surface having scratches, pitting, puncture, etc. is deemed to be unsuitable for commercialization. By using a magnification of at least x7, either with a hand held instrument or a projection comparator, under illuminating conditions, these characteristics can be examined [37].

4.4. First commercially available drug delivery contact lens – Acuvue Theravision

Acuvue Theravision, a ketotifen-loaded soft hydrogel lens is officially the first commercially available drug delivery contact lens for the prevention of itch associated with allergic conjunctivitis while still correcting refractive ametropia (i.e. myopia and hyperopia). The lens material is etafilcon A, a copolymer of HEMA and MAA crosslinked with EGDMA and 1,1,1-trimethylol propane trimethacrylate. Physical, optical, and dimensional properties of this drug-loaded lens were fully evaluated to ensure the lens' critical properties to commercial standard. As such, the lens was shown to exhibit over 90% light transmission, a refractive index of 1.40, 59% water content and 21.4×10^{-11} (cm^2/sec) (ml O_2/ml × mmHg) at 35 °C for its oxygen permeability [206]. The lens diameter was determined to be 14.2 mm, with other required lens parameters outlined in the relevant ISO standards [36,38] fulfilled. The tensile strength of non-drug loaded Acuvue lens was previously investigated by Bhamra *et al.* to be 0.2 MPa [156].

5. Conclusions and future perspectives

Over the past few decades, extensive research investigating novel ODDS has been carried out. These studies aim to develop a new analyte-loaded carrier that can provide a more targeted delivery and controlled release, while reducing side effects. Additionally, following the advancement of nanotechnology, nano-sized drug-loaded carrier systems as a mode of drug administration have received great interest by ocular scientists. To enhance ocular bioavailability and overcome several ocular barriers and limitations associated with conventional ODDSs, drug-loaded nanoparticle (NP)-laden soft contact lens (SCLs) have received special attention from scientists and have been identified to be a promising ODDS.

Based on successful *in vitro* release and *in vivo* animal studies of these technologies, the majority of work has focused on testing the lens physical and chemical properties upon the incorporation of drug-loaded NPs to study their feasibility in treating ocular diseases. These tests include optical transparency, water content, wettability, modulus, tribology, refractive index, and oxygen and ion permeability. These parameters are known to have an impact on the clinical performance since they can influence the quality of the commercialised SCLs and patient compliance.

This review notes that several lens testing methodologies still lack standardised methods of analysis as well as corresponded accepted values. In addition, following the above extensive review, it can be observed that the majority of works in this area were not carried out using lenses that have comparable mechanical, physical, and chemical properties to commercial lenses. Instead, sheets of similar lens materials were used to investigate the feasibility of this technology and determine the lens properties. This is in turn significantly influences two critical lens parameters including but not limited to lens thickness and lens shape. Hence, it can be expected that the physical and chemical properties of lenses studied in such work would change significantly when applying such technology in a commercial lens. Based on the current contact lens international standards, several essential lens properties such as: dimensions, power, extractable profiles, edge profiles and surface morphology have not been addressed within the scope of many investigations. Since the incorporation of drug can potentially change these lens properties, it is critical to assess such parameters after the loading of drug.

With the advanced development of using therapeutic CL as an ODDS for the treatment of ocular diseases, future studies should involve the characterisation of the lens features to gain an in-depth understanding of the real potential of this exciting drug delivery approach. Furthermore, to ensure the safety, efficacy, and quality of the products for clinical trial of this system, physical and chemical stability of drug-nanoparticulate systems should also be taken into consideration throughout the development process.

Funding

This work was supported by the Irish Research Council-Enterprise Partnership Scheme [grant number: EPSPG/2017/236, 2017].

Declaration of Competing Interest

The authors declare that they have no known competing financial interests or personal relationships that could have appeared to influence the work reported in this paper.

References

[1] W. H. Organization. "Blindness and vision impairment." https://www.who.int/news-room/fact-sheets/detail/blindness-and-visual-impairment (accessed 17 November, 2019).

[2] Gaudana R, Ananthula HK, Parenky A, Mitra AK. "Ocular drug delivery," (in eng). AAPS J 2010;12(3):348–60. https://doi.org/10.1208/s12248-010-9183-3.

[3] Kumar A, Malviya R, Sharma P. Recent Trends in Ocular Drug Delivery: A Short Review. Am J Appl Sci 2011;3:86–92.

[4] Patel A, Cholkar K, Agrahari V, Mitra AK. "Ocular drug delivery systems: An overview," (in eng). World J Pharmacol 2013;2(2):47–64. https://doi.org/10.5497/wjp.v2.i2.47.

[5] Pandey, S. Kunsel, T. "Eye Drops and Lubricants Market by Type (Antibiotics, Hormones, Artificial Tears, and Others) and Application (Eye Diseases, Eye Care, and Others): Global Opportunity Analysis and Industry Forecast, 2018 - 2025," doi: https://www.alliedmarketresearch.com/eye-drop-and-lubricants-market.

[6] Weng Y, Liu J, Jin S, Guo W, Liang X, Hu Z. Nanotechnology-based strategies for treatment of ocular diseases. Acta Pharmaceut Sin B 2017;7(3):281–91.

[7] Stone JL, Robin AL, Novack GD, Covert DW, Cagle GD. An Objective Evaluation of Eyedrop Instillation in Patients With Glaucoma. Arch Ophthalmol 2009;127(6):732–6. https://doi.org/10.1001/archophthalmol.2009.96.

[8] Zhao C, Zhang Z, Chen L, Wang F, Xu D. "Effectiveness of Intravitreal Injection of Ranibizumab for Neovascular Age-Related Macular Degeneration with Serous Pigment Epithelial Detachment," (in eng). Med Sci Monit 2016;22:833–9. https://doi.org/10.12659/msm.895528.

[9] Lim RHF, Gupta B, Simcock P. "Intravitreal aflibercept in neovascular age-related macular degeneration previously treated with ranibizumab," (in eng). Int J Ophthalmol 2017;10(3):423–6. https://doi.org/10.18240/ijo.2017.03.15.

[10] Yang W, Tan Y, Li C, Liu Yi, Lu G, Bianchini P. Observation of curative effect of intravitreal injection of conbercept in wet age-related macular degeneration: Optical coherence tomography analysis after injection. Microsc Res Tech 2018;81(4):384–8. https://doi.org/10.1002/jemt.v81.410.1002/jemt.22989.

[11] Falavarjani KG, Nguyen QD. "Adverse events and complications associated with intravitreal injection of anti-VEGF agents: a review of literature," (in eng). Eye (Lond) 2013;27(7):787–94. https://doi.org/10.1038/eye.2013.107.

[12] Nagarwal RC, Kant S, Singh PN, Maiti P, Pandit JK. Polymeric nanoparticulate system: A potential approach for ocular drug delivery. J Control Release 2009;136(1):2–13. https://doi.org/10.1016/j.jconrel.2008.12.018.

[13] Meng R, Li K, Chen Z, Shi C. Multilayer Coating of Tetrandrine-loaded PLGA nanoparticles: Effect of surface charges on cellular uptake rate and drug release profile. J. Huazhong Univers. Sci. Technol. [Medical Sciences] 2016/02/01 2016,;36(1):14–20. https://doi.org/10.1007/s11596-016-1535-5.

[14] Stella B, Peira E, Dianzani C, Gallarate M, Battaglia L, Gigliotti C, et al. "Development and Characterization of Solid Lipid Nanoparticles Loaded with a Highly Active Doxorubicin Derivative," (in eng). Nanomaterials (Basel) 2018;8(2):110. https://doi.org/10.3390/nano8020110.

[15] Baskar G, Garrick BG, Lalitha K, Chamundeeswari M. Gold nanoparticle mediated delivery of fungal asparaginase against cancer cells. J Drug Delivery Sci Technol 2018;44:498–504. https://doi.org/10.1016/j.jddst.2018.02.007.

[16] Weng Y, Liu J, Jin S, Guo W, Liang X, Hu Z. "Nanotechnology-based strategies for treatment of ocular disease," (in eng). Acta Pharm Sin B 2017;7(3):281–91. https://doi.org/10.1016/j.apsb.2016.09.001.

[17] Xu J, Xue Y, Hu G, Lin T, Gou J, Yin T, et al. A comprehensive review on contact lens for ophthalmic drug delivery. J Control Release 2018;281:97–118. https://doi.org/10.1016/j.jconrel.2018.05.020.

[18] Battaglia L, Serpe L, Foglietta F, Muntoni E, Gallarate M, Del Pozo Rodriguez A, et al. Application of lipid nanoparticles to ocular drug delivery. Expert Opinion on Drug Delivery 2016;13(12):1743–57. https://doi.org/10.1080/17425247.2016.1201059.

[19] Nayak K, Misra M. A review on recent drug delivery systems for posterior segment of eye. Biomed Pharmacother 2018;107:1564–82. https://doi.org/10.1016/j.biopha.2018.08.138.

[20] Lee D, Cho S, Park HS, Kwon I. Ocular Drug Delivery through pHEMA-Hydrogel Contact Lenses Co-Loaded with Lipophilic Vitamins. Sci Rep 2016;6(1):34194. https://doi.org/10.1038/srep34194.

[21] Horne RR, Judd KE, Pitt WG. Rapid loading and prolonged release of latanoprost from a silicone hydrogel contact lens. J Drug Delivery Sci Technol 2017;41:410–8. https://doi.org/10.1016/j.jddst.2017.08.011.

[22] D. F. Maulvi, T. Soni, and D. Shah, "Extended release of hyaluronic acid from hydrogel contact lenses for dry eye syndrome," J Biomater Sci. Polymer edition, vol. 26, pp. 1-26, 07/15 2015, doi: 10.1080/09205063.2015.1072902.

[23] Hsu K-H, Carbia BE, Plummer C, Chauhan A. Dual drug delivery from vitamin E loaded contact lenses for glaucoma therapy. Eur J Pharm Biopharm 2015;94:312–21. https://doi.org/10.1016/j.ejpb.2015.06.001.

[24] Yang M, Yang Y, Lei M, Ye C, Zhao C, Xu J, et al. Experimental studies on soft contact lenses for controlled ocular delivery of pirfinedone: in vitro and in vivo. Drug Delivery 2016;23(9):3538–43. https://doi.org/10.1080/10717544.2016.1204570.

[25] Korhonen E, Rönkkö S, Hillebrand S, Riikonen J, Xu W, Järvinen K, et al. Cytotoxicity assessment of porous silicon microparticles for ocular drug delivery. Eur J Pharm Biopharm 2016;100:1–8. https://doi.org/10.1016/j.ejpb.2015.11.020.

[26] Park J-H, Jeong H, Hong J, Chang M, Kim M, Chuck RS, et al. The Effect of Silica Nanoparticles on Human Corneal Epithelial Cells. Sci Rep 2016;6(1). https://doi.org/10.1038/srep37762.

[27] Ubani-Ukoma U, Gibson D, Schultz G, Silva BO, Chauhan A. Evaluating the potential of drug eluting contact lenses for treatment of bacterial keratitis using an ex vivo corneal model. Int J Pharm 2019;565:499–508. https://doi.org/10.1016/j.ijpharm.2019.05.031.

[28] A. R. Desai et al., "Co-delivery of timolol and hyaluronic acid from semi-circular ring-implanted contact lenses for the treatment of glaucoma: in vitro and in vivo evaluation," Biomaterials Science, 10.1039/C8BM00212F vol. 6, no. 6, pp. 1580-1591, 2018, doi: 10.1039/C8BM00212F.

[29] Kapoor Y, Dixon P, Sekar P, Chauhan A. Incorporation of drug particles for extended release of Cyclosporine A from poly-hydroxyethyl methacrylate hydrogels. Eur J Pharm Biopharm 2017;120:73–9. https://doi.org/10.1016/j.ejpb.2017.08.007.

[30] Maulvi FA, Lakdawala DH, Shaikh AA, Desai AR, Choksi HH, Vaidya RJ, et al. In vitro and in vivo evaluation of novel implantation technology in hydrogel contact lenses for controlled drug delivery. J Control Release 2016;226:47–56. https://doi.org/10.1016/j.jconrel.2016.02.012.

[31] ElShaer A, Mustafa S, Kasar M, Thapa S, Ghatora B, Alany RG. "Nanoparticle-Laden Contact Lens for Controlled Ocular Delivery of Prednisolone: Formulation Optimization Using Statistical Experimental Design," (in eng). Pharmaceutics 2016;8(2):14. https://doi.org/10.3390/pharmaceutics8020014.

[32] Silva D, Sousa HCd, Gil MH, Santos LF, Moutinho GM, Serro AP, et al. Antibacterial layer-by-layer coatings to control drug release from soft contact lenses material. Int J Pharm 2018;553(1-2):186–200. https://doi.org/10.1016/j.ijpharm.2018.10.041.

[33] Mehta P, Al-Kinani AA, Arshad MS, Singh N, van der Merwe SM, Chang M-W, et al. Engineering and Development of Chitosan-Based Nanocoatings for Ocular Contact Lenses. J Pharm Sci 2019;108(4):1540–51. https://doi.org/10.1016/j.xphs.2018.11.036.

[34] García-Millán E, Koprivnik S, Otero-Espínar FJ. Drug loading optimization and extended drug delivery of corticoids from pHEMA based soft contact lenses hydrogels via chemical and microstructural modifications. Int J Pharm 2015;487(1):260–9. https://doi.org/10.1016/j.ijpharm.2015.04.037.

[35] Ophthalmic optics – Contact lenses – Part 1: Vocalbulary, classification system and recommendations or labelling specifications (ISO 18369-1:2017), S. S. Institute, 2017.

[36] Ophthalmic optics – Contact lenses – Part 2: Tolerances (ISO 18369-2:2017), S. S. Institute, 2017.

[37] Ophthalmic optics - Contact lenses - Part 3: Measurement methods (ISO 18369-3:2017), S. S. Institute, 2017.

[38] Ophthalmic optics - Contact lenses - Part 4: Physicochemical properties of contact lens materials (ISO 18369-4:2017), S. S. Institute, 2017.

[39] Alipour F, Khaheshi S, Soleimanzadeh M, Heidarzadeh S, Heydarzadeh S. "Contact Lens-related Complications: A Review," (in eng). J Ophthalmic Vis Res 2017;12(2):193–204. https://doi.org/10.4103/jovr.jovr_159_16.

[40] Peng C-C, Kim J, Chauhan A. Extended delivery of hydrophilic drugs from silicone-hydrogel contact lenses containing Vitamin E diffusion barriers. Biomaterials 2010;31(14):4032–47. https://doi.org/10.1016/j.biomaterials.2010.01.113.

[41] Phan C-M, Subbaraman LN, Jones L. In Vitro Uptake and Release of Natamycin From Conventional and Silicone Hydrogel Contact Lens Materials. Eye & Contact Lens 2013;39(2):162–8. https://doi.org/10.1097/ICL.0b013e31827a7a07.

[42] J. J. Kang-Mieler, W. F. Mieler, "Thermo-Responsive Hydrogels for Ocular Drug Delivery," in Retinal Pharmacotherapeutics, vol. 55, Q. D. Nguyen, E. B. Rodrigues, M. E. Farah, W. F. Mieler, and D. V. Do Eds., (Dev Ophthalmol. Basel: Karger, 2016, pp. 104-111.

[43] Fathi M, Barar J, Aghanejad A, Omidi Y. Hydrogels for ocular drug delivery and tissue engineering. BioImpacts : BI 2015;5(4):159–64. https://doi.org/10.15171/bi.2015.31.

[44] Kirchhof S, Goepferich AM, Brandl FP. Hydrogels in ophthalmic applications. Eur J Pharm Biopharm 2015;95:227–38. https://doi.org/10.1016/j.ejpb.2015.05.016.

[45] Buwalda SJ, Boere KWM, Dijkstra PJ, Feijen J, Vermonden T, Hennink WE. Hydrogels in a historical perspective: From simple networks to smart materials. J Control Release 2014;190:254–73. https://doi.org/10.1016/j.jconrel.2014.03.052.

[46] Galante R, Ghisleni D, Paradiso P, Alves VD, Pinto TJA, Colaço R, et al. Sterilization of silicone-based hydrogels for biomedical application using ozone gas. Compar Convent Techn 2017;78:389–97.

[47] G. A. Hirani A, Lee YW, Pathak Y, Sutariya V, "Polymer-based Therapies for Posterior Segment Ocular Disease," J Biomol Res Ther, vol. 3, no. 1, pp. 1-2, 2013, doi: 10.4172/2167-7956.1000e122.

[48] J. J. Nichols and D. Fisher, "Contact Lenses 2018: The industry saw slightly higher growth last year due to a continued conversion to daily disposable lenses coupled with a stabilization in patient rebate rates.," Contact lens spectrum, vol. 34, no. January 2019, pp. 18-23, 2019. [Online]. Available: https://www.clspectrum.com/issues/2019/january-2019/contact-lenses-2018.

[49] Musgrave CSA, Fang F. "Contact Lens Materials: A Materials Science Perspective," (in eng). Materials (Basel) 2019;12(2):261. https://doi.org/10.3390/ma12020261.

[50] STERN JUDITH, WONG REGINALD, NADUVILATH THOMASJ, STRETTON SERINA, HOLDEN BRIENA, SWEENEY DEBORAHF. Comparison of the Performance of 6- or 30-night Extended Wear Schedules with Silicone Hydrogel Lenses over 3 Years. Optom Vis Sci 2004;81(6):398–406. https://doi.org/10.1097/01.opx.0000135092.69383.fd.

[51] Fonn D, Sweeney D, Holden BA, Cavanagh D. Corneal Oxygen Deficiency. Eye & Contact Lens 2005;31(1):23–7. https://doi.org/10.1097/01.icl.0000151949.30730.9d.

[52] Alvarez-Lorenzo C, Hiratani H, Gómez-Amoza JL, Martínez-Pacheco R, Souto C, Concheiro A. Soft Contact Lenses Capable of Sustained Delivery of Timolol. J Pharm Sci 2002;91(10):2182–92. https://doi.org/10.1002/jps.10209.

[53] Hiratani H, Alvarez-Lorenzo C. Timolol uptake and release by imprinted soft contact lenses made of N, N-diethylacrylamide and methacrylic acid. J Control Release 2002;83(2):223–30. https://doi.org/10.1016/S0168-3659(02)00213-4.

[54] Li C-C, Chauhan A. Modeling Ophthalmic Drug Delivery by Soaked Contact Lenses. Ind Eng Chem Res 2006;45(10):3718–34. https://doi.org/10.1021/ie0507934.

[55] White CJ, Tieppo A, Byrne ME. Controlled drug release from contact lenses: a comprehensive review from 1965-present. J Drug Delivery Sci Technol 2011;21(5):369–84. https://doi.org/10.1016/S1773-2247(11)50062-0.

[56] Topete A, Oliveira AS, Fernandes A, Nunes TG, Serro AP, Saramago B. Improving sustained drug delivery from ophthalmic lens materials through the control of temperature and time of loading. Eur J Pharm Sci 2018;117:107–17. https://doi.org/10.1016/j.ejps.2018.02.017.

[57] Galante R, Oliveira AS, Topete A, Ghisleni D, Braga M, Pinto TJA, et al. Drug-eluting silicone hydrogel for therapeutic contact lenses: Impact of sterilization methods on the system performance. Colloids Surf B 2018;161:537–46. https://doi.org/10.1016/j.colsurfb.2017.11.021.

[58] Maulvi FA, Patil RJ, Desai AR, Shukla MR, Vaidya RJ, Ranch KM, et al. Effect of gold nanoparticles on timolol uptake and its release kinetics from contact lenses: In vitro and in vivo evaluation. Acta Biomater 2019;86:350–62. https://doi.org/10.1016/j.actbio.2019.01.004.

[59] Malakooti N, Alexander C, Alvarez-Lorenzo C. Imprinted Contact Lenses for Sustained Release of Polymyxin B and Related Antimicrobial Peptides. J Pharm Sci 2015;104(10):3386–94. https://doi.org/10.1002/jps.24537.

[60] Wulff G, Sarhan A. Angewandte Chemie. Angew Chem Int Ed Engl 1972;341(11):84–364.

[61] Wulff G. Molecular Imprinting in Cross-Linked Materials with the Aid of Molecular Templates—A Way towards Artificial Antibodies. Angew Chem Int Ed Engl 1995;34(17):1812–32. https://doi.org/10.1002/(ISSN)1521-377310.1002/anie.v34:1710.1002/anie.199518121.

[62] Ali M, Byrne ME. Controlled Release of High Molecular Weight Hyaluronic Acid from Molecularly Imprinted Hydrogel Contact Lenses. Pharm Res 2009;26(3):714–26. https://doi.org/10.1007/s11095-008-9818-6.

[63] Omranipour H, Tabassi S, Kowsari R, Rad M, Mohajeri S. Brimonidine Imprinted Hydrogels and Evaluation of Their Binding and Releasing Properties as New Ocular Drug Delivery Systems. Curr Drug Deliv 2015;12. https://doi.org/10.2174/1567201812666150316110838.

[64] Kloomars S, Heidari S, Malaekeh-Nikouei B, Shayani Rad M, Khameneh B, Mohajeri SA. Ciprofloxacin-imprinted hydrogels for drug sustained release in aqueous media. Pharm Dev Technol 2017;22(1):122–9. https://doi.org/10.1080/10837450.2016.1230131.

[65] Bengani LC, Hsu K-H, Gause S, Chauhan A. Contact lenses as a platform for ocular drug delivery. Exp Opin Drug Deliv 2013;10(11):1483–96. https://doi.org/10.1517/17425247.2013.821462.

[66] C. Gomes, G. Sadoyan, R. C. S. Dias, and M. R. P. F. N. Costa, "Development of Molecularly Imprinted Polymers to Target Polyphenols Present in Plant Extracts," Processes, vol. 5, no. 4, p. 72, 2017. [Online]. Available: https://www.mdpi.com/2227-9717/5/4/72.

[67] Hiratani H, Mizutani Y, Alvarez-Lorenzo C. Controlling Drug Release from Imprinted Hydrogels by Modifying the Characteristics of the Imprinted Cavities. Macromol Biosci 2005;5(8):728–33. https://doi.org/10.1002/(ISSN)1616-519510.1002/mabi.v5:810.1002/mabi.200500065.

[68] Alvarez-Lorenzo C, Yañez F, Barreiro-Iglesias R, Concheiro A. Imprinted soft contact lenses as norfloxacin delivery systems. J Control Release 2006;113(3):236–44. https://doi.org/10.1016/j.jconrel.2006.05.003.

[69] Tieppo A, Pate KM, Byrne ME. In vitro controlled release of an anti-inflammatory from daily disposable therapeutic contact lenses under physiological ocular tear flow. Eur J Pharm Biopharm 2012;81(1):170–7. https://doi.org/10.1016/j.ejpb.2012.01.015.

[70] White CJ, McBride MK, Pate KM, Tieppo A, Byrne ME. Extended release of high molecular weight hydroxypropyl methylcellulose from molecularly imprinted, extended wear silicone hydrogel contact lenses. Biomaterials 2011;32(24):5698–705. https://doi.org/10.1016/j.biomaterials.2011.04.044.

[71] Behl G, Iqbal J, O'Reilly NJ, McLoughlin P, Fitzhenry L. Synthesis and Characterization of Poly(2-hydroxyethylmethacrylate) Contact Lenses Containing Chitosan Nanoparticles as an Ocular Delivery System for Dexamethasone Sodium Phosphate. Pharm Res 2016;33(7):1638–48. https://doi.org/10.1007/s11095-016-1903-7.

[72] Zhu Q, Cheng H, Huo Y, Mao S. Sustained ophthalmic delivery of highly soluble drug using pH-triggered inner layer-embedded contact lens. Int J Pharm 2018;544(1):100–11. https://doi.org/10.1016/j.ijpharm.2018.04.004.

[73] J. Mun, J. w. Mok, S. Jeong, S. Cho, C.-K. Joo, and S. K. Hahn, "Drug-eluting contact lens containing cyclosporine-loaded cholesterol-hyaluronate micelles for dry eye syndrome," RSC Advances, 10.1039/C9RA02858G vol. 9, no. 29, pp. 16578-16585, 2019, doi: 10.1039/C9RA02858G.

[74] Liu S, Jones L, Gu FX. Nanomaterials for ocular drug delivery. Macromol Biosci 2012;12(5):608–20. https://doi.org/10.1002/mabi.v12.510.1002/mabi.201100419.

[75] Mehanna MM, Elmaradny HA, Samaha MW. Mucoadhesive liposomes as ocular delivery system: physical, microbiological, and in vivo assessment. Drug Dev Ind Pharm 2010;36(1):108–18. https://doi.org/10.3109/03639040903099751.

[76] Nasr FH, Khoee S, Dehghan MM, Chaleshtori SS, Shafiee A. Preparation and Evaluation of Contact Lenses Embedded with Polycaprolactone-Based Nanoparticles for Ocular Drug Delivery. Biomacromolecules 2016;17(2):485–95. https://doi.org/10.1021/acs.biomac.5b01387.s001.

[77] Jung HJ, Chauhan A. Temperature sensitive contact lenses for triggered ophthalmic drug delivery. Biomaterials 2012;33(7):2289–300. https://doi.org/10.1016/j.biomaterials.2011.10.076.

[78] Kapoor Y, Thomas JC, Tan G, John VT, Chauhan A. Surfactant-laden soft contact lenses for extended delivery of ophthalmic drugs. Biomaterials 2009;30(5):867–78. https://doi.org/10.1016/j.biomaterials.2008.10.032.

[79] Kakisu K, Matsunaga T, Kobayakawa S, Sato T, Tochikubo T. Development and Efficacy of a Drug-Releasing Soft Contact Lens. Invest Ophthalmol Vis Sci 2013;54(4):2551–61. https://doi.org/10.1167/iovs.12-10614.

[80] Sekar P, Chauhan A. Effect of vitamin-E integration on delivery of prostaglandin analogs from therapeutic lenses. J Colloid Interface Sci 2019;539:457–67. https://doi.org/10.1016/j.jcis.2018.12.036.

[81] Maulvi FA, Desai AR, Choksi HH, Patil RJ, Ranch KM, Vyas BA, et al. Effect of surfactant chain length on drug release kinetics from microemulsion-laden contact lenses. Int J Pharm 2017;524(1-2):193–204. https://doi.org/10.1016/j.ijpharm.2017.03.083.

[82] Gebreel RM, Edris NA, Elmofty HM, Tadros MI, El-Nabarawi MA, Hassan DH. "Development and Characterization of PLGA Nanoparticle-Laden Hydrogels for Sustained Ocular Delivery of Norfloxacin in the Treatment of Pseudomonas Keratitis: An Experimental Study," (in eng). Drug Des Devel Ther 2021;15:399–418. https://doi.org/10.2147/DDDT.S293127.

[83] Anirudhan TS, Nair AS, Parvathy J. Extended wear therapeutic contact lens fabricated from timolol imprinted carboxymethyl chitosan-g-hydroxy ethyl methacrylate-g-poly acrylamide as a onetime medication for glaucoma. Eur J Pharm Biopharm 2016;109:61–71. https://doi.org/10.1016/j.ejpb.2016.09.010.

[84] Hui A, Willcox M, Jones L. In Vitro and In Vivo Evaluation of Novel Ciprofloxacin-Releasing Silicone Hydrogel Contact Lenses. Invest Ophthalmol Vis Sci 2014;55(8):4896–904. https://doi.org/10.1167/iovs.14-14855.

[85] Fuentes R, Fernández E, Pascual I, García C. UV-Visible Transmittance of Silicone-Hydrogel Contact Lenses measured with a fiber optic spectrometer. Proc SPIE 2013;8785. https://doi.org/10.1117/12.2025710.

[86] N. Efron and C. Maldonado-Codina, "6.633 - Development of Contact Lenses from a Biomaterial Point of View – Materials, Manufacture, and Clinical Application," in Comprehensive Biomaterials, P. Ducheyne Ed. Oxford: Elsevier, 2011, pp. 517-541.

[87] Silva D, Fernandes AC, Nunes TG, Colaço R, Serro AP. The effect of albumin and cholesterol on the biotribological behavior of hydrogels for contact lenses. Acta Biomater 2015;26c184–94. https://doi.org/10.1016/j.actbio.2015.08.011.

[88] Paradiso P, Galante R, Santos L, Alves de Matos AP, Colaço R, Serro AP, et al. Comparison of two hydrogel formulations for drug release in ophthalmic lenses. J Biomed Mater Res B Appl Biomater 2014;102(6):1170–80. https://doi.org/10.1002/jbm.b.v102.610.1002/jbm.b.33099.

[89] Paradiso P, Serro AP, Saramago B, Colaço R, Chauhan A. Controlled Release of Antibiotics From Vitamin E-Loaded Silicone-Hydrogel Contact Lenses. J Pharm Sci 2016;105(3):1164–72. https://doi.org/10.1016/S0022-3549(15)00193-8.

[90] Paradiso P, Colaço R, Mata JLG, Krastev R, Saramago B, Serro AP. Drug release from liposome coated hydrogels for soft contact lenses: the blinking and temperature effect. J Biomed Mater Res B Appl Biomater 2017;105(7):1799–807. https://doi.org/10.1002/jbm.b.v105.710.1002/jbm.b.33715.

[91] Maulvi FA, Mangukiya MA, Patel PA, Vaidya RJ, Koli AR, Ranch KM, et al. Extended release of ketotifen from silica shell nanoparticle-laden hydrogel contact lenses: in vitro and in vivo evaluation. J Mater Sci - Mater Med 2016;27(6). https://doi.org/10.1007/s10856-016-5724-3.

[92] Insua Pereira E, Lira M. "Comfort, Ocular Dryness, and Equilibrium Water Content Changes of Daily Disposable Contact Lenses,". Eye Contact Lens 2018;44:S233–40. https://doi.org/10.1097/icl.0000000000000441.

[93] Tranoudis I, Efron N. Parameter stability of soft contact lenses made from different materials. Contact Lens Anterior Eye 2004;27(3):115–31. https://doi.org/10.1016/j.clae.2004.03.001.

[94] Pritchard N, Fonn D. Dehydration, lens movement and dryness ratings of hydrogel contact lenses. Ophthalmic Physiol Opt 1995;15(4):281–6. https://doi.org/10.1016/0275-5408(95)00004-W.

[95] Little SA, Bruce AS. Environmental influences on hydrogel lens dehydration and the postlens tear film. Int Contact Lens Clinic 1995;22(7):148–55. https://doi.org/10.1016/0892-8967(95)00049-Z.

[96] Fink B, Hill RM. Corneal oxygen uptake: A review of polarographic techniques, applications, and variables. Cont Lens Anterior Eye 2006;29(5):221–9. https://doi.org/10.1016/j.clae.2006.09.005.

[97] Chi JM, Fink BA, Hill RM, Mitchell GL. Factors influencing the measurement of oxygen shortfall of the human cornea: Sequencing of test conditions. Cont Lens Anterior Eye 2007;30(1):17–21. https://doi.org/10.1016/j.clae.2006.10.002.

[98] Ramamoorthy P, Sinnott LT, Nichols JJ. Contact lens material characteristics associated with hydrogel lens dehydration. Ophthal Physiol Opt 2010;30(2):160–6. https://doi.org/10.1111/j.1475-1313.2009.00705.x.

[99] Mirejovsky D, Patel AS, Young G. Water properties of hydrogel contact lens materials: a possible predictive model for corneal desiccation staining. Biomaterials 1993/11/01/ 1993,;14(14):1080–8. https://doi.org/10.1016/0142-9612(93)90209-K.

[100] Efron N, Brennan NA. The clinical relevance ofhydrogel lens water content. J Br Contact Lens Associat 1987;10:9–14. https://doi.org/10.1016/S0141-7037(87)80040-X.

[101] R. E. Gundel and C. Hi, "Soft Lens Dehydration: Thin Low Water vs. Thick High Water Lenses," Eyecare, vol. 2, 1986.

[102] Lattimore MR, Harding TH, Williams ST. Hydrogel Contact Lens Water Content is Dependent on Tearfilm pH. Mil Med 2018;183(no. suppl_1):224–30. https://doi.org/10.1093/milmed/usx233.

[103] Høvding G. The fluid content of hydrophilic contact lenses on the eye. Acta Ophthalmol 1983;61(5):889–97. https://doi.org/10.1111/j.1755-3768.1983.tb01471.x.

[104] Jones L, May C, Nazar L, Simpson T. In vitro evaluation of the dehydration characteristics of silicone hydrogel and conventional hydrogel contact lens materials. Contact Lens Anterior Eye 2002;25(3):147–56. https://doi.org/10.1016/S1367-0484(02)00033-4.

[105] Gonzalez-Meijome JM, Lira M, Lopez-Alemany A, Almeida JB, Parafita MA, Refojo MF. Refractive index and equilibrium water content of conventional and silicone hydrogel contact lenses. Ophthalmic Physiol Opt 2006;26(1):57–64. https://doi.org/10.1111/opo.2006.26.issue-110.1111/j.1475-1313.2005.00342.x.

[106] González-Méijome JoséM, López-Alemany A, Lira M, Almeida JoséB, Oliveira MECDR, Parafita MA. Equivalences between refractive index and equilibrium water content of conventional and silicone hydrogel soft contact lenses from automated and manual refractometry. J Biomed Mater Res B Appl Biomater 2007;80B(1):184–91. https://doi.org/10.1002/(ISSN)1552-498110.1002/jbm.b.v80b:110.1002/jbm.b.30583.

[107] Ruel-Gariépy E, Leroux J-C. In situ-forming hydrogels—review of temperature-sensitive systems. Eur J Pharm Biopharm 2004;58(2):409–26. https://doi.org/10.1016/j.ejpb.2004.03.019.

[108] Maulvi FA, Singhania SS, Desai AR, Shukla MR, Tanna AS, Ranch KM, et al. Contact lenses with dual drug delivery for the treatment of bacterial conjunctivitis. Int J Pharm 2018;548(1):139–50. https://doi.org/10.1016/j.ijpharm.2018.06.059.

[109] Varikooty J, Keir N, Woods CA, Fonn D. Measurement of the Refractive Index of Soft Contact Lenses During Wear. Eye Contact Lens 2010;36(1):2–5. https://doi.org/10.1097/ICL.0b013e3181c8135f.

[110] Lira M, Santos L, Azeredo J, Yebra-Pimentel E, Real Oliveira MECD. The effect of lens wear on refractive index of conventional hydrogel and silicone-hydrogel contact lenses: A comparative study. Contact Lens Anterior Eye 2008;31(2):89–94. https://doi.org/10.1016/j.clae.2007.09.001.

[111] Gavara R, Compañ V. Oxygen, water, and sodium chloride transport in soft contact lenses materials. J Biomed Mater Res B Appl Biomater 2017;105(8):2218–31. https://doi.org/10.1002/jbm.b.v105.810.1002/jbm.b.33762.

[112] Lee SE, Kim SR, Park M. "Oxygen permeability of soft contact lenses in different pH, osmolality and buffering solution," (in eng). Int J Ophthalmol 2015;8(5):1037–42. https://doi.org/10.3980/j.issn.2222-3959.2015.05.33.

[113] K. A. Lebow and D. Campbell-Burns, "Understanding the Values that Describe Oxygen Flux Through a Contact Lens," Contact lens spectrum, no. Jan 1998, 1998. [Online]. Available: https://www.clspectrum.com/issues/1998/january-1998/understanding-the-values-that-describe-oxygen-flux.

[114] Holden BA, Mertz GW. Critical oxygen levels to avoid corneal edema for daily and extended wear contact lenses. Invest Ophthalmol Vis Sci 1984;25(10):1161–7.

[115] Young MD, Benjamin WJ. Calibrated Oxygen Permeability of 35 Conventional Hydrogel Materials and Correlation with Water Content. Eye Contact Lens 2003;29(2):126–33. https://doi.org/10.1097/01.icl.0000062463.64717.86.

[116] N. Efron, P. B. Morgan, I. D. Cameron, N. A. Brennan, and M. Goodwin, "Oxygen Permeability and Water Content of Silicone Hydrogel Contact Lens Materials," Optometry and Vision Science, vol. 84, no. 4, 2007. [Online]. Available: https://journals.lww.com/optvissci/Fulltext/2007/04000/Oxygen_Permeability_and_Water_Content_of_Silicone.16.aspx.

[117] González-Chomón C, Silva M, Concheiro A, Alvarez-Lorenzo C. Biomimetic contact lenses eluting olopatadine for allergic conjunctivitis. Acta Biomater 2016;41:302–11. https://doi.org/10.1016/j.actbio.2016.05.032.

[118] J. R. Larke, S. T. Parrish, and C. G. Wigham, "Apparent Human Corneal Oxygen Uptake Rate," Optometry and Vision Science, vol. 58, no. 10, pp. 803-805, 1981. [Online]. Available: https://journals.lww.com/optvissci/Fulltext/1981/10000/Apparent_Human_Corneal_Oxygen_Uptake_Rate.4.aspx.

[119] Fatt I. Comparison of the single-chamber polarographic and the coulometric carrier gas procedures for measuring oxygen permeability. Int Contact Lens Clinic 1989;16(7):226–31. https://doi.org/10.1016/0892-8967(89)90037-0.

[120] Fatt I. "Measurement of oxygen flux into the cornea by pressing a sensor onto a soft contact lens on the eye," (in eng). Am J Optom Physiol Opt 1978;55(5):294–301. https://doi.org/10.1097/00006324-197805000-00002.

[121] Quinn TG, Schoessler JP. "Solubility effects on corneal oxygen measurement," (in eng). Am J Optom Physiol Opt 1983;60(5):360–3. https://doi.org/10.1097/00006324-198305000-00003.

[122] A. Barber, B. A. Fink, and R. M. Hill, "(CL-163)human cornea: Its rapid response to anoxia—the first 540 seconds: Poster # 59," Optometry and Vision Science, vol. 77, no. 12, p. 170, 2000. [Online]. Available: https://journals.lww.com/optvissci/Fulltext/2000/12001/_CL_163_HUMAN_CORNEA__ITS_RAPID_RESPONSE_TO.278.aspx.

[123] Holden BA, Sweeney DF, Vannas A, Nilsson KT, Efron N. Effects of long-term extended contact lens wear on the human cornea. Invest Ophthalmol Vis Sci 1985;26(11):1489–501.

[124] M. J. Jauregui and I. Fatt, "Estimation of oxygen tension under a contact lens*," Optometry and Vision Science, vol. 48, no. 3, pp. 210-218, 1971. [Online]. Available: https://journals.lww.com/optvissci/Fulltext/1971/03000/ESTIMATION_OF_OXYGEN_TENSION_UNDER_A_CONTACT_LENS_.4.aspx.

[125] Benjamin WJ, Hill RM. Closed-lid factors influencing human corneal oxygen demand. Acta Ophthalmol 1986;64(6):644–8. https://doi.org/10.1111/j.1755-3768.1986.tb00681.x.

[126] Benjamin WJ, Hill RM. Human cornea: Oxygen uptake immediately following graded deprivation. Graefe's Arch Clin Exp Ophthalmol 1985;223(1):47–9. https://doi.org/10.1007/BF02150573.

[127] Efron N, Fitzgerald JP. "Distribution of oxygen across the surface of the human cornea during soft contact lens wear," (in eng). Optom Vis Sci 1996;73(10):659–65. https://doi.org/10.1097/00006324-199610000-00005.

[128] R. M. Hill, G. E. Lowther, "Oxygen flux across the tear-epithelial interface as an index of corneal wound repair*," Optometry and Vision Science, vol. 44, no. 5, pp. 267-275, 1967. [Online]. Available: https://journals.lww.com/optvissci/Fulltext/1967/05000/OXYGEN_FLUX_ACROSS_THE_TEAR_EPITHELIAL_INTERFACE.1.aspx.

[129] Papas EB. The significance of oxygen during contact lens wear. Contact Lens Anterior Eye 2014;37(6):394–404. https://doi.org/10.1016/j.clae.2014.07.012.

[130] S. E. Lee, S. R. Kim, and M. Park, "Influence of Tear Protein Deposition on the Oxygen Permeability of Soft Contact Lenses," (in eng), J Ophthalmol, vol. 2017, pp. 5131764-513176, 2017, doi: 10.1155/2017/5131764.

[131] Pozuelo J, Compañ V, González-Méijome JM, González M, Mollá S. Oxygen and ionic transport in hydrogel and silicone-hydrogel contact lens materials: An experimental and theoretical study. J Membr Sci 2014;452:62–72. https://doi.org/10.1016/j.memsci.2013.10.010.

[132] Austin D, Kumar RV. Ionic conductivity in hydrogels for contact lens applications. Ionics 2005;11(3):262–8. https://doi.org/10.1007/BF02430387.

[133] Peng C-C, Chauhan A. Ion transport in silicone hydrogel contact lenses. J Membr Sci 2012;399–400:95–105. https://doi.org/10.1016/j.memsci.2012.01.039.

[134] Lin MC, Svitova TF. "Contact lenses wettability in vitro: effect of surface-active ingredients," (in eng). Optom Vis Sci 2010;87(6):440–7. https://doi.org/10.1097/OPX.0b013e3181dc9a1a.

[135] Campbell D, Carnell SM, Eden RJ. Applicability of Contact Angle Techniques Used in the Analysis of Contact Lenses, Part 1: Comparative Methodologies. Eye Contact Lens 2013;39(3):254–62. https://doi.org/10.1097/ICL.0b013e31828ca174.

[136] J. R. A. Pearson, "Interfacial Phenomena - Equilibrium and Dynamic Effects (2nd Edition) By Clarence A Miller and P Neogi," AIChE Journal, vol. 54, no. 11, pp. 3032-3032, 2008, doi: 10.1002/aic.11631.

[137] de Gennes PG. Wetting: statics and dynamics. Rev Mod Phys 1985;57(3):827–63. https://doi.org/10.1103/RevModPhys.57.827.

[138] Shanker RM, Ahmed I, Bourassa PA, Carola KV. An in vitro technique for measuring contact angles on the corneal surface and its application to evaluate corneal wetting properties of water soluble polymers. Int J Pharm 1995;119(2):149–63. https://doi.org/10.1016/0378-5173(94)00381-E.

[139] Maldonado-Codina C, Efron N. Dynamic wettability of pHEMA-based hydrogel contact lenses. Ophthalmic Physiol Opt 2006;26(4):408–18. https://doi.org/10.1111/opo.2006.26.issue-410.1111/j.1475-1313.2006.00394.x.

[140] Cheng I, Muller SJ, Radke CJ. Wettability of silicone-hydrogel contact lenses in the presence of tear-film components. Curr Eye Res 2004;28(2):93–108. https://doi.org/10.1076/ceyr.28.2.93.26231.

[141] Tonge S, Jones L, Goodall S, Tighe B. The ex vivo wettability of soft contact lenses. Curr Eye Res 2001;23(1):51–9. https://doi.org/10.1076/ceyr.23.1.51.5418.

[142] Li L, Xin Z. Surface-hydrophilic and protein-resistant tris(trimethylsiloxy)-3-methacryloxypropylsilane-containing polymer by the introduction of phosphorylcholine groups. Colloids Surf A 2011;384(1):713–9. https://doi.org/10.1016/j.colsurfa.2011.05.049.

[143] Brozova T, Raudensky M. Determination of surface wettability of polymeric hollow fibres. J Elastomers Plast 2018/12/01 2018,;50(8):737–46. https://doi.org/10.1177/0095244318765041.

[144] D. Campbell, R. Eden, S. Carnell, B. Tighe, "Dynamic contact angle analysis of silicone hydrogel contact lenses using the Wilhelmy plate technique," Contact Lens Anterior Eye, vol. 36, pp. 25-26, 12/01 2013, doi: 10.1016/j.clae.2013.08.093.

[145] Park J, Pasaogullari U, Bonville L. Wettability measurements of irregular shapes with Wilhelmy plate method. Appl Surf Sci 2018/01/01/ 2018,;427:273–80. https://doi.org/10.1016/j.apsusc.2017.08.186.

[146] Karl CW, Krauklis AE, Lang A, Giese U. Characterization of Rough PTFE Surfaces by the Modified Wilhelmy Balance Technique. Polymers (Basel) 2020;12(7):1–17. https://doi.org/10.3390/polym12071528.

[147] L. Jones, "Understanding the Link Between Wettability and Comfort," Contact lens spectrum, no. June, 2007.

[148] M. Vuckovac, M. Latikka, K. Liu, T. Huhtamäki, and R. H. A. Ras, "Uncertainties in contact angle goniometry," Soft Matter, 10.1039/C9SM01221D vol. 15, no. 35, pp. 7089-7096, 2019, doi: 10.1039/C9SM01221D.

[149] Dumbleton K, Caffery B, Dogru M, Hickson-Curran S, Kern J, Kojima T, et al. The TFOS International Workshop on Contact Lens Discomfort: Report of the Subcommittee on Epidemiology. Invest Ophthalmol Vis Sci 2013;54(11):TFOS20. https://doi.org/10.1167/iovs.13-13125.

[150] Guryča V, Hobzová R, Přádný M, Širc J, Michálek J. Surface morphology of contact lenses probed with microscopy techniques. Contact Lens Anterior Eye 2007;30(4):215–22. https://doi.org/10.1016/j.clae.2007.02.010.

[151] Giraldez M, Serra-Rodríguez C, Lira M, Real Oliveira ME, Yebra-Pimentel E. Soft Contact Lens Surface Profile by Atomic Force Microscopy. Optom Vis Sci 2010;87: E475–81. https://doi.org/10.1097/OPX.0b013e3181e170c5.

[152] Lee SJ, Bourne GR, Chen X, Sawyer WG, Sarntinoranont M. Mechanical Characterization of Contact Lenses by Microindentation: Constant Velocity and Relaxation Testing. Acta Biomater 2008;4(5):1560–8. https://doi.org/10.1016/j.actbio.2008.02.021.

[153] Tranoudis I, Efron N. Tensile properties of soft contact lens materials. Contact Lens Anterior Eye 2004;27(4):177–91. https://doi.org/10.1016/j.clae.2004.08.002.

[154] Nicolson PC, Vogt J. Soft contact lens polymers: an evolution. Biomaterials 2001; 22(24):3273–83. https://doi.org/10.1016/S0142-9612(01)00165-X.

[155] Holden BA, Stephenson A, Stretton S, Sankaridurg PR, O'Hare N, Jalbert I, et al. Superior Epithelial Arcuate Lesions with Soft Contact Lens Wear. Optom Vis Sci 2001;78(1):9–12. https://doi.org/10.1097/00006324-200101010-00008.

[156] Bhamra TS, Tighe BJ. Mechanical properties of contact lenses: The contribution of measurement techniques and clinical feedback to 50 years of materials development. Contact Lens Anterior Eye 2017;40(2):70–81. https://doi.org/10.1016/j.clae.2016.11.005.

[157] Kim E, Saha M, Ehrmann K. Mechanical Properties of Contact Lens Materials. Eye Contact Lens 2018;44:S148–56. https://doi.org/10.1097/icl.0000000000000442.

[158] Tighe B. A Decade of Silicone Hydrogel Development: Surface Properties, Mechanical Properties, and Ocular Compatibility. Eye Contact Lens 2013;39: 3–11. https://doi.org/10.1097/ICL.0b013e318275452b.

[159] Horst CR, Brodland B, Jones LW, Brodland GW. Measuring the Modulus of Silicone Hydrogel Contact Lenses. Optom Vis Sci 2012;89(10):1468–76. https://doi.org/10.1097/OPX.0b013e3182691454.

[160] Young G, Garofalo R, Harmer O, Peters S. The effect of soft contact lens care products on lens modulus. Contact Lens Anterior eye : J Br Contact Lens Associat 2010;33(5):210–4. https://doi.org/10.1016/j.clae.2010.06.002.

[161] Bozukova D, Bertrand V, Pagnoulle C, De Pauw-Gillet M-C. Evaluation of a class of polyurethane materials for intraocular lens manufacturing. J Biomed Mater Res B Appl Biomater 2015;103(6):1274–86. https://doi.org/10.1002/jbm.b.v103.610.1002/jbm.b.33305.

[162] Gulsen D, Chauhan A. Dispersion of microemulsion drops in HEMA hydrogel: a potential ophthalmic drug delivery vehicle. Int J Pharm 2005;292(1):95–117. https://doi.org/10.1016/j.ijpharm.2004.11.033.

[163] Jones L, Subbaraman L, Rogers R, Dumbleton K. Surface treatment, wetting and modulus of silicone hydrogels. Optician 2006;232:28–34.

[164] Szczotka-Flynn L. Looking at silicone hydrogels across generations. Optom Manag 2008;43:68–71.

[165] Iskeleli G, Karakoc Y, Ozkok A, Arici C, Ozcan O, Ipcioglu O. "Comparison of the effects of first and second generation silicone hydrogel contact lens wear on tear film osmolarity," (in eng). Int J Ophthalmol 2013;6(5):666–70. https://doi.org/10.3980/j.issn.2222-3959.2013.05.22.

[166] M. Lin and T. Yeh, "Mechanical Complications Induced by Silicone Hydrogel Contact Lenses," Eye Contact Lens, vol. 39, 2012, doi: 10.1097/ICL.0b013e31827c77fd.

[167] Rennie AC, Dickrell PL, Sawyer WG. Friction coefficient of soft contact lenses: Measurements and modeling. Tribol Lett 2005;18(4):499–504. https://doi.org/10.1007/s11249-005-3610-0.

[168] V. Ngai, J. B. Medley, L. Jones, J. Forrest, and J. Teichroeb, "Friction of Contact Lenses: Silicone Hydrogel versus Conventional Hydrogel," in Tribology and Interface Engineering Series, vol. 48, D. Dowson, M. Priest, G. Dalmaz, and A. A. Lubrecht Eds.: Elsevier, 2005, pp. 371-379.

[169] Dunn AC, Cobb JA, Kantzios AN, Lee SJ, Sarntinoranont M, Tran-Son-Tay R, et al. Friction Coefficient Measurement of Hydrogel Materials on Living Epithelial Cells. Tribol Lett 2008;30(1):13–9. https://doi.org/10.1007/s11249-008-9306-5.

[170] Van Beek M, Jones L, Sheardown H. Hyaluronic acid containing hydrogels for the reduction of protein adsorption. Biomaterials 2008;29(7):780–9. https://doi.org/10.1016/j.biomaterials.2007.10.039.

[171] Young G, Keir N, Hunt C, Woods CA. Clinical Evaluation of Long-Term Users of Two Contact Lens Care Preservative Systems. Eye Contact Lens 2009;35(2):50–8. https://doi.org/10.1097/ICL.0b013e31819630d3.

[172] Keir N, Woods CA, Dumbleton K, Jones L. Clinical performance of different care systems with silicone hydrogel contact lenses. Contact Lens Anterior Eye 2010;33 (4):189–95. https://doi.org/10.1016/j.clae.2010.01.006.

[173] Malet F. An acute clinical comparison of corneal staining and comfort associated with contact lens care solutions. Contact Lens Anterior Eye 2014/10/01/ 2014,; 37(5):351–7. https://doi.org/10.1016/j.clae.2014.05.007.

[174] Guillon M, Maissa C, Wong S, Patel T, Garofalo R. The influence of lens care systems on eyelid tissue changes during silicone hydrogel contact lens wear. Contact Lens Anterior Eye 2018;41(4):362–8. https://doi.org/10.1016/j.clae.2018.02.141.

[175] Santodomingo-Rubido J, Barrado-Navascués E, Rubido-Crespo M-J, Sugimoto K, Sawano T. Compatibility of two new silicone hydrogel contact lenses with three soft contact lens multipurpose solutions*. Ophthalmic Physiol Opt 2008;28(4): 373–81. https://doi.org/10.1111/j.1475-1313.2008.00573.x.

[176] Barabino S, Rolando M, Camicione P, Chen W, Calabria G. Effects of a 0.9% sodium chloride ophthalmic solution on the ocular surface of symptomatic contact lens wearers. Can J Ophthalmol 2005;40(1):45–50. https://doi.org/10.1016/S0008-4182(05)80116-4.

[177] Zigler L, Cedrone R, Evans D, Helbert-Green C, Shah T. Clinical Evaluation of Silicone Hydrogel Lens Wear With a New Multipurpose Disinfection Care Product. Eye Contact Lens 2007;33(5):236–43. https://doi.org/10.1097/ICL.0b013e318030c959.

[178] Sterner O, Aeschlimann R, Zürcher S, Scales C, Riederer D, Spencer ND, et al. Tribological Classification of Contact Lenses: From Coefficient of Friction to Sliding Work. Tribol Lett 2016;63(1). https://doi.org/10.1007/s11249-016-0696-5.

[179] Muntz A, Subbaraman LN, Sorbara L, Jones L. Tear exchange and contact lenses: A review. J Optom 2015/01/01/ 2015,;8(1):2–11. https://doi.org/10.1016/j.optom.2014.12.001.

[180] Mann A, Tighe B. Contact lens interactions with the tear film. Exp Eye Res 2013/ 12/01/ 2013,;117:88–98. https://doi.org/10.1016/j.exer.2013.07.013.

[181] Jones L, Brennan NA, González-Méijome J, Lally J, Maldonado-Codina C, Schmidt TA, et al. The TFOS International Workshop on Contact Lens Discomfort: Report of the Contact Lens Materials, Design, and Care Subcommittee. Invest Ophthalmol Vis Sci 2013;54(11):TFOS37. https://doi.org/10.1167/iovs.13-13215.

[182] Sterner O, Aeschlimann R, Zürcher S, Osborn Lorenz K, Kakkassery J, Spencer ND, et al. Friction Measurements on Contact Lenses in a Physiologically Relevant Environment: Effect of Testing Conditions on Friction. Investigat Opthalmol Visual Sci 2016;57(13):5383. https://doi.org/10.1167/iovs.16-19713.

[183] Roba M, Duncan EG, Hill GA, Spencer ND, Tosatti SGP. Friction Measurements on Contact Lenses in Their Operating Environment. Tribol Lett 2011;44(3):387–97. https://doi.org/10.1007/s11249-011-9856-9.

[184] h. D. Conway and M. Richman, "Effects of Contact Lens Deformation on Tear Film Pressures Induced during Blinking," Optometry and Vision Science, vol. 59, no. 1, pp. 13-20, 1982. [Online]. Available: https://journals.lww.com/optvissci/Fulltext/1982/01000/Effects_of_Contact_Lens_Deformation_on_Tear_Film.3.aspx.

[185] Shaw AJ, Collins MJ, Davis BA, Carney LG. Eyelid Pressure and Contact with the Ocular Surface. Invest Ophthalmol Vis Sci 2010;51(4):1911–7. https://doi.org/10.1167/iovs.09-4090.

[186] Kim SH, Marmo C, Somorjai GA. Friction studies of hydrogel contact lenses using AFM: non-crosslinked polymers of low friction at the surface. Biomaterials 2001; 22(24):3285–94. https://doi.org/10.1016/S0142-9612(01)00175-2.

[187] Zhou B, Li Y, Randall NX, Li L. A study of the frictional properties of senofilcon-A contact lenses. J Mech Behav Biomed Mater 2011;4(7):1336–42. https://doi.org/10.1016/j.jmbbm.2011.05.002.

[188] Samsom M, Chan A, Iwabuchi Y, Subbaraman L, Jones L, Schmidt TA. In vitro friction testing of contact lenses and human ocular tissues: Effect of proteoglycan 4 (PRG4). Tribol Int 2015;89:27–33. https://doi.org/10.1016/j.triboint.2014.11.022.

[189] Ghosh S, Mutalib HA, Sharanjeet K, Ghoshal R, Retnasabapathy S. "Effects of contact lens wearing on keratoconus: a confocal microscopy observation," (in eng). Int J Ophthalmol 2017;10(2):228–34. https://doi.org/10.18240/ijo.2017.02.08.

[190] Lau C, Tosatti S, Mundorf M, Ebare K, Osborn Lorenz K. "Comparison of the Lubricity and Surface Roughness of 5 Cosmetic Contact Lenses," (in eng). Eye Contact Lens 2018;vol. 44 Suppl 2(2):S256–65. https://doi.org/10.1097/ICL.0000000000000482.

[191] Young G, Veys J, Pritchard N, Coleman S. A multi-centre study of lapsed contact lens wearers. Ophthalmic Physiol Opt 2002;22(6):516–27. https://doi.org/10.1046/j.1475-1313.2002.00066.x.

[192] Jones L, Dumbleton K. 10 - Soft Contact Lens Fitting. In: Phillips AJ, Speedwell L, editors. Contact Lenses (Sixth Edition). London: Elsevier; 2019. p. 207–22.

[193] Sorbara L, Mueller K. "Effect of lens diameter on lens performance and initial comfort of two types of GP lenses for keratoconus: a pilot study," (in eng). J Optomet 2011;4(1):22–9. https://doi.org/10.1016/S1888-4296(11)70036-X.

[194] El-Nimri NW, Walline JJ. "Centration and Decentration of Contact Lenses during Peripheral Gaze," (in eng). Optom Vis Sci 2017;94(11):1029–35. https://doi.org/10.1097/OPX.0000000000001127.

[195] Shen M, Cui L, Riley C, Wang MR, Wang J. "Characterization of soft contact lens edge fitting using ultra-high resolution and ultra-long scan depth optical coherence tomography," (in eng). Invest Ophthalmol Vis Sci 2011;52(7):4091–7. https://doi.org/10.1167/iovs.10-6507.

[196] Wolffsohn JS, Drew T, Dhallu S, Sheppard A, Hofmann GJ, Prince M. Impact of Soft Contact Lens Edge Design and Midperipheral Lens Shape on the Epithelium and Its Indentation With Lens Mobility. Invest Ophthalmol Vis Sci 2013;54(9): 6190–6. https://doi.org/10.1167/iovs.13-12425.

[197] Pearson RM, Evans BJW. A comparison of in-air and in-saline focimeter measurement of the back vertex power of spherical soft contact lenses. Ophthalmic Physiol Opt 2012;32(6):508–17. https://doi.org/10.1111/opo.2012.32.issue-610.1111/j.1475-1313.2012.00932.x.

[198] Woods CA. Verification of the vertex powers of varifocal rigid contact lenses. Contact Lens Anterior Eye 2003;26(4):181–7. https://doi.org/10.1016/S1367-0484(03)00050-X.

[199] Hough T, Livnat A, Keren E. Inter-laboratory reproducibility of power measurement of toric hydrogel lenses using the focimeter and the Moiré deflectometer. J Br Contact Lens Associat 1996;19(4):117–27. https://doi.org/10.1016/S0141-7037(96)80004-8.

[200] Fowler CW. Technical note: Apparatus for comparison of progressive addition spectacle lenses. Ophthalmic Physiol Opt 2006;26(5):502–6. https://doi.org/10.1111/opo.2006.26.issue-510.1111/j.1475-1313.2006.00399.x.

[201] Phan, C.-M. Weber,S. Mueller, J. Yee, A. Jones, L. "A Rapid Extraction Method to Quantify Drug Uptake in Contact Lenses," (in eng), Transl Vis Sci Technol, vol. 7, no. 2, pp. 11-11, 2018, doi: 10.1167/tvst.7.2.11.

[202] Ciolino JB, et al. "In vivo performance of a drug-eluting contact lens to treat glaucoma for a month," (in eng). Biomaterials 2014;35(1):432–9. https://doi.org/10.1016/j.biomaterials.2013.09.032.
[203] S. Imafuku, "Silicone hydrogel soft contact lens having wettable surface (EP2840431B1)," 2016.
[204] Alli, A. Guzman, A. "Silicone hydrogels comprising polyamides (US20180011222)," 2019. [Online]. Available: https://patents.justia.com/patent/10371865.
[205] Pimenta AFR, Ascenso J, Fernandes JCS, Colaço R, Serro AP, Saramago B. Controlled drug release from hydrogels for contact lenses: Drug partitioning and diffusion. Int J Pharm 2016;515(1):467–75. https://doi.org/10.1016/j.ijpharm.2016.10.047.
[206] Acuvue® Theravision Product Information, Product information I. Johnson & Johnson Vision Care, USA, 2021.

Appendix 1.2: Research Article

International Journal of Pharmaceutics 621 (2022) 121793

Contents lists available at ScienceDirect

International Journal of Pharmaceutics

journal homepage: www.elsevier.com/locate/ijpharm

Controlled release of naringenin from soft hydrogel contact lens: An investigation into lens critical properties and *in vitro* release

Dan (Chau Thuy) Nguyen [a,*], Joseph Dowling [b], Richie Ryan [a], Peter McLoughlin [a], Laurence Fitzhenry [a]

[a] Ocular Therapeutics Research Group (OTRG), Pharmaceutical & Molecular Biotechnology Research Centre (PMBRC), South East Technological University (SETU), Waterford City, County Waterford X91 K0EK, Ireland
[b] Research and Development Department, Bausch + Lomb Ireland Ltd., Waterford City, County Waterford X91 V383, Ireland

ARTICLE INFO

Keywords:
Ocular drug delivery
Hydrogel contact lens
Therapeutic lens
In vitro release
Physical properties
Chemical properties

ABSTRACT

The naringenin (NAR)-impregnated hydrogel lenses (nesofilcon A material) were manufactured in this study with the feasibility to achieve controlled daily drug release. The lenses were fabricated using a comparable commercial-standard process, utilizing injection molding and thermal curing approaches. NAR-loaded lenses were prepared by both direct entrapment and 'soak and release' methods. Their critical properties were tested to ISO standards and comparable to the commercial lenses. NAR was fully characterized by studying its physical and chemical stability throughout the manufacturing processes using thermal analysis, high performance liquid chromatography and X-ray diffraction analysis. The NAR-loaded lenses showed > 97% light transmission, >75% water content, 0.50–0.53 ± 0.06 MPa tensile strength, with a lens diameter of 14.1 ± 0.1 mm. Lens polymerization kinetics were studied using differential scanning calorimetry. NAR released from the lens, prepared by a direct entrapment approach, followed a diffusion-controlled mechanism, and provided a controlled drug release of 72–82% for 24 h. A faster release rate was observed for NAR-loaded lenses prepared by a soak and release method, with over 90% of NAR was released in the first five hours.

1. Introduction

The treatment of ocular disorders of the anterior segment has relied upon a topical delivery strategy, which is often associated with low drug bioavailability (Weng et al., 2017). Where clinically relevant, intravitreal or periocular routes have been employed (Yang et al., 2018), which, while improving therapeutic bioavailability, can result in a higher number of systemic adverse effects and ocular complications (Falavarjani and Nguyen, 2013). Several studies have demonstrated controlled and sustained drug delivery using contact lenses while examining their critical physical properties such as swelling, optical transparency, ionic permeability, modulus, refractive index, wettability, and morphological characterization (Nguyen et al., 2021). Hydrogels are commonly used in the manufacture of soft conventional and daily disposable contact lens and have been investigated for the application in various biomedical applications such as ocular drug delivery systems (Nguyen et al., 2021). The interaction between the polymer and the water that the polymer binds or adsorbs is said to be the main factor governing the majority of hydrogel material properties (e.g. the functionality of soft contact lens on the human eye) (Tranoudis and Efron, 2004).

Furthermore, by using a therapeutic soft contact lens (SCL) as an ocular drug delivery system, the drug bioavailability can increase from<5% in topical administration up to 50% (Peng et al., 2010; Li and Chauhan, 2006). The first therapeutic-loaded contact lens, Acuvue® Theravision®, was recently in the market in 2021, which is ketotifen-loaded hydrogel lens (etafilcon A) by Johnson & Johnson Inc. (J.J. Inc, 2022). Such product has added the interest in the development of various therapeutic-loaded lens to provide a better care for patients who both need vision correction and suffering from various ocular disease.

Naringenin (NAR), 5,7-dihydroxy-2-(4-hydroxyphenyl)-2,3-dihydrochromen-4-one, is a type of flavonoid that has a molecular weight of 272.3 g/mol. NAR concentration varies from 1.47 to 11.15 mg/100 g in oranges and 14.17–53 mg/100 g in grapefruit (Nogata et al., 2006). Having two hydroxyl groups at position 5 and 7 of the A ring and a carbonyl group at position 4 of the C ring (Fig. 1), NAR can interact with

* Corresponding author at: Ocular Therapeutics Research Group, Ireland.
E-mail address: danchauthuy.nguyen@postgrad.wit.ie (D. (Chau Thuy) Nguyen).

https://doi.org/10.1016/j.ijpharm.2022.121793
Received 23 December 2021; Received in revised form 28 April 2022; Accepted 29 April 2022
Available online 6 May 2022

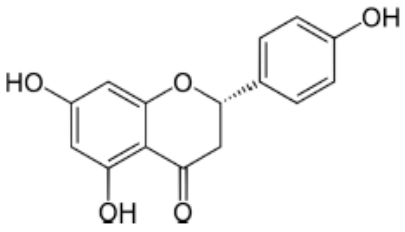

Fig. 1. Molecular structure of naringenin.

iron and copper ions to quench free radicals and ROS (reactive oxygen species) as reviewed by Alam *et al.* (Alam et al., 2014). NAR was demonstrated to exhibit several protective effects such as antiestrogenic activity (Ruh et al., 1995), inhibition of oxidative stress and UVB irradiation-induced skin damage (Martinez at al., 2015). NAR was also shown to have anti-inflammatory and antioxidant properties, with an ability to reduce neutrophil-derived reactive oxygen species (ROS) (Manchope, et al., 2016). By triggering the synthesis of reduced glutathione, which is known as the most abundant nonenzymatic antioxidant in cells, NAR can also enhance ROS detoxification (Ramprasath et al., 2014). NAR was also demonstrated to be able to tackle oxidative stress diseases such as cardiovascular, neurodegenerative, and age-related macular degeneration (Zaidun et al., 2018). Administration of NAR can also reduce lipid peroxidation while increasing antioxidant levels (Rashmi et al., 2018). As an eye-drop, with its anti-inflammatory and anti-oxidant properties, NAR at high dose (80 μg/eye) was found to inhibit corneal neovascularization (Oguido et al., 2017). Daily treatment with NAR eye drops was shown to significantly reduce the area of neovascularization (mm^2) after 3 and 7 days. Therefore, NAR has received increasing attention for ophthalmological applications via a topical route to treat posterior segment diseases (Zhang et al., 2016; Wang, 2020; Lin, 2015).

There are several methodologies and technologies used to create a SCL-based ocular drug delivery system (ODDS), and these techniques have been extensively reviewed (Dixon et al., 2015). Such approaches include 'soak and release', direct entrapment, molecularly imprinted SCL, nanoparticle-loaded SCL, and surface modified SCL, to name but a few. Additionally, with the improvement of the daily-disposable SCL market worldwide, as well as extended wear SCL, this technology can potentially reduce redness and irritation as it limits the eye contact with other preservatives used in many topical formulations. Many early studies on the incorporation of drugs into SCLs focused on soaking the lenses in drug solution (Maulvi et al., 2014). This approach is widely known as the 'soak and release' method, which is the simplest and the cheapest approach to loading drugs into SCLs. Another commonly used approach in the preparation of drug-loaded SCL is by directly adding a therapeutic agent into the SCL by adding it directly into the pre-polymerized monomer mixture before polymerization process, known as direct entrapment (Maulvi at al., 2017).

Considering the advantages of using SCL as an ODDS to increase drug bioavailability and controlled drug release, this work involved the manufacture and characterization of a hydrogel SCL impregnated with NAR. Although there has been an extensive amount of work carried out in the development of a therapeutic-loaded hydrogel, the majority of those did not involve the manufacturing of a commercial-quality SCL using a commercial-standard manufacturing process. As such, out of 50 articles published from 2016 to 2022 in various scientific journals, reviewed by the author, there are 16 works used a sheet of hydrogel/silicone hydrogel lens materials (e.g., (Pereira-da-Mota et al., 2021; Silva et al., 2020) and 18 works used commercial lens and modified it rather than fabricating them to commercial standards on-site (e.g., (Dixon et al., 2018; Pulliero et al., 2021). It was noted that the remaining 16 studies used cast molding technique to fabricate a lens, and all used an approximation of lens' polymeric materials rather than a commercial formulation. Furthermore, the synthesis of SCLs in those articles generally involved prolonged curing hours (e.g., 8–24 h) and harsh extracting conditions (e.g., boiling water for 5 h to 3 days) (e.g., (Pereira-da-Mota et al., 2021; Wang at al., 2021). These lens' manufacturing approaches, to the best of the authors' knowledge, are not commonly used in the industrial manufacturing process of a commercial SCL. In addition, most of the hydrogel lenses that have been studied are HEMA-based and are not commercial monomers, while in this study, the chosen lens material is predominantly NVP-based and is used in the manufacturing of a commercial lens. Therefore, it is of scientific value and interest to study and investigate the impact of loading a therapeutic agent in a different hydrogel-material of a commercial contact lens.

Furthermore, as mentioned by Brian Pall, a director at Johnson & Johnson Vision Care, there are various challenges with the commercialization of the first therapeutic SCLs (Ford, 2022). As such, after being successful incorporated into the lens matrix, the drug must be able to diffuse out of the lens matrix once it is placed on the eye. Therefore, besides ensuring that the developed drug-loaded lens exhibits all the critical commercialized lens parameters, the preliminary study should involve the investigation on its release behaviour.

In this work, a daily disposable SCL (nesofilcon A material, Biotrue® ONEDay) was chosen. Nesofilcon A lens is a daily disposable SCLs that are capable of maintaining nearly 100% of moisture for 16 h (B.L. Incorporated, 2021). The aim of this research was to investigate the feasibility of manufacture NAR-loaded lens prepared by both direct entrapment and 'soak and release' approaches to act as a potential therapeutic lens that has comparable properties to an unloaded commercial lens based on the relevant ISO standards.

2. Materials and Methods

2.1. Materials

Monomer components, nesofilcon A pre-polymerized monomer mixture and Biotrue® ONEday contact lens' molds and contact lens (-3.00 SVS was used as the control lens throughout this study), N-vinyl pyrrolidone (NVP, purity: >97%), 2-hydroxyethyl methacrylate (HEMA, purity: >99%), ethylene glycol dimethacrylate (EGDMA, purity: >98%), allyl methacrylate (AMA, purity: >99%), e-Butyl-hydroxycyclohexyl (TBE, purity: >97%), Poloxamer 407 dimethacrylate (purity: N/A) were provided by Bausch + Lomb Ireland Ltd (Waterford City, Ireland). 2,2-azobisisobutyronitrile (AIBN, purity: >98%), naringenin (purity: >98%), acetic acid (purity: ≥99%) and Tween 80 (CMC: 0.012 mM, purity: not specified) were purchased from Sigma-Aldrich Ireland (Wicklow, Ireland). PBS (phosphate buffered saline tablets, purity: not specified) and Methanol (HPLC grade, purity: >99%) were purchased from Fisher Scientific (Dublin, Ireland). Ultrapure deionized water obtained from WhiteWater equipment (Dublin, Ireland) was used throughout the study.

2.2. Preparation methodologies

2.2.1. Manufacturing of soft hydrogel contact lens

The SCL (nesofilcon A) was prepared by mixing NVP, HEMA, EGDMA, AMA, TBE, Poloxamer 407dimethacrylate, and AIBN in a container for an hour. An injection moulding approach was used to fabricate the contact lenses. After removing the posterior part of the moulds, 23 μL of liquid pre-polymerization monomer mixture was injected into the anterior segment. This was followed by manually capping the anterior and posterior parts of the mould together before curing. A forced convection oven (UF50, Memmert) was used to cure SCLs in an ambient gaseous environment. The full curing cycle is demonstrated in Table 1. Once the curing cycle was completed, the tower of moulds was allowed to cool for at least 30 min inside the oven. Lenses were then removed from the moulds using a dry-release process.

Table 1
Description of lenses used in this study.

Lens ID	Description
Control	Commercial Biotrue® ONEDay (nesofilcon A) contact lens.
Blank WM	Unloaded lens produced onsite using nesofilcon A pre-polymerized monomer mixture.
L1	NAR-loaded WM lens prepared by direct entrapment approach at a concentration of 14.6–20.7 μg/lens.
L2	NAR-loaded WM lens prepared by direct entrapment approach at a concentration of 23.3–33.1 μg/lens.
L3	NAR-loaded WM lens prepared by direct entrapment approach at a concentration of 37.9–53.7 μg/lens.
L4	NAR-loaded WM lens prepared by direct entrapment approach at a concentration of 46.6–66.1 μg/lens.
L5	NAR-loaded WM lens prepared by 'soak and release' approach at a concentration of 46.6–66.1 μg/lens.

Lenses were then hydrated in 2 mL of 60 °C DI H_2O and washed three times individually using 60 °C DI H_2O (2 mL each time) to remove any unreacted monomers. The finished lenses were subjected to thermal sterilization (autoclave) at 123 °C for 66 min. The preparation process for making SCLs is illustrated in the Fig. 2.

Directly entrapped NAR-lenses, coded L1, L2, L3 and L4 were prepared in the same way as described above with 2.18, 3.48, 5.66 and 6.96 mg/mL, respectively, of NAR were added to and dissolved in the pre-polymerized monomer mixture by stirring for one hour.

'Soak and release' NAR-lens, coded L5, was prepared by soaking a dry lens in the NAR solution of a concentration 0.85 mg/ 3 mL in 0.1% Tween 80 in PBS, pH 7.4 for 72 h. The L5 lens was then extracted and sterilized using the same procedure as described earlier on in this section.

2.2.1.1. Stability of naringenin. **TGA:** a TGA (Q50 model, TA Instrument) was used in this study. Approximately 5 mg of NAR was accurately weighed into a sample pan. Each sample was ramped from 20 to 500 °C at 10 °C/min heating rate.

XRD: a XRD, Bruker D8 Advance diffractometer equipped with a copper source, operating at 4 kV and 40 mA using an SSD-160 detector, was used in this study. The instrument was operated in Bragg-Brentano geometry from 5 to 60 (2θ) with a CHC^+ Temperature and Relative Humidity Chamber (Anton Parr). An Internal air scatter was equipped to limit beam divergence and reduce background interference. Prior to sample analysis the system was validated using a certified corundum reference standard. All samples were analysed using DIFFRAC.EVA software. XRD of NAR sample was analysed using the method described in Table 2 (non-ambient condition), using a 0.019° step size with 1 s per step from 5 to 60° (2θ).

HPLC: the stability of NAR in the release media (i.e., PBS + 0.1% Tween 80, pH 7.4) was investigated by implementing the HPLC method as outlined in Section 2.4.1 below. Briefly, a NAR solution of 1 mg/mL was prepared in release media in a 15 mL centrifuge tube and was placed in a 37 °C incubator and shaken at 50 rpm for over 7 days. After each day, an amount of NAR solution was withdrawn from the tube for HPLC analysis. In addition, NAR stability in water at 123 °C (based on the sterilization condition) was also assessed in this study by analyzing the water solution of NAR-loaded lens after sterilization.

Table 2
Experimental parameters for SCL curing cycle, DSC and XRD analysis.

Pre-polymerized monomer mixture/Curing cycle/XRD analysis	
Test parameter	Setting
Equilibrate	20 °C
Ramp rate	10° C/min 64 °C
Isothermal hold	20 min
Ramp rate	2 °C/min to 93 °C
Isothermal hold	30 min
Ramp rate	1 °C/min to 110 °C
Isothermal hold	60 min
Contact lens (dry state)	
Test parameter	**Setting**
Equilibrate	20 °C
Ramp rate	5 °C/min to 200 °C

2.3. Characterisation of naringenin-loaded soft hydrogel contact lenses

A total of 7 contact lens' systems were studied and characterized in this study, which is described in Table 1 Below:

2.3.1. Differential scanning calorimetry

A DSC (Q2000 model, TA Instrument) was used in this study. A calibration with indium was carried out before testing any samples to ensure the accuracy and precision of the measurements. Approximately 2–10 mg of each sample was accurately weighed into a sample pan. The pan lid was pierced with a pin to ensure no pressure build up within the pan during the experiment. An empty aluminium pan was used as a reference. Parameters of this test are illustrated in Table 2.

2.3.2. Light transmission

A Shimadzu UV-2401 PC, UV–Vis spectrophotometer was used to

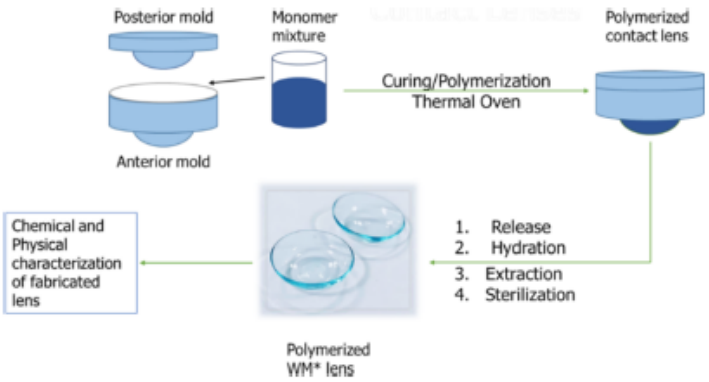

Fig. 2. Schematic diagram on the manufacturing process of SCL (WM lens = lens made by the author on-site at Waterford Institute of Technology using a Memmert oven).

measure the light transmission through the hydrated WM and control lens. Measurement was carried out using a wavelength range from 800 to 400 nm at 1 nm intervals and referenced to air. Lenses were suspended in the light path using a quartz cuvette. Values presented are averages of three measurements for each lens.

2.3.3. Water content

SCL swelling studies evaluated the equilibrium water content (EWC) over a 24-hour period. Three measurements were carried out for each type of lens at room temperature. The dry lenses (W_D) were weighed and then immersed in DI H_2O in separate containers. At specific intervals of time, each sample was carefully blotted with white absorbent paper (free from residues) and weighed immediately (W_w). The equilibrium water content (%EWC) was calculated based on Equation (1):

$$\%EWC = \frac{W_w - W_D}{W_w} \times 100 \quad (1)$$

2.3.4. Wettability

Contact angle of the developed lenses were measured using a captive air bubble technique (Nguyen et al., 2021). Fully hydrated lens was cut into a small rectangle section, flattened, and fixed using parafilm, which was then immersed in water. A micrometer syringe with a curved needle was used to create air bubbles on the surface of the lens. A contact angle measure system G10 (Krüss Scientific, Germany) was used in this study. Values presented are averages of nine measurements for each lens.

2.3.5. Tensile strength

Each hydrated lens (in water) was cut into a dog-bone shape using a 'dog-bone' shaped cutting template (Figure S1, Supplementary Information). The TA.XT Express Enhanced (Stable Micro System) instrument was used in this study to measure the tensile properties of the lenses. Tensile grips (which were modified with sponges) were used to stretch the lens until breakage occurred. In order to eliminate any ambiguity from the slope area used, it was suggested that the modulus can be derived from a tangent within the first 10% of the extension range, which was previously used by Kim *et al.* (Kim et al., 2018) to measure the mechanical properties of commercial lenses. The velocity of the two grips was set to 0.11 mm/s and the applied force was 1 g. Values presented are averages of ten measurements for each lens.

2.3.6. Refractive index

The RFM340 refractometer (Bellingham + Stanley Ltd.) with a wavelength of 589 nm (sodium D-line) was used to measure the refractive index (RI) of all lenses. Temperature was controlled at 20 °C throughout the measurement. Tested lenses were immersed in ultrapure water for at least 30 min prior to testing. To verify the performance of the refractometer, the RI of water was measured prior to testing samples, which is 1.333. The hydrated individual lens was then placed directly on top of the lens holder, which was attached to an appropriate spring to create a force to push the lens in contact with the prism.

2.3.7. Fourier-transform infrared spectroscopy

A calibration with a polystyrene sample was carried out before testing any samples to ensure the accuracy and precision of the measurements. Each sample spectrum was generated from 64 scans recorded in the range from 600 to 4000 cm^{-1}, with a resolution of 2 cm^{-1}. Each sample was tested in triplicate. Sample spectra were recorded using:

- Naringenin: A small quantity (2–4 mg) was finely ground in a 1:5 ratio with KBr. This mixture was then made into a solid disc (applied pressure: 3 N for 3 min) for further analysis.
- Liquid samples (monomers): A ZnSe crystal with a six-reflection geometry and 45° angle of incidence (70 mm × 10 mm) was used: A thin layer of liquid monomer was injected onto the ATR crystal to cover the entire crystal surface.
- For dry lenses, spectra were recorded using FT-IR spectrophotometer equipped with an ATR (attenuated total reflectance) microscope. The spectrum was obtained upon contacting between the Ge metal ball and the surface of the lens.

2.3.8. Lens dimensions

Lens diameter, sagittal depth and centre thickness were measured using the Micrometer Caliper measurement tool through magnified glass at 5X. Values presented are averages of ten measurements for each lens. The generated results are comparative only and may not be reflective of the true value of nesofilcon A lenses. Dimensional measurements are dependent on temperature and test solution, which were carried out in air at room temperature in this work. Centre thickness results depend on the force used during the measurement due to the sponge type nature of the material.

2.4. In vitro release

2.4.1. HPLC analysis of naringenin

Naringenin (NAR) was assayed by a gradient, reversed phase high performance liquid chromatography (RP-HPLC) methodology using a Waters, Symmetry® C18 column (150 mm × 4.6 mm, 5 µm particle size). Method conditions were adapted from the study carried out by Zhang *et al.* (Zhang et al., 2016) with a reduction in running time, from 20 min down to 15 min. The mobile phase consisted of 0.1% acetic acid in water (A) and methanol (B) and each solvent was degassed in an ultrasonic bath before use for at least 45 min. Chromatographic separation was achieved using a gradient programme: 0–5 min (60:40 v/v A:B), 5–11 min (40:60 v/v A:B), 11–12.5 min (30:70 v/v A:B), and 12.5–15 min (60:40 v/v A:B). Column temperature was held constant at 30 °C with a 1 mL/min flow rate. The injection volume was 20 µL with each injection carried out in triplicate, and ultraviolet detection at 288 nm.

2.4.2. In vitro release

Soaked and directly entrapped NAR-loaded SCL (sterilized lens stored in DI water) were placed in 5 mL of 0.1% Tween 80 in PBS in glass vials, kept at 37 °C in an incubator with shaking at 50 rpm. At a predetermined interval, 500 µL of release media was withdrawn and replaced immediately with the same volume of fresh release media to maintain sink conditions. The concentration of NAR was determined by HPLC, according to the procedure described in Section 2.4.1. The percentage cumulative drug release from a lens was calculated following the below equation (Equation (2)):

$$\%\text{Cumulative drug release} = \left(\frac{Testedvolume}{Bathvolume} * P_t\right) + P_{tc} \quad (2)$$

Where: P_t and P_{tc} are the percentage release at time 't' and percentage release previous to time 't', respectively; Tested volume (mL): volume of release media was withdrawn at a specified interval for HPLC analysis; Bath volume (mL): total volume of release media in a glass vial.

2.5. Statistical analysis

A paired *t*-test (two-tailed) was used to compare various fabricated WM lens properties to the control lens (i.e., RI, EWC, optical transparency, contact angle, tensile strength, dimensions, and thermal analysis). A p-value < 0.05 was considered statistically significant, while a p-value > 0.05 was considered statistically insignificant. All analyses were performed using Minitab 17.

3. Results and discussion

3.1. Estimation of naringenin therapeutic window

As mentioned in Section 1, NAR ophthalmic drops were studied to

treat retinal diseases. A study carried out by Lin *et al.* demonstrated that 1 μg/mL NAR can increase the proliferation of retinal pigment epithelium cells while inhibiting the growth of human umbilical vein endothelial cells (Lin and Chiou, 2008). Therefore, it was essential to estimate the appropriate NAR concentrations to be used in this study that are within its therapeutic window to potentially treat posterior segment diseases. A required daily dose of approximately 500 μg was calculated based on the ocular pharmacokinetics of 1% NAR eye drops in rabbits (Lin at al., 2015). It is widely concluded that SCL can significantly enhance drug residence time (Dixon et al., 2015), and thus, its ocular bioavailability, from 1 to 5% in eye drops to as high as 50% in SCL. Hence, the NAR therapeutic concentration range to be loaded into the lens was calculated for this study to be 14 – 66 μg/day.

In addition, given that there are several processes involved in the fabrication of the SCLs, it is essential to accurately quantify the amount of drug loss through each stage of the process, and subsequently, the precise amount of drug uptake in the lens. Hence, to accurately determine the amount of NAR presented in the finished NAR-loaded lens before carrying out an *in vitro* release study, the amount of NAR loss through each stage of the process (i.e., drug leaching). The percentage of NAR uptake in a finished NAR-loaded lens was quantified with respect to the initial amount of added NAR into the pre-polomerized monomer mixture (for direct entrapped lens), and the amount of added NAR into the soaking solution (for soak and release) lens (Table 3).

3.2. Stability of naringenin

It is essential to investigate the thermal stability of NAR to ensure its activity was maintained throughout the curing cycle, extraction, and sterilization steps. This was confirmed by TGA (Fig. 3A) and X-Ray Diffraction (Fig. 3B).

As could be observed from the generated thermal graph, NAR is thermally stable up to 296.55 ± 2.89 °C. XRD is commonly used to analyze the amorphous or crystalline state of materials, as well as their type of crystalline phase and chemical nature of a compound (Manaia et al., 2017). Fig. 4B showed that the crystallinity of NAR maintained throughout the whole curing cycle.

Additionally, HPLC analysis on NAR presented in NAR-loaded lens solution after sterilization step was also carried out to determine its stability in aqueous environment. NAR stability in water and release media (i.e., PBS + 0.1% Tween 80, pH 7) were studied. The outcome from this analysis indicated NAR is stable in both water and release media at 37 °C for over 4 weeks.

3.3. Polymerisation kinetics of hydrogel contact lens and drug-loaded lens

A controlled and repeatable polymerization process is essential in producing a commercial-quality lens. Differential scanning calorimetry (DSC) was previously used to investigate polymeric materials structure and properties by heating such materials at a certain rate in a specified temperature range (Alves at al., 2011), as well as to monitor polymerization reactions for several systems (Achilias and Siafaka, 2017). To obtain an insight into the polymerisation kinetics of the WM lens, pre-polymerization monomer mixture and five individual monomers including NVP, HEMA, EGDMA, AMA, and TBE were investigated. An adequate amount of initiator (AIBN, which was used in this study) of approximate 0.5 %w/v was added into each individual monomer solution to initiate the polymerization process, which was assessed by DSC. The chosen DSC cycle for this study was based on the lens curing cycle used in this study (Table 2).

Due to the addition reaction to the monomer's double bond, free radical polymerization of vinyl monomers produces a substantial heat release (polymerization enthalpy). The bulk radical polymerization of NVP with AIBN was previously carried out at 60 °C as cited by Wan *et al.* (Wan et al., 2005).

The DSC data of the pre-polymerized monomer mixture with and without NAR at various concentrations was analysed by the heat flow curves, where the heating rates mimicked the curing cycle. All three stages included initiation (i.e. decomposition of an initiator to form the primary radicals), propagation (of radicals by reacting with monomer molecules) and termination (of two macro-radicals to form polymer chains) were observed in Fig. 4 as expected to be seen in a radical polymerization mechanism (Achilias, 2014).

As could be observed from Fig. 4, the polymerization kinetics of the lens pre-polymerization mixture with and without the presence of NAR provided similar thermal curves. Following the thermal data generated from this experiment, illustrated in Table 4 and Figure S2 (supplementary information), it was found that the addition of NAR did not alter the polymerization of the pre-polymerized mixture of the lens monomer. Therefore, it was suggested that the formulated NAR-loaded lens could still exhibit the lens' critical properties that are comparable to the control lens.

An investigation into the polymerization kinetics of each monomer component with the presence of AIBN was carried out to confirm this observation (Figure S3, Supplementary Information). It should be noted that due to the small quantity of some components in the final mixture, the test was carried out using a larger volume to facilitate initiation with AIBN. Therefore, the intensities of each exothermic reaction in the individual component did not reflect its real concentration in the monomer mixture. Instead, this analysis aimed to provide insight into the polymerization process of the monomer mixture, to determine which component was correlated to the first and second stages of polymerization.

There was no energy release at Stage 1 (Fig. 4) of the process (ramp 10 °C/min from 20 °C to 64 °C). An exothermic peak, which indicated the start of the propagation, occurred at Stage 2 (isothermal at 64 °C for 20 min, Fig. 4), which was corresponded to the initiation of HEMA, EGDMA and TBE (Figure S3, Supplementary Information). This occurred due to the decomposition of AIBN initiator, which produced free radicals at approximately 64 °C to initiate the polymerization process to give a rapid increase in energy evolved in the reaction (Achilias and Siafaka, 2017; Koetzier et al., 1980). It was noticed that the peak at this stage carried a shoulder (Fig. 4). Huang *et al.* suggested that this was due to the presence of crosslinker (EGDMA) (Huang et al., 1997). Study carried out by Achilias *et al.* postulated that the free radical polymerization was diffusion-controlled (Achilias and Siafaka, 2017). As the chemical crosslinking of the polymer matrix increased, diffusion through the matrix was considered as a limiting factor since a higher degree of crosslinking could result in more residual vinyl groups in the network (Huang et al., 1997). Thus, the isothermal conversion and the associated heat release would be decreased. It was postulated that the presence of a shoulder peak or peak splitting from EGDMA was due to a later reaction of the trapped monomers and pendant vinyl groups, which could limit both the reaction rate and final conversion.

When the polymerization process proceeded into Stage 3 (ramp 2 °C/min to 93 °C), a noticeable amount of heat release was recorded,

Table 3
Summary table illustrating an actual NAR loading concentration for L1-L5 lenses, as well as the percentage drug loss through the manufacturing processes, and the percentage of NAR uptake for all five lens systems.

Lens ID	%Drug loss through hydration, extraction, and sterilization	% NAR uptake	NAR (μg/lens)
L1	17.65 ± 0.47	47.08 ± 3.32	23.54 ± 1.66
L2			28.45 ± 1.92
L3			39.63 ± 1.16
L4			51.14 ± 1.09
L5	33.45 ± 0.06	18.10 ± 1.50	55.51 ± 0.83

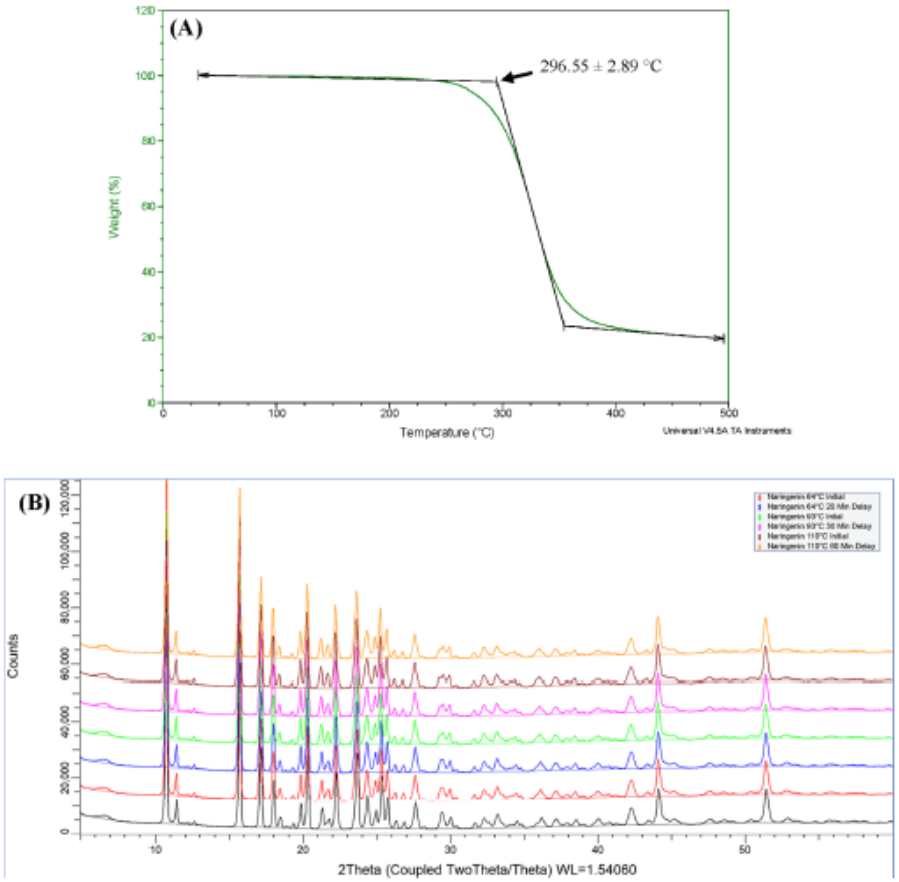

Fig. 3. Naringenin thermal and crystalline profiles through TGA (A) and XRD (B) analysis, respectively.

indicating the propagation stage of the reaction (Fig. 4). This stage corresponded to the initiation of NVP, AMA and EGDMA monomers that release heat in the system (Figure S3, Supplementary Information). Since NVP accounts for over 75% of the monomer mixture, the majority of the monomers have been cured at this step. Stage 4 of the polymerization (isothermal at 93 °C for 30 min) showed a heat release from EGDMA (Figure S3, Supplementary Information). This step was suggested to be essential to increase the overall conversion rate of the polymerization of the lens. At a higher reaction temperature, both monomers and polymer network would have higher energy to decrease the limitation of diffusion due to a reduction in the degree of cross-linking (Huang et al., 1997). Stages 5 (ramp 1 °C/min to 110 °C) and 6 (isothermal at 110 °C for 60 min) of the polymerization process recorded little or no heat release from the system (Fig. 4) suggesting that the reaction entered the termination/completion stage and the formation of polymer chains (i.e., SCLs).

3.4. Characterisation of naringenin-loaded lenses

The manufacturing of the 'soak and release' NAR-lens required a higher amount of added NAR (Table 2) and a longer preparation time in comparison to directly entrapped NAR-lens due to the additional soaking period (3 days). Moreover, the initial observation of the prepared directly entrapped NAR-lens showed no noticeable differences to the control lens. Hence, while there were four concentrations of directly entrapped NAR-lens investigated, only 'soak and release' NAR-lens at the highest concentration (comparable to L4 lens) were fabricated and characterized to compare with those prepared using a direct entrapment approach.

3.4.1. Light transmission

One of the most essential parameters in SCLs is their light transmission. Hence, this feature should be studied for both the control lens and lens upon any modifications to examine its optical quality. The result data obtained in this study is summarized in Table 5 and Figure S4 (Supplementary Information).

From the generated data, an average transmittance of 99% (in the visible region) relative to the control lenses was observed in the fabricated blank WM lenses. An optical transparency>97% was observed for all NAR-loaded lenses at different concentrations and was within the ISO tolerance limits for optical transparency of a SCL (ISO, 2017). This result indicated that the WM and NAR-loaded WM lenses produced by both direct entrapment and soak and release approaches provided sufficient optical clarity for commercial use as ophthalmic medical devices.

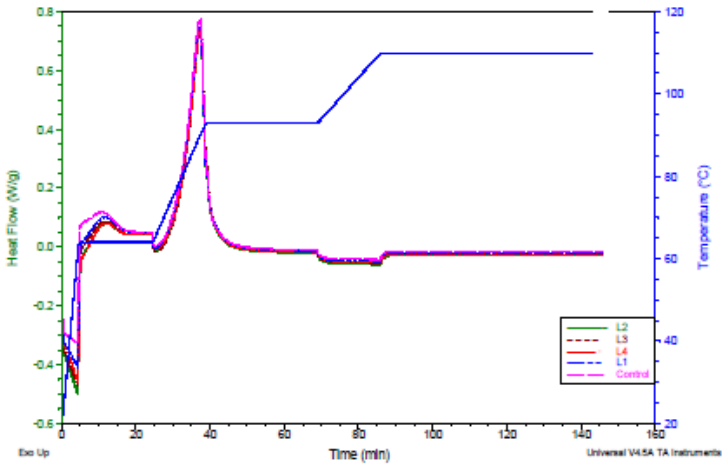

Fig. 4. Polymerization kinetics of the pre-polymerization monomer mixture (with and without NAR) as a function of time and temperature (n = 3).

Table 4
Thermal data on peak temperatures and reaction enthalpy derived from the polymerization of pre-polymerized monomer mixture with and without the presence of NAR (n = 3, p-value > 0.05).

Sample	Peak 1		Peak 2	
	Temperature (°C)	Reaction enthalpy (J/g)	Temperature (°C)	Reaction enthalpy (J/g)
Control/ Blank WM	63.99	268.9 ± 17.1	90.16 ± 0.27	260.1 ± 4.9
L1		278.2 ± 16.0	90.28 ± 0.08	261.8 ± 10.9
L2		302.8 ± 11.3	90.26 ± 0.10	261.2 ± 8.2
L3		305.8 ± 10.4	90.32 ± 0.11	251.3 ± 4.0
L4		284.2 ± 6.8	90.33 ± 0.04	245.7 ± 2.4

3.4.2. Water content

It is essential to study the water content of the prepared SCLs since it is related to the comfort of the lens and is also closely related to their dehydration rate (Nguyen et al., 2021). To determine the lens hydrophilicity and water uptake, swelling studies were carried out on the WM lens, NAR-loaded WM lenses, and the control lens. As discussed in the recently published review of the author (Nguyen et al., 2021), there are several limitations associated to this technique which could result in a significant difference between different operators. Hence, it should be noted that the value of the control lens in this test was only for comparative purposes only and does not reflect the true value of nesofilcon A materials, which is 78%.

The average percentage EWC and its standard deviation for each lens type are tabulated in Table 5. The obtained data demonstrated that the %EWC values of the NAR-loaded WM lenses (e.g. 75.5 ± 0.6% for L1 lens) was similar to those obtained in the control lenses (76.0 ± 0.5% for the control lens and 75.8 ± 0.2% for blank WM lens) at 25 °C (p-values > 0.05 at 25 °C), which was within the ISO tolerance limits for water content of a soft hydrogel lens (ISO, 2017). Additionally, low standard deviation in %EWC values implied that the WM lenses were manufactured uniformly.

3.4.3. Refractive index

The RI of SCL materials was measured at 589 nm (sodium D-line), which is within the requirement as stated in ISO18369-4:2017 (ISO, 2017). The required RI value for a commercial SCL typically should not exceed 1.55 (ISO, 2017). Table 5 demonstrated that the fabricated WM NAR-loaded lenses produced similar RI values in comparison to the unloaded WM lens (p-value > 0.05), which was 1.373. Additionally, following the ISO 18369–2 standard, this difference is within the tolerance limit (±0.005) for RI values of SCLs (ISO, 2017). Hence, the WM lenses with varying NAR concentrations produced a comparable RI value to the control lenses. In addition, given that the standard deviation is low in both cases, the tests provided reproducible and reliable results.

3.4.4. Wettability

Wettability is a crucial characteristic since it illustrates the spreading ability of the tear film along the material surface. Hence, this property is

Table 5
Summary table of the fabricated lens' physicochemical and mechanical properties.

Lens sample	%T (n = 3)	%EWC (n = 3)	Refractive index (n = 3)	Contact angle (n = 10)	Tensile strength (n = 10)	T_g (°C)
Control	98.1 ± 0.7	76.0 ± 0.5	1.373 ± 0.000	41.22 ± 0.57	0.53 ± 0.05	80.2 ± 1.5
WM	98.2 ± 0.8	75.8 ± 0.2	1.373 ± 0.000	40.35 ± 0.66	0.54 ± 0.06	79.7 ± 1.6
L1	98.9 ± 0.5	75.5 ± 0.6	1.373 ± 0.000	42.23 ± 0.88^{+}	0.52 ± 0.04	77.5 ± 2.5
L2	98.2 ± 0.4	75.4 ± 0.5	1.373 ± 0.000	44.33 ± 0.49^{+}	0.51 ± 0.05	76.3 ± 1.9
L3	97.8 ± 0.3	75.1 ± 0.6	1.373 ± 0.000	46.03 ± 0.70^{+}	0.50 ± 0.06	75.0 ± 4.5
L4	97.6 ± 0.5	75.6 ± 0.6	1.373 ± 0.000	45.76 ± 0.87^{+}	0.53 ± 0.06	71.9 ± 3.6^{+}
L5	98.2 ± 0.6	75.9 ± 1.0	1.373 ± 0.000	44.47 ± 0.97^{+}	0.53 ± 0.07	N/A
ISO tolerance (ISO, 2017)	± 5% absolute*	± 2% absolute*	± 0.005 absolute*	N/A	N/A	N/A

*: values from the blank WM lens.
$^{+}$: values exhibit a p-value < 0.05 in comparison to the control lens.

directly related to the comfort and performance of manufactured SCLs (Nguyen et al., 2021). The smaller the CA, the better the wetting ability of the material over a substrate (Campbell et al., 2013). Water contact angles (CAs) of the studied lenses in the hydrated state were measured by a captive bubble method.

From Table 5, it can be observed that the CA of the lens increased slightly with the increase in the amount of NAR loaded into the lens for the direct entrapment approach (p-value < 0.05). As an example, the CA value increased from 40.35 ± 0.66 in blank WM lens, to 42.23 ± 0.88° and 45.76 ± 0.87° for L1 and L4 lenses, respectively. This is expected due to the hydrophobicity of NAR. The CA of the HEMA/PVP lenses (water content: 60.7 ± 0.3%) was previously determined to be 42.00° ± 3.00° using a captive bubble method (Silva et al., 2015), and the CA range in this work was between 40 and 46°. Lin *et al.* (Lin and Svitova, 2010) cited that the acceptable range of CA of commercial SCLs is 11°-83°, demonstrating that the produced WM lenses have a suitable hydrophilicity to be used as ophthalmic medical devices. Although tear fluid and water have distinctive characteristics, this study was carried out in water rather than simulated tear fluid (STF) to investigate the raw material's property. As such, if the measurement was done in STF, the lens matrix could potentially take up the components that are present in the solution, which in turn could affect the outcome of the inherent wettability of the SCL material. Additionally, this is in agreement with a number of other studies that have also used water (Campbell et al., 2013; Silva et al., 2015; Korogiannaki et al., 2017).

3.4.5. Tensile strength

In order to investigate the tensile strength of the SCL, it was first cut into a standard shape (Nguyen et al., 2021). ISO 18369–1:2017 (E) (ISO, 2017) states that the tensile modulus of elastic material is a constant ratio between the tensile stress and the tensile strain, which should be in the range of linear elastic behaviour of the material. As cited by Bhamra and Tighe (Bhamra and Tighe, 2017), studies on tension of a material provide a measured modulus, tensile strength and elongation to break of that material, which all relate to both handling and durability. The tensile strength of eight different types of lenses was investigated. Since this test required a lot of manual handling, at least ten samples for each lens type were required to produce representative data.

From the generated data, calculations for mechanical properties of the material were carried out to determine the Young's Modulus of the SCLs. Generally, in the case of stress–strain graphs in experimental cases, the slope of the curve changes between the origin and terminus of the graph (Bhamra and Tighe, 2017). The Young's modulus values for the eight lens' systems are compared, Table 5. All 8 types of fabricated lenses showed no statistically significant difference in tensile strength in comparison to the control lenses (p-value > 0.05). The standard deviation was low in all cases, which implied that this technique is feasible in determining the hydrogel tensile strength, and WM lenses were produced consistently.

The Young's modulus value for hydrogels such as pHEMA is expected to be approximately 0.5 MPa (Materials Data Book, Cambridge University Engineering Department, 2003). The Young's modulus values in a range of 0.1–1.9 MPa were recorded for conventional hydrogel lenses, depending on the lens' components and its water content (Bhamra and Tighe, 2017). Since the Young's modulus values of the NAR-loaded WM lenses from this experiment are within the range of other hydrogel materials with similar composition, they can be considered as appropriate material for commercialized hydrogel SCLs.

3.4.6. Thermal analysis

The thermotropic behaviour of dry-state (Fig. 5) SCLs was investigated throughout this study. DSC determines the material's glass transition temperature (T_g) by measuring material heat capacity as a function of temperature (Efremov et al., 2004). T_g is the temperature at which a material changes from a glassy to a rubbery state, which is related to a material's chemical and physical stabilities as well as its viscoelastic properties (Hancock and Zografi, 1994). The T_g value is also linked to the stiffness and flexibility of the polymer chains as it is determined by steric and electrostatic interactions (Klähn et al., 2019). The DSC cycle used in this study was previously used to determine the T_g value of a material (Silva et al., 2015; ElShaer et al., 2016).

The addition of NAR resulted in a reduction in the T_g value (Table 5) of the fabricated lens, and the higher the concentration of added NAR, the lower the T_g value (p-value < 0.05 for DE_NAR-160 lens). This is believed to be due to the presence of NAR in the polymer matrix, which had a plasticising effect (Hancock and Zografi, 1994). T_g of a SCL is correlated to the lens' water content, and hence, this value can influence on-eye comfort, lens movement, as well as water, ion, and oxygen

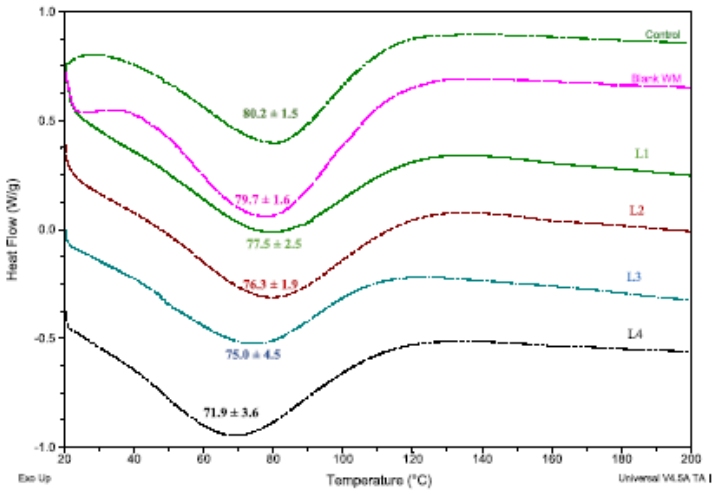

Fig. 5. DSC thermograms of the control, blank-WM lens and NAR-loaded WM lenses (L1-L4 denoting different concentrations of NAR loaded through direct entrapment). All lens' systems are in the dry state (n = 3) and the instrumental value for Tg was reported.

transport in the lens (Fornasiero et al., 2005). In polymers, the ability of an analyte to transport within the matrix increases when the T_g of such material decreases, which is determined by the relaxation state of the polymer host matrix (Lira et al., 2020). As such, a lower T_g value indicates that there is less intermolecular constrain in the motion of the chain segment of the main polymer in the lens, and thus, the higher its water content (Fornasiero et al., 2005; Lira et al., 2020). However, as could be observed from Table 5, the water content of all four concentrations of NAR-loaded lenses, prepared by a direct entrapment approach, showed no statistically significant difference to each other (p-value > 0.05).

The T_g of the fabricated lens (predominantly NVP-based) in this study was compared with the literature value T_g for PVP polymer of 10 k Da, which falls in a range between 66 and 124 °C (M. d. P. Buera, G. Levi, and M. Karel, , 1992). This value is dependent on the molecular weight of PVP and can also vary upon interacting with the other monomer components in the pre-polymerization mixture (Guan et al., 2011). It should be noted that only T_g values of a material prepared using the same procedure should be compared to each other. This is because T_g values depend on various experimental factors experimental such as drying method, heating rate, as well as degree of cross-linking and MW distribution.

3.4.7. Lens dimension

One of the critical lens properties that must be assessed in order to evaluate the feasibility of commercialization of the developed drug-loaded lens is its dimensional properties (Nguyen et al., 2021). Due to the comparative nature of this test as noted in Section 2.3.8, it should be noticed that the measured values of the control lens are for comparative purposes only and did not represent the true values of commercial nesofilcon A lens. The published dimensions for nesofilcon A lens are: 14.20 mm in diameter, sagittal depth of 3.820 mm and centre thickness of 0.100 mm. The developed lens diameter, sagittal depth and centre thickness are shown in Table 6.

It should be taken into consideration that this part of characterization was carried out by mainly manual observation with a ruler rather an instrument and hence, the results were estimated only and not a definitive value. Although some values showed a statistically significant difference to the blank lens, the tolerance limits for each dimensional parameter of all the measured lenses were within the acceptance criteria according to ISO 18369–2:2017 (E) (ISO, 2017). Therefore, the results demonstrated that the developed NAR-loaded lens exhibited adequate lens dimensional properties for commercialization.

3.4.8. Fourier-transform infrared spectroscopy

The spectroscopic characterization of hydrogel SCL and their monomer components was performed by Fourier-transform infrared spectroscopic analysis (FT-IR). The FT-IR spectra of blank WM, NAR-loaded WM and control lenses, all were at dry state, are shown in Fig. 6, with NAR spectrum is illustrated in Figure S5 (Supplementary Information). A detailed of each main peak value was illustrated in Table S1 (Supplementary Information).

Because NVP is the main component in the Nesofilcon A monomer mixture (>75%), it was expected that the FTIR spectra of the developed WM lenses and the control lens would exhibit the characteristic peaks of PVP (poly-vinylpyrrolidone). An intense peak at 1721 cm^{-1} observed in the control and blank WM lenses spectra represented the C = O stretching from an aliphatic ketone in NVP, which was also observed in other FTIR analysis on NVP (Lai et al., 2018; Safo et al., 2019; Loría-Bastarrachea et al., 2011), shifted to 1726 cm^{-1} in L4 lens spectrum. The two characteristic peaks (C-N stretching) at 1287 cm^{-1}, indicative of NVP (the major monomer component of the formed SCLs) could be observed in all cases. As for the developed NAR-loaded lenses formed through a direct entrapment approach, all characteristic bands present in FT-IR spectra of control and blank WM lenses appeared in the FT-IR spectrum of the obtained hydrogel. A shift in wavenumbers of the two characteristic peaks represented C = O stretching and C = C stretch could be seen in NAR-loaded lens in comparison to blank WM lens. This may have been due to the weak dipole–dipole interaction between the lens' polymeric matrix and NAR. A characteristic NAR peak at 1711 cm^{-1} (C= O stretch) could be observed in the NAR-loaded lenses spectra and NAR spectrum (Figure 6 and S5, respectively), which was not visible in the FT-IR spectra of control and blank WM lenses.

Table 6
Diameter, sagittal depth, and centre thickness values of the control and developed SCLs (n = 10).

Lens type	Diameter (mm)	Sagittal depth (mm)	Centre thickness (mm)
Control lens	14.18 ± 0.10	3.82 ± 0.09	0.116 ± 0.008
Blank WM	14.15 ± 0.09	3.79 ± 0.06	0.117 ± 0.008
L1	14.03 ± 0.08	3.91 ± 0.07	0.116 ± 0.008^{+}
L2	14.09 ± 0.10^{+}	3.77 ± 0.11^{+}	0.118 ± 0.007^{+}
L3	14.12 ± 0.05^{+}	3.83 ± 0.08^{+}	0.128 ± 0.006
L4	14.08 ± 0.09^{+}	3.75 ± 0.14	0.128 ± 0.009^{+}
L5	14.13 ± 0.09^{+}	3.86 ± 0.12^{+}	0.124 ± 0.007^{+}
ISO tolerance limit (ISO, 2017)	± 0.20 absolute*	± 0.05 absolute*	± 0.010 + 0.10 absolute*

*: values from the blank WM lens.
$^{+}$: values exhibit a p-value < 0.05 in comparison to the control lens.

3.5. In vitro release study

Since NAR is sparingly soluble in aqueous solution, the *in vitro* release study of the NAR-loaded lens was carried out in 0.1% Tween 80, in PBS (pH 7.4) to increase its water solubility, from 20.1 μg/mL (in PBS) to 152.5 μg/mL. Solubility and dissolution rate are vital factors to investigate the ocular bioavailability of a drug, and thus, it is essential to increase the dissolution of a poorly water-soluble drug (i.e., NAR). Tween 80 has been commonly used in the development of ocular drug delivery (Garrigue et al., 2017) and *in vitro* release studies for many different drug delivery systems to enhance the solubility of a therapeutic agent (Dandamudi, et al., 2021; Abouelmagd et al., 2015). Human tear film is comprised of three layers including: the outer lipid layer, the middle aqueous layer and the inner mucin layer that interacts with the corneal epithelial surface (Hodges and Dartt, 2013). Each layer in the tear film contains different compounds, including proteins, polar and nonpolar lipids, electrolytes, mucins, and water. The most abundant lipids present in human tear fluid are phospholipids, free fatty acids (FFAs), triglycerides (TGs), cholesteryl esters (CEs), and wax esters (Telenius et al., 2012). Of those, FFAs, TGs and CEs are known as neutral lipids. Hence, to better mimic the human tear film, 0.1% Tween 80 was used in this study to ensure the perfect sink condition was maintained for the release of NAR. In addition, being a nonionic surfactant, the use of 0.1% Tween 80 in the release media can ensure that there will be no interaction with NAR.

The percentage cumulative drug release (%) profiles for an initial daily release (24 h) and a 7-day release for L1-L5 lenses are shown in Fig. 7 below and Figure S6 (Supplementary Information), respectively.

As can be observed in Fig. 7, all five batches showed a controlled and sustained NAR release in the first 24 h, followed by a stabilized release of NAR over the next seven days (Figure S6, Supplementary Information). Fig. 7 illustrated that there is no correlation between the loaded NAR concentration and the lens' release profile. The outcome demonstrated that NAR release from the five developed NAR-loaded lens' systems is within the estimated therapeutic range, which was calculated at the end of the first 24 h of release (17.88, 19.04, 28.03, 40.46 and 54.42 μg/day L1, L2, L3, L4 and L5, respectively). Since this is a daily disposable SCL, it was expected that the majority of drug would be released within a day

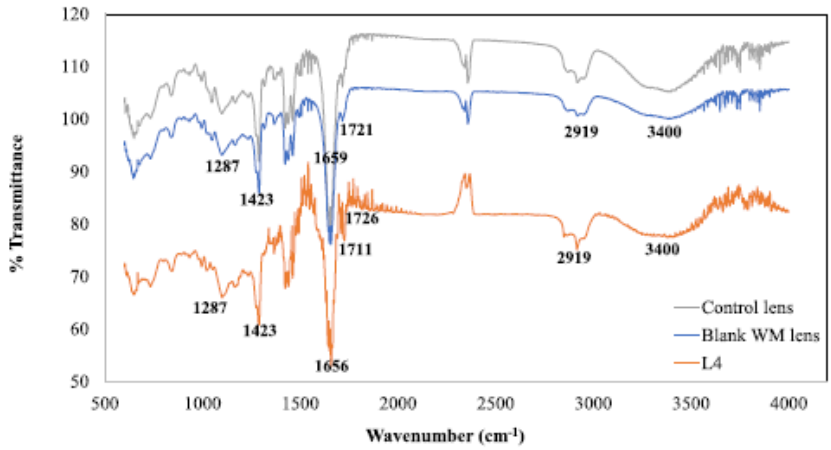

Fig. 6. Comparative FT-IR spectra of control lens, blank WM lens vs. L4 lens.

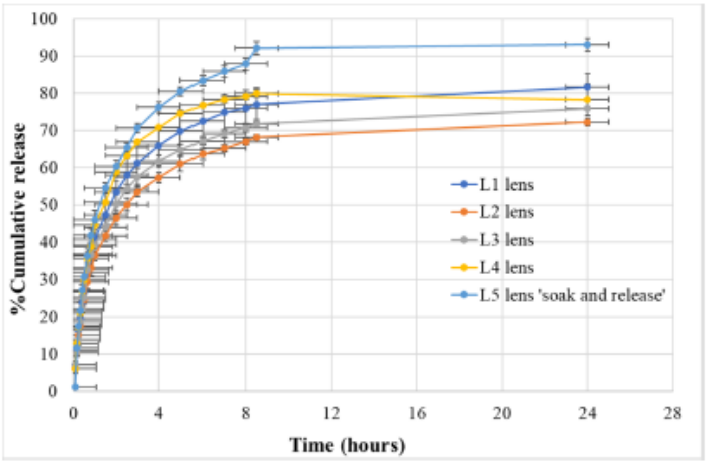

Fig. 7. *In vitro* release profiles of NAR-loaded lenses in 24 h, prepared by both direct entrapment and 'soak and release' approaches (n = 3).

for it to be therapeutically relevant. When compared with a similar work published previously (Kwak et al., 2021); which investigated the *in vitro* release profiles of a hydrophilic drug naringin from the pHEMA hydrogel lenses, a different release pattern was observed. The work carried out by Kwak *et al.* demonstrated a sustained release of naringin from the hydrogel SCL for a month, however, a controlled drug release for 24 h in this study was obtained. It is worth noting that the developed lens in this study is NVP-based, while the majority of hydrogel's material used in the development of therapeutic lens is HEMA-based. Thus, it was expected that there would be a difference in lens' properties and behaviour upon the incorporation of a drug. Additionally, as mentioned previously, the lens in this studied was manufactured using a comparable commercial process with a significantly shorter curing time and milder hydration and extraction steps.

By applying various mathematical models: zero-order, first-order, Higuchi and Korsmeyer-Peppas, the release mechanism of NAR-loaded lenses at various NAR concentrations was investigated. The applicability of all the models was tested up to 8 h (i.e., 480 min, initial release). From the generated data, the correlation coefficient (R^2) values were calculated to identify the best fit model to describe the release mechanism of the NAR-loaded lens. The R^2 values and diffusion exponent (n) and rate parameter (k) values are listed in Table 8.

As can be observed from Table 8, based on the R^2 values generated from each of the mathematical models, the initial release of NAR (in the first 8 h) from the fabricated lens in all five systems indicated a good fit for both Higuchi and Korsmeyer-Peppas models. This observation suggested that the mechanism of NAR release is mainly governed by diffusion. The diffusion exponent values 'n' obtained from the Korsmeyer-Peppas model for L5 lens was higher than 0.5 (i.e., 0.6759), indicating a non-Fickian release type. Hence, the mechanism of NAR release is governed by both diffusion and swelling for this system (Bruschi, 2015; Vigata et al., 2020). The remained four systems, L1-L4, showed the 'n' values that are very close to 0.5 (i.e., L1: 0.5001 and L4: 0.5096) or less (i.e., L2:0.4893 and L3:0.4946), suggested that these

Table 8
Release kinetic data for initial release phase (first 8 h) obtained from zero order, first order, Higuchi and Korsmeyer-Peppas mathematical models from the prepared NAR-loaded lenses.

Lens type	Drug release during initial release			
	Zero order (k unit: M/s)	First order (k unit: 1/M)	Higuchi (k unit: $M/s^{1/2}$)	Korsmeyer-Peppas
L1	R^2: 0.8114 k = 0.1373	R^2: 0.5939 k = 0.0015	R^2: 0.9433 k = 3.5792	R^2: 0.9533 n = 0.5001
L2	R^2:0.8120 k = 0.1182	R^2: 0.5814 k = 0.0015	R^2: 0.9432 k = 3.0794	R^2: 0.9451 n = 0.4893
L3	R^2: 0.7493 k = 0.1257	R^2: 0.5799 k = 0.0015	R^2: 0.9315 k = 3.2893	R^2: 0.9447 n = 0.4946
L4	R^2: 0.7808 k = 0.1426	R^2: 0.5492 k = 0.0015	R^2: 0.9247 k = 3.7497	R^2: 0.9292 n = 0.5096
L5	R^2: 0.7991 k = 0.1624	R^2: 0.3920 k = 0.0019	R^2: 0.9355 k = 4.2472	R^2: 0.7727 n = 0.6759

systems are driven by diffusion mechanism through the swollen polymeric network. The above observation agrees with previous studies on drug-loaded hydrogels. As an example, a work carried out by Pereira-da-Mota *et al.* on atorvastatin-loaded hydrogel (HEMA-based) demonstrated that the best fitted mathematical model for the developed system is Higuchi (Pereira-da-Mota et al., 2021). Aiming to investigate the novel material for the development of drug-loaded hydrogel lens, Jeencham *et al.* studied the used of chitosan and regenerated silk fibroin blended films as SCL for the delivery of diclofenac sodium (Jeencham et al., 2020). The *in vitro* drug release results from all tested drug-loaded hydrogels in this study implied that Higuchi is the best fitted model. These previous observations suggested that the release of drug from the hydrogel is governed by a diffusion-controlled mechanism.

The kinetic data from Table 8 also demonstrated that L5 exhibited a faster release rate in comparison to those fabricated using a direct entrapment approach. As such, the k values in the Higuchi model for L1-L4 lenses are in a range of 2.8–3.8 $M/s^{1/2}$, while a value of 4.8 $M/s^{1/2}$ was obtained for L5 lens. This observation was in agreement with the previous study (Maulvi at al., 2014), which was postulated to be due to the loosely binding of drug in the polymer matrix in the 'soak and release' lens in comparison to the directly entrapped lenses. Additionally, it has been suggested that the soaking duration of a lens in the drug solution could make an impact on the distribution of drug throughout the lens matrix, which in turn, can potentially impact on the diffusivity of a drug, therefore, its release profile (Lanier et al., 2021).

4. Conclusion

The development of a therapeutic-loaded hydrogel contact lens for a controlled and prolonged release of a drug has received considerable focus as an alternative approach to eye drops to treat various ocular diseases. This work was carried out using a commercial-standard process in the manufacturing of a SCL to ensure the developed lens exhibited all the critical properties that could be directly compared with a commercial lens.

Due to the favorable ocular pharmacology and pharmacokinetics of NAR in the treatment of posterior segment diseases, topical installation of NAR through daily disposable SCLs can potentially act as an effective alternative delivery system. This work investigated the feasibility for use of a NAR-loaded hydrogel contact lens fabricated using direct entrapment and 'soak and release' approaches to provide an extended release of NAR to treat diseases affecting the back of the eye.

In vitro release studies under sink conditions showed that the loaded NAR in the lens can be control released for 24 h within the estimated therapeutic window. All the formulated NAR-lens' batches were found to be suitable as a daily disposable SCL with respect to optical clarity, physicochemical, and dimensional properties when compared to the unloaded control lens (nesofilcon A). Therefore, the outcome from this work suggested that the developed NAR-loaded SCLs can potentially be used as an alternative ocular drug delivery system to treat posterior segment diseases of the eye caused by oxidative stress.

CRediT authorship contribution statement

Dan (Chau Thuy) Nguyen: Carry out experimental work, Data analysis, Conceptualization, Investigation, Writing – original draft, Writing – review & editing, Visualization, Data curation, Validation, Funding acquisition. **Joseph Dowling:** Conceptualization, Investigation, Writing – review & editing, Supervision, Validation, Funding acquisition. **Richie Ryan:** Conceptualization, Investigation, Writing – review & editing, Supervision, Validation, Funding acquisition. **Peter McLoughlin:** Conceptualization, Investigation, Writing – review & editing, Supervision, Validation, Funding acquisition. **Laurence Fitzhenry:** Conceptualization, Investigation, Writing – review & editing, Supervision, Validation, Funding acquisition.

Declaration of Competing Interest

The authors declare that they have no known competing financial interests or personal relationships that could have appeared to influence the work reported in this paper.

Acknowledgement

The authors would like to thank Sean Roche at the Pharmaceutical & Molecular Biotechnology Research Centre, South East Technological University, for his help in carrying out the XRD analysis of naringenin. We would also like to thank Adrián Martín Prado (3D-NEONET, project's grant number: 734907) for his contribution in examining the robustness of the lens characterization techniques including equilibrium water content and refractive index. We want to extend our acknowledgement to Professor Ana Paula Serro's lab (Instituto Superior Técnico, Lisbon, Portugal) for their training on the lens characterization techniques including wettability and tensile strength.

Funding sources

This work was supported by the Irish Research Council-Enterprise Partnership Scheme [grant number: EPSPG/2017/236, 2017].

Appendix A. Supplementary data

Supplementary data to this article can be found online at https://doi.org/10.1016/j.ijpharm.2022.121793.

References

Abouelmagd, S.A., Sun, B., Chang, A.C., Ku, Y.J., Yeo, Y., 2015. Release Kinetics Study of Poorly Water-Soluble Drugs from Nanoparticles: Are We Doing It Right? Mol. Pharm. 12 (3), 997–1003. https://doi.org/10.1021/mp500817h.

Achilias, D.S., 2014. Investigation of the radical polymerization kinetics using DSC and mechanistic or isoconversional methods. J. Therm. Anal. Calorim. 116 (3), 1379–1386. https://doi.org/10.1007/s10973-013-3633-y.

S. D. Achilias and I. P. Siafaka, "Polymerization Kinetics of Poly(2-Hydroxyethyl Methacrylate) Hydrogels and Nanocomposite Materials," *Processes*, vol. 5, no. 2, 2017, 10.3390/pr5020021.

Alam, M.A., Subhan, N., Rahman, M.M., Uddin, S.J., Reza, H.M., Sarker, S.D., 2014. "Effect of citrus flavonoids, naringin and naringenin, on metabolic syndrome and their mechanisms of action," (in eng). Adv Nutr 5 (4), 404–417. https://doi.org/10.3945/an.113.005603.

Alves, T.V.G., et al., 2011. Thermal analysis characterization of PAAm-co-MC hydrogels. J. Therm. Anal. Calorim. 106 (3), 717–724. https://doi.org/10.1007/s10973-011-1572-z.

Bhamra, T.S., Tighe, B.J., 2017. Mechanical properties of contact lenses: The contribution of measurement techniques and clinical feedback to 50 years of materials development. Contact Lens and Anterior Eye 40 (2), 70–81. https://doi.org/10.1016/j.clae.2016.11.005.

Bruschi, M.L., 2015. 5 - Mathematical models of drug release. In: *Strategies to Modify the Drug Release from Pharmaceutical Systems*. Woodhead Publishing, pp. 63–86.

Campbell, D., Carnell, S.M., Eden, R.J., 2013. Applicability of Contact Angle Techniques Used in the Analysis of Contact Lenses, Part 1: Comparative Methodologies. Eye & Contact Lens 39 (3), 254–262. https://doi.org/10.1097/ICL.0b013e31828ca174.

M. Dandamudi et al., "Chitosan-Coated PLGA Nanoparticles Encapsulating Triamcinolone Acetonide as a Potential Candidate for Sustained Ocular Drug Delivery," *Pharmaceutics*, vol. 13, no. 10, p. 1590, 2021. [Online]. Available: https://www.mdpi.com/1999-4923/13/10/1590.

Dixon, P., Shafor, C., Gause, S., Hsu, K.-H., Powell, K.C., Chauhan, A., 2015. Therapeutic contact lenses: a patent review. Expert Opin. Ther. Pat. 25 (10), 1117–1129. https://doi.org/10.1517/13543776.2015.1057501.

Dixon, P., Fentzke, R.C., Bhattacharya, A., Konar, A., Hazra, S., Chauhan, A., 2018. In vitro drug release and in vivo safety of vitamin E and cysteamine loaded contact lenses. Int. J. Pharm. 544 (2), 380–391. https://doi.org/10.1016/j.ijpharm.2017.11.059.

Efremov, M.Y., Olson, E.A., Zhang, M., Zhang, Z., Allen, L.H., 2004. Probing Glass Transition of Ultrathin Polymer Films at a Time Scale of Seconds Using Fast Differential Scanning Calorimetry. Macromolecules 37 (12), 4607–4616. https://doi.org/10.1021/ma035909r.

ElShaer, A., Mustafa, S., Kasar, M., Thapa, S., Ghatora, B., Alany, R.G., 2016. "Nanoparticle-Laden Contact Lens for Controlled Ocular Delivery of Prednisolone: Formulation Optimization Using Statistical Experimental Design," (in eng). Pharmaceutics 8 (2), 14. https://doi.org/10.3390/pharmaceutics8020014.

Falavarjani, K.G., Nguyen, Q.D., 2013. "Adverse events and complications associated with intravitreal injection of anti-VEGF agents: a review of literature," (in eng). Eye (Lond) 27 (7), 787–794. https://doi.org/10.1038/eye.2013.107.

O. Ford, "J&J's 'Limit-Breaking' Contact Lens Win FDA Nod," *The company's drug-eluting product treats allergic eye itch for contact lens wearers and reduces the need for eyedrops.*, March 02,2022, https://www.mddionline.com/technologies/jjs-limit-breaking-contact-lens-win-fda-nod?ADTRK=InformaMarkets&elq_mid=21119&elq_cid=882233.

Fornasiero, F., Ung, M., Radke, C.J., Prausnitz, J.M., 2005. Glass-transition temperatures for soft-contact-lens materials. Dependence on water content. Polymer 46 (13), 4845–4852. https://doi.org/10.1016/j.polymer.2005.03.084.

Garrigue, J.-S., Amrane, M., Faure, M.-O., Holopainen, J.M., Tong, L., 2017. "Relevance of Lipid-Based Products in the Management of Dry Eye Disease," (in eng), *Journal of ocular pharmacology and therapeutics : the official journal of the Association for Ocular*. Pharmacol. Ther. 33 (9), 647–661. https://doi.org/10.1089/jop.2017.0052.

Guan, L., Xu, H., Huang, D., 2011. The investigation on states of water in different hydrophilic polymers by DSC and FTIR. J. Polym. Res. 18, 681–689. https://doi.org/10.1007/s10965-010-9464-7.

Hancock, B.C., Zografi, G., 1994. The Relationship Between the Glass Transition Temperature and the Water Content of Amorphous Pharmaceutical Solids. Pharm. Res. 11 (4), 471–477. https://doi.org/10.1023/A:1018941810744.

Hodges, R.R., Dartt, D.A., 2013. Tear film mucins: front line defenders of the ocular surface; comparison with airway and gastrointestinal tract mucins. Exp. Eye Res. 117, 62–78. https://doi.org/10.1016/j.exer.2013.07.027.

Huang, C.-W., Sun, Y.-M., Huang, W.-F., 1997. Curing kinetics of the synthesis of poly(2-hydroxyethyl methacrylate) (PHEMA) with ethylene glycol dimethacrylate (EGDMA) as a crosslinking agent. J. Polym. Sci., Part A: Polym. Chem. 35 (10), 1873–1889. https://doi.org/10.1002/(SICI)1099-0518(19970730)35:10<1873::AID-POLA2>3.0.CO;2-P.

J. J. Inc. "Acuvue Theravision with Ketotifen." https://www.jnjvisionpro.ca/products/acuvue-theravision (accessed 2022).

B. L. Incorporated. "Biotrue ONEDay Contact Lenses." https://www.bausch.com/ecp/our-products/contact-lenses/myopia-hyperopia/biotrue-oneday-contact-lenses (accessed 2021).

ISO18369-1:2017: Ophthalmic optics-Contact lenses, S. S. Institute, CEN-CENELEC Management Centre: Avenue Marnix 17, B-1000 Brussels, 2017. [Online]. Available: https://www.iso.org/obp/ui/#iso:std:iso:18369:-1:ed-2:v2:en:sec:3.1.6.1.

ISO18369-2:2017: Ophthalmic optics-Contact lenses, S. S. Institute, CEN-CENELEC Management Centre: Avenue Marnix 17, B-1000 Brussels, 2017. [Online]. Available: https://www.iso.org/obp/ui/#iso:std:iso:18369:-2:ed-3:v1:en.

ISO18369-4:2017: Ophthalmic optics-Contact lenses, S. S. Institute, CEN-CENELEC Management Centre: Avenue Marnix 17, B-1000 Brussels, 2017. [Online]. Available: https://www.iso.org/obp/ui/#iso:std:iso:18369:-4:ed-2:v2:en.

Jeencham, R., Sutheenawattananonda, M., Rungchang, S., Tiyaboonchai, W., 2020. Novel daily disposable therapeutic contact lenses based on chitosan and regenerated silk fibroin for the ophthalmic delivery of diclofenac sodium. Drug Delivery 27 (1), 782–790. https://doi.org/10.1080/10717544.2020.1765432.

E. Kim, M. Saha, and K. Ehrmann, "Mechanical Properties of Contact Lens Materials," *Eye & Contact Lens*, vol. 44, 2018. [Online]. Available: https://journals.lww.com/claojournal/Fulltext/2018/11002/Mechanical_Properties_of_Contact_Lens_Materials.26.aspx.

Klähn, M., Krishnan, R., Phang, J.M., Lim, F.C.H., van Herk, A.M., Jana, S., 2019. Effect of external and internal plasticization on the glass transition temperature of (Meth) acrylate polymers studied with molecular dynamics simulations and calorimetry. Polymer 179. https://doi.org/10.1016/j.polymer.2019.121635, 121635.

Koetsier, D.W., Tan, Y.Y., Challa, G., 1980. Radical polymerization of N-vinylpyrrolidone in the presence of syndiotactic poly(methacrylic acid) templates. Journal of Polymer Science: Polymer Chemistry Edition 18 (6), 1933–1943. https://doi.org/10.1002/pol.1980.170180629.

Korogiannaki, M., Zhang, J., Sheardown, H., 2017. Surface modification of model hydrogel contact lenses with hyaluronic acid via thiol-ene "click" chemistry for enhancing surface characteristics. J. Biomater. Appl. 32 (4), 446–462. https://doi.org/10.1177/0885328217733443.

Kwak, G., Kim, H., Jang, W.-D., Ryu, G.-C., Kim, I.-S., 2021. Antibacterial Effect of Naringin-containing Soft Contact Lens. Bull. Korean Chem. Soc. 42 (10), 1345–1350. https://doi.org/10.1002/bkcs.12375.

Lai, C.-F., Li, J.-S., Fang, Y.-T., Chien, C.-J., Lee, C.-H., 2018. UV and blue-light anti-reflective structurally colored contact lenses based on a copolymer hydrogel with amorphous array nanostructures. RSC Adv. 8, 4006–4013. https://doi.org/10.1039/C7RA12753G.

Lanier, O.L., Manfre, M., Kulkarni, S., Bailey, C., Chauhan, A., 2021. Combining modeling of drug uptake and release of cyclosporine in contact lenses to determine partition coefficient and diffusivity. Eur. J. Pharm. Sci. 164 https://doi.org/10.1016/j.ejps.2021.105891, 105891.

Li, C.-C., Chauhan, A., 2006. Modeling Ophthalmic Drug Delivery by Soaked Contact Lenses. Ind. Eng. Chem. Res. 45 (10), 3718–3734. https://doi.org/10.1021/ie0507934.

Lin, J., et al., 2015. "Ocular pharmacokinetics of naringenin eye drops following topical administration to rabbits," (in eng), *Journal of ocular pharmacology and therapeutics : the official journal of the Association for Ocular*. Pharmacol. Ther. 31 (1), 51–56. https://doi.org/10.1089/jop.2014.0047.

B. Q. Lin and G. Chiou, "Antioxidant activity of naringenin on various oxidants induced damages in ARPE-19 cells and HUVEC," *Int J Ophthalmol*, vol. 8, pp. 1963-1967, 10/25 2008.

Lin, M.C., Svitova, T.F., 2010. "Contact lenses wettability in vitro: effect of surface-active ingredients," (in eng). Optom. Vis. Sci. 87 (6), 440–447. https://doi.org/10.1097/OPX.0b013e3181dc9a1a.

M. Lira, C. Lourenço, M. Silva, and G. Botelho, "Physicochemical stability of contact lenses materials for biomedical applications," (in eng), *J Optom*, vol. 13, no. 2, pp. 120-127, Apr-Jun 2020, 10.1016/j.optom.2019.10.002.

Loría-Bastarrachea, M., Herrera, W., Cauich, J., Vázquez, H., Avila-Ortega, A., Cervantes, M., 2011. A TG/FTIR study on the thermal degradation of poly(vinyl pyrrolidone). J. Therm. Anal. Calorim. 104, 737–742. https://doi.org/10.1007/s10973-010-1061-9.

M. d. P. Buera, G. Levi, and M. Karel, "Glass transition in poly(vinylpyrrolidone): effect of molecular weight and diluents," *Biotechnology Progress*, vol. 8, no. 2, pp. 144-148, 1992, 10.1021/bp00014a008.

Manaia, E.B., Abuçafy, M.P., Chiari-Andréo, B.G., Silva, B.L., Oshiro Junior, J.A., Chiavacci, L.A., 2017. "Physicochemical characterization of drug nanocarriers," (in eng). Int. J. Nanomed. 12, 4991–5011. https://doi.org/10.2147/IJN.S133832.

M. F. Manchope *et al.*, "Naringenin Inhibits Superoxide Anion-Induced Inflammatory Pain: Role of Oxidative Stress, Cytokines, Nrf-2 and the NO-cGMP-PKG-KATP Channel Signaling Pathway," (in eng), *PLoS One*, vol. 11, no. 4, 2016, 10.1371/journal.pone.0153015.

Martínez, R.M., et al., 2015. Naringenin Inhibits UVB Irradiation-Induced Inflammation and Oxidative Stress in the Skin of Hairless Mice. J. Nat. Prod. 78 (7), 1647–1655. https://doi.org/10.1021/acs.jnatprod.5b00198.

Materials Data Book, *Cambridge University Engineering Department*, 2003 ed. Cambridge, UK: Cambridge University Engineering Department, 2003. [Online]. Available: http://www-mdp.eng.cam.ac.uk/web/library/enginfo/cueddatabooks/materials.pdf. Accessed on: 15 April, 2019.

Maulvi, F.A., 2014. Effect of Timolol Maleate Concentration on Uptake and Release from Hydrogel Contact Lenses using Soaking Method. J. Pharmacy Applied Sciences 1, 16–22.

Maulvi, F.A., et al., 2017. pH triggered controlled drug delivery from contact lenses: Addressing the challenges of drug leaching during sterilization and storage. Colloids Surf., B 157, 72–82. https://doi.org/10.1016/j.colsurfb.2017.05.064.

Nguyen, D.C.T., Dowling, J., Ryan, R., McLoughlin, P., Fitzhenry, L., 2021. Pharmaceutical-loaded contact lenses as an ocular drug delivery system: A review of critical lens characterization methodologies with reference to ISO standards. Contact Lens and Anterior Eye. https://doi.org/10.1016/j.clae.2021.101487, 101487.

Nogata, Y., Sakamoto, K., Shiratsuchi, H., Ishii, T., Yano, M., Ohta, H., 2006. Flavonoid Composition of Fruit Tissues of Citrus Species. Biosci. Biotechnol. Biochem. 70 (1), 178–192. https://doi.org/10.1271/bbb.70.178.

Oguido, A.P.M.T., et al., 2017. Naringenin Eye Drops Inhibit Corneal Neovascularization by Anti-Inflammatory and Antioxidant Mechanisms. Invest. Ophthalmol. Vis. Sci. 58 (13), 5764–5776. https://doi.org/10.1167/iovs.16-19702.

Peng, C.-C., Kim, J., Chauhan, A., 2010. Extended delivery of hydrophilic drugs from silicone-hydrogel contact lenses containing Vitamin E diffusion barriers. Biomaterials 31 (14), 4032–4047. https://doi.org/10.1016/j.biomaterials.2010.01.113.

A. F. Pereira-da-Mota, M. Vivero-Lopez, A. Topete, A. P. Serro, A. Concheiro, and C. Alvarez-Lorenzo, "Atorvastatin-Eluting Contact Lenses: Effects of Molecular Imprinting and Sterilization on Drug Loading and Release," *Pharmaceutics*, vol. 13, no. 5, p. 606, 2021. [Online]. Available: https://www.mdpi.com/1999-4923/13/5/606.

A. Pulliero, A. Profumo, C. Rosano, A. Izzotti, and S. C. Saccà, "Therapeutic Hydrogel Lenses and the Antibacterial and Antibiotic Drugs Release," *Applied Sciences*, vol. 11, no. 4, 2021, 10.3390/app11041931.

Ramprasath, T., Senthamizharasi, M., Vasudevan, V., Sasikumar, S., Yuvaraj, S., Selvam, G.S., 2014. Naringenin confers protection against oxidative stress through upregulation of Nrf2 target genes in cardiomyoblast cells. J. Physiol. Biochem. 70 (2), 407–415. https://doi.org/10.1007/s13105-014-0318-3.

R. Rashmi, S. Bojan Magesh, K. Mohanram Ramkumar, S. Suryanarayanan, and M. Venkata SubbaRao, "Antioxidant Potential of Naringenin Helps to Protect Liver Tissue from Streptozotocin-Induced Damage," (in eng), *Rep Biochem Mol Biol*, vol. 7, no. 1, pp. 76-84, 2018. [Online]. Available: https://pubmed.ncbi.nlm.nih.gov/30324121.

Ruh, M.F., Zacharewski, T., Connor, K., Howell, J., Chen, I., Safe, S., 1995. Naringenin: A weakly estrogenic bioflavonoid that exhibits antiestrogenic activity. Biochem. Pharmacol. 50 (9), 1485–1493. https://doi.org/10.1016/0006-2952(95)02061-6.

Safo, I.A., Werheid, M., Dosche, C., Oezaslan, M., 2019. The role of polyvinylpyrrolidone (PVP) as a capping and structure-directing agent in the formation of Pt nanocubes. Nanoscale Advances 1 (8), 3095–3106. https://doi.org/10.1039/C9NA00186G.

Silva, D., et al., 2020. Diclofenac sustained release from sterilised soft contact lens materials using an optimised layer-by-layer coating. Int. J. Pharm. 585 https://doi.org/10.1016/j.ijpharm.2020.119506, 119506.

Silva, D., Fernandes, A.C., Nunes, T.G., Colaço, R., Serro, A.P., 2015. The effect of albumin and cholesterol on the biotribological behavior of hydrogels for contact lenses. Acta Biomater. 26, 184–194. https://doi.org/10.1016/j.actbio.2015.08.011.

Telenius, J., Koivuniemi, A., Kulovesi, P., Holopainen, J.M., Vattulainen, I., 2012. Role of Neutral Lipids in Tear Fluid Lipid Layer: Coarse-Grained Simulation Study. Langmuir 28 (49), 17092–17100. https://doi.org/10.1021/la304366d.

Tranoudis, I., Efron, N., 2004. Water properties of soft contact lens materials. Contact Lens and Anterior Eye 27 (4), 193–208. https://doi.org/10.1016/j.clae.2004.08.003.

M. Vigata, C. Meinert, D. W. Hutmacher, and N. Bock, "Hydrogels as Drug Delivery Systems: A Review of Current Characterization and Evaluation Techniques," *Pharmaceutics*, vol. 12, no. 12, p. 1188, 2020. [Online]. Available: https://www.mdpi.com/1999-4923/12/12/1188.

Wan, D., Satoh, K., Kamigaito, M., Okamoto, Y., 2005. Xanthate-Mediated Radical Polymerization of N-Vinylpyrrolidone in Fluoroalcohols for Simultaneous Control of Molecular Weight and Tacticity. Macromolecules 38 (25), 10397–10405. https://doi.org/10.1021/ma0515230.

Wang, H., et al., 2020. Nanocomplexes based polyvinylpyrrolidone K-17PF for ocular drug delivery of naringenin. Int. J. Pharm. 578 https://doi.org/10.1016/j.ijpharm.2020.119133, 119133.

Wang, Z., et al., 2021. "Novel Contact Lenses Embedded with Drug-Loaded Zwitterionic Nanogels for Extended Ophthalmic Drug Delivery," (in eng). Nanomaterials (Basel) 11 (9), 2328. https://doi.org/10.3390/nano11092328.

Weng, Y., Liu, J., Jin, S., Guo, W., Liang, X., Hu, Z., 2017. Nanotechnology-based strategies for treatment of ocular diseases. Acta Pharmaceutica Sinica B 7 (3), 281–291.

Yang, W., Tan, Y., Li, C., Liu, Y., Lu, G., 2018. Observation of curative effect of intravitreal injection of conbercept in wet age-related macular degeneration: Optical coherence tomography analysis after injection. Microsc. Res. Tech. 81 (4), 384–388. https://doi.org/10.1002/jemt.22989.

Zaidun, N.H., Thent, Z.C., Latiff, A.A., 2018. Combating oxidative stress disorders with citrus flavonoid: Naringenin. Life Sci. 208, 111–122. https://doi.org/10.1016/j.lfs.2018.07.017.

Zhang, P., Liu, X., Hu, W., Bai, Y., Zhang, L., 2016. Preparation and evaluation of naringenin-loaded sulfobutylether-β-cyclodextrin/chitosan nanoparticles for ocular drug delivery. Carbohydr. Polym. 149, 224–230. https://doi.org/10.1016/j.carbpol.2016.04.115.